

Development and Study of Aminocatalyzed Asymmetric
Organic Reactions

by

Jorge Manuel de Carvalho Marques Dourado

A Thesis Submitted to the Faculty of Graduate Studies of
the University of Manitoba
in partial fulfilment of the requirements of the degree of

DOCTOR OF PHILOSOPHY

Department of Chemistry
University of Manitoba
Winnipeg

Copyright © 2021 by Jorge Manuel de Carvalho Marques Dourado

Abstract

Chirality is an important feature that many Organic molecules possess and can have huge repercussions in the activity of Organic compounds. Therefore, the development of stereoselective methodologies in Organic chemistry has been an area of focus for many years. In the 2000s, organocatalysis emerged as an excellent tool for asymmetric synthesis and quickly received a great deal of attention by chemists namely, the field of aminocatalysis, where small amine-based chiral organic molecules could be used as catalysts to, not only activate carbonyl compounds but also, to provide the required facial differentiation during the chemical transformations these carbonyl molecules underwent and thus, produce enantioenriched products.

The activation of carbonyl compounds, namely aldehydes and ketones can take place either by increasing their nucleophilicity (enamine pathway or HOMO-activation pathway) or by increasing their electrophilicity (iminium ion pathway or LUMO-lowering pathway). These small chiral amine-based molecules are easily accessible from natural sources like amino acids and cinchona alkaloids. Taking advantage of the vinylogy principle, reactivity of the carbonyl substrates can be extended to more remote positions whilst maintaining total control over the stereo-outcome of the transformations. In more recent years, aminocatalysis has been proven to be an excellent way of achieving several cycloaddition reactions with excellent levels of enantiocontrol, yielding highly functionalized products bearing multiple contiguous stereocenters.

The focus of this Thesis will be in the computational study and subsequent application of aminocatalysis in the development of asymmetric pericyclic reactions, namely cycloadditions. Four projects will be discussed, starting with a DFT study (M06-2X/6-31+G(d,p)) on the aminocatalyzed induced dearomatization of heteroaromatic aldehydes which, following the results obtained, allowed us to develop two distinct approaches to the synthesis of dihydropyrido[1,2-a]indole scaffolds, either through an intramolecular Michael addition reaction or through an aza-Diels-Alder reaction.

The exploration of aminocatalysis as a tool for higher-order cycloadditions was also explored in this Thesis, by use of an oxo-fulvene system. However, this fulvene system proved troublesome to synthesize and the desired reactions were never studied.

Asymmetric Ireland-Claisen rearrangements were also explored in this Thesis using either H-bond catalysis or APTC. Unfortunately, lack of reactivity of the starting materials and side reactions failed to give the desired rearranged products.

Acknowledgments

I would like to thank my parents, Manuel Dourado and Ana Cristina de Carvalho Marques Dourado, for their patience, support and encouragement since my days as a toddler until now as well as for making sure that I would always be able to go back to Portugal, once a year, to run away from Canadian Winter for a couple of weeks and bring back some sunshine and warmth with me.

I would also like to thank my supervisor Dr. Rebecca Davis for accepting me as her PhD student. I am very grateful for her guidance and mentorship during my PhD. I learnt a lot during my years as a graduate student under her supervision and I developed quite a taste for pericyclic reactions despite some frustrating results.

I would like to thank all of Dr. Davis' group members both present and past for all the help and fruitful discussions. I would particularly like to acknowledge Simarpreet Singh for his help in the computational project described in this Thesis, Michael Packer for his help on the Ireland-Claisen project, and Erin Liebrecht for her help with the intramolecular Michael additions project.

I would like to thank Dr. Kirk Murat and Dr. David Davidson for keeping the NMR apparatus always running and for their availability to help in any questions or issues I might come about.

I would like to thank all my friends for all their support, both the ones I made here in Canada who made my staying here more memorable as well as the ones I left in Portugal who would always find the time for a nice diner party when I went back on holidays!

Last but not least, I would like to thank the members of my PhD Committee, both past and present, for all their support and constructive feedback during our meetings.

I would like to dedicate this Thesis to Dr. Philip Hultin

Contents

Abstract	ii
List of Tables	viii
List of Figures	x
List of Schemes	xii
List of Abbreviations	xviii
Part I – Introduction	23
Chapter I – Asymmetric Synthesis	24
Chapter II – Pericyclic Reactions	26
Chapter III – Organocatalysis	38
Chapter IV – Aminocatalysis	41
Part II – Results and Discussion	76
Chapter I – Computational Study on Dearomative Aminocatalysis	77
Chapter II - Organocatalyzed Asymmetric Synthesis of Dihydropyrido[1,2-a]indoles ...	96
Chapter III – Higher-Order Cycloadditions	114
Chapter IV – Organocatalyzed Asymmetric Ireland-Claisen Rearrangement	131
Part III – Conclusions	149
Part IV – Experimental Section	154
General Methods	155

Chapter I – Synthesis and Characterization of Organocatalysts	156
Chapter II – General Procedures for the Synthesis of Dihydropyrido[1,2-a]indole Scaffolds	166
Chapter III – General Procedures for the High Order Cycloadditions.....	171
Chapter III – Ireland-Claisen Rearrangement	180
Chapter IV – Energies and Reaction Coordinates.....	187
Part V – References	275
Part VI – Annexes	304

List of Tables

Table 1. 1 – Summary of the selection rules for pericyclic reactions (where p+q denote the total number of electrons involved in the process, n is an integer number like 0,1,2,3,..., s stands for suprafacial and a stands for antarafacial).....	29
Table 1. 2 –Effect of silyl group (R ₁) of catalyst family III in enantioselectivity.	50
Table 1. 3 – High Order cycloadditions developed by Jørgensen and co-workers.	71
Table 2. 1 – Hyperhomodesmotic equations for Model System A (relative free energies in kcal/mol). ...	79
Table 2. 2 – Orbital coefficients of the HOMO of Model System A.	81
Table 2. 3 – Hyperhomodesmotic equations for Model System B (relative free energies in kcal/mol). ...	83
Table 2. 4 – Comparison between the bond lengths (Å) for aldehydes B1-3 and iminium ions B9-11 , in Model System B.....	83
Table 2. 5 – Orbital coefficients of the HOMO of Model System B.	84
Table 2. 6 – Hyperhomodesmotic equations for Model System C (relative free energies in kcal/mol). ...	86
Table 2. 7 – Orbital coefficients for the HOMO of Model System C.	87
Table 2. 8 – Hyperhomodesmotic equations for Model System D (relative free energies in kcal/mol). ...	89
Table 2. 9 – Orbital coefficients for the HOMO of Model System D.....	90
Table 2. 10 – Hyperhomodesmotic equations for Model System E (relative free energies in kcal/mol)...	91
Table 2. 11 – Bond distances (Å) and angles (°) in thiophene, iminium ion E11 and trienamine E15	92
Table 2. 12 – Orbital coefficients for the HOMO of Model System E.	93
Table 2. 13 – Initial screening for the intramolecular Michael addition of 133	98
Table 2. 14 – Screening of reaction conditions for the intramolecular Michael addition of 131	100
Table 2. 15 – Screening of conditions for the intramolecular Michael addition reaction of 131 catalyzed by Va·3HCl.	100
Table 2. 16 – Screening of reaction conditions for the intramolecular Michael addition of 131 using secondary amine organocatalysts.....	102

Table 2. 17 – Scope of secondary aminocatalysts for the intramolecular Michael addition of 131	105
Table 2. 18 – Screening of catalysts and dienophiles for the aza-Diels-Alder reaction of 134	109
Table 2. 19 – Screening of catalysts for the cooperative iminium ion/dienamine process.	111
Table 2. 20 – Oxidation reactions tested for the conversion of 146 into 143 (for detailed experimental procedures see Chapter IV).....	117
Table 2. 21 – Attempts to generate tetraenamine 144 and/or hemiaminal 163	129
Table 2. 22 – Test reactions for the enantioselective IC of 169 , under APTC conditions.	135
Table 2. 23 – Test reactions for the enantioselective IC under APTC conditions.	137
Table 2. 24 – Test reactions for the enantioselective IC of 175 under APTC conditions.	140
Table 2. 25 – Test reactions for the enantioselective IC of 175 under APTC conditions.	141
Table 2. 26 – Thiourea XVIII induced IC reaction.....	143
Table 2. 27 – Schreiner’s thiourea (XIX) catalyzed IC reaction.....	144
Table 2. 28 – Guanidine induced IC rearrangement.....	146
Table 2. 29 – Primary amine induced IC rearrangement of ester 175	147

List of Figures

Figure 1. 1 – Selected examples of pairs of enantiomers and their respective biological activity.....	24
Figure 1. 2 – Orbital diagram for the Diels-Alder reaction showcasing the two possible HOMO/LUMO interactions, (a) and (b), with path (a) being favoured over path (b) due to the lower energy gap associated.	28
Figure 1. 3 – Frontier orbital coefficients of cyclopentadiene 1 and tropone 9 (top view of the orbitals).	35
Figure 1. 4 – Activation modes in aminocatalysis (A) enamine pathway, and (B) iminium ion pathway.	41
Figure 1. 5 – Stereoselectivity in aminocatalysis (A) induced by steric bulk; (B) induced by H-bond interactions.....	42
Figure 1. 6 – Relevant enamine and iminium ion intermediates (Ar = 3,5-(CF ₃) ₂ C ₆ H ₃ ; relative energies in kcal/mol calculated at the B3LYP/6-31 G(d) level of theory).....	48
Figure 1. 7 –Enamine (left) and iminium ion (right) conformations from catalyst IIIa	49
Figure 1. 8 – Catalytic cycles for primary amine catalysis: (A) enamine pathway and, (B) iminium ion pathway.....	56
Figure 1. 9 – Possible conformations of trienamine 66 (relative energies in kcal/mol calculated at the B3LYP/6-31G(d) level of theory; Orbital coefficients calculated at the HF/STO-3G level of theory).....	62
Figure 1. 10 – Modes of remote activation in aminocatalysis.	69
Figure 2. 1 – HOMO of trienamines A13-A15 for Model System A (isovalue (0.035).	81
Figure 2. 2 – HOMO of trienamines B12-15 for Model System B (isovalue 0.035).....	84
Figure 2. 3 – HOMO of trienamines C12-15 for Model System C (isovalue 0.035).....	87
Figure 2. 4 – HOMO of trienamines D12-15 for Model System D (isovalue 0.035).	90
Figure 2. 5 – HOMO of trienamines E12-15 for Model System E (isovalue 0.035).	93
Figure 2. 6 – Selection of biologically active alkaloids with a dihydropyrido[1,2-a]indole core structure.	96
Figure 2. 7 – ¹ H NMR of reaction from Table 2.13, entry 1 (300 MHz, CDCl ₃).	98

Figure 2. 8 – ^1H NMR of reaction from Table 2.13, entry 2. Signals from imine 137 highlighted in red (300 MHz, CDCl_3).	99
Figure 2. 9 – ^1H NMR spectrum of hydroamination product, 138 (300 MHz in CDCl_3).	104
Figure 2. 10 – Reaction scheme and ^1H NMR of the DMP/ H_2O oxidation of 143 (recorded in CDCl_3 at 300 MHz).	121
Figure 2. 11 – ^1H NMR spectra of DMP/ H_2O oxidation of 146 ; red spectrum – after work up; blue spectrum – after column chromatography (both spectra recorded in CDCl_3 at 300 MHz).	122
Figure 2. 12 – Enthalpies of dissociation for 7-hydroxy fulvenes and their nonallylic analogues (relative energies in kcal/mol calculated at the G3MP2 level of theory).	124
Figure 2. 13 – Transition states for the formation of the E- and Z-enolates with LDA.	132
Figure 2. 14 – Overlap of the ^1H -NMR zoomed in the double bond region,: red – trans-2-penten-1-ol, green – 169 , and blue – crude reaction mixture of entry 3 from Table 2.23 (300 MHz in CDCl_3).	136
Figure 2. 15 – ^1H NMR spectrum of alcohol 171 (300 MHz in CDCl_3).	138

List of Schemes

Scheme 1. 1 – First example of a Diels-Alder reaction between cyclopentadiene 1 and 1,4-benzoquinone 2	26
Scheme 1. 2 – Comparisson between the allowed [4+2]-cycloaddition and the forbidden [2+2]-cycloaddition between 1 and 2	31
Scheme 1. 3 – Regioselectivity and endo vs exo approach in the Diels-Alder reaction between 1 and 2 ..	33
Scheme 1. 4 – Regioselectivity of Diels-Alder reactions when the asymmetric diene 6 and dienophile 7 are used.	33
Scheme 1. 5 – Periselectivity in the cycloaddition between cyclopentadiene 1 and tropone 9	34
Scheme 1. 6 – Selected examples of seminal high order cycloadditions.	35
Scheme 1. 7 – General representation of a (n,m)-sigmatropic rearrangement.	36
Scheme 1. 8 – Generic examples of electrocyclic reactions, (top) involving 8π ($4n$) electrons, and (bottom) involving 6π ($4n+2$) electrons.	37
Scheme 1. 9 – Hajos-Parrish-Eder-Sauer-Wiechert intramolecular aldol cyclization catalyzed by S-proline (I).	39
Scheme 1. 10 – (1) List's and co-workers S-proline (I) catalyzed aldol reaction; and (2) MacMillan's and co-workers oxazolidinone (II) catalyzed Diels-Alder reaction.	39
Scheme 1. 11 – Mechanism of the S-proline (I) catalyzed aldol reaction.....	43
Scheme 1. 12 – Mechanism of the imidazolidinone (II) catalyzed Diels-Alder reaction.	44
Scheme 1. 13 – Hayashi's highly enantioselective Michael addition catalyzed by IIIa	45
Scheme 1. 14 – Jørgensen's highly enantioselective α -functionalizations of aldehydes catalyzed by IIIb	46
Scheme 1. 15 – Catalyst design for improved reactivity and selectivity.....	47
Scheme 1. 16 – Divergent reaction pathways via iminium ion activation of enals 25 with different catalysts and reaction conditions.	51

Scheme 1. 17 –Michael addition of α,α -dicyanoalkenes 36 to enones 37 catalyzed by Va (dr's not reported in original paper).....	54
Scheme 1. 18 – α -Functionalization of ketones (39 and 43) and aldehydes (40) via enamine activation with cinchona alkaloids; (1) Connon et. al. Michael addition to nitroolefins 29 catalyzed by Vb , and (2) Chen et. al. amination of ketones with 44 catalyzed by Vc	55
Scheme 1. 19 – Enantioselective γ -amination of enals 46 catalyzed by IIIb (Ar = 3,5-(CF ₃) ₂ C ₆ H ₃).	56
Scheme 1. 20 – Proposed mechanism for the dienamine-mediated γ -amination reaction reported by Jørgensen and co-workers (Ar = 3,5-(CF ₃) ₂ C ₆ H ₃ ; relative energies in kcal/mol calculated at the B3LYP/6-31G(d) level of theory).	57
Scheme 1. 21 – Entrapment of the catalyst by a carbon-based dienophile (Ar = 3,5-(CF ₃) ₂ C ₆ H ₃).	57
Scheme 1. 22 – Eliminative regeneration of aminocatalysts in dienamine/iminium ion-mediated [4+2]-cycloadditions, (1) reported by Hong and co-workers and, (2) reported by Christmann and co-workers..	59
Scheme 1. 23 – Synthesis of steroid scaffolds, via dienamine intermediates, reported by Jørgensen and co-workers.....	60
Scheme 1. 24 – Cross-dienamine-mediated Diels-Alder reaction reported by Jørgensen and co-workers.	60
Scheme 1. 25 – Trienamine-mediated Diels-Alder reactions reported by Jørgensen, Chen, and co-workers.	61
Scheme 1. 26 – Selected examples of trienamine-mediated asymmetric Diels-Alder reactions.....	62
Scheme 1. 27 – Cross-trienamine-mediated Diels-Alder reactions reported by Jørgensen and co-workers.	63
Scheme 1. 28 – Houk's computational study on the cross-trienamine-mediated Diels-Alder reaction (relative free energies in kcal/mol, calculated at the M06-2X/def2-TZVPP/IEFPCM(CHCl ₃)/B97D/6-31+G(d,p)/IEFPCM (CHCl ₃)).....	64
Scheme 1. 29 – Heterocyclic ortho-quinomethane mediated Diels-Alder reaction reported by Melchiorre and co-workers.....	65

Scheme 1. 30 – One-pot Aminocatalysis/NHC sequential Diels-Alder/Benzoin reaction reported by Melchiorre and co-workers.	66
Scheme 1. 31 – Dearomatized trienamine mediated ϵ -functionalization of furfural derivatives reported by Albrecht and co-workers.	66
Scheme 1. 32 – Tetraenamine mediated [4+2]-cycloaddition reported by Jørgensen and co-workers.	67
Scheme 1. 33 – Dienamine mediated protocol with consequent trapping of the catalyst.	67
Scheme 1. 34 – oxa-Diels-Alder reaction via a dearomatized tetraenamine intermediate, reported by Chen and co-workers.	68
Scheme 1. 35 – Intramolecular [6+2]-cycloaddition reported by Hayashi, Uchimaro and co-workers.	69
Scheme 1. 36 – [6+2]-Cycloaddition reported by Ouyang, Chen, and co-workers.	70
Scheme 1. 37 – Switchable periselectivity of the reaction reported by Ouyang, Chen, and co-workers. ...	72
Scheme 1. 38 – [8+2]-Cycloaddition reported by Jørgensen and co-workers.	73
Scheme 1. 39 – [10+4]-Cycloaddition reported by Jorgensen and co-workers.	73
Scheme 1. 40 – [10+2]-Cycloaddition reported by Jørgensen and co-workers.	74
Scheme 1. 41 – Hetero-[6+4]- and [6+2]-cycloadditions reported by Jørgensen and co-workers.	75
Scheme 1. 42 – [8+2]-Cycloaddition reported by Albrecht and co-workers.	75
Scheme 2. 1 – Model Systems studied in this section.	77
Scheme 2. 2 – Michael addition reaction between furfural 124 and 3-olefinic oxindoles 125 , reported by Chen and co-workers.	85
Scheme 2. 3 – Diels-Alder reaction between 3-olefinic oxindoles 67 and pyrrole 127 or furan 128 , reported by Melchiorre and co-workers.	88
Scheme 2. 4 – Energy differences between trienamines and possible fulvene systems for Model Systems A-E (relative free energies in kcal/mol).....	94

Scheme 2. 5 – Proposed synthetic paths for the synthesis of chiral tetrahydroisoquinolines 133 and 136 ; (1) via dienamine catalyzed intramolecular Michael addition and (2) via hetero-cross-trienamine catalyzed aza-Diels-Alder.....	97
Scheme 2. 6 – Test reaction for the intramolecular Michael addition, using 100 mol% of pyrrolidine... 103	103
Scheme 2. 7 – Test reaction to trap dienamine 132a	107
Scheme 2. 8 – Formation of the stable vinylogous iminium ion intermediary 142	110
Scheme 2. 9 – Cooperative iminium ion/dienamine processes for the synthesis of dihydropyrido[1,2-a]indole scaffolds.....	111
Scheme 2. 10 – Cross-aldol of trans-2-hexenal promoted by catalyst XV	112
Scheme 2. 11 – Test reactions to trap either iminium ion 142 or cross-trienamine 135	112
Scheme 2. 12 – Proposed biosynthetic paths for spinosyn A, heronamide A and streptoseomycin.	115
Scheme 2. 13 – Proposed strategy for the tetraenamine mediated higher-order cycloadditions.	116
Scheme 2. 14 – Synthetic path for oxo-fulvene 143	116
Scheme 2. 15 – Rational for the use of DDQ for the formation of 143	118
Scheme 2. 16 – Proposed mechanism for the TEMPO/BAIB oxidation of alcohols.	118
Scheme 2. 17 – Erden and co-workers NaIO ₄ oxidation of 148 and our approach to 143	119
Scheme 2. 18 – Reactivity of 6-(chloromethyl)-6-methylfulvene 150 towards different strength nucleophiles (adapted from ref. 209).	123
Scheme 2. 19 – Reactivity of 150 towards methoxide reported by Erden, Gronert and co-workers.	124
Scheme 2. 20 – Possible reason for the failure to oxidize 146 into 143	125
Scheme 2. 21 – New synthetic route to oxo-fulvene 143	126
Scheme 2. 22 – Synthetic route to 156 via mesylation of 157	127
Scheme 2. 23 – Attempt to synthesize 3-oxobutanenitrile 159 for subsequent synthesis of fulvene 157 .127	127
Scheme 2. 24 – New synthetic route for fulvene 143 with unexpected synthesis of fulvene 162	128
Scheme 2. 25 – Attempts to convert acetal 162 into aldehyde 143	128
Scheme 2. 26 – General example of an Ireland-Claisen rearrangement.....	131

Scheme 2. 27 – Relative stereo-outcome of the Ireland-Claisen rearrangement based on the configuration of the R ₂ substituent.	132
Scheme 2. 28 – Enantioselective IC reported by Corey and co-workers.	134
Scheme 2. 29 – Approaches envisioned for the stereoselective IC; path a: asymmetric phase-transfer approach and; path b: asymmetric H-bond approach (R ₂ * denotes the chiral moiety of the catalyst).....	134
Scheme 2. 30 – Test reaction to study the hydrolysis of the starting ester.	136
Scheme 2. 31 – Mechanism for the elimination of N-Boc glycinate group in ester 169b with subsequent production of alcohol 171	138
Scheme 2. 32 – Enolate trapping experiments.	139
Scheme 2. 33 – Test reaction for the APTC IC reaction using ester 173	140
Scheme 2. 34 – Required conformation of the enolate for the TS of the IC reaction (top) vs non-viable conformation of the enolate (bottom).	142
Scheme 2. 35 – Rationale for the new approach to the IC rearrangement.	146
Scheme 4. 1 – Synthesis of catalyst IIIa	156
Scheme 4. 2 – Synthetic route for catalysts IV and XII	157
Scheme 4. 3 – Synthesis of primary amine catalyst XIII	159
Scheme 4. 4 – Synthesis of primary amine XIV	159
Scheme 4. 5 – Reaction scheme for the synthesis of Schreiner’s thiourea.	160
Scheme 4. 6 – Reduction of S-phenylalanine.	160
Scheme 4. 7 – General reaction scheme for the synthesis of catalyst XX	161
Scheme 4. 8 – Synthetic route for the synthesis of catalyst XV	163
Scheme 4. 9 – Synthetic path to compound 131	166
Scheme 4. 10 – Synthetic path for substrate 134	168
Scheme 4. 11 – Synthetic route to the 3-olefinic oxindole 67	170

Scheme 4. 12 – General reaction scheme for the synthesis of fulvenes.	171
Scheme 4. 13 – General reaction scheme for the oxidation of 146 to 143	173
Scheme 4. 14 – General reaction scheme for the cyanation of 157	177
Scheme 4. 15 – Synthetic route for the formation of fulvene 156	178
Scheme 4. 16 – General reaction Scheme for the synthesis of allylic alcohols 194a and 194b via Grignard reaction.....	182
Scheme 4. 17 – General procedure for the Steglich esterification reactions.	183
Scheme 4. 18 – General reaction scheme for the transesterification of ethyl acetoacetate.	185
Scheme 4. 19 – Reaction scheme for the esterification of potassium isocyanoacetate.	186

List of Abbreviations

°C	degrees Celsius
Å	Angstrom
Ac	Acetyl
APTC	Asymmetric Phase-Transfer Catalysis
aq.	aqueous
Ar	Aryl
B3LYP	Becke, 3-parameter, Lee-Yang-Parr
B97D	Grimme's functional
BA	Benzoic acid
BAIB	(Bisacetoxyiodo)benzene
Bn	Benzyl
Boc	<i>tert</i> -Butoxycarbonyl
cat.	catalytic
CSA	Camphor sulfonic acid
d	doublet
DABCO	1,4-Diazabicyclo[2.2.2]octane
DBU	1,8-Diazabicyclo[5.4.0]undec-7-ene
DCE	Dichloroethane
dd	doublet of doublets
DDQ	2,3-Dichloro-5,6-dicyano- <i>p</i> -benzoquinone
DEAD	Diethyl azodicarboxylate
def2-TZVPP	Valence triple-zeta with two sets of polarization functions
DFT	Density Functional Theory
DIBAL-H	Diisobutylaluminium hydride

DMAP	4-Dimethylaminopyridine
DMF	Dimethylformamide
DMP	Dess-Martin periodane
DMSO	Dimethyl sulfoxide
DNA	Deoxyribonucleic acid
DNP	Dinitrophenylhydrazine
DPMS	Diphenylmethylsilyl
dr	diastereomeric ration
dt	doublet of triplets
E ⁺	Electrophile
E _a	Activation Energy
EDC	<i>N</i> -(3-Dimethylaminopropyl)- <i>N'</i> -ethylcarbodiimide hydrochloride
ee	enantiomeric excess
<i>ent</i>	enantiomer
equiv.	equivalent
Et	Ethyl
eV	electron Volt
EWG	electron-withdrawing group
FC	Flash Column
FMO	Frontier Molecular Orbital
g	gram
h	hour
HF	Hartree-Fock
HOMO	Highest Occupied Molecular Orbital
IBX	2-Iodoxybenzoic acid

IC	Ireland-Claisen
IEFPCM	Integral equation formalism polarizable continuum model
iPr	<i>iso</i> -Propyl
<i>J</i>	Coupling Constant
kcal/mol	kilocalory per mole
KHMDS	Potassium bis(trimethylsilyl)amide
LDA	Lithium diisopropylamide
LiCA	Lithioisopropylcyclohexylamine
LUMO	Lowest Unoccupied Molecular Orbital
M	molarity (mol/liter)
m	multiplet
M06	Minnesota functional
Me	Methyl
mg	milligram
MHz	Megahertz
mL	millilitre
mmol	millimole
MO	Molecular Orbital
MS	Molecular Sieves
Ms	Mesyl
MTBE	<i>tert</i> -Butyl methyl ether
NFSI	<i>N</i> -Fluorobenzenesulfonimide
NHC	<i>N</i> -Heterocyclic Carbene
NMR	Nuclear Magnetic Resonance
<i>n</i> Pr	<i>normal</i> -Propyl

Nu ⁻	Nucleophile
<i>o</i> FBA	<i>ortho</i> -Fluorobenzoic acid
PCC	Pyridinium Chlorochromate
Ph	Phenyl
PMP	<i>para</i> -Methoxyphenyl
<i>p</i> Ts	<i>para</i> -Toluenesulfonyl
q	quartet
rf	retention factor
rt	room temperature
s	singlet
SM	Starting material
SOMO	Single occupied molecular orbital
STO	Slater-type orbital
T	temperature
t	triplet
TBD	1,5,7-Triazabicyclo[4.4.0]dec-5-ene
TBDPS	<i>tert</i> -Butyldiphenylsilyl
TBS	<i>tert</i> -Butyldimethylsilyl
tBu	<i>tert</i> -Butyl
td	triplet of doublets
TEMPO	2,2,6,6-Tetramethyl-1-piperidinyloxy
TES	Triethylsilyl
Tf	Triflyl
TFA	Trifluoroacetic acid
THF	Tetrahydrofuran

TLC	Thin Layer Chromatography
TMBA	2,4,6-Trimethyl benzoic acid
TMS	Trimethylsilyl
TOF	Turn over frequency
TON	Turn over number
TS	Transition State
UV	Ultra-violet
δ	Chemical shift

Part I – Introduction

Chapter I – Asymmetric Synthesis

Nature is asymmetrical, it possesses a left and right hand and can distinguish between the two. On our planet, and possibly in the Universe, life exists in a single-handed form with some saying that without homochirality life would not be possible. On Earth, almost all chiral molecules in living organisms are found in just one form: sugars are right-handed, amino acids are left-handed, and DNA coils into right-handed helices.¹

The homochirality observed in those building blocks causes biological systems to be chiral environments and therefore, different enantiomers of the same molecule can have different biological activities. Figure 1.1 illustrates these differences on a few selected molecules.^{2,3}

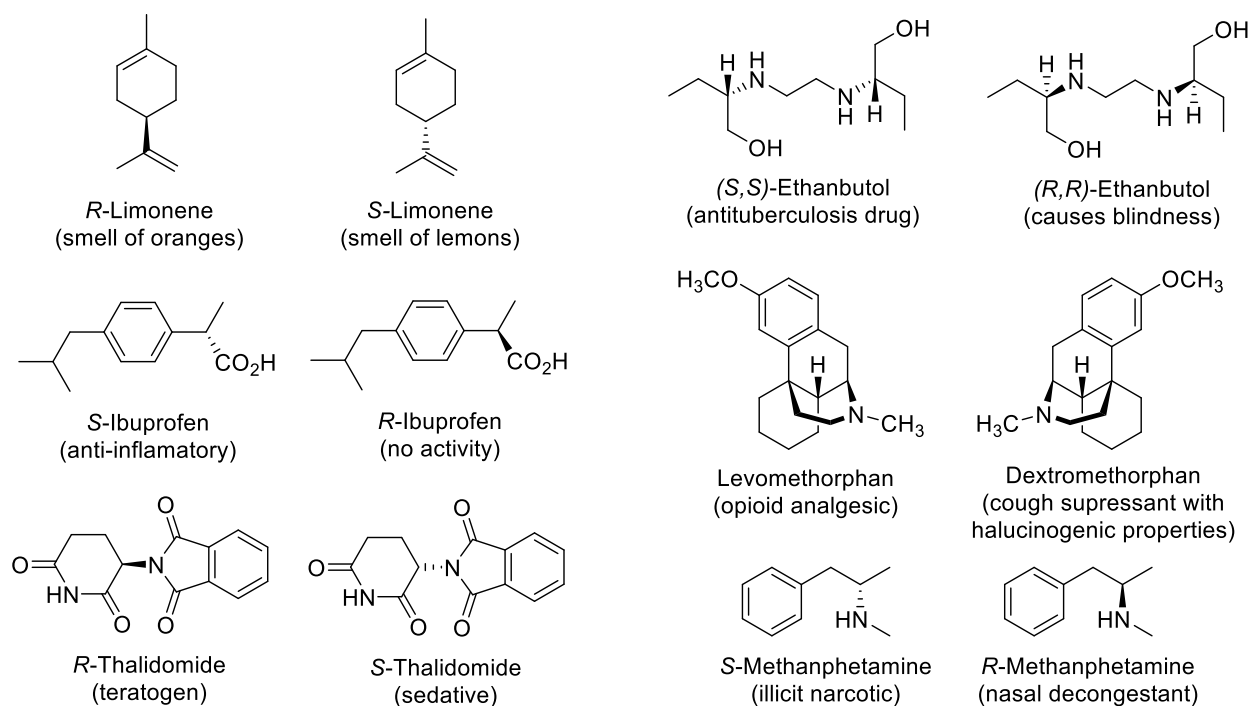


Figure 1. 1 – Selected examples of pairs of enantiomers and their respective biological activity.

From the innocuous limonene and ibuprofen to the infamous thalidomide and methamphetamine it is clearly necessary to account for the stereochemistry when designing and testing new drugs. The example of thalidomide, which was commercialized as a racemic mixture back in the 1960s, caused governmental

agencies to tighten regulations surrounding chiral pharmaceuticals and more recently, those regulations have been extended to agrochemicals as well. Therefore, the need to develop stereoselective protocols has been a focal point in synthetic Organic Chemistry for many years now.⁴

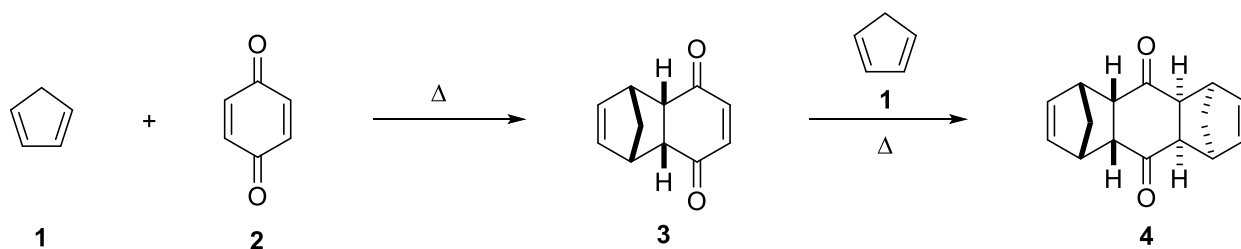
There are three main ways of achieving stereoselectivity in Organic synthesis: (i) chiral pool; (ii) chiral auxiliaries and reagents; and (iii) chiral catalysts. The chiral pool approach makes use of cheap, readily available, and enantiomerically pure natural products, such as amino acids or sugars, as the building blocks for the target molecule. The transformations performed in these compounds occur in a stereoselective fashion, due to the stereocenters already present, and the building blocks chosen end up being part of the final product. Chiral auxiliaries and chiral reagents are enantiomerically pure compounds, usually derived from the chiral pool, which are attached to a pro-chiral starting material. A diastereoselective reaction is then carried out followed by removal of the chiral auxiliary, leaving an enantiomerically pure compound behind. Stoichiometric amounts of chiral auxiliaries or reagents must be employed; however, it is sometimes possible to recover/regenerate them for use in other reactions. Finally, the chiral catalyst approach can also be used. The catalysts can also be derived from the chiral pool, are used in sub-stoichiometric amounts, and provide activation of the pro-chiral substrate towards the desired reaction as well as facial differentiation to the transformation since they themselves are chiral.⁵

In this Dissertation we will explore the use of chiral organocatalysts in asymmetric pericyclic reactions. Pericyclic reactions, as we will discuss later, are usually diastereoselective and easy to predict the major diastereomer produced. Allying this feature of pericyclic reaction with chiral organocatalysts we hope to achieve highly enantio- and diastereoselective transformations which could allow us to access complex and biologically relevant molecules bearing multiple stereocenters.

Chapter II – Pericyclic Reactions

A pericyclic reaction is one that involves a transition state where the electrons involved in the process of bond formation and breaking are aligned in a cyclic array with an associated cyclic array of interacting orbitals and a rearrangement of σ and π bonds occurs within this cyclic system. These reactions are also concerted meaning, the electrons move around in a concerted way and there are no positive or negative charges in any intermediate; as a matter of fact, there are no intermediates at all.⁶ The three main categories of pericyclic reactions are (i) cycloadditions; (ii) sigmatropic rearrangements; and (iii) electrocyclizations. Of these three types, cycloadditions are, probably, the most widely used and are the ones that have found wider application in asymmetric aminocatalyzed processes which we will discuss later in this Thesis. Therefore, we will mostly focus on the factors that influence the mechanism of cycloaddition reactions, with the other two types being briefly mentioned for completeness sake. In Part II of this Dissertation, we will discuss in slightly more detail one specific example of a sigmatropic rearrangement – the Ireland-Claisen rearrangement – and illustrate which factors contribute to this reaction.

Cycloaddition reactions involve the combination of two molecules to form a new ring through a concerted reorganization of the π -electron systems of the reactants, forming two new σ -bonds. One of the most famous examples of a cycloaddition reaction is the Diels-Alder reaction which was developed in 1928 by Otto Diels and Kurt Alder^{7,8} with the authors having been awarded the Nobel Prize for its discovery in 1950.⁹ This reaction consisted on heating cyclopentadiene **1** and 1,4-benzoquinone **2** to afford the cycloadduct **3**, which, upon treatment of with another equivalent of **1** afforded product **4** (Scheme 1.1).



Scheme 1.1 – First example of a Diels-Alder reaction between cyclopentadiene **1** and 1,4-benzoquinone **2**.

The Diels-Alder reaction is a type of cycloaddition also denominated as [4+2]-cycloaddition, where the numbers denote how many electrons are involved in the overall process. It requires a diene possessing 4 π -electrons and a dienophile with 2 π -electrons.¹⁰ In the original report illustrated in Scheme 1.1, the diene is cyclopentadiene **1** and the dienophile is 1,4-benzoquinone **2**.

The mechanisms of pericyclic reactions can be understood within the framework of molecular orbital theory (MO). Consideration of the MOs of reagents and products reveals that in many cases a smooth transformation of the orbitals of reactants to those of products is possible.¹¹ MO theory assumes that electrons move freely within molecular orbitals, which are originated from linear combination of atomic orbitals. This description of electronic structure has been around since the early 20th century and has proven to be very useful especially in molecules that contain conjugated π -systems.¹² Frontier Molecular Orbital (FMO) theory was first proposed in the 1970s by Fukui¹³ and has been widely used in Organic chemistry to explain/predict reactivity. Broadly speaking, FMO states that, in order for two molecules to come together and react with one another, one only needs to account for the interaction between the highest occupied molecular orbital (HOMO) of one molecule, with the lowest unoccupied molecular orbital (LUMO) of the other molecule. This interaction gives rise to the lowest energy gap between the two molecules and, therefore, the more favoured reaction pathway. Going back to the Diels-Alder reaction depicted in Scheme 1.1, and using FMO analysis, we can visualize the orbitals in each of the starting reagents **1** and **2** and, based on their relative energies, predict which interactions are occurring (Figure 1.2).⁵

The electron-deficient dienophile which, in the given example, is 1,4-benzoquinone **2**, has a low-energy LUMO while the electron-rich diene, in this particular example cyclopentadiene **1**, possesses a high-energy HOMO. Therefore, the combination of these orbitals gives better overlap in the transition state (path (a) in Figure 1.2). Conversely, path (b) (Figure 1.2) has a higher energy gap causing the overlap between these orbitals to be disfavoured. However, there are cases where electron-rich dienophiles possess a high-energy HOMO which can interact with a low-energy LUMO of an electron-deficient diene. These reactions are called inverse electron demand Diels-Alder and in Chapter III of Part I we will see some examples.

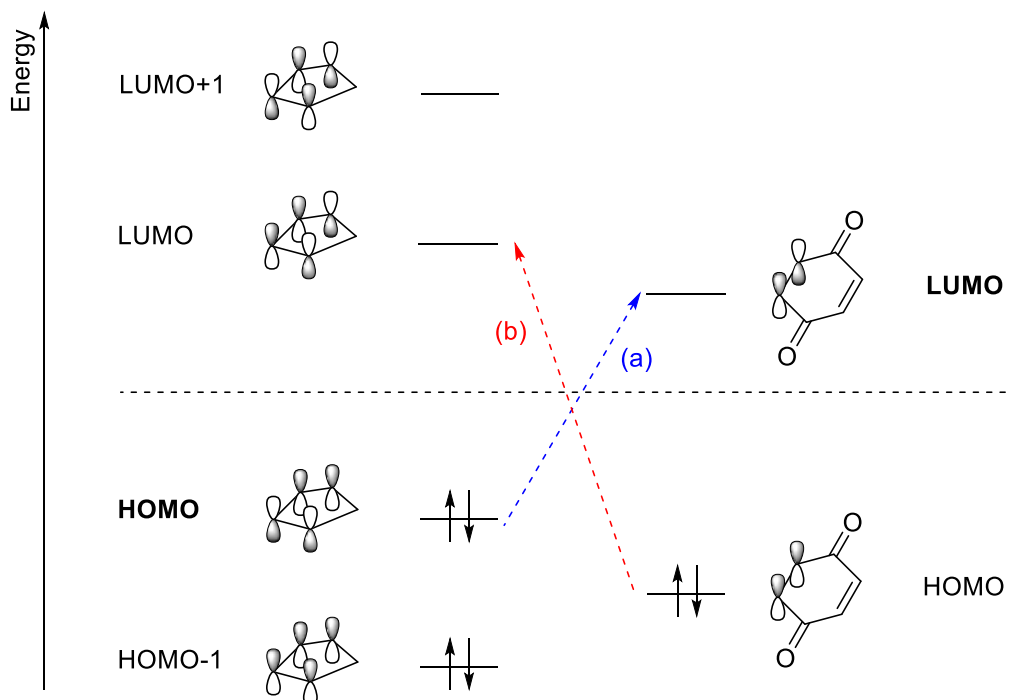


Figure 1. 2 – Orbital diagram for the Diels-Alder reaction showcasing the two possible HOMO/LUMO interactions, (a) and (b), with path (a) being favoured over path (b) due to the lower energy gap associated.

The Diels-Alder reaction illustrated in Scheme 1.1, as mentioned already, is a [4+2]-cycloaddition. However, there are more types of cycloadditions, which are described by how many π -electrons are involved in the transition state. Therefore, there can be [2+2]-, [4+2]-, [6+2]-, [6+4]-cycloadditions and so on. Looking at the example illustrated in Scheme 1.1, why do we not see the cycloadduct corresponding to the [2+2]-cycloaddition? If the diene and dienophile possess the required number of electrons to undergo a [4+2] than, they clearly also possess the electrons to undergo a [2+2]-cycloaddition, yet they do not.

The reason why we observe certain cycloaddition pathways and not others, for the same substrates, has to do with selection rules that govern pericyclic reactions. The most widely used and general set of selection rules was first proposed by Woodward and Hoffmann in 1965¹⁴ where the authors rationalized the different reactivities and relative stereo-outcomes observed when performing electrocyclization reactions under thermal and photochemical conditions, for a series of conjugated systems. These selection rules were further expanded in 1969, by the same authors,¹⁵ to account for the same issues observed in other pericyclic reactions and became known as the Woodward-Hoffmann rules which state that orbital symmetry must be

maintained in any given pericyclic reaction, and its general formulation is as follows: “A *ground-state pericyclic change is symmetry-allowed when the total number of $(4q+2)_s$ and $(4r)_a$ components is odd*”.^{12,15} Where q and r are integer numbers (0,1,2,3, etc); and the subscripts s and a stand for suprafacial (i.e. both bonds forming on the same face) and antarafacial (i.e. new bonds being formed on different faces), respectively. Another way to formulate the Woodward-Hoffmann rules is by considering a given $[p+q]$ -cycloaddition. If $p+q = 4n+2$ (with n being an integer number 0,1,2,3,...) then, orbital symmetry is maintained only when the components approach in a supra/suprafacial or antara/antarafacial fashion, for a thermal process, or supra/antarafacial approach for a photochemical process and therefore, the reaction is allowed. On the other hand, if $p+q = 4n$ then, orbital symmetry is only maintained in a supra/antarafacial fashion for thermal processes and supra/suprafacial or antara/antarafacial approach for photochemical processes. Table 1.1 summarizes these rules for better clarity.⁶

Table 1. 1 – Summary of the selection rules for pericyclic reactions (where $p+q$ denote the total number of electrons involved in the process, n is an integer number like 0,1,2,3,..., s stands for suprafacial and a stands for antarafacial).

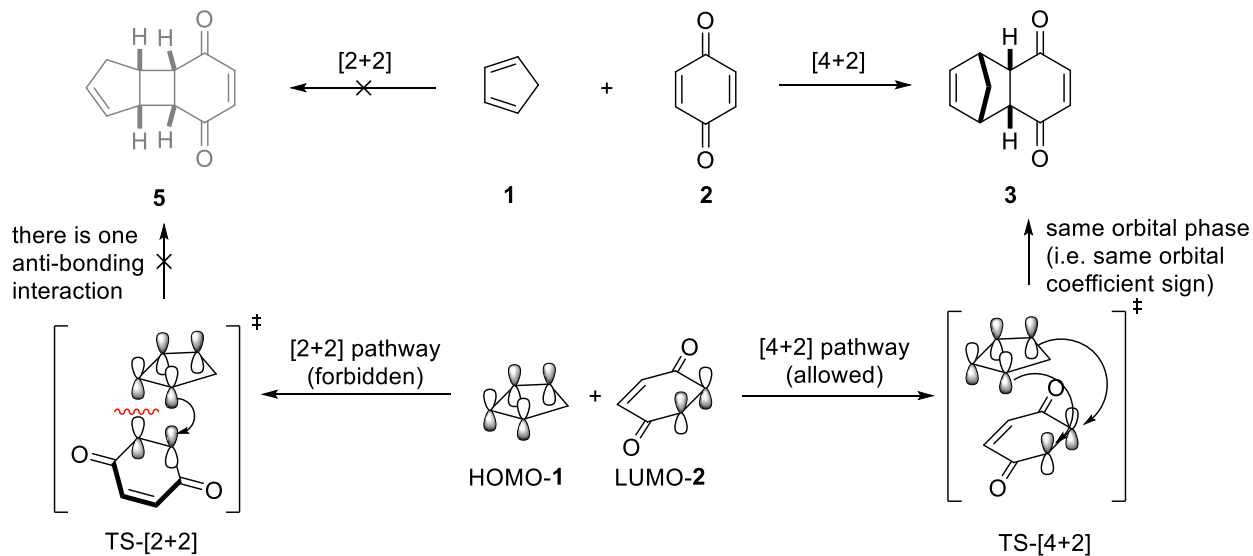
p+q	Thermal Process		Photochemical Process	
	Allowed	Forbidden	Allowed	Forbidden
4n+2	(s,s) or (a,a)	(s,a) or (a,s)	(s,a) or (a,s)	(s,s) or (a,a)
4n	(s,a) or (a,s)	(s,s) or (a,a)	(s,s) or (a,a)	(s,a) or (a,s)

The Woodward-Hoffmann rules are always obeyed and one finds that the signs of the coefficients of the frontier molecular orbitals regularly account for the conservation of orbital symmetry making the selection rules as well as FMO theory the most powerful model of prediction for reaction selectivity. Hoffmann and Fukui were awarded the Nobel prize in Chemistry in 1981.¹⁶ R. B. Woodward passed away in 1979 making him not eligible for what would have been his second Nobel prize.

In 1966, independent works from Zimmerman¹⁷ on cyclization reactions and Dewar¹⁸ on cycloaddition reactions showed that the type of aromaticity, either Hückel or Möbius, in the transition state

plays a role in the observed reactivity, with systems that present $4n+2$ electrons showcasing Hückel aromaticity and Möbius anti-aromaticity while systems with $4n$ electrons exhibit Möbius aromaticity but are Hückel anti-aromatic (n being an integer number such as 0,1,2,3,...). This aromaticity/anti-aromaticity also determines if a given pericyclic reaction is allowed or forbidden and is also called the aromatic transition state theory. All these rules have shown to be complementary of one other and they can be easily applied to any given system to predict if, and under what conditions, a specific pericyclic reaction takes place.

Let us examine the Diels-Alder reaction illustrated in Scheme 1.1 whilst comparing it to the [2+2]-reaction that we know was not observed. Firstly, the reaction was performed under thermal conditions and, as clear from Table 1.1, this is an important factor to be considered as it will affect which FMOs need to be analyzed. Considering FMO theory, the two components in the Diels-Alder reaction are the HOMO of the diene (**1**) and the LUMO of the dienophile (**2**). If they both approach each other from the same face both FMOs will have a constructive interaction and a new bond can be formed (see TS-[4+2] in Scheme 1.2). This is called a supra/supra approach and is in agreement with the Woodward-Hoffmann rules. We have one component with 2 electrons, which is a $(4q+2)_s$ component and no $(4r)_a$ components thus, the No. of $(4q+2)_s + (4r)_a = 1 + 0 = 1$ as it is required. Conversely, the [2+2]-cycloadduct would require a $(4q+2)_s = 1$ but also, a $(4r)_a = 1$ giving a total of 2 and hence, the [2+2] process is forbidden. In respect to the FMO theory, there is one destructive interaction between the HOMO of **1** and the LUMO of **2** in the TS-[2+2] (Scheme 1.2) . Therefore, the process is forbidden or would have to take place in a stepwise fashion and thus, would no longer be a pericyclic reaction (Scheme 1.2).



Scheme 1.2– Comparison between the allowed [4+2]-cycloaddition and the forbidden [2+2]-cycloaddition between **1** and **2**.

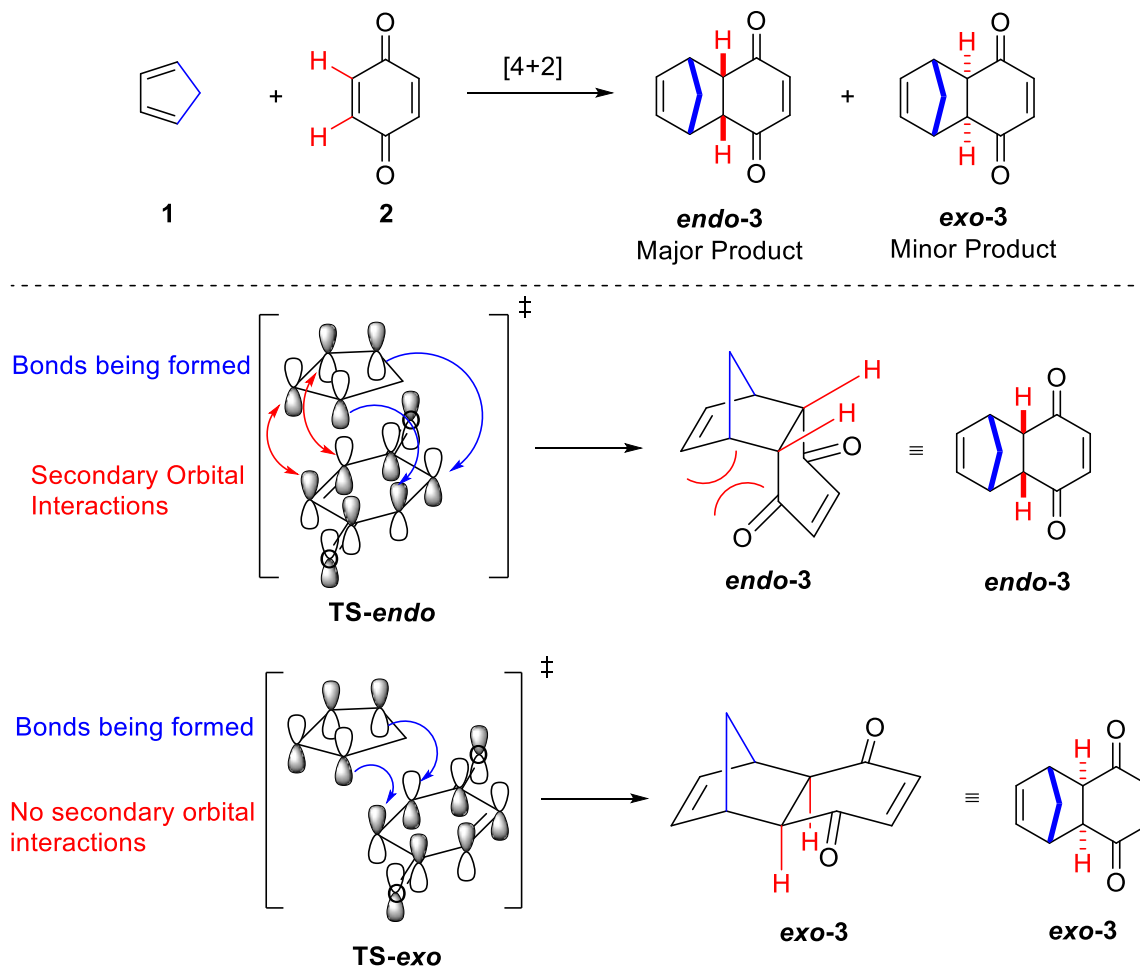
As it is evident in Scheme 1.2, the interaction between the HOMO of the diene and the LUMO of the dienophile, for the [4+2]-cycloaddition, have the same coefficient sign meaning they interact in a constructive way allowing for the reaction to take place. On the contrary, in the [2+2] pathway, those same orbitals would have a point with destructive interaction which creates an anti-bonding orbital hence, the [2+2]-cycloaddition is forbidden which is in agreement with what is observed experimentally. Finally, in the transition state, we have 6 electrons being displaced. According to the Dewar-Zimmerman model, this makes the transition state aromatic with a Hückel topology and therefore, the reaction is allowed. The [2+2]-cycloaddition between **1** and **2** would be a 4-electron process which could only be allowed if one of the components would approach in an antarafacial way, allowing for a $4n$ aromatic Möbius transition state. However, for a thermal, close-shell process, this would then violate the remaining rules or would require the transformation to take place in a stepwise fashion meaning it would no longer be a pericyclic reaction.

Moreover, these selection rules can also provide insights into the relative stereochemistry of the products. We already mentioned the suprafacial vs antarafacial approaches between the two components of the Diels-Alder reaction where the supra/suprafacial approach means that both components interact through the same face which, inevitably, conserves the relative relationship between the substituents from the

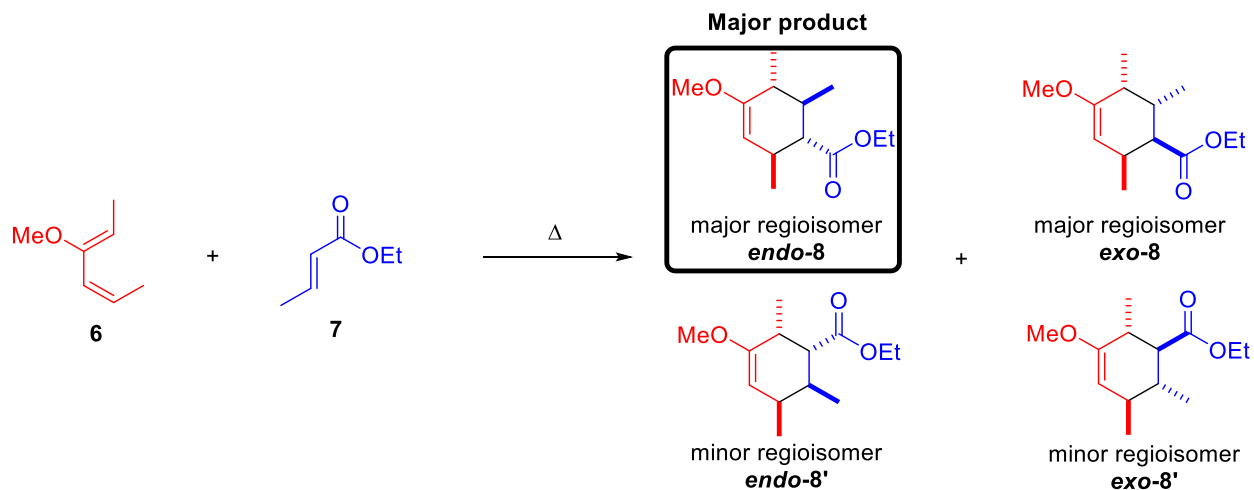
reagent to the product. This supra/suprafacial approach makes Diels-Alder reactions stereospecific where the stereochemistry of the reagents is maintained in the final product. For the example given in Scheme 1.1, the dienophile **2** has a *cis* relationship between its hydrogens therefore, that relationship is maintained in the final product **3**. The same type of stereospecificity is also observed for the diene **1** however, it can, sometimes, be a little bit harder to understand.

Another interesting feature of the Diels-Alder reaction is the ability to predict its diastereoselective. When the diene and dienophile approach each other, they can do so in two distinct ways denoted as *endo* or *exo* giving rise to products that are diastereomers of one another. The *endo* vs *exo* approaches are more noticeable when the dienophile possesses electron withdrawing groups that can interact with the backbone of the diene through secondary orbital interactions.¹⁹⁻²² These interactions make the transition state for the *endo*-product preferred and will give rise to the kinetic product while the *exo*-approach produces the thermodynamic product. Scheme 1.3 illustrates both the stereospecificity as well as the *endo* vs *exo* approaches for the Diels-Alder reaction between diene **1** and dienophile **2** (Scheme 1.3).

Furthermore, the regioselectivity of Diels-Alder reactions can also be easily predicted. The example we have been exploring so far, between diene **1** and dienophile **2**, does not allow us to see this feature but, if we consider the asymmetric alkenes depicted in Scheme 1.4 then we can see the different regioisomers that can be formed. Due to the presence of an electron-donating group in the diene **6**, the lobes of its HOMO have different coefficients and similarly, in the dienophile **7**, the presence of an electron-withdrawing group also affects the coefficients of the lobes of its LUMO. The HOMO/LUMO interaction will take place between the lobes with a similar coefficient as the overlap is more efficient. Therefore, the regioselectivity of these reactions becomes easy to predict (Scheme 1.4).^{5,12}



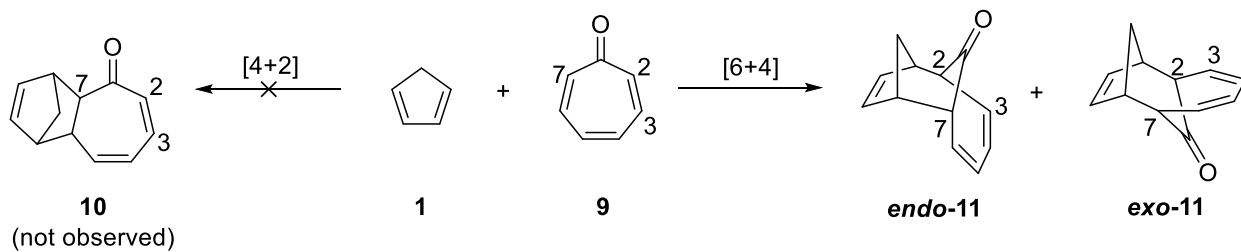
Scheme 1.3 – Regioselectivity and *endo vs exo* approach in the Diels-Alder reaction between **1** and **2**.



Scheme 1.4 – Regioselectivity of Diels-Alder reactions when the asymmetric diene **6** and dienophile **7** are used.

As we venture into cycloadditions involving higher conjugated systems, a new problem arises relating to how many electrons and, therefore, which site of the highly conjugated system are going to be involved in the cycloaddition. This is called periselectivity and the Woodward-Hoffmann rules do not provide any help in this matter. Those rules state that, for all suprafacial reactions, only a total of 6, 10, 14, etc. electrons are allowed but, if both the 6 and 10 processes are feasible, the rules do not tell us which one is preferred.¹²

If we consider the reaction between cyclopentadiene **1** and tropone **9**, there is the possibility of a Diels-Alder reaction (6 electrons process) to take place, using 2 electrons from **9** and 4 electrons from **1** to give the cycloadduct **10** but, there is also an equally allowed [6+4]-cycloaddition (10 electrons process) making use of 6 electrons from **9** and 4 electrons from **1** to give the cycloadduct **11** which is actually the observed product (Scheme 1.5).^{23,24} The observed product **11** is probably not thermodynamically much preferred over product **10**, if at all, so that will not be a very compelling argument to account for this example of periselectivity.



Scheme 1.5 – Periselectivity in the cycloaddition between cyclopentadiene **1** and tropone **9**.

Nevertheless, FMO theory seems to provide a good explanation for the periselectivity observed in this particular example with the longer conjugated system of tropone **9** appearing more reactive than the shorter one as it is clear by the larger orbital coefficients at C2 and C7 of **9** (in either HOMO or LUMO) making reactivity along these carbons more likely than across the C2 and C3 carbons (Figure 1.3).^{25,26}

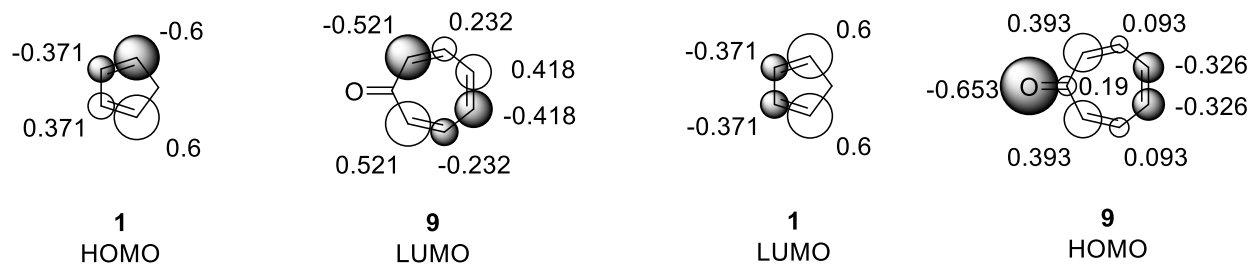
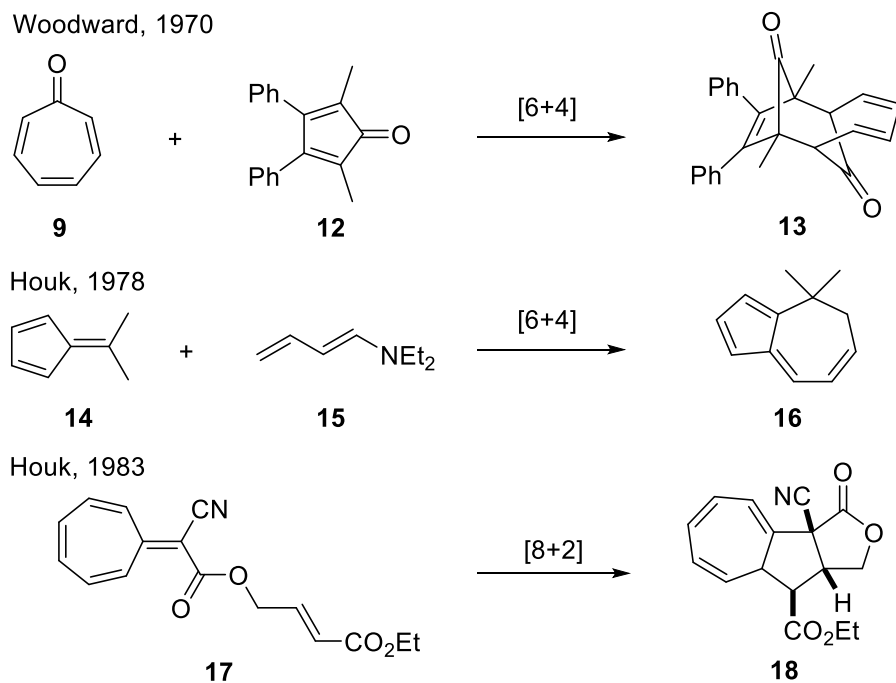


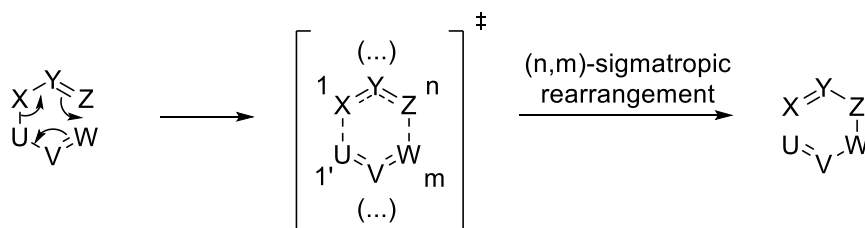
Figure 1.3 – Frontier orbital coefficients of cyclopentadiene **1** and tropone **9** (top view of the orbitals).

In general, the ends of conjugated systems carry the largest coefficients in the frontier orbitals, and we should therefore expect pericyclic reactions to use the longest part of a conjugated system compatible with the Woodward-Hoffmann rules. In Scheme 1.6 are illustrated some selected seminal examples of high order cycloadditions namely, a [6+4]-cycloaddition between tropone **9** and a cyclopentadienone **12**, reported by Woodward and co-workers,²⁷ another [6+4]-cycloaddition between fulvene **14** and dienamine **15** and an intramolecular [8+2]-cycloaddition with an alkenylheptafulvene **17**, both reported by Houk and co-workers (Scheme 1.6).^{28,29}



Scheme 1.6 – Selected examples of seminal high order cycloadditions.

Another type of pericyclic reaction is the sigmatropic rearrangements. In these reactions, a σ -bond changes its position within a molecule and they are denoted not by how many electrons are involved in the process but instead by the number of atoms from which said bond was displaced. The Woodward-Hoffmann rules also apply to these reactions however, geometric constraints must be considered as the selection rules may deem the process to be allowed but, in reality, not take place due to the inability of the orbitals to overlap (e.g. 1,3-hydrogen shifts). There are many types of sigmatropic rearrangements such as Hydrogen shifts, ene-reactions,³⁰⁻³² Ireland-Claisen rearrangements, Cope rearrangements,³³⁻³⁵ and Wittig rearrangements,³⁶⁻³⁸ amongst others.^{39,40} In Scheme 1.7 is depicted a general representation of a sigmatropic rearrangement, where a σ -bond migrates between atoms X and U (1 and 1') to atoms Z and W located n and m atoms away, respectively.⁵

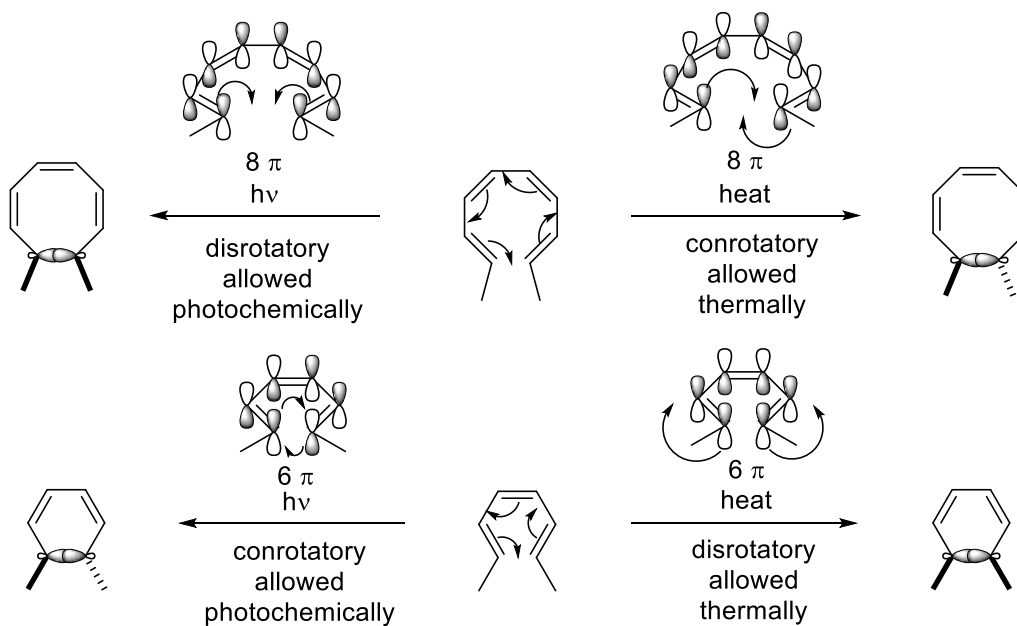


Scheme 1.7 – General representation of a (n,m)-sigmatropic rearrangement.

The last major class of reactions in the family of pericyclic reactions is called electrocyclic reactions. These reactions fall beyond the scope of this Dissertation so, we will not go into too much detail and only a few key aspects will be briefly discussed.

In electrocyclic reactions a ring is either formed, at the ends of a conjugated π -system, or a ring is broken giving rise to a π -system with extra conjugation. The terms antarafacial and suprafacial are no longer applicable since there are no components coming together to form a new molecule. Consequently, orbital symmetry is always maintained making electrocyclic reactions always allowed. The only analysis that needs to be done is regarding the frontier orbitals which must possess the same orbital coefficient sign in order to overlap in a constructive manner. If the orbitals in question rotate in the same fashion (they both rotate either clockwise or anticlockwise) the reaction is said to be conrotatory. On the other hand, if the

orbitals rotate in opposite directions of one another, the reaction is said to be disrotatory.⁵ Thermal electrocyclic reactions involving $4n+2$ electrons are always disrotatory while thermal electrocyclic reactions with $4n$ electrons are always conrotatory. Conversely, photochemical electrocyclic reactions with $4n+2$ electrons become conrotatory and the ones with $4n$ electrons disrotatory. The conrotatory/disrotatory nature will determine the relative stereochemistry of the substituents present in the atoms involved. In Scheme 1.8 are illustrated two generic examples of electrocyclizations, under both thermal and photochemical conditions, one involving $4n+2$ electrons and another involving $4n$ electrons with their respective frontier orbitals being showcased for clarity (Scheme 1.8).⁵



Scheme 1.8 – Generic examples of electrocyclic reactions, (top) involving 8π ($4n$) electrons, and (bottom) involving 6π ($4n+2$) electrons.

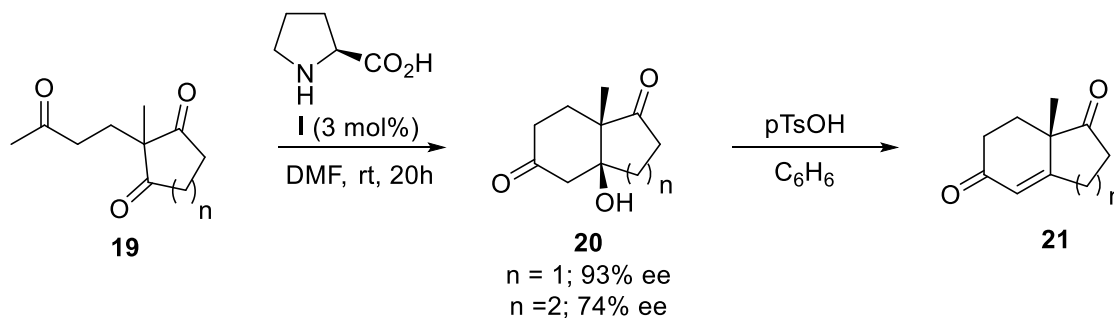
Chapter III – Organocatalysis

The use of catalysts in Organic Chemistry is of great importance and it is an area that has been widely consolidated throughout the years. A textbook definition of a catalyst is that of a species which increases the rate of a chemical reaction without changing the overall standard Gibbs energy. The catalyst is both a reagent and a product, meaning, it is not consumed in the overall course of the reaction. The increase in reaction rate is achieved by the ability of the catalyst to lower the Activation energy (E_a) of the chemical process.⁴¹ Furthermore, the use of catalysts can allow chemists to perform reactions that would otherwise not take place and grant great regio-, chemio-, and stereocontrol. There are two main types of catalysis, homogeneous, where both the reagents and catalyst are in the same physical phase and heterogeneous, where the reagents and the catalyst are in different physical phases (e.g.: solid/liquid, liquid/liquid, etc). For the purpose of this Thesis, I will mostly be focusing on homogeneous catalysis. In Part II of this Thesis, we will briefly introduce asymmetric phase-transfer catalysis which is a type of heterogeneous catalysis.

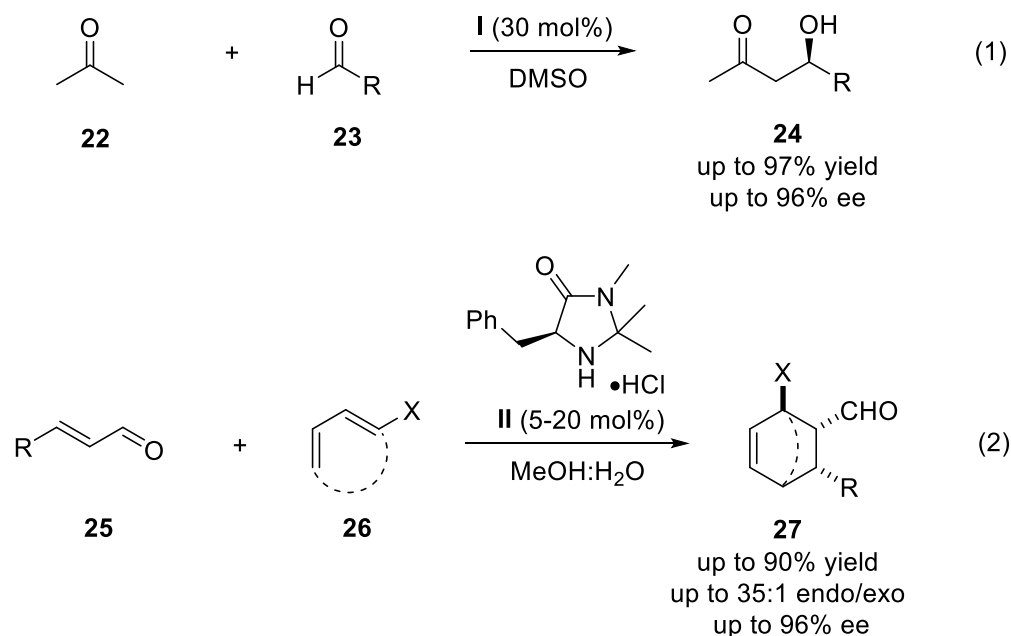
There are three main families in homogeneous catalysis (i) transition metal catalysis; (ii) enzymatic catalysis and; (iii) organocatalysis. Since the focus of this Dissertation will be on organocatalysis, I will not be discussing the other two methods. Organocatalysis is a relatively new area in synthetic Organic Chemistry and, despite some sporadic examples of small organic molecules being used as catalysts, with the Hajos-Parrish-Eder-Sauer-Wiechert reaction being, probably, the most famous example (Scheme 1.9),^{42,43} the term organocatalysis was only coined in the 2000's with the independent works by List *et. al.*⁴⁴, on a *S*-proline (**I**) catalyzed aldol condensation (Scheme 1.10, eq. 1) and MacMillan *et. al.*⁴⁵, on an oxazolidinone (**II**) catalyzed Diels-Alder reaction (Scheme 1.10, eq. 2).

The inspiration for organocatalysis came from nature with the ability of metal-free enzymes to catalyze chemical transformations in a stereospecific fashion by employing Hydrogen bond and electrostatic interactions as activation modes. So, organocatalysts are small organic molecules comprised

of carbon, hydrogen, oxygen, nitrogen and/or sulfur that can be used to facilitate organic transformations mimicking some of the activation modes observed in nature.⁴⁶⁻⁴⁸



Scheme 1. 9 – Hajos-Parrish-Eder-Sauer-Wiechert intramolecular aldol cyclization catalyzed by *S*-proline (**I**).



Scheme 1. 10 – (1) List's and co-workers *S*-proline (**I**) catalyzed aldol reaction; and (2) MacMillan's and co-workers oxazolidinone (**II**) catalyzed Diels-Alder reaction.

With the advent of organocatalysis, the field grew quickly becoming one of the most powerful methods for asymmetric synthesis. Some of the main factors that make organocatalysis a preferred tool in asymmetric synthesis, when compared to transition metals and enzymatic catalysis, are its versatility, i.e. the catalysts work for a wide range of substrates, catalysts can be easily modified to improve results, and both enantiomers of the catalyst are usually available. Moreover, organocatalysts are relatively cheap and

green as they are derived from readily available natural products meaning they come from renewable sources and, for the most part, they are non-toxic and robust against the presence of oxygen and/or water in the reaction allowing for easy bench chemistry techniques without the need of laborious and expensive methodologies to exclude oxygen and water from solvents and reagents.⁴⁹

There are four main types of organocatalysis namely, (i) asymmetric phase-transfer catalysis (APTC),^{50,51} (ii) Hydrogen bond catalysis (H-bond),⁵²⁻⁵⁵ (iii) aminocatalysis,⁵⁶⁻⁶⁰ and (iv) *N*-heterocyclic carbenes (NHC) catalysis.⁶¹ In the next Chapter, we will be focusing on aminocatalysis and its uses in the promotion of asymmetric pericyclic reactions, namely, cycloadditions. Unfortunately, the other types of organocatalysis fall beyond the scope of this work nonetheless, a brief introduction to H-bond catalysis and APTC will be given in Part II in the context of the Ireland-Claisen rearrangement.

Chapter IV – Aminocatalysis

One of the most widely used families of organocatalysts is aminocatalysis⁵⁸ which uses chiral secondary or primary amines to activate aldehydes or ketones making these molecules excellent nucleophiles, by raising the energy of the HOMO (enamine pathway),^{56,60} or great electrophiles, by lowering the energy of the LUMO (iminium ion pathway)⁶² (Figure 1.4). SOMO-activation⁶³⁻⁶⁶ (single occupied molecular orbital) is also a known pathway but it will not be discussed in this Dissertation.

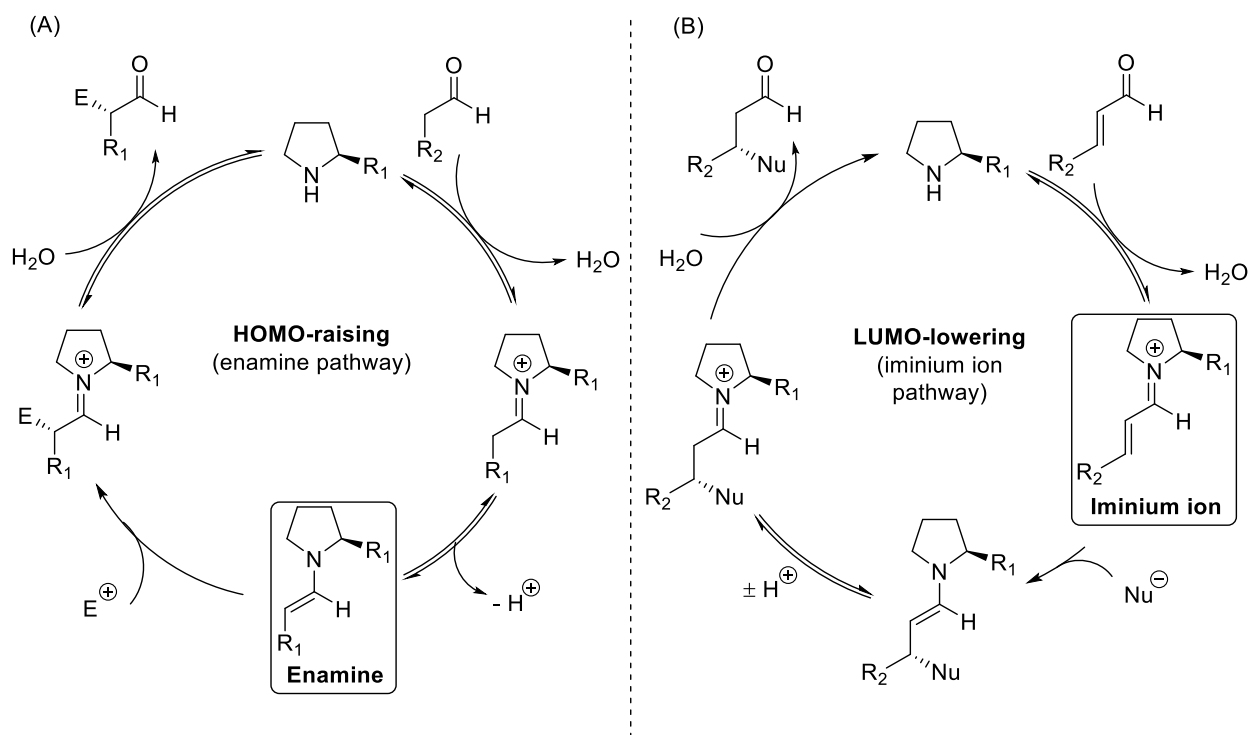


Figure 1.4 – Activation modes in aminocatalysis: (A) enamine pathway, and (B) iminium ion pathway.

The catalytic cycles depicted in Figure 1.4 showcase the use of a secondary amine catalyst, however, it is worth mentioning that primary amine catalysts can also be used and undergo similar cycles with the main difference being the initial formation of an imine upon condensation of the aldehyde or ketone with the catalyst. This imine can then equilibrate to an enamine or iminium ion, with said equilibrium being, usually, aided by an acid co-catalyst.

The achievement of stereocontrol in aminocatalyzed reactions can be attained by two approaches (i) steric bulk and (ii) H-bond direction. The use of chiral aminocatalysts, which possess bulky substituents, allows shielding of one of the faces of the (poly-)enamine or iminium ion forcing the electrophile (in the case of enamine catalysis) or nucleophile (in the case of iminium ion catalysis) to approach from the opposite face (Figure 1.5 – A). If the catalyst has a H-bond donor moiety than this feature will interact with the electrophile through H-bond and the electrophile will approach from the same face where the H-bond donor moiety is. Furthermore, in the case of poly-enamines, this H-bond feature can provide additional control on regioselectivity by placing the electrophile in close proximity to a more remote position and thus, preventing reactivity at the α -position (Figure 1.5 – B).^{67–69}

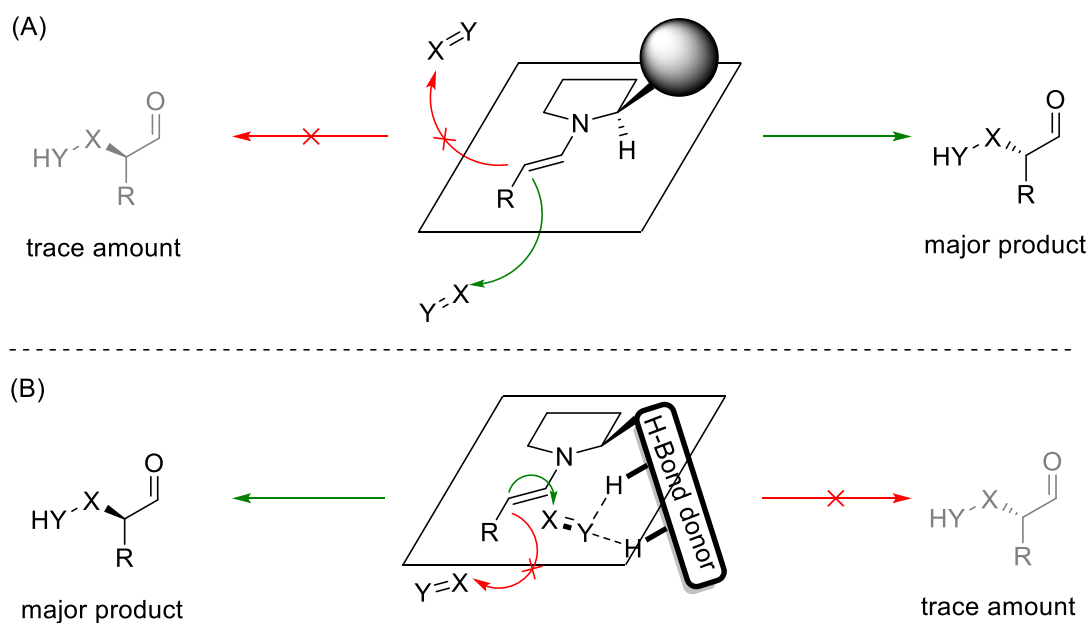
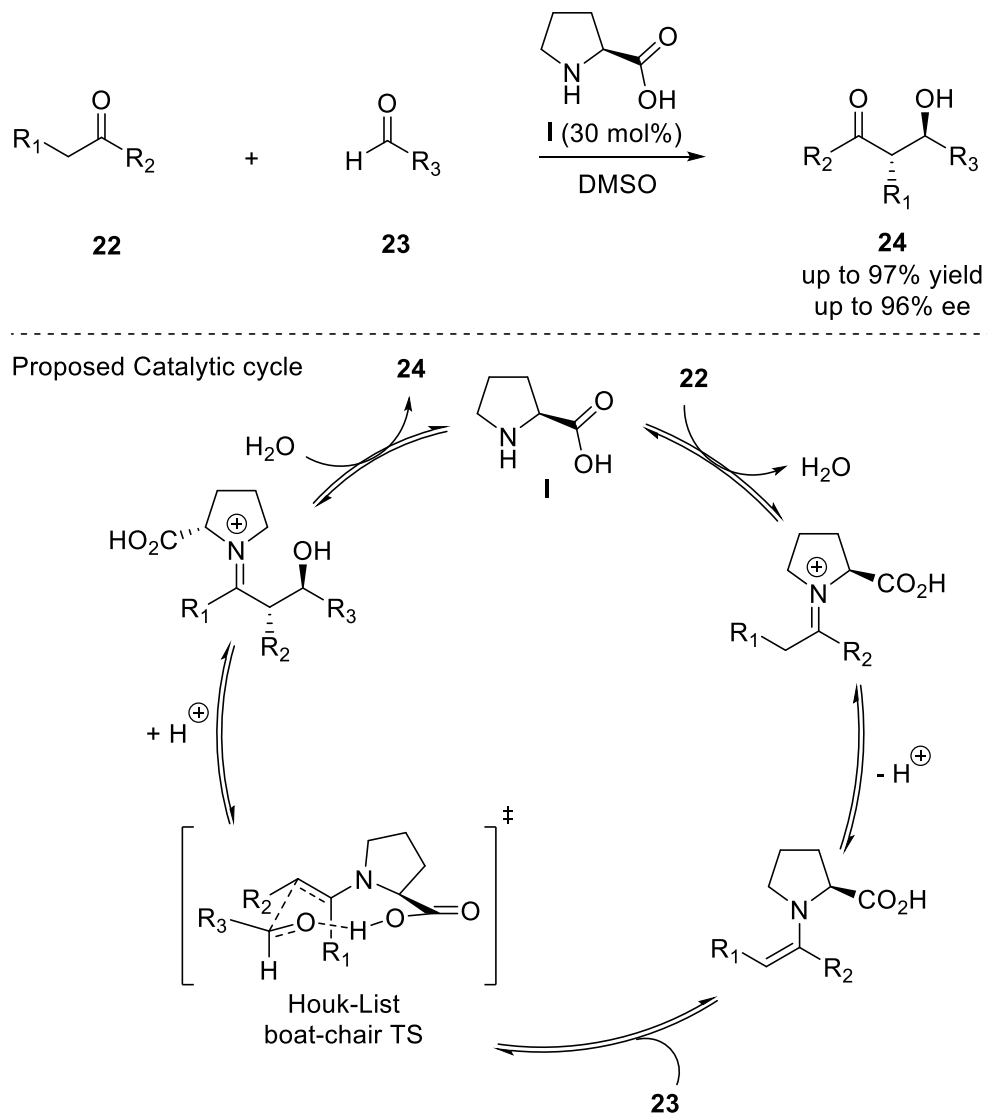


Figure 1.5 – Stereoselectivity in aminocatalysis (A) induced by steric bulk; (B) induced by H-bond interactions.

To better illustrate the nature of this directing groups in determining stereoselectivity, we can go back to the *S*-proline (**I**) catalyzed aldol reaction reported by List and co-workers⁴⁴ and the oxazolidinone (**II**) Diels-Alder reaction described by MacMillan and co-workers⁴⁵ (Scheme 1.10). In the aldol reaction the stereoselectivity was explained by the authors through a Zimmerman-Traxler metal-free type transition state⁷⁰ with a tricyclic H-bond framework. However, later computational work by Houk, List and co-

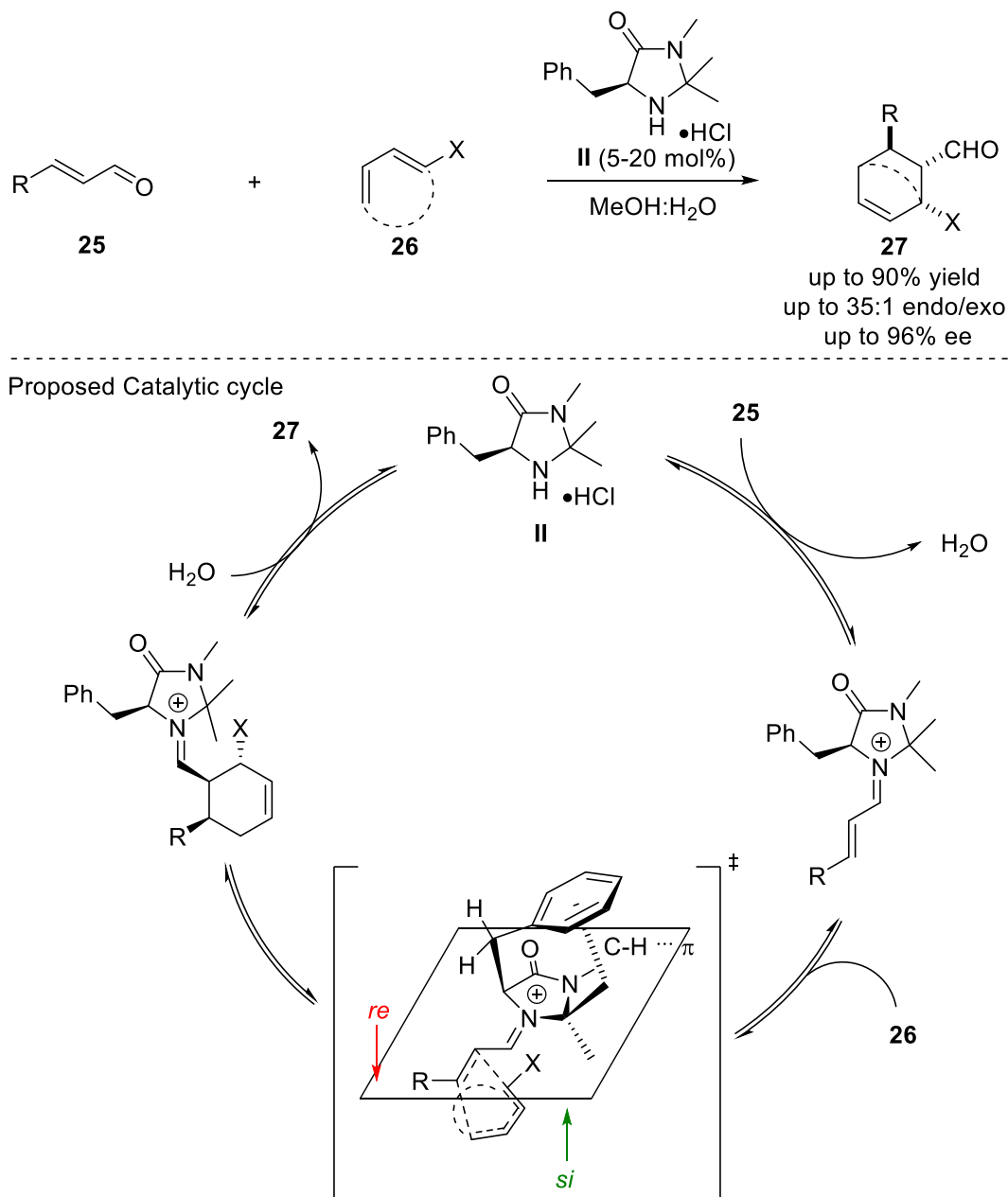
workers⁷¹⁻⁷³ showed a boat-chair 9-member ring transition state with the Hydrogen from proline interacting only with the Oxygen of aldehyde **23** in an (*E*)-configured enamine with the substituent of **23** (R_3) in a pseudoequatorial position (Scheme 1.11).



Scheme 1. 11 – Mechanism of the *S*-proline (**I**) catalyzed aldol reaction.

In respect to the imidazolidinone (**II**) catalyzed Diels-Alder reaction, the mechanism appears to be simpler with the benzyl group of the catalysts providing steric shielding to the *re*-face of the iminium ion which forces the diene **26** to approach from the *si*-face. Subsequent computational studies have shown

C – H \cdots π interactions between the methyl groups and the phenyl ring of the catalyst as well as an *E-s-trans* conformation of the iminium ion to further explain the good diastereoselectivity (Scheme 1.12).^{73–76}

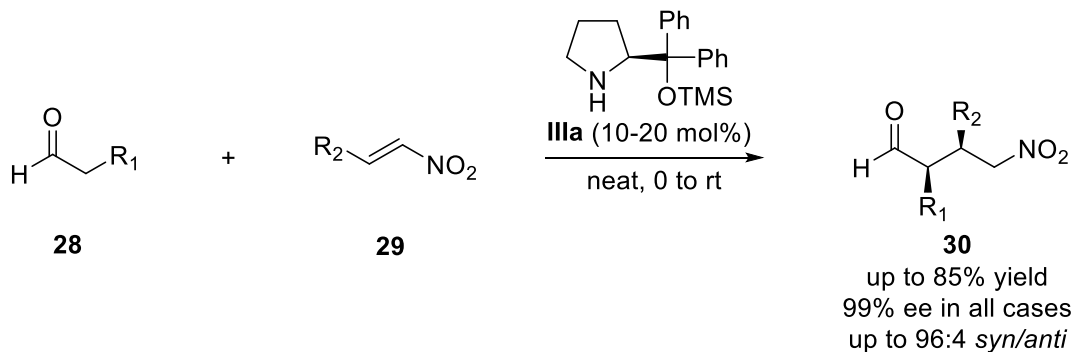


Scheme 1.12 – Mechanism of the imidazolidinone (**II**) catalyzed Diels-Alder reaction.

With these two seminal works by List and MacMillan, the field of aminocatalysis grew quickly with several examples of the activation of aldehydes towards α -functionalization, through enamine formation, with aldol reactions,^{44,77–81} Mannich reactions,^{82–88} Michael additions,^{89–93} α -aminations,^{94–97} α -

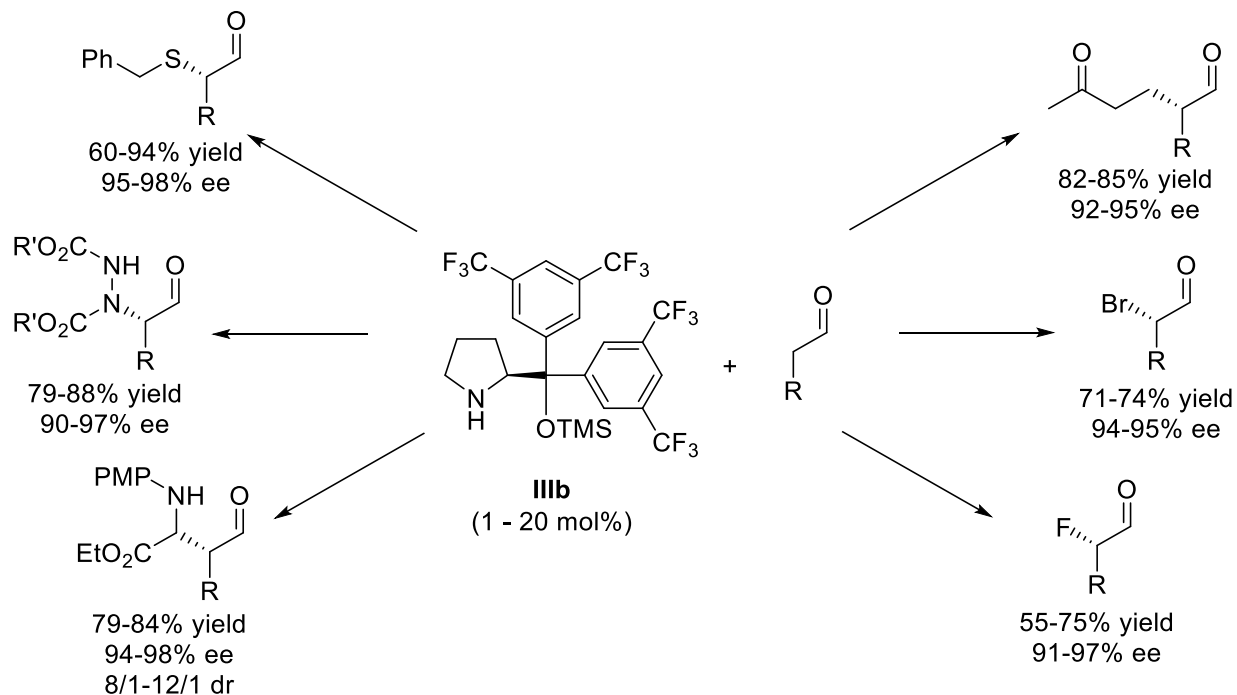
oxygenations,⁹⁸⁻¹⁰⁰ and even Diels-Alder reactions were achieved yielding the α ,*ipso*-functionalized products with excellent enantioselectivities.^{101,102} Conversely, the activation of α,β -unsaturated aldehydes via iminium ion formation remained restricted to Diels-Alder reactions⁴⁵ and very soon after, to 1,3-dipolar cycloadditions.¹⁰³

Despite the extensive list of chemical transformations that were achieved in the early days of aminocatalysis, the lack of a general catalyst resulted in extensive screening of reaction conditions and catalysts prior to the development of new reactions, with only MacMillan's oxazolidinones **II** proving to be more general in iminium ion activation chemistry. This situation changed, in 2005, with the seminal, independent, works from Hayashi *et. al.* and Jørgensen *et. al.* who developed a diarylprolinol silyl ether catalyst – **III** (Schemes 1.13 and 1.14, respectively). Hayashi used the diphenylprolinol silyl ether (**IIIa**) for the Michael addition between aldehydes **28** and nitroolefins **29** giving their respective Michael adducts in good yields and excellent enantioselectivities (Scheme 1.13).¹⁰⁴



Scheme 1. 13 – Hayashi's highly enantioselective Michael addition catalyzed by **IIIa**.

Jørgensen and co-workers developed a di(3,5-bis(trifluoromethyl)phenyl)prolinol silyl ether catalyst (**IIIb**) and showed its robustness with several α -functionalizations of aldehydes, namely, through sulfenylations, aminations, Mannich reactions, Michael additions and halogenations, all yielding their respective α -functionalized products with good yields and excellent enantioselectivities (Scheme 1.14).¹⁰⁵

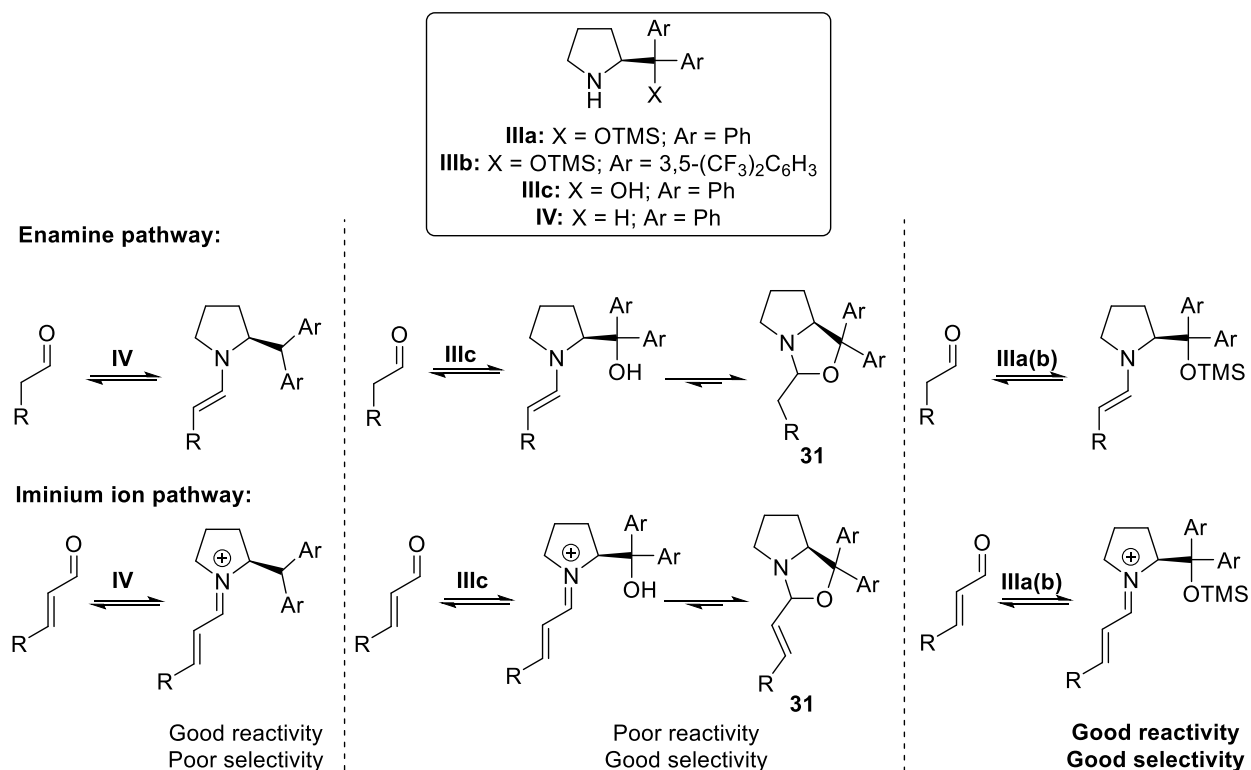


Scheme 1.14 – Jørgensen's highly enantioselective α -functionalizations of aldehydes catalyzed by **IIIb**.

Soon after, the same group proved the utility of catalyst **IIIb** in the activation of enals through iminium ion activation with the conjugate addition of malonates to cinnamaldehyde derivatives¹⁰⁶ and Enders and co-workers developed a three component reaction between nitroolefins and enals through an enamine-iminium-enamine activation sequence catalyzed by **IIIa**.¹⁰⁷ Both these reports helped proving the generality of these catalysts by showcasing their abilities to provide either HOMO-raising activation or LUMO-lowering activation.

Further studies by Jørgensen and co-workers helped elucidate the generality of catalysts of type **IIIa** and **IIIb** by comparing them to the diraylmethylpyrrolidine (**IV**) and the *O*-unprotected diarylprolinol (**IIIc**) versions. Diraylmethylpyrrolidine catalysts **IV**, albeit exhibiting good reactivities, seldomly provided good enantioselectivities whilst the unprotected dirayprolinols (**IIIc**) could afford good enantioselectivities but, lower reactivity due to the formation of a parasitic oxazolidine species (**31**) which would poison the catalyst and reduce its turnover frequency (Scheme 1.15). None of these results were observed for catalysts

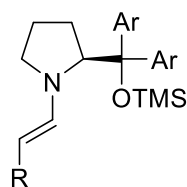
IIIa and **IIIb** which consistently yielded products in good yields and enantioselectivities, making them the most widely used aminocatalysts for the activation of aldehydes to this day.^{67,105}



Scheme 1. 15 – Catalyst design for improved reactivity and selectivity.

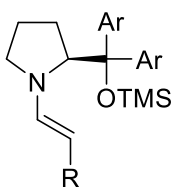
In order to gain further insight into the operating mechanism of catalysts **IIIa** and **IIIb**, relevant intermediates were studied by several groups using various methods including X-ray analysis,^{108,109} NMR analysis,^{110,111} and computational methods.^{112,113} These studies were motivated by the observation that very high enantioselectivities can be achieved although several enamine or iminium ion intermediates conformations may be present in solution with different faces expected to be shielded (Figure 1.6). A study of the distribution of the possible enamine intermediates using DFT calculations revealed that the two enamines both with *E*-configuration were similar in energy. Yet, the *s-cis*-enamines gave rise to a transition state with a higher energy than the *s-trans* conformer for the tested α -fluorination reaction. This energy increment was caused by increased steric repulsion between the substituent of the parent aldehyde and the catalyst face-differentiating element and between the fluorinating reagent computed (NFSI).¹¹²

Enamine intermediate conformations

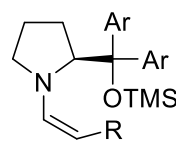


E-s-trans
R = Me: 0.0
R = tBu: 0.0

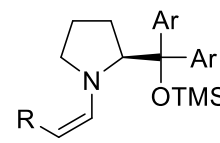
Reactive Intermediate



E-s-cis
R = Me: -0.1
R = tBu: +0.5

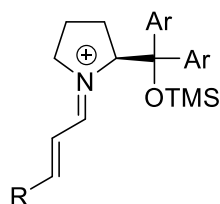


Z-s-cis
R = Me: +5.6
R = tBu: +12.1



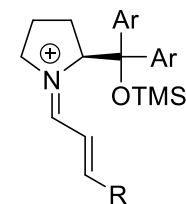
Z-s-trans
R = Me: +1.9
R = tBu: +7.5

Iminium ion intermediate conformations



E,E-iminium ion
R = Me: 0.0

Reactive intermediate



Z,E-iminium ion
R = Me: +1.56

Figure 1. 6 – Relevant enamine and iminium ion intermediates (Ar = 3,5-(CF₃)₂C₆H₃; relative energies in kcal/mol calculated at the B3LYP/6-31 G(d) level of theory).

NMR studies performed by Gschwind and co-workers,^{110,111} on enamine formation, revealed that the *E-s-trans* enamine was primarily present in solution. Furthermore, the studies showed an influence of the aromatic ring substituent of the catalyst on enamine rate formation. The reactive enamine intermediate was formed faster with the phenyl substituent (**IIIa**) than with the 3,5-bis(trifluoromethyl)phenyl substituent (**IIIb**). Moreover, the bulk of the catalyst was found to influence the equilibrium between condensed and hydrolysed substrates resulting in a larger amount of the enamine intermediate being present in solution for catalyst **IIIa**.

Regarding the iminium ion, NMR studies performed by Seebach and co-workers¹¹⁴ have revealed that some intermediates exist in an equilibrium between the *E,E* and *Z,E* isomers. Although reaction through these isomers would presumably provide opposite products, leading to poor stereocontrol, excellent stereoselectivity is often observed with catalysts **IIIa** and **IIIb**. A plausible explanation for this is that nucleophilic attack on the *Z,E* iminium ion isomer is associated with increased steric repulsion in the

transition state. Consequently, high enantioselectivities can be achieved by the preferential reaction through *E,E* iminium ion intermediate in accordance with the Curtin-Hammett principle, which is also in agreement with the observed absolute stereochemistry of the products.

Looking at the stereocontrol provided by the diralylprolinol ether catalysts **IIIa** and **IIIb**, X-ray analysis has shown that in both enamines and iminium ions the OTMS group adopts a *sc-exo* conformation with the aromatic rings lying mostly over the pyrrolidine ring and the OTMS group providing the required steric shielding of the *re*-face of the enamine/iminium ion (Figure 1.7).¹¹⁵ This feature was thoroughly studied by Seebach and Hayashi with the addition of bis(phenylsulfonyl)methane **32** to iminium ions derived from crotonaldehydes **25b** using aminocatalysts with different silyl groups (Table 1.2).¹¹⁶ The authors observed a direct relationship between the bulk of the silyl group and enantioselectivity whilst the yields were kept fairly constant for the catalysts containing a phenyl ring. The same trend was observed when the phenyl rings were replaced with the 3,5-bis(trifluoro)methylphenyl albeit, the yields dropped substantially which could be explained by the observations reported by Gschwind *et. al.* (*vide supra*). A similar trend has been observed in other iminium ion based reactions.^{117–120}

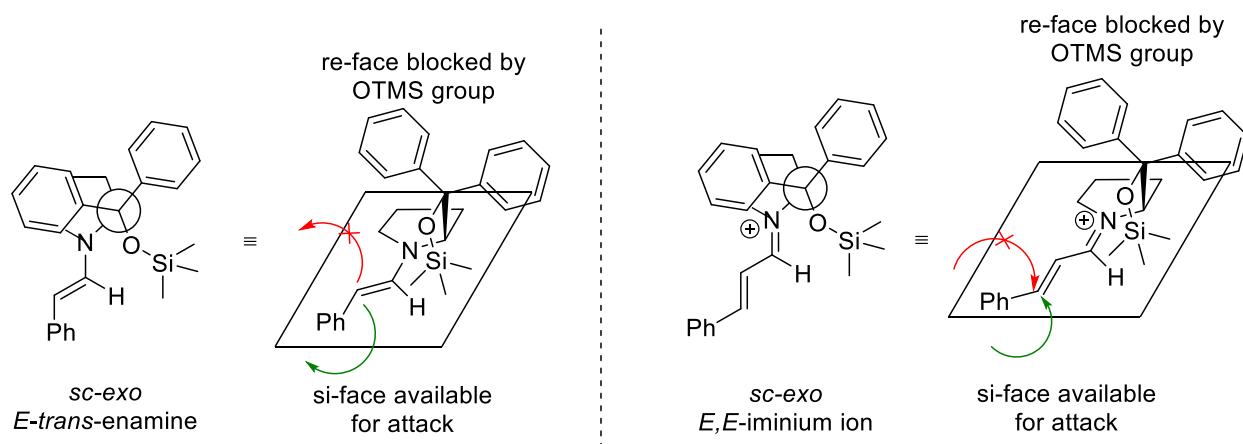


Figure 1. 7 –Enamine (left) and iminium ion (right) conformations from catalyst **IIIa**.

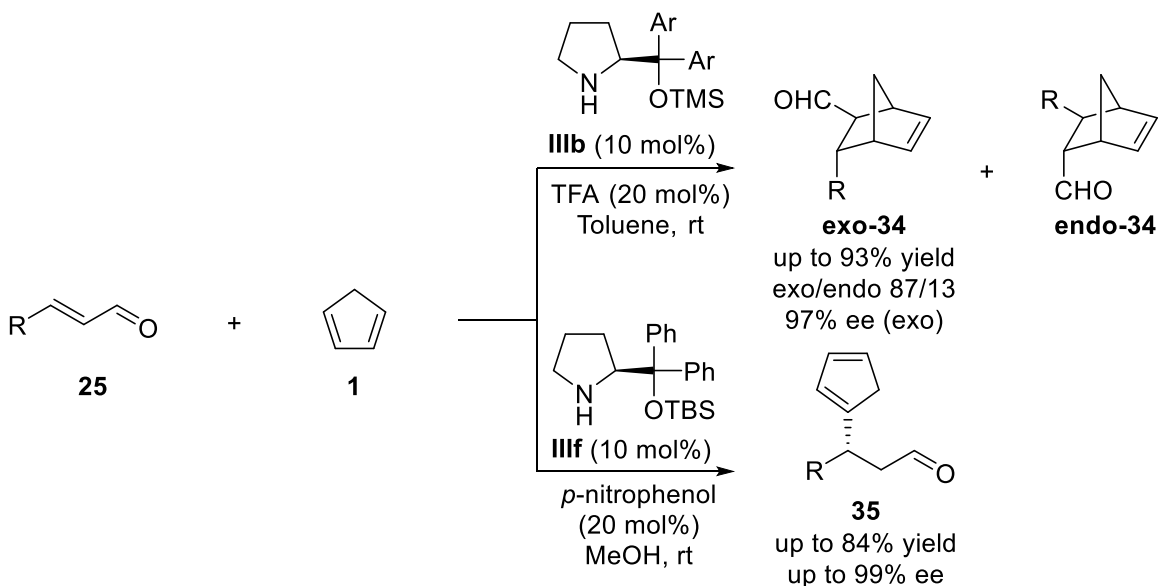
Table 1. 2 –Effect of silyl group (R_1) of catalyst family **III** in enantioselectivity.

Entry	Catalyst	R_1	R_2	T (°C)	Yield (%)	ee (%)
1	IIIa	SiMe ₃	H	23	90	71
2	IIIe	SiEt ₃	H	23	83	73
3	IIIf	SiMe ₂ tBu	H	23	92	79
4	IIIg	SiMe ₂ Ph	H	23	78	81
5	IIIh	SiMePh ₂	H	23	88	83
6	IIIi	SiPh ₃	H	23	90	84
7	IIIh	SiMePh ₂	H	0	94	90
8	IIIi	SiPh ₃	H	0	87	89
9	IIIb	SiMe ₃	CF ₃	23	15	80
10	IIIj	SiEt ₃	CF ₃	23	12	85

After extensive X-ray and computational conformational analysis of diverse iminium ions, the authors concluded that the diphenylmethylsilyl (DPMS) group of catalyst **IIIh** completely shielded the β -position of the *re*-face of the iminium ion affording the addition product with the highest enantioselectivity (entries 5 and 7 of Table 1.2). Nevertheless, this observation does not hold true for all types of reactions namely cycloadditions, where both the α and β positions participate in the TS, as well as additions of strong anionic species such as nitronate anions, where strong electrostatic interactions provide a well-organized TS. In these cases, the smaller trimethylsilyl (TMS) group of catalyst **IIIa** is sufficient to provide good enantioselectivities. Furthermore, the same observation has been done for α -functionalizations of aldehydes, via enamine intermediates, where the small TMS group yields products with excellent enantioselectivities and the use of bulkier silyl groups can be detrimental to the catalyst's reactivity.¹²¹

Based on these observations, Hayashi and co-workers demonstrated that, by judicious selection of catalyst system and reaction conditions, the same substrates could undergo distinct reactivities. Specifically,

the reaction between enals **25** and cyclopentadiene **1** catalyzed by two different catalyst systems proceeds through two different reaction pathways, furnishing either the [4+2]-cycloadduct **34** or the Michael product **35** (Scheme 1.16).¹²² The reactivity is rationalized by the higher electrophilicity of the iminium ion created from catalyst **IIIb**, owing to the electron-withdrawing effect of the aryl groups. On the other hand, when catalyst **IIIc** is used along with weak acids in MeOH, the conjugate addition is promoted. In this case, the generation of the reactive iminium species is faster under the influence of the more electron-rich catalyst **IIIc**. In both cases, suitable acidic additives are key in promoting the intended reactivity. In fact, the strong trifluoroacetic acid (TFA) increases the iminium ion concentration in the reaction medium, while the weaker acid *p*-nitrophenol enables the formation of the anionic nucleophilic species in sufficient reactive concentration. This is an excellent example of how the appropriate catalyst structure, together with suitable reaction conditions, determines divergent reaction pathways. The same concept has been exploited using remotely enolizable dicyanodienes as pro-vinylogous nucleophiles.¹²³



Scheme 1.16 – Divergent reaction pathways via iminium ion activation of enals **25** with different catalysts and reaction conditions.

At this point, whilst elucidating the mechanisms of action of aminocatalysts and how they can activate substrates and induce stereoselectivity, one clear disadvantage of aminocatalysis may have become

apparent to the more careful reader, which is the high catalyst loadings required, usually ranging from 10 – 30 mol%, while transition metal catalysts usually have catalyst loadings of less than 5 mol% with 1 mol% loadings being a common feature. This high catalyst loadings in aminocatalysis, and in organocatalysis in general, hampers the wide implementation of organocatalysts in large-scale industrial processes.^{124,125} These high catalyst loadings are associated with the turnover number (TON) and turnover frequency (TOF). TON denotes the number of moles of product formed per one mole of catalyst before the catalyst gets deactivated. TOF is determined by the turnover per unit of time. In the case of the diarylprolinol silyl ether family of catalysts (**III**), TON can be low due to cleavage of the silyl protecting group which gives rise to the free hydroxyl group catalyst **IV** which, as shown in Scheme 1.15, can form a parasitic oxazolidine **31** species deactivating the catalyst. In 2012, Zeitler and Gschwind *et. al.* reported an *in situ* NMR study on the rate of degradation of biphenylprolinol silyl ether **IIIa** under different, commonly employed, reaction conditions.¹²⁶ The study revealed that the cleavage rates are significant in highly polar solvents with strong H-bond acceptor properties, reaching 0.84%·h⁻¹ for DMF-d₇ and 0.27%·h⁻¹ for methanol-d₄. More commonly used solvents such as chloroform-d and acetonitrile-d₃ showed residual cleavage rates of 0.0003 and 0.005%·h⁻¹, respectively. The effect of additives in catalyst decomposition was also investigated by the authors in DMSO-d₆. It was discovered that weak acids strongly accelerate the deactivation pathway with benzoic acid, a common additive in aminocatalyzed reactions, decreasing the amount of available catalyst **IIIa** from 84% to 10% in only 6h. Taking into account the fact that most common reaction times span from several hours to days, catalyst degradation should be considered in order to enable the development of robust and more efficient catalytic processes.

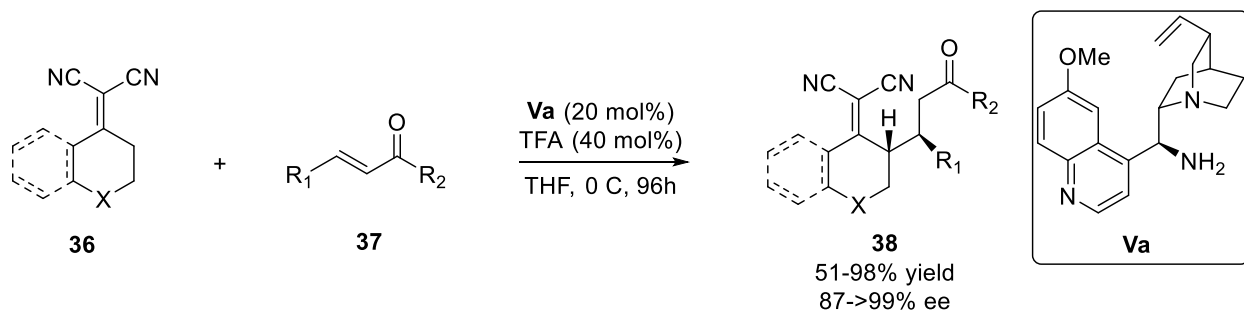
On the other hand, if deactivation is not significant under certain reaction conditions, the low catalyst efficiency may be caused by low TOF. Recently, in 2017, Burés *et. al.* reported an excellent protocol to study the distribution of catalytic species and used it as an indicator to evaluate and optimize the performance of catalyst **IIIa** in the conjugate addition of carbon-based nucleophiles to enals under iminium activation.¹²⁷ The authors, using NMR analysis, were able to correlate the different catalyst species present during the reaction (i.e. free catalyst, iminium ion, and product enamine) with its associated TOF

and adjust reaction conditions to improve the catalyst's TOF. The authors also realized that at very low catalyst loadings, even if the catalyst is properly optimized at its maximum performance, acid impurities formed by aldehyde oxidation drastically reduce the efficiency of the catalyst. The use of distribution of catalytic species enables the *in situ* correction of this detrimental perturbation by consequent addition of a suitable additive, maintaining the catalyst at optimum TOF. With their protocol, and using non-D NMR¹²⁸ techniques for the optimization, the authors were able to perform a gram-scale Michael addition of dimethyl malonate to cinnamaldehyde catalyzed by as little as 0.1 mol% loading of catalyst **IIIa** achieving completion at 60h affording the final product with 91% ee.

Despite the generality of the diarylprolinol silyl ethers catalyst family, and their derivatives, in the activation of aldehydes through enamine or iminium ion intermediates towards several different functionalizations, it soon became apparent that other carbonyl compounds, namely ketones, failed to produce the desired reactive intermediates when treated with those catalysts. For a while, proline (**I**) was the catalyst of choice when dealing with ketones but, even with this catalyst, the type of substrates was restricted to simple methyl or cyclic ketones. More sterically demanding ketones, enones and even sterically demanding α -branched aldehydes could not be activated by the current aminocatalysts available.

Therefore, a new class of catalysts had to be developed for these substrates and chemists turned into chiral primary amines of which, the cinchona alkaloids derived compounds appeared to be good candidates due to their bulky nature, natural abundance, availability of different stereoisomers, and fairly easy process to modify the hydroxyl group at C(9) to its primary amine counterpart by a simple Mitsunobu reaction, with sodium azide as the nucleophile, followed by reduction of the azide to the desired primary amine.^{129–131}

The first example of the use of a 9-amino-9-deoxyquinine **Va**, as an aminocatalyst in asymmetric synthesis, dates back to 2007 and was reported by Chen, Deng and co-workers in the Michael addition of α,α -dicyanoalkenes **36** to several linear and cyclic enones **37** (Scheme 1.17).¹³²

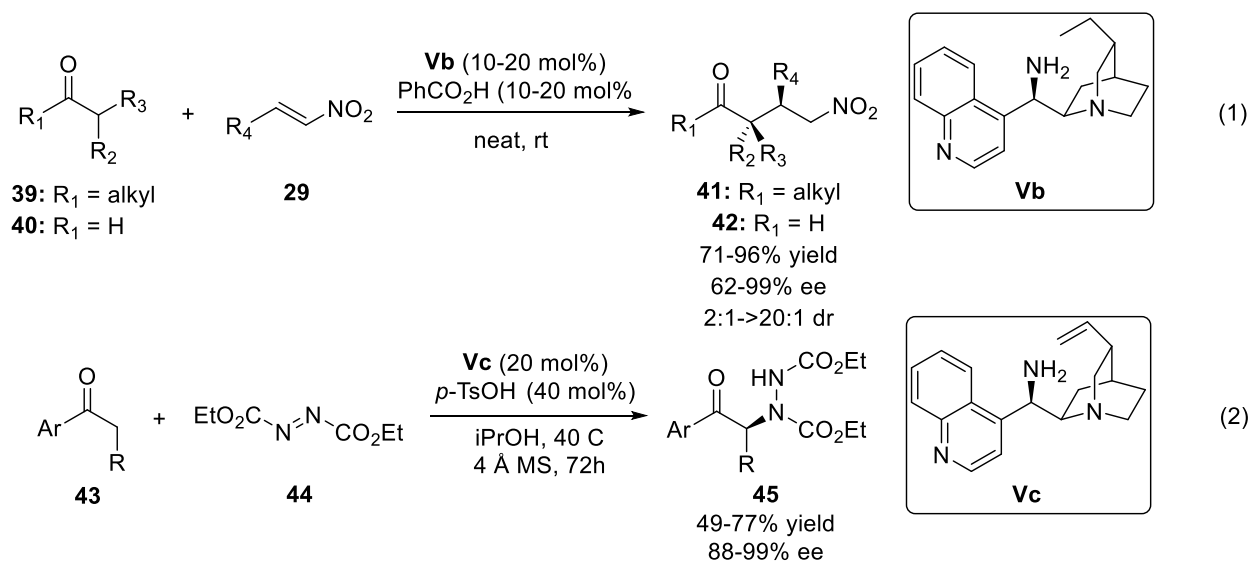


Scheme 1.17 –Michael addition of α,α -dicyanoalkenes **36** to enones **37** catalyzed by **Va** (dr's not reported in original paper).

The Michael adducts **38** were obtained with overall good yields and excellent enantioselectivities; unfortunately, the diastereomeric ratios were not reported by the authors. The use of trifluoroacetic acid (TFA) as a co-catalyst proved to be crucial to stereoselectivity as the screening of other acids such as perchloric, hydrochloric and triflic acid all decreased enantioselectivity, probably by promoting the same transformation under achiral Brønsted acid catalysis.

In the same year, Connon and co-workers developed a Michael addition between sterically demanding ketones and aldehydes (**39** and **40**, respectively), to nitroolefins **29** catalyzed by 9-*epi*-amino dehydroquinidine (**Vb**) via enamine activation (Scheme 1.18, eq. 1)¹³³ and Chen and co-workers reported the use of a 9-amino-9-deoxyepicinchonine (**Vc**) catalyst for the enantioselective α -amination of ketones **43** with DEAD (**44**) also through enamine activation (Scheme 1.18, eq. 2).¹³⁴

In both examples, the authors theorize that protonation of quinuclidine nitrogen of the catalyst takes place by the acid co-catalyst, allowing for the presence of an H-bond donor moiety in the catalyst which could provide further activation but, most importantly, face differentiation and concomitant stereocontrol to the electrophiles **29** and **44**.



Scheme 1.18 – α -Functionalization of ketones (**39** and **43**) and aldehydes (**40**) via enamine activation with cinchona alkaloids; (1) Connon *et. al.* Michael addition to nitroolefins **29** catalyzed by **Vb**, and (2) Chen *et. al.* amination of ketones with **44** catalyzed by **Vc**.

With the aforementioned seminal works, C(9)-amino cinchona alkaloids found their place as general aminocatalysts for sterically demanding carbonyl compounds that do not form enamines or iminium ions with the dirayprolinol silyl ether catalysts **III** and have been widely used as catalysts¹³⁵ with small alterations to the catalytic system namely, regarding the choice of acid co-catalyst and the general scaffold of the cinchona alkaloid. This type of catalysts can achieve both enamine and iminium ion activation and their catalytic cycles are similar to those depicted in Figure 1.3 for the secondary amines but, with the slight difference that an initial imine is formed in both cases which can then tautomerize to the reactive enamine or become protonated and generate the reactive iminium ion (Figure 1.8).

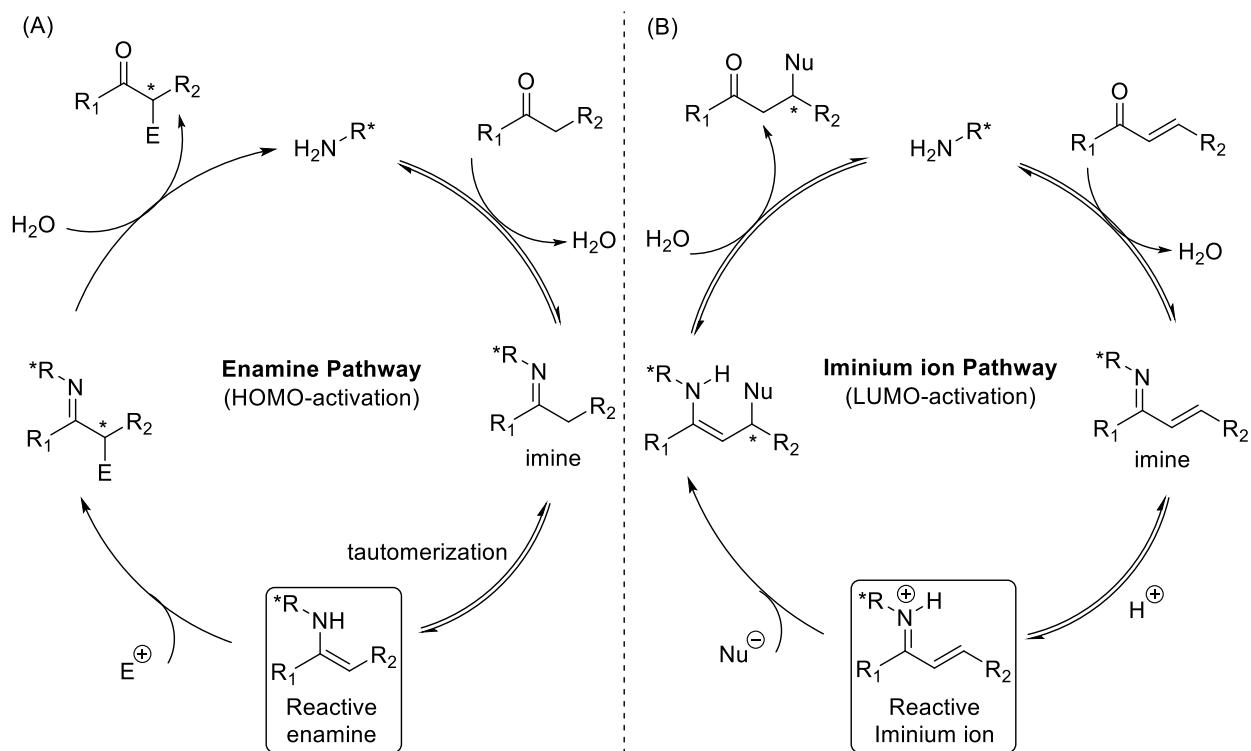
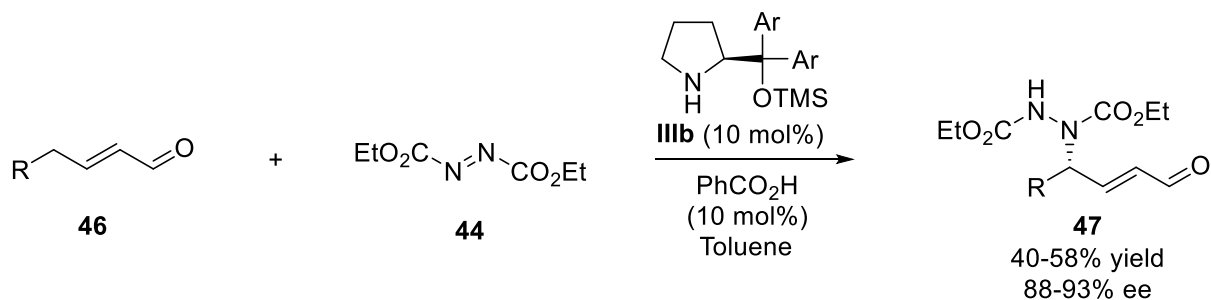


Figure 1. 8 – Catalytic cycles for primary amine catalysis: (A) enamine pathway and, (B) iminium ion pathway.

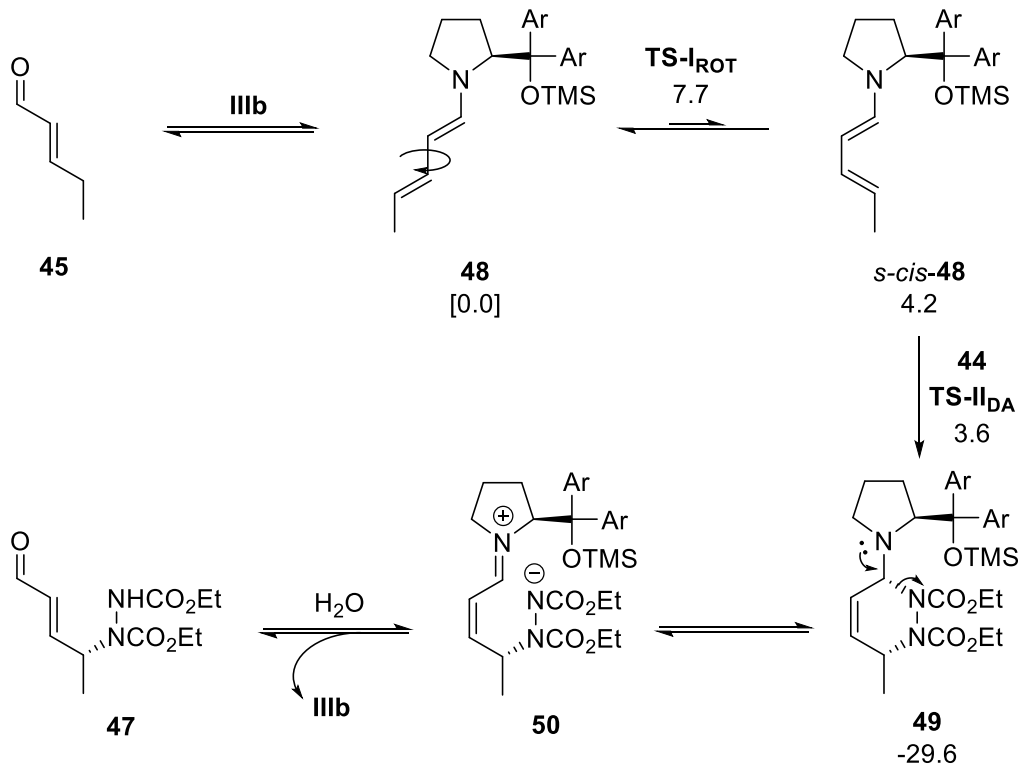
In 2006, Jørgensen and co-workers reported what is perhaps one of the most important milestones of aminocatalysis, when they performed an enantioselective γ -amination of enals **46** with DEAD **44**, using **IIIb** as catalyst (Scheme 1.19).¹³⁶



Scheme 1. 19 – Enantioselective γ -amination of enals **46** catalyzed by **IIIb** (Ar = 3,5-(CF₃)₂C₆H₃).

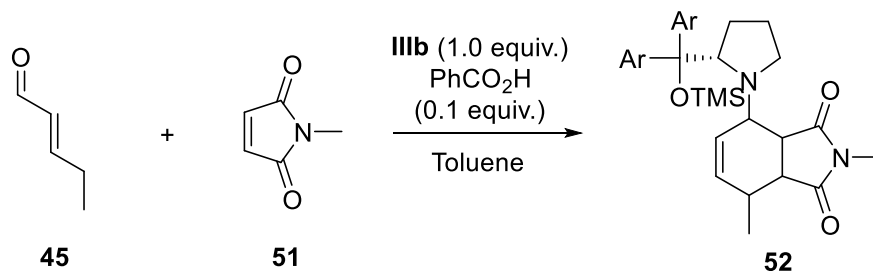
Surprisingly, the stereochemistry of the product appears to be the opposite of what would be expected based on how catalyst **IIIb** operates. To explain this odd observation, the authors, with the aid of computational methods, proposed that the dienamine intermediate **48** undergoes a bond rotation to form the

s-cis-**48** conformer which reacts with **44** through a Diels-Alder reaction forming intermediate **49** which could collapse to the zwitterion **50** with consequent ring opening and hydrolysis of the catalyst affording product **47** (Scheme 1.20).



Scheme 1. 20 – Proposed mechanism for the dienamine-mediated γ -amination reaction reported by Jørgensen and co-workers (Ar = 3,5-(CF₃)₂C₆H₃; relative energies in kcal/mol calculated at the B3LYP/6-31G(d) level of theory).

To further support this mechanism, the authors performed a reaction with enal **45** and *N*-methylmaleimide **50**, using 1.0 equiv. of **IIIb**, and observed the cycloadduct **51** with the trapped catalyst (Scheme 1.21).

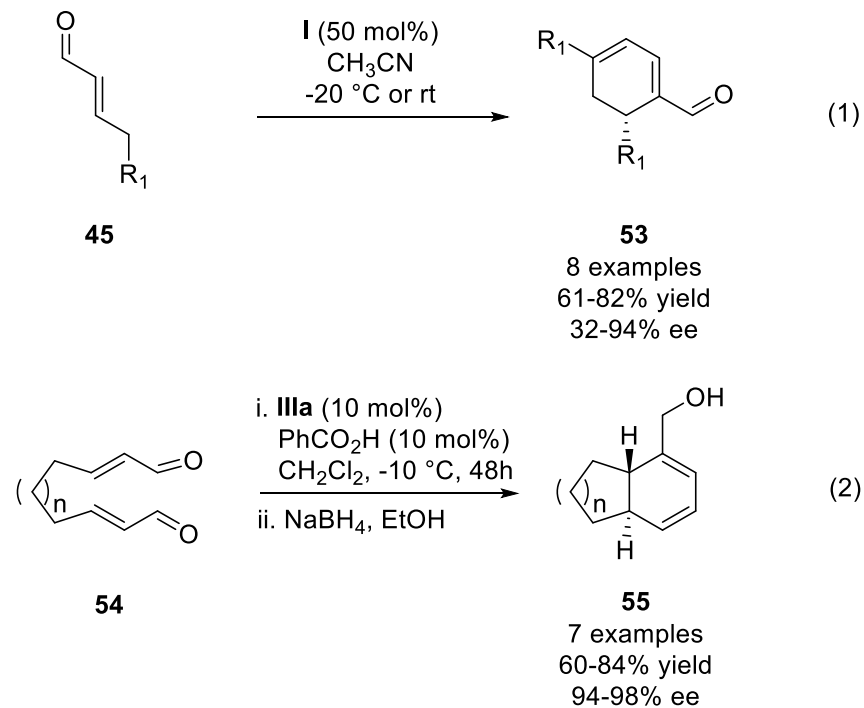


Scheme 1. 21 – Entrapment of the catalyst by a carbon-based dienophile (Ar = 3,5-(CF₃)₂C₆H₃).

This work was the first example of a dienamine-mediated functionalization of γ -enolizable α,β -unsaturated aldehydes which allowed the field of aminocatalysis to expand its scope of reactions allowing for functionalizations at more remote positions with good stereocontrol. However, this work also showed a particular challenge in dienamine catalysis which is the catalyst turn over specially, if asymmetric [4+2]-cycloadditions are to be developed, using carbon-based dienophiles.

Fortunately, interesting solutions to this problem soon appeared, independently, from the groups of Hong^{137–139} and Christmann.¹⁴⁰ The authors demonstrated the possibility of an eliminative release of the catalyst which proved to be quite general for various linear and β -branched enals (Scheme 1.22). In both reports, a dual dienamine/iminium ion activation is achieved between the aldehydes and the aminocatalyst allowing for a stepwise (4+2)-cyclization reaction to take place followed by α -deprotonation and subsequent elimination of the aminocatalyst. Hong and co-workers used Proline (**I**) as their catalyst and linear dienals **45** affording products **53** in moderate yields and low to good enantioselectivities (Scheme 1.22, eq. 1) whilst Christmann and co-workers used catalyst **IIIa** to perform a similar intramolecular [4+2]-cyclization of compounds **54** yielding the bicyclic scaffolds **55** in higher yields and enantioselectivities than those reported by Hong (Scheme 1.22, eq. 2).

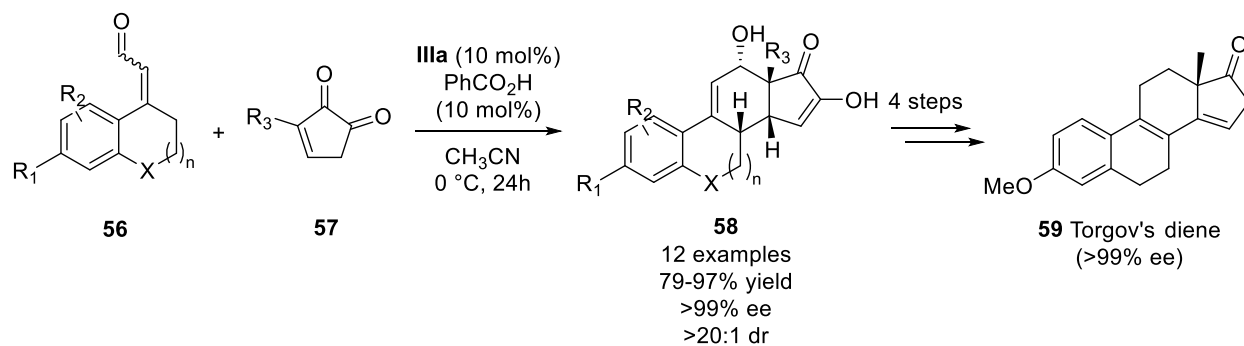
However, despite the works by Hong and Christmann the regeneration of the catalyst proved to be troublesome and highly reliant on the nature of the substrates used, so, most cycloaddition reactions involving dienamine intermediates used the dienamine as an electron rich dienophile for inverse-electron-demand-Diels-Alder reactions with the functionalization taking place in the β,γ -double bond of the dienamine, where trapping of the catalyst is not a concern.¹⁴¹



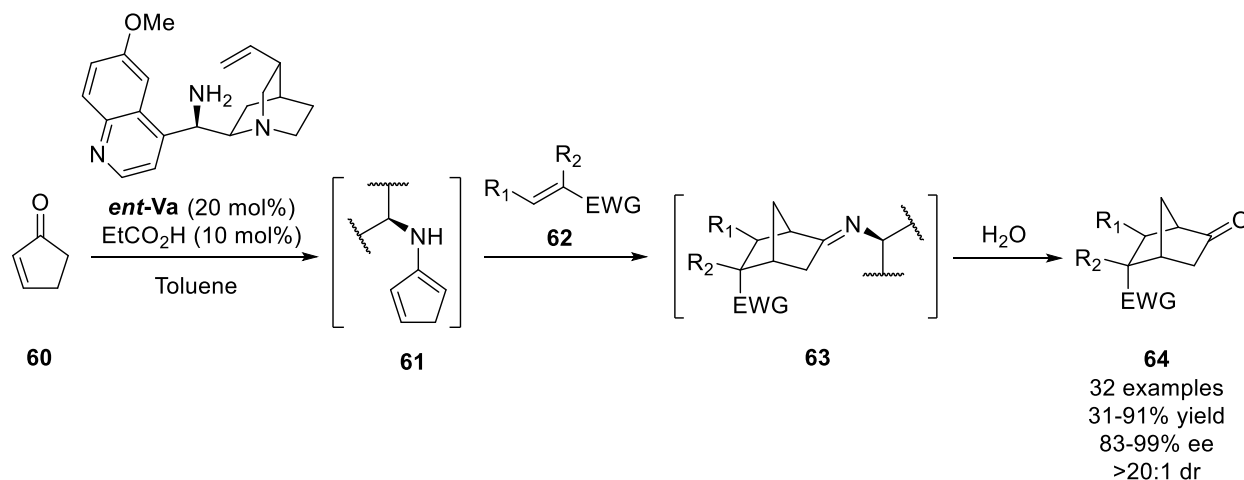
Scheme 1.22 – Eliminative regeneration of aminocatalysts in dienamine/iminium ion-mediated [4+2]-cycloadditions, (1) reported by Hong and co-workers and, (2) reported by Christmann and co-workers.

Nonetheless, Jørgensen and co-workers, in 2014, developed a stepwise asymmetric (4+2)-cyclization reaction between enals **56** and diketones **57**, using aminocatalyst **IIIa** to obtain the steroidal skeleton **58** with overall excellent results. Moreover, the authors were able to use this methodology for the synthesis of Torgov's diene **59**, an important precursor for the synthesis of several steroids (Scheme 1.23).¹⁴²

More recently, in 2015, Jørgensen and co-workers proposed the use of a cross-dienamine **61**, formed from the condensation between 2-cyclopentenone **60** and a cinchona alkaloid primary aminocatalyst (*ent*-**Va**), as electron rich dienes for Diels-Alder reactions with electron poor dienophiles **62** yielding functionalized norcamphor scaffolds **64** in moderate to good yields and excellent enantio- and diastereoselectivities (Scheme 1.24).¹⁴³ This approach has overridden the necessity to eliminate the catalyst as the imine intermediate **63** is susceptible to hydrolysis.

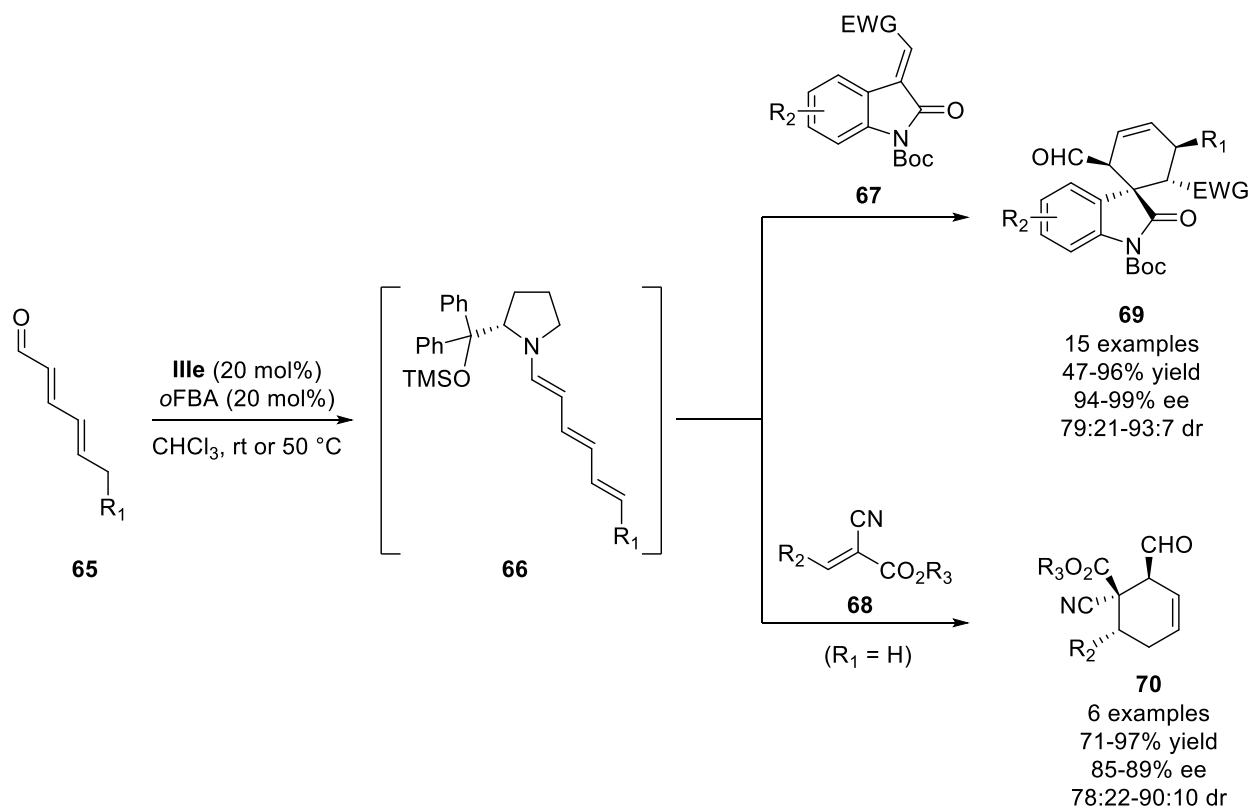


Scheme 1.23 – Synthesis of steroid scaffolds, via dienamine intermediates, reported by Jørgensen and co-workers.



Scheme 1.24 – Cross-dienamine-mediated Diels-Alder reaction reported by Jørgensen and co-workers.

The ability to perform remote functionalizations was further expanded in 2011 with the collaborative work of Jørgensen, Chen and co-workers, where the authors used dienals **65** to generate trienamines **66** *in situ* by condensation with aminocatalyst **IIIe**. The authors then envisioned these trienamine intermediates as electron rich dienes that could react with electron deficient alkenes, such as 3-olefinic oxindoles **67** and cyanoacetates **68** through a Diels-Alder reaction affording the corresponding cycloadducts **69** and **70**, respectively, with excellent enantio- and diastereoselectivities (Scheme 1.25).¹⁴⁴



Scheme 1.25 – Trienamine-mediated Diels-Alder reactions reported by Jørgensen, Chen, and co-workers.

In order for these reactions to take place, trienamine **66** must undergo a σ -bond rotation to form the reactive *s-cis* diene, required for Diels-Alder reactions. Computational studies by the authors showed that both rotation around C2 – C3 or C4 – C5, in trienamine **66**, could take place leading to the 2,3-*s-cis-66* intermediate or the 4,5-*s-cis-66* intermediate, respectively, with the latter being slightly preferred both kinetically and thermodynamically (Figure 1.9). Population analysis was also performed by the authors and showed that the coefficients of the atoms of interest were -0.23 (C3 in 4,5-*s-cis-66*) and 0.34 (C6 in 4,5-*s-cis-66*) vs -0.32 (C1 in 2,3-*s-cis-66*) and 0.43 (C4 in 1,4-*s-cis-66*) (Figure 1.9). These results pointed towards conformer 2,3-*s-cis-66* to be more reactive than 4,5-*s-cis-66*, however, the HOMO of 2,3-*s-cis-66* was 2.17 eV lower in energy than that of the 4,5-*s-cis-66* conformer. Therefore, trienamine **66** exhibits a preference to react with suitable dienophiles through the 4,5-*s-cis-66* conformer yielding the cycloadducts at the more remote locations.

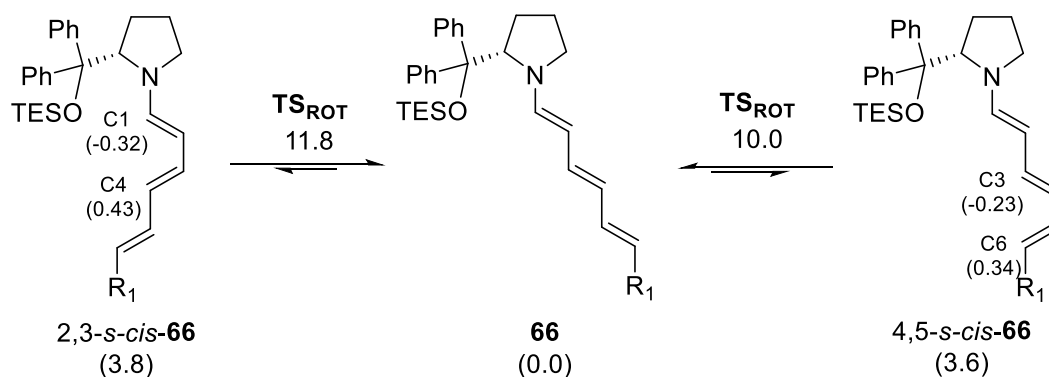
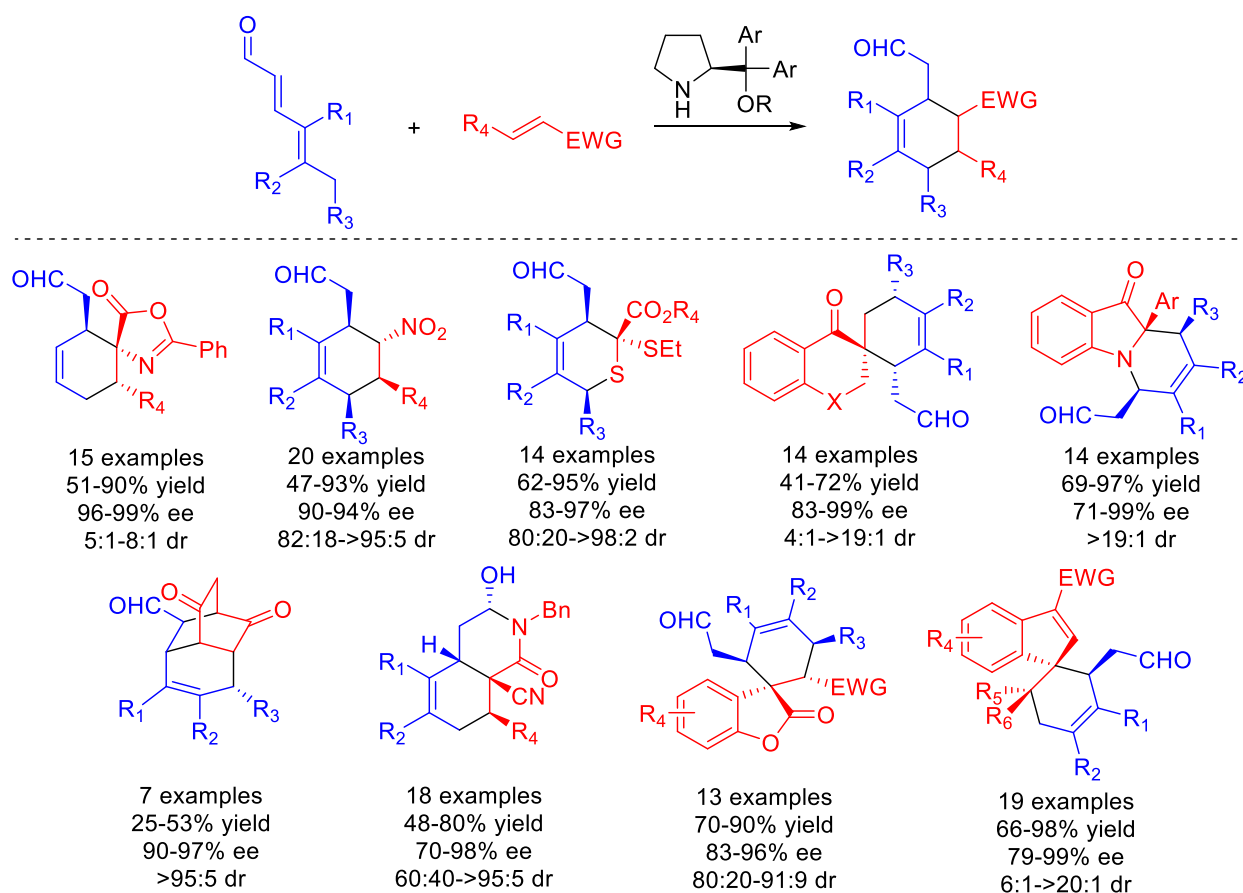


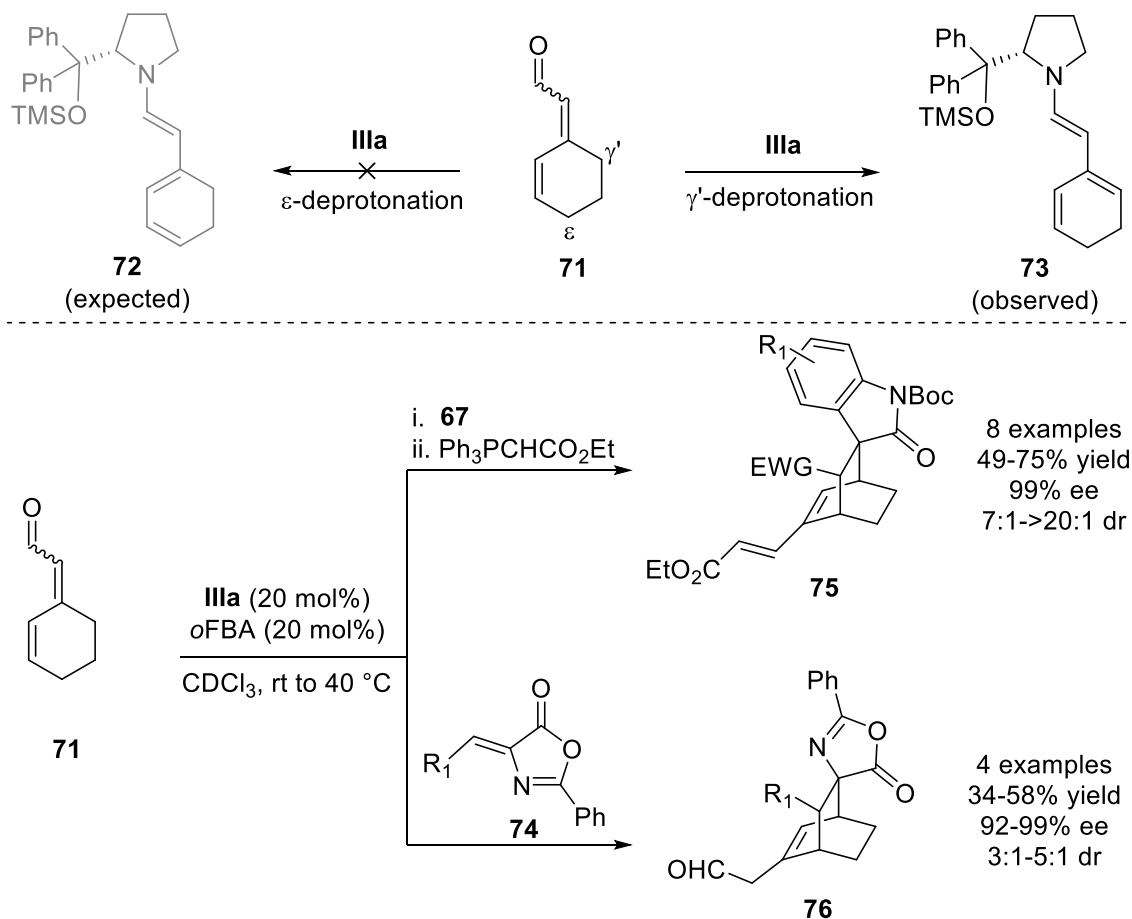
Figure 1. 9 – Possible conformations of trienamine **66** (relative energies in kcal/mol calculated at the B3LYP/6-31G(d) level of theory; Orbital coefficients calculated at the HF/STO-3G level of theory).



Scheme 1. 26 – Selected examples of trienamine-mediated asymmetric Diels-Alder reactions.

With the seminal work from Jørgensen and Chen, several trienamine-mediated asymmetric Diels-Alder reactions were soon reported using a wide variety of dienophiles and *O*-protected bisarylpiprolinol aminocatalysts **III** (Scheme 1.26).^{145–154} The selected examples illustrated above showcased the versatility

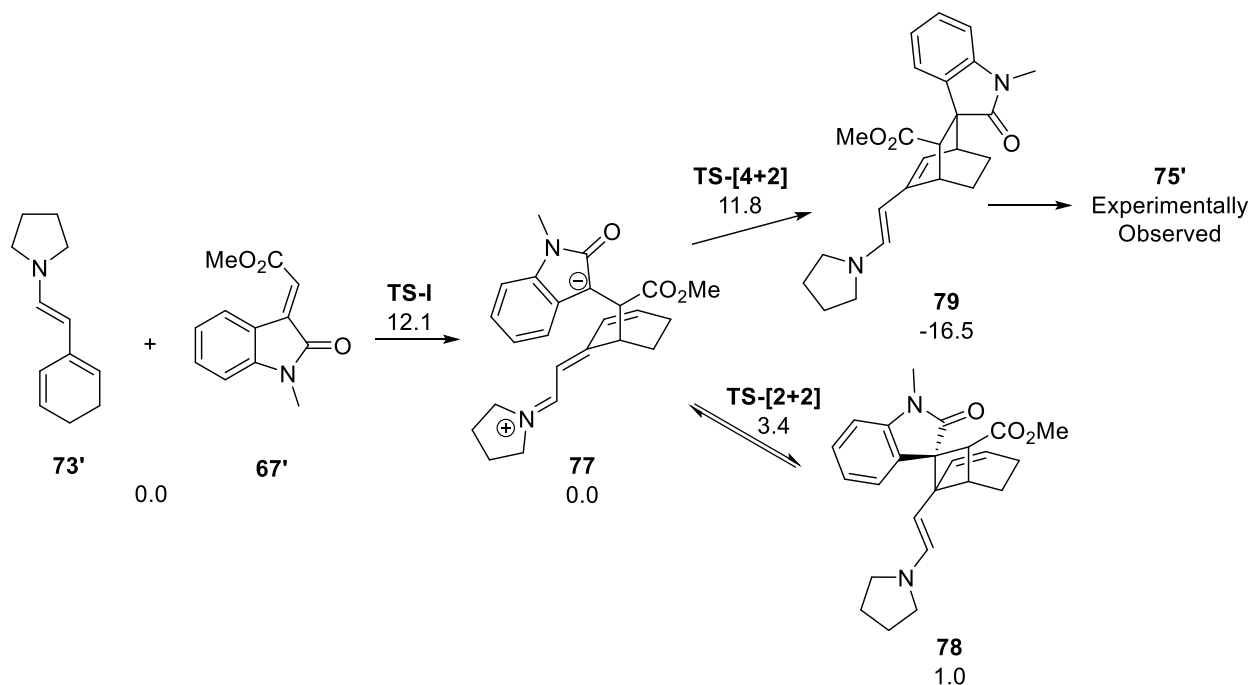
of linear trienamines, like **66**, to undergo asymmetric Diels-Alder reactions with a wide variety of dienophiles. However, from the beginning, it became apparent that regio- and diastereocontrol remained somewhat difficult. To circumvent this issue, Jørgensen and co-workers designed an aldehyde (**71**) which, they expected, would always form a 4,5-*s-cis*-trienamine (**72**) and thus allow for better control of the reaction. However, upon condensation with an aminocatalyst, aldehyde **71** underwent deprotonation at the γ' -position forming the cross-trienamine **73**. Nevertheless, treatment of intermediate **73** with 3-olefinic oxindoles **67** or azalactones **74** also took place through a Diels-Alder reaction giving the bicycloadducts **75** and **76**, respectively in moderate yields but excellent enantio- and diastereoselectivities (Scheme 1.27).¹⁵⁵



Scheme 1.27 – Cross-trienamine-mediated Diels-Alder reactions reported by Jørgensen and co-workers.

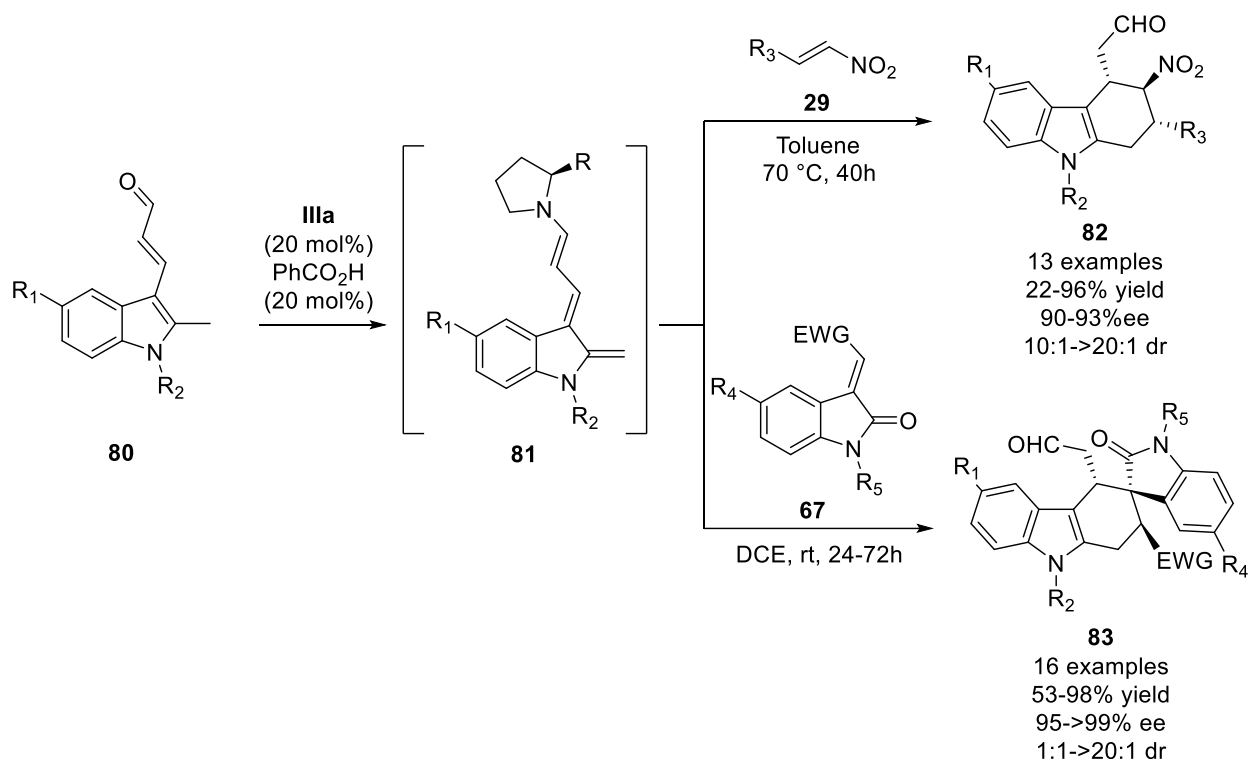
Later computational work by Houk and co-workers showed that the reaction between **73'** and **67'** took place in a stepwise fashion via zwitterion **77** which could readily cyclize to give the [2+2]-cycloadduct

78. Regardless, the (2+2)-cyclization is reversible and hence only the [4+2]-cycloadduct **79** is formed which readily hydrolysis to give the experimentally observed compound **75'** (Scheme 1.28).¹⁵⁶



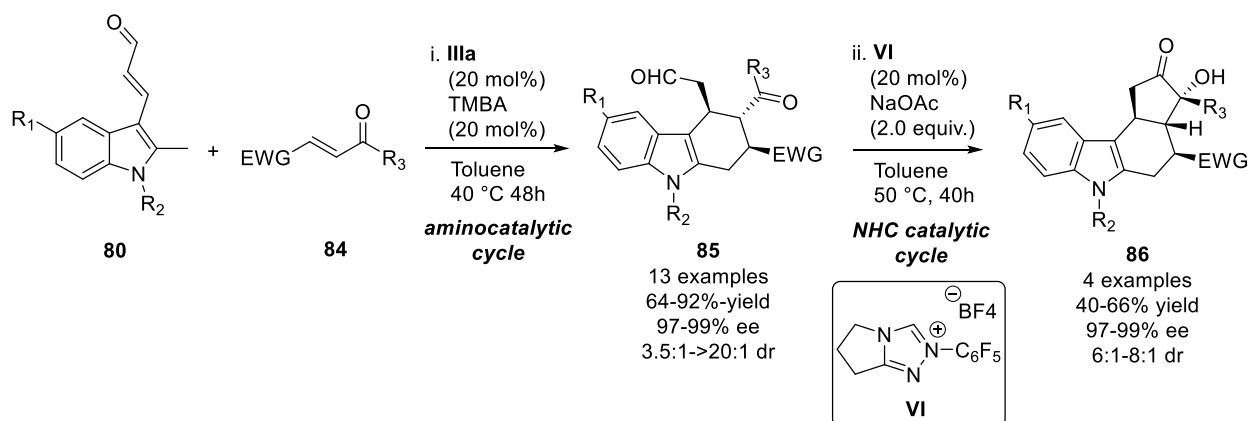
Scheme 1. 28 – Houk’s computational study on the cross-trienamine-mediated Diels-Alder reaction (relative free energies in kcal/mol, calculated at the M06-2X/def2-TZVPP/IEFPCM(CHCl₃)/B97D/6-31+G(d,p)/IEFPCM(CHCl₃)).

Parallel to Jørgensen’s work, Melchiorre and co-workers designed another aldehyde that, upon condensation with an aminocatalyst, would form a 4,5-*s-cis*-trienamine which could be employed in Diels-Alder reactions. For that purpose, the authors used the *N*-Boc protected 3-(2-methyl-3-indol-3-yl)acrylaldehyde **80** which generated an heterocyclic *ortho*-quinodimethane trienamine **81** upon treatment with **IIIa**. Trienamine intermediate **81** was then reacted with nitrostyrene **29** and 3-olefinic oxindoles **67** to give the corresponding tetrahydrocarbazoles **82** and **83**, respectively, in moderate to good yields and overall excellent enantio- and diastereoselectivities (Scheme 1.29).¹⁵⁷ Moreover, this was the first example where an aminocatalyst (**IIIa**) was used to generate heterocyclic *ortho*-quinodimethanes **81** *in situ*.



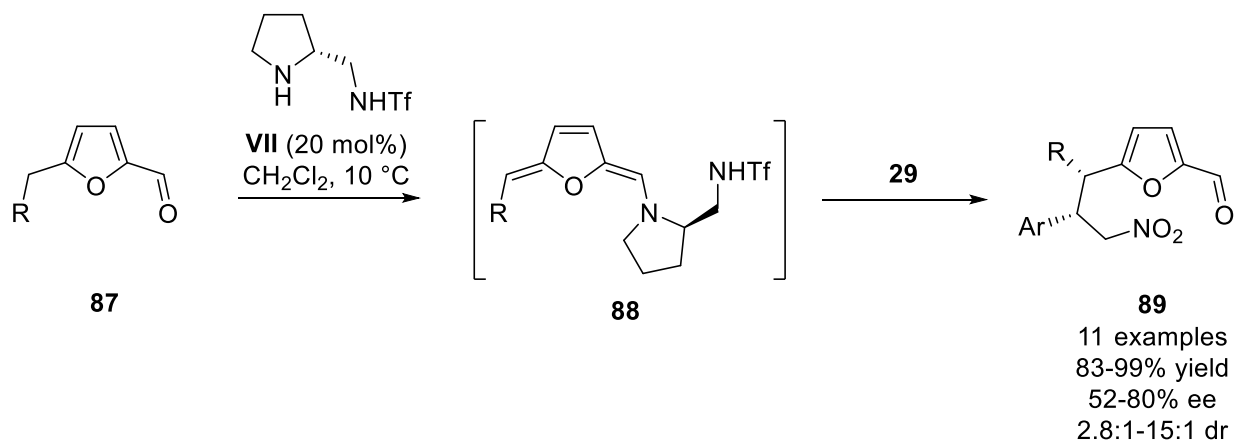
Scheme 1.29 – Heterocyclic *ortho*-quinomethane mediated Diels-Alder reaction reported by Melchiorre and co-workers.

Reaction with nitrostyrene **29** afforded the *exo*-product while the 3-olefinic oxindole **67** gave the *endo*-cycloadduct. The authors rationalized this selectivity with electrostatic repulsions between the nitro group of **29** and the π -system of the trienammine that disfavour the *exo*-approach of **29**. Conversely, when oxindole **67** was used, secondary orbital interactions caused the *endo*-approach to be preferred. One year later, in 2012, the same group used this strategy and catalyst to perform a Diels-Alder reaction between **80** and α,β -unsaturated ketones **84** giving the corresponding tetrahydrocarbazoles **85** in moderate to good yields, good to excellent diastereoselectivities and overall excellent enantioselectivities. Furthermore, the authors were able to treat products **85** with a NHC catalyst (**VI**) and perform a one-pot sequential Diels-Alder/Benzoin reaction via a dual aminocatalytic/NHC catalytic cycle obtaining the corresponding products **86** in moderate yields, good diastereoselectivities and excellent enantioselectivities (Scheme 1.30).¹⁵⁸



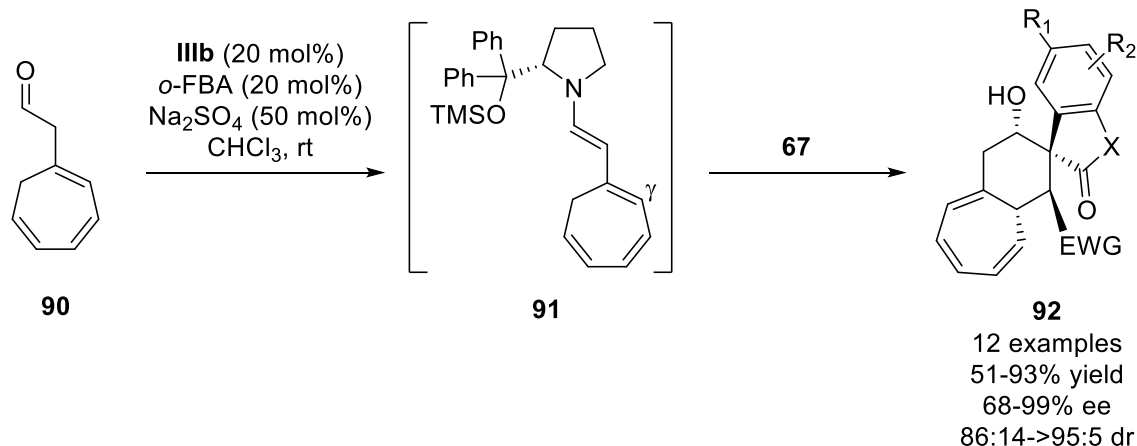
Scheme 1.30 – One-pot Aminocatalysis/NHC sequential Diels-Alder/Benzoin reaction reported by Melchiorre and co-workers.

In 2015 Albrecht and co-workers developed an ϵ -functionalization of furfural derivatives **87** with nitrostyrene compounds **29** through a dearomatized trienamine intermediary **88** (Scheme 1.31).¹⁵⁹ This work opened the door for the use of heteroaromatic aldehyde derivatives as possible substrates for aminocatalyzed asymmetric transformations with higher conformational control of the polyenamine intermediates leading to several reports of cycloadditions and cascade cyclization procedures.¹⁶⁰ The insights into the formation and reactivity of these systems are the topic of one of the Chapters in Part II of this Dissertation.



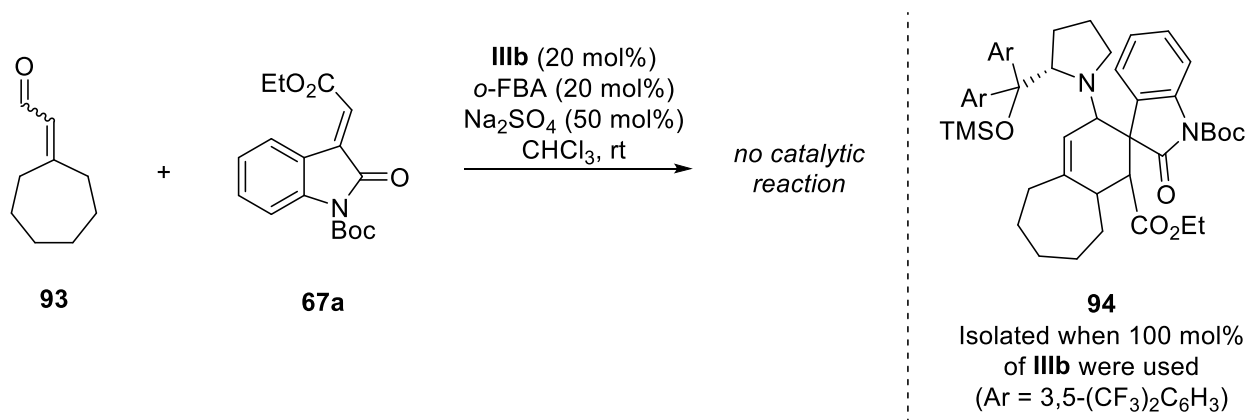
Scheme 1.31 – Dearomatized trienamine mediated ϵ -functionalization of furfural derivatives reported by Albrecht and co-workers.

However, the remote activation modes in aminocatalysis did not stop at trienamamine and, in 2014, Jørgensen and co-workers reported the first example of a tetraenamamine **91** mediated [4+2]-cycloaddition between aldehyde **90** and 3-olefinic oxindoles **67** (Scheme 1.32).¹⁶¹



Scheme 1.32 – Tetraenamamine mediated [4+2]-cycloaddition reported by Jørgensen and co-workers.

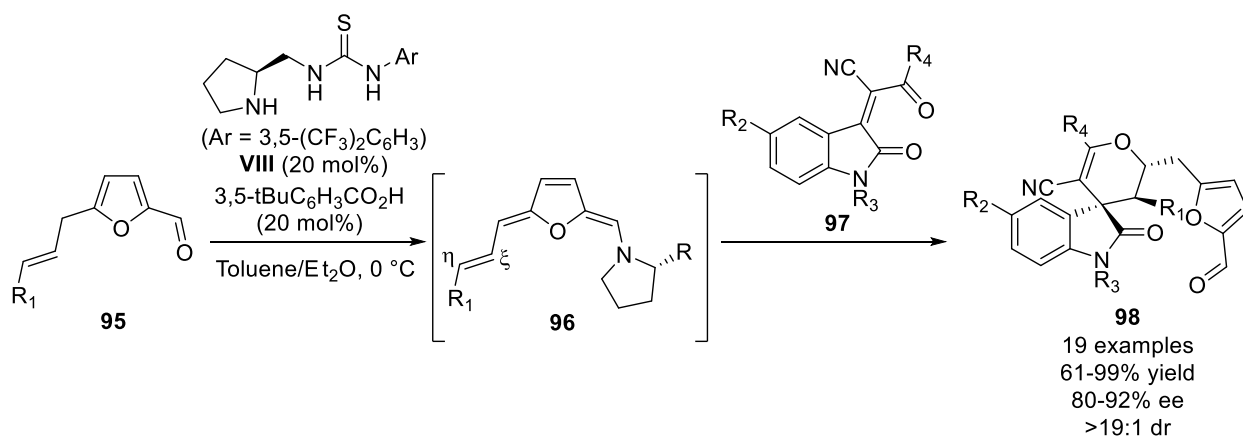
The reaction proceeded in a stepwise fashion with initial addition of the γ -carbon of tetraenamamine **91** to oxindole **67**. The resulting iminium ion, due to the extended conjugation, was long lived enough to undergo hydrolysis of the catalyst and subsequent cyclization. This rationale was further proved by the authors who, by trying a dienamine variation of this protocol via aldehyde **93**, observed no catalytic reaction. Only cycloadduct **94**, with the trapped catalyst, was observed when **IIIa** was used in 100 mol% loading (Scheme 1.33).



Scheme 1.33 – Dienamine mediated protocol with consequent trapping of the catalyst.

It was not until 2018 that Chen and co-workers were able to functionalize the most remote positions of a tetraenamine through an oxa-Diels-Alder reaction, taking advantage a bifunctional H-bond aminocatalyst and the regio- and conformational control provided by heteroaromatic aldehydes showcased by the work of Albrecht and co-workers (*vide supra*).

In this remote oxa-Diels-Alder, the authors used furfural **95** and the bifunctional catalyst **VIII** to form the desired tetraenamine **96** which, upon reaction with oxindoles **97**, afforded the cycloadduct **98** with overall excellent results (Scheme 1.34).¹⁶²



Scheme 1. 34 – oxa-Diels-Alder reaction via a dearomatized tetraenamine intermediate, reported by Chen and co-workers.

With these reports, the field of aminocatalysis established itself as a powerful tool to perform various transformations, namely cycloadditions, with transfer of reactivity to extended π -systems obtaining products bearing new stereocenters located several bonds away from the face differentiating element of the catalyst without loss of stereoselectivity. In Figure 1.10 are illustrated the modes of activation in aminocatalysis for remote functionalizations i.e. dienamine¹⁴¹ and cross-dienamine^{143,163}, trienamine and cross-trienamine, tetraenamine^{161,162,164}, vinylogous iminium ion and bis-vinylogous iminium ion (Figure 1.10).^{59,67-69,165,166}

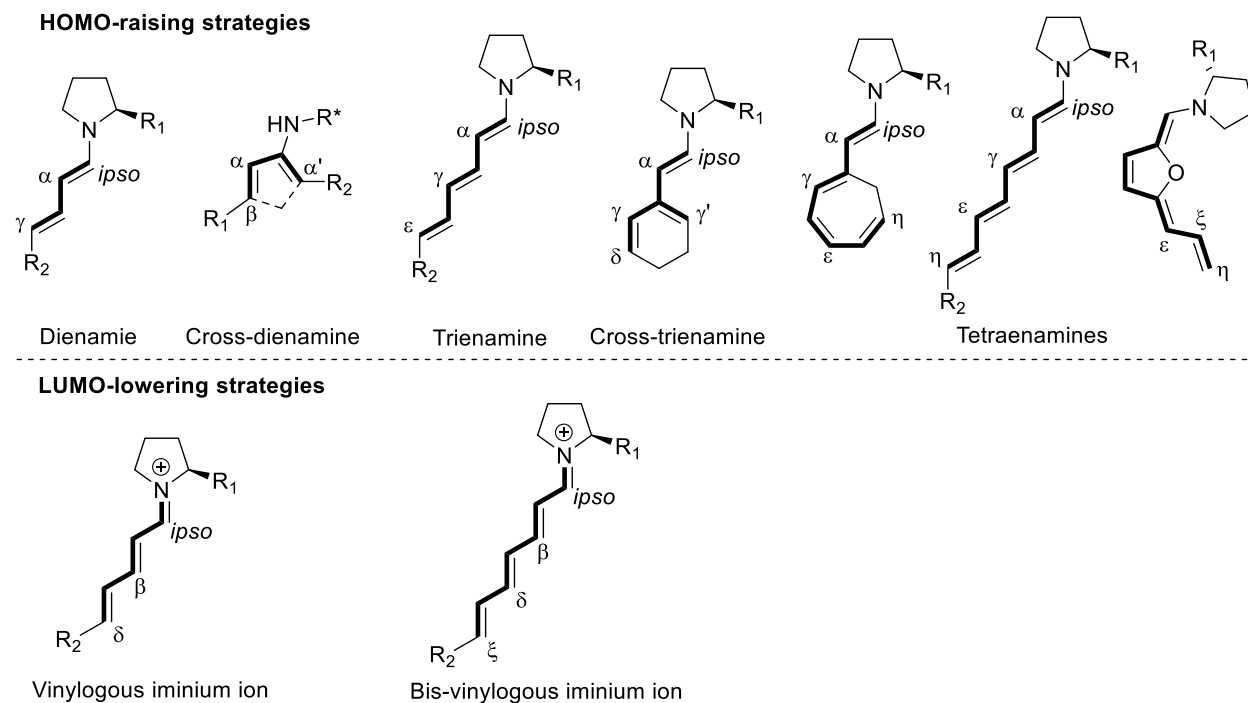
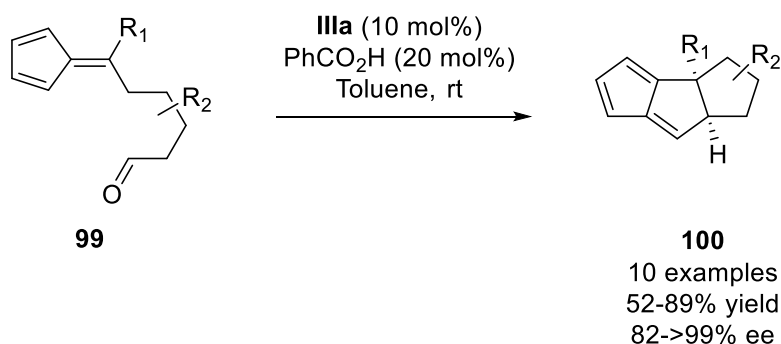


Figure 1. 10 – Modes of remote activation in aminocatalysis.

Another landmark for aminocatalysis has been established in more recent years, with its use in catalyzing high order cycloadditions, in most cases, with excellent periselectivity. The first example of an aminocatalyzed asymmetric high order cycloaddition dates to 2011 when Hayashi, Uchimaro and co-workers performed an intramolecular [6+2]-cycloaddition in oxo-fulvenes **99**, using catalyst **IIIa**, affording the corresponding cycloadducts **100** in moderate yields but excellent enantioselectivities (Scheme 1.35).¹⁶⁷

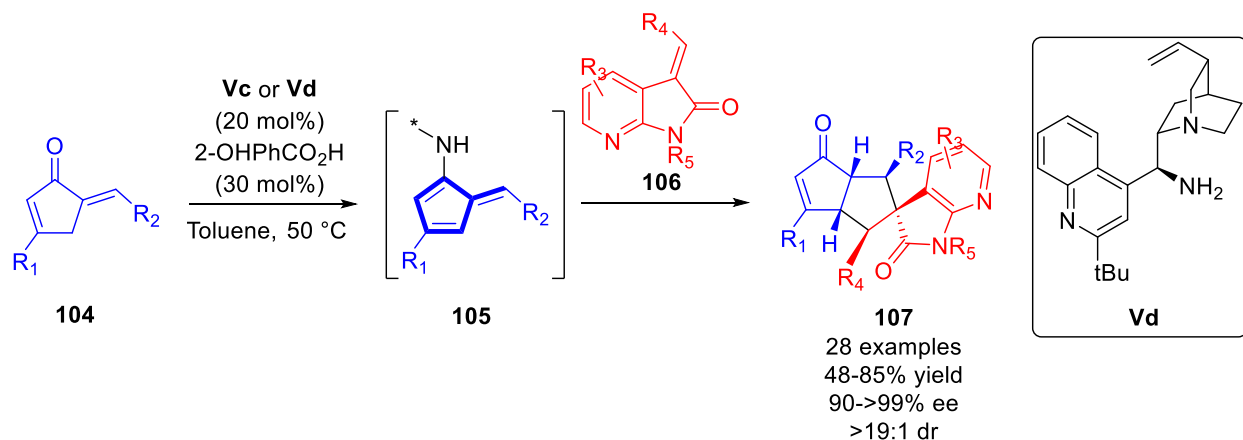


Scheme 1. 35 – Intramolecular [6+2]-cycloaddition reported by Hayashi, Uchimaro and co-workers.

However, it was not until 2017, with the independent works by Jørgensen and co-workers and Ouyang, Chen and co-workers, that the search for new methods to perform asymmetric high order

cycloadditions, through aminocatalysis, gained attention from chemists. Jørgensen's work focused on the use of a cross-dienamine obtained by condensation between cyclic enones **60a-c** with primary aminocatalysts *ent-Va* or *ent-Vc* and subsequent treatment with heptafulvenes **9a-b** to afford the corresponding cycloadducts **101-103**, which correspond to the [4+2]-, [6+4]- and [8+2]-cycloadditions, respectively (Table 1.3).¹⁶⁸ Despite the poor periselectivities observed by the authors, this seminal work illustrated the possibility of aminocatalysts to perform asymmetric high order cycloadditions with reasonably good enantioselectivities and overall excellent diastereoselectivities. Furthermore, it opened the door for the possibility of improvement of both catalyst systems as well as choice of reagents.

Parallel to this work, Ouyang, Chen and co-workers developed a highly periselective [6+2]-cycloaddition between α' -alkylidene-2-cyclopentenones **104** and highly electrophilic 3-olefinic-7-azaoxindoles **106**, yielding the [6+2]-cycloadducts **107** in moderate to good yields but, excellent enantio- and diastereoselectivities (Scheme 1.36).¹⁶⁹ The reaction proceeded via a 4-aminofulvene trienamine intermediary **105** produced after condensation of **104** with the primary aminocatalysts **Vc** or **Vd**.



Scheme 1. 36 – [6+2]-Cycloaddition reported by Ouyang, Chen, and co-workers.

Table 1. 3 – High Order cycloadditions developed by Jørgensen and co-workers.

ent-Va

ent-Vc

60a: $n = 1$
60b: $n = 2$
60c: $n = 3$

9a: $X = O$
9b: $X = C(CN)_2$
9c: $X = C(CN)CO_2Et$

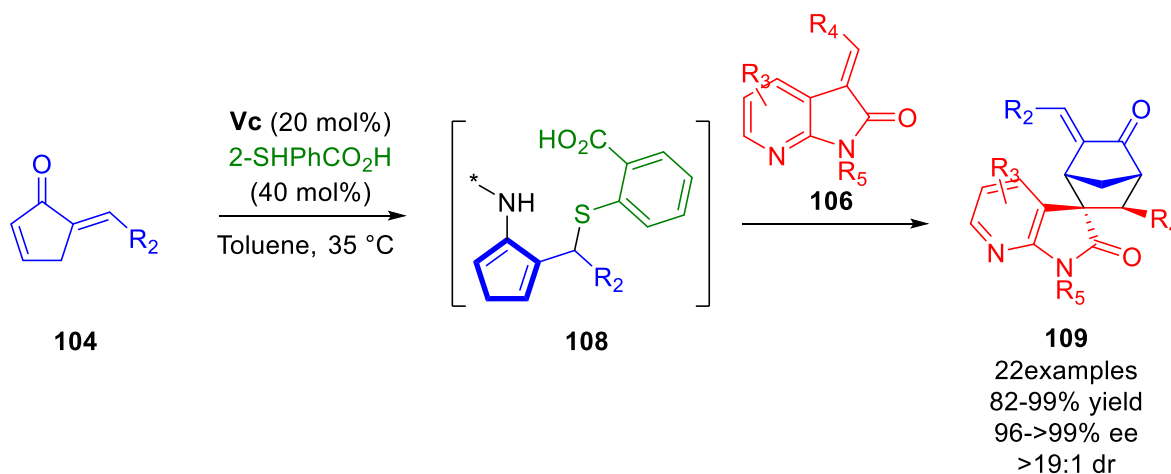
101 **102** **103**

Entry	60	9	[4+2]-cycloadduct	[6+4]-cycloadduct	[8+2]-cycloadduct
1*	60a	9a	—	102aa , 51% yield; 95% ee; >20:1 dr	—
2†	60a	9b	—	102ab , 50% yield; 42% ee; >20:1 dr	—
3*†	60a	9c	NR	NR	NR
4*	60b	9a	101ab , 72% yield; 71% ee; >20:1 dr	—	—
5†	60b	9b	101bb , 56% yield; 87% ee; >20:1 dr	—	—
6†	60b	9c	—	—	103bc , 58% yield; 98% ee; 85:15 dr
7*†	60c	9a	NR	NR	NR
8†	60c	9b	—	102cb , 5% yield; 52% ee; >20:1 dr	103cb , 48% yield; >99% ee; 9:1 dr
9†	60c	9c	—	—	103cc , 61% yield; 99% ee; >20:1 dr

* Conditions A: **ent-Vc** (20 mol%), (-)-CSA (40 mol%), dioxane, 60 °C; † Conditions B: **ent-Va** (20 mol%), EtCO₂H (20-60 mol%), Toluene, 60 °C; NR, no reaction; Dashes indicate no product was observed.

Moreover, the authors were able to switch the regioselectivity of these reactions by manipulation of the reaction conditions and obtain the [4+2]-cycloadducts when using 2-mercaptobenzoic acid instead of salicylic acid as an additive. The authors suspect that intermediary **105** gets trapped through nucleophilic

attack of the sulfur to form dienamine **108** which undergoes the [4+2]-cycloaddition with **106** to produce the [4+2]-cycloadducts **109** in excellent results, overall (Scheme 1.37).

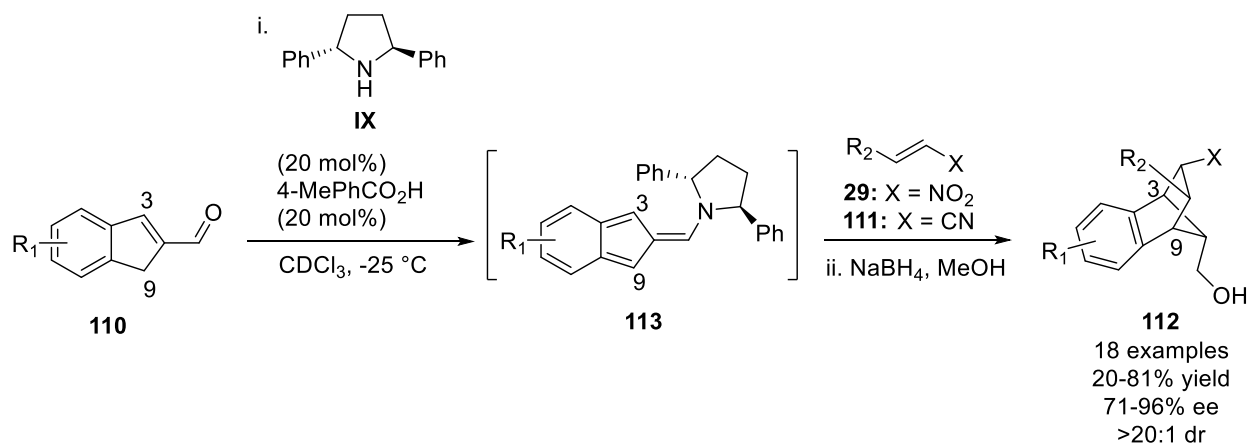


Scheme 1. 37 – Switchable periselectivity of the reaction reported by Ouyang, Chen, and co-workers.

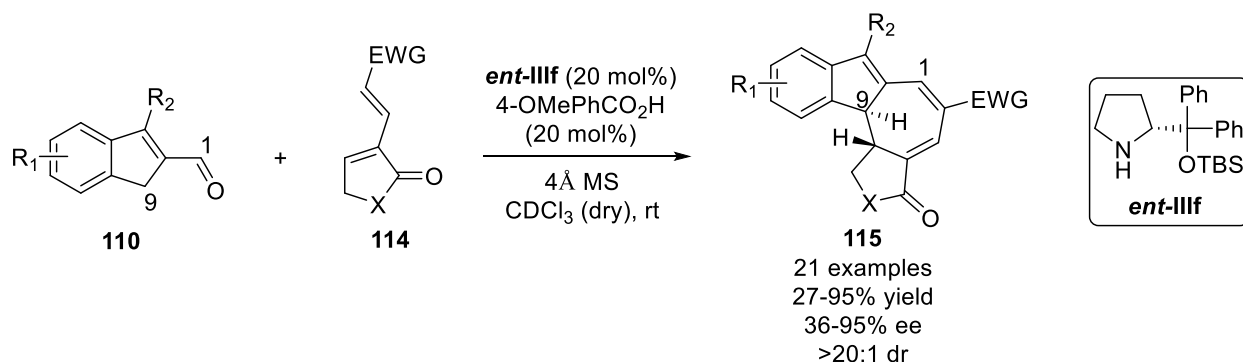
One year later, in 2018, Jørgensen and co-workers reported a highly peri- and stereoselective [8+2]-cycloaddition between indene-2-carbaldehyde **110** and electron deficient alkenes **29** and **111** catalyzed by the C_2 -symmetric aminocatalyst **IX** producing the corresponding [8+2]-cycloadducts which were reduced *in situ* with NaBH_4 to afford the more stable alcohols **112** in moderate yields and excellent enantioselectivities (Scheme 1.38).¹⁷⁰ In the same work, DFT calculations suggested that the high order cycloaddition took place in a stepwise fashion and stereoselectivity was governed by the kinetics of the first bond forming event. Moreover, the authors proposed that π -stacking and electrostatic interactions present between the nitro group of **29** and the amino isobenzofulvene intermediate **113** were essential for reactivity and stereoselectivity.

Following the promising reactivity observed for the amino isobenzofulvene system **113**, the same group soon published a [10+4]-cycloaddition between **110** and electron deficient dienes **114** using aminocatalyst *ent*-**III**f. The cycloadducts **115** were obtained in generally good results and the authors were able to expand the scope of indenenes used. However, on the side of the diene **114**, only full carbon systems

afforded good results as the only example with a lactone gave the corresponding cycloadduct **115** in only 27% yield and 76% ee (Scheme 1.39).¹⁷¹

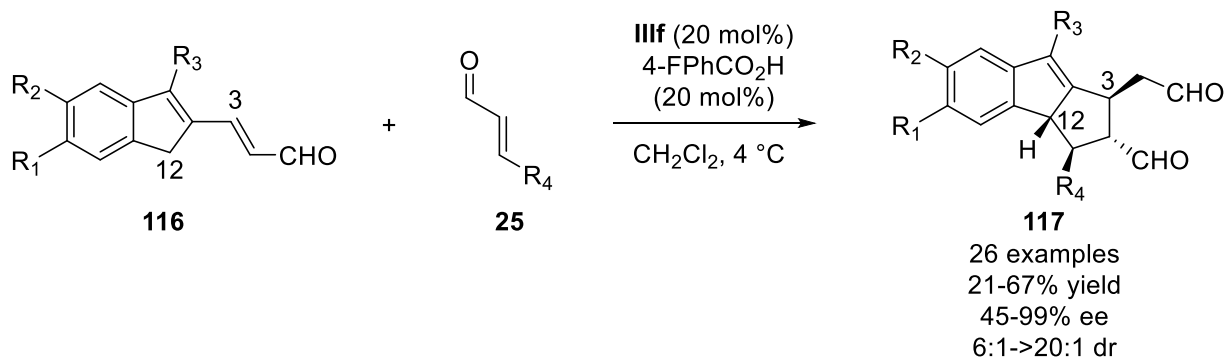


Scheme 1. 38 – [8+2]-Cycloaddition reported by Jørgensen and co-workers.



Scheme 1. 39 – [10+4]-Cycloaddition reported by Jørgensen and co-workers.

Very recently, in 2020, the same group reported the use of homologated indene-2-carbaldehydes **116** as precursors for a poly-enamine which reacted smoothly with α,β-unsaturated aldehydes **25** in a highly periselective [10+2]-cycloaddition, using catalyst **III**f. The authors were able to employ a wide scope of cinnamyl aldehydes as well as alkynyl and alkyl substituents. However, the scope of **116** was fairly limited. The cycloadducts **117** were obtained in moderate yields but excellent enantio- and diastereoselectivities (Scheme 1.40).¹⁷²

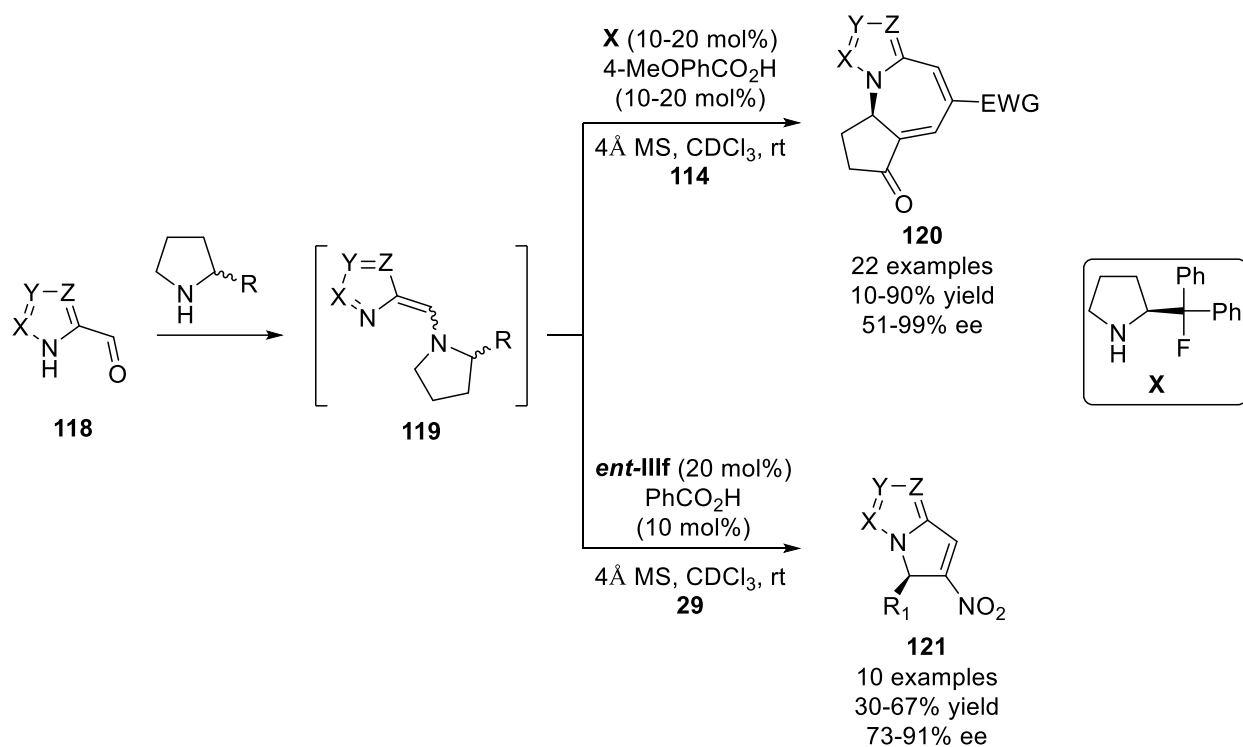


Scheme 1.40 – [10+2]-Cycloaddition reported by Jørgensen and co-workers.

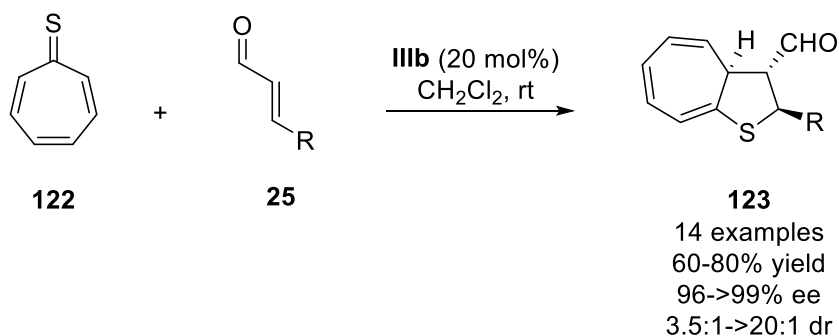
The excellent periselectivity of this reaction is quite impressive and was studied by the authors using DFT calculations, which showed that a stepwise mechanism was in place with the first addition occurring almost instantly with a virtually barrierless transition state. Cyclization to the [10+2]-product was kinetically favoured over other possible cycloadducts.

In 2019, the same group reported the use of 6-amino azafulvene intermediates **119** as 6π -electron systems for selective hetero- [6+4]- and [6+2]-cycloadditions. For this purpose, Jørgensen and co-workers treated 2-formyl substituted pyrroles, imidazoles and pyrazoles **118** with aminocatalysts *ent*-**III f** or **X** to generate intermediate **119**. These hetero-trienes were then subjected to compounds **114** or **29** to achieve the desired [6+4]- or [6+2]-cycloadducts **120** and **121**, respectively (Scheme 1.41).¹⁷³

In the same year, Albrecht and co-workers reported the inversion of reactivity of troponoid systems by replacement of the oxygen of tropone **9** with a sulfur atom. This new troprothione **122** was then employed by the authors in [8+2]-cycloadditions with iminium ions derived from α,β -unsaturated aldehydes **25** and aminocatalyst **III b** (Scheme 1.42). The use of cinnamyl aldehyde derivatives afforded cycloadducts **123** in moderate to good yields and good enantio- and diastereoselectivities however, alkyl substituted aldehydes gave poorer results.¹⁷⁴



Scheme 1.41 – Hetero-[6+4]- and [6+2]-cycloadditions reported by Jørgensen and co-workers.



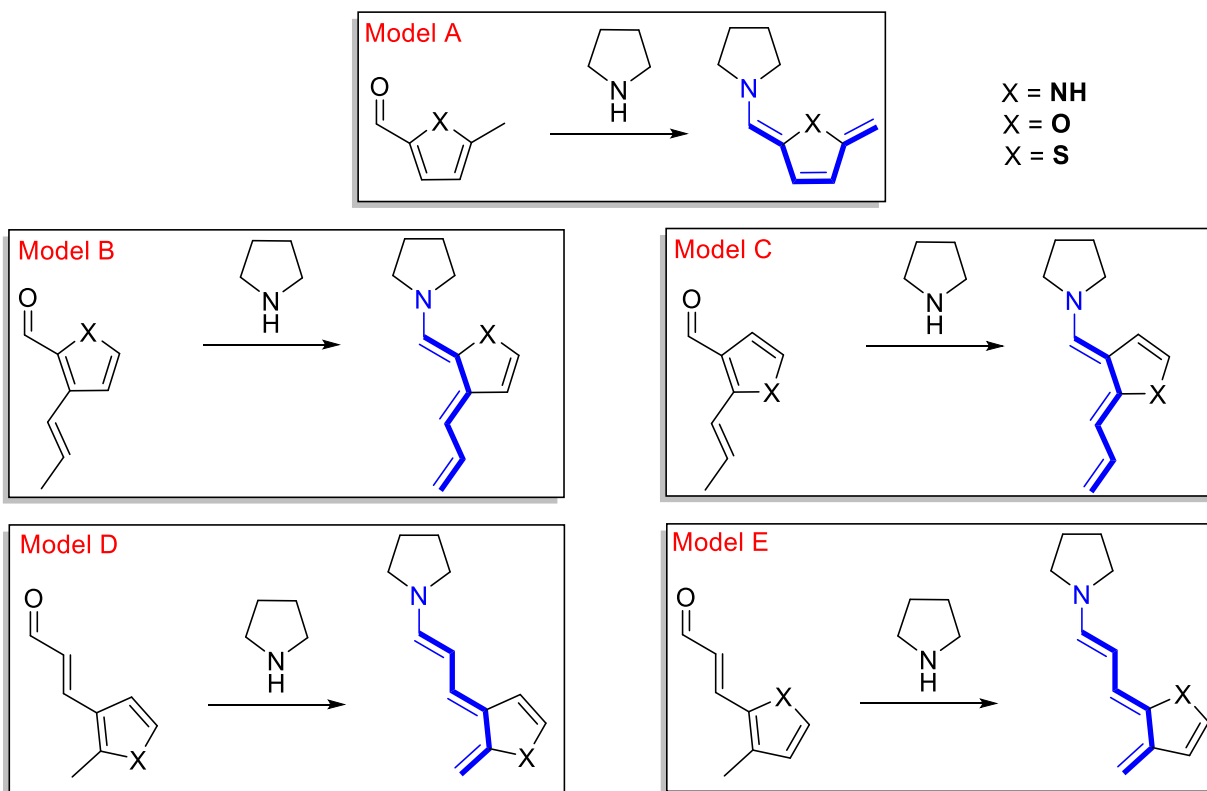
Scheme 1.42 – [8+2]-Cycloaddition reported by Albrecht and co-workers.

In this Chapter, we illustrated some of the landmarks of aminocatalysis namely, in HOMO-raising strategies such as enamine, dienamine, (cross-)trienamine and tetraenamine, and their efficiency in performing several asymmetric cycloaddition reactions between a wide variety of aldehydes and dienophiles allowing the synthesis of enantioenriched, complex (hetero-)cyclic structures. The more recent reports in higher-order cycloadditions will definitely bring the possibility of synthesizing even more complex and functionalized scaffolds.

Part II – Results and Discussion

Chapter I – Computational Study on Dearomative Aminocatalysis

In Chapter III of Part I of this Dissertation we saw some examples of the use of aminocatalysis in dearomatizing heteroaromatic aldehydes to form the reactive poly-enamines that could then react with desired electrophiles with higher conformational control than their linear counterparts (Schemes 1.28-1.30 and 1.33). To us, this mode of activation of heteroaromatic aldehydes, with aminocatalysts, was quite intriguing so, we decided to examine a series of heteroaromatic aldehydes (Scheme 2.1) in order to explore what effect the formation of the iminium ion intermediate, the precursor to the trienamine, could have on promoting the loss of aromaticity in those heterocyclic systems using DFT calculations.



Scheme 2.1 – Model Systems studied in this section.

The model systems depicted in Scheme 2.1 were studied using hyperhomodesmotic equations^{175,176} to assess the energy penalty associated with dearomatization, and population analysis of the HOMO of the

formed trienamines to better understand if the heteroatom has any influence in the conjugated system and if so, what could one expect in terms of regioselectivity for the substrates depicted in Scheme 2.1.

Computational Methods

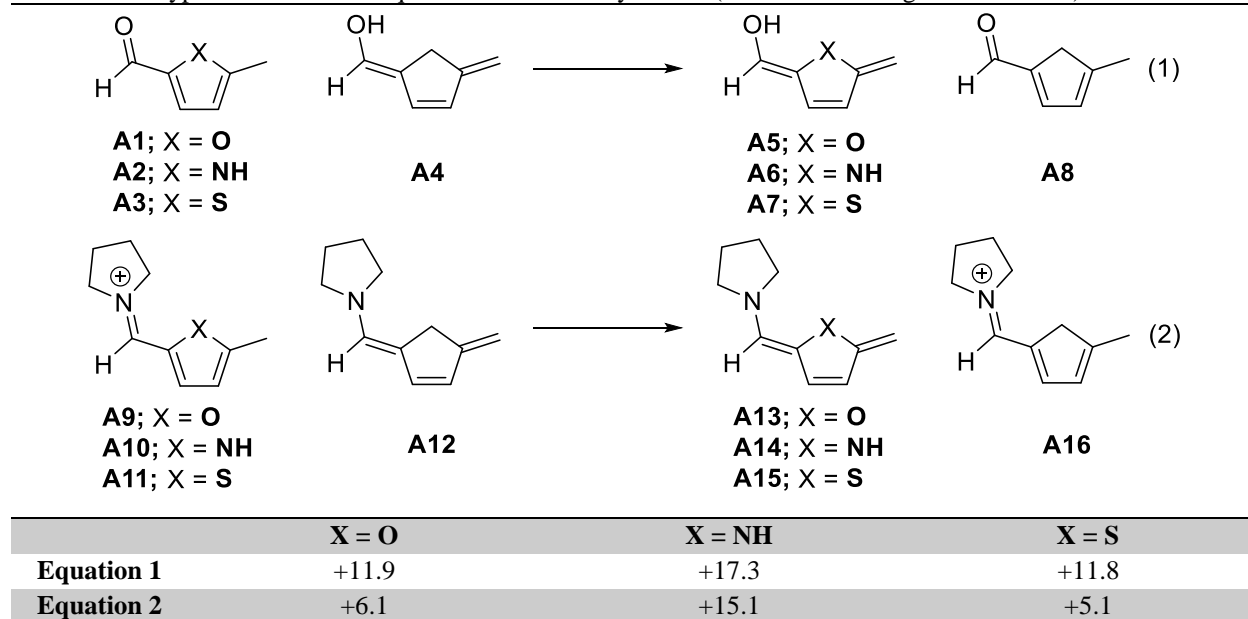
All structures were optimized using M06-2X¹⁷⁷ with the double- ζ split valence 6-31+G(d,p)^{178,179} basis set and vibrational analysis verified that each structure was a minimum. All optimizations were performed in Gaussian 09.e01.¹⁸⁰ Orbital coefficients were generated with QMForge v2.1.¹⁸¹ All figures produced using VESTA v4.5.0.¹⁸²

Model System A

To begin this study, we explored the simplest heteroaromatic system bearing an aldehyde at the 2-position and a methyl group at the 5-position (Model System A). This represents one of the first compounds that employed the dearomatization approach in the formation of polyenamines for the remote alkylation of furfural derivatives (Scheme 1.30).¹⁵⁹ We decided to focus on the influence that the transient iminium ion has on the formation of the dearomatized trienamine intermediate using the hyperhomodesmotic equations outlined in Table 2.1. The first equation examines the energetic cost of breaking the aromaticity of the furfural derivative by forming its enol tautomer while the second equation evaluates the same energetic penalty with the iminium ion derived from furfural. In examining the energetics of equations 1 and 2 it can be seen that dearomatization of the heteroaromatic ring in both the aldehydes **A1-3** (X = O, NH, S, respectively) and the corresponding iminium ions **A9-11** are disfavored. However, the presence of the iminium ion decreases the energetic penalty for loss of aromaticity in all heterocycles **A9-11** by 5.8, 2.2, and 6.7 kcal/mol for X = O, NH, and S, respectively, when compared to the corresponding aldehydes **A1-**

3. This decrease in the energy penalty suggests that the presence of the iminium ion facilitates dearomatization.

Table 2. 1 – Hyperhomodesmotic equations for Model System A (relative free energies in kcal/mol).



In examining equations 1 and 2, we see that in both the dearomatization of the pyrrole is more unfavorable than dearomatization of the furan or thiophene. Perhaps the most interesting observation noted is in the comparison of the influence of the iminium ion across the three heterocyclic systems. The presence of the iminium ion in the furan and thiophene systems has a significant influence on the dearomatization, in each case lowering it by ~6 kcal/mol, relative to the corresponding aldehydes. In the case of the pyrrole system, the effect of the iminium ion is significantly less, lowering it by only 2.2 kcal/mol relative to the aldehyde.

To understand how the choice of heteroatom in the heteroaromatic ring influences the dearomatization energy penalty in Model System A, we examined the geometries of all structures involved in equations 1 and 2. While no large geometric changes were noted in comparing the structures or the aldehydes (**A1-3** and **A8**) and iminium ions (**A9-11** and **A16**), comparison of the enols and enamines did reveal a significant change in geometry in **A14** relative to **A6**. In trienamine **A14**, the pyrrolidine ring is

bent so that the nitrogen lone pair is not fully aligned for donation into the pi system of the triene. This twisting appears to be due to steric clash of the alkyl ring of the catalyst with the N-H bond of the pyrrole and is not present in the system containing the furan. Comparing the $N_{\text{cat}}\text{---C}$ bond lengths of the enamines, 1.36 Å for **A13**, 1.38 Å for **A12**, 1.38 Å for **A15**, and 1.39 Å for **A14**, suggests that the trienamine **A14** is the least conjugated. In the corresponding enol **A5** the pyrrole -NH is not bent out of conjugation, hence, shows more sp² character than the enamine **A14**. The combination of steric clash between the pyrrolidine and -NH of the ring, the bending of this group, and the longer $N_{\text{cat}}\text{---C}$ bond length in **A14** suggests the loss of conjugation, resulting in increase in energy for the formation of trienamine.

We next wanted to assess the influence of the heteroaromatic ring on the regioselectivity of the addition reaction. To do this, we performed population analysis of the HOMO of the trienamine systems **A12-15** (Figure 2.1 and Table 2.2). In order to evaluate the possible synergistic effects between the conjugation provided by the aminocatalyst and the heteroatom, the all-carbon trienamine **A12** was also computed to serve as a means of comparing the results. While examining the HOMO orbital coefficients of the trienamine derived from cyclopentadiene **A12** it was observed that it follows the general vinylogy principle¹⁸³, with the α -carbon having the largest coefficient followed by γ -carbon and then the ε -carbon (Table 2.2). The presence of the heteroatom in the ring system of Model System A (trienamines **A13-15**) significantly increases the orbital coefficient at the ε -carbon whereas the orbital coefficients for β - and γ -carbon decrease relative to those in **A12**. An interesting feature of this model is the very low orbital coefficient observed at the γ -carbon in trienamines **A13-15**, when compared to **A12**. It would appear that the heteroatom in the ring is influencing the conjugated trienamine backbone in two ways; it donates into the terminal double bond, increasing the orbital coefficient at the ε -carbon and it also disrupts the donating abilities of the amine via cross-conjugation with the enamine, decreasing the orbital coefficients at the α - and γ -carbons.

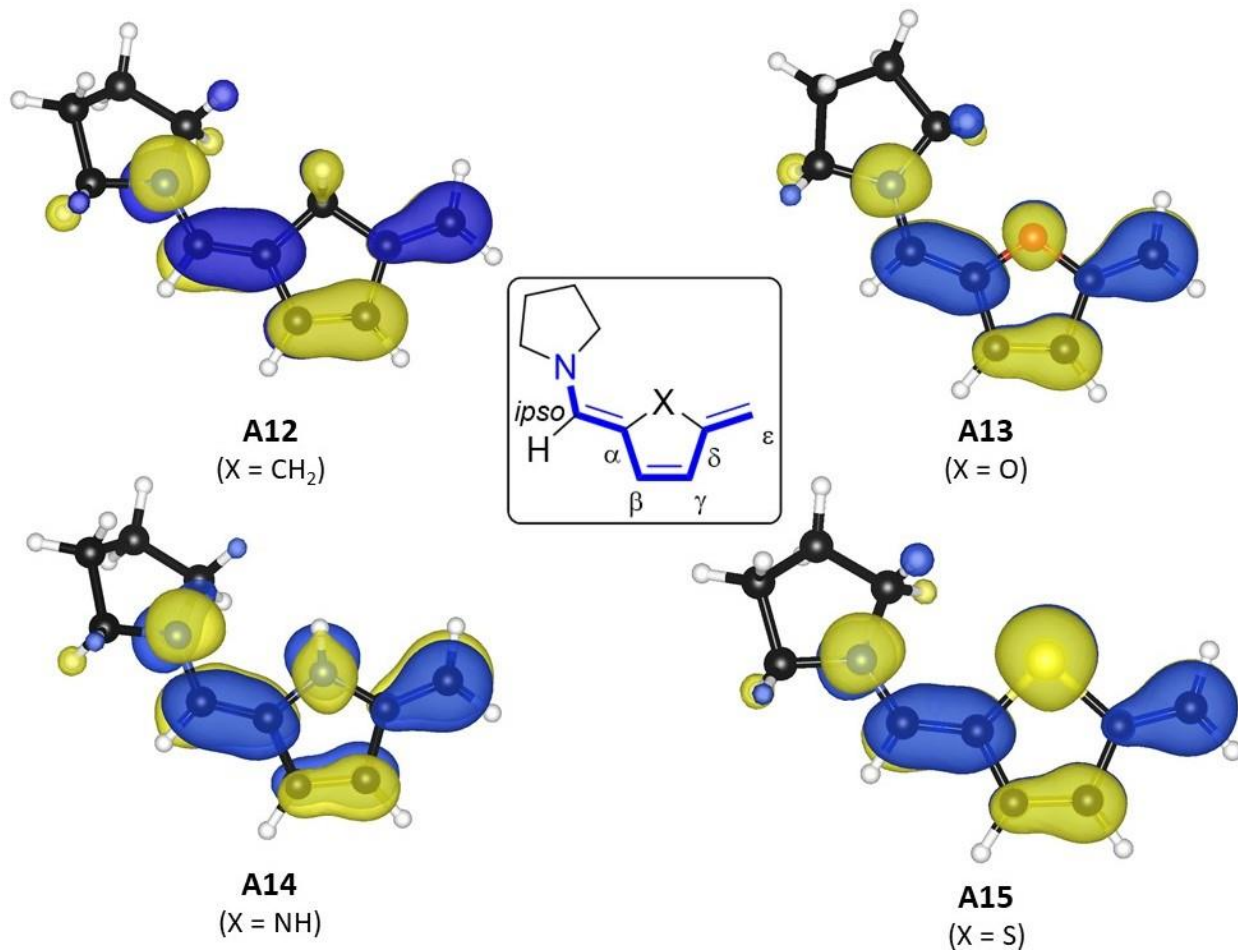


Figure 2. 1 – HOMO of trienamines A13-A15 for Model System A (isovalue (0.035).

Table 2. 2 – Orbital coefficients of the HOMO of Model System A.

Carbon	A12 (X = CH ₂)	A13 (X = O)	A14 (X = NH)	A15 (X = S)
<i>ipso</i>	13.6	11.8	15.2	10.8
α	18.7	11.3	8.4	11.2
β	7.5	3.4	3.3	3.3
γ	16.0	8.0	5.6	7.6
δ	2.5	3.3	3.7	3.4
ϵ	12.3	19.7	20.6	16.7

Overall, the decreased energy penalty associated with the dearomatization of the trienamine system and the regiochemical preferences suggested by the orbital analysis of the various trienamines are in agreement with the experimental results been reported by Albrecht and co-workers.¹⁵⁹ Our results also

suggest that other heteroaromatic rings follow a similar trend so, similar reactivity may be achieved employing those systems.

Model System B

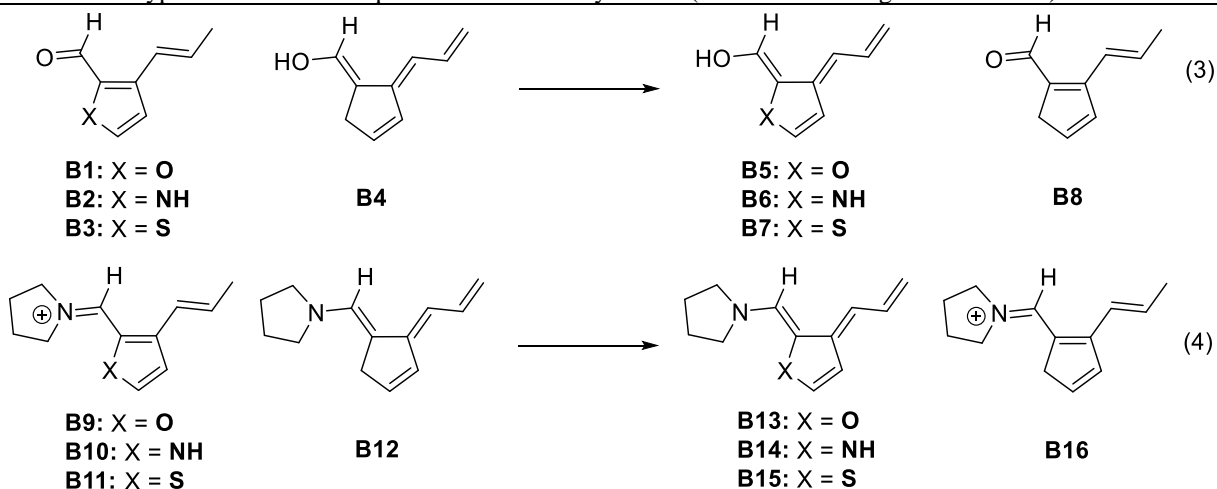
We next explored a family of heterocyclic systems with an allyl group on the 3-position (Model System B). Upon deprotonation at the ϵ -carbon of the corresponding iminium ion, aromaticity in the ring is disrupted as the trienammine intermediate is formed (Scheme 2.1). While these ortho-olefinated, heterocyclic aldehydes have been synthesized and have found use as intermediates in the design of photoswitches and optoelectronics^{184–186}, to the best of our knowledge, they have yet to be used as substrates in organocatalytic reactions. However, the rigidity provided by the heterocyclic scaffold suggests that they would serve as optimal substrates for organocatalytic remote functionalization and, therefore, we decided to perform a similar study to that made for Model System A to provide insights into what features this scaffold may present for future organocatalytic reaction development.

Assessment of the impact of the catalyst on the energetic penalty for dearomatization of the substrate was achieved through hyperhomodesmotic equations 3 and 4. It was observed that dearomatization of aldehydes **B1-3** (eq 3) and iminium ions **B9-11** (eq 4) is, again, disfavored. Similar to Model System A, the iminium ion decreases the energetic penalty for the loss of aromaticity in all heterocycles **B9-11** by 4.2 kcal/mol, 4.9 kcal/mol, and 6.1 kcal/mol for X=O, NH, and S respectively, when compared to the corresponding aldehydes **B1-3** (Table 2.3).

The decrease in the relative energy penalty for the dearomatization of the iminium ions **B9-11** can be explained by the increased polarization of the iminium ion vs the parent aldehyde which results in increased delocalization of the electrons of the heterocycle out of the ring and into the exocyclic C=N bond of the iminium ion. This can be observed by the decrease in the $C_{ipso} - C_{\alpha}$ bond lengths in the iminium ions **B9-11** vs the parent aldehydes **B1-3** (Table 2.4, entry 1). Further analysis of the bond distances in the

aldehyde and iminium ion derived from pyrrole (**B2** vs **B8**) shows slight decreases in the $X - C_{\delta}$, $C_{\gamma} - C_{\delta}$, and $C_{\beta} - C_{\gamma}$ bonds indicating some cross-conjugation through the ring to stabilize the positively charged nitrogen of the aminocatalyst moiety (Table 2.4, entries 5 to 8).

Table 2.3 – Hyperhomodesmotic equations for Model System B (relative free energies in kcal/mol).



	X = O	X = NH	X = S
Equation 1	+10.5	+17.3	+11.4
Equation 2	+6.3	+12.4	+5.3

Table 2.4 – Comparison between the bond lengths (Å) for aldehydes **B1-3** and iminium ions **B9-11**, in Model System B.



Entry	Bond	B1 (X = O)	B2 (X = NH)	B3 (X = S)	B9 (X = O)	B10 (X = NH)	B11 (X = S)
1	$C_{ipso} - C_{\alpha}$	1.46	1.45	1.46	1.41	1.40	1.41
2	$C_{\alpha} - C_{\beta}$	1.38	1.40	1.39	1.40	1.42	1.41
3	$C_{\beta} - C_{\gamma}$	1.46	1.46	1.47	1.45	1.46	1.46
4	$C_{\gamma} - C_{\delta}$	1.34	1.34	1.34	1.34	1.34	1.34
5	$C_{\alpha} - X$	1.46	1.37	1.73	1.41	1.39	1.73
6	$X - C_{\delta}$	1.34	1.36	1.71	1.34	1.35	1.70
7	$C_{\gamma} - C_{\delta'}$	1.36	1.38	1.37	1.36	1.39	1.37
8	$C_{\beta} - C_{\gamma'}$	1.43	1.42	1.43	1.43	1.41	1.42

To assess the influence of the heteroaromatic ring in Model System B on the potential regioselectivity of an addition reaction we performed a population analysis of the HOMO of the trienamine systems **B12-15** (Figure 2.2). It was observed that for all trienamines **B12-B15**, the vinylogy principle does not seem to be obeyed as the coefficient at C_γ is higher than any of the other carbons in the trienamine backbone (Table 2.5).

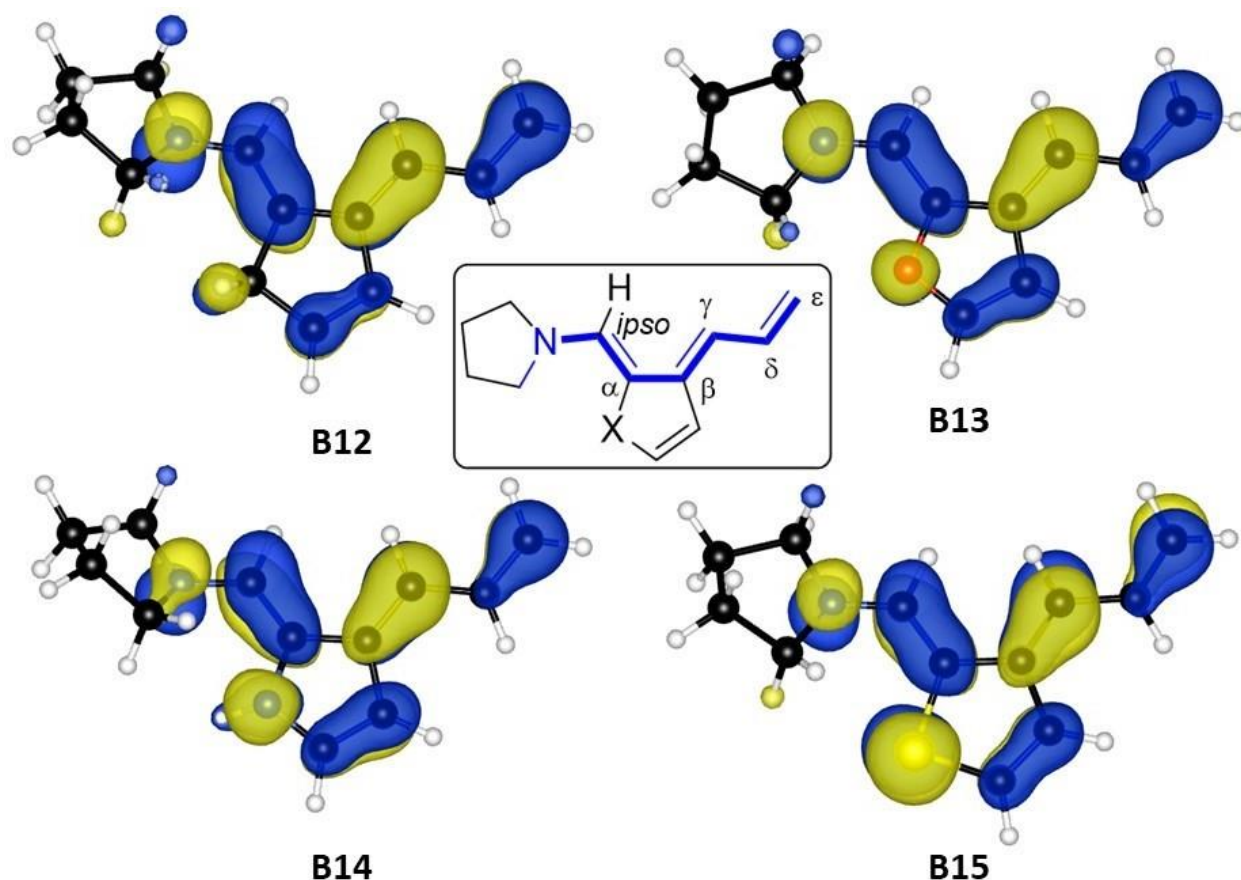


Figure 2. 2 – HOMO of trienamines **B12-15** for Model System B (isovalue 0.035).

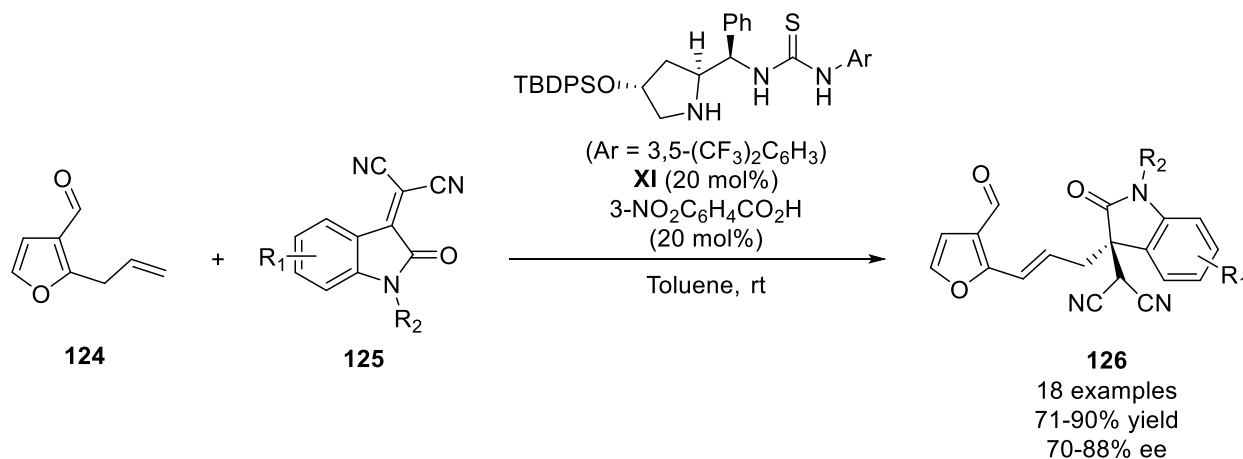
Table 2. 5 – Orbital coefficients of the HOMO of Model System B.

Carbon	B12 (X = CH ₂)	B13 (X = O)	B14 (X = NH)	B15 (X = S)
<i>ipso</i>	10.8	10.9	14.4	10.8
α	15.2	11.6	8.1	10.5
β	8.6	4.9	4.8	4.2
γ	21.0	21.4	19.4	17.8
δ	2.5	1.5	1.4	1.2
ϵ	12.4	11.2	10.1	9.0

One possible explanation for the high coefficient at the C_γ can be attributed to the loss of planarity between the catalyst and the rest of the π -system which could affect resonance and thus, electron donation. While the dihedral angles between $C_{cat}, N_{cat}, C_{ipso}, C_\alpha$, in the parent iminium ions **B9-11** and **B16** are fairly planar (between 0.6 and 2.7°), they get fairly distorted in the enamines to 33.5° in **B12**, 4.2° in **B13**, 46.6° in **B14** and 27.5° in **B15**. These changes are caused by increased steric repulsion between the CH_2 unit of the catalyst and hydrogens and/or lone pairs of X in the cyclic substrate.

Model system C

We then inverted the position of the aldehyde and allyl group relative to the heteroatom from Model system B and came across Model system C. This System has been recently used by Chen and co-workers to perform remote Michael additions, catalyzed by the bifunctional organocatalyst **XI**, between the furfural derivative **124** and electron-deficient 3-olefinic oxindoles **125** via trienamine intermediary to give the corresponding Michael adducts **126** in good yields and moderate enantioselectivities (Scheme 2.2).¹⁸⁷



Scheme 2.2 – Michael addition reaction between furfural **124** and 3-olefinic oxindoles **125**, reported by Chen and co-workers.

As with the previous model systems, hyperhomodesmotic equations (Table 2.6) suggest that the conversion of aldehydes **C1-3** and iminium ions **C9-11** to the corresponding trienes is an unfavourable

process. The penalty for loss of aromaticity in iminium ion **C9** ($X = O$) is 3.2 kcal/mol lower than that of the parent aldehyde **C1**, suggesting the iminium ion is decreasing the penalty for dearomatization. This is also the case in the thiophene system (**C11** vs **C3**) where the presence of the iminium ion decreases the penalty for loss of aromaticity by 3.9 kcal/mol. Conversely, the loss of aromaticity in iminium ion **C10** ($X = NH$) is 1.2 kcal/mol higher than that for the dearomatization of aldehyde **C2**. This can be explained by the additional loss of delocalization of the pyrrole lone pair into the iminium ion upon formation of the trienamine. This delocalization can be seen in the increased length of the C_α - C_β double bond (see Figure 2.3 for atom labels) in **C10** (1.42 Å) relative to that in **C2** (1.40 Å).

Table 2. 6 – Hyperhomodesmotic equations for Model System C (relative free energies in kcal/mol).

<p>C1: $X = O$ C2: $X = NH$ C3: $X = S$</p> <p>C4</p> <p>C5: $X = O$ C6: $X = NH$ C7: $X = S$</p> <p>C8</p>	<p>C9: $X = O$ C10: $X = NH$ C11: $X = S$</p> <p>C12</p> <p>C13: $X = O$ C14: $X = NH$ C15: $X = S$</p> <p>C16</p>	(5)												
	<table border="1"> <thead> <tr> <th></th> <th>$X = O$</th> <th>$X = NH$</th> <th>$X = S$</th> </tr> </thead> <tbody> <tr> <td>Equation 5</td> <td>+10.7</td> <td>+15.7</td> <td>+10.3</td> </tr> <tr> <td>Equation 6</td> <td>+7.5</td> <td>+16.9</td> <td>+6.4</td> </tr> </tbody> </table>		$X = O$	$X = NH$	$X = S$	Equation 5	+10.7	+15.7	+10.3	Equation 6	+7.5	+16.9	+6.4	
	$X = O$	$X = NH$	$X = S$											
Equation 5	+10.7	+15.7	+10.3											
Equation 6	+7.5	+16.9	+6.4											

Population analysis shows that for trienamine **C12** ($X = CH_2$) the vinylogy principle is obeyed, i.e. the highest orbital coefficient in the HOMO is at C_α followed by C_γ and finally C_ϵ . When $X =$ heteroatom, carbon C_γ exhibits the highest orbital coefficient in the HOMO. Similarly to Model System B, there appears to be a synergistic effect between the N_{cat} and the heteroatom of the substrate ring which increases the electron density at carbon C_γ (Table 2.7 and Figure 2.3). It is also observed that C_α and C_ϵ have similar values in their orbital coefficients which could indicate some cross conjugation between the heteroatom and C_{ipso} .

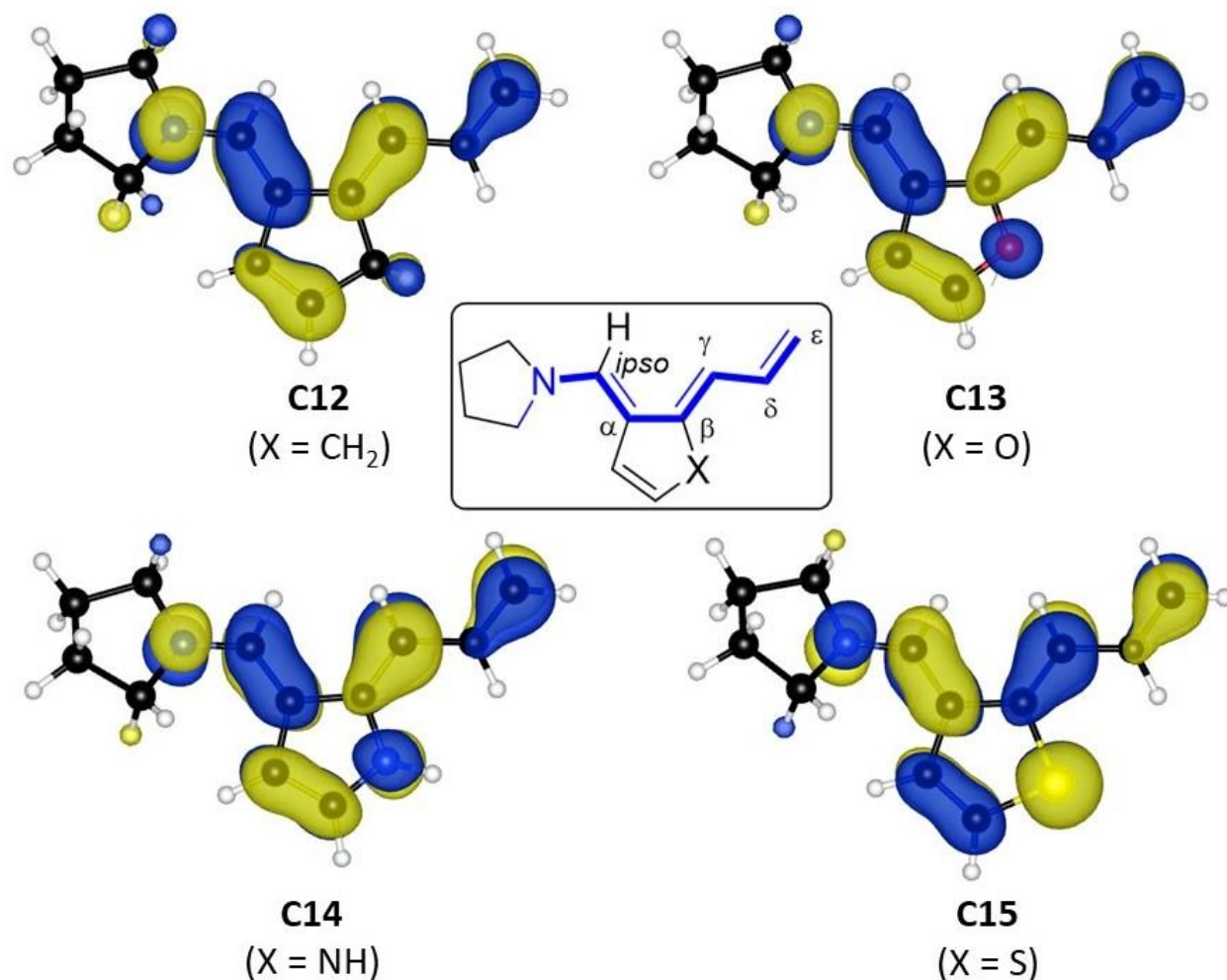


Figure 2. 3 – HOMO of trienamines **C12-15** for Model System C (isovalue 0.035).

Table 2. 7 – Orbital coefficients for the HOMO of Model System C.

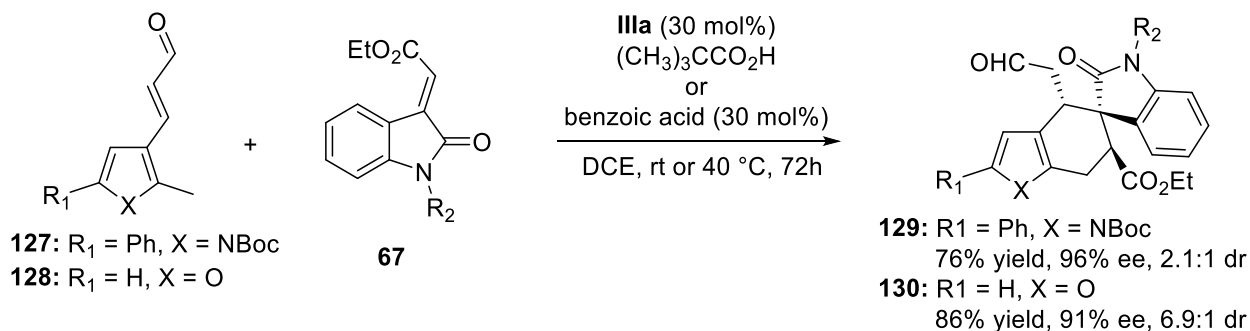
Carbon	C12 (X = CH ₂)	C13 (X = O)	C14 (X = NH)	C15 (X = S)
<i>ipso</i>	13.2	11.2	10.7	10.3
α	19.0	12.6	10.2	11.4
β	4.7	3.7	3.0	3.4
γ	14.4	20.3	22.6	17.9
δ	1.3	1.6	1.2	1.1
ϵ	7.5	10.7	11.3	8.7

In the work published by Chen and co-workers (Scheme 2.2)¹⁸⁷, the authors observed functionalization at the epsilon position which can be explained by the choice of catalyst used. The authors

used a bifunctional H-bond aminocatalyst which directed the electrophile to the most remote position, overcoming the inherent nucleophilicity of the gamma carbon.

Model System D

Next, we explored Model System D where an α,β -unsaturated aldehyde is at the 3-position and a methyl substituent on 2-position. In Chapter III of Part I of this Thesis we already saw that the indole-based version of this system has been reported by Melchiorre and co-workers to undergo a Diels-Alder reaction via formation of an *ortho*-quinodimethane trienamine intermediate (Schemes 1.28 and 1.29).^{157,158} However, in the same paper, the authors also explored the reactivity of these systems towards Diels-Alder reaction using pyrrole **127** or furan **128** with 3-olefinic oxindoles **67** as the dienophile, catalyzed by **IIIa** (Scheme 2.3).¹⁵⁷

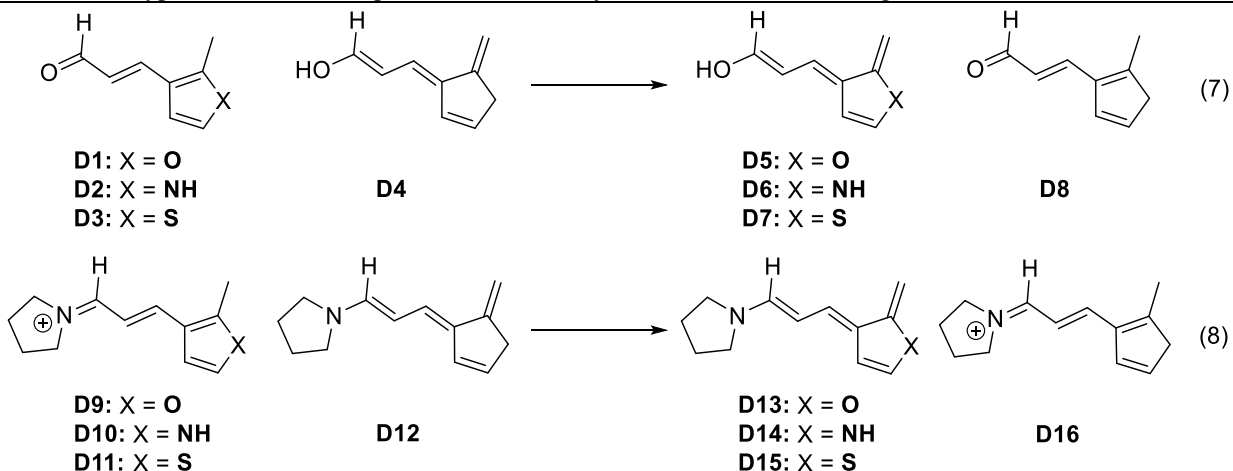


Scheme 2. 3 – Diels-Alder reaction between 3-olefinic oxindoles **67** and pyrrole **127** or furan **128**, reported by Melchiorre and co-workers.

As with the previous model systems, hyperhomodesmotic equations (Table 2.8) suggest that the conversion of aldehydes **D1-3** and iminium ions **D9-11** to the corresponding trienes is an unfavourable process. However, in this system, it appears that the formation of the iminium ions does not have a major influence in the energy penalty for loss of aromaticity. According to Table 2.8, the iminium ions **D9** and **D11** (X = O and S, respectively) are only favoured to undergo dearomatization by 1.3 and 1.8 kcal/mol compared to their respective parent aldehydes **D1** and **D3**. On the other hand, the loss of aromaticity in

iminium ion **D10** ($X = \text{NH}$) is 3.9 kcal/mol higher than that for the dearomatization of aldehyde **D2**. It appears that the introduction of an alkene moiety between the aldehyde group and the heteroaromatic ring weakens the inductive effects of the iminium ion which were most likely responsible for the general favourability of dearomatization observed in the previous models.

Table 2. 8 – Hyperhomodesmotic equations for Model System D (relative free energies in kcal/mol).



	X = O	X = NH	X = S
Equation 7	+11.1	+16.9	+11.3
Equation 8	+9.8	+20.8	+9.5

Population analysis of the trienamine shows that for this model, C_ϵ carries the highest coefficient of the HOMO in trienamines **D13-15** while **D12** ($X = \text{CH}_2$) follows the vinylogy principle (Table 2.9). This observation is similar to that of Model System A and is due to the synergistic effect between the aminocatalyst electron pair and the heteroatom in the aromatic ring that help increase the electron density at the terminal position of the trienamine system (Figure 2.4).

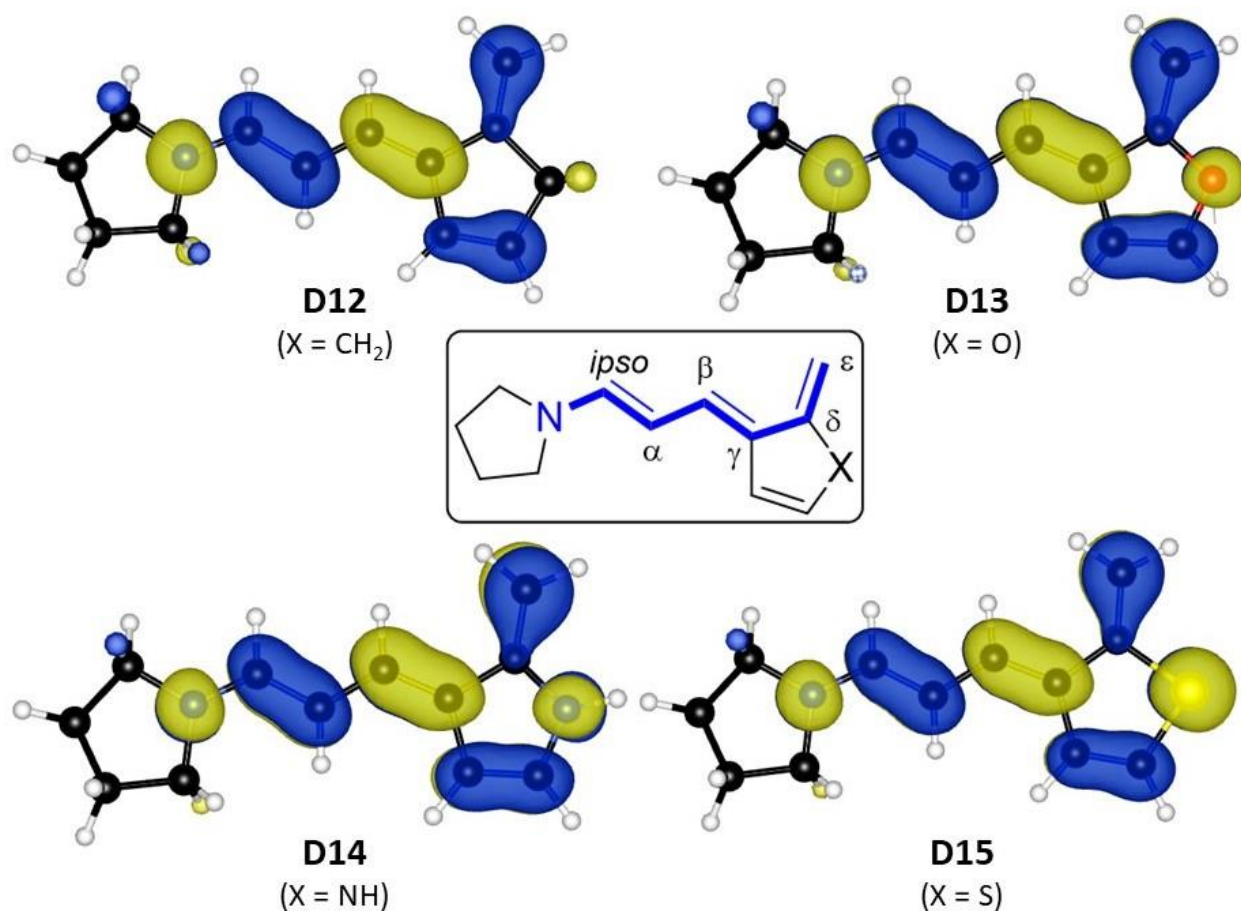


Figure 2. 4 – HOMO of trienamines **D12-15** for Model System D (isovalue 0.035).

Table 2. 9 – Orbital coefficients for the HOMO of Model System D.

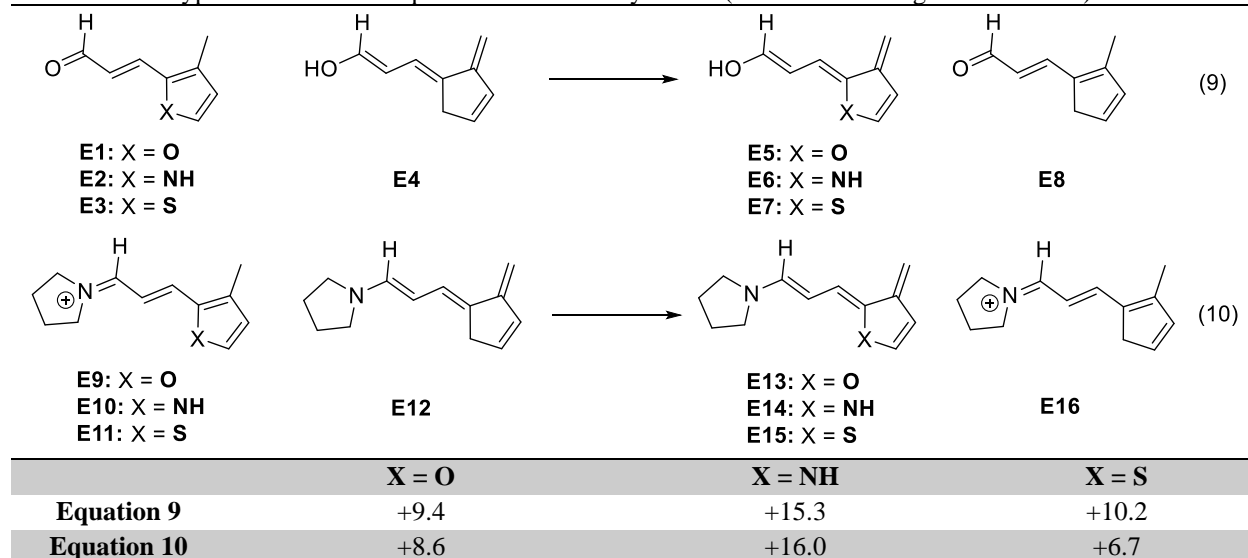
Carbon	D12 (X = CH ₂)	D13 (X = O)	D14 (X = NH)	D15 (X = S)
<i>Ips</i> o	10.7	8.6	9.1	8.0
α	16.7	10.2	12.9	10.8
β	11.0	12.0	11.2	10.3
γ	17.5	11.5	13.9	12.5
δ	1.4	1.1	1.2	1.3
ϵ	8.8	17.0	14.8	13.9

Our calculations show that aminocatalysis does not have a major influence on the dearomatization of this type of systems. Nonetheless, Melchiorre's work (*vide supra*) show that they can still be exploited for Diels-Alder reactions and the regioselectivity observed in his work supports the orbital coefficients calculated in our work.

Model system E

Finally, we explored Model System E where an α,β -unsaturated aldehyde is at the 2-position and a methyl substituent on 3-position. This system has not been explored in any asymmetric synthetic approach but, due to its similarities with the previous Model, we decided it would be interesting to explore in this paper. The hyperhomodesmotic equations are illustrated in Table 2.10 and, similarly to Model System D, the increased distance between the aldehyde group and the heteroaromatic ring system seems to attenuate the effect of the aminocatalyst to decrease the energy cost for dearomatization. Iminium ion **E9** ($X = O$) is just slightly more favourable to undergo dearomatization when compared to its parent aldehyde **E1** (0.8 kcal/mol difference) while, the dearomatization of the iminium ion derived from the pyrrole system **E10** is disfavoured by 0.7 kcal/mol when compared to its parent aldehyde **E2**. Interestingly, when $X = S$ the iminium ion (**E11**) undergoes dearomatization more easily than its parent aldehyde (**E3**) by a difference of 3.5 kcal/mol.

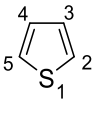
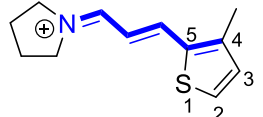
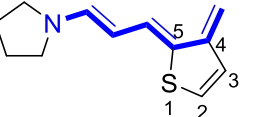
Table 2. 10 – Hyperhomodesmotic equations for Model System E (relative free energies in kcal/mol).



The decrease of in the energy penalty for dearomatization of the sulfur system could arise from geometry changes in the thiophene ring between the iminium ion **E11** and the trienamine **E15**, when

compared to an unsubstituted thiophene.^{188–190} The bond distances between S – C₅ and C₅ – C₄, in **E11**, are elongated when compared to an unsubstituted thiophene while the bond angles remain virtually unchanged. This bond distortion is likely to destabilize the iminium ion intermediate. Upon dearomatization, the new bond angles and distances observed in **E15** attenuate the ring strain of **E11** making the dearomatization more favoured (Table 2.11).

Table 2. 11 – Bond distances (Å) and angles (°) in thiophene, iminium ion **E11** and trienamine **E15**.

	 Thiophene	 E11	 E15
1,2	1.71	1.71	1.75
1,5	1.71	1.74	1.78
2,3	1.37	1.37	1.34
3,4	1.42	1.41	1.47
4,5	1.37	1.40	1.48
5,1,2	92.2	91.1	90.8
1,2,3	111.5	113.0	114.2
2,3,4	112.5	112.9	114.7
3,4,5	112.5	111.5	109.0
4,5,1	111.5	111.5	110.5

Nonetheless, in all cases considered, the energy penalty to undergo dearomatization seems to be very close for either aldehydes **E1-3** and the respective iminium ions **E9-11** and is low enough to be accessible in reactions performed at room temperature making the trienamines **E13-15** easily accessible.

Population analysis on the HOMO of trienamines **E12-15** shows that C_ε possesses the largest orbital coefficient for all heteroaromatic trienamines (Table 2.12). This can be explained by the conjugation of the lone pairs of the heteroatom donating to the epsilon position. This is also easily visualized by the orbital pictures (Figure 2.5). Predictably, the carbon system follows the vinylogy principle with α-carbon having the largest coefficient. It is also observed that when X = CH₂, there seems to be no contribution of the double bond of the ring into the HOMO, however, when X=O,N,S, the π-system is delocalized in the respective trienamine intermediates (Figure 2.5).

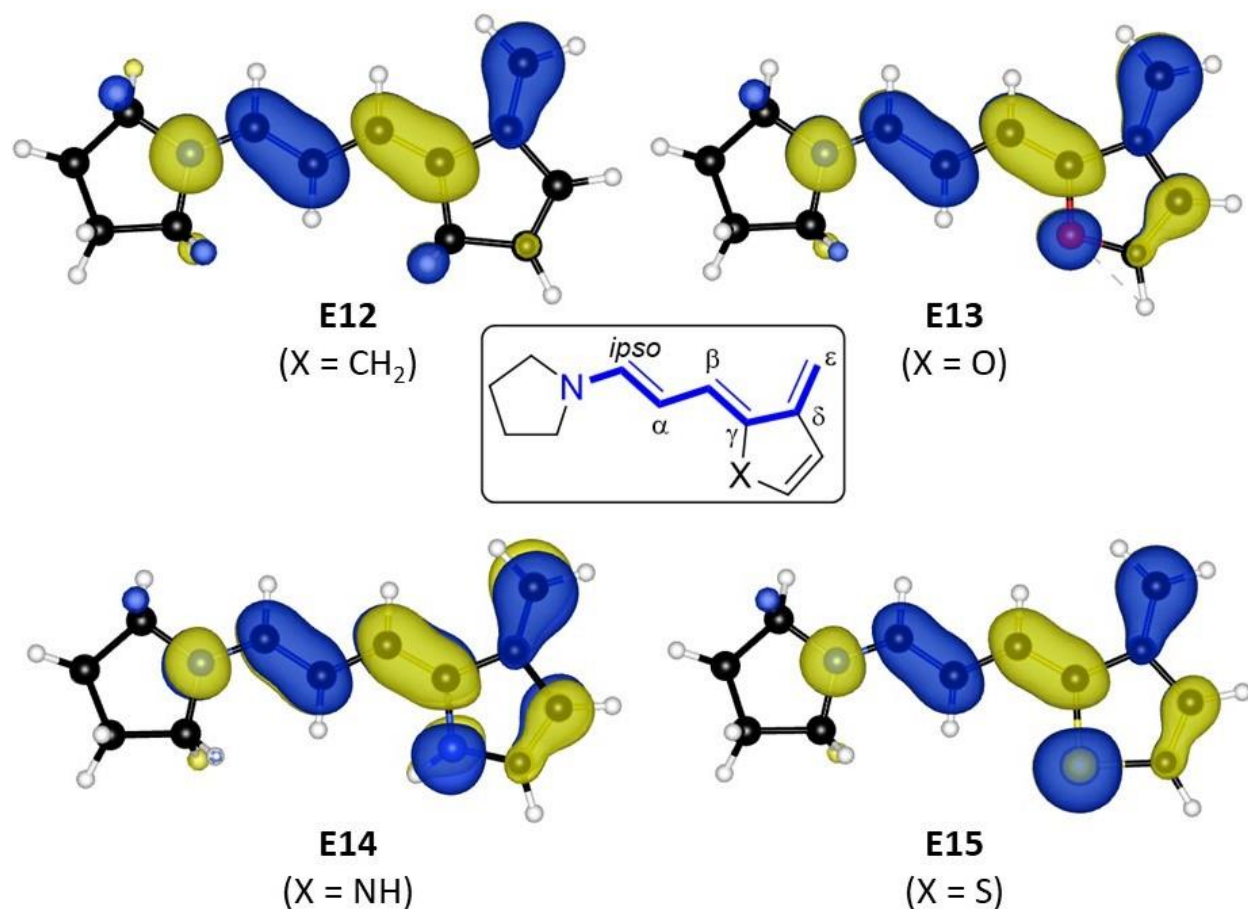


Figure 2. 5 – HOMO of trienamines **E12-15** for Model System E (isovalue 0.035).

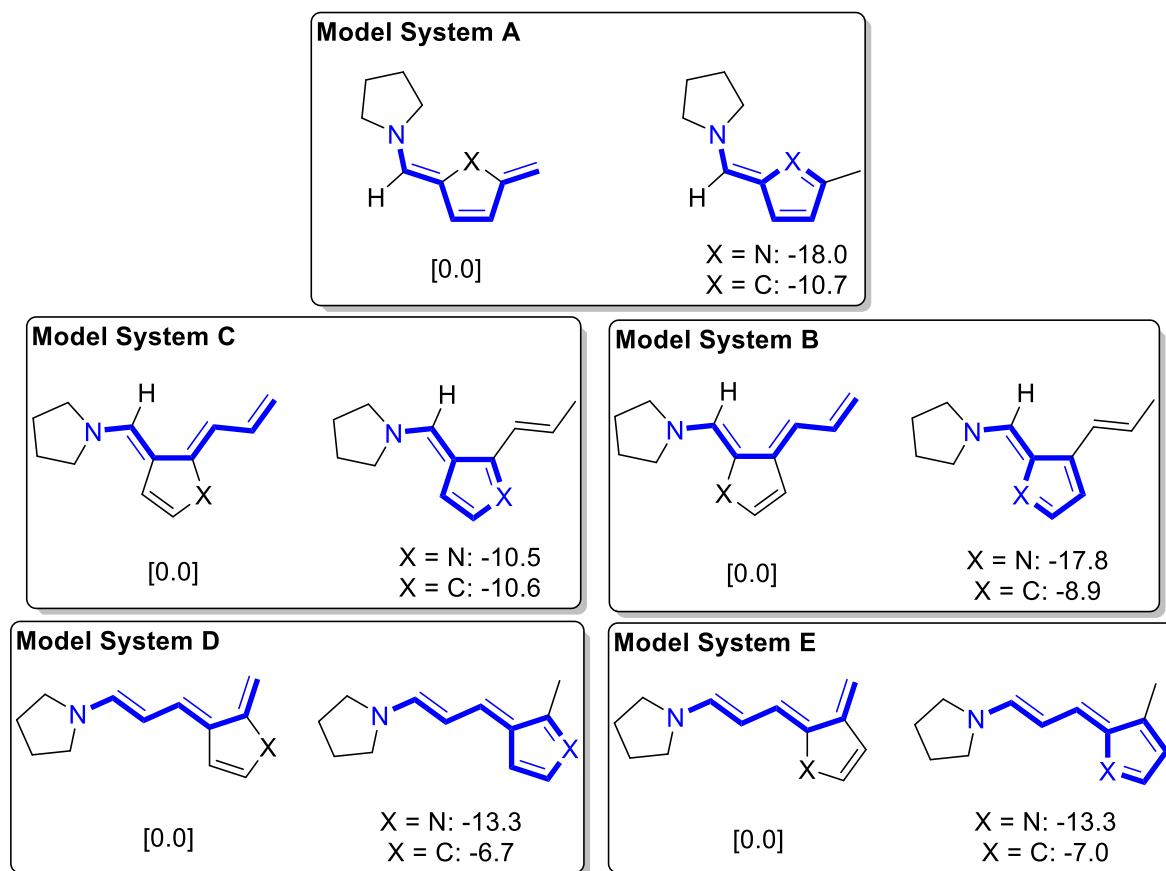
Table 2. 12 – Orbital coefficients for the HOMO of Model System E.

Carbon	E12 (X = CH ₂)	E13 (X = NH)	E14 (X = O)	E15 (X = S)
<i>Ips</i> o	10.6	9.7	9.3	8.2
α	19.2	14.5	11.4	11.6
β	8.9	10.8	13.3	10.6
γ	18.5	13.0	11.1	11.9
δ	2.4	1.8	1.7	1.6
ϵ	12.7	15.5	15.3	13.5

The high orbital coefficient at the ϵ position, allied with the relatively low energy penalties associated with dearomatization, make these systems excellent candidates to be explored in asymmetric aminocatalyzed remote functionalizations.

Fulvene Systems

During the study of the Model Systems illustrated in Figure 2.1, it became evident that in all cases, when $X = \text{CH}_2$ or NH another trienammine intermediate could be formed by deprotonation on the ring system instead of the studied ϵ -deprotonation. This other possibility opens the doors to the formation of (hetero)fulvenes which can then be used as 6 electron systems for higher-order cycloadditions. In fact, some examples have already been reported by Jørgensen and co-workers such as the [10+2]- and [10+4]-cycloadditions using isobenzofulvenes derived from compounds **110** and **116** (Schemes 1.38 to 1.40 of Chapter III of Part I of this Dissertation) and the hetero-[6+4]- and [6+2]-cycloadditions using compounds **118** as the heterofulvene precursor (Scheme 1.41 of Chapter III of Part I of this Dissertation).



Scheme 2.4 – Energy differences between trienammine and possible fulvene systems for Model Systems A-E (relative free energies in kcal/mol)

Consequently, we decided to explore the energy differences between the trienamines depicted in the previous models to the possible fulvenes (Scheme 2.4). It is clear from Scheme 2.4 that, in all Model Systems, the fulvenes are thermodynamically preferred over the trienamines previously explored. This feature expands the scope of these substrates as possible polyenes for higher-order cycloadditions as well as non-classical modes of activation. In Chapter II we will be exploring an analogue of the fulvene of Model System C as an hetero-cross-trienamine for aza-Diels-Alder reactions.

In conclusion, in this Chapter we investigated the influences of an aminocatalyst in the dearomatization of several heteroaromatic systems in order to form a trienamine reactive intermediate. Our calculations suggest that all Models are good candidates for further synthetic studies namely when Oxygen is used as the heteroatom, as this allows for a smaller energy penalty on the dearomatization step. Orbital analysis seems to indicate that the closer the heteroatom is to the epsilon position of the trienamine the more likely it is for the carbon to possess a higher electron density and, therefore allow for remote functionalizations. Experimental work cited in this Chapter as well as in Chapter III of Part I helps to support our findings for Model Systems A, C and D. Model Systems B and E, to the best of our knowledge, have yet to be used in asymmetric aminocatalysis and, hopefully this paper can help guide chemists in the development of their chemistry. Furthermore, it has been illustrated that, when cyclopentadienes or pyrroles are used, it is thermodynamically possible to obtain electron-rich (hetero)fulvene systems that can be exploited in higher-order cycloadditions.

Chapter II - Organocatalyzed Asymmetric Synthesis of Dihydropyrido[1,2-a]indoles

Chiral pyridoindoles derived from indoles have unique tricyclic structures, which have received much attention due to their interesting and potent biological activities.^{191–193} For example, cryptaustoline,¹⁹⁴ cladoniamides,^{195,196} goniomitine,^{197–199} and vincamine²⁰⁰ alkaloids are known to possess a broad range of biological properties (Figure 2.6). Due to the remarkable biological activities of these types of compounds we decided to develop an asymmetric protocol for the synthesis of dihydropyrido[1,2-a]indole scaffolds. For this purpose, we devised two different strategies, one involving an intramolecular Michael addition of substrate **131**, via formation of an *ortho*-quinonedimethide type dienamine (**132**), catalyzed by a chiral secondary amine, to give the desired product **133** (Scheme 2.5, eq. 1), and another approach which involved an asymmetric aza-Diels-Alder reaction between an hetero-cross-trienamine **135**, derived from substrate **134**, and a chiral secondary amine catalyst and an electron deficient dienophile (Scheme 2.5, eq. 2).

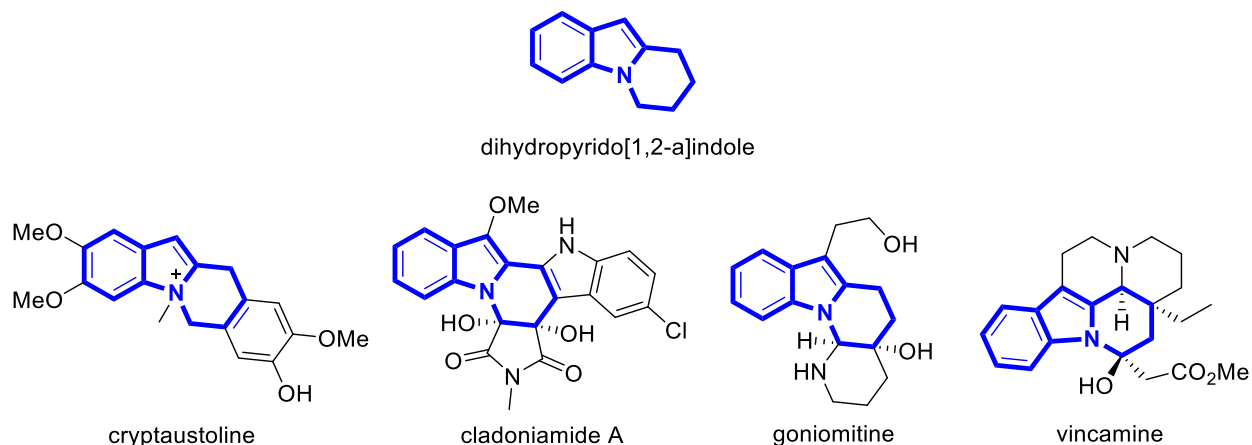
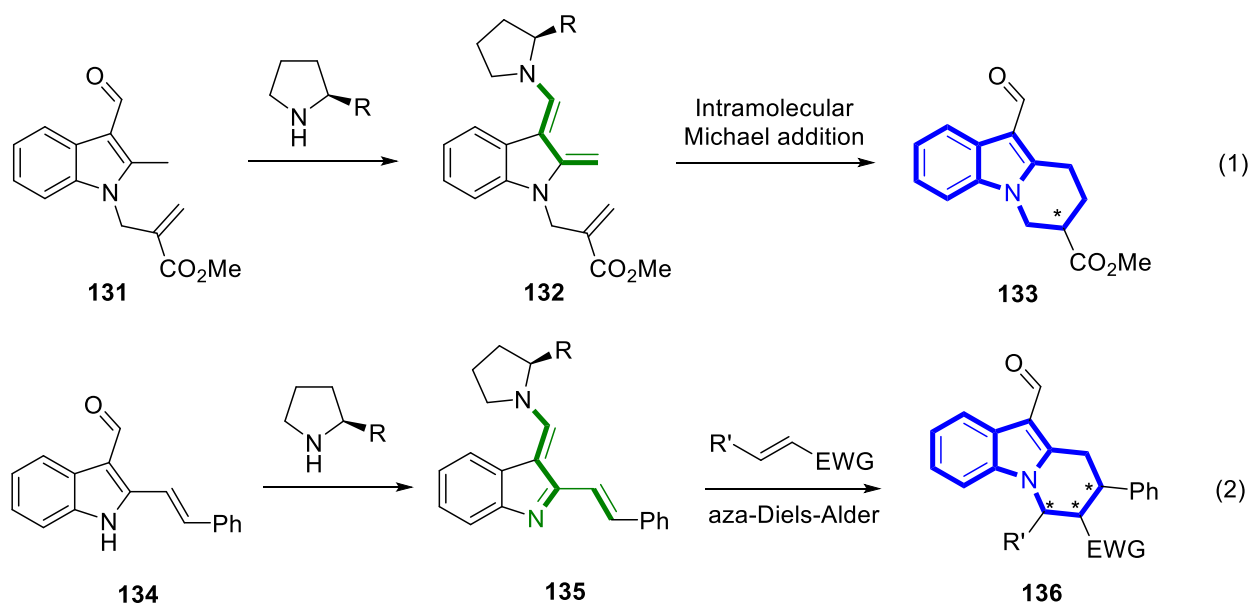


Figure 2. 6 – Selection of biologically active alkaloids with a dihydropyrido[1,2-a]indole core structure.



Scheme 2. 5 – Proposed synthetic paths for the synthesis of chiral tetrahydroisoquinolines **133** and **136**; (1) via diamine catalyzed intramolecular Michael addition and (2) via hetero-cross-trienamine catalyzed aza-Diels-Alder.

Intramolecular Michael Addition

The starting material **131**, required for the intramolecular Michael addition reaction, was conveniently synthesized starting from commercially available 2-methylindole through a Vilsmeier-Haack formylation followed by *N*-alkylation with methyl 3-bromo-2-(bromomethyl)propionate, in 86% yield over two steps (see Part IV for detailed experimental procedures).

With the desired reagent **131** in hand, we subjected it to a few different reaction conditions to get a feel of **131**'s reactivity (Table 2.13). The initial attempts showed some promising results. Pyrrolidine was used as a surrogate of the more expensive Hayashi's and Jørgensen's catalysts **IIIa** and **IIIb**, respectively, and after 4 days, it showed some small conversion ($\approx 8\%$) to a new product, by comparing the integration of the aldehyde proton signals in ^1H NMR (Table 2.13, entry 1; Figure 2.7). Primary amine **XII** was also tested to overcome possible problems relating to steric hindrance that could prevent condensation of a secondary amine catalyst to the α -substituted aldehyde and indeed, around 29% conversion to the imine intermediary was observed by crude ^1H NMR (Table 2.13, entry 2; Figure 2.8). Finally, L-proline **I** was

also tested but no conversion was observed. Isopropanol was used as a co-solvent to help in the solubility of **I** (Table 2.13, entry 3).

Table 2.13 – Initial screening for the intramolecular Michael addition of **133**.

Catalyst (20 mol%)
Additive (20 mol%)
Solvent, T, time

Catalysts screened:

I

XII

pyrrolidine

Entry	Catalyst	Additive	Solvent	T	time	Conversion (%) ^a
1	Pyrrolidine	BA	CDCl ₃	rt	4 days	8
2	XII	BA	CDCl ₃	rt	24h	29
3	I	BA	CDCl ₃ /iPrOH (9/1)	rt	24h	—

All reactions performed on a 0.2 mmol scale, in respect to **133** in solvent (0.5 mL); (a) determined by ¹H NMR

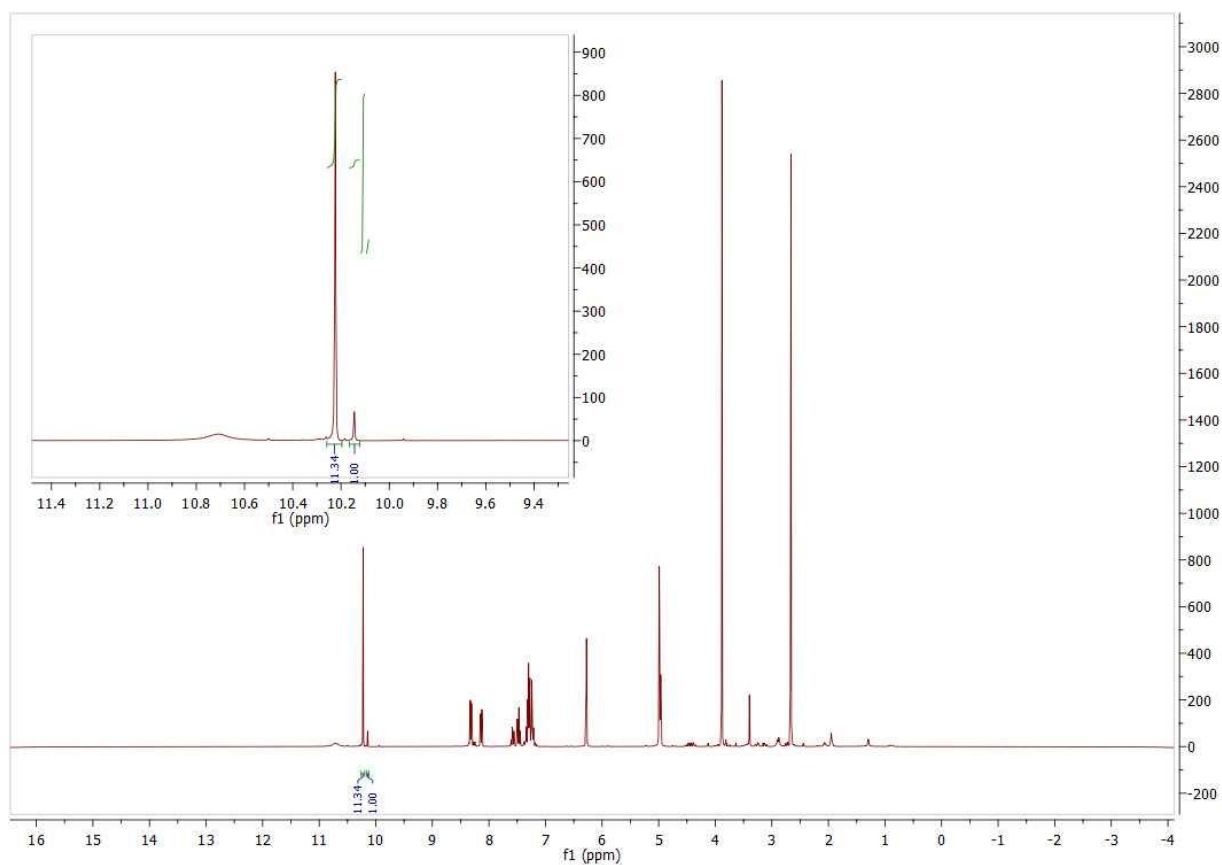


Figure 2.7 – ¹H NMR of reaction from Table 2.13, entry 1 (300 MHz, CDCl₃).

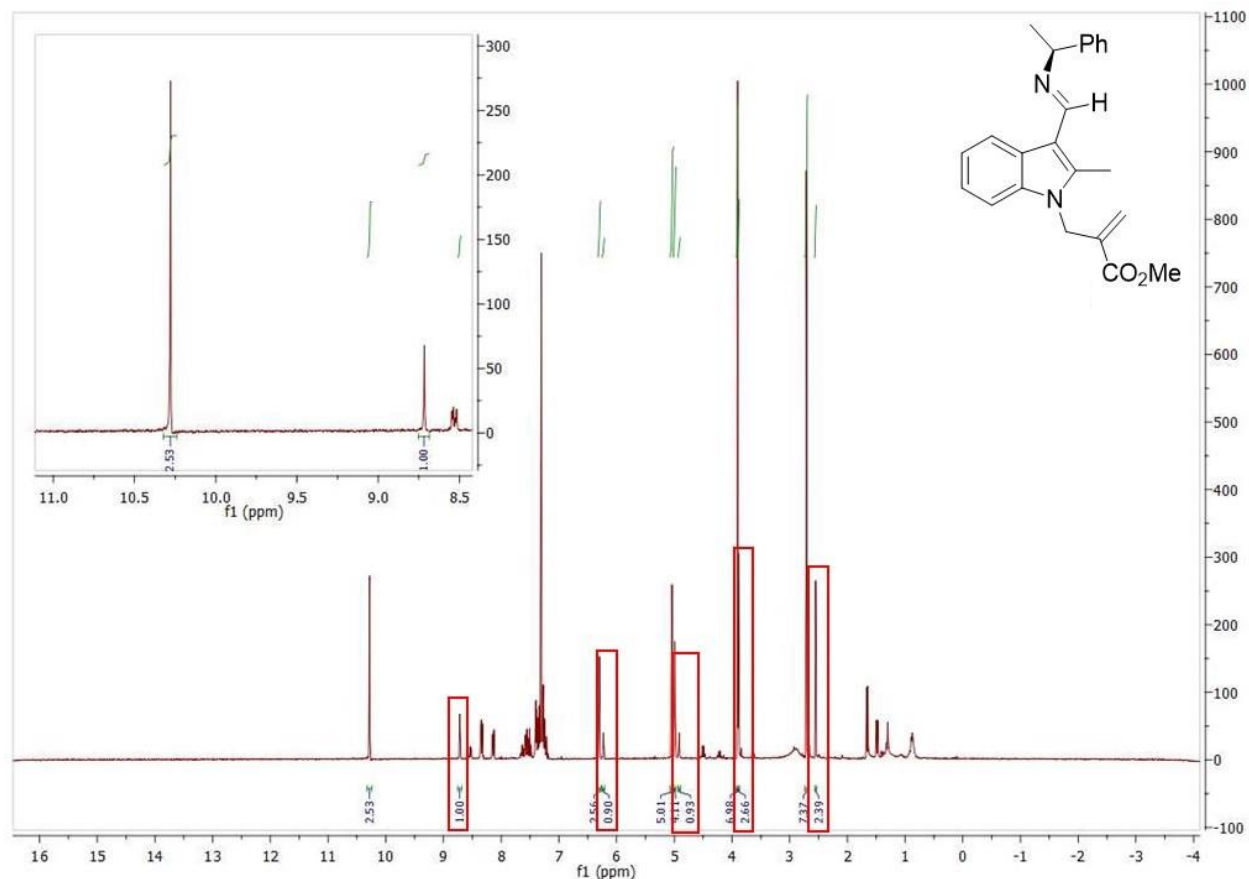


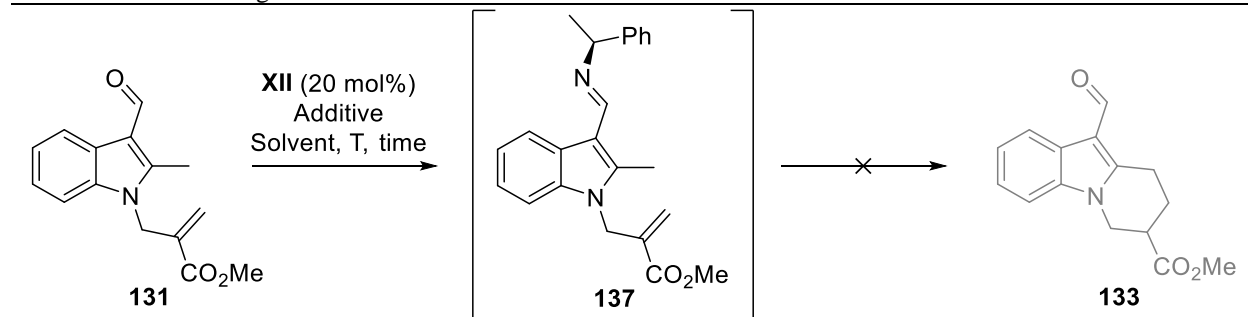
Figure 2. 8 – ^1H NMR of reaction from Table 2.13, entry 2. Signals from imine **137** highlighted in red (300 MHz, CDCl_3).

With these preliminary results, we decided to focus on catalyst **XII** and try to explore reaction conditions that could lead to the formation of the desired dienamine **132**, by heating the reaction as well as changing the acid additive (Table 2.14). Unfortunately, the only conversion observed was to the corresponding imine **137** which, regardless of the reaction conditions employed, failed to tautomerize to the corresponding dienamine **132**.

We then decided to test the commercially available catalyst **Va**·**3HCl** (Table 2.15). We hoped that since catalyst **Va**·**3HCl** already possessed 3.0 equiv. of a strong acid, it could promote the desired tautomerization of imine to dienamine. Unfortunately, it did not afford the desired Michael adduct product **133**. Initial testing was performed in CDCl_3 but, due to poor solubility of the catalyst salt in this solvent, no conversion was observed by ^1H NMR, even after heating to 40°C (Table 2.15, entries 1 and 2) and the same

was observed when toluene was used as a solvent (Table 2.15, entry 3). The more polar solvent MeOH was also tested as it could help improving catalyst solubility as well as act as a proton shuttle which could facilitate the formation of the reactive dienamine and concomitant Michael addition step. Unfortunately, solubility also proved to be an issue (Table 2.15, entry 4).

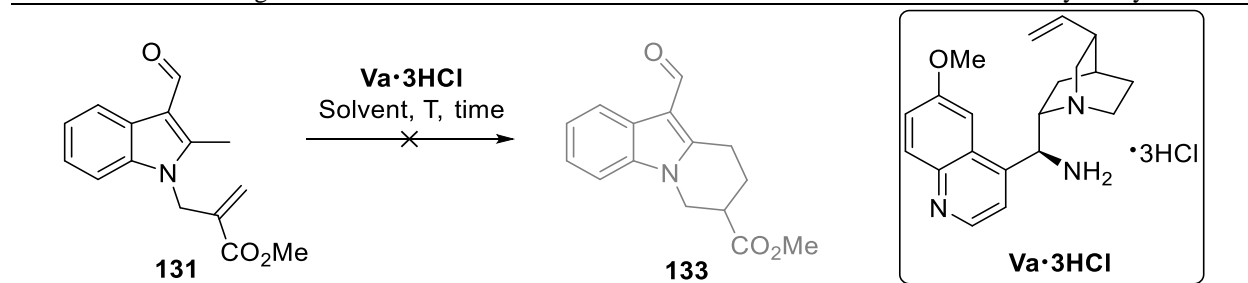
Table 2. 14 – Screening of reaction conditions for the intramolecular Michael addition of **131**.



Entry	Additive (mol%)	Solvent	T (°C)	Time (h)	Conversion (%) ^a
1	BA (20 mol%)	Toluene	60	48	22 ^b
2	<i>p</i> TsOH·H ₂ O (40 mol%)	MeOH	60	24	— ^c
3	TFA (40 mol%)	MeOH	60	72	15 ^b
4	<i>p</i> TsOH·H ₂ O (40 mol%)	Toluene	120	24	— ^c

All reactions performed on a 0.2 mmol scale, in respect to **131**, in solvent (0.4 M); (a) determine by ¹H NMR; (b) conversion to imine **137** and; (c) followed by TLC analysis.

Table 2. 15 – Screening of conditions for the intramolecular Michael addition reaction of **131** catalyzed by **Va·3HCl**.



Entry	Solvent	T	Time (h)	Conversion (%) ^a
1	CDCl ₃	rt	24	—
2	CDCl ₃	40 °C	24	—
3	Toluene	rt	48	—
4	MeOH	rt	48	—

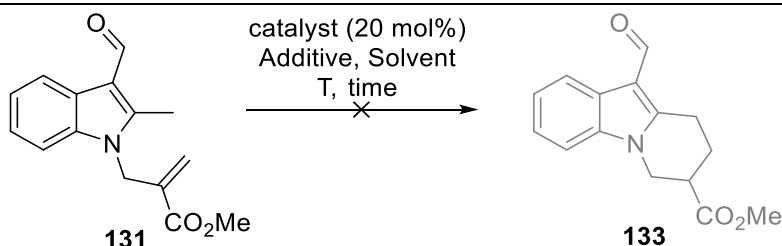
All reactions performed in a 0.2 mmol scale in respect to **131**, in solvent (0.6 mL); (a) reactions followed by ¹H NMR, with no evidence of conversion to either product or imine **137**.

Due to the inability to tautomerize imine **137** to the reactive dienamine **132**, we decided to go back to the secondary amine catalysts of which pyrrolidine had given some conversion to a new product. Therefore, we decided to test L-proline **I** under different solvent and additive conditions as well as try Jørgensen's catalyst **IIIb**. We also tested pyrrolidine with Lewis acid additives to see if further activation of the ester group of **131** could facilitate the intramolecular Michael addition and thus improving the conversions initially observed with this catalyst (Table 2.16).

Catalyst **IIIb** failed to give any detectable conversion by ^1H NMR (Table 2.16, entry 1) even when heated to 90 °C in toluene (Table 2.16, entry 2). Similarly, **I** also failed to yield any detectable product regardless of heating and the use of strong Brønsted acid additives (Table 2.16, entries 3 to 5). From the preliminary results from Table 2.13, we decided to explore pyrrolidine again, and use Lewis acids as additives to provide further activation of the ester group which, we theorized, could be responsible for yielding a weak Michael acceptor. Benzoic acid was also used in these experiments to ensure that all free aminocatalyst would be protonated and therefore preventing the formation of Lewis acid/base pair between pyrrolidine and the metals.²⁰¹ Of the Lewis acids tested (Table 2.16, entries 6 to 11, 17 and 18) the one that seemed to produce the most promising results was BiCl_3 (Table 2.16, entry 8) giving around 9% conversion to a new product after 48h at rt (determined by integration of the aldehyde peaks in the ^1H NMR). Increasing the temperature to 50 °C gave 14% conversion after the same amount of time (Table 2.16, entry 11). Using a higher loading of BA (100 mol%) did not improve the conversion (6% after 24h at 50 °C; Table 2.16, entry 12). Catalyst **IIIb** was also tested under these new cooperative conditions (Table 2.16, entry 13) but no new product was detected by ^1H NMR.

To discard the possibility of a Brønsted/Lewis acid catalyzed transformation, a test reaction was performed in the absence of pyrrolidine and no product was observed by ^1H NMR indicating that this aminocatalyst was crucial to the observed product (Table 2.16, entry 14).

Table 2. 16 – Screening of reaction conditions for the intramolecular Michael addition of **131** using secondary amine organocatalysts.

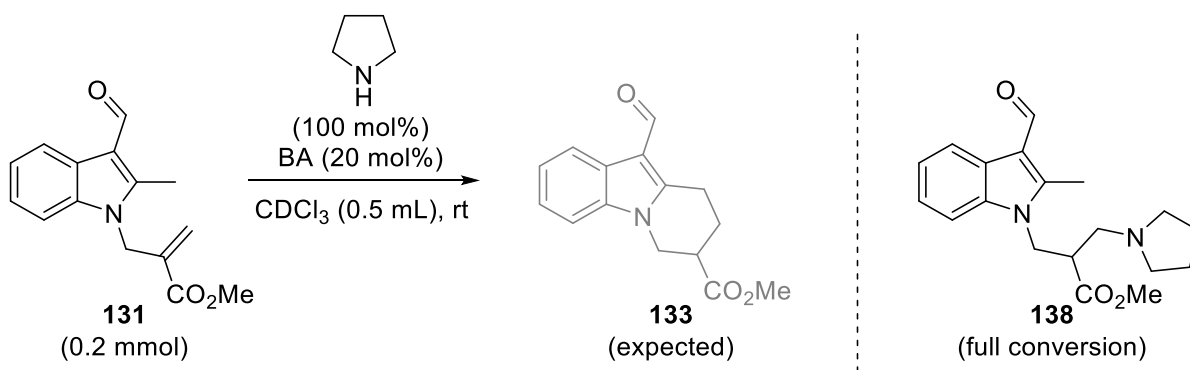


Entry	Catalyst	Additive (mol%)	Solvent	T (°C)	Time (h)	Conversion (%) ^a
1	IIIb	BA (20 mol%)	CDCl ₃	rt	72	<5
2	IIIb	BA (20 mol%)	Toluene	90	96	<5
3	I	BA (20 mol%)	Toluene/iPrOH (9/1)	60	48	<5
4	I	<i>p</i> TsOH·H ₂ O (40 mol%)	MeOH	60	96	<5
5	I	TFA (40 mol%)	MeOH	60	24	<5
6	pyrrolidine	BA (20 mol%) Zn(OTf) ₂ (10 mol%)	CH ₂ Cl ₂	rt	48	<5
7	pyrrolidine	BA (20 mol%) FeCl ₃ (10 mol%)	CH ₂ Cl ₂	rt	48	— ^b
8	pyrrolidine	BA (20 mol%) BiCl ₃ (10 mol%)	CH ₂ Cl ₂	rt	48	9
9	pyrrolidine	BA (20 mol%) MnCl ₄ ·4H ₂ O (10 mol%)	CH ₂ Cl ₂	rt	48	— ^b
10	pyrrolidine	BA (20 mol%) Yb(OTf) ₃ (10 mol%)	CH ₂ Cl ₂	rt	48	— ^b
11	pyrrolidine	BA (20 mol%) BiCl ₃ (10 mol%)	CDCl ₃	50	48	14
12	pyrrolidine	BA (100 mol%) BiCl ₃ (10 mol%)	CDCl ₃	50	24	6
13	IIIb	BA (20 mol%) BiCl ₃ (10 mol%)	CDCl ₃	50	24	<5
14	—	BA (20 mol%) BiCl ₃ (10 mol%)	CDCl ₃	50	24	<5
15	pyrrolidine	BiCl ₃ (10 mol%)	THF	75	48	10
16	pyrrolidine	BA (20 mol%) BiCl ₃ (10 mol%)	THF	75	48	10
17	pyrrolidine	BA (20 mol%) CsF (10 mol%)	Toluene	120	24	25
18	pyrrolidine	BA (20 mol%) CsF (10 mol%)	Toluene	120	72	17
19	pyrrolidine	BA (20 mol%) BiCl ₃ (50 mol%)	Toluene	120	24	25
20	pyrrolidine	BA (20 mol%) BiCl ₃ (10 mol%)	Toluene	120	24	9
21	pyrrolidine	BA (20 mol%)	Toluene	120	24	16

All reactions performed on a 0.2 mmol scale in respect to **133** in solvent (0.5 mL); (a) determined by ¹H NMR; (b) followed by TLC.

To see if BA was having any influence of reactivity, a test reaction was performed in its absence (Table 2.16, entry 15) and a 10% conversion was observed after 48h at 75 °C in THF. Standard conditions (20 mol% of pyrrolidine and BA, and 10 mol% BiCl₃) under higher temperatures in THF did not provide any improvement (Table 2.16, entry 16). Changing the Lewis acid to the stronger CsF and performing the reaction in refluxing toluene did not improve conversions and, as a matter of fact, these conditions were detrimental to the reaction as the starting material **131** was decomposing over time (Table 2.16, entries 17 and 18). Increased loading of BiCl₃ to 50 mol% did not provide any substantial improvement on conversions (Table 2.16, entry 19) neither did just heating of the reaction to reflux conditions in toluene (Table 2.16, entry 20). Finally, another test reaction was done to try and assess if the Lewis acid played any role, and to our surprise, 16% conversion was observed after 24h under refluxing toluene (Table 2.16 entry 21).

With these results, we decided to perform a test reaction using 100 mol% pyrrolidine (Scheme 2.6) and try to see if the dienamine **132** was being formed and what would happen to the conversion as until now, conversions were in the range of the pyrrolidine loading (20 mol%) or in the range of the free pyrrolidine that did not have any Lewis acid to react with.



Scheme 2.6 – Test reaction for the intramolecular Michael addition, using 100 mol% of pyrrolidine.

With the test reaction depicted in Scheme 2.6 we realized that instead of the observed Michael adduct **133** we were obtaining the hydroamination product **138** as can be seen by its ¹H NMR spectra depicted in Figure 2.9. To our frustration, it became evident that the conversions observed in previous trials were not only derived from product **138** but were also consistent with the amount of free pyrrolidine present

in solution. Therefore, the Lewis acids used so far were hindering the formation of **138** by formation of a Lewis acid/base pair with pyrrolidine leaving only around 10 mol% of free pyrrolidine. The benzoic acid seemed to not have any influence whatsoever in the reaction and, if anything, even facilitated the proton transfer in the zwitterionic intermediary that leads to **138**.

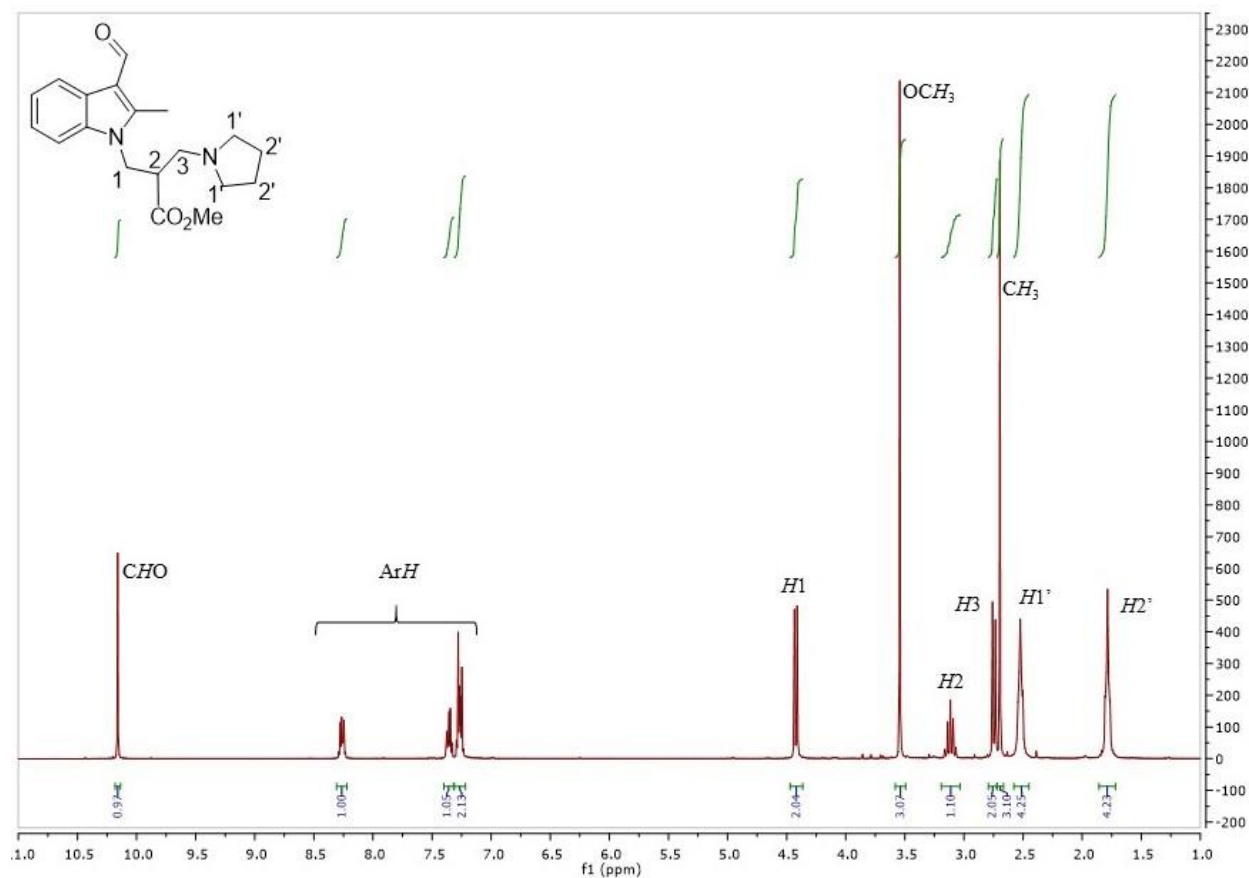
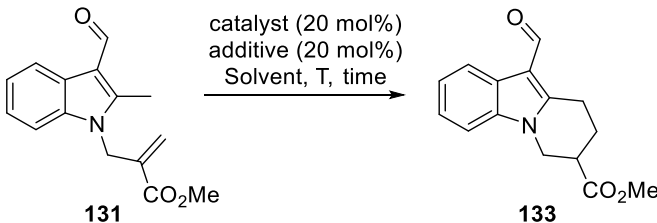


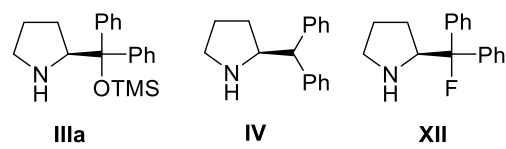
Figure 2. 9 – ¹H NMR spectrum of hydroamination product, **138** (300 MHz in CDCl₃).

Clearly, pyrrolidine could not be used as surrogate for other secondary aminocatalysts nor as an achiral catalyst in itself. Nonetheless, the hydroamination product was never observed when **I** or **IIIb** were used as catalysts, and it has been shown that silyl protected prolinols are capable of activating substrates similar to **131** in a fashion similar to that envisioned for this reaction.¹⁶⁰ Therefore, we decided to synthesize a few other secondary aminocatalysts (see Chapter IV for more information) and test them in our dienamine mediated intramolecular Michael addition (Table 2.17).

Table 2. 17 – Scope of secondary aminocatalysts for the intramolecular Michael addition of **131**.



Catalysts tested:



Entry	Catalyst	Solvent	Additive	T (°C)	Time (h)
1	IIIa	CDCl ₃	—	rt	48
2	IIIa	CDCl ₃	BA	rt	48
3	IIIa	CDCl ₃	NEt ₃	rt	48
4	IIIa	CDCl ₃	—	40	24
5	IIIa	CDCl ₃	BA	40	24
6	IIIa	CDCl ₃	NEt ₃	40	24
7	IIIa	THF	—	rt	48
8	IIIa	THF	BA	rt	48
9	IIIa	THF	NEt ₃	rt	48
10	IIIa	THF	—	75	24
11	IIIa	THF	BA	75	24
12	IIIa	THF	NEt ₃	75	24
13	IIIa	Toluene	—	90	48
14	IIIa	Toluene	BA	90	48
15	IIIa	Toluene	NEt ₃	90	48
16	IIIa	CH ₃ CN	BA	rt	48
17	IIIa	CH ₃ CN	BA	75	48
18	IV	CDCl ₃	—	40	24
19	IV	CDCl ₃	BA	40	24
20	IV	CDCl ₃	NEt ₃	40	24
21	IV	CH ₃ CN	—	75	24
22	IV	CH ₃ CN	BA	75	24
23	IV	CH ₃ CN	NEt ₃	75	24
24	IV	Toluene	BA	90	24
25	XII	THF	—	rt	48
26	XII	THF	BA	rt	48
27	XII	THF	NEt ₃	rt	48

- Table 2.17 continues next page -

- Table 2.17 continuation -

Entry	Catalyst	Solvent	Additive	T (°C)	Time (h)
28	XII	THF	—	75	24
29	XII	THF	BA	75	24
30	XII	THF	NEt ₃	75	24
31	XII	Toluene	—	90	24
32	XII	Toluene	BA	90	24
33	XII	Toluene	NEt ₃	90	24
34	XII	CH ₃ CN	—	75	24
35	XII	CH ₃ CN	BA	75	24
36	XII	CH ₃ CN	NEt ₃	75	24

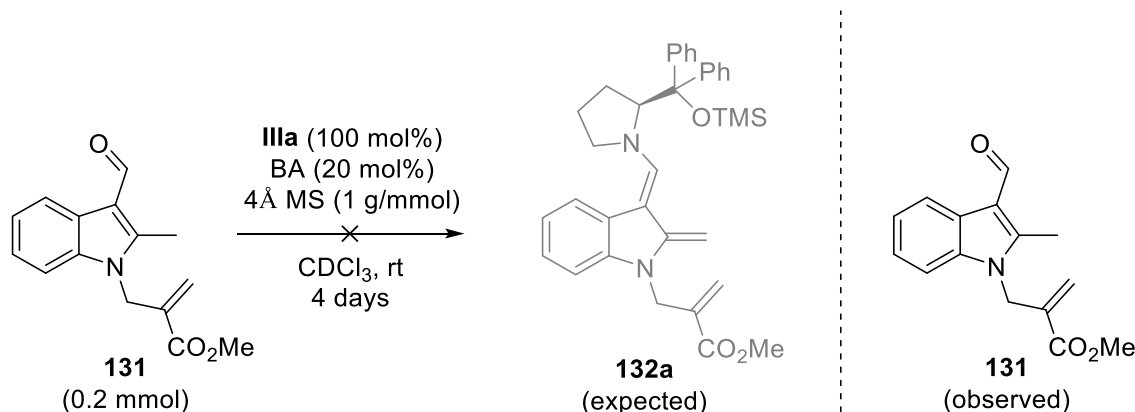
All reactions performed on a 0.2 mmol scale in respect to **131** with 20 mol% catalyst loading and 20 mol% additive loading, in solvent (0.6 mL).

Unfortunately, none of the catalysts and reaction conditions employed afforded the desired dihydropyrido[1,2-a]indole **133**. Benzoic acid (BA) is a commonly used additive in aminocatalysis, as it facilitates the condensation between the catalyst and the substrate as well as its hydrolysis once the reaction is completed, thus speeding up the reaction. Triethylamine was also tested as an additive and, even though it usually hinders the condensation between the catalyst and the substrate, it can, sometimes, aid in the formation of enamine intermediaries by acting as a proton shuttle. Several organic solvents with different polarities and boiling points were also tested allowing us to perform the reaction at different temperatures as well as providing stabilization of charged species that could form in the desired process.

Catalyst **IIIa** was tested because it possesses less steric bulk than the previously tested **IIIb** which did not provide any conversion. We hoped that the biphenyl groups could allow condensation of the catalyst and subsequent dienamine formation. However, it did not afford any product nor any indication of iminium and/or dienamine formation. Likewise, catalyst **IV** was also tested as this catalyst is more nucleophilic than either **IIIa** or **IIIb** and possesses less steric bulk. Therefore, we rationalized it could form the desired dienamine more easily without the hydroamination side reaction taking place. However, as evident from Table 2.17, no product was observed.

Finally, catalyst **XII** was also tested but afforded no conversion either. This catalyst was chosen as it forms a very electron deficient reactive iminium ion, which we thought, it could facilitate the subsequent deprotonation of said iminium ion to the desired dienamine **132**. This step could be hindered when the other catalysts were tested because of the presence of the electron donor indole Nitrogen that decreases the acidity of the Hydrogens of the methyl group at the 2-position of the indole.

One final reaction was performed with this substrate to try and assess why this simple intramolecular Michael addition was not taking place. We decided to use catalyst **IIIa** in a 100 mol% loading in the presence of BA (20 mol%) and 4Å molecular sieves, in CDCl₃, hoping that we could trap either the iminium ion or the transient dienamine **132a** (Scheme 2.7) and observe them by ¹H NMR. However, and to our surprise, no alteration of the ¹H NMR signals of the starting material **131** were observed which hinted at the fact that no condensation between the catalyst and substrate **131** was taking place.



Scheme 2.7 – Test reaction to trap dienamine **132a**.

These results suggest that there might be an issue with the condensation between secondary aminocatalysts and **131**. As demonstrated in the previous Chapter of this Dissertation, the required dearomatization to form the reactive enamine should take place at room temperature (+16.9 kcal/mol for the formation of the trienamine system in Model System C, which is analogous to the required activation for this project). However, even when 100 mol% of catalyst **IIIa** is used, no dienamine is observed by ¹H

NMR and when 100 mol% pyrrolidine is used, the product observed is the hydroamination of the α,β -unsaturated ester meaning that this group is more reactive than the aldehyde moiety. The lack of electrophilicity of the aldehyde could be caused by the presence of the electron-donating Nitrogen atom of the indole ring and, in fact, this type of systems has only been explored using furfural derivatives.

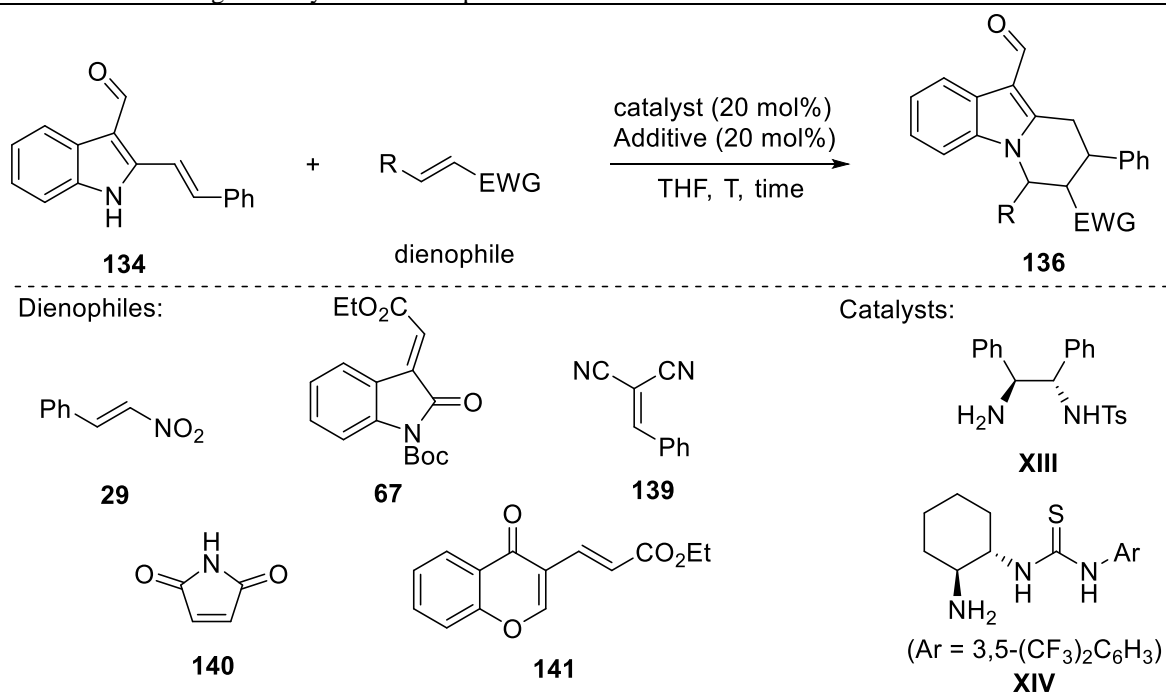
A possible way to circumvent the lack of electrophilicity of the aldehyde would be to extend the conjugation and use a trienamine, analogous to that described in Model System D and used by Melchiorre and co-workers.

Aza-Diels-Alder Reaction

To the other approach to dihydropyrido[1,2-a]indole scaffolds we decided to synthesize substrate **134** which was obtained in 49% yield over four steps, starting from commercially available indole-2-carboxylic acid (see Chapter IV for more details). However, for this substrate we had to optimize both catalyst and reaction conditions as well as find a suitable dienophile which would react in the desired aza-Diels-Alder mechanism we envisioned in Scheme 2.5.

During the synthesis and purification of **134**, it was discovered that this substrate had some solubility issues so, we tested its solubility in a wide range of organic solvents and discovered that THF was a suitable solvent at reasonable working concentrations and, of the solvents that solubilize **134**, was the most favorable at avoiding side reactions between catalysts and solvents as well as allowing for an easy recovery of any product that could form. Thus, with these solubility issues in mind we focused on screening catalysts and dienophiles in THF before we could explore other solvents (Table 2.18).

Initially, we tried to discover a hit-dienophile that would undergo the desired aza-Diels-Alder reaction using Hayashi's catalyst **IIIa** without any additives but, unfortunately, no product **134** was observed by ^1H NMR at either rt or upon heating the reaction to 75 °C (Table 2.18, entries 1 to 10).

Table 2. 18 – Screening of catalysts and dienophiles for the aza-Diels-Alder reaction of **134**.

Entry	Dienophile	Catalyst	Additive	T (°C)	Time (h)	Conversion (%) ^a
1	29	IIIa	—	rt	24	0
2	29	IIIa	—	75	72	0
3	67	IIIa	—	rt	24	0
4	67	IIIa	—	75	72	0
5	139	IIIa	—	rt	24	0
6	139	IIIa	—	75	72	0
7	140	IIIa	—	rt	24	0
8	140	IIIa	—	75	72	0
9	141	IIIa	—	rt	24	0
10	141	IIIa	—	75	72	0
11	29	IIIa	BA	75	48	0
12	29	IIIa	NEt ₃	75	48	0
13	29	IIIa	DBU	75	48	0
14	29	IIIa	DABCO	75	48	0
15	29	IIIa	Imidazole	75	48	0
16	29	I	BA	75	48	0
17	29	pyrrolidine	BA	75	48	0
18	29	XIII	BA	75	48	0
19	29	XIV	BA	75	48	0

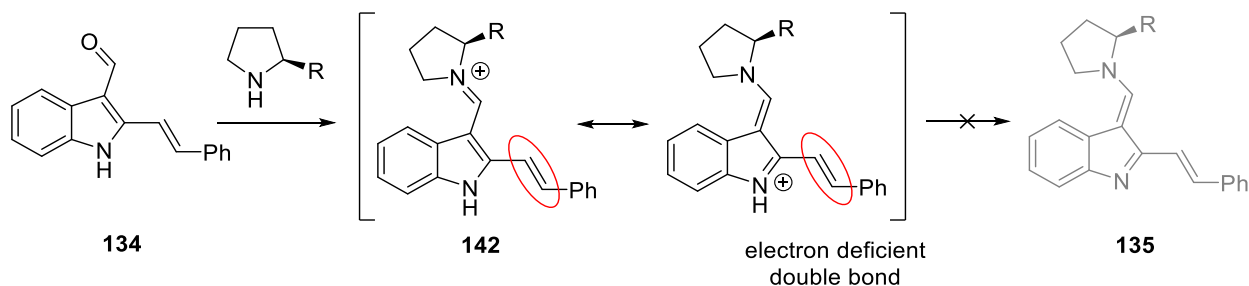
All reactions performed on a 0.5 mmol scale in respect to **134**, in THF (2 mL), with 1.2 equiv. of dienophile; (a) determine by ¹H NMR.

We then decided to screen a few different additives maintaining catalyst **IIIa** and chose nitrostyrene (**29**) as the target dienophile as it has been shown to be a commonly used molecule for this type of reactions.

We started by adding benzoic acid which is widely used as an additive in aminocatalysis for reasons described before but, no reaction took place (Table 2.18, entry 11). At this point we suspected that, perhaps, the iminium ion formed by condensation between **134** and **IIIa** may be too stable, and therefore, not collapsing to the desired reactive hetero-cross-trienamine **135**. Thus, we tested a few organic bases to see if we could facilitate the formation of the enamine **135** but these reactions were also met with disappointing results (Table 2.18, entries 12 to 15).

Finally, maintaining nitrostyrene as the dienophile, we tested some different aminocatalysts. L-proline, **I**, was chosen for its ability to activate **29** via H-bond activation (Table 2.18, entry 16). However, it afforded no product. Pyrrolidine and the primary amine catalysts **XIII** and **XIV** were also tested for their higher nucleophilicity and/or less steric hindrance to condense with substrate **134**, but no product was observed either (Table 2.18, entries 17 to 19).

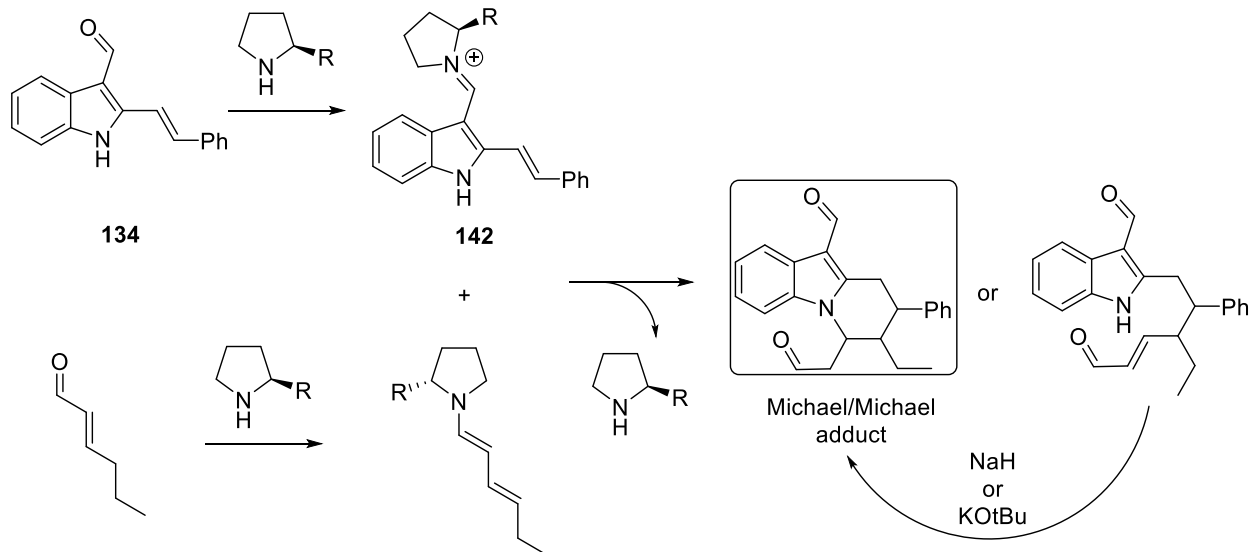
Looking back at the intermediaries formed during this reaction as well as the results from Table 2.18, entries 12 to 15, where Brønsted base additives were used, we suspected that perhaps the desired hetero-cross-trienamine **135** was not being formed at all and the condensation between **134** and the aminocatalysts was stopping at the stable vinylogous iminium ion **142**. This substrate does possess an electron deficient double bond that could be explored (Scheme 2.8).



Scheme 2.8 – Formation of the stable vinylogous iminium ion intermediary **142**.

We decided to test a cooperative iminium ion/dienamine approach by using *trans*-2-hexenal as the precursor to the nucleophilic dienamine. This substrate was chosen because it could still give rise to the desired dihydropyrido[1,2-*a*]indole scaffolds that we were interested in synthesizing by either an *in situ*

step-wise Michael/Michael cascade or via a simple Michael addition followed by treatment with a strong base to produce the desired cyclized product (Scheme 2.9). The catalysts and reaction conditions tested are depicted in Table 2.19.



Scheme 2. 9 – Cooperative iminium ion/dienamine processes for the synthesis of dihydropyrido[1,2-a]indole scaffolds.

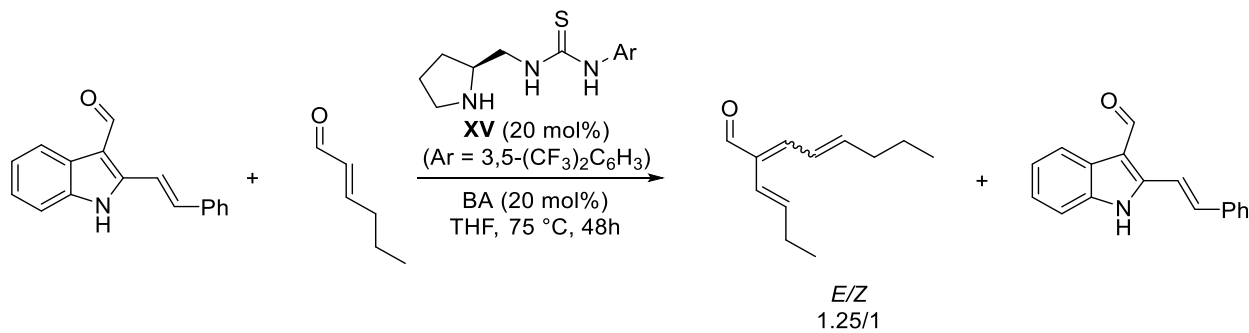
Table 2. 19 – Screening of catalysts for the cooperative iminium ion/dienamine process.

Entry	Catalyst	Time (h)	Conversion (%) ^a
1	IIIb	48	0
2	XV	48	100 ^b
3	IIIa	48	0
4	I	48	0

All reactions performed on a 0.5 mmol scale in respect to **134**, in 2 mL of THF, with 1.2 equiv. of *trans*-2-hexenal; (a) determined by ¹H NMR; (b) determined in respect to *trans*-2-hexenal.

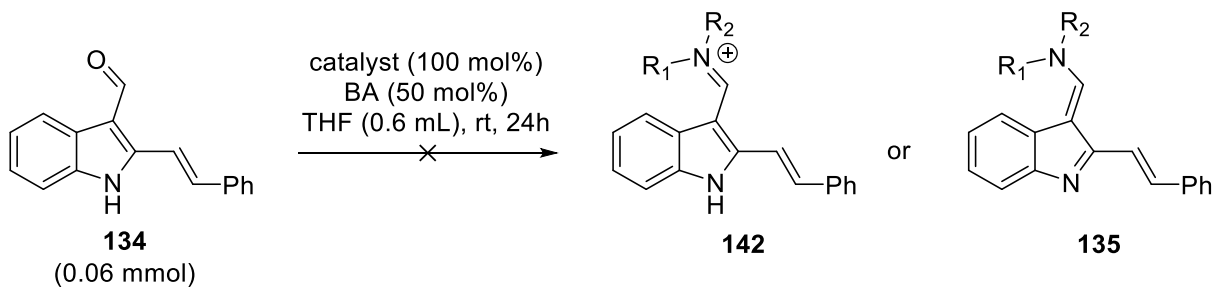
Of the catalysts tested, only **XV** (Scheme 2.10) showed new signals in the ¹H NMR of the crude reaction mixture (Table 2.19, entry 2 vs entries 1, 3 and 4). However, the ¹H signals of **134** were still present

and only the *trans*-2-hexenal was changed and consumed. TLC analysis of this reaction provided further evidence that the starting *trans*-2-hexenal had been consumed and a new product was formed whilst **134** was still present in the reaction mixture. Isolation of this new product showed it was the cross-aldol product of *trans*-2-hexenal with an *E/Z* ratio of 1.25/1 (Scheme 2.10).

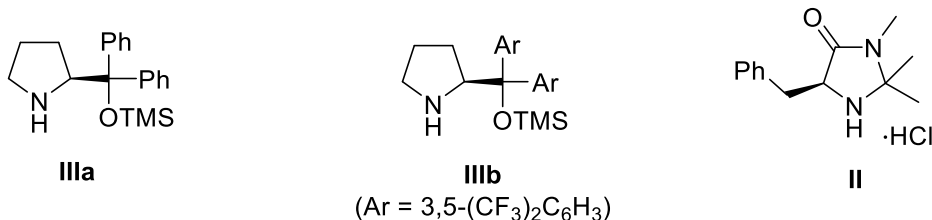


Scheme 2. 10 – Cross-aldol of *trans*-2-hexenal promoted by catalyst **XV**.

Lastly, we performed a few test reactions with three different aminocatalysts, in 100 mol% loading, to see if the iminium ion **142** and/or cross-trienamine **135** were being formed but, none of those intermediates were found by ¹H NMR (Scheme 2.11).



Catalysts screened:



Scheme 2. 11 – Test reactions to trap either iminium ion **142** or cross-trienamine **135**.

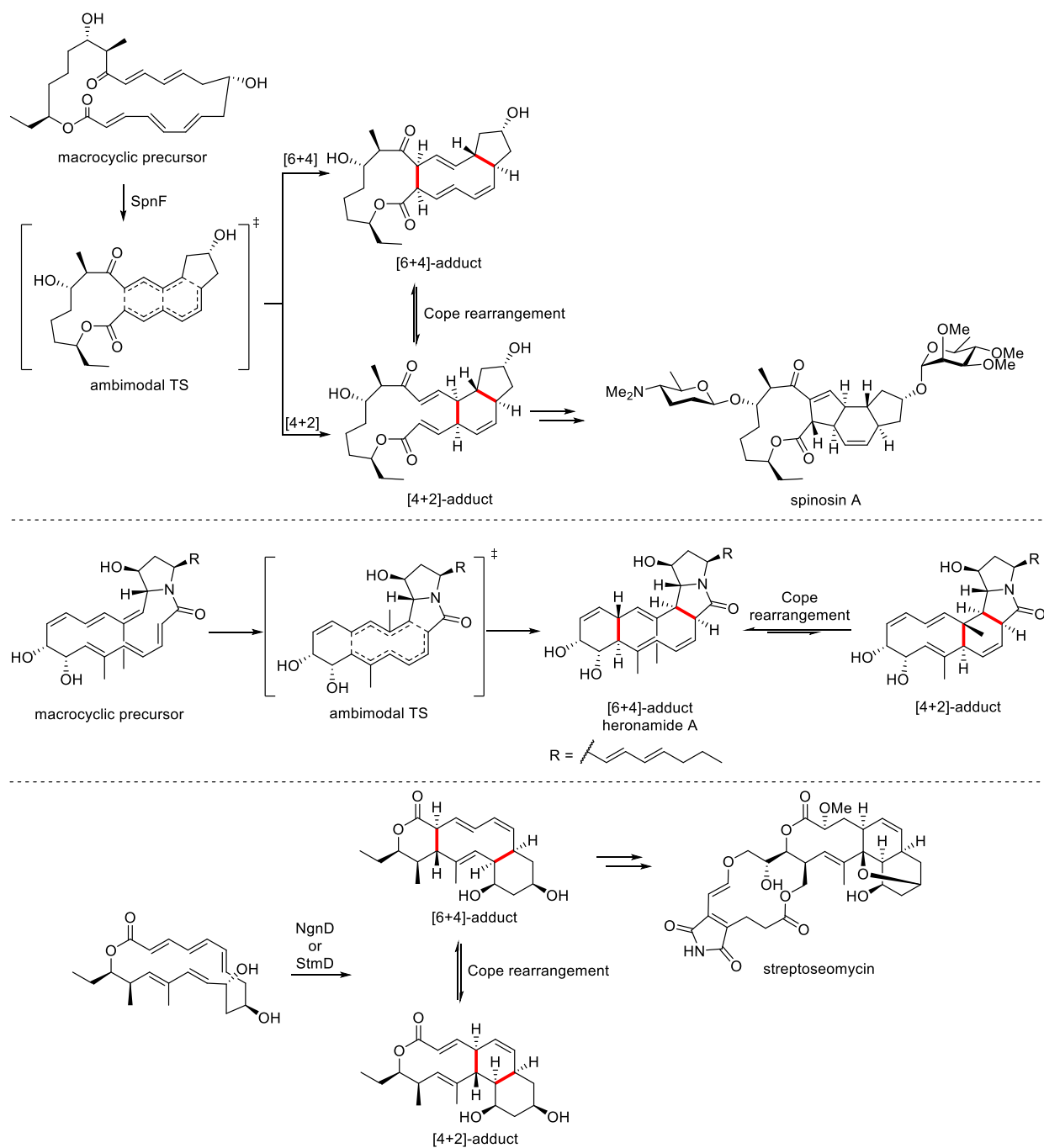
In conclusion, it appears that the relative position of the aldehyde moiety in respect to the indole Nitrogen atom is detrimental to the ability of the aminocatalyst to condense with the aldehyde to form the reactive intermediary species. This can be caused by electronic effects which decrease the nucleophilicity of the carbonyl carbon. It is also possible that some of the catalysts tested may have been too bulky to condense with this aldehyde. Therefore, neither of these two approaches, the intramolecular Michael of **131** nor the aza-Diels-Alder reaction of **134**, were successful at achieving the desired dihydropyrido[1,2-a]indole scaffolds. Nonetheless, further studies on the reactivity of **134** could be performed as perhaps a more suitable dienophile or a stronger nucleophile may react in the desired fashion. Moreover, H-bond catalysis may prove to be a better way of achieving the desired reactivity for substrate **134** however, changes to its structure may be required namely, the addition of a better H-bond acceptor group.

Chapter III – Higher-Order Cycloadditions

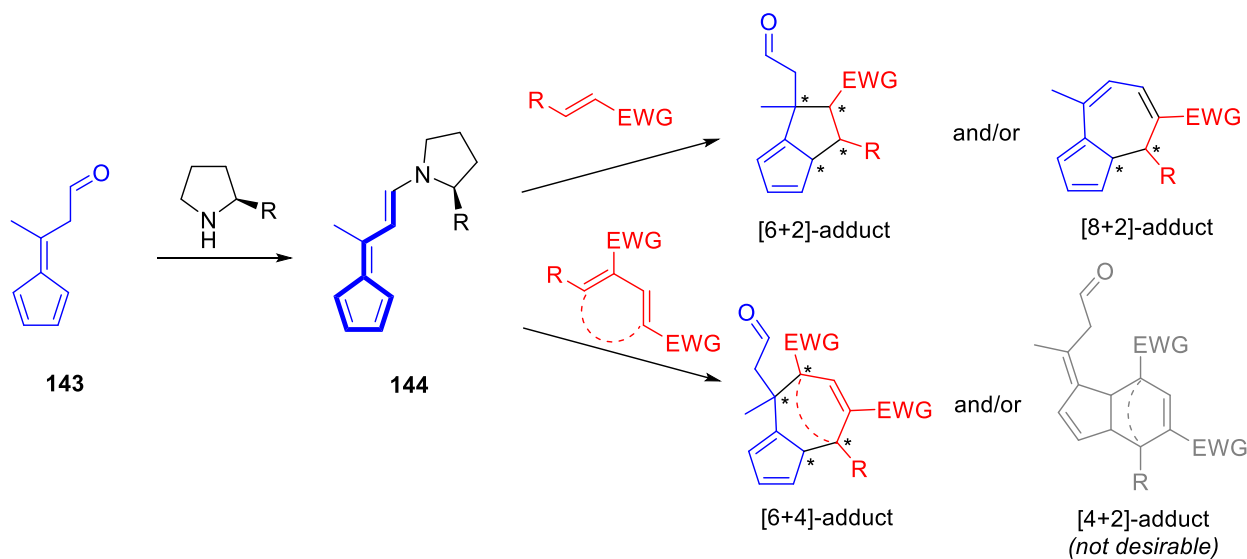
The introduction of orbital symmetry selection rules for cycloadditions in the mid-1960's, by Woodward and Hoffmann, allowed for a classification of these types of reactions in terms of electronic characteristics and opened the path to expand the scope beyond six-electron processes with reports of higher-order cycloadditions soon being reported in the following years.²⁰² In this century, it has been found that some higher-order cycloadditions, namely [6+4]-cycloadditions, also occur in enzyme-catalyzed reactions in the biosynthesis of spinosyn²⁰³, heronamide²⁰⁴ and streptoseomycin²⁰⁵ natural products (Scheme 2.12) with a whole new class of enzymes, the pericyclases that catalyze pericyclic reactions, being discovered.²⁰⁶

As it has been shown in Chapter IV of Part I, the first asymmetric aminocatalyzed intramolecular [6+2]-cycloaddition was reported in 2011, by Hayashi, Uchimaru and co-workers¹⁶⁷ but it was not until the end of 2017, with the independent works by Jørgensen and co-workers¹⁶⁸ and Chen and co-workers²⁰⁷, that the use of aminocatalysts was shown to be an effective method for performing asymmetric higher-order cycloadditions (see Schemes 1.35 to 1.42 and Table 1.3 from Chapter IV of Part I).

With this in mind, we decided to develop our own variants of higher-order cycloaddition reactions and for that purpose, we envisioned that a tetraenamine intermediary **143**, containing a fulvene moiety, could show to be quite effective at achieving the desired cycloadditions. Fulvenes are known to undergo higher-order cycloadditions by contributing with 6π electrons²⁰⁸ while the condensation of an aminocatalyst with the oxo-fulvene **143** to form the desired tetraenamine **144** would provide HOMO-raising activation to the system, making it more reactive towards the desired cycloadditions (Scheme 2.13).

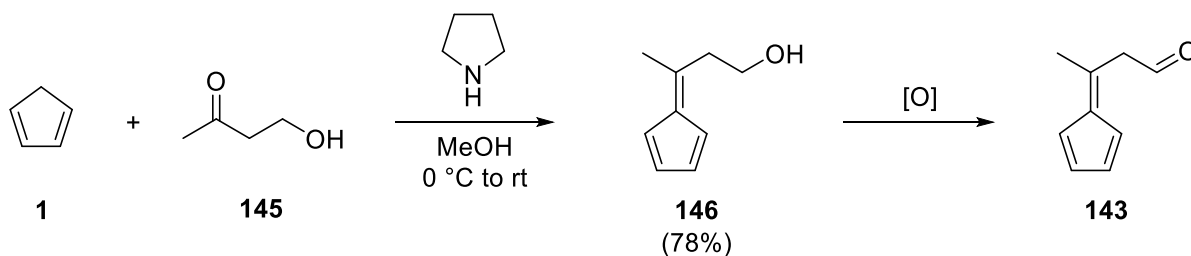


Scheme 2.12 – Proposed biosynthetic paths for spinosin A, heronamide A and streptosemycin.



Scheme 2.13 – Proposed strategy for the tetraenamine mediated higher-order cycloadditions.

To prepare substrate **143**, we decided to perform a condensation reaction between cyclopentadiene **1** and 4-hydroxy-2-butanone **145** in the presence of pyrrolidine (see Chapter IV for the detailed experimental procedure) forming the hydroxy-fulvene intermediate **146** which we could then oxidize to obtain the oxo-fulvene **143** (Scheme 2.14).



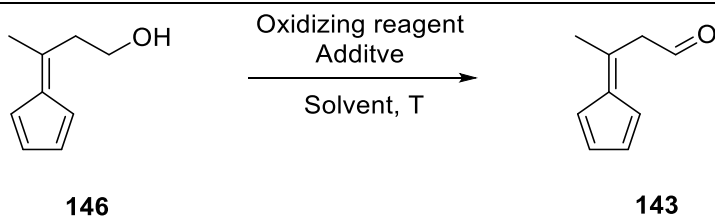
Scheme 2.14 – Synthetic path for oxo-fulvene **143**.

Hydroxy-fulvene **146** was easily obtained in 78% yield and with that in hand we envisioned that a Swern oxidation would certainly yield **143**. However, to our surprise, the Swern oxidation of **146** failed to give **143** and only starting material was obtained. Another attempt on the Swern oxidation was done with slight changes in timings and work up (see Chapter IV for experimental procedures) but that also failed.

Swern oxidations are widely employed in total synthesis of natural products, meaning that they are highly chemoselective and can tolerate a wide range of functional groups. Moreover, this oxidation

protocol usually provides the respective aldehyde or ketone in excellent yields thus, this method being our first choice to obtain compound **143**. With the failure to obtain the desired aldehyde **143** via Swern oxidation, we decided to try other standard oxidation methods as well as some more exotic (Table 2.20) but, surprisingly, they all failed to produce the desired compound **143**.

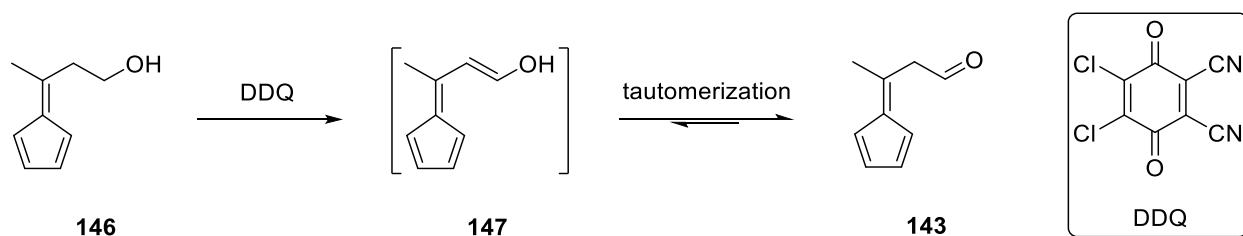
Table 2. 20 – Oxidation reactions tested for the conversion of **146** into **143** (for detailed experimental procedures see Chapter IV).



Entry	Oxidizing reagent/method	Additive	Solvent	T (°C)
1	Swern	—	CH ₂ Cl ₂	-78 to rt
2	DDQ	—	CH ₂ Cl ₂	rt
3	DDQ	—	1,4-dioxane	reflux
4	TEMPO (cat.)	BAIB	CH ₂ Cl ₂	rt
5	PCC	SiO ₂	CH ₂ Cl ₂	rt
6	PCC	—	CH ₂ Cl ₂	0
7	PCC	—	CH ₂ Cl ₂	rt
8	NaIO ₄	—	H ₂ O/MeOH	0
9	NaIO ₄	—	H ₂ O/1,4-dioxane	0
10	DMP	—	CH ₂ Cl ₂	rt
11	DMP	H ₂ O	CH ₂ Cl ₂	rt
12	IBX	—	THF/DMSO	rt

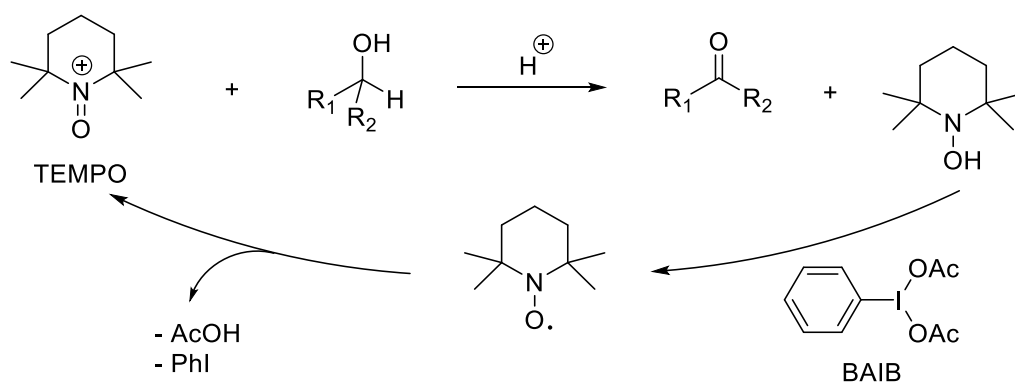
As mentioned above, the Swern oxidation failed to produce the desired fulvene **143** (Table 2.20, entry 1) so, we decided to try DDQ that, we hoped, would generate enol **147** via dehydrogenation which would tautomerize to the desired aldehyde **143** (Scheme 2.15). This method was a little bit far fetched but, if it worked, it could give rise to a new method for the formation of enols which could have interesting applications for aldol chemistry. However, standard conditions commonly employed with DDQ (see

Chapter IV for detailed experimental procedures) failed to give the desired product (Table 2.20, entries 2 and 3).



Scheme 2.15 – Rational for the use of DDQ for the formation of **143**.

Next, based on a report by Margarita, Piancatelli and co-workers²⁰⁹, we decided to try the oxidation of our alcohol **146** using TEMPO as a catalytic oxidizing reagent in the presence of stoichiometric amounts of BAIB which would regenerate the reactive oxidizing TEMPO *in situ* (see Chapter IV for detailed experimental procedure). Unfortunately, this approach also failed to produce compound **143** (Table 2.20, entry 4). The mechanism of this oxidation, proposed by the authors, is illustrated in Scheme 2.16.



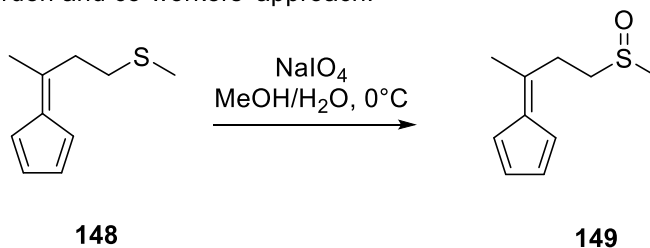
Scheme 2.16 – Proposed mechanism for the TEMPO/BAIB oxidation of alcohols.

With the failure to obtain the desired aldehyde using the above-mentioned methods, we decided to try the very common PCC method (see Chapter IV for detailed experimental procedures). We tested three different approaches. The first one was based on a report by Luzzio and co-workers²¹⁰, where SiO₂ was used as an additive. This method is an improvement on the standard PCC reaction conditions firstly, by maintaining an anhydrous environment which reduces the formation of carboxylic acids through oxidation

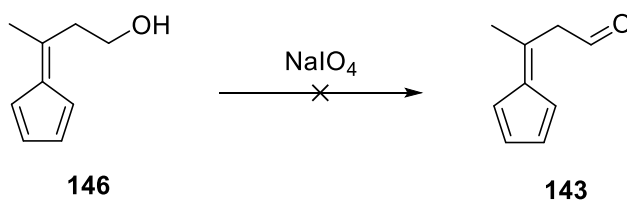
of aldehyde hydrates and secondly, by substantially facilitating the removal of the reduced chromium tars that form in this reaction (Table 2.20, entry 5). Visually, the reaction appeared promising as the bright orange suspension of PCC/SiO₂ in CH₂Cl₂ turned a very dark brown color upon addition of alcohol **146** which is consistent with these reactions. However, TLC analysis showed that no new product was being formed and upon quenching the reaction mixture and ¹H NMR analysis of the crude, only alcohol **146** was present. We decided to try this method yet again removing the SiO₂ and letting the reaction proceed at either 0 °C or rt but, no oxidation took place (Table 2.20, entries 6 and 7).

The use of NaIO₄ as an oxidizing reagent was based on a report by Erden and co-workers²¹¹ where the authors used this method to oxidize 6-[2-(methylthio)ethyl]fulvene **148** to its corresponding sulfoxide **149** in 83% yield and without oxidation of the unsaturated fulvene system (Scheme 2.17).

Erden and co-workers' approach:



Our approach:



Scheme 2. 17 – Erden and co-workers NaIO₄ oxidation of **148** and our approach to **143**.

The authors performed their oxidation in a MeOH/H₂O mixture however, they were oxidizing a softer, more reactive sulfur atom while, in our case, we wanted an alcohol to be oxidized so, it was not surprising when our first attempt in MeOH/H₂O failed to give any product (Table 2.20, entry 8). We then decided to change the organic solvent to 1,4-dioxane which is miscible with H₂O and non-oxidizable by NaIO₄ but, this attempt was also met with failure (Table 2.20, entry 9).

We then decided to use DMP which is also a widely used reagent in total synthesis of natural products, to convert alcohols into aldehydes. We first tested this oxidation under standard conditions i.e. stirring in CH₂Cl₂ at rt but, no product was observed (Table 2.20, entry 10). It is known that addition of water or performing the reaction with “wet” solvents enhances the reactivity of DMP by *in situ* hydrolysis of this reagent into the stronger oxidizing IBX²¹² so, we decided to test this protocol and TLC analysis did indicate a new product was formed after 5h stirring at rt (Table 2.20, entry 11). We then proceeded to work up the reaction (see Chapter IV for detailed experimental procedure) and submit a sample for ¹H NMR analysis (Figure 2.10).

Even though the ¹H NMR spectrum is fairly dirty, it does appear that the desired aldehyde **143** may be present. There is a triplet of one proton at 9.74 ppm with a coupling constant (*J*) of 2.1 Hz which is consistent with the proton at the carbonyl group (depicted in red in Figure 2.10). This triplet seems to be coupling with a doublet of two protons at 3.65 ppm (*J* also 2.1 Hz). This doublet could be produced by the α-protons (depicted in blue in Figure 2.10). However, these *J* values are not consistent with vicinal couplings, specifically, when there are no conformational constraints between the two groups where the protons are. Additionally, a singlet of three protons at 1.95 ppm as well as a multiplet of five protons between 6.58 and 6.55 ppm are also detectable and could be caused by the methyl group and cyclopentadiene moiety of the fulvene, respectively.

Attempts to isolate the product of this reaction by flash column chromatography caused the product to decompose as the NMR spectra of the product that came out of the column was substantially different than the one recorded after work up (Figure 2.10).

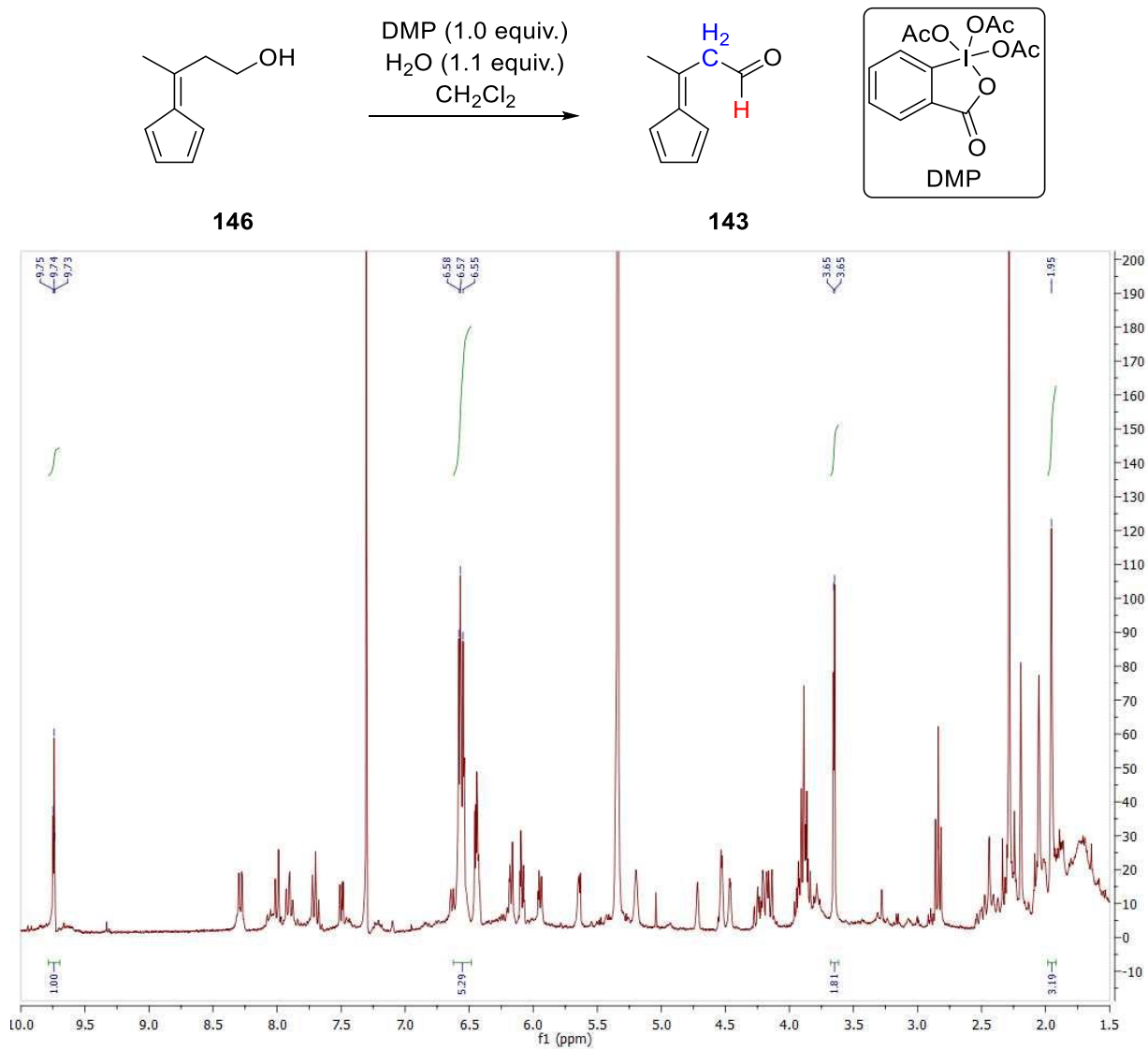


Figure 2. 10 – Reaction scheme and ¹H NMR of the DMP/H₂O oxidation of **143** (recorded in CDCl₃ at 300 MHz).

From my experience, reactions with DMP or IBX are usually very clean and tend to give the desired product virtually pure after work up. However, as it can be seen from Figure 2.10, this was not the case. The *in situ* hydrolysis of DMP releases 3.0 equiv. of acetic acid and we suspect that a possible Brønsted acid catalyzed polymerization side-reaction could be occurring under the conditions employed and hence, the complex NMR spectrum. Furthermore, if indeed the desired product **143** was being formed, the attempt to purify it and isolate it resulted in its destruction (Figure 2.11, blue spectrum). To overcome these problems, we decided to synthesize and test IBX (Table 2.20, entry 11) hoping that the lack of acetic acid

would provide a cleaner reaction. Unfortunately, this approach did not produce the desired aldehyde **143** either.

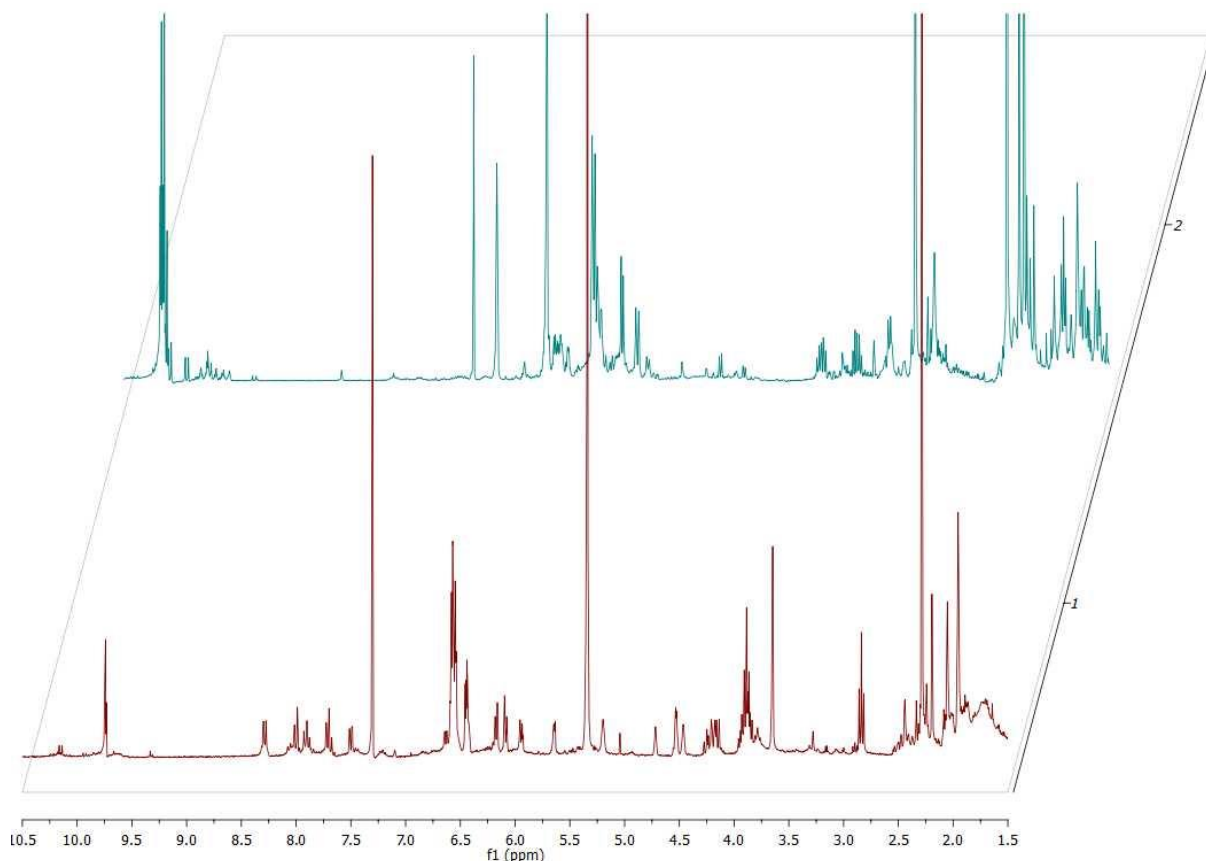
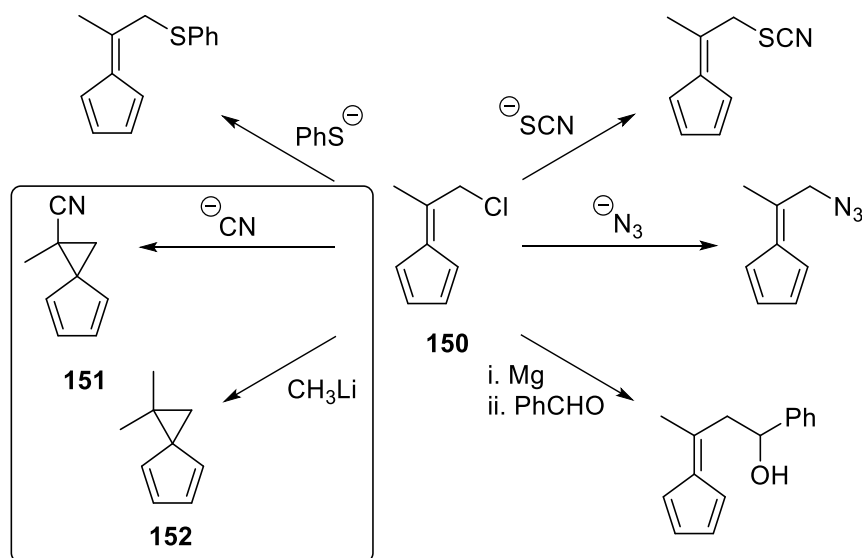


Figure 2.11 – ^1H NMR spectra of DMP/ H_2O oxidation of **146**; red spectrum – after work up; blue spectrum – after column chromatography (both spectra recorded in CDCl_3 at 300 MHz).

With these results, especially the ones with the Swern and DMP protocols, we decided to take a step back and try to understand the reactivity, or in our case, lack thereof, of fulvene **146**. According to the reported paper by Erden and co-workers, from which we based the synthesis of our fulvene **146**, the authors observed that treating 6-(chloromethyl)-6-methylfulvene **150** with several nucleophiles would not always result in substitution of the chlorine atom through a $\text{S}_{\text{N}}2$ reaction pathway. The authors observed that soft nucleophiles would give rise to the expected $\text{S}_{\text{N}}2$ product. However, the hard nucleophiles like ^-CN and $^-\text{CH}_3$ would add to the exocyclic double bond of the fulvene with subsequent cyclization and displacement of the chlorine atom to afford the corresponding spirocyclopropanes **151** and **152**, respectively (Scheme

2.18).²¹³ These results strongly suggest that the exocyclic double bond of the fulvene is highly polarized making it the hardest electrophilic centre of the molecule.



Scheme 2.18 – Reactivity of 6-(chloromethyl)-6-methylfulvene **150** towards different strength nucleophiles (adapted from ref. 209).

A few years after their synthetic work, the same group reported a computational study on the displacement of the chlorine atom of **150** by a chloride anion and compared those results with other similar systems (both structurally and electronically). The authors concluded that the fulvenyl group accelerates the rate of substitution when compared to the dihydro and nonallylic analogues (structural similarity) as well as when compared to benzylic and allylic groups (electronic similarity). These results were rationalized with electrostatic interactions between the electron rich chlorides and the electron deficient exocyclic double bond which provided stabilization of the transition state for the chlorine displacement with additional increment of the negative character of the fulvenyl ring providing extra stabilization. The anion-stabilizing effect of the fulvenyl group was further illustrated with the computed enthalpies of dissociation of 7-hydroxy-fulvenes, which were lower than those of their nonallylic analogues by c.a. 10 kcal/mol (Figure 2.12).²¹⁴

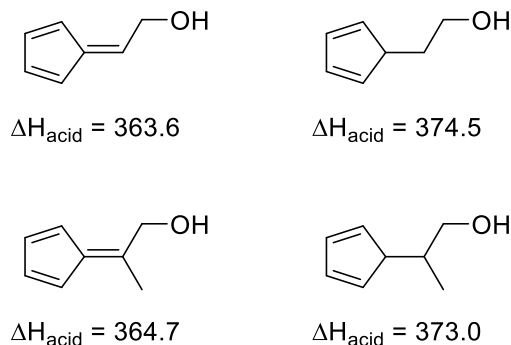
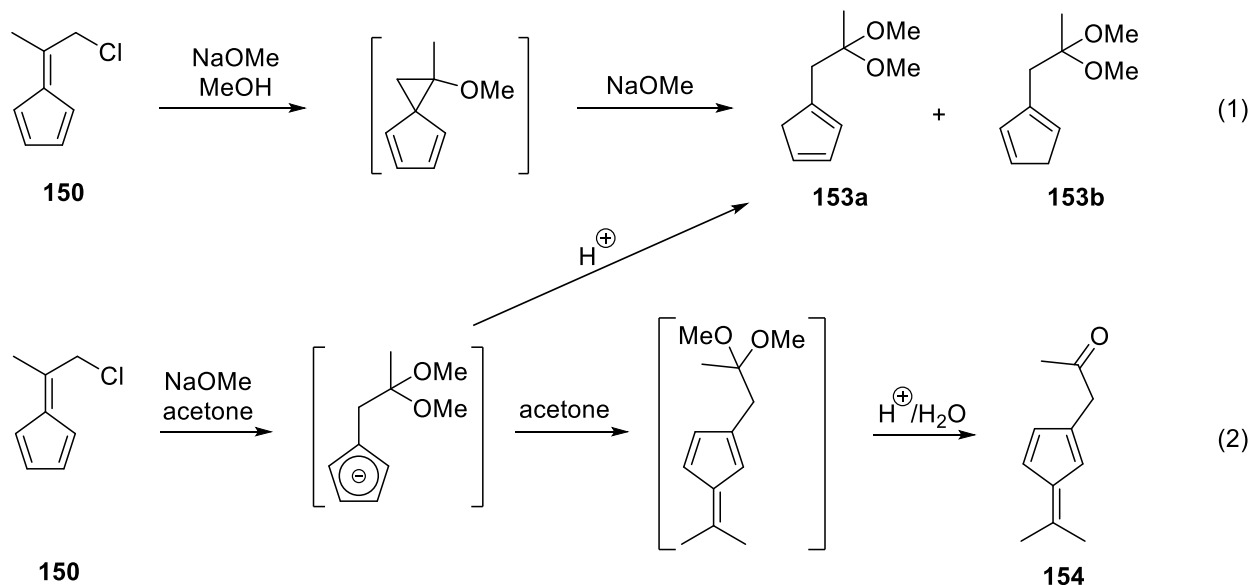


Figure 2. 12 – Enthalpies of dissociation for 7-hydroxy fulvenes and their nonallylic analogues (relative energies in kcal/mol calculated at the G3MP2 level of theory).

More recently, the Erden, Gronert and co-workers provided further proofs of the high reactivity of the exocyclic double bond of **150**. Upon treatment with NaOMe in MeOH the authors observe the formation of acetals **153a** and **153b** (Scheme 2.19, eq. 1) but, when acetone was used as solvent the authors isolated the new fulvene **154** (Scheme 2.19, eq. 2).²¹⁵

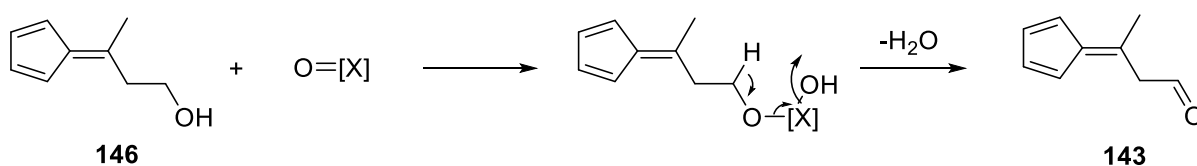


Scheme 2. 19 – Reactivity of **150** towards methoxide reported by Erden, Gronert and co-workers.

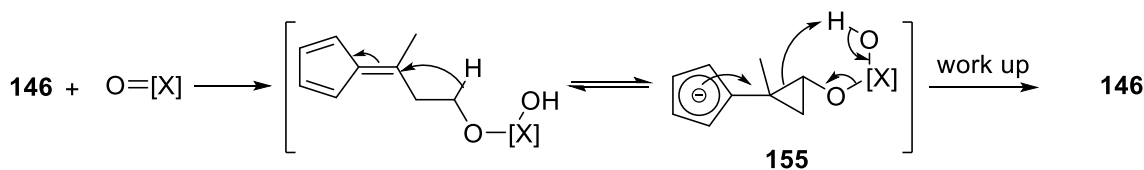
Looking at the synthetic and computational work developed by Erden and co-workers on the chemistry of fulvenes' side chains, it starts to become evident why our oxidations failed to produce the desired oxo-fulvene **143**. The mechanism of the oxidation of **146** is fairly similar for all the protocols we

explored and a key step in all of them is the deprotonation of the *ipso*-Carbon with the electrons from the former C – H bond moving towards the formation of the new C = O double bond with concomitant elimination of the reduced oxidizing reagent and production of the desired aldehyde. However, due to the ability of the fulvenyl ring to stabilize negative charges allied to the highly polarized exocyclic double bond of the fulvene, it is very likely that upon deprotonation (if it even takes place), the electrons move towards the fulvene ring forming the anionic, aromatic intermediary **155** which upon quenching and working up of the reactions collapses back to the starting alcohol **146**. In this likely scenario, complexation between **146** and the oxidizing reagent takes place which could explain the color change observed in the PCC reactions (Scheme 2.20).

Expected mechanism:



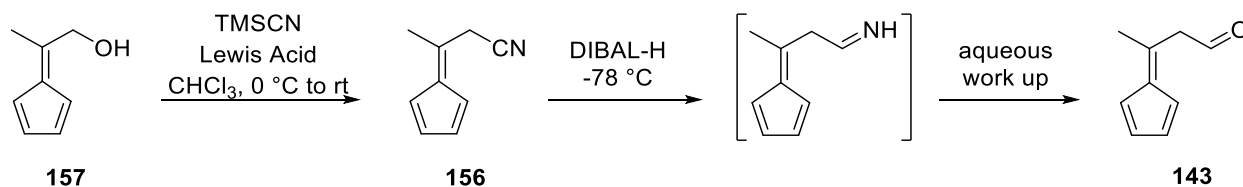
Likely scenario:



Scheme 2.20 – Possible reason for the failure to oxidize **146** into **143**.

Nevertheless, we did not give up on this project, yet and, if oxidations do not provide the desired oxo-fulvene **143**, then we could try to obtain it through a reduction reaction. To do so, we envisioned preparing fulvene **156** and then performing a reduction with DIBAL-H which would generate an aldimine intermediate that would spontaneously collapse to the desired aldehyde moiety upon aqueous work up. To prepare fulvene **156** and based on the reactivity observed by Erden and co-workers (see Scheme 2.18), we had to devise a different approach from the standard S_N2 with KCN as the nucleophile. So, we decided to adapt the procedure reported by Ding and co-workers who were able to effect a direct cyanation of alcohols

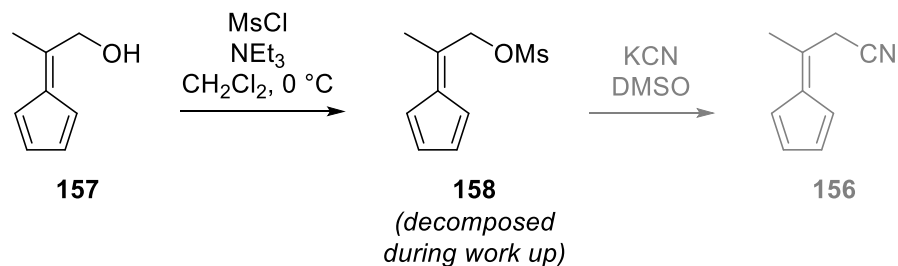
using TMSCN and a Lewis acid catalyst, and try this protocol with the newly prepared 6-(hydroxymethyl)-6-methylfulvene **157** (Scheme 2.21).²¹⁶



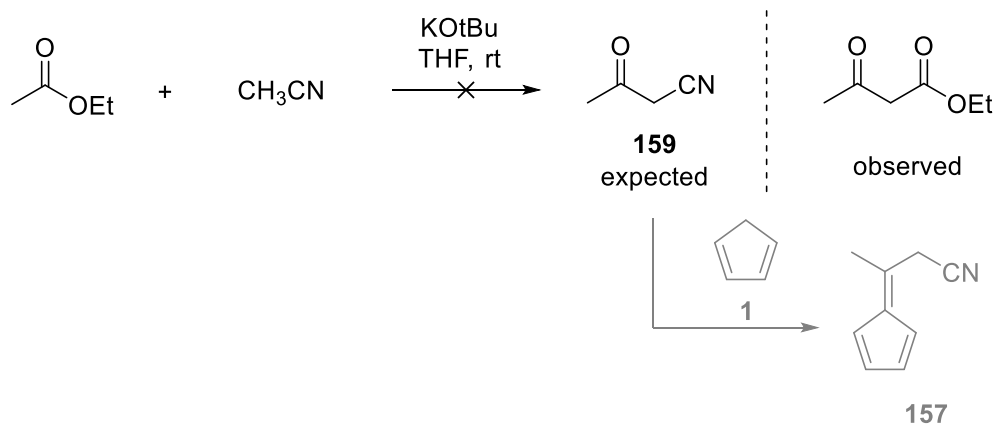
Scheme 2. 21 – New synthetic route to oxo-fulvene **143**.

Fulvene **157** was prepared in 43% yield using the same procedure used for fulvene **146** (see Chapter IV for experimental procedure). Unfortunately, treatment of **157** with a Lewis acid immediately led to its decomposition. In our first trial, we decided to use BiCl₃ as the Lewis acid but, as soon as the fulvene was added to the mixture of BiCl₃ and TMSCN in CHCl₃, reaction immediately turned black with a black solid suspended and TLC analysis showed no spots whatsoever on the reaction lane. BF₃·OEt₂ was also tested but it showed similar behavior to BiCl₃ (see Chapter IV for detailed experimental procedures).

We then thought that we could perhaps circumvent the chemoselectivity of the S_N2 reaction with cyanide by making a fulvene with a better leaving group than a chloride. In other words, we hoped that mesylation of the hydroxyl group of **157** would cause the cyanide to perform an S_N2 reaction instead of a conjugate addition as observed by Erden and co-workers with **150** (*vide supra*). Therefore, we set up to mesylate **157** (see Chapter IV for detailed experimental procedure) but, after the work up of the reaction, while the solvent was being evaporated, the bright yellow solution turned black and left a black solid in the flask that was not soluble in CDCl₃, DMSO-d₆, acetone, MeOH or H₂O (Scheme 2.22). Attempts to prepare **156** directly from the condensation between cyclopentadiene **1** and 3-oxobutanenitrile **159** were also unsuccessful (Scheme 2.23).



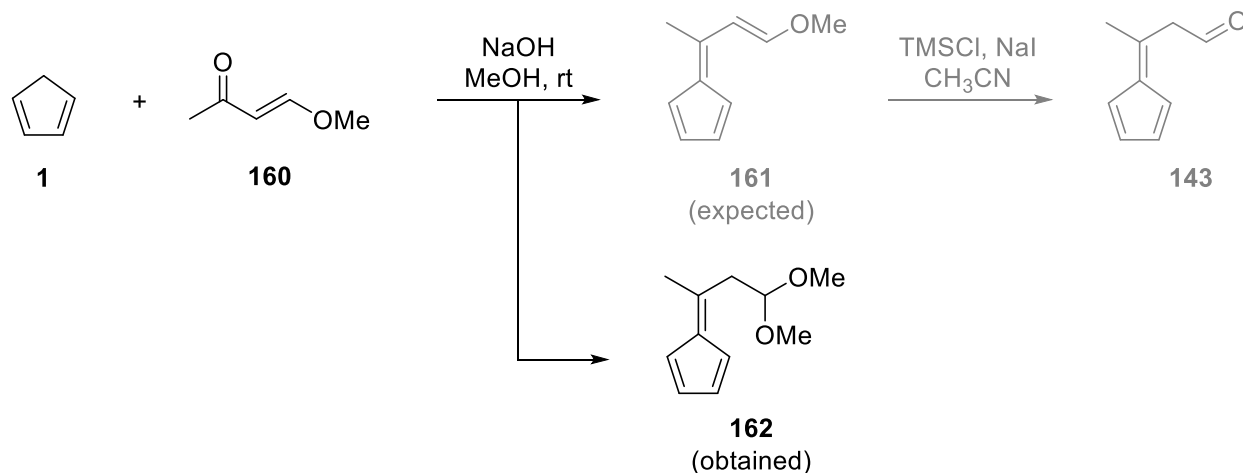
Scheme 2.22 – Synthetic route to **156** via mesylation of **157**.



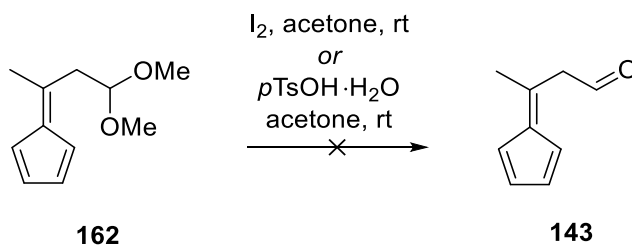
Scheme 2.23 – Attempt to synthesize 3-oxobutanenitrile **159** for subsequent synthesis of fulvene **157**.

With these results we abandoned our attempts to synthesize **157**. Instead we decided to use *trans*-4-methoxy-3-buten-2-one **160** and condense it with cyclopentadiene **1** to get fulvene **161** which we could then convert to the desired oxo-fulvene **143** by treatment with TMSCl and NaI in CH₃CN as reported by Cohen and co-workers.²¹⁷ Our initial attempt of synthesizing fulvene **161** was not successful even after allowing the reaction to stir at rt over night but, changing the base from pyrrolidine to sodium hydroxide did provide a fulvene, albeit not the one expected and instead fulvene **162** was obtained (Scheme 2.24).

After all these attempts we finally were able to obtain the desired fulvene **143** as its dimethyl acetal (**162**). With this substrate in hand, we first decided to deprotect the acetal under standard conditions using either *p*TsOH·H₂O or I₂ in acetone (see Chapter IV for detailed experimental procedures) but, unfortunately, as soon as these reagents were mixed with fulvene **162**, reaction mixtures turned from orange solutions into black suspensions and TLC analysis would show no spots in the reaction lane (Scheme 2.25).



Scheme 2.24 – New synthetic route for fulvene **143** with unexpected synthesis of fulvene **162**.



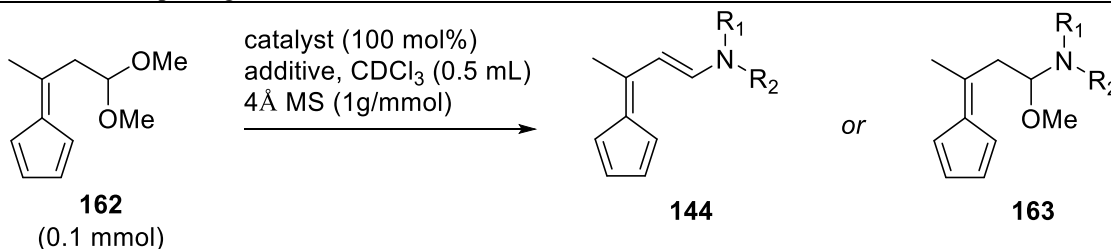
Scheme 2.25 – Attempts to convert acetal **162** into aldehyde **143**.

The unexpected obtention of **162** instead of **161** as well as the saddening results on the deprotection of acetal **162** hinted at yet another issue that may have been responsible for the inability to synthesize fulvene **143**. The CH₂ unit of **143** is linking two very electron deficient carbons which means that, probably, the pK_a of these protons is very low and, therefore, **143** may be a very unstable molecule. Looking back at the oxidation procedures, not only was there a kinetic issue as illustrated in Scheme 2.20, there may also be a thermodynamic barrier with **143** being too unstable to form and it either collapses back to whatever precursor we tried or, if it can not go back to its precursor, it just decomposes through other paths and thus, the black insoluble solids obtained.

Nevertheless, we decided to explore the protected aldehyde **162** and subject it to several aminocatalysts to see if we could form the desired tetraenamine **144** or the methyl heminaminal **163** both

of which could then be tested towards the initial goal of this project of developing asymmetric higher-order cycloadditions (Table 2.21).

Table 2. 21 – Attempts to generate tetraenamine **144** and/or hemiaminal **163**.



Entry	Catalyst	Additive (mol%)
1	IIIb	BA (20 mol%)
2	IIIb	TFA (20mol%)
3	IIIb	<i>p</i> TsOH·H ₂ O (20 mol%)
4	II	—
5	IIIb	TFA (100 mol%)
6	IIIb	<i>p</i> TsOH·H ₂ O (100 mol%)
7	XII	—
8	XII	<i>p</i> TsOH·H ₂ O (20 mol%)
9	XII	<i>p</i> TsOH·H ₂ O (100 mol%)

Since there were no major issues of solubility, CDCl₃ was used as the solvent in all cases to facilitate monitoring the reaction by ¹H NMR. The aminocatalysts were added in stoichiometric amounts (100 mol% loading) to ensure that the tetraenamine **144** and/or hemiaminal **163** could be observed in the NMR spectra. 4Å MS were also added to trap MeOH, generated from the condensation of the aminocatalysts and **162**, ensuring that enough tetraenamine **144** or the methyl hemiaminal **163** could be visible in ¹H NMR spectrum. Initially we used Jorgensen's catalyst **IIIb** with several Brønsted acid additives of different strengths (pKa's), hopefully, to facilitate the elimination of the methoxy groups of **162**. Unfortunately, ¹H NMR analysis did not show any indication of the presence of tetraenamine **144** or hemiaminal **163** (Table 2.21, entries 1 to 3). We also tested MacMillan's oxazolidinone **II**, which did not require an acid additive as it is

commercialized and used as its HCl salt so, a strong acid is already present but, it too failed to produce the desired compounds according to the ^1H NMR spectrum (Table 2.21, entry 4).

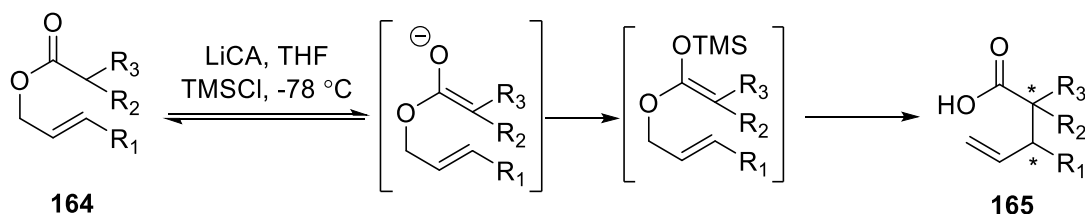
We then decided to go back to catalyst **IIIb** but, this time, we used more acidic conditions and decided to test TFA and *p*TsOH·H₂O in 100 mol% loading but, again no compound **144** or **163** could be seen by ^1H NMR analysis (Table 2.21, entries 5 and 6).

Lastly, we decided to test primary amine **XII** that, albeit being less nucleophilic than secondary amines, the lack of steric bulk around the nitrogen atom could facilitate its condensation with **162**. We used it without any acid additive (Table 2.21, entry 7) as well as with the strong *p*TsOH·H₂O in both sub-stoichiometric (Table 2.21, entry 8) and stoichiometric amounts (Table 2.21, entry 9) but again neither **144** nor **163** were observed by ^1H NMR.

At this stage, we decided to abandon substrate **162** as well as any further attempts to obtain oxo-fulvene **143** which appears to be impossible to synthesize. Ongoing studies are being performed to try to understand the inability to oxidize hydroxyfulvene **144** to the oxo-fulvene **143**.

Chapter IV – Organocatalyzed Asymmetric Ireland-Claisen Rearrangement

The Ireland-Claisen rearrangement (abbreviated from now on to IC) is a powerful tool in organic synthesis for the synthesis of γ,δ -unsaturated carboxylic acids **165** from simple, easy to prepare, allylic esters **164** (Scheme 2.26). It was first reported by Robert E. Ireland in 1972²¹⁸ with further studies on the mechanism and optimization of reaction conditions, performed by the author in subsequent years.^{219,220} In addition to the well established protocol for the IC rearrangement, its corresponding products can be obtained with high enantiocontrol when the starting material possesses a stereocenter making the IC a widely used tool in the synthesis of natural products.^{34,221}



Scheme 2. 26 – General example of an Ireland-Claisen rearrangement.

There are two main features of the IC that must be considered in order to predict the stereo-outcome of these reactions: (i) the configuration of the reactive enolate and, (ii) the configuration of the starting allylic ester. The first report of an IC rearrangement used lithioisopropylcyclohexylamine (LiCA) as a base. However, it has been found that other lithium bases, namely lithium diisopropyl amine (LDA), also produce the desired enolate.²²⁰ LDA usually gives rise to the *E*-enolate which can be explained by a cyclic TS where the proton is abstracted from the stereoelectronically favoured orientation more or less perpendicular to the carbonyl group. On the other hand, steric repulsions between the α -substituent of the ester and the alkyl groups of the base disfavour the TS which gives rise to the *Z*-enolate (Figure 2.13).^{220,222}

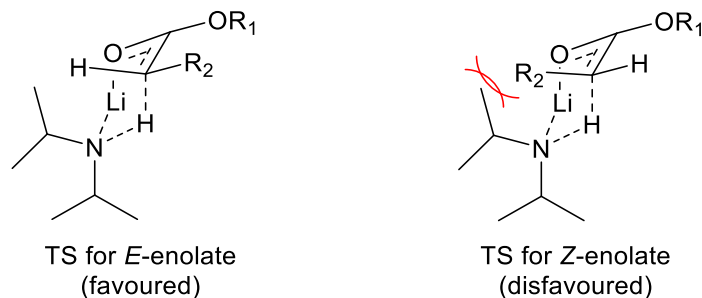
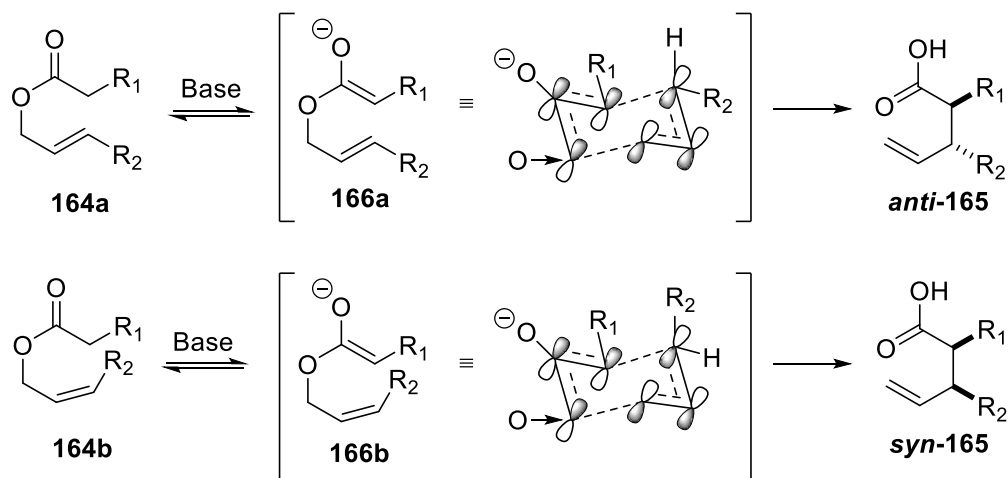


Figure 2.13 – Transition states for the formation of the *E*- and *Z*-enolates with LDA.

It has been discovered that the use of hexamethylphosphoramide (HMPA), as a co-solvent, produces the *Z*-enolate preferentially and, even though it is not very clear why, it is theorized that the cyclic TS depicted in Figure 2.13 is disrupted due to increased solvation of the lithium counterion by HMPA and the deprotonation takes place through an acyclic TS giving the kinetic *Z*-enolate.²²³ Moreover, the presence of chelating groups in R_2 can also favour the formation of the *Z*-enolate as it has been recently demonstrated by Zakarian and co-workers with their stereodivergent Ireland-Claisen protocol for α -alkoxyesters.²²⁴

Since the configuration of the enolate can be predicted by the type of base used, the configuration of the double bond of the starting ester is known and, given the concerted nature of this pericyclic reaction, one can effortlessly predict the relative stereo-outcome of the final product (Scheme 2.27).



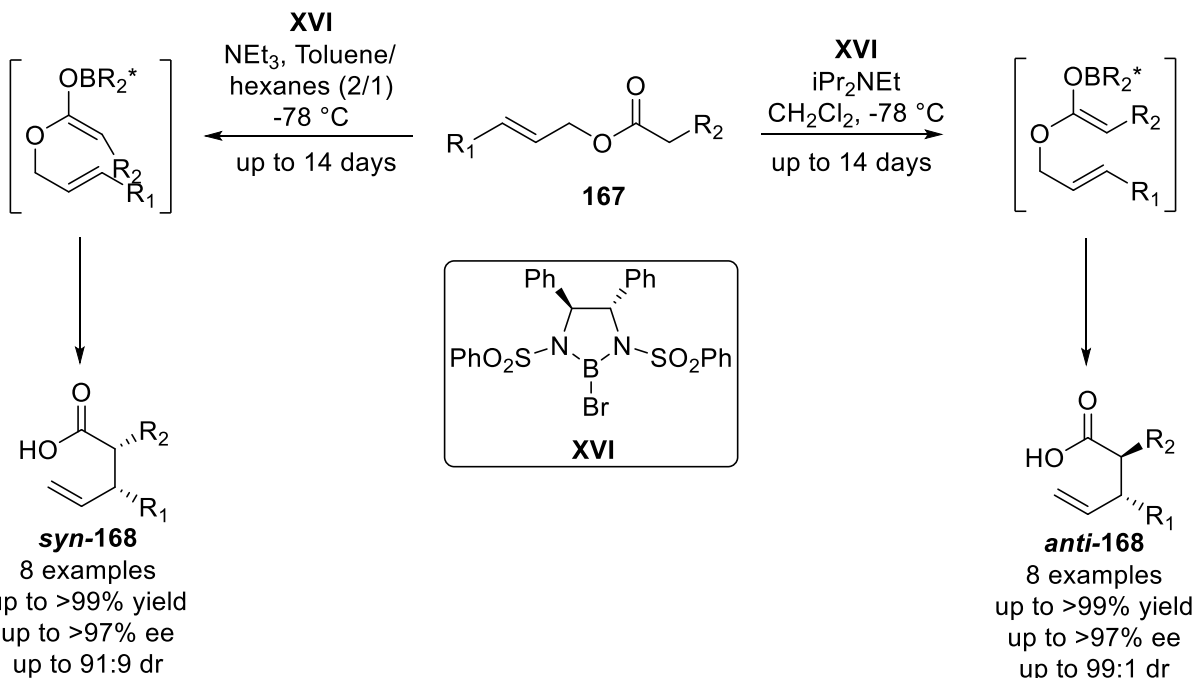
Scheme 2.27 – Relative stereo-outcome of the Ireland-Claisen rearrangement based on the configuration of the R_2 substituent.

The only difference between **164a** and **164b** is the configuration around the allylic substituent which is *E* in **164a** and *Z* in **164b**. As seen above, careful choice of base and/or co-solvents can allow for an almost exclusive formation of the *Z*-enolate (**166**), which is what is depicted in Scheme 2.27. Therefore, using the Woodward-Hoffmann rules and FMO theory, not only do we know that the reaction is thermally allowed through a supra/suprafacial approach. We can also predict that **164a** gives rise to a major product with a relative *anti*-configuration between R₁ and R₂ (*anti*-**165**) whilst, **164b** will give a major product with the relative *syn*-configuration between the R₁ and R₂ groups (*syn*-**165**).

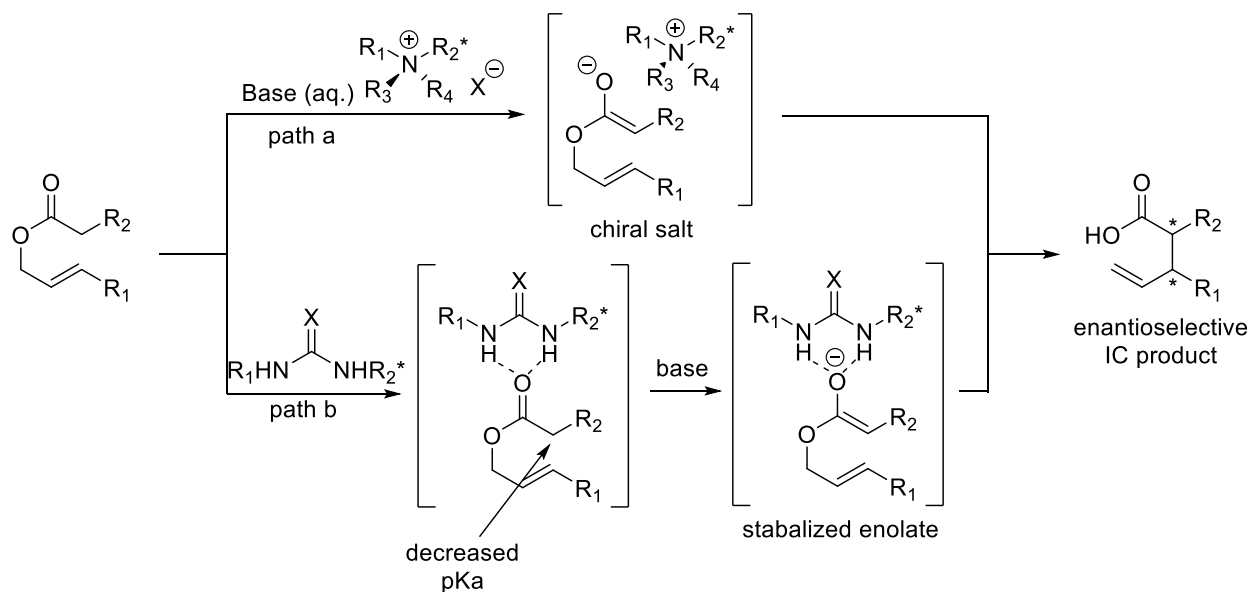
In respect to enantioselective versions of this reaction, most examples in the literature make use of stoichiometric inorganic Lewis acids with chiral ligands²²⁵ which makes this methods not very appealing due to high costs and environmental hazards posed by the metals used. To the best of our knowledge, the only organic Lewis acid enantioselective IC was reported in 1991 by Corey and co-workers where the authors used a boron sulfonamide chiral auxiliary to promote the IC with excellent yields and enantio- and diastereoselectivities (Scheme 2.28).²²⁶

Albeit the excellent results obtained by Corey and co-workers, the reactions were very long (up to 14 days) and the Lewis acid used is highly sensitive to moisture. As a result, we decided that the enantioselective IC could be improved and organocatalysis could prove useful in that objective. So, we envisioned two distinct approaches for the activation of the starting esters and consequent enantioselective IC (Scheme 2.29).

The first approach relied on APTC, where we theorized that a basic aqueous solution would deprotonate the starting ester to form the reactive enolate which could form a chiral ionic salt with an asymmetric phase-transfer catalyst which would in turn allow for the IC to take place in a stereoselective fashion (Scheme 2.29, path a). The second approach was based on H-bond catalysis, where a chiral thiourea catalyst could increase the acidity of the α -protons of the starting ester, via H-bond activation, forming the desired enolate that could proceed to undergo the IC with the asymmetric catalyst providing the necessary chiral environment for an enantioselective IC to take place (Scheme 2.29, path b).



Scheme 2.28 – Enantioselective IC reported by Corey and co-workers.

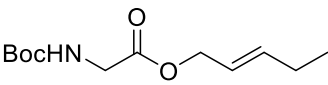


Scheme 2.29 – Approaches envisioned for the stereoselective IC; path a: asymmetric phase-transfer approach and; path b: asymmetric H-bond approach (R_2^* denotes the chiral moiety of the catalyst).

Another aspect that we were interested in was to be able to synthesize, in an enantioselective manner, non-natural α -substituted amino-acids which are highly important substrates in fine chemistry with a wide range of applications from proteomics and protein structure and function elucidation²²⁷ to peptidomimetics and the synthesis of novel pharmaceutical drugs.²²⁸

We started by preparing the required allylic esters **169** via Steglich esterification²²⁹ protocol starting from *N*-Boc glycine and *trans*-2-penten-1-ol which smoothly produced to desired products in good yields (see Chapter IV for more information). With the substrates in hand, we subjected them to our first trials for the enantioselective IC with the chiral APTC **XVII**, a widely used type of catalyst families for these type of conditions (Table 2.22).^{50,51,230}

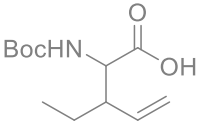
Table 2.22 – Test reactions for the enantioselective IC of **169**, under APTC conditions.



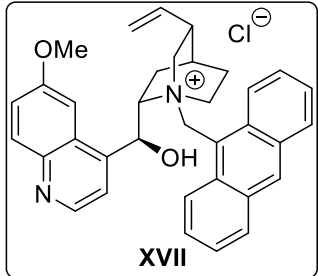
169

XVII (20 mol%)
Solvent, rt
1.0 M aq. NaOH

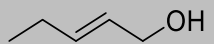
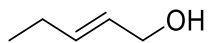
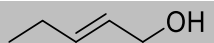
→



170



XVII

Entry	Solvent	Time (h)	Product ^a
1	Hexanes	6	
2	Toluene	6	
3	CH ₂ Cl ₂	6	

All reactions performed on a 0.2 mmol scale in respect to **169** using a 1/1 ration of Solvent/aq. base; (a) followed by TLC.

Unfortunately, our initial approaches did not afford the desired IC product **170**, but instead led to hydrolysis of the starting ester within 6h at rt. TLC analysis showed that the starting ester was absent from the reaction mixture and a new spot appeared which, upon comparison with the starting alcohol, *trans*-2-penten-1-ol, exhibited the same *r_f*. A crude NMR was then performed (Figure 2.14) which confirmed that indeed the ester was mostly consumed. The two multiplets from the double bond of **169**, at 5.85 and 5.55 ppm were mostly gone (Figure 2.14; green spectrum vs blue spectrum) and instead, one multiplet, at 5.7 ppm, was present in the double bond region, consistent with the double bond pattern observed for the starting alcohol (Figure 2.14; blue spectrum vs red spectrum). Furthermore, the appearance of a signal at 4.1 ppm can also be observed corresponding to the CH₂OH protons from the alcohol (Figure 2.14; blue spectrum vs red spectrum).

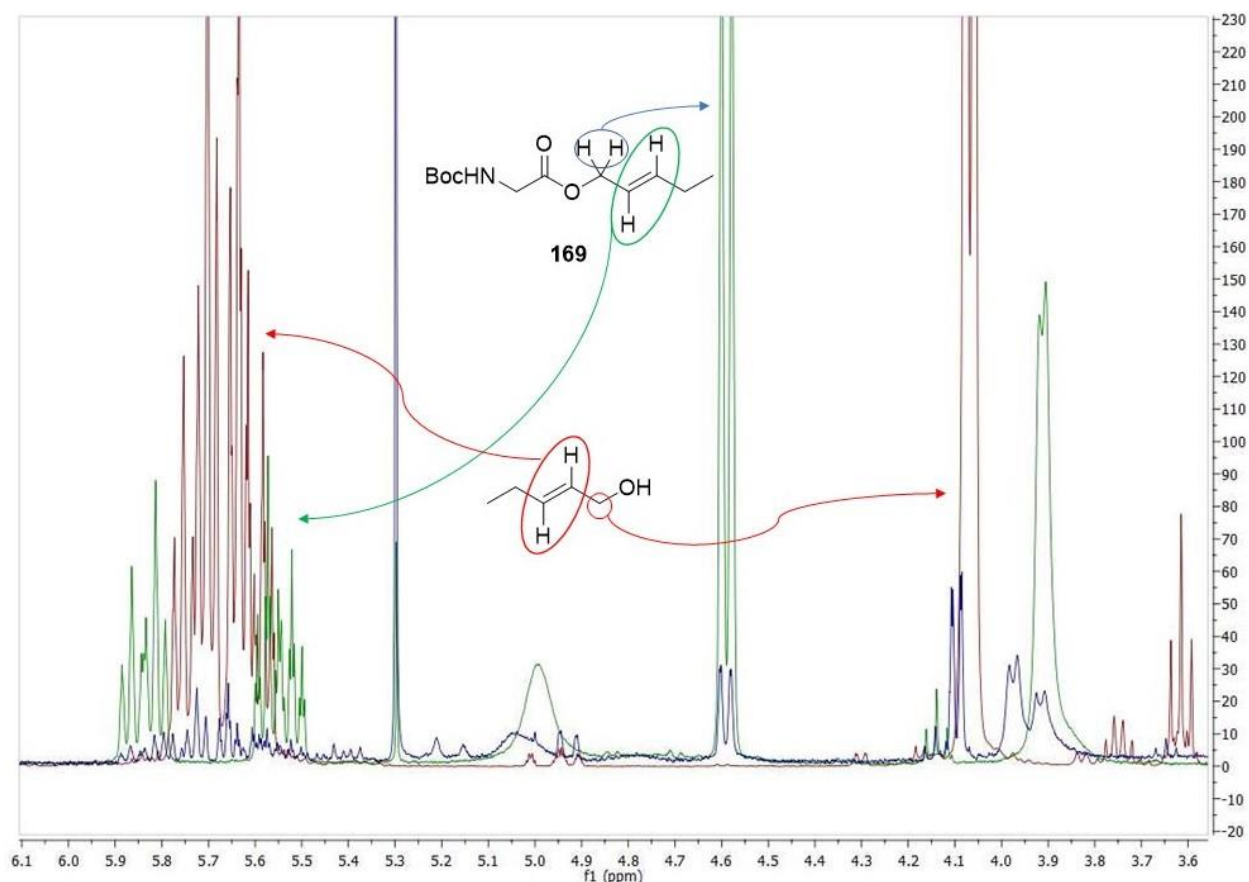
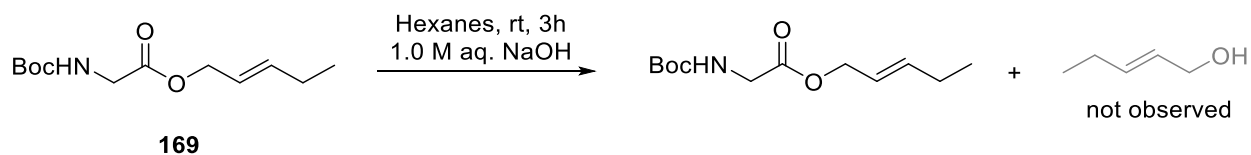


Figure 2. 14 – Overlap of the $^1\text{H-NMR}$ zoomed in the double bond region,.: red – *trans*-2-penten-1-ol, green – **169**, and blue – crude reaction mixture of entry 3 from Table 2.23 (300 MHz in CDCl_3).

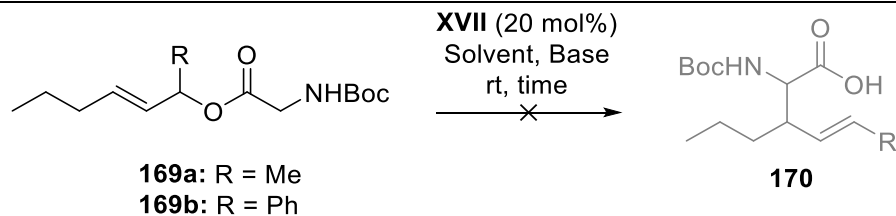
To determine if the hydrolysis side-reaction was inherent to the reaction conditions employed or if **XVII** was involved, a test reaction was done under the same conditions but without the addition of **XVII** (Scheme 2.30). After the same amount of time (6h), no hydrolysis product was observed by TLC leading us to believe that the ester was not being destroyed in the interface between the two solvents and that indeed **XVII** was bringing the hydroxyl anions to the organic layer but, they were acting as nucleophiles and not as a bases like we wished.



Scheme 2. 30 – Test reaction to study the hydrolysis of the starting ester.

Based on these results, we decided to test a new series of esters derived from secondary allylic alcohols in an attempt to hinder the hydrolysis reaction (Table 2.23).

Table 2. 23 – Test reactions for the enantioselective IC under APTC conditions.

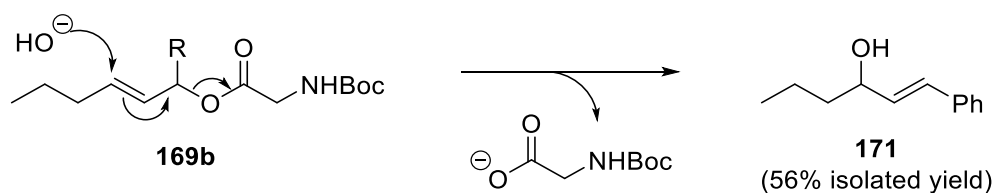


Entry	Substrate	R	Solvent	Base	Time (h)
1	169b	Ph	Toluene	NaOH (1.0 M)	24
2	169b	Ph	Hexanes	NaOH (1.0 M)	24
3	169b	Ph	CH ₂ Cl ₂	NaOH (1.0 M)	24
4	169b	Ph	Et ₂ O	KOH (5.0 M)	24
5	169b	Ph	Toluene	KOH (5.0 M)	24
6	169b	Ph	Hexanes	KOH (5.0 M)	24
7	169a	Me	iPrOH	KOtBu (2.5 equiv)	4.5
8	169a	Me	iPrOH	KOtBu (5.0 equiv)	4.5
9	169a	Me	iPrOH	KOtBu (10.0 equiv)	4.5

All reactions performed on a 0.2 mmol scale in respect to **169a** or **169b**.

The addition of a methyl substituent in the alcohol (R = Me, substrates **169a**) did not hinder the hydrolysis side-reaction as TLC analysis indicated hydrolysis to the starting alcohol, probably from adventitious water from the iPrOH and the hygroscopic base (Table 2.23, entries 7 – 9). On the other hand, adding a bulkier phenyl ring to the alcohol moiety (R = Ph, substrates **169b**) did prevent the standard hydrolysis to take place, i.e. direct attack on the carbonyl carbon. TLC analysis of these reaction (Table 2.23, entries 1 – 6) indicated the formation of a new product, with a lower *rf* than the starting ester which would be consistent with the IC product. Furthermore, NMR analysis of the reaction performed in CH₂Cl₂ (this reaction was chosen because it showed the highest conversion by TLC) also seemed to indicate that the desired IC product was present as the double bond region as well as the aromatic protons became deconvoluted with the multiplicities and chemical shifts consistent with the IC product. However, careful

analysis of the ^1H NMR spectrum indicated the absence of the expected doublet corresponding to the α -proton of the IC product as well as the lack of the 9 protons singlet of the Boc group (Figure 2.15). ^{13}C NMR was also inconsistent with the IC product as the carbonyl carbon of the carboxylic acid (at c.a. 170 ppm) and the carbonyl carbon of the Boc group (at c.a. 148 ppm) were missing (see Annexes). With these results, we concluded that hydrolysis of this substrate also took place but, by a different path than direct attack on the carbonyl carbon (Scheme 2.31). Alcohol **171** is indeed the observed product of this reaction as the NMR spectra are consistent with it.



Scheme 2.31 – Mechanism for the elimination of *N*-Boc glycinate group in ester **169b** with subsequent production of alcohol **171**.

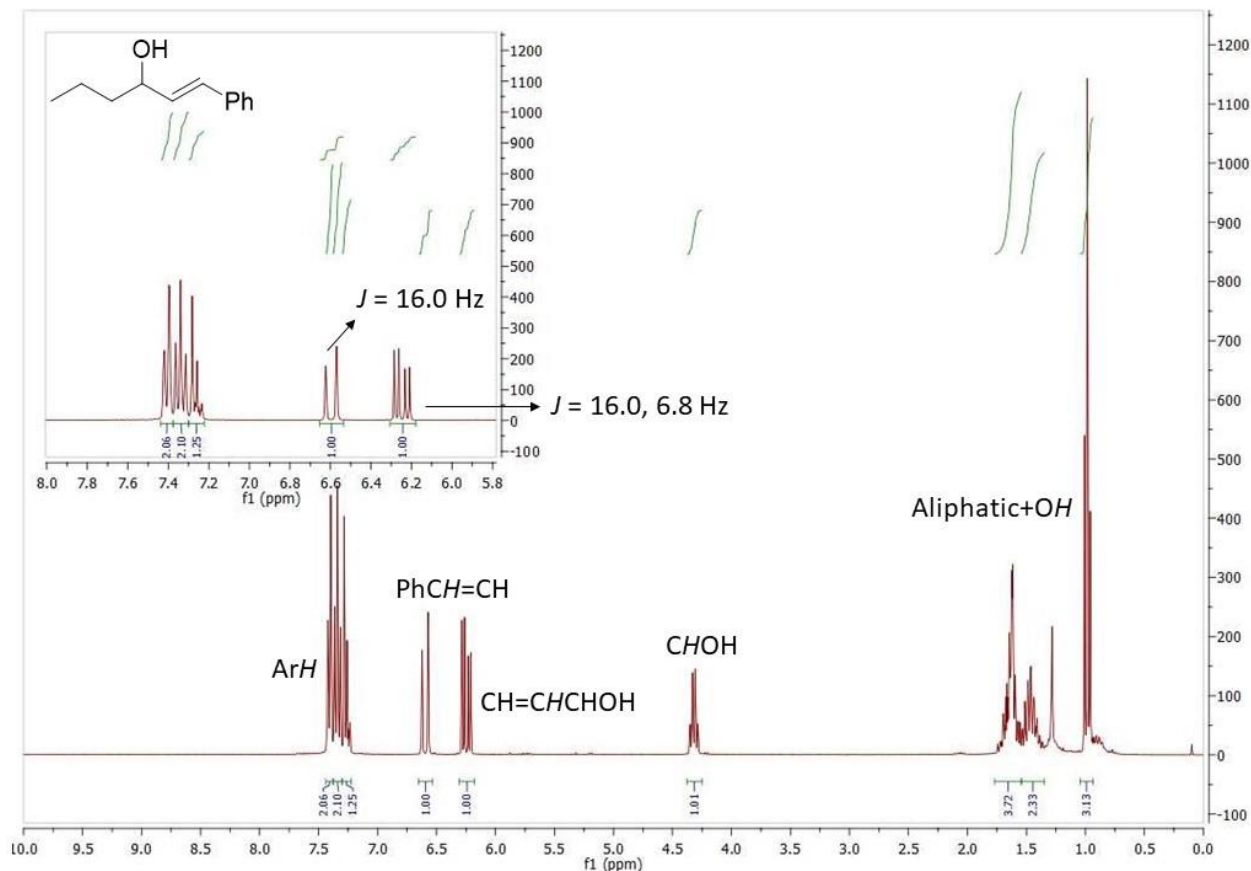
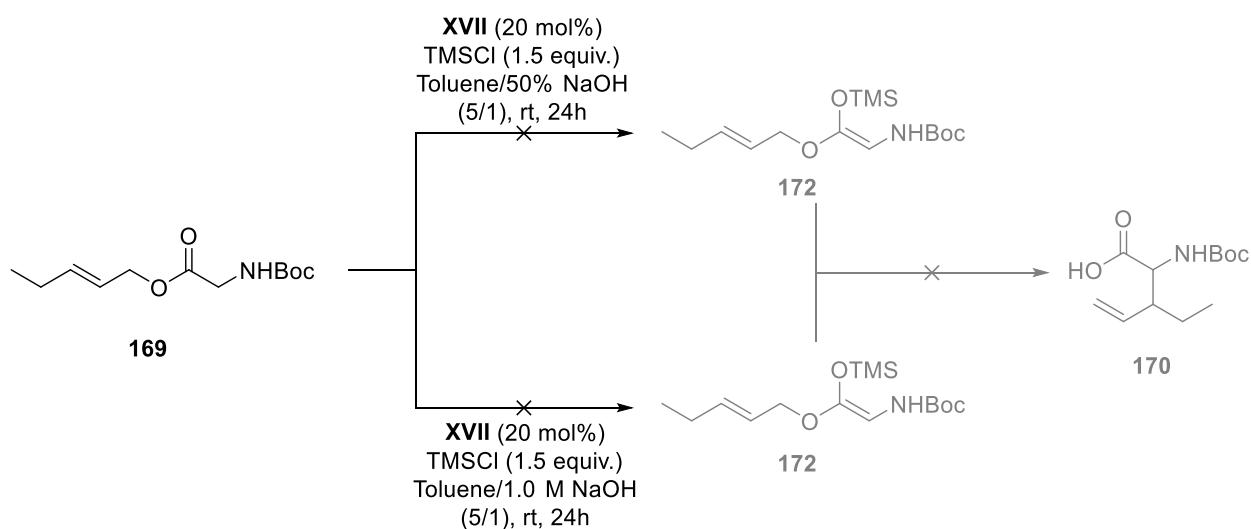


Figure 2.15 – ^1H NMR spectrum of alcohol **171** (300 MHz in CDCl_3).

According to the literature, in this type of phase-transfer catalysis, the deprotonation usually takes place in the interface between the two solvents.²³¹ With that in mind, a couple of test reactions were performed, following similar conditions to those employed by Lygo and co-workers for the alkylation of glycine imine esters²³² with addition of TMSCl as an attempt to trap the enolate **172** and hopefully allow it to undergo the desired IC reaction (Scheme 2.32). To be noted though, that an enantioenriched product was not expected via this approach as the enolate would now exist as a silyl ether and therefore, would not form any chiral salt with the APTC.

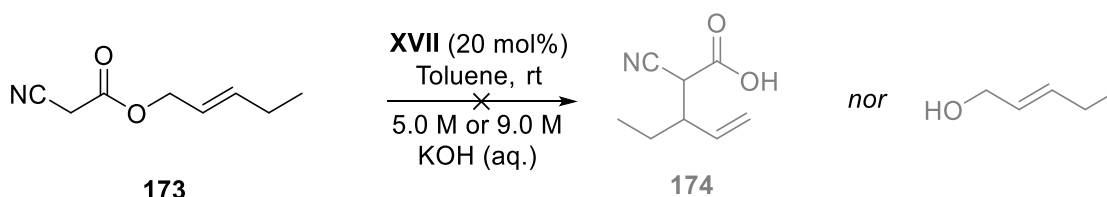


Scheme 2.32 – Enolate trapping experiments.

Two reactions were attempted, one with under highly basic conditions (50% aq. NaOH), following Lygo's procedure, and another with milder basic conditions (1.0 M aq. NaOH) but, TLC analysis showed, like before, hydrolysis of the starting materials and no indication of the formation of the trapped enolate and/or IC product. It is possible that the enolate forms to some extent under the reaction conditions employed but the acid/base equilibrium between enolate/ester and subsequent hydrolysis of the ester takes place faster than the desired IC.

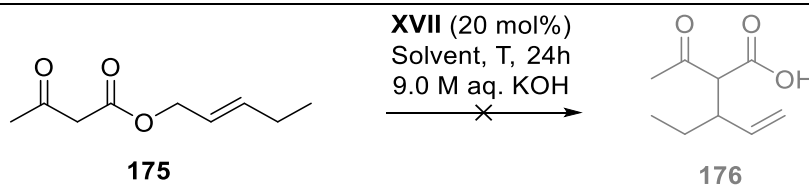
With the results obtained so far, it became evident that the substrates were keener to undergo hydrolysis under APTC than to form the enolate and subsequent desired IC. Ergo, we decided to use more acidic esters which, hopefully, undergo enolate formation more easily and subsequent IC rearrangement.

Initial screening was done using cyanoacetate ester **173**, prepared from cyanoacetic acid and *trans*-2-penten-1-ol (see Chapter IV for more details) in toluene using either 5.0 M or 9.0 M aq. KOH but, after 24h at room temperature, no new spots were observed in the TLC (Scheme 2.33). Curiously, hydrolysis of this ester was not observed which could indicate that the required enolate could be forming and therefore, hydrolysis was hindered due to the increased electron density around the carbonyl carbon. Unfortunately, the IC was not taking place either possibly caused by the fact that the enolate of ester **173** is too stable to undergo the desired rearrangement under the reaction conditions employed.



Scheme 2.33 – Test reaction for the APTC IC reaction using ester **173**.

Table 2.24 – Test reactions for the enantioselective IC of **175** under APTC conditions.



Entry	Solvent	T (°C)
1	Toluene	rt
2	Toluene	40
3	CH ₂ Cl ₂	rt

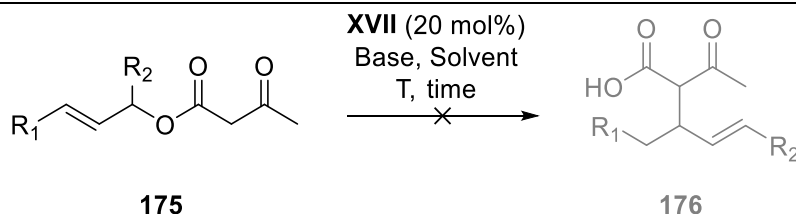
All reactions performed on a 0.2 mmol scale, in respect to **175**, a 1/1 ratio of organic solvent/aq. KOH was used.

The other substrate we decided to use was the β -ketoester **175** (Table 2.24), which could be prepared through a *trans*-esterification of ethyl acetoacetate and *trans*-2-penten-1-ol (see Chapter IV for more information). Unfortunately, no IC product was observed after 24h under the reaction conditions depicted in Table 2.24. Performing the reaction in Toluene at rt seemed to indicate, by TLC, that the starting material was consumed after 24h, however, upon acidic work up and extraction only the starting ester was

recovered (Table 2.24, entry 1). Increasing the temperature to 40 °C, under the same conditions, led to hydrolysis of the starting material as well as the use of CH₂Cl₂ as solvent (Table 2.24, entries 2 and 3).

With these disappointing results, it is obvious that the presence of water and/or the use of hydroxyl bases is detrimental to the desired IC reaction and only hydrolysis of the starting esters is observed. We decided to switch gears and try a solid/liquid phase-transfer approach using strong, non-nucleophilic bases in organic solvents with catalyst **XVII** being used to aid in the solubility of the bases via cation exchange, as well as keep using the more acidic β -ketoesters **175** which have a pK_a \approx 14 for the α -proton making them more likely to undergo the required α -deprotonation and subsequent formation of the reactive enolate (Table 2.25).

Table 2. 25 – Test reactions for the enantioselective IC of **175** under APTC conditions.



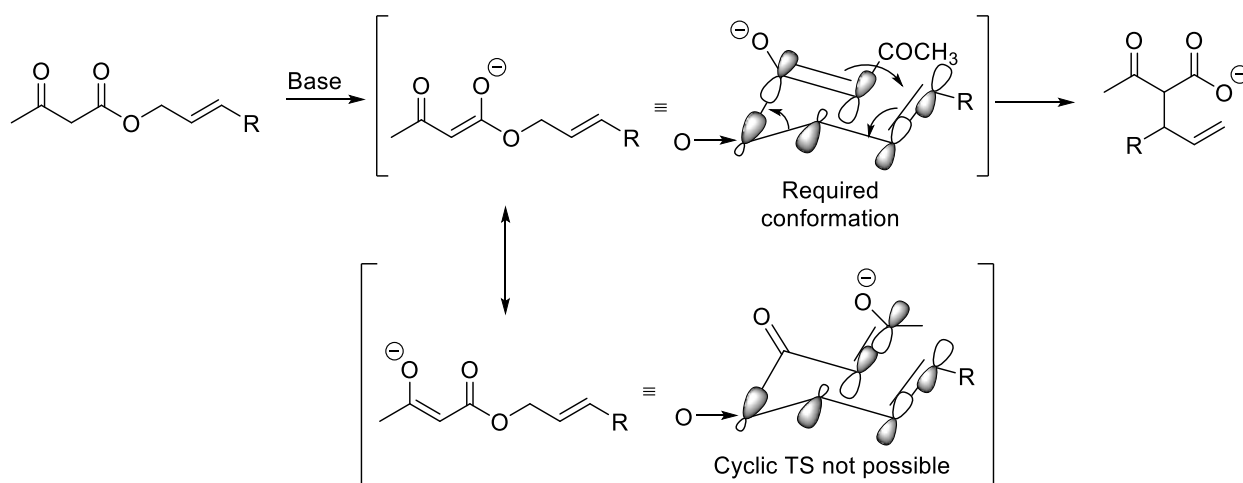
Entry	R1	R2	Solvent	Base (equiv.)	T (°C)	Time (h)	Product
1	Et	H	iPrOH	KOtBu (2.5)	rt	24	SM
2	Et	H	DMSO	KOtBu (2.5)	rt	4	SM
3	Et	H	DMSO	KOtBu (2.5)	rt	120	SM
4	Et	H	Diglyme	KOtBu (2.0)	90	96	SM
5 ^a	Et	H	Diglyme	NaOH (2.0)	90	96	Hydrolysis
6	Ph	H	1,4-Dioxane	KOtBu (2.5)	rt	24	SM
7	Pr	Me	Toluene	KOtBu (2.5)	rt	24	SM
8	Pr	Me	Toluene	KOtBu (2.5)	reflux	24	SM
10 ^a	Ph	H	THF	NaOH (1.0)	reflux	24	SM

All reactions performed on a 0.2 mmol scale in respect to **175**; (a) freshly grinded NaOH was used; SM – starting material.

As it is clear from Table 2.25, none of these trials afforded the desired IC product. The reaction in DMSO appeared to indicate, by TLC, that a new product was being formed after 4h. This may have been caused by the high polarity of DMSO that distorted the *r_f* values in the TLC because, after acidic work up

and extraction, only starting material was isolated. The reaction was repeated and left for a longer period of time which also failed to give the IC product (Table 2.25 entries 2 and 3). Heating the reaction did not seem to help either (Table 2.25 entries 4, 5, 8 and 10). Also, the use of NaOH as a base was further proven to be detrimental to this reaction with hydrolysis being observed when diglyme was used as solvent. However, when using the same base in THF, only SM was observed after 24h under reflux (Table 2.25, entry 5 vs entry 10). This fact could be explained by the amount of base used but, most likely, it was due to the higher solubility of NaOH in diglyme over THF.

However, the results using KOtBu were intriguing. The difference in pKa's between the base and the ester used (pKa \approx 17 and 14.2, respectively) should allow for complete deprotonation of the starting ester and consequent formation of the desired enolate with a Keq \approx $10^{2.8}$ for the corresponding acid base equilibrium. The inability of KOtBu to promote the desired IC rearrangement of ester **175** could be caused by two factors, the first, the enolate is formed but the electrons do not align themselves in the required cyclic array for the IC to take place, preferring to populate the ketone oxygen (Scheme 2.34) and second, the enolate is too stable due to the delocalization of the electrons between the two carbonyl groups which increases the barrier for the IC to occur once the enolate is formed.



Scheme 2.34 – Required conformation of the enolate for the TS of the IC reaction (top) vs non-viable conformation of the enolate (bottom).

Parallel to the APTC approach, we also tried the use of thioureas to promote the activation and subsequent IC rearrangement of allylic esters. Our initial attempts focused on using the non-chiral and commercially available thiourea **XVIII** in stoichiometric amounts and several bases, to see if the desired IC product was formed. If a positive outcome was to be accomplished, we would then proceed to test the viability of this protocol with catalytic amounts of thiourea **XVIII** as well as starting to develop a chiral variant that could induce asymmetry to the transformation (Table 2.26).

Table 2. 26 – Thiourea **XVIII** induced IC reaction.

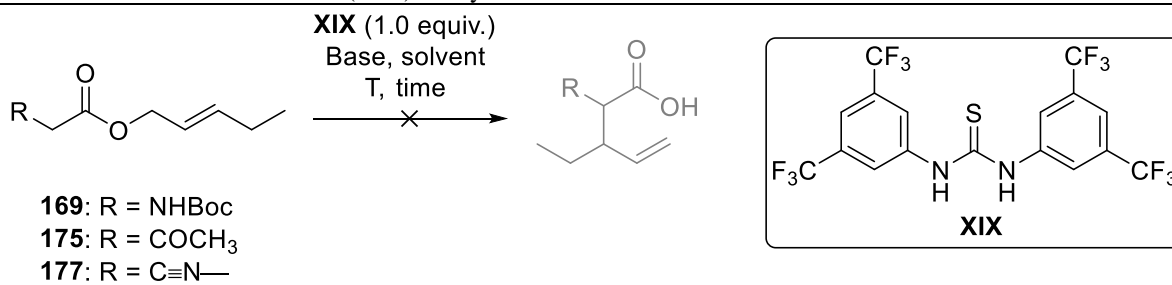
Entry	Base (equiv.)	Solvent	T (°C)	time (h)	Product
1	Cyclohexylamine (1.0 equiv.)	Toluene	rt	48	x1a
2	Cyclohexylamine (1.0 equiv.)	Toluene	60	24	x1a
3	DMAP (1.0 equiv.)	Toluene	rt	48	x1a
4	DMAP (1.0 equiv.)	Toluene	40	24	x1a
5	DBU (1.0 equiv.)	Toluene	rt	48	x1a
6	DBU (1.0 equiv.)	Toluene	90	24	x1a

Unfortunately, our initial attempts did not provide the desired IC product regardless of base or temperature tested. Furthermore, it was observed that the thiourea employed was not very soluble in organic solvents which could have contributed to the failure of these reactions. So, we decided to test Schreiner's thiourea **XIX**, which exhibits better solubility in a wide range of organic solvents as well as being a better H-bond donor due to the presence of the electron deficient aromatic rings attached to the nitrogen atoms (Table 2.27).

For these initial experiments, we used three different substrates, **169**, **175** and **177**. However, none produced the desired IC product. The reaction depicted in Table 2.27, entry 1, which made use of the strongest base, did not provide the IC product, most likely due to the higher acidity of the thiourea protons

vs the α -protons of the ester, making it possible that the thiourea got deprotonated instead of the ester, leading to a weaker base present in solution and also, disabling H-bond activation process desired. Not surprisingly, pyrrolidine did not afford any product (Table 2.27, entry 2) nonetheless, we thought it would be interesting to test it as it would be an easy scaffold to introduce in the thiourea should this mode of activation prove favourable for the IC rearrangement. The use of the stronger organic base 1,8-diazabicyclo[5.4.0]undec-7-ene (DBU) also failed to produce the desired product (Table 2.27 entry 9) Sadly, the use of stronger inorganic bases in high loadings, did not provide any viable alternative for the reaction we wanted and only starting materials were observed under the reaction conditions employed (Table 2.27, entries 3 to 6 and 8). Treatment of ester **175** with a primary amine base and a thiourea also failed to provide the desired product (Table 2.27, entry 7).

Table 2. 27 – Schreiner’s thiourea (**XIX**) catalyzed IC reaction.



Entry	R	Base (equiv.)	Solvent	T (°C)	time	Product
1	NHBoc	KHMDS (1.5 equiv.)	THF	-78 to rt	24h	169
2	CN—	Pyrrolidine (1.5 equiv.)	Dioxane	rt	7 days	177
3	NHBoc	Cs ₂ CO ₃ (3.0 equiv.)	Dioxane	rt	24h	169
4	CN—	Cs ₂ CO ₃ (3.0 equiv.)	Diglyme	rt	24h	177
5	NHBoc	KOtBu (3.0 equiv.)	Diglyme	rt	8 days	169
6	CN—	KOtBu (3.0 equiv.)	Diglyme	rt	8 days	177
7	COCH ₃	 (2.0 equiv.)	CDCl ₃	rt	48h	175
8	NHBoc	NaH (2.0 equiv.)	Toluene	rt	48h	169
9	NHBoc	DBU (2.0 equiv.)	CH ₃ CN	rt	48h	169

Very recently, in 2019, Mečiarová and Šebesta reported a mechanistic study employing both computational methods and synthetic experiments, to study the effects of thiourea and squaramide catalysts in the IC rearrangement and discovered that these type of catalysts not only fail to provide good stereo- and diastereocontrol but also seem to slow down the reaction.²³³ The authors treated cinnamyl ester with a large excess of NEt_3 and TMSOTf and obtained the IC products in good yields albeit low diastereoselectivities and upon addition of either a thiourea or a squaramide catalyst, the yields started to drop, under the same reaction conditions. Upon DFT calculations the authors concluded that the H-bond catalyst would form a very stable complex with the silyl ether enolate which would inherently increase the activation energy for the IC process therefore, slowing the reaction down.

In view of the results obtained and with this recent report, it is not surprising that the H-bond approach did not furnish the desired IC product.

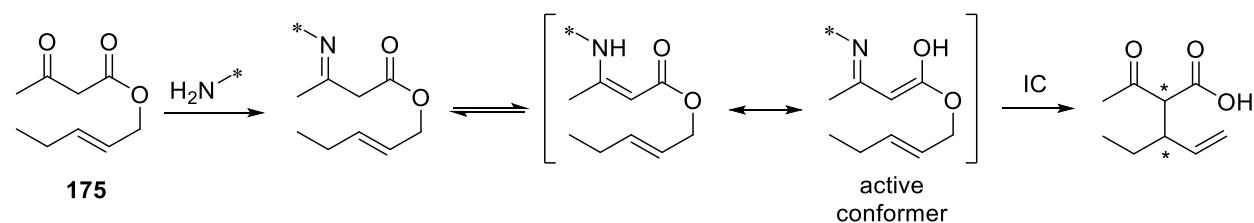
Nonetheless, a few more attempts were done to achieve an asymmetric variant of the IC rearrangement but this time we decided to try and use chiral auxiliaries instead of catalysts. The first trials involved the use of guanidines which are strong organic bases that could possibly promote the required α -deprotonation of the starting ester, to form the required enolate. For this purpose, commercially available TBD was used in stoichiometric amounts and as a last attempt, the chiral bifunctional guanidine **XX** was also tested (Table 2.28). Furthermore, we used malonate **178** to facilitate the formation of the enolate with the required conformation to undergo the IC rearrangement.

The commercially available TBD did not afford the desired IC product under the reaction conditions employed. Guanidine **XX** was still prepared (see Chapter IV for more information) as its H-bond/Brønsted base bifunctionality could prove useful in activating, deprotonating, and stabilizing the starting material. Since guanidine **XX** was isolated as its HCl salt, K₂CO₃ was added to free base the guanidine in situ leaving it available to deprotonate the ester. Furthermore, the pK_a of K₂CO₃ also allowed for the deprotonation of **178** which could still form H-bond with **XX** and hopefully undergo the IC rearrangement in an asymmetric fashion. Unfortunately, no reaction was observed with **XX**.

Table 2. 28 – Guanidine induced IC rearrangement.

Entry	Guanidine	Base (equiv.)	Solvent	T	Time (h)	Product
1	TBD	—	CH ₂ Cl ₂	rt	96	178
2	TBD	—	THF	rt	96	178
3	TBD	—	Toluene	rt	96	178
4	X	KOtBu (1.5 equiv.)	THF	rt	96	178

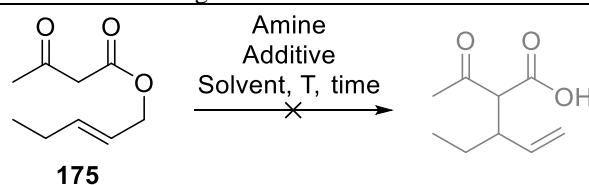
Up to this point, only fairly weak, non-covalent interactions had been used between the catalysts and the esters (ionic forces and H-bond interactions). Hence, heating was mostly avoided to ensure proper activation. Since the IC rearrangement, sometimes, requires reflux conditions, we decided to use primary amine catalysts with the keto-ester **175**. With this substrate and catalyst system, covalent bonds would be formed and, therefore, higher temperatures could be tried without compromising any possible enantioselectivity (Scheme 2.9).

**Scheme 2. 35** – Rationale for the new approach to the IC rearrangement.

For this purpose, two primary amine catalysts, **XIII** and **XIV** were prepared (see Chapter IV for more information) and used with ester **175** (Table 2.29). We decided to test the primary amines both in catalytic amounts as well as in stoichiometric amounts in the presence of Brønsted acid or base additives which could prove useful in facilitating either enamine formation (acid additive) or enol formation (base additive).

Surprisingly, none of these reactions afforded the desired IC product, regardless of the high temperatures used and extended reaction times (up to 9 days). It is highly unlikely that the catalysts failed to condense with the ketone moiety of the starting material, however, it is possible that the condensation led to the imine product only and no enamine was formed and thus, no active conformer of the enol was ever present in the reaction medium so, no IC rearrangement took place.

Table 2. 29 – Primary amine induced IC rearrangement of ester **175**.



Entry	Amine (mol%)	Additive	Solvent	T (°C)	Time (days)	Product
1	XIV (20 mol%)	—	THF	50	9	175
2	XIV (20 mol%)	NEt ₃	THF	50	9	175
3	XIV (20 mol%)	BA	THF	50	9	175
4	XIII (20 mol%)	—	THF	50	9	175
5	XIII (20 mol%)	NEt ₃	THF	50	9	175
6	XIII (20 mol%)	BA	THF	50	9	175
7	XIV (100 mol%)	NEt ₃	Toluene	120	7	175
8	XIV (100 mol%)	BA	Toluene	120	7	175
9	XIII (100 mol%)	NEt ₃	Toluene	120	7	175
10	XIII (100 mol%)	BA	Toluene	120	7	175

After all these experiments, it seems that the IC rearrangement is a tricky reaction, and an asymmetric organocatalyzed approach is not viable. Phase-transfer catalysis led to decomposition of starting materials and/or to formation of non-active enolates (Figure 2.2). H-bond catalysis did not provide an answer either and, with the recent studies from Mečiarová and Šebesta (*vide supra*), can prove to be detrimental to reactivity. Primary amines in conjunction with keto-esters also failed to deliver the desired reaction. However, guanidines could prove useful, specially if used as a chiral auxiliary. Their reactivity was not thoroughly tested but, perhaps, a wise choice of chiral guanidine and substrate could lead to the

desired product. Addition of a scavenger base such as DBU or DABCO could even allow for a catalytic variant with guanidines however, a wider range of these compounds would have to be prepared and tested.

Part III – Conclusions

In this Dissertation, we explored the role of organocatalysts in asymmetric Organic synthesis, more specifically, the applications and mechanistic considerations of aminocatalysts in pericyclic reactions. We performed a DFT study on the role of aminocatalysts in promoting the dearomatization of several heteroaromatic aldehydes in order to form electron-rich trienamine intermediates, some of which have already been explored in asymmetric synthesis. Our discoveries suggest that, upon condensation of the aminocatalyst with the parent aldehyde and subsequent iminium ion formation, the energy penalty for loss of aromaticity was generally decreased in all systems studied, making them excellent candidates for further applications in asymmetric Organic Synthesis. Population analysis of the trienamine systems was also performed and showed that careful design of the starting materials could impact the regioselectivity of these systems by increasing the electron density at either the more remote ϵ -position or at the γ -position. This regioselectivity could also be manipulated by careful choice of the aminocatalyst to employ as some literature work by Chen and co-workers seems to support.

Furthermore, it was also demonstrated that the Nitrogen containing heteroaromatic aldehydes as well as the all-carbon systems could give rise to (hetero)fulvene which proved to be thermodynamically more favoured than their corresponding trienamine counterparts. These fulvenes could open the door to new approaches in higher-order cycloaddition reactions.

Following the results obtained from the aforementioned project, we decided to explore some of its systems in the asymmetric synthesis of dihydropyrido[1,2-*a*]indole scaffolds. For this purpose, two approaches were envisioned. The first approach relied on an intramolecular Michael addition reaction proceeding through a dienamine intermediate whilst the second approach consisted of an aza-Diels-Alder reaction using a hetero-cross-trienamine intermediate. In respect to the intramolecular Michael addition, our initial screening of catalysts failed to produce the desired product. The use of a primary amine catalyst gave only the imine intermediate which, regardless of our efforts, did not tautomerize to the desired reactive dienamine, while the use of secondary aminocatalysts either failed to produce the dienamine intermediate or gave rise to the hydroamination product of our Michael acceptor. Further screening of secondary

aminocatalysts was performed but no reaction was observed and, when one full equiv. of catalyst was used, no indication of the presence of the dienamine intermediate was observed by ^1H NMR spectroscopy.

Similarly, the aza-Diels-Alder approach also failed to produce the desired product. Several dienophiles, including the highly reactive nitrostyrene and *N*-Boc-3-olefinic oxindoles were tested but no reaction was observed. Screening of multiple secondary aminocatalysts was also performed and again, even when one equiv. of catalyst was used, no aza-cross-trienamine (or iminium ion precursor) were observed by ^1H NMR. It appears that the relative position of the aldehyde moiety in respect to the indole Nitrogen atom is detrimental to the ability of the aminocatalyst to condense with the aldehyde to form the reactive intermediary species. This can be caused by electronic effects which decrease the nucleophilicity of the carbonyl carbon. A possible way to circumvent the lack of electrophilicity of the aldehyde would be to extend the conjugation and use a trienamine, analogous to that described in Model System D and used by Melchiorre and co-workers. It is also possible that some of the catalysts tested may have been too bulky to condense with this aldehyde. Therefore, neither of these two approaches, the intramolecular Michael addition nor the aza-Diels-Alder reaction, were successful at achieving the desired dihydropyrido[1,2-*a*]indole scaffolds. Nonetheless, further studies on the reactivity of these systems could be performed as perhaps a more suitable dienophile or a stronger nucleophile may react in the desired fashion. Moreover, H-bond catalysis may prove to be a better way of achieving the desired reactivity. However, changes to its structure may be required namely, the addition of a better H-bond acceptor group.

Another project explored in this Dissertation was the attempt to synthesize an oxo-fulvene and use it as a precursor to an electron-rich tetraenamine intermediate, upon condensation with a suitable aminocatalyst. This tetraenamine would incorporate the fulvene moiety and hopefully higher-order cycloadditions could be achieved between this intermediate and suitable alkenes. Unfortunately, it appeared that the fulvene moiety was preventing the formation of the desired aldehyde. After several synthetic approaches no oxo-fulvene was obtained and in some cases complete decomposition of the starting material was observed. Upon more careful analysis of the literature, it became clearer how the polarization on the exocyclic double bond of the fulvene could be affecting the reactivity on the side chain of the fulvene. The

starting material for this project was never obtained and studies are underway to provide a better explanation on why, and how this fulvene proved to be so elusive.

Finally, the last project studied in this Dissertation was the development of an organocatalyzed, asymmetric Ireland-Claisen rearrangement. Two approaches were initially envisioned, one based on H-bond catalysis which would, hopefully, provide activation to the starting ester with consequent decrease of the pKa of the α -protons and stabilization of the enolate intermediary and the second approach was based on asymmetric phase-transfer catalysis where, strong inorganic bases could be used in aqueous solution and be brought into the organic phase, by the APTC to perform the required α -deprotonation and formation of the necessary enolate. In both approaches chiral organocatalysts would be used to provide the necessary facial differentiation. Another objective of this project would be the ability to synthesize enantioenriched non-natural α -substituted amino acids. After all the experiments, it seems that the IC rearrangement is a tricky reaction, and an asymmetric organocatalyzed approach is not viable. Phase-transfer catalysis led to decomposition of starting materials and/or to formation of non-active enolates while H-bond catalysis did not provide an answer either and, with the recent studies from Mečiarová and Šebesta, (*vide supra*)²³³ can prove to be detrimental to reactivity. Primary amines in conjunction with keto-esters also failed to deliver the desired reaction. However, guanidines could prove useful, specially if used as a chiral auxiliary. Their reactivity was not thoroughly tested but, perhaps, a wise choice of chiral guanidine and substrate could lead to the desired product. Addition of a scavenger base such as DBU or DABCO could even allow for a catalytic variant with guanidines however, a wider range of these compounds would have to be prepared and tested.

Overall, in this Dissertation we studied and showcased some of the advantages of aminocatalysis as well as its limitations. The computational study on the dearomatization of heteroaromatic aldehydes illustrated the ability of aminocatalysts to form what could be theorized as an improbable intermediate – a dearomatized system. However, the computational analysis started from the premise that the aminocatalyst would condense with the starting aldehyde. In the subsequent project, on the synthesis of dihydropyrido[1,2-*a*]indole scaffolds, it became apparent that not all systems will undergo condensation

between the aldehyde moiety and the aminocatalyst to form the corresponding iminium ion which can undergo dearomatization to form an electron-rich poly-enamine system. The effects on fulvene systems on the reactivity of their side chain groups also become apparent in our pursuit of an oxo-fulvene compound that could be a useful precursor to tetraenamine systems that could undergo higher-order cycloadditions. Finally, the development of an asymmetric and catalytic methodology for the Ireland-Claisen rearrangement proved to be a very challenging due to both the inherent liability of esters under basic aqueous conditions as well as the very high pKa's of the α -protons. Therefore, it is not surprising that the asymmetric variants for this reaction all use chiral auxiliaries in stoichiometric amounts.

Part IV – Experimental Section

General Methods

NMR spectra were acquired on Bruker Avance 300 spectrometer at 300 MHz and 75 MHz for ^1H and ^{13}C , respectively. Chemical shifts (δ) are reported in ppm in respect to the solvents' residual signals. The following abbreviations are used to indicate the multiplicity in NMR spectra: s, singlet; d, doublet; t, triplet; q, quartet; p, pentet; dd, doublet of doublets; dt, doublet of triplets; td, triplet of doublets; ddd, doublet of doublets of doublets; m, multiplet; and br, broad resonance.

Thin layer chromatography (TLC) was performed using pre-coated aluminium-backed plates (Merck Kieselgel 60 F254) and visualized using either UV light, KMnO_4 dip, dinitrophenylhydrazine (DNP) dip or Iodine chamber. For flash column chromatography (FC) silica flash 40-63 μm (230-400 mesh), from Silicycle, was used.

All reagents and solvents were purchased from Sigma Aldrich or Fisher and, unless noted otherwise, were used as received without further purification. Anhydrous solvents were distilled according to standard laboratory techniques using the appropriate drying agent²³⁴ and were stored in 4Å molecular sieves under Argon atmosphere.

2-Iodoxybenzoic acid (IBX) was synthesized based on a literature procedure²³⁵ and stored in the freezer ($T \approx -20\text{ }^\circ\text{C}$). (*CAUTION! IBX is explosive under impact or heating to $>200\text{ }^\circ\text{C}$*) The synthesis of IBX went as follows: 2-Iodobenzoic acid (10 g, 40.3 mmol) was added in one portion to a solution of Oxone® (37.1813 g, 60.5 mmol, 1.5 equiv.) in H_2O (135 mL) in a 500 mL round bottom flask. Reaction was heated to $70\text{ }^\circ\text{C}$ and magnetically stirred at this temperature for 3h, adjusting stirring speed to ensure that the mixture went from a hard to stir slur to an easy to stir, finely dispersed suspension. After 3h, reaction was cooled to $0\text{ }^\circ\text{C}$ and left at this temperature, with slow stirring, for 1.5h. Resulting suspension was filtered through a medium porosity sintered glass funnel and solid was rinsed with H_2O (6x20 mL) and acetone (2x20 mL). Resulting solid was air dried over night, giving IBX as a white amorphous solid, in 87% yield with purity consistently $\approx 85\%$, determined by ^1H NMR. Mother and washing liquors were acidic and oxidizing so, they were treated with solid $\text{Na}_2\text{S}_2\text{O}_3$ followed by neutralization with NaOH pellets and

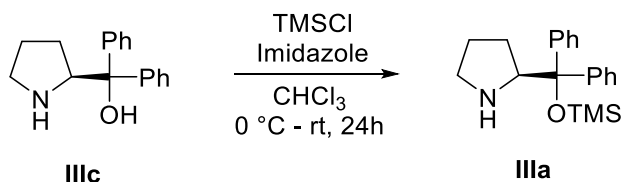
disposed down the sink. ^1H NMR (300 MHz, DMSO) δ 8.14 (d, $J = 7.8$ Hz, 1H), 8.07 – 7.95 (m, 2H), 7.84 (t, $J = 7.3$ Hz, 1H).

Cyclopentadiene was freshly distilled before use, by cracking commercially available dicyclopentadiene at 170-180 °C using a Vigreux column and collected in a flask cooled to -78 °C.

2,3-Dichloro-5,6-dicyano-*p*-benzoquinone (DDQ) was recrystallized from benzene prior to use.

Chapter I – Synthesis and Characterization of Organocatalysts

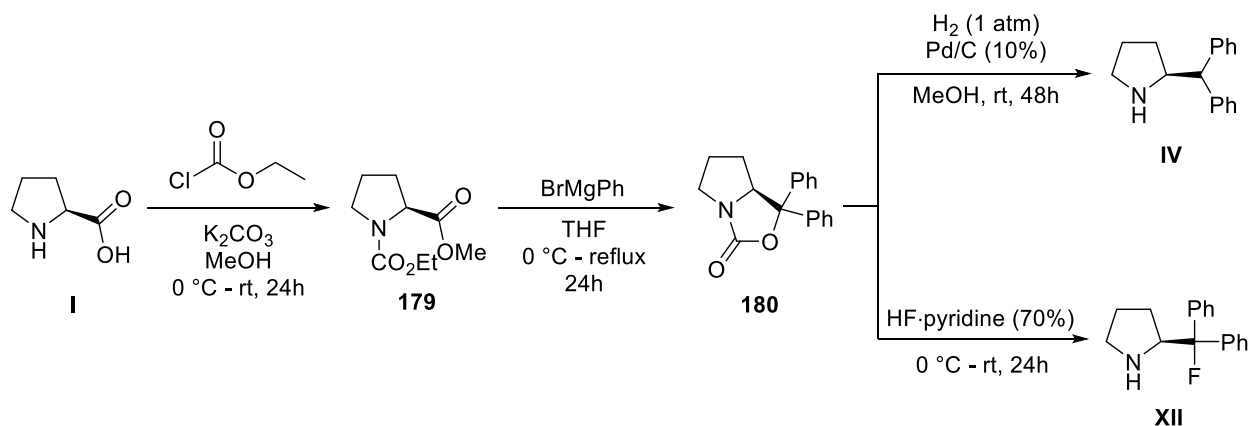
Synthesis of (*S*)-(-)- α,α -diphenyl-2-pyrrolidinemethanol trimethyl silyl ether (**IIIa**):¹⁰⁴



Scheme 4. 1 – Synthesis of catalyst **IIIa**.

(*S*)-(-)- α,α -diphenyl-2-pyrrolidinemethanol, **IIIc**, (1.0 g, 3.95 mmol) was taken in CHCl_3 (10 mL) and cooled to 0 °C. Imidazole (0.81 g, 11.9 mmol 3.0 equiv.) was added, in one portion, followed by dropwise addition of TMSCl (1.25 mL, 9.87 mmol, 2.5 equiv.) and reaction was allowed to warm up to rt. After stirring for 24h at rt, MTBE (25 mL) was added and mixture filtered. Mother liquors were washed sequentially with H_2O (10 mL) and brine (2x10 mL), dried over Na_2SO_4 , filtered and purified by FC using a mixture of EtOAc/Hexanes (4/1) as eluent affording the title catalyst **IIIa** as a yellow oil in 78% yield. ^1H NMR (300 MHz, CDCl_3) δ 7.54 – 7.46 (m, 2H), 7.45 – 7.36 (m, 2H), 7.36 – 7.20 (m, 6H), 4.12 – 4.02 (m, 1H), 2.98 – 2.76 (m, 2H), 1.75 – 1.70 (m, 2H), 1.68 – 1.52 (m, 3H), 1.51 – 1.35 (m, 1H), -0.06 (s, 9H).

Synthesis of (S)-(-)-2-(diphenylmethyl)pyrrolidine (IV)²³⁶ and (S)-(-)-2-(fluorodiphenylmethyl)pyrrolidine (XII):²³⁷



Scheme 4. 2 – Synthetic route for catalysts **IV** and **XII**.

Synthesis of (S)-N-(Ethoxycarbonyl)proline methyl ester (179): Ethyl chloroformate (3.0 mL, 30 mmol, 2.3 equiv.) was added dropwise to a 0 °C mixture of L-proline, **I**, (1.5 g, 13 mmol) and K₂CO₃ (1.80 g, 13 mmol, 1.0 equiv.) in MeOH (12 mL). Reaction was gradually warmed up to rt and left stirring for 24h. Reaction was filtered, mother liquors were concentrated and then taken in Et₂O and washed with brine. Volatiles were removed under reduced pressure to give carbamate **179** as a white solid in 92% yield, which was used in the next step without further purification. ¹H NMR (300 MHz, CDCl₃) δ 4.37 (ddd, *J* = 20.0, 8.5, 3.5 Hz, 1H), 4.25 – 4.04 (m, 2H), 3.76 (d, *J* = 5.5 Hz, 3H), 3.70 – 3.40 (m, 2H), 2.36 – 2.14 (m, 1H), 2.14 – 1.83 (m, 3H), 1.26 (dt, *J* = 21.4, 7.1 Hz, 3H).

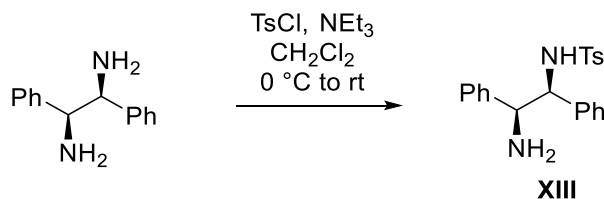
Synthesis of (7aS)-Tetrahydro-1,1-diphenyl-1H,3H-pyrrolo[1,2-c]oxazol-3-one (180): Carbamate **179** (2.39 g, 12 mmol) was taken in dry THF (65 mL) and cooled to 0 °C. A 1.0 M solution of BrMgPh in THF (26.4 mmL, 26.4 mmol, 2.2 equiv.) was added dropwise and resulting mixture was allowed to warm to rt and then heated to reflux for 24h. Reaction was cooled to rt, quenched by careful addition of sat. aq. NH₄Cl and extracted twice with Et₂O. The combined organic extracts were washed with brine, dried over Na₂SO₄, filtered, and purified by FC, using a mixture EtOAc/Hexanes (1/3) as eluent, to give the cyclic carbamate **180** as a white solid in 85% yield. ¹H NMR (300 MHz, CDCl₃) δ 7.60 – 7.50 (m, 2H), 7.49 – 7.21 (m, 8H),

4.59 (dd, $J = 10.5, 5.5$ Hz, 1H), 3.77 (dt, $J = 11.4, 8.0$ Hz, 1H), 3.29 (ddd, $J = 11.5, 9.4, 3.8$ Hz, 1H), 2.14 – 1.84 (m, 2H), 1.84 – 1.69 (m, 1H), 1.17 (dtd, $J = 12.4, 10.7, 8.9$ Hz, 1H). ^{13}C NMR (75 MHz, CDCl_3) δ 160.5, 143.3, 140.3, 128.6, 128.4, 128.3, 127.7, 126.0, 125.5, 85.9, 69.3, 46.1, 29.0, 24.9.

Synthesis of (S)-(-)-2-(diphenylmethyl)pyrrolidine (IV): (*CAUTION: 10% Pd/C is an explosive solid. Reagents and solvent were mixed under Argon atmosphere and then purged with H_2 . During the filtration process, copious amounts of MeOH were used to ensure the Pd would not go dry!*) Carbamate **180** (1.0 g, 3.6 mmol) and 10% Pd/C (242.2 mg) in MeOH (30 mL) were stirred, under an atmosphere of H_2 , for 48h at rt. Upon completion, Pd/C was removed by vacuum filtration, over celite and washed thoroughly with MeOH. Volatiles were removed under reduced pressure and residue purified by FC using MeOH/ CH_2Cl_2 (1/9) as eluent to give catalyst **IV** as a colorless oil, which solidified to a white solid upon storing in the freezer, in 65% yield. ^1H NMR (300 MHz, CDCl_3) δ 7.45 – 7.38 (m, 2H), 7.38 – 7.26 (m, 6H), 7.26 – 7.16 (m, 2H), 3.92 – 3.82 (m, 1H), 3.79 (d, $J = 10.2$ Hz, 1H), 3.14 – 3.01 (m, 1H), 2.97 – 2.82 (m, 1H), 1.94 – 1.69 (m, 4H), 1.53 – 1.36 (m, 1H).

Synthesis of (S)-(-)-2-(fluorodiphenylmethyl) pyrrolidine (XII): Pre-cooled 70% HF·pyridine complex (12.5 mL) was added to carbamate **180** (0.85 g, 3.1 mmol) in a cooled plastic vial. Reaction was gradually warmed up to rt and after stirring for 24h, mixture was cooled down to 0 °C, diluted with Et_2O (12.5 mL) and quenched by very careful addition of 9.0 M aq. KOH to pH \approx 14. Phases were separated and aqueous layer was extracted with Et_2O (3x25 mL). Combined organic extracts were dried over Na_2SO_4 , filtered, and purified by FC using MeOH/ CH_2Cl_2 (1/9) to give catalyst **XII**, as a pale-yellow oil, in 87% yield. ^1H NMR (300 MHz, CDCl_3) δ 7.61 – 7.54 (m, 2H), 7.50 – 7.21 (m, 8H), 4.35 – 4.14 (m, 1H), 3.15 – 3.05 (m, 1H), 3.00 – 2.85 (m, 1H), 2.28 (s, 1H), 1.92 – 1.62 (m, 4H).

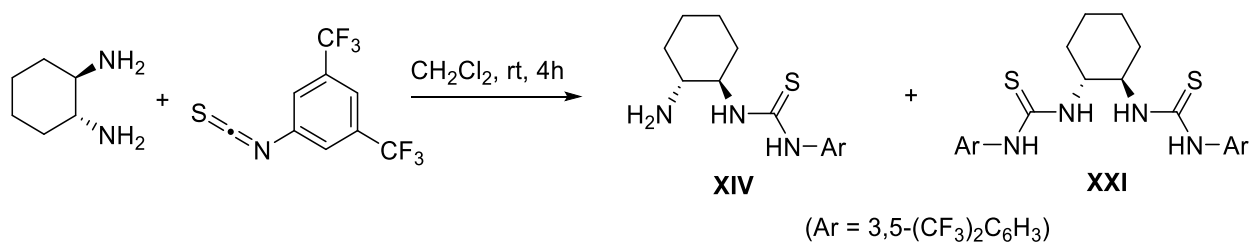
Synthesis of Bifunctional Primary Aminocatalyst (1*S*,2*S*)-(+)-*N*-(4-Toluenesulfonyl)-1,2-diphenylethylenediamine (XIII)²³⁸



Scheme 4. 3 – Synthesis of primary amine catalyst **XIII**.

(1*S*,2*S*)-1,2-Diphenylethylenediamine (0.50 g, 2.4 mmol) was dissolved in CH₂Cl₂ (35 mL) and cooled to 0 °C. NEt₃ (0.38 mL, 2.7 mmol, 1.1 equiv.) was added followed by *p*TsCl (0.47 g, 2.5 mmol, 1.05 equiv.). Reaction was allowed to warm up to rt and stirred for 16h. Reaction was quenched by addition of H₂O (15 mL) and phases were separated. Organic layer was washed with brine (15 mL), dried over Na₂SO₄, filtered, and volatiles removed under reduced pressure. The crude product was purified by FC using a mixture of EtOAc/hexanes (2/1) to give the desired compound **XIII** as a white solid in 76% yield. ¹H NMR (300 MHz, CDCl₃) δ 7.35 (d, *J* = 8.3 Hz, 2H), 7.26 – 7.10 (m, 10H), 7.02 (d, *J* = 8.0 Hz, 2H), 6.07 (s, 1H), 4.41 (d, *J* = 5.1 Hz, 1H), 4.17 (d, *J* = 5.2 Hz, 1H), 2.37 (s, 3H), 1.45 (s, 2H).

Synthesis of Bifunctional Primary Aminocatalyst *N*-[(1*R*,2*R*)-2-Aminocyclohexyl]-*N'*-[3,5-bis(trifluoromethyl)phenyl]thiourea (XIV)²³⁹

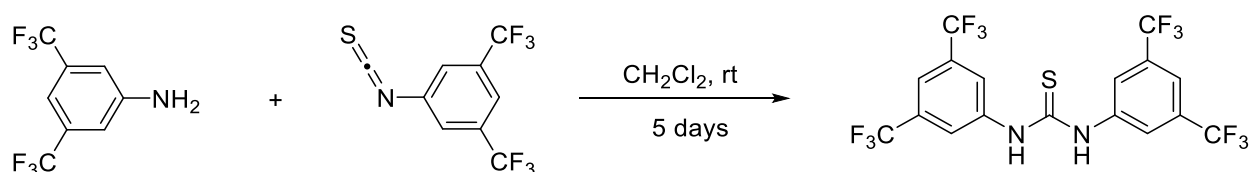


Scheme 4. 4 – Synthesis of primary amine **XIV**.

A solution of 3,5-bis(trifluoromethyl)phenyl isothiocyanate (0.91 mL, 5.0 mmol) in dry CH₂Cl₂ (10 mL) was added dropwise to a solution of (1*R*,2*R*)-1,2-diaminocyclohexane (0.57 g, 5.0 mmol) in

CH₂Cl₂ (10 mL). Reaction was stirred at rt for 4h. Volatiles were removed and residue purified by FC using a gradient starting with CH₂Cl₂ to CH₂Cl₂/MeOH (9/1) to give the desired primary amine **XIV** as a white solid, in 70% yield as well as the bistiourea **XXI** as a pale yellow foam, in 13% yield. *N*-[(1*R*,2*R*)-2-Aminocyclohexyl]-*N'*-[3,5-bis(trifluoromethyl)phenyl]thiourea **XIV**: ¹H NMR (300 MHz, CDCl₃) δ 8.08 (s, 2H), 7.61 (s, 1H), 6.34 (s, 1H), 3.42 (s, 1H), 2.87 – 2.65 (m, 1H), 2.20 – 2.05 (m, 1H), 2.05 – 1.92 (m, 1H), 1.92 – 1.67 (m, 2H), 1.45 – 1.15 (m, 4H); and *N,N'*-(1*R*,2*R*)-1,2-Cyclohexanediylbis[*N'*-[3,5-bis(trifluoromethyl)phenyl]thiourea **XXI**: ¹H NMR (300 MHz, CDCl₃) δ 8.17 (s, 2H), 7.84 (s, 4H), 7.73 (s, 2H), 7.09 (s, 2H), 4.50 – 4.32 (m, 2H), 2.30 – 2.15 (m, 2H), 1.95 – 1.70 (m, 2H), 1.50 – 1.19 (m, 4H).

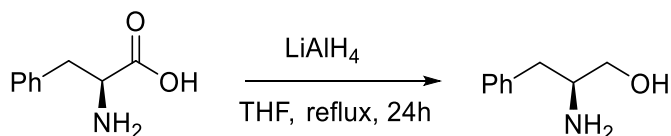
Synthesis of Schreiner's thiourea **XIX**²⁴⁰



Scheme 4. 5 – Reaction scheme for the synthesis of Schreiner's thiourea.

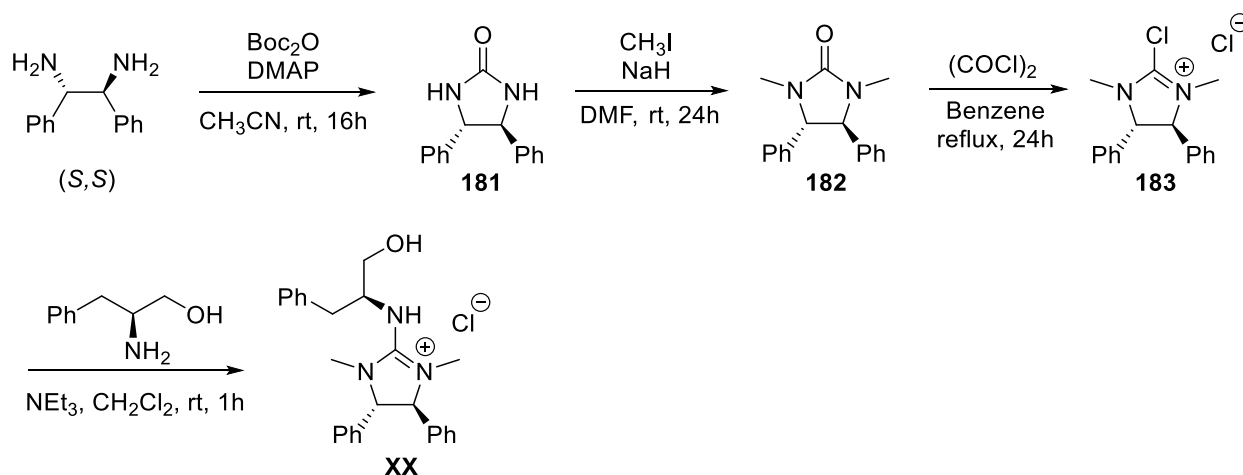
To a stirred solution of 3,5-bis(trifluoromethyl)phenyl isocyanate (0.37 mL, 2.0 mmol) in dry CH₂Cl₂ (4 mL) was added 3,5-bis(trifluoromethyl)aniline (0.31 mL, 2.0 mmol, 1.0 equiv.). The resulting solution was stirred at rt for 5 days, and then filtered. The filtrate cake was washed with cold CH₂Cl₂ (3x5 mL) to give Schreiner's thiourea as a white solid in 67% yield; ¹H NMR (300 MHz, DMSO) δ 10.64 (s, 1H), 8.21 (s, 2H), 7.87 (s, 1H).

Synthesis of Guanidinium **XX**



Scheme 4. 6 – Reduction of *S*-phenylalanine.

LiAlH₄ (0.46 g, 12.0 mmol, 4.0 equiv.) was suspended in dry THF (15 mL) and cooled to 0 °C. *S*-phenylalanine (0.50 g, 3.0 mmol) was added portion-wise and the resulting mixture was heated to reflux for 24h. Reaction was allowed to cool down to rt and was further cooled to 0 °C. Reaction was quenched by slow addition of sat. aq. K₂CO₃ and the resulting slurry was filtered under vacuum. The filtrate cake was thoroughly washed with H₂O and EtOAc. Phases were separated and aqueous layer washed with EtOAc (3x). Combined organic extracts were washed with brine, dried over Na₂SO₄, filtered, concentrated and air dried over night to give the desired *S*-phenylalalinol product, as a pale yellow crystalline solid, in >99% yield. ¹H NMR (300 MHz, CDCl₃) δ 7.43 – 7.18 (m, 1H), 3.67 (dd, *J* = 10.6, 3.9 Hz, 1H), 3.43 (dd, *J* = 10.6, 7.2 Hz, 1H), 3.22 – 3.09 (m, 1H), 2.83 (dd, *J* = 13.5, 5.2 Hz, 1H), 2.56 (dd, *J* = 13.5, 8.6 Hz, 1H). ¹³C NMR (75 MHz, CDCl₃) δ 138.7, 129.2, 128.6, 126.4, 66.4, 54.2, 41.0.



Scheme 4.7 – General reaction scheme for the synthesis of catalyst **XX**.

Guanidinium **XX** was synthesized based on literature procedures^{241,242} and it went as follows:

Synthesis of (4*S*,5*S*)-diphenyl-imidazolidin-2-one (181): (1*S*,2*S*)-Diphenylethylenediamine (0.50 g, 2.4 mmol) and DMAP (0.32 g, 2.6 mmol, 1.1 equiv.) were dissolved in CH₃CN (35 mL). Boc₂O (0.57, 2.6 mmol, 1.1 equiv.) was added, in one portion, and reaction stirred at rt overnight. Volatiles were removed under reduced pressure and residue purified by FC using a mixture of EtOAc/CH₂Cl₂ (1/1) to give the title compound **181** as a white solid in 86% yield. ¹H NMR (300 MHz, CDCl₃) δ 7.47 – 7.35 (m, 6H), 7.35 –

7.26 (m, 4H), 5.21 (s, 2H), 4.63 (s, 2H). ¹³C NMR (75 MHz, CDCl₃) δ 162.7, 140.1, 128.9, 128.4, 126.5, 66.0.

Synthesis of (4*S*,5*S*)-1,3-dimethyl-4,5-diphenyl-imidazolidin-2-one (182): Urea **181** (0.46 g, 1.9 mmol) was dissolved in dry DMF (6 mL) and cooled to 0 °C. NaH (0.20 g, 5.0 mmol, 2.6 equiv.) was added and mixture was stirred for 30 min at 0 °C. MeI (0.41 mL, 6.65 mmol, 3.5 equiv.) was added dropwise and reaction allowed to warm up to rt and left stirring for 16h. Upon completion, reaction was quenched by careful addition of 1.0 M aq. HCl and product was extracted with EtOAc (3x). Combined organic extracts were washed with H₂O (3x) and brine (3x), dried over Na₂SO₄, filtered, concentrated, and purified by FC using a mixture of EtOAc/Hex (1/1) to give the title compound as a white solid in 88% yield. ¹H NMR (300 MHz, CDCl₃) δ 7.43 – 7.34 (m, 6H), 7.22 – 7.14 (m, 4H), 4.12 (s, 2H), 2.75 (s, 6H). ¹³C NMR (75 MHz, CDCl₃) δ 161.8, 138.1, 128.8, 128.4, 127.3, 70.3, 30.0.

Synthesis of (4*S*,5*S*)-2-chloro-1,3-dimethyl-4,5-diphenyl-imidazolidium chloride (183): To a solution of compound **182** (0.50 g, 1.9 mmol) in toluene (12 mL) was added (COCl)₂ (0.90 mL, 10.5 mmol, 5.5 equiv.) and reaction was heated to reflux for 24h. Reaction was then cooled to rt and volatiles were removed under reduced pressure. Residue was washed with toluene (3x) and dried under high vacuum overnight, giving the title compound, as a white solid, in 89% yield, which was used in the next step without further purification.

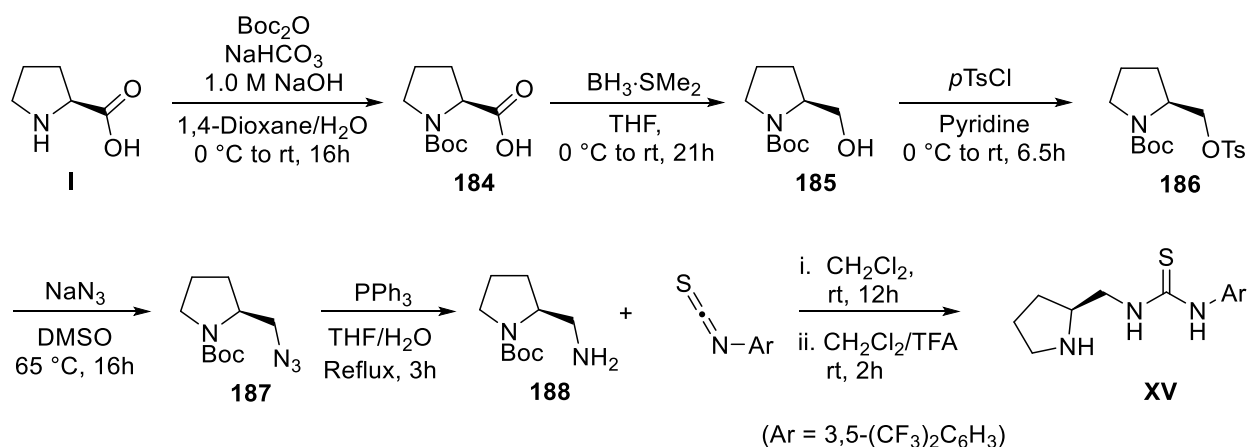
Synthesis of guanidinium XX: To a solution of previously synthesized *S*-phenylalalinol (0.21 g, 1.37 mmol, 1.05 equiv.) and NEt₃ (0.45 mL, 3.25 mmol, 2.5 equiv.) in dry CH₂Cl₂ (14 mL), was added compound **183** (0.40 g, 1.3 mmol, 1.0 equiv.). Reaction was stirred at rt for 2h and then poured into 5% aq. HCl. The product was extracted with CH₂Cl₂ (3x) and the combined organic extracts were concentrated and purified by FC using a mixture of MeOH/CH₂Cl₂ (1/9) to give guanidinium **XX** as a white solid in 79% yield.ⁱ ¹H NMR (300 MHz, CDCl₃) δ 8.79 (d, *J* = 10.1 Hz, 1H), 7.51 – 7.43 (m, 2H), 7.43 – 7.19 (m, 10H), 7.19 – 7.08 (m, 4H), 5.52 (t, *J* = 4.0 Hz, 1H), 4.29 (s, 2H), 4.21 (td, *J* = 9.7, 5.2 Hz, 1H), 4.12 – 3.99 (m,

ⁱ Attempts to free-base the guanidinium prior to purification by FC failed to give the desired compound in a pure form suitable for use, free-basing after FC gave a pale-yellow oil which was hard to handle.

1H), 4.00 – 3.90 (m, 1H), 3.53 (dd, $J = 13.6, 10.2$ Hz, 1H), 3.03 – 2.78 (m, 7H). ^{13}C NMR (75 MHz, CDCl_3) δ 162.4, 138.5, 136.2, 129.9, 129.44, 129.3, 128.5, 127.1, 126.6, 74.0, 65.5, 61.7, 36.6, 34.8.

Synthesis of catalyst **XV**

Catalyst **XV** was prepared following the synthetic route illustrated in Scheme 4.8, which was based on literatures procedures.^{243,244}



Scheme 4.8 – Synthetic route for the synthesis of catalyst **XV**.

Synthesis of *N*-Boc-(*S*)-proline (184**):** L-Proline **I** (1.15 g, 10 mmol) was dissolved in a 2/1 mixture of 1,4-dioxane and H₂O (30 mL) and made alkaline by addition of 1.0 M aq. NaOH (10 mL). The resulting mixture was cooled to 0 °C and Boc₂O (3.27 g, 15 mmol, 1.5 equiv.) and NaHCO₃ (0.804 g, 10 mmol, 1.0 equiv.) were added sequentially. Reaction was stirred at rt over night and then evaporated to half the volume. Residue was cooled to 0 °C and acidified to 2 < pH < 3 by addition of 1.0 M aq. HCl. Resulting mixture was diluted with EtOAc (40 mL) and transferred to a separatory funnel. Phases were separated and aqueous layer was further extracted with EtOAc (2x20 mL). The combined organic extracts were washed with H₂O (20 mL) and brine (20 mL), dried over Na₂SO₄, filtered, concentrated to give the title compound as a white crystalline solid, in >99% yield, as a mixture of rotamers which was used in the next step without further purification. ^1H NMR (300 MHz, CDCl_3) δ 10.95 (s, 2H), 4.39 (dd, $J = 8.1, 2.6$ Hz, 1H), 4.27 (dd,

$J = 8.5, 4.2$ Hz, 1H), 3.67 – 3.32 (m, 4H), 2.40 – 2.20 (m, 2H), 2.21 – 1.83 (m, 6H), 1.49 (s, 9H), 1.45 (s, 9H). ^{13}C NMR (75 MHz, CDCl_3) δ 179.0, 175.4, 156.3, 153.9, 146.7, 85.2, 81.4, 80.3, 59.1, 58.9, 47.0, 46.4, 30.9, 28.7, 28.4, 28.3, 27.4, 24.3, 23.7.

Synthesis of N-Boc-(S)-prolinol (185): In a 250 mL round bottom flask equipped with a magnetic stirring bar and a pressure-equalizer addition funnel was added **184** (2.37 g, 10.9 mmol) and dry THF (17 mL), under an Argon atmosphere. Solution was cooled to 0 °C and a 2.0 M solution of $\text{BH}_3\cdot\text{SMe}_2$ in THF (11 mL, 21.8 mmol, 2.0 equiv.) was added very slowly through the addition funnel. After complete addition of the $\text{BH}_3\cdot\text{SMe}_2$, reaction was stirred for 5h at 0 °C and then allowed to warm up to rt overnight. Reaction was quenched by very careful addition of H_2O (40 mL) (*CAUTION! Substantial gas evolution and temperature increase will occur in this step*). Mixture was further diluted with EtOAc (250 mL) and transferred to a separatory funnel. Phases were separated and organic layer was washed with brine (40 mL), sat. aq. NaHCO_3 (40 mL), H_2O (2x40 mL) and brine again (40 mL), dried over Na_2SO_4 , filtered, concentrated, and residue purified by FC using EtOAc/Hexanes (1/1) as eluent to give the title compound as a white crystalline solid in 70% yield. ^1H NMR (300 MHz, CDCl_3) δ 4.76 (s, 1H), 3.98 (s, 1H), 3.78 – 3.55 (m, 3H), 3.52 – 3.44 (m, 1H), 3.40 – 3.26 (m, 1H), 2.14 – 1.93 (m, 1H), 1.93 – 1.66 (m, 3H), 1.49 (s, 9H).

Synthesis of N-Boc-(S)-2-(4-toluenesulfonyloxy)methylpyrrolidine (186): Compound **185** (0.50 g, 2.5 mmol) was dissolved in pyridine (2.6 mL) and cooled to 0 °C. *p*TsCl (0.57 g, 3.0 mmol, 1.2 equiv.) was added and reaction stirred for 6.5h, at rt. Reaction was extracted with Et_2O (23 mL) and organic layer was washed with 10% aq. HCl (3x9 mL), sat. aq. NaHCO_3 (3x9 mL) and brine (2x9 mL), dried over Na_2SO_4 , filtered, and volatiles were removed under reduced pressure to give the title compound as a colorless oil in 85% yield which was immediately used in the next step without any further purification.

Synthesis of N-Boc-(S)-2-azidomethylpyrrolidine (187): Compound **186** (0.75 g, 2.1 mmol) was taken in DMSO (22 mL) and NaN_3 (0.82 g, 12.6 mmol, 6.0 equiv.) was added. Reaction was heated to 65 °C overnight and then allowed to cool down to rt and diluted with Et_2O (45 mL). The organic phase was separated and washed with H_2O (3x40 mL) and brine (20 mL), dried over Na_2SO_4 , filtered, and volatiles removed under reduced pressure to give the title compound as a white solid, in 67% yield which was used

in the next step without further purification. ^1H NMR (300 MHz, CDCl_3) δ 4.06 – 3.84 (m, 1H), 3.71 – 3.24 (m, 4H), 2.12 – 1.77 (m, 4H), 1.51 (s, 9H).

Synthesis of *N*-Boc-(*S*)-2-(aminomethyl)pyrrolidine (188): Azide **187** (0.32 g, 1.4 mmol) was dissolved in THF (12 mL). PPh_3 (0.75 g, 2.87 mmol, 2.05 equiv.) and H_2O (53 μL , 2.94 mmol, 2.1 equiv.) were added sequentially. Mixture was heated to reflux and upon completion (TLC monitoring), reaction was allowed to cool down to rt and volatiles removed under reduced pressure. Residue was dissolved in Et_2O (30 mL) and pH was adjusted to ≈ 2 by addition of 1.0 M aq. HCl with vigorous stirring. Phases were separated and aqueous layer was washed with Et_2O (2x10 mL). Ethereal extracts were discarded, and the aqueous phase was made alkaline (pH ≈ 13) by addition of 2.0 M aq. NaOH and extracted with CH_2Cl_2 (6x15 mL). Combined organic extracts were dried over K_2CO_3 , filtered and volatiles removed under reduced pressure to give the title compound in 62% yield as a thick pale-yellow oil which was used in the next step without further purification. ^1H NMR (300 MHz, CDCl_3) δ 3.90 – 3.65 (m, 1H), 3.60 – 3.26 (m, 2H), 2.95 – 2.75 (m, 1H), 2.70 (dd, $J = 12.8, 7.0$ Hz, 1H), 2.06 – 1.72 (m, 4H), 1.50 (s, 9H).

Synthesis of (*S*)-1-(3,5-bis(trifluoromethyl)phenyl)-3-(pyrrolidine-2-ylmethyl)thiourea (XV): To a solution of amine **188** (0.41 g, 2.1 mmol) in dry CH_2Cl_2 (15 mL) was added 3,5-bis(trifluoromethyl)phenyl isothiocyanate (0.36 mL, 2.1 mmol, 1.0 equiv.) and reaction was stirred at rt for 12h. Solvent was removed under reduced pressure and residue was taken in a 1/1 mixture of $\text{CH}_2\text{Cl}_2/\text{TFA}$ (30 mL) and stirred at rt. Upon completion (TLC monitoring), volatiles were removed under reduced pressure. With vigorous stirring, sat. aq. NaHCO_3 was added until pH ≈ 9 and product was extracted thrice with CH_2Cl_2 . Combined organic extracts were dried over K_2CO_3 , filtered, and purified by FC using a mixture of MeOH/EtOAc (1/7) to give the title compound in 55% yield over the two steps, as a white solid. ^1H NMR (300 MHz, CDCl_3) δ 8.05 (s, 2H), 7.61 (s, 1H), 3.65 – 3.52 (m, 1H), 3.52 – 3.47 (m, 1H), 3.47 – 3.27 (m, 1H), 3.20 – 3.07 (m, 1H), 2.95 – 2.85 (m, 1H), 2.07 – 1.87 (m, 1H), 1.86 – 1.69 (m, 1H), 1.69 – 1.50 (m, 1H).

Chapter II – General Procedures for the Synthesis of Dihydropyrido[1,2-a]indole Scaffolds

General Procedures for the Organocatalyzed reactions

Intramolecular Michael addition

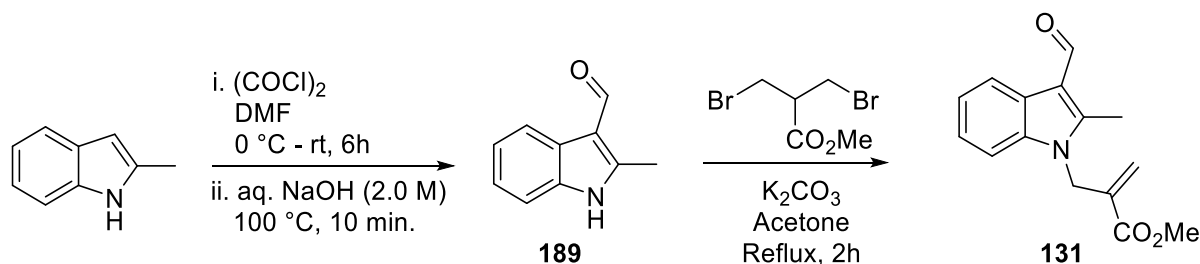
In a screw cap vial equipped with a magnetic stirring bar, was added **131** (51.5 mg, 0.2 mmol), organocatalyst (0.04 mmol, 0.2 equiv.) and additive (from 0.1 to 0.5 equiv.) and mixture dissolved in the appropriated solvent (0.4 M). Reaction was stirred at the appropriated temperature for the time depicted in the Tables from Part II, Chapter I and monitored by ^1H NMR.

aza-Diels-Alder reaction

In a screw cap vial equipped with a magnetic stirring bar, indole **134** (0.5 mmol) was dissolved in THF (2 mL) and aminocatalyst (0.1 mmol, 0.2 equiv.), additive (0.1 mmol, 0.2 equiv.) and dienophile (0.12 mmol, 1.2 equiv.) were added. Reaction was stirred at 75 °C and monitored by ^1H NMR and/or TLC.

Synthesis of compounds **131** and **134**

Compound **131** was prepared in two steps, starting from commercially available 2-methylindole, following the reaction depicted in Scheme 4.9.

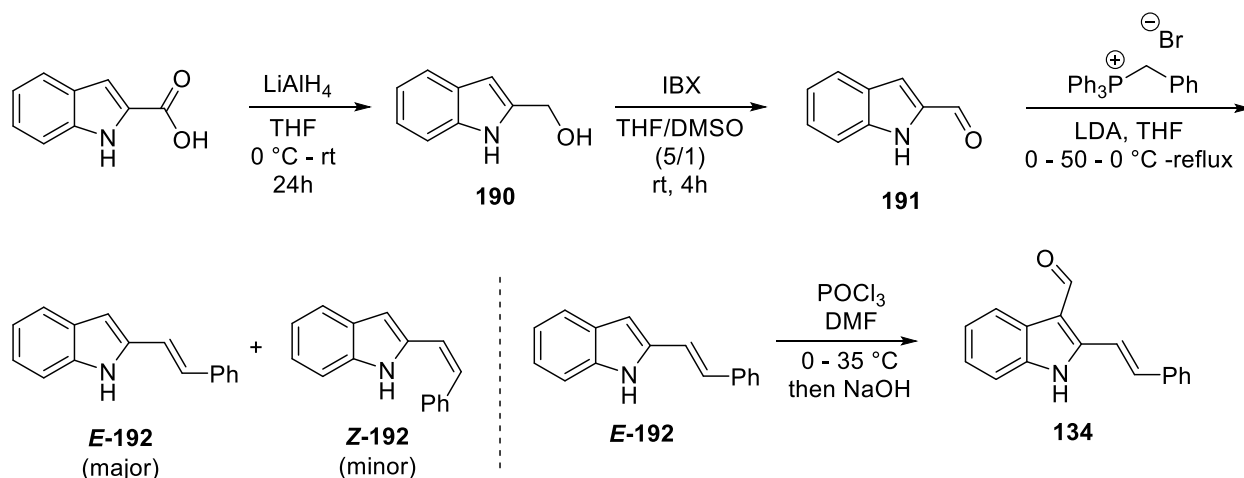


Scheme 4.9 – Synthetic path to compound **131**.

Synthesis of 2-methylindole-3-carboxaldehyde (189): Oxalyl chloride (1.5 mL) was added dropwise, over several minutes, to ice cold DMF (14 mL) and the mixture was left stirring at 0 °C for 1h. 2-Methylindole (2.5 g, 19.06 mmol) in DMF (7 mL) was added dropwise and mixture was brought up to rt and left stirring for 5h. A 2.0 M solution of NaOH (9.5 mL) was slowly added and reaction heated to 100 °C for 10 min. Mixture was cooled to rt and extracted with EtOAc (3x100 mL). The combined organic extracts were washed with water (3x100 mL) and brine (3x100 mL), dried over Na₂SO₄, filtered, and concentrated to give the final compound, as a brick colored crystalline solid, in 89% yield, which was used in the next step without further purification. ¹H NMR (300 MHz, DMSO) δ 11.97 (s, 1H), 10.06 (s, 1H), 8.08 – 8.00 (m, 1H), 7.43 – 7.34 (m, 1H), 7.21 – 7.11 (m, 2H), 2.69 (s, 3H).

Synthesis of 131:²⁴⁵ 2-Methylindole-3-carboxaldehyde **189** (0.5 g, 3.14 mmol), K₂CO₃ (2.17 g, 15.7 mmol, 5.0 equiv.) and methyl 3-bromo-2-(bromomethyl)propionate (0.45 mL, 3.14 mmol, 1.0 equiv.) were taken in dry acetone (30 mL) and heated to reflux. Reaction was monitored by TLC and upon completion (2-3h) mixture was allowed to cool down to rt and filtered. Volatiles were removed under reduced pressure and residue purified by FC (EtOAc/Hexanes 1/1) to give the desired product **131**, as a white solid, in 97% yield. ¹H NMR (300 MHz, CDCl₃) δ 10.26 (s, 1H), 8.37 – 8.27 (m, 1H), 7.39 – 7.20 (m, 3H), 6.29 (t, *J* = 1.7 Hz, 1H), 5.03 (t, *J* = 1.9 Hz, 2H), 4.98 (t, *J* = 2.0 Hz, 1H), 3.90 (s, 3H), 2.70 (s, 3H).

Compound **134** was synthesized in four steps, starting from commercially available indole-2-carboxylic acid, following the synthetic route depicted in Scheme 4.10 which, was adapted from the literature.²⁴⁶



Scheme 4.10 – Synthetic path for substrate **134**.

Synthesis of indole-2-methanol (190): LiAlH₄ (2.40 g, 62 mmol, 2.0 equiv.) was suspended in dry THF (90 mL) and cooled to 0 °C. Indole-2-carboxylic acid (5.00 g, 31 mmol) was added portion-wise and reaction allowed to warm up to rt and left stirring at this temperature for 24h. Reaction was then quenched by careful addition of sat. aq. NaHCO₃ and resulting slurry was filtered through celite and washed with H₂O and EtOAc. Phases were separated and aqueous layer was washed thrice with EtOAc. Combined organic extracts were washed with brine, dried over Na₂SO₄, filtered, and concentrated to dryness affording alcohol **190** as a pale yellow solid, in 90% yield, which could be stored for long periods of time in the freezer but decomposed upon standing on the bench. Alcohol **190** was used in the next step without further purification. ¹H NMR (300 MHz, CDCl₃) δ 8.40 (s, 1H), 7.63 (dd, *J* = 7.7, 0.5 Hz, 1H), 7.41 – 7.33 (m, 1H), 7.24 (dt, *J* = 7.04, 1.27 Hz, 1H), 7.15 (dt, *J* = 7.04, 1.27 Hz, 1H), 6.47 – 6.41 (m, 1H), 4.83 (s, 2H), 2.09 (s, 1H). ¹³C NMR (75 MHz, DMSO) δ 140.57, 136.62, 128.30, 120.96, 120.07, 119.07, 111.50, 98.90, 57.34.

Synthesis of indole-2-carboxaldehyde (191): Freshly prepared IBX (*vide supra*, 10.00 g, 36 mmol, 1.5 equiv.) was suspended in DMSO (20 mL) and alcohol **190** (3.50 g, 24 mmol) in THF (100 mL) was added. Reaction was stirred at rt and monitored by TLC. Upon completion (usually, 4h) Et₂O (600 mL) was added and resulting mixture was filtered through celite. Mother liquors were washed with sat. aq. NaHCO₃ and

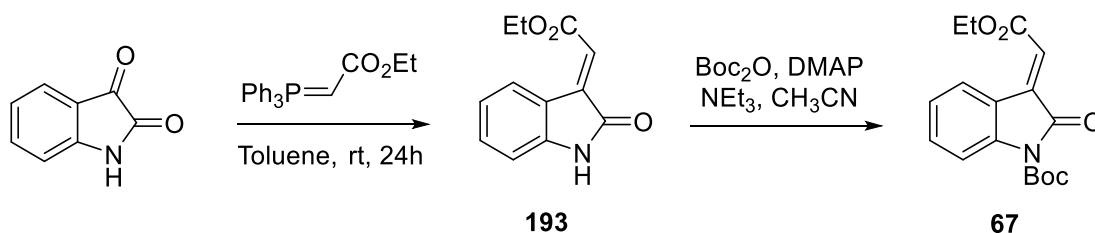
brine, dried over Na₂SO₄, filtered, concentrated and residue purified by FC using EtOAc/Hexanes (1/5) as eluent to give the title compound as an off-white crystalline solid, in 82% yield. ¹H NMR (300 MHz, CDCl₃) δ 9.91 (s, 1H), 9.64 (s, 1H), 7.80 (d, *J* = 8.1 Hz, 1H), 7.54 (d, *J* = 8.4 Hz, 1H), 7.45 (dt, *J* = 7.0, 1.0 Hz, 1H), 7.34 (d, *J* = 1.2 Hz, 1H), 7.22 (dt, *J* = 7.0, 1.0 Hz, 1H).

Synthesis of 2-[(*E*)-2'-phenylethenyl]-1*H*-indole (192**):** A commercially available 2.0 M solution of LDA (11 mL, 22 mmol, 1.3 equiv.) was added dropwise to an ice cold solution of benzyltriphenylphosphonium bromide (8.79 g, 20.3 mmol, 1.2 equiv.) in dry THF (27 mL). Mixture was stirred at rt for 45 min and at 50 °C for 30 min. Resulting mixture was then cooled again to 0 °C and aldehyde **191** (2.46 g, 16.9 mmol, 1.0 equiv.) in dry THF (19 mL) was added slowly and reaction was heated to reflux and monitored by TLC. Upon completion (usually, 5h), mixture was poured into sat. aq. NaHCO₃ (90 mL) and phases were separated. Aqueous layer was extracted with EtOAc (5x60 mL) and combined organic extracts were washed with H₂O (2x60 mL) and brine (60 mL). Organic extracts were dried over Na₂SO₄, filtered, absorbed in SiO₂ and evaporated to dryness under reduced pressure. Resulting solid was charged into a column and eluted with EtOAc/Hexanes (1/20 to 1/5, directly) to afford complete separation of the two isomers, *E*-**192** and *Z*-**192**, in 91% overall yield. *Z*-**192** (minor isomer) eluted first and was isolated in 21% yield as a pale yellow solid ¹H NMR (300 MHz, CDCl₃) δ 7.91 (s, 1H), 7.60 (dd, *J* = 7.7, 0.7 Hz, 1H), 7.54 – 7.38 (m, 5H), 7.23 – 7.07 (m, 3H), 6.70 (d, *J* = 12.2 Hz, 1H), 6.63 (d, *J* = 12.2 Hz, 1H), 6.57 (d, *J* = 2.0 Hz, 1H). *E*-**192** (major isomer) eluted afterwards and was isolated in 70% yield as a yellow solid ¹H NMR (300 MHz, CDCl₃) δ 8.29 (s, 1H), 7.63 (d, *J* = 7.9 Hz, 1H), 7.55 (d, *J* = 7.3 Hz, 2H), 7.49 – 7.28 (m, 5H), 7.25 (dt, *J* = 7.1, 1.1 Hz, 1H), 7.21 – 7.10 (m, 2H), 6.95 (d, *J* = 16.5 Hz, 1H), 6.67 (d, *J* = 1.3 Hz, 1H).

Synthesis of 2-[(*E*)-2'-phenylethenyl]-1*H*-indole-3-carboxaldehyde (134**):** POCl₃ (0.8 mL, 8.2 mmol, 1.2 equiv.) was added dropwise to ice cold DMF (2 mL). Mixture was stirred at 0 °C for 20 min. and then indole *E*-**192** (1.5 g, 6.8 mmol) in DMF (3 mL) was slowly added and mixture allowed to warm up to rt and then further heated to 35 °C. Upon completion (usually, 2h, by TLC monitoring), reaction was cooled down to rt and ice (≈3.5 g) was added followed by 5.0 M aq. NaOH. Reaction was heated to 95 °C for 30 min. and then allowed to cool down to rt. Ice (≈3.5 g) was added again and mixture stirred for 30 min.

Product was collected by vacuum filtration and washed thoroughly with H₂O and dried under high vacuum overnight, giving the title compound **134** as a bright yellow amorphous solid in 95% yield. ¹H NMR (300 MHz, DMSO) δ 12.33 (s, 1H), 10.42 (s, 1H), 8.13 (d, *J* = 7.7 Hz, 1H), 7.91 (d, *J* = 16.5 Hz, 1H), 7.75 (d, *J* = 7.5 Hz, 2H), 7.57 (d, *J* = 16.4 Hz, 1H), 7.46 (t, *J* = 7.0 Hz, 3H), 7.42 – 7.33 (m, 1H), 7.28 (t, *J* = 7.4 Hz, 1H), 7.20 (t, *J* = 7.4 Hz, 1H). ¹³C NMR (75 MHz, DMSO) δ 185.77, 145.47, 137.09, 136.39, 134.07, 129.43, 127.67, 126.11, 124.67, 122.64, 121.28, 115.65, 115.05, 111.97.

The 3-olefinic oxindole **67** was prepared from commercially available isatin following the synthetic route depicted in Scheme 4.11 which, was adapted from the literature.²⁴⁷



Scheme 4.11 – Synthetic route to the 3-olefinic oxindole **67**.

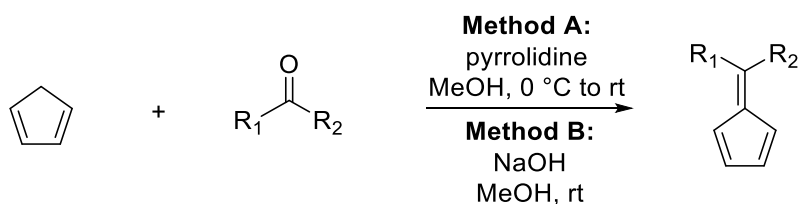
Synthesis of Ethyl 2-(1,2-dihydro-2-oxo-3H-indol-3-ylidene)acetate (193): A solution of isatin (1.50 g, 10.2 mmol), and (carbethoxymethylene)triphenylphosphorane (3.91 g, 11.2 mmol, 1.1 equiv.), in toluene (30 mL) was stirred at rt for 24h. Volatiles were removed under reduced pressure and the solid residue taken in CH₂Cl₂/MeOH and absorbed in SiO₂, solvents were removed under reduced pressure and crude mixture charged into a column and purified using EtOAc/Hexanes (1/1) to give the title compound **193** in 85% yield as a bright orange crystalline solid. ¹H NMR (300 MHz, CDCl₃) δ 8.59 (d, *J* = 7.7 Hz, 1H), 8.28 (s, 1H), 7.36 (td, *J* = 7.7, 1.2 Hz, 1H), 7.09 (dt, *J* = 7.7, 1.2 Hz, 1H), 6.96 – 6.86 (m, 2H), 4.38 (q, *J* = 7.2 Hz, 2H), 1.42 (t, *J* = 7.2 Hz, 3H).

1,1-Dimethylethyl 3-(2-ethoxy-2-oxoethylidene)-2,3-dihydro-2-oxo-1H-indole-1-carboxylate (67): A solution of oxindole **193** (0.50 g, 2.3 mmol), DMAP (0.03 g, 0.23 mmol, 0.1 equiv.), and NEt₃ (0.42 mL, 2.99 mmol, 1.3 equiv.), in CH₃CN (5 mL) was cooled to 0 °C. A solution of di-*tert*-butyl dicarbonate

(0.60 g, 2.8 mmol, 1.2 equiv.) in CH₃CN (3 mL) was added dropwise and mixture was allowed to warm up to rt and left stirring overnight. Volatiles were removed under reduced pressure and residue purified by FC eluting with EtOAc/Hexanes (1/10) to give the title compound **67** in 74% yield as a yellow solid. ¹H NMR (300 MHz, CDCl₃) δ 8.73 (d, *J* = 7.8 Hz, 1H), 7.94 (d, *J* = 8.2 Hz, 1H), 7.47 (dt, *J* = 7.8 1.0 Hz, 1H), 7.23 (td, *J* = 7.8, 1.0 Hz, 1H), 6.96 (d, *J* = 4.0 Hz, 1H), 4.37 (q, *J* = 7.1 Hz, 2H), 1.72 (s, 9H), 1.41 (t, *J* = 7.1 Hz, 3H).

Chapter III – General Procedures for the High Order Cycloadditions

Synthesis of Fulvenes

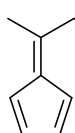


Scheme 4.12 – General reaction scheme for the synthesis of fulvenes.

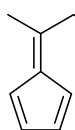
Method A:^{213,248} To an ice cold solution of freshly distilled cyclopentadiene (1.25 equiv.) and the required aldehyde or ketone (1.0 equiv.) in MeOH (1.1 M), under Argon atmosphere, was added pyrrolidine (0.6 equiv.) dropwise. After complete addition of pyrrolidine, ice bath was removed, and reaction stirred until TLC analysis indicated full conversion of starting aldehyde or ketone (between 2 to 4h). Reaction was cooled again to 0 °C and glacial acetic acid was added dropwise. Solution was diluted with H₂O and extracted thrice with Et₂O. The combined organic extracts were washed with sat. aq. NaHCO₃ and brine, dried over Na₂SO₄, filtered, and concentrated under reduced pressure. Residue was purified by FC using EtOAc/Hex mixture as eluent.

Method B: NaOH pellets (0.6 equiv.) were taken in MeOH (4.0 M) and upon complete solubilization, freshly distilled cyclopentadiene (1.0 equiv.) was added followed by the ketone (1.0 equiv.). Mixture was

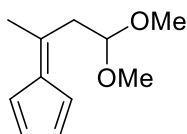
stirred at rt and monitored by TLC (usually 2h is sufficient). Reaction was quenched by dilution with H₂O and product was extracted with Et₂O (2x). Combined organic extracts were washed with 0.5 M HCl (2x) and brine, dried over Na₂SO₄, filtered, concentrated and residue purified by FC using EtOAc/Hex mixture as eluent.



3-(2,4-cyclopentadien-1-ylidene)-1-butanol (146): Prepared according to the general procedure, method A, by stirring cyclopentadiene (5.0 mL, 61 mmol, 1.25 equiv.), 4-hydroxy-2-butanone (4.2 mL, 48.5 mmol, 1.0 equiv.) and pyrrolidine (3.1 mL, 37 mmol, 0.6 equiv.) in MeOH (45 mL) for 2h. Purified by FC using EtOAc/Hexanes 1/1, to give the title compound as a bright yellow liquid in 78%. ¹H NMR (300 MHz, CDCl₃) δ 6.60 – 6.52 (m, 4H), 3.88 (t, *J* = 6.5 Hz, 2H), 2.84 (t, *J* = 6.5 Hz, 2H), 2.29 (s, 3H), 1.55 (s, 1H). ¹³C NMR (75 MHz, CDCl₃) δ 148.98, 144.55, 131.51, 131.46, 120.66, 120.52, 61.33, 39.91, 21.26.

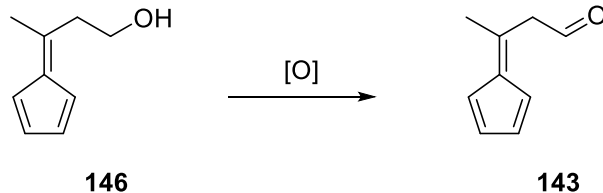


2-(2,4-cyclopentadien-1-ylidene)-1-propanol (157): Prepared according to the general procedure, method A, by stirring cyclopentadiene (10 mL, 121.3 mmol, 1.25 equiv.), hydroxyacetone (7.4 mL, 97.1 mmol, 1.0 equiv.) and pyrrolidine (6.1 mL, 72.8 mmol, 0.6 equiv.) in MeOH (90 mL) for 3h. Purified by FC using EtOAc/Hex 1/2, to give the title compound as bright yellow crystalline solid in 43% yield. ¹H NMR (300 MHz, CDCl₃) δ 6.61 – 6.51 (m, 4H), 4.58 (d, *J* = 5.4 Hz, 2H), 2.33 (s, 3H), 1.66 – 1.56 (m, 1H).



5-(3,3-Dimethoxy-1-methylpropylidene)-1,3-cyclopentadiene (162): Prepared according to the general procedure, method B, by dissolving NaOH pellets (0.73 g, 18.2 mmol, 0.6 equiv.) in MeOH (7.5 mL) and adding cyclopentadiene (2.5 mL, 30.3 mmol, 1.0 equiv.) followed by *trans*-4-methoxy-3-buten-2-one (3.1 mL, 30.3 mmol, 1.0 equiv.) and stirring at rt for 2h. Purified by FC using EtOAc/Hex 1/5, to give the title compound as a red liquid in 61% yield. ¹H NMR (300 MHz, CDCl₃) δ 6.61 – 6.48 (m, 4H), 4.65 (t, *J* = 5.7 Hz, 1H), 3.40 (s, 6H), 2.90 (d, *J* = 5.5 Hz, 2H), 2.31 (s, 3H).

Experimental Procedures for the Oxidation Reactions



Scheme 4. 13 – General reaction scheme for the oxidation of **146** to **143**.

Swern Oxidation (procedure #1): To a solution of oxalyl chloride (2.5 mL, 29.4 mmol, 2.0 equiv.) in dry CH_2Cl_2 (115 mL), at $-78\text{ }^\circ\text{C}$ and under Argon atmosphere, was added DMSO (3.2 mL, 44.1 mmol, 3.0 equiv.) dropwise and the mixture was stirred for 15 min. A solution of 3-(2,4-cyclopentadien-1-ylidene)-1-butanol **146** (2.00 g, 14.7 mmol) in CH_2Cl_2 (9 mL) was added dropwise and resulting mixture stirred at $-78\text{ }^\circ\text{C}$ for 3h. Then, NEt_3 (14.5 mL, 102.9 mmol, 7.0 equiv.) was added dropwise and mixture stirred at $-78\text{ }^\circ\text{C}$ for an additional 15 min and then allowed to warm up to $0\text{ }^\circ\text{C}$ and stirred for 1h. Dilution was performed with 0.5 M aq. HCl (120 mL) and the whole was extracted with CH_2Cl_2 (3x120 mL). The combined organic extracts were washed with sat. aq. NaHCO_3 (120 mL) and brine (120 mL), dried over Na_2SO_4 , and filtered. TLC analysis (EtOAc/Hexanes 1/1) appeared to indicate only starting alcohol was present. Volatiles were removed under reduced pressure and ^1H NMR submitted which confirmed that no reaction took place.

Swern Oxidation (procedure #2): To a solution of oxalyl chloride (1.9 mL, 22.0 mmol, 3.0 equiv.) in CH_2Cl_2 (70 mL), at $-78\text{ }^\circ\text{C}$ and under Argon atmosphere, was added DMSO (1.72 mL, 24.1 mmol, 3.3 equiv.) dropwise. Reaction was stirred at $-78\text{ }^\circ\text{C}$ for 30 min. and then, a solution of 3-(2,4-cyclopentadien-1-ylidene)-1-butanol **146** (1.00 g, 7.3 mmol) in CH_2Cl_2 (5 mL) was added dropwise. Reaction was stirred at $-78\text{ }^\circ\text{C}$ for 30 min and NEt_3 (5.2 mL, 37.2 mmol, 5.1 equiv.) was added slowly and reaction allowed to warm up to rt and left stirring for 1h at this temperature. Reaction was then quenched with H_2O (150 mL) and the resulting mixture was extracted with CH_2Cl_2 (3x150 mL). Combined organic extracts were washed with brine (150 mL), dried over Na_2SO_4 , and filtered. TLC analysis (EtOAc/Hexanes

1/1) indicated that no oxidation took place. Volatiles were removed and ^1H NMR submitted which confirmed the presence of starting alcohol.

DDQ Dehydrogenation (procedure #1): 3-(2,4-cyclopentadien-1-ylidene)-1-butanol **146** (0.14 g, 1.0 mmol) was taken in CH_2Cl_2 (10 mL) and DDQ (0.34 g, 1.5 mmol, 1.5 equiv.) was added. Reaction was stirred at rt and monitored by TLC (EtOAc/Hexanes 1/3) and after 5h it appeared that starting material was consumed. Reaction was diluted with CH_2Cl_2 (10 mL) and quenched by addition of 1.0 M aq. NaOH (20 mL). Phases were separated and organic layer was washed with H_2O (10 mL) and brine (10 mL), dried over Na_2SO_4 , and filtered. New TLC was performed, and it appeared that starting alcohol was in fact still present which was confirmed by ^1H NMR analysis.

DDQ Dehydrogenation (procedure #2): 3-(2,4-cyclopentadien-1-ylidene)-1-butanol **146** (0.14 g, 1.0 mmol) was taken in 1,4-dioxane (10 mL) and DDQ (0.34 g, 1.5 mmol, 1.5 equiv.) was added. Reaction was heated to reflux and monitored by TLC (EtOAc/Hexanes 1/1). After 24h reaction was allowed to cool down to rt and filtered and filtrate cake washed with CH_2Cl_2 . Volatiles were removed under reduced pressure and ^1H NMR analysis was performed showing a very messy spectrum with mostly starting alcohol present but, no indication of the desired aldehyde.

TEMPO/BAIB Oxidation:²⁰⁹ 3-(2,4-cyclopentadien-1-ylidene)-1-butanol **146** (0.50 g, 3.7 mmol) and TEMPO (0.06 g, 0.37 mmol, 0.1 equiv.) were dissolved in CH_2Cl_2 (4 mL) and BAIB (1.29 g, 4.0 mmol, 1.1 equiv.) was added. Reaction was stirred at rt and monitored by TLC (EtOAc/Hexanes 1/3) and after 5h it appeared to indicate that starting material was consumed. Reaction was then diluted with CH_2Cl_2 (20 mL) and quenched with sat. aq. $\text{Na}_2\text{S}_2\text{O}_3$ (20 mL). Phases were separated and aqueous layer extracted with CH_2Cl_2 (4x20 mL). Combined organic extracts were washed with sat. aq. NaHCO_3 (20 mL) and brine (20 mL), dried over Na_2SO_4 , and filtered. ^1H NMR was submitted and showed a very messy spectrum with no evidence of aldehyde and with the major product being iodobenzene.

PCC/SiO₂ Oxidation:²¹⁰ A mixture of PCC (3.17 g, 14.7 mmol, 2.0 equiv.) and SiO₂ 40-63 μm (230-400 mesh) (≈3.2 g, 1/1 (w/w) in respect to PCC) were grounded to a fine powder using a mortar and pestle. The obtained orange mixture was placed in a round bottom flask equipped with a magnetic stirring bar and CH₂Cl₂ (35 mL) was added, under Argon atmosphere. With mild stirring, 3-(2,4-cyclopentadien-1-ylidene)-1-butanol **146** (1.00 g, 7.3 mmol) was added in one portion and reaction immediately went from bright orange to very dark brown. Mixture was stirred at rt and monitored by TLC (EtOAc/Hexanes 1/1) and left for 24h. After this period of time, TLC analysis did not showcase any new product and only starting alcohol was observed. Reaction was, nonetheless, quenched by dilution with Et₂O (70 mL) and filtered through a pad of basic alumina. Volatiles were removed under reduced pressure and ¹H NMR analysis showed only starting alcohol.

PCC Oxidation (procedure #1): PCC (3.17 g, 14.7 mmol, 2.0 equiv.) was taken in CH₂Cl₂ (35 mL) and cooled to 0 °C. 3-(2,4-cyclopentadien-1-ylidene)-1-butanol **146** (1.00 g, 7.3 mmol) was added and reaction was kept stirring at 0 °C and monitored by TLC (EtOAc/Hexanes 1/1). After 4h, TLC analysis showed no conversion of starting alcohol, so reaction was quenched by dilution with Et₂O (70 mL) and filtration through a short pad of celite and silica. Volatiles were removed and ¹H NMR analysis indicated that only starting material was present.

PCC Oxidation (procedure #2): PCC (3.17 g, 14.7 mmol, 2.0 equiv.) was taken in CH₂Cl₂ (35 mL) and cooled to 0 °C. 3-(2,4-cyclopentadien-1-ylidene)-1-butanol **146** (1.00 g, 7.3 mmol) was added and reaction was kept stirring at 0 °C and monitored by TLC (EtOAc/Hexanes 1/3). After 5h, TLC analysis showed no conversion of starting alcohol, so reaction was quenched by dilution with Et₂O (70 mL) and filtration through a short pad of celite and silica. Volatiles were removed and ¹H NMR analysis indicated that only starting material was present.

NaIO₄ Oxidation (procedure #1):²¹¹ 8.2 mL of a 0.5 M aq. solution of NaIO₄ (4.1 mmol, 1.1 equiv.) was cooled to 0 °C and 3-(2,4-cyclopentadien-1-ylidene)-1-butanol **146** (0.50 g, 3.7 mmol) in MeOH (11 mL) was added. Reaction was stirred at 0 °C and monitored by TLC (4h should suffice according to the literature).

After 4h no new product was observed by TLC and only starting alcohol seemed to be present. Reaction was stopped, filtration was performed to remove any solid NaI that may have formed, and mother liquors were extracted with CH₂Cl₂ (2x50 mL). Combined organic extracts were dried over MgSO₄, filtered and concentrated. ¹H NMR analysis confirmed that no reaction took place.

NaIO₄ Oxidation (procedure #2): 8.2 mL of a 0.5 M aq. solution of NaIO₄ (4.1 mmol, 1.1 equiv.) was cooled to 0 °C and 3-(2,4-cyclopentadien-1-ylidene)-1-butanol **146** (0.50 g, 3.7 mmol) in 1,4-dioxane (11 mL) was added. Reaction was stirred at 0 °C and monitored by TLC. After 4h reaction was filtered, and mother liquors were extracted with Et₂O (2x50 mL). Combined organic extracts were dried over Na₂SO₄, filtered and concentrated. ¹H NMR analysis showed no reaction took place.

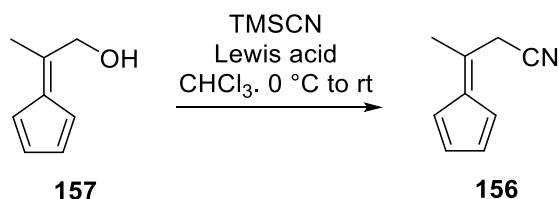
DMP Oxidation (procedure #1): 3-(2,4-cyclopentadien-1-ylidene)-1-butanol **146** (0.50 g, 3.7 mmol) was taken in CH₂Cl₂ (50 mL) and cooled to 0 °C. Dess-Martin periodane (1.73 g, 4.1 mmol, 1.1 equiv.) was carefully added and reaction stirred at this temperature for 1h. After 1h, TLC analysis indicated no evolution so, reaction was allowed to warm to rt and left stirring for 5h, and still no evolution by TLC analysis. Reaction was quenched by careful addition of sat. aq. Na₂S₂O₃ (50 mL) and vigorously stirred for 15 min. Phases were separated and organic layer was washed with sat. aq. NaHCO₃, (50 mL) and brine (50 mL), dried over Na₂SO₄, filtered and concentrated. ¹H NMR analysis showed no indication of the desired aldehyde.

DMP Oxidation (procedure #2):²¹² 3-(2,4-cyclopentadien-1-ylidene)-1-butanol **146** (0.25 g, 1.84 mmol) was taken in CH₂Cl₂ (40 mL) and H₂O (36.4 μL, 0.2 mmol, 1.1 equiv.) was added and mixture vigorously

stirred. Dess-Martin periodane (1.17 g, 2.75 mmol, 1.5 equiv.) was added in one portion and reaction was monitored by TLC. After 2h TLC analysis seemed to indicate that starting material was consumed and a new product was present in the reaction mixture. Reaction was then quenched by addition of sat. aq. $\text{Na}_2\text{S}_2\text{O}_3$ (50 mL) and vigorously stirred for 15 min. Phases were separated and organic layer was washed with sat. aq. NaHCO_3 (50 mL), H_2O (50 mL) and brine (50 mL). Organic layer was dried over Na_2SO_4 , filtered, concentrated and ^1H NMR analysis did indicate that perhaps the desired aldehyde was present so, crude was purified by FC using EtOAc/Hex 1/3 as eluent. ^1H NMR after column chromatography was complex, inconsistent with the desired product and different from the spectrum recorded after work up. Reaction was repeated under the exact same conditions but, at a slightly higher scale (3.7 mmol in respect to fulvene) with the difference that the column was performed using a $\text{Et}_2\text{O}/\text{PE}$ (1/1) mixture as eluent and volatiles were evaporated at 0°C instead of the usual 40°C at which we keep the water bath of the rotorvaps in an attempt to prevent thermal decomposition of the product. Unfortunately, the same decomposition took place.

IBX oxidation: IBX (0.46 g, 1.7 mmol, 1.5 equiv.) was suspended in DMSO (1.0 mL). A solution of 3-(2,4-cyclopentadien-1-ylidene)-1-butanol **146** (0.15 g, 1.1 mmol) in THF (4 mL) was then added and resulting mixture was stirred at rt and monitored by TLC. After stirring for 24h, no conversion was observed however, reaction was quenched nonetheless by diluting with Et_2O (10 mL) and filtration through celite. Mother liquors were washed with sat. aq. NaHCO_3 (10 mL) and brine (10 mL). Organic layer was dried over Na_2SO_4 , filtered and concentrated. ^1H NMR analysis showed no indication of the desired aldehyde.

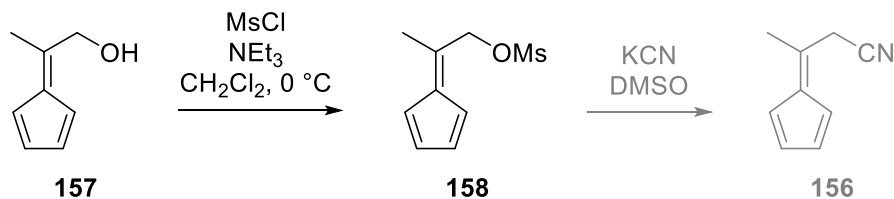
Procedures for the Cyanation Reactions



Scheme 4. 14 – General reaction scheme for the cyanation of **157**.

Cyanation Using BiCl₃ as the Lewis Acid:²¹⁶ In a round bottom flask, under Argon atmosphere, was added BiCl₃ (0.13 g, 0.41 mmol, 0.1 equiv.), dry CHCl₃ (8 mL) and TMSCN (1.0 mL, 8.2 mmol, 2.0 equiv.). Mixture was cooled down to 0 °C and a solution of **157** (0.50 g, 4.1 mmol, 1.0 equiv.) in CHCl₃ (8 mL) was added dropwise. Reaction was allowed to warm up to rt and monitored by TLC. After 3h, reaction was cooled down again to 0 °C and quenched by careful addition of sat. aq. NaHCO₃ (8 mL) and filtered through a short pad of celite. Phases were separated and aqueous layer was extracted with CHCl₃ (3x4mL). Combined organic extracts were washed with H₂O (8 mL) and brine (8 mL), dried over Na₂SO₄, filtered and volatiles removed under reduced pressure. During the addition of the fulvene solution, reaction mixture became black and an insoluble black solid could be seen suspended. Reaction was nonetheless left stirring for 3h before work up was performed. ¹H NMR analysis of the residue extracted showed complete decomposition of starting material and no evidence of the desired nitrile was observed.

Cyanation Using BF₃·OEt₂ as the Lewis Acid: Hydroxyfulvene **157** (0.50 g, 4.1 mmol) was taken in CHCl₃ (15 mL) and cooled to 0 °C. BF₃·OEt₂ (1.0 mL, 8.2 mmol, 2.0 equiv.) was added dropwise followed by TMSCN (1.0 mL, 8.2 mmol, 2.0 equiv.). Reaction immediately turned into a black goo right after addition of the Lewis acid and was allowed to warm up to rt and stirred for 1h. Reaction was then filtered through celite and filtrate cake thoroughly washed with CH₂Cl₂ and sat. aq. NaHCO₃. Phases were separated and organic layer was washed with brine, dried over Na₂SO₄, filtered and volatiles removed under reduced pressure. ¹H NMR analysis was performed, and only solvent signals were observed in the spectrum.



Scheme 4. 15 – Synthetic route for the formation of fulvene **156**.

Mesylation procedure: Fulvene **157** (0.50 g, 4.1 mmol) in dry CH₂Cl₂ (17 mL) was cooled to 0 °C. NEt₃ (0.7 mL, 4.9 mmol, 1.2 equiv.) was added and mixture was stirred for 15 min. MsCl (0.6 mL, 6.1 mmol, 1.5 equiv.) was then added dropwise and reaction was stirred at 0 °C and monitored by TLC. Upon complete consumption of starting material (2.5h) reaction was diluted with CH₂Cl₂ (10 mL) and transferred to a separatory funnel where it was washed sequentially with 10% HCl (10 mL), sat. aq. NaHCO₃ (10 mL) and brine (10 mL). Organic layer was dried over Na₂SO₄, filtered and volatiles were removed under reduced pressure. During this stage, the bright yellow solution gave rise to a black insoluble solid.

Synthesis of 3-oxobutanenitrile (159): To an ice-cold solution of acetonitrile (0.5 mL, 9.6 mmol) in THF (35 mL) was added KOtBu (3.23 g, 28.8 mmol, 3.0 equiv.), carefully, followed by EtOAc (3.7 mL, 38.3 mmol, 4.0 equiv.). Reaction was allowed to warm up to rt and stirred for 24h. Upon completion (TLC monitoring), reaction was quenched by careful addition of 1.0 M aq. HCl (100 mL) followed by dilution with H₂O (200 mL) and EtOAc (200 mL). Organic layer was extracted, washed with H₂O (2x100 mL) and brine (2x100 mL), dried over Na₂SO₄, filtered, concentrated, and purified by FC using EtOAc/Hex 1/5 as eluent to give, not the desired 3-oxobutanenitrile but instead, ethyl acetoacetate as the only product, as a colorless liquid in 26% yield. ¹H NMR (300 MHz, CDCl₃) δ 4.23 (q, *J* = 7.1 Hz, 2H), 3.47 (s, 2H), 2.30 (s, 3H), 1.31 (t, *J* = 7.1 Hz, 3H).

Procedures for the Deprotection of Acetal 162

Iodine Method: Acetal **162** (0.2 g, 1.11 mmol) was taken in acetone (4 mL) and I₂ (0.03 g, 0.11 mmol, 0.1 equiv.) was added. Reaction immediately went from an orange solution to a black suspension and TLC analysis showed no spots in the reaction lane. Reaction was quenched by solvent removal and the remaining black solid was taken in CH₂Cl₂ (15 mL) and washed with sat. aq. Na₂S₂O₃ (5 mL), H₂O (5 mL) and brine (5 mL). The black solid was not soluble in CH₂Cl₂ nor any of the aqueous solutions and was removed by

filtration. ^1H NMR analysis of the concentrated filtrate residue showed only solvent signals and no evidence of starting acetal or desired aldehyde product.

***para*-Toluenesulfonic Acid Method:** Acetal **162** (0.2 g, 1.11 mmol) was taken in acetone (4 mL) and *p*TsOH·H₂O (0.11 g, 0.55 mmol, 0.5 equiv.) was added. Reaction was stirred at rt and after 3h, the reaction went from an orange solution to a black suspension. TLC analysis showed no spots on the reaction lane so, volatiles were removed and the resulting black insoluble solid was suspended in CH₂Cl₂ (15 mL) and washed sequentially with sat. aq. NaHCO₃ (5 mL), H₂O (5 mL) and brine (5 mL). Black solid was removed by filtration and resulting residue subjected to ^1H NMR analysis where only solvent signals were observed.

Chapter III – Ireland-Claisen Rearrangement

General Procedures for the Asymmetric Ireland-Claisen Reaction under Asymmetric Liquid/Liquid Phase-Transfer Catalysis

A screw cap vial equipped with a magnetic stirring bar, was charged with the ester (0.2 mmol), **XVII** (0.2 equiv.) and organic solvent (1.1 mL). Aqueous basic solution (1.1 mL) was then added, and mixture was vigorously stirred, at rt, and monitored by TLC and/or ^1H NMR. When applicable, reactions were acidified to pH \approx 2 by careful addition of 1.0 M HCl, phases were separated, and aq. layer extracted with EtOAc (3 x 2 mL). Combined organic extracts were dried over Na₂SO₄, filtered, and concentrated under reduced pressure.

Synthesis and isolation of alcohol 171: Ester **169b** (33.5 mg, 0.1 mmol) and **XVII** (10.4 mg, 0.02 mmol, 0.2 equiv.) were dissolved in CH₂Cl₂ (0.4 mL), and aq. 1.0 M NaOH (0.4 mL) was added. Reaction was stirred vigorously at rt and monitored by TLC. After 48h a new, higher *rf* spot was visible in the TLC so, reaction was acidified with careful addition of aq. 2.0 M HCl (until pH \approx 2) and extracted thrice with Et₂O. Combined organic extracts were washed with brine, dried over solid Na₂SO₄, filtered and purified by FC,

eluting with EtOAc/Hexanes (1/3), to give alcohol **171** in 56% yield as a pale-yellow oil. ^1H NMR (300 MHz, CDCl_3) δ 7.44 – 7.37 (m, 2H), 7.38 – 7.30 (m, 2H), 7.30 – 7.22 (m, 1H), 6.60 (d, $J = 15.9$ Hz, 1H), 6.25 (dd, $J = 15.9, 6.8$ Hz, 1H), 4.33 (q, $J = 6.7$ Hz, 1H) 1.73 – 1.54 (m, 4H), 1.54 – 1.35 (m, 2H), 1.30 (s, 1H), 0.98 (t, $J = 7.2$ Hz, 3H). ^{13}C NMR (75 MHz, CDCl_3) δ 136.79, 132.64, 130.23, 128.60, 127.64, 126.47, 72.88, 39.52, 18.70, 14.03.

General Procedures for Enolate Trapping, under APTC conditions

In a screw cap vial equipped with a magnetic stirring bar, was charged ester (0.5 mmol) and toluene (5 mL) and mixture treated sequentially with TMSCl (95 μL , 0.75 mmol, 1.5 equiv.), **XVII** (56 mg, 0.1 mmol, 0.2 equiv.) and aq. NaOH solution (1 mL of either 1.0 M or 50% w/v). Reaction was vigorously stirred at rt for 24h upon which TLC was performed.

General Procedures for the Asymmetric Ireland-Claisen Reaction under Asymmetric Solid/Liquid Phase-Transfer Catalysis

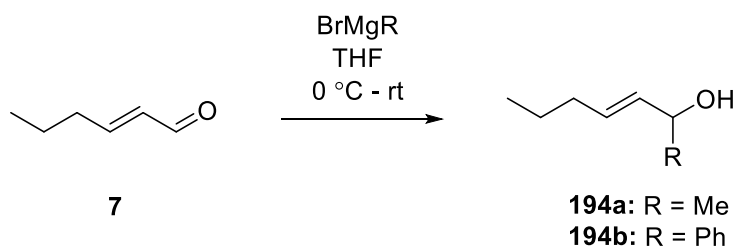
In a screw cap vial equipped with a magnetic stirring bar, was charged the corresponding ester (0.2 mmol), **XVII** (0.2 equiv.), base (see equiv. in the Tables from Part II, Chapter IV) and solvent (0.6 mL). Reaction was vigorously stirred under the appropriate temperature and monitored by ^1H NMR and/or TLC. Reaction was acidified by addition of 1.0 M aq. HCl and product extracted with EtOAc (3x1 mL) and combined organic extracts were washed with brine, dried over Na_2SO_4 , filtered and volatiles removed under reduced pressure.

General Procedures for the Ireland-Claisen Reaction under H-Bond Catalysis

In a screw cap vial equipped with a magnetic stirring bar, ester (0.2 mmol), thiourea (0.2 or 1.0 equiv.) and base (see equiv. in Tables from Part II Chapter IV). Reaction was stirred at the appropriate temperature and monitored by ^1H NMR and/or TLC.

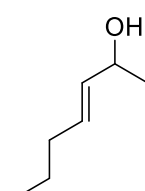
Synthesis and Characterization of the Substrates for the Ireland-Claisen Rearrangement

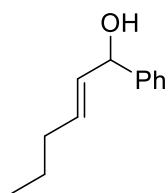
General Procedure for the Synthesis of Allylic Alcohols via Grignard Reaction



Scheme 4. 16 – General reaction Scheme for the synthesis of allylic alcohols **194a** and **194b** via Grignard reaction.

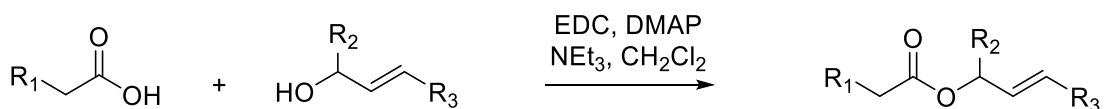
trans-2-Hexenal **7c** (1.0 equiv.) was taken in dry THF (0.25 M) and cooled to 0 °C. An ethereal solution of the Grignard reagent (1.2 equiv.) was added dropwise. Mixture was stirred at 0 °C for 30 min and then allowed to warm up to rt and monitored by TLC. Upon completion, sat. aq. NH_4Cl was added and product extracted with Et_2O (3x). Combined organic layers were washed with brine, dried over Na_2SO_4 , filtered, concentrated, and purified by FC eluting with EtOAc/Hexanes mixture.

 **3-E-hepten-2-ol (194a)**: prepared following the general procedure using *trans*-2-hexenal **7c** (0.6 mL, 5.09 mmol) and BrMgMe 1.0 M in Et_2O (6.1 mL, 6.2 mmol, 1.2 equiv.) in THF (20 mL). Purified by FC using EtOAc/Hexanes (1/5) to give the product as a pale-yellow oil in 70% yield; ^1H NMR (300 MHz, CDCl_3) δ 5.71 – 5.58 (m, 1H), 5.58 – 5.47 (m, 1H), 4.35 – 4.20 (m, 1H), 2.09 – 1.94 (m, 2H), 1.53 (br s, 1H), 1.48 – 1.32 (m, 2H), 1.27 (dd, $J = 6.3, 0.4$ Hz, 3H), 0.91 (t, $J = 7.4$ Hz, 3H).



1-Phenyl-2-*E*-hexen-1-ol (194b): prepared according to the general procedure using *trans*-2-hexenal **7c** (1.18 mL, 10.2 mmol) and BrMgPh 1.0 M in THF (12.2 mL, 12.2 mmol, 1.2 equiv.) in THF (40 mL). Purified by FC using EtOAc/Hexanes (1/9) to give the pure final product as a colorless liquid in 72% yield. ¹H NMR (300 MHz, CDCl₃) δ 7.47 – 7.22 (m, 5H), 5.90 – 5.60 (m, 2H), 5.19 (d, *J* = 6.4 Hz, 1H), 2.14 – 1.98 (m, 2H), 1.90 (s, 1H), 1.54 – 1.33 (m, 2H), 0.93 (t, *J* = 7.4 Hz, 3H).

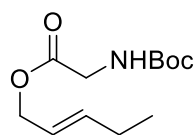
General Procedure for the Steglich Esterification



169: R₁ = NHBoc, R₂ = H, R₃ = Et
169a: R₁ = NHBoc, R₂ = Me, R₃ = *n*Pr
169b: R₁ = NHBoc, R₂ = Me, R₃ = *n*Pr
173: R₁ = CN, R₂ = Me, R₃ = *n*Pr
178: R₁ = CO₂Et, R₂ = H, R₃ = Et

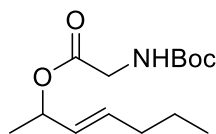
Scheme 4. 17 – General procedure for the Steglich esterification reactions.

A mixture of the carboxylic acid (1.0 equiv.), allylic alcohol (1.13 equiv.) and DMAP (0.5 equiv.), in dry CH₂Cl₂ (0.25 M), was cooled to 0 °C. Then, EDC (1.1 equiv.) was added, and the reaction was stirred at 0 °C for 2h and then at rt overnight. The reaction mixture was then concentrated, and the residue taken in EtOAc and H₂O (5/1). The organic layer was separated and washed sequentially with sat. aq. NaHCO₃ (2x) and H₂O (2x), dried over Na₂SO₄, filtered, concentrated, and purified by FC eluting with EtOAc/Hexanes mixture.



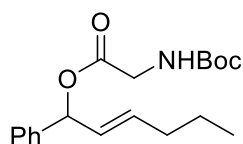
2-*E*-penten-1-yl *N*-Boc glycinate (169): prepared according to the general procedure using *N*-Boc glycine (0.50 g, 2.85 mmol) and *trans*-2-penten-1-ol (0.3 mL, 3.23 mmol, 1.13 equiv.) in CH₂Cl₂ (11.5 mL). Purified by FC using EtOAc/Hexanes (1/5) to give the final product as a pale yellow oil in 89% yield; ¹H NMR (300 MHz, CDCl₃) δ 5.97 – 5.77 (m, 1H), 5.59

(dt, $J = 14.9, 6.6, 1.6$ Hz, 1H), 5.04 (s, 1H), 4.63 (dd, $J = 6.6, 0.9$ Hz, 2H), 3.95 (d, $J = 5.4$ Hz, 2H), 2.20 – 2.01 (m, 2H), 1.49 (s, 9H), 1.04 (td, $J = 7.4, 2.6$ Hz, 3H).



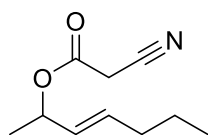
3-E-hepten-2-yl *N*-Boc glycinate (169a): prepared according to the general procedure using *N*-Boc glycine (0.50 g, 2.85 mmol) and alcohol **194a** (0.37 g, 3.23 mmol, 1.13 equiv.) in CH_2Cl_2 (11.5 mL). Purified by FC using EtOAc/Hexanes (1/3) to give the

final product as a pale yellow oil in 83% yield; ^1H NMR (300 MHz, CDCl_3) δ 5.81 – 5.64 (m, 1H), 5.52 – 5.28 (m, 2H), 5.01 (s, 1H), 3.88 (t, $J = 8.9$ Hz, 2H), 2.02 (q, $J = 6.0$ Hz, 2H), 1.47 (s, 9H), 1.41 (dd, $J = 14.8, 7.4$ Hz, 2H), 1.32 (d, $J = 5.3$ Hz, 3H), 0.91 (t, $J = 7.5$ Hz, 3H).



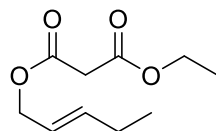
2-Phenyl-3-E-hexen-2-yl *N*-Boc glycinate x1ab (169b): prepared according to the general procedure using *N*-Boc glycine (0.50 g, 2.85 mmol) and alcohol **194b** (0.57 g, 3.23 mmol, 1.13 equiv.) in CH_2Cl_2 (11.5 mL). Purified by FC using

EtOAc/Hexanes (1/3) to give the final product as a pale-yellow oil in 86% yield. ^1H NMR (300 MHz, CDCl_3) δ 7.47 – 7.21 (m, 2H), 6.30 (d, $J = 6.7$ Hz, 1H), 5.86 – 5.71 (m, 1H), 5.66 (dd, $J = 15.4, 6.7$ Hz, 1H), 5.03 (s, 1H), 3.97 (qd, $J = 18.2, 5.4$ Hz, 1H), 2.12 – 1.98 (m, 1H), 1.54 – 1.33 (m, 5H), 0.91 (t, $J = 17.1$ Hz, 1H). ^{13}C NMR (75 MHz, CDCl_3) δ 169.49, 155.66, 139.26, 135.36, 132.54, 132.51, 128.55, 128.46, 128.11, 127.83, 126.90, 126.17, 42.73, 34.26, 28.32, 21.99, 13.65.



3-E-hepten-2-yl cyanoacetate (173): prepared according to the general procedure using cyanoacetic acid (0.50 g, 5.88 mmol) and alcohol **194a** (0.76 g, 6.64 mmol, 1.13 equiv.) in CH_2Cl_2 (23 mL). Purified by FC using EtOAc/Hexanes (1/3) to give the

final product as a pale-yellow oil in 63% yield; ^1H NMR (300 MHz, CDCl_3) δ 5.78 (dt, $J = 12.0, 9.0$ Hz, 1H), 5.54 – 5.34 (m, 2H), 3.44 (s, 2H), 2.09 – 1.97 (m, 2H), 1.47 – 1.33 (m, 5H), 0.91 (t, $J = 7.5$ Hz, 3H).

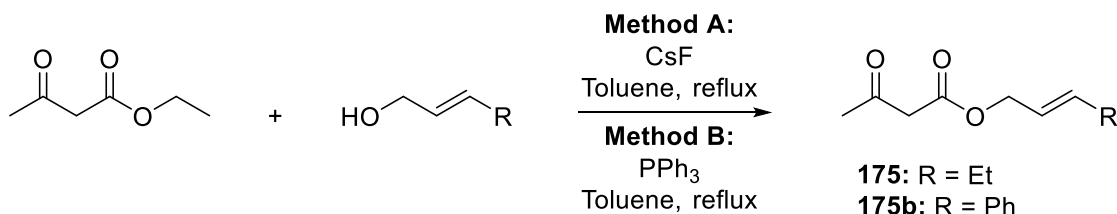


Ethyl-2-E-penten-1-yl malonate (178): prepared according to the general procedure using mono-ethyl malonate (0.5 mL, 4.2 mmol) and *trans*-2-penten-1-ol (0.5 mL, 4.7 mmol, 1.1 equiv.) in CH_2Cl_2 (17 mL). Purified by FC using EtOAc/Hexanes (1/7)

to give the final product as a pale yellow oil in 81% yield; ^1H NMR (300 MHz, CDCl_3) δ 5.96 – 5.79 (m,

1H), 5.67 – 5.49 (m, 1H), 4.62 (dd, $J = 6.5, 0.9$ Hz, 2H), 4.24 (q, $J = 7.1$ Hz, 2H), 3.41 (s, 2H), 2.11 (p, $J = 6.2$ Hz, 2H), 1.31 (t, $J = 7.1$ Hz, 3H), 1.03 (t, $J = 7.5$ Hz, 3H).

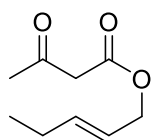
General Procedure for the transesterification of ethyl acetoacetate



Scheme 4. 18 – General reaction scheme for the transesterification of ethyl acetoacetate.

Method A: In a pyrex® test tube (2.5x20 cm) equipped with a drying tube, a vigorously stirred mixture of ethyl acetoacetate (1.0 equiv.), alcohol (1.3 equiv.) and CsF (0.1 equiv.) in toluene (0.5 M) was heated so that toluene refluxed up to halfway of the tube, for 18h. Toluene was decanted and the CsF residue washed with Et₂O. The combined organics were concentrated and purified by FC using a mixture of EtOAc/Hexanes as eluent.

Method B: A round bottom flask equipped with a magnetic stirring bar, condenser, and drying tube, was charged ethylacetoacetate (1.0 equiv.), alcohol (1.0 equiv.), triphenylphosphine (0.1 equiv.) and toluene (0.2 M) and mixture was heated to reflux overnight. Upon completion, SiO₂ was added and residue evaporated to dryness and purified by FC eluting with EtOAc/Hexanes mixture.

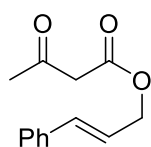


(E)-3-oxo-butanoic acid 2-pentenyl ester (175): Prepared according to method A, using ethyl acetoacetate (1.3 mL, 10 mmol) and *trans*-2-penten-1-ol (1.3 mL, 13 mmol, 1.3 equiv.) in toluene (20 mL). Purified by FC using EtOAc/Hexanes (1/5) to give the final product as

a colorless oil in 50% yield. ¹H NMR (300 MHz, CDCl₃) δ 5.93 – 5.79 (m, 1H), 5.64 – 5.49 (m, 1H), 4.64 – 4.55 (m, 2H), 3.46 (s, 2H), 2.28 (s, 3H), 2.16 – 2.03 (m, 2H), 1.01 (t, $J = 7.5$ Hz, 3H).

Prepared according to method B, using ethyl acetoacetate (0.25 mL, 2.0 mmol), *trans*-2-pentenol (0.2 mL, 2.0 mmol) and PPh₃ (0.05 g, 0.2 mmol, 0.1 equiv.) in toluene (10 mL). Purified by FC using

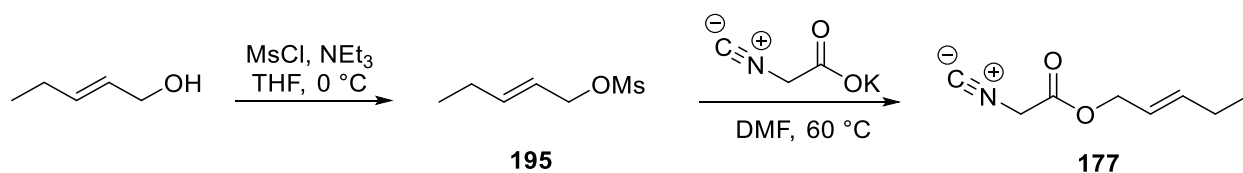
EtOAc/Hexanes (1/5) to give the final product as a colorless oil in 90% yield. $^1\text{H NMR}$ (300 MHz, CDCl_3) δ 5.97 – 5.79 (m, 1H), 5.68 – 5.50 (m, 1H), 4.68 – 4.56 (m, 2H), 3.49 (s, 2H), 2.31 (s, 3H), 2.12 (p, $J = 6.3$ Hz, 2H), 1.04 (t, $J = 7.5$ Hz, 3H).



4-Phenyl-2-buten-1-yl acetoacetate (175b): Prepared according to method A, using ethyl acetoacetate (0.72 mL, 5.73 mmol) and cinnamyl alcohol (1.04 g, 7.45 mmol, 1.3 equiv.) in toluene (11 mL). Purified by FC using EtOAc/Hexanes (1/3) to give the final product as

pale-yellow oil in 37% yield. $^1\text{H NMR}$ (300 MHz, CDCl_3) δ 7.46 – 7.41 (m, 2H), 7.41 – 7.27 (m, 3H), 6.72 (d, $J = 15.9$ Hz, 1H), 6.32 (dt, $J = 15.9, 6.5$ Hz, 1H), 4.84 (dd, $J = 6.5, 1.2$ Hz, 2H), 3.54 (s, 2H), 2.32 (s, 3H).

Esterification of potassium isocyanoacetate



Scheme 4. 19 – Reaction scheme for the esterification of potassium isocyanoacetate.

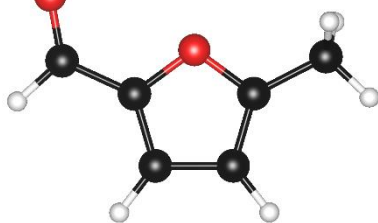
Under argon atmosphere, *trans*-2-penten-1-ol (0.60 mL, 5.8 mmol) was added to a 1.0 M solution of triethylamine in THF (11.6 mL, 11.6 mmol, 2.0 equiv.) and cooled to 0 °C. MsCl (0.70 mL, 8.7 mmol, 1.5 equiv.) was added dropwise and reaction was stirred, at 0 °C and monitored by TLC. Upon completion (usually, 1h), reaction was diluted with Et_2O (60 mL) and washed sequentially with 10% aq. HCl, brine, and sat. aq. NaHCO_3 (30 mL each). The organic layer was dried over Na_2SO_4 , filtered and concentrated and to give the mesylated alcohol as a colorless liquid, in 90% yield which, was used in the next step without further purification. $^1\text{H NMR}$ (300 MHz, CDCl_3) δ 5.97 (tt, $J = 16.5, 8.2$ Hz, 1H), 5.71 – 5.54 (m, 1H), 4.70 (d, $J = 6.8$ Hz, 2H), 3.02 (s, 3H), 2.21 – 2.04 (m, 2H), 1.04 (t, $J = 7.4$ Hz, 3H).

To a suspension of potassium isocyanoacetate (0.64 g, 5.2 mmol) in DMF (4 mL) was added the mesylated alcohol from the previous step (0.85 g, 5.2 mmol) and the mixture was stirred at 60 °C for 3h

(TLC monitoring). Upon completion, reaction was cooled down to rt and H₂O (4 mL) was added, and product extracted with EtOAc (3x4 mL). The combined organic extracts were washed with H₂O (6x6 mL) and sat. aq. NaCl (2x6 mL), dried over Na₂SO₄, filtered, concentrated, and purified by FC EtOAc/Hexanes (1/5) to give the title compound as a colorless liquid in 30% yield. ¹H NMR (300 MHz, CDCl₃) δ 5.90 (dq, *J* = 20.0, 6.2 Hz, 1H), 5.58 (dtt, *J* = 15.1, 6.7, 1.5 Hz, 1H), 4.68 (d, *J* = 6.7 Hz, 2H), 4.24 (s, 2H), 2.20 – 2.01 (m, 2H), 1.03 (t, *J* = 7.5 Hz, 3H); ¹³C NMR (75 MHz, CDCl₃) δ 163.75, 140.03, 121.44, 67.47, 43.55, 25.26, 12.97.

Chapter IV – Energies and Reaction Coordinates

Aldehyde A1



HF (M062X/6-31+G(d,p)) = -382.5277955 Hartrees

Imaginary Frequencies: none found

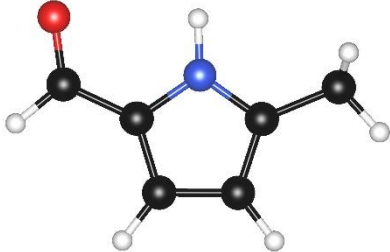
Zero-point correction = 0.108322 (Hartree/Particle)

Thermal correction = 0.076441 Hartrees

Coordinates from last standard orientation:

Center Number	Atomic Number	Atomic Type	Coordinates (Angstroms)		
			X	Y	Z
1	6	0	1.375744	-0.126055	-0.000039
2	6	0	1.299606	1.240881	-0.000011
3	1	0	2.137053	1.922463	0.000080
4	6	0	-0.088014	1.560053	0.000004
5	1	0	-0.543457	2.540475	0.000096
6	6	0	-0.754104	0.364370	-0.000024
7	8	0	0.137251	-0.661068	-0.000044
8	6	0	-2.181796	0.069935	0.000005
9	1	0	-2.818917	0.976375	0.000020
10	6	0	2.514381	-1.080950	0.000034
11	1	0	2.478849	-1.722943	-0.884593
12	1	0	3.457153	-0.532319	0.000007
13	1	0	2.478872	-1.722851	0.884728
14	8	0	-2.660308	-1.042757	0.000025

Aldehyde A2



HF (M062X/6-31+G(d,p)) = -362.6872371 Hartrees

Imaginary Frequencies: none found

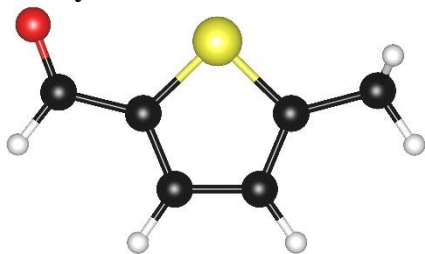
Zero-point correction = 0.121432 (Hartree/Particle)

Thermal correction = 0.089606 Hartrees

Coordinates from last standard orientation:

Center Number	Atomic Number	Atomic Type	Coordinates (Angstroms)		
			X	Y	Z
1	6	0	-1.388959	-0.144738	-0.000005
2	6	0	-1.289247	1.241453	0.000009
3	6	0	0.083412	1.572549	0.000000
4	6	0	0.790787	0.379993	-0.000020
5	7	0	-0.125513	-0.644201	-0.000021
6	1	0	0.146813	-1.618146	-0.000017
7	1	0	-2.127298	1.923694	0.000026
8	1	0	0.520001	2.561822	-0.000006
9	6	0	-2.593252	-1.028401	0.000009
10	1	0	-2.616925	-1.670573	-0.886035
11	1	0	-2.617038	-1.670398	0.886175
12	1	0	-3.497466	-0.417921	-0.000107
13	6	0	2.211180	0.096703	0.000004
14	1	0	2.875750	0.980476	0.000014
15	8	0	2.663903	-1.035612	0.000014

Aldehyde A3



HF (M062X/6-31+G(d,p)) = -705.4955175 Hartrees

Imaginary Frequencies: none found

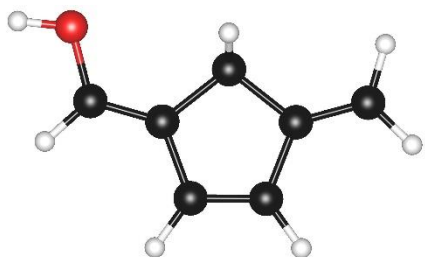
Zero-point correction = 0.104736 (Hartree/Particle)

Thermal correction = 0.070700 Hartrees

Coordinates from last standard orientation:

Center Number	Atomic Number	Atomic Type	Coordinates (Angstroms)		
			X	Y	Z
1	6	0	-0.904114	0.406018	0.000078
2	6	0	-0.180906	1.573719	0.000046
3	6	0	1.220542	1.346593	-0.000070
4	6	0	1.543305	0.011991	-0.000086
5	1	0	-0.646691	2.553622	0.000110
6	1	0	1.968404	2.131347	-0.000133
7	16	0	0.129805	-0.982765	-0.000004
8	6	0	2.913383	-0.593874	0.000039
9	1	0	3.072886	-1.218606	-0.883578
10	1	0	3.664247	0.199244	-0.001502
11	1	0	3.073792	-1.215983	0.885357
12	6	0	-2.359849	0.283404	0.000007
13	1	0	-2.896894	1.253285	-0.000024
14	8	0	-2.963349	-0.768221	-0.000030

Enol A4



HF (M062X/6-31+G(d,p)) = -346.5931717 Hartrees

Imaginary Frequencies: none found

Zero-point correction = 0.131596 (Hartree/Particle)

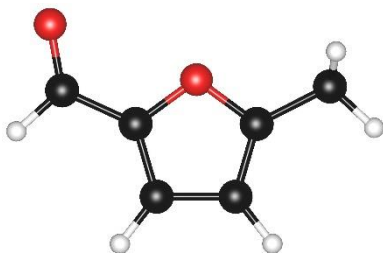
Thermal correction = 0.099574 Hartrees

Coordinates from last standard orientation:

Center Number	Atomic Number	Atomic Type	Coordinates (Angstroms)		
			X	Y	Z

1	6	0	1.583220	-0.291727	-0.000109
2	6	0	1.439401	1.168394	0.000162
3	1	0	2.284272	1.847830	0.000309
4	6	0	0.138321	1.523998	0.000210
5	1	0	-0.240401	2.540783	0.000556
6	6	0	-0.719189	0.343465	-0.000336
7	6	0	-2.055285	0.336594	-0.000431
8	1	0	-2.644403	1.250420	-0.000299
9	6	0	2.732576	-0.977473	-0.000353
10	1	0	2.745972	-2.062922	-0.000708
11	1	0	3.689954	-0.465487	-0.000488
12	8	0	-2.740394	-0.846393	0.002435
13	1	0	-3.688099	-0.685655	-0.014639
14	6	0	0.177203	-0.877822	0.000056
15	1	0	-0.000924	-1.503524	-0.881060
16	1	0	-0.000702	-1.502873	0.881646

Enol A5



HF (M062X/6-31+G(d,p)) = -382.4882319 Hartrees

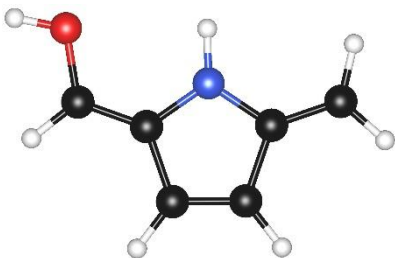
Imaginary Frequencies: none found

Zero-point correction = 0.107953 (Hartree/Particle)

Thermal correction = 0.076513 Hartrees

Coordinates from last standard orientation:

Center Number	Atomic Number	Atomic Type	Coordinates (Angstroms)		
			X	Y	Z
1	6	0	1.472947	-0.310612	0.000145
2	6	0	1.470349	1.150388	-0.000030
3	1	0	2.367223	1.753900	0.000023
4	6	0	0.190456	1.564747	-0.000096
5	1	0	-0.182181	2.580352	-0.000005
6	6	0	-0.652523	0.383111	0.000329
7	8	0	0.157017	-0.727622	0.000465
8	6	0	-1.989768	0.295686	-0.000219
9	1	0	-2.589699	1.199198	-0.000565
10	6	0	2.487729	-1.181719	-0.000218
11	1	0	2.304721	-2.248351	-0.000307
12	1	0	3.506223	-0.816782	-0.000947
13	8	0	-2.620485	-0.909123	-0.000267
14	1	0	-3.573680	-0.783965	0.000745

Enol A6

HF (M062X/6-31+G(d,p)) = -362.6370567 Hartrees

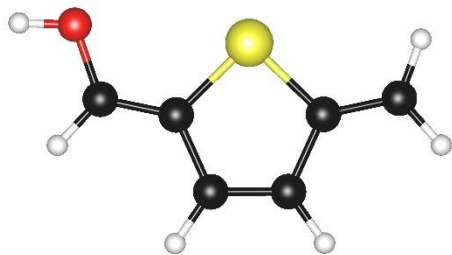
Imaginary Frequencies: none found

Zero-point correction = 0.119909 (Hartree/Particle)

Thermal correction = 0.087709 Hartrees

Coordinates from last standard orientation:

Center Number	Atomic Number	Atomic Type	Coordinates (Angstroms)		
			X	Y	Z
1	6	0	-1.503442	-0.316760	0.000030
2	6	0	-1.458566	1.152729	0.000066
3	1	0	-2.346119	1.771075	0.000128
4	6	0	-0.175706	1.562136	0.000020
5	1	0	0.192039	2.579752	0.000036
6	6	0	0.687264	0.385075	-0.000082
7	6	0	2.028144	0.325937	-0.000062
8	1	0	2.646147	1.215280	-0.000007
9	6	0	-2.589984	-1.111325	0.000050
10	1	0	-2.509377	-2.191917	0.000008
11	1	0	-3.578034	-0.670466	0.000122
12	8	0	2.637654	-0.904564	0.000145
13	1	0	3.593640	-0.806371	-0.001082
14	7	0	-0.168551	-0.711780	-0.000055
15	1	0	0.154075	-1.665137	-0.000119

Enol A7

HF (M062X/6-31+G(d,p)) = -705.4574365 Hartrees

Imaginary Frequencies: none found

Zero-point correction = 0.104529 (Hartree/Particle)

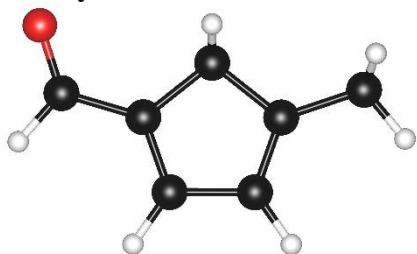
Thermal correction = 0.071959 Hartrees

Coordinates from last standard orientation:

Center	Atomic	Atomic	Coordinates (Angstroms)		
--------	--------	--------	-------------------------	--	--

Number	Number	Type	X	Y	Z
1	6	0	-1.674854	-0.112802	0.000076
2	6	0	-1.373476	1.319149	0.000137
3	1	0	-2.174042	2.050523	0.000240
4	6	0	-0.061874	1.613624	0.000068
5	1	0	0.346517	2.618870	0.000107
6	6	0	0.809543	0.448104	-0.000078
7	6	0	2.149281	0.467685	-0.000068
8	1	0	2.700532	1.404107	-0.000018
9	6	0	-2.894566	-0.670051	0.000122
10	1	0	-3.039977	-1.744046	0.000063
11	1	0	-3.776512	-0.038367	0.000224
12	8	0	2.859943	-0.691066	0.000051
13	1	0	3.804831	-0.512421	-0.000865
14	16	0	-0.154076	-1.040274	-0.000106

Aldehyde A8



HF (M062X/6-31+G(d,p)) = -346.6127503 Hartrees

Imaginary Frequencies: none found

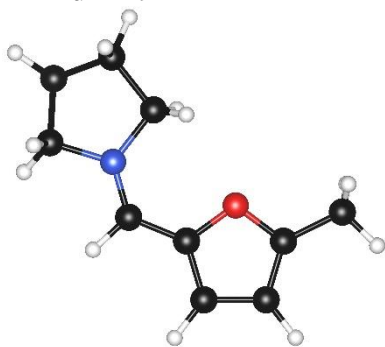
Zero-point correction = 0.130759 (Hartree/Particle)

Thermal correction = 0.098492 Hartrees

Coordinates from last standard orientation:

Center Number	Atomic Number	Atomic Type	Coordinates (Angstroms)		
			X	Y	Z
1	6	0	-0.830027	0.295577	-0.000011
2	6	0	-0.159055	1.474461	-0.000091
3	6	0	1.275807	1.216431	-0.000142
4	6	0	1.489414	-0.120877	-0.000064
5	1	0	-0.616249	2.459337	-0.000163
6	1	0	2.045007	1.980624	-0.000259
7	6	0	2.798092	-0.841239	0.000002
8	1	0	2.887947	-1.487244	-0.880251
9	1	0	3.635476	-0.140054	-0.000817
10	1	0	2.888565	-1.485870	0.881209
11	6	0	-2.279187	0.140251	-0.000018
12	1	0	-2.856745	1.087657	0.000009
13	8	0	-2.850382	-0.933219	0.000156
14	6	0	0.161350	-0.829900	0.000102
15	1	0	0.040310	-1.478554	-0.877663
16	1	0	0.040379	-1.478373	0.878011

Iminium A9



HF (M062X/6-31+G(d,p)) = -519.028205 Hartrees

Imaginary Frequencies: none found

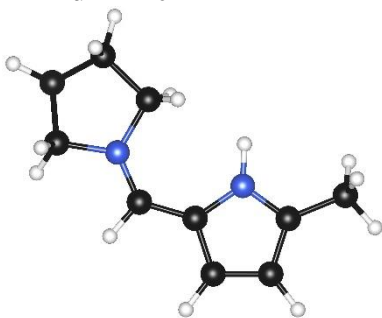
Zero-point correction = 0.228589 (Hartree/Particle)

Thermal correction = 0.191270 Hartrees

Coordinates from last standard orientation:

Center Number	Atomic Number	Atomic Type	Coordinates (Angstroms)		
			X	Y	Z
1	6	0	2.071803	-1.678665	0.004074
2	6	0	3.184241	-0.819227	-0.030374
3	6	0	0.950806	-0.867405	0.026282
4	6	0	-0.408699	-1.239534	0.054838
5	6	0	2.686100	0.466379	-0.029158
6	6	0	3.336769	1.796960	-0.058705
7	7	0	-1.452144	-0.466013	0.073777
8	6	0	-1.443953	1.019389	0.063279
9	6	0	-2.842598	-0.991811	0.079932
10	6	0	-2.919511	1.387633	0.230088
11	1	0	-0.795916	1.386907	0.860248
12	6	0	-3.660028	0.202663	-0.399668
13	1	0	-2.903403	-1.874993	-0.558052
14	1	0	-3.169167	1.470108	1.292257
15	1	0	-4.702076	0.133023	-0.085526
16	1	0	-1.037387	1.348507	-0.898293
17	1	0	-3.150762	2.340271	-0.247802
18	1	0	-3.631665	0.264958	-1.491982
19	1	0	-0.599647	-2.311252	0.057511
20	1	0	2.072254	-2.760433	0.012738
21	1	0	4.228939	-1.091055	-0.053606
22	1	0	3.059039	2.378063	0.825286
23	1	0	-3.100152	-1.265023	1.108880
24	1	0	4.419962	1.679037	-0.078654
25	8	0	1.340123	0.443781	0.005360
26	1	0	3.024424	2.355435	-0.945855

Iminium A10



HF (M062X/6-31+G(d,p)) = -499.1821833 Hartrees

Imaginary Frequencies: none found

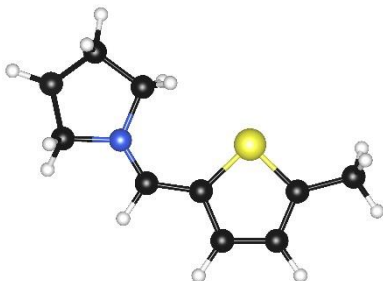
Zero-point correction = 0.241203 (Hartree/Particle)

Thermal correction = 0.202793 Hartrees

Coordinates from last standard orientation:

Center Number	Atomic Number	Atomic Type	Coordinates (Angstroms)		
			X	Y	Z
1	6	0	1.996639	-1.668470	0.027647
2	6	0	3.172804	-0.930468	-0.010649
3	6	0	0.915231	-0.766556	0.026176
4	6	0	-0.432047	-1.151890	0.050023
5	6	0	2.819682	0.425304	-0.039192
6	6	0	3.687395	1.636511	-0.068385
7	7	0	-1.516532	-0.421401	0.068411
8	6	0	-1.567167	1.053771	0.082810
9	6	0	-2.881402	-1.005074	0.064175
10	6	0	-3.058864	1.369223	0.238010
11	1	0	-0.966175	1.434694	0.914624
12	6	0	-3.746083	0.159803	-0.405841
13	1	0	-2.905873	-1.878895	-0.588889
14	1	0	-3.317224	1.432134	1.299134
15	1	0	-4.785746	0.047346	-0.096183
16	1	0	-1.172792	1.427985	-0.870211
17	1	0	-3.322879	2.316372	-0.233682
18	1	0	-3.716760	0.234818	-1.497326
19	1	0	-0.597018	-2.227882	0.051474
20	1	0	1.899207	-2.745760	0.055098
21	1	0	4.185037	-1.306966	-0.019788
22	1	0	3.712983	2.117006	0.914987
23	1	0	-3.136363	-1.306299	1.086108
24	1	0	4.706845	1.356759	-0.334227
25	1	0	3.328477	2.366414	-0.799114
26	7	0	1.471294	0.509456	-0.014389
27	1	0	0.967823	1.382965	-0.048808

Iminium A11



HF (M062X/6-31+G(d,p)) = -841.9915834 Hartrees

Imaginary Frequencies: none found

Zero-point correction = 0.225272 (Hartree/Particle)

Thermal correction = 0.186669 Hartrees

Coordinates from last standard orientation:

Center Number	Atomic Number	Atomic Type	Coordinates (Angstroms)		
			X	Y	Z
1	6	0	-1.720310	1.720016	0.020273
2	6	0	-2.995287	1.139557	-0.020358
3	6	0	-0.690694	0.782140	0.036786
4	6	0	0.669088	1.177416	0.061959
5	6	0	-2.956852	-0.242082	-0.037188
6	6	0	-4.116709	-1.185038	-0.063100
7	7	0	1.742356	0.444838	0.079098
8	6	0	1.791852	-1.035784	0.073044
9	6	0	3.112215	1.022841	0.079989
10	6	0	3.283625	-1.352559	0.214134
11	1	0	1.184190	-1.426914	0.893287
12	6	0	3.969756	-0.135808	-0.416371
13	1	0	3.135135	1.912600	-0.550918
14	1	0	3.550490	-1.433813	1.271986
15	1	0	5.011824	-0.028657	-0.112955
16	1	0	1.382776	-1.389160	-0.880286
17	1	0	3.541294	-2.292605	-0.274737
18	1	0	3.931750	-0.192626	-1.508670
19	1	0	0.841218	2.253715	0.063738
20	1	0	-1.536596	2.789280	0.036413
21	1	0	-3.923091	1.697979	-0.038656
22	1	0	-4.217720	-1.699675	0.897187
23	1	0	3.367293	1.296920	1.109261
24	1	0	-5.036174	-0.629560	-0.253372
25	1	0	-3.999595	-1.941921	-0.842529
26	16	0	-1.344337	-0.835852	-0.003653

Trienamine A12



HF (M062X/6-31+G(d,p)) = -482.7037554 Hartrees

Imaginary Frequencies: none found

Zero-point correction = 0.238156 (Hartree/Particle)

Thermal correction = 0.200257 Hartrees

Coordinates from last standard orientation:

Center Number	Atomic Number	Atomic Type	Coordinates (Angstroms)		
			X	Y	Z
1	6	0	2.986169	0.525401	0.090684
2	6	0	3.224370	-0.890424	-0.193906
3	6	0	2.053807	-1.560554	-0.274431
4	6	0	0.914644	-0.680760	-0.058783
5	1	0	4.213500	-1.317128	-0.313847
6	1	0	1.949128	-2.623620	-0.469634
7	6	0	-0.364344	-1.113596	0.005601
8	1	0	-0.551416	-2.184647	-0.079402
9	7	0	-1.496680	-0.356546	0.197985
10	6	0	3.910472	1.483933	0.237675
11	1	0	4.968826	1.258491	0.150892
12	1	0	3.634737	2.512362	0.450269
13	6	0	-2.799636	-1.009066	0.279490
14	1	0	-2.840244	-1.679950	1.143176
15	1	0	-3.011532	-1.600813	-0.627711
16	6	0	-3.763206	0.168656	0.390808
17	1	0	-3.774771	0.540132	1.420930
18	1	0	-4.784531	-0.093033	0.105329
19	6	0	-3.120024	1.201026	-0.542189
20	1	0	-3.449570	2.224287	-0.348606
21	1	0	-3.364983	0.958284	-1.581625
22	6	0	-1.613387	1.015036	-0.305882
23	1	0	-1.036162	1.127396	-1.231953
24	1	0	-1.225987	1.736727	0.423880
25	6	0	1.475178	0.711776	0.191346
26	1	0	1.191715	1.074725	1.186454
27	1	0	1.133799	1.454035	-0.536530

Fulvene trienamine A12'



HF (M062X/6-31+G(d,p)) = -482.720686 Hartrees

Imaginary Frequencies: none found

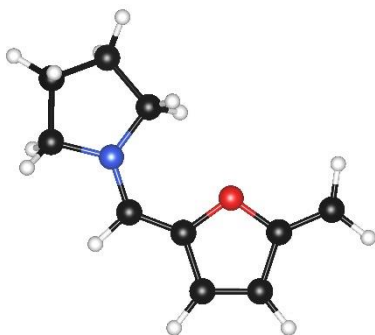
Zero-point correction = 0.238397 (Hartree/Particle)

Thermal correction = 0.200207 Hartrees

Coordinates from last standard orientation:

Center Number	Atomic Number	Atomic Type	Coordinates (Angstroms)		
			X	Y	Z
1	6	0	2.868597	0.454201	0.031474
2	6	0	3.160927	-0.968990	-0.018590
3	6	0	1.985378	-1.658380	-0.047083
4	6	0	0.891804	-0.698183	-0.022925
5	1	0	4.158497	-1.393450	-0.029803
6	1	0	1.854234	-2.733793	-0.086343
7	6	0	-0.413795	-1.120447	-0.038348
8	1	0	-0.585430	-2.196641	-0.048984
9	7	0	-1.546153	-0.399018	-0.039632
10	6	0	-2.878625	-1.005029	-0.034747
11	1	0	-2.911636	-1.850111	0.658871
12	1	0	-3.142797	-1.367444	-1.038604
13	6	0	-3.780342	0.155887	0.382432
14	1	0	-3.772120	0.257793	1.472808
15	1	0	-4.813559	0.022393	0.055274
16	6	0	-3.089642	1.361604	-0.266138
17	1	0	-3.379903	2.315918	0.177781
18	1	0	-3.328913	1.396747	-1.334295
19	6	0	-1.599233	1.059706	-0.076607
20	1	0	-0.978014	1.437989	-0.895308
21	1	0	-1.209761	1.470557	0.864811
22	6	0	1.510593	0.620644	0.027420
23	1	0	1.006356	1.576379	0.073724
24	6	0	3.906864	1.533666	0.082882
25	1	0	3.443436	2.522744	0.135042
26	1	0	4.556985	1.418007	0.957441
27	1	0	4.550523	1.507961	-0.803617

Triamine A13



HF (M062X/6-31+G(d,p)) = -518.6058491 Hartrees

Imaginary Frequencies: none found

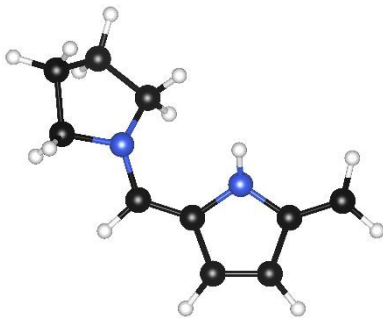
Zero-point correction = 0.213928 (Hartree/Particle)

Thermal correction = 0.175216 Hartrees

Coordinates from last standard orientation:

Center Number	Atomic Number	Atomic Type	Coordinates (Angstroms)		
			X	Y	Z
1	6	0	2.745192	0.599225	0.040828
2	6	0	3.244851	-0.767393	-0.035214
3	6	0	2.180404	-1.597980	-0.073379
4	6	0	0.984532	-0.797959	-0.023546
5	1	0	4.294025	-1.025899	-0.054817
6	1	0	2.185420	-2.678734	-0.130920
7	6	0	-0.308772	-1.201441	-0.026831
8	1	0	-0.476739	-2.274060	-0.063818
9	7	0	-1.434911	-0.439954	0.025448
10	6	0	3.391627	1.773288	0.099996
11	1	0	4.473192	1.788434	0.094450
12	1	0	2.848655	2.707707	0.154995
13	6	0	-2.766022	-1.033351	-0.003701
14	1	0	-2.841491	-1.852471	0.719833
15	1	0	-3.003213	-1.433705	-1.002591
16	6	0	-3.672495	0.147999	0.339848
17	1	0	-3.704936	0.284655	1.426068
18	1	0	-4.693889	0.013111	-0.022768
19	6	0	-2.944664	1.325690	-0.319117
20	1	0	-3.245953	2.296659	0.079918
21	1	0	-3.142050	1.325127	-1.396667
22	6	0	-1.464806	1.021085	-0.061154
23	1	0	-0.811203	1.375387	-0.863251
24	1	0	-1.109913	1.466989	0.876919
25	8	0	1.366674	0.533938	0.047267

Trienamamine A14



HF (M062X/6-31+G(d,p)) = -498.7478339 Hartrees

Imaginary Frequencies: none found

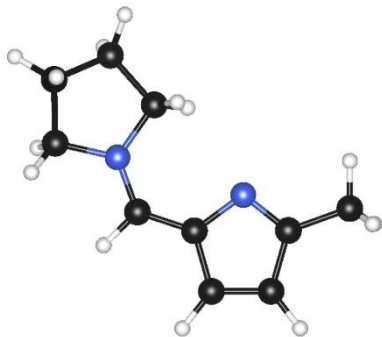
Zero-point correction = 0.226391 (Hartree/Particle)

Thermal correction = 0.188996 Hartrees

Coordinates from last standard orientation:

Center Number	Atomic Number	Atomic Type	Coordinates (Angstroms)		
			X	Y	Z
1	6	0	2.829793	0.569448	0.106917
2	6	0	3.211752	-0.784762	-0.307677
3	6	0	2.107037	-1.555518	-0.376476
4	6	0	0.945933	-0.751857	-0.027353
5	7	0	1.431912	0.547781	0.184725
6	1	0	0.933279	1.196431	0.774274
7	1	0	4.233420	-1.077107	-0.509965
8	1	0	2.050578	-2.600391	-0.653932
9	6	0	-0.344221	-1.147847	0.055164
10	1	0	-0.573822	-2.205030	-0.063971
11	7	0	-1.413410	-0.299447	0.310760
12	6	0	3.632216	1.620059	0.364573
13	1	0	4.705196	1.513046	0.273203
14	1	0	3.236071	2.582317	0.667397
15	6	0	-2.721337	-0.909461	0.543053
16	1	0	-2.767170	-1.361328	1.538982
17	1	0	-2.924096	-1.699689	-0.201002
18	6	0	-3.695431	0.252046	0.366099
19	1	0	-3.725768	0.856623	1.279097
20	1	0	-4.710458	-0.081866	0.139434
21	6	0	-3.045561	1.042091	-0.774043
22	1	0	-3.403518	2.071489	-0.850872
23	1	0	-3.242905	0.540431	-1.727833
24	6	0	-1.550400	0.960462	-0.444271
25	1	0	-0.916551	0.939488	-1.336890
26	1	0	-1.242464	1.819290	0.167771

Fulvene trienamine A14'



HF (M062X/6-31+G(d,p)) = -498.7768887 Hartrees

Imaginary Frequencies: none found

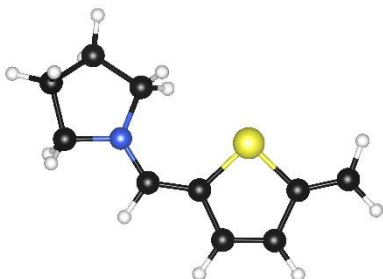
Zero-point correction = 0.227128 (Hartree/Particle)

Thermal correction = 0.189429 Hartrees

Coordinates from last standard orientation:

Center Number	Atomic Number	Atomic Type	Coordinates (Angstroms)		
			X	Y	Z
1	6	0	2.692671	0.481895	0.026678
2	6	0	3.178172	-0.880804	0.015161
3	6	0	2.066997	-1.677579	-0.016139
4	6	0	0.942446	-0.777379	-0.024065
5	1	0	4.216558	-1.187257	0.029303
6	1	0	2.017508	-2.759682	-0.033153
7	6	0	-0.374391	-1.184693	-0.050228
8	1	0	-0.562355	-2.257509	-0.061540
9	7	0	-1.474110	-0.431614	-0.059064
10	6	0	-2.825811	-0.998428	-0.068463
11	1	0	-2.882023	-1.861841	0.600558
12	1	0	-3.095563	-1.323777	-1.082837
13	6	0	-3.695179	0.176488	0.376632
14	1	0	-3.685494	0.251199	1.469281
15	1	0	-4.731096	0.077308	0.045774
16	6	0	-2.968279	1.376841	-0.241176
17	1	0	-3.237668	2.327830	0.222601
18	1	0	-3.200938	1.442503	-1.309756
19	6	0	-1.488001	1.037726	-0.046131
20	1	0	-0.827573	1.425675	-0.823678
21	1	0	-1.093341	1.394171	0.912262
22	6	0	3.546325	1.711766	0.062109
23	1	0	4.179548	1.725047	0.955578
24	1	0	4.209354	1.754718	-0.808615
25	1	0	2.913381	2.600901	0.066281
26	7	0	1.378396	0.545287	0.003590

Trienammine A15



HF (M062X/6-31+G(d,p)) = -841.5716629 Hartrees

Imaginary Frequencies: none found

Zero-point correction = 0.210916 (Hartree/Particle)

Thermal correction = 0.171406 Hartrees

Coordinates from last standard orientation:

Center Number	Atomic Number	Atomic Type	Coordinates (Angstroms)		
			X	Y	Z
1	6	0	-3.055180	-0.346298	0.026575
2	6	0	-3.062135	1.102553	-0.150453
3	6	0	-1.838690	1.667574	-0.180820
4	6	0	-0.728078	0.749543	-0.036290
5	1	0	-3.997682	1.641832	-0.245034
6	1	0	-1.660578	2.731652	-0.303701
7	6	0	0.567522	1.153284	-0.002579
8	1	0	0.740098	2.227447	-0.059326
9	7	0	1.704859	0.414634	0.112913
10	6	0	-4.119293	-1.163239	0.090603
11	1	0	-5.118806	-0.750368	0.007663
12	1	0	-4.020571	-2.234036	0.224608
13	6	0	3.016371	1.056607	0.154104
14	1	0	3.068547	1.778395	0.975568
15	1	0	3.225683	1.588679	-0.787915
16	6	0	3.969654	-0.122597	0.336902
17	1	0	4.014637	-0.401804	1.394943
18	1	0	4.982564	0.100327	-0.005192
19	6	0	3.284907	-1.228782	-0.473454
20	1	0	3.625552	-2.232471	-0.210712
21	1	0	3.471005	-1.073842	-1.541617
22	6	0	1.796487	-1.019756	-0.170152
23	1	0	1.156534	-1.283277	-1.018283
24	1	0	1.476445	-1.610291	0.697772
25	16	0	-1.367927	-0.904876	0.157139

Iminium A16



HF (M062X/6-31+G(d,p)) = -483.1133476 Hartrees

Imaginary Frequencies: none found

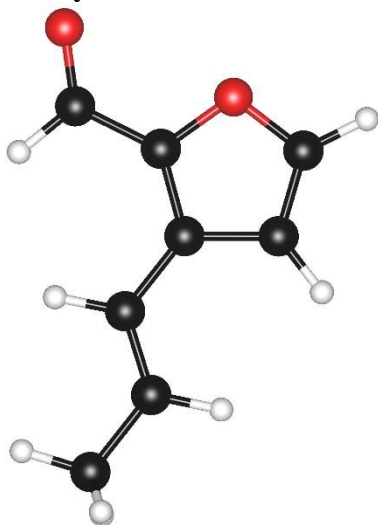
Zero-point correction = 0.251329 (Hartree/Particle)

Thermal correction = 0.213321 Hartrees

Coordinates from last standard orientation:

Center Number	Atomic Number	Atomic Type	Coordinates (Angstroms)		
			X	Y	Z
1	6	0	-1.886537	-1.632074	-0.005783
2	6	0	-3.159509	-0.975359	0.040865
3	6	0	-0.865688	-0.707269	-0.044241
4	6	0	0.482677	-1.130099	-0.070862
5	6	0	-2.963655	0.373338	0.031017
6	6	0	-3.997190	1.443894	0.064806
7	7	0	1.567462	-0.407366	-0.075299
8	6	0	1.632738	1.071582	-0.035825
9	6	0	2.929699	-0.999671	-0.086535
10	6	0	3.122754	1.374434	-0.211741
11	1	0	1.006168	1.492960	-0.824010
12	6	0	3.807807	0.148021	0.400483
13	1	0	2.949204	-1.888255	0.546478
14	1	0	3.366094	1.453901	-1.275577
15	1	0	4.843713	0.032365	0.079673
16	1	0	1.261928	1.406915	0.938833
17	1	0	3.403342	2.310643	0.272180
18	1	0	3.788641	0.200822	1.493555
19	1	0	0.651129	-2.206974	-0.082626
20	1	0	-1.745815	-2.709167	-0.007318
21	1	0	-4.118064	-1.477421	0.079215
22	1	0	-3.942072	2.060843	-0.838755
23	1	0	3.175415	-1.280860	-1.116285
24	1	0	-5.000507	1.022370	0.136176
25	1	0	-3.835386	2.110297	0.918710
26	6	0	-1.491390	0.666817	-0.030379
27	1	0	-1.264441	1.247653	-0.933811
28	1	0	-1.181829	1.273787	0.829821

Aldehyde B1



HF (M062X/6-31+G(d,p)) = -459.8920817 Hartrees

Imaginary Frequencies: none found

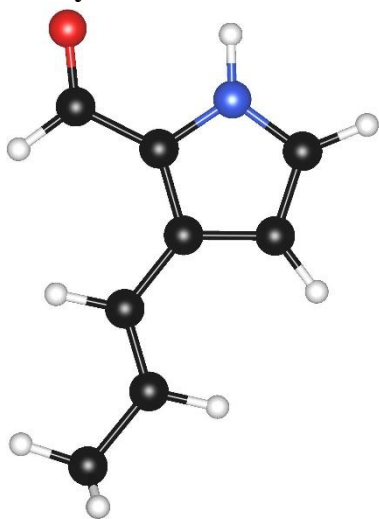
Zero-point correction = 0.142254 (Hartree/Particle)

Thermal correction = 0.107009 Hartrees

Coordinates from last standard orientation:

Center Number	Atomic Number	Atomic Type	Coordinates (Angstroms)		
			X	Y	Z
1	6	0	0.156592	0.332642	0.000118
2	6	0	-1.124296	-0.179309	-0.000104
3	6	0	-1.618166	-1.550818	-0.000173
4	1	0	-0.825187	-2.322712	-0.000582
5	6	0	1.401428	-0.432246	0.000331
6	6	0	2.623805	0.112161	-0.000054
7	6	0	3.899091	-0.671982	-0.000090
8	1	0	4.505492	-0.429055	0.878932
9	1	0	3.703921	-1.747239	0.001843
10	1	0	1.312386	-1.517116	0.000871
11	1	0	2.720925	1.197655	-0.000481
12	6	0	-1.349960	1.981493	0.000067
13	1	0	-1.942345	2.883819	0.000063
14	6	0	-0.008109	1.757558	0.000055
15	1	0	0.763585	2.512637	0.000161
16	1	0	4.503512	-0.431944	-0.881302
17	8	0	-2.036948	0.826516	-0.000184
18	8	0	-2.791127	-1.856896	0.000133

Aldehyde B2



HF (M062X/6-31+G(d,p)) = -440.0542266 Hartrees

Imaginary Frequencies: none found

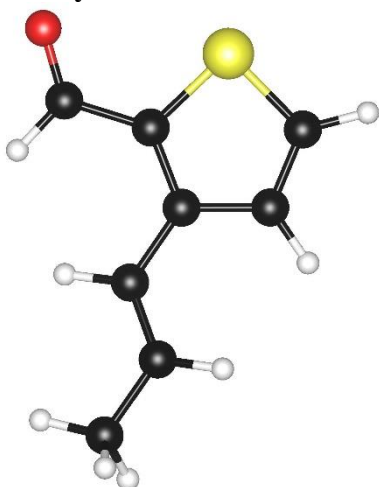
Zero-point correction = 0.155004 (Hartree/Particle)

Thermal correction = 0.119651 Hartrees

Coordinates from last standard orientation:

Center Number	Atomic Number	Atomic Type	Coordinates (Angstroms)		
			X	Y	Z
1	6	0	0.170557	0.344118	0.000294
2	6	0	-1.113486	-0.207302	0.000152
3	6	0	-1.593894	-1.574674	0.000029
4	1	0	-0.825434	-2.368153	0.000292
5	6	0	1.420573	-0.414254	0.000492
6	6	0	2.645751	0.123997	-0.000261
7	6	0	3.917927	-0.666789	-0.000212
8	1	0	4.526751	-0.429396	0.878934
9	1	0	3.716092	-1.741149	0.001731
10	1	0	1.332808	-1.500150	0.001360
11	1	0	2.747641	1.209094	-0.001064
12	6	0	-1.360946	2.008493	-0.000144
13	1	0	-1.894774	2.947372	-0.000345
14	6	0	-0.002751	1.754788	0.000230
15	1	0	0.773333	2.506068	0.000388
16	1	0	4.524921	-0.432292	-0.881427
17	8	0	-2.781778	-1.853912	-0.000277
18	7	0	-2.018887	0.823082	-0.000165
19	1	0	-3.017293	0.668069	0.000032

Aldehyde B3



HF (M062X/6-31+G(d,p)) = -782.8629443 Hartrees

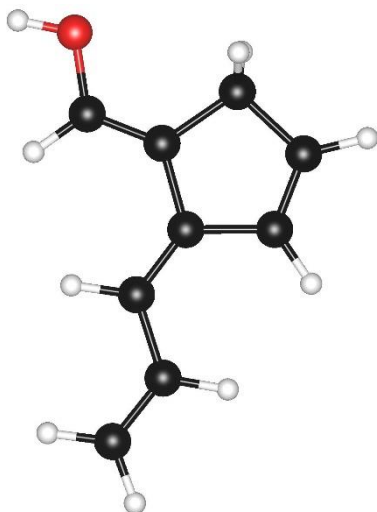
Imaginary Frequencies: none found

Zero-point correction = 0.138668 (Hartree/Particle)

Thermal correction = 0.102485 Hartrees

Coordinates from last standard orientation:

Center Number	Atomic Number	Atomic Type	Coordinates (Angstroms)		
			X	Y	Z
1	6	0	-0.346814	-0.274220	-0.068014
2	6	0	0.863826	0.401062	-0.025519
3	6	0	1.101979	1.842626	-0.000699
4	1	0	0.199003	2.479863	-0.021404
5	6	0	-1.659162	0.379713	-0.125736
6	6	0	-2.827082	-0.232556	0.104243
7	6	0	-4.161055	0.443817	0.035167
8	1	0	-4.683485	0.373690	0.995173
9	1	0	-4.057680	1.500216	-0.225293
10	1	0	-1.674469	1.439573	-0.371163
11	1	0	-2.833113	-1.289184	0.370055
12	6	0	1.176432	-2.033636	-0.001317
13	1	0	1.591211	-3.032799	0.008566
14	6	0	-0.144064	-1.690428	-0.056519
15	1	0	-0.943562	-2.418934	-0.109864
16	1	0	-4.802421	-0.034604	-0.712885
17	8	0	2.207938	2.342223	0.044619
18	16	0	2.219791	-0.673368	0.033764

Enol B4

HF (M062X/6-31+G(d,p)) = -423.962005 Hartrees

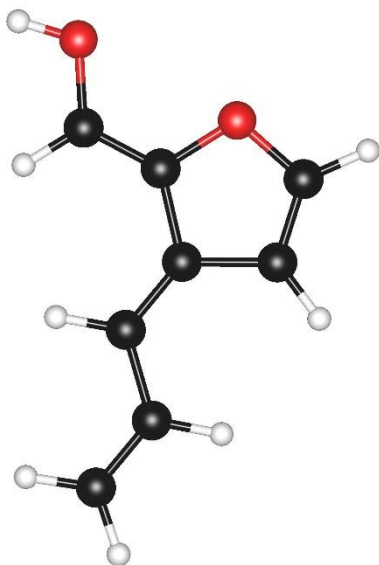
Imaginary Frequencies: none found

Zero-point correction = 0.165626 (Hartree/Particle)

Thermal correction = 0.130196 Hartrees

Coordinates from last standard orientation:

Center Number	Atomic Number	Atomic Type	Coordinates (Angstroms)		
			X	Y	Z
1	6	0	-0.338758	0.264310	0.000026
2	6	0	1.076592	-0.165825	-0.000039
3	6	0	1.534391	-1.419239	0.000128
4	1	0	0.882328	-2.289208	0.000318
5	6	0	-1.438569	-0.523758	-0.000098
6	6	0	-2.810125	-0.048347	0.000043
7	6	0	-3.881241	-0.855807	-0.000064
8	1	0	-4.890588	-0.460108	0.000061
9	1	0	-3.770003	-1.937185	-0.000278
10	1	0	-1.312150	-1.606048	-0.000320
11	1	0	-2.967748	1.028445	0.000260
12	6	0	0.965582	2.185159	0.000026
13	1	0	1.254164	3.230646	0.000034
14	6	0	-0.298314	1.735944	0.000162
15	1	0	-1.180390	2.364792	0.000314
16	6	0	1.967252	1.059445	-0.000187
17	1	0	2.623661	1.087570	-0.879163
18	1	0	2.624001	1.087530	0.878536
19	8	0	2.878252	-1.661293	-0.000064
20	1	0	3.049848	-2.607385	0.000770

Enol B5

HF (M062X/6-31+G(d,p)) = -459.8540095 Hartrees

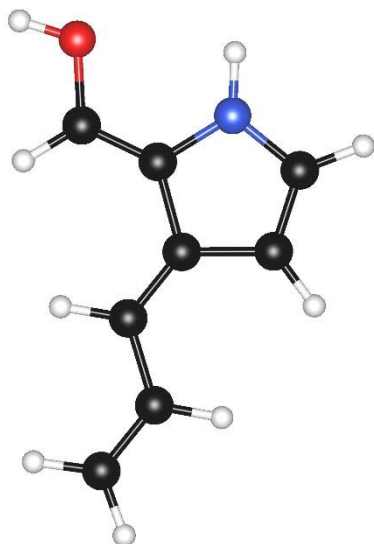
Imaginary Frequencies: none found

Zero-point correction = 0.141517 (Hartree/Particle)

Thermal correction = 0.106321 Hartrees

Coordinates from last standard orientation:

Center Number	Atomic Number	Atomic Type	Coordinates (Angstroms)		
			X	Y	Z
1	6	0	-0.350825	0.264652	0.000063
2	6	0	1.063419	-0.144250	0.000032
3	6	0	1.621940	-1.360345	0.000087
4	1	0	0.999224	-2.248373	0.000162
5	6	0	-1.442305	-0.538923	0.000035
6	6	0	-2.809674	-0.060985	-0.000030
7	6	0	-3.887598	-0.860485	-0.000070
8	1	0	-4.893381	-0.456151	-0.000167
9	1	0	-3.785325	-1.942601	-0.000017
10	1	0	-1.305317	-1.619116	0.000057
11	1	0	-2.958075	1.017615	-0.000095
12	8	0	1.865207	0.986859	-0.000010
13	6	0	1.023095	2.057127	-0.000093
14	1	0	1.513580	3.020366	-0.000086
15	6	0	-0.277143	1.725747	0.000126
16	1	0	-1.105074	2.417643	0.000304
17	8	0	2.971270	-1.516077	-0.000282
18	1	0	3.197087	-2.450868	0.001281

Enol B6

HF (M062X/6-31+G(d,p)) = -440.0033034 Hartrees

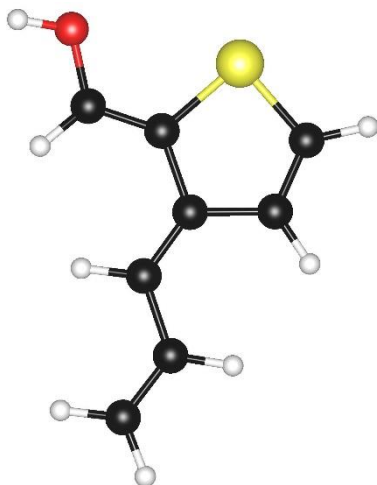
Imaginary Frequencies: none found

Zero-point correction = 0.152735 (Hartree/Particle)

Thermal correction = 0.116901 Hartrees

Coordinates from last standard orientation:

Center Number	Atomic Number	Atomic Type	Coordinates (Angstroms)		
			X	Y	Z
1	6	0	-0.356701	0.274819	0.000033
2	6	0	1.056893	-0.169372	0.000443
3	6	0	1.584701	-1.402207	-0.000013
4	1	0	0.982242	-2.302049	-0.000626
5	6	0	-1.449809	-0.531306	0.000238
6	6	0	-2.816112	-0.055424	-0.000043
7	6	0	-3.896480	-0.853342	-0.000101
8	1	0	-4.901644	-0.447312	-0.000387
9	1	0	-3.796151	-1.935738	0.000098
10	1	0	-1.311820	-1.611526	0.000572
11	1	0	-2.963693	1.023366	-0.000291
12	6	0	1.018638	2.093959	-0.000152
13	1	0	1.447794	3.087094	-0.000358
14	6	0	-0.287204	1.735112	-0.000254
15	1	0	-1.124588	2.415147	-0.000395
16	8	0	2.951331	-1.529565	-0.001222
17	1	0	3.203512	-2.457111	0.005278
18	7	0	1.840591	0.989771	0.000898
19	1	0	2.846008	0.982824	-0.001299

Enol B7

HF (M062X/6-31+G(d,p)) = -782.8244225 Hartrees

Imaginary Frequencies: none found

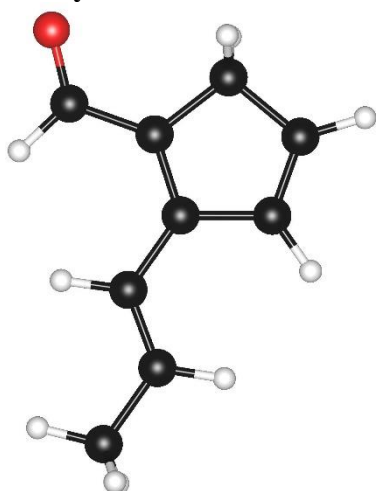
Zero-point correction = 0.138690 (Hartree/Particle)

Thermal correction = 0.102729 Hartrees

Coordinates from last standard orientation:

Center Number	Atomic Number	Atomic Type	Coordinates (Angstroms)		
			X	Y	Z
1	6	0	0.530561	-0.211753	-0.032191
2	6	0	-0.822248	0.384908	0.001438
3	6	0	-1.142555	1.682648	-0.077888
4	1	0	-0.389028	2.456814	-0.190392
5	6	0	1.689649	0.491100	0.040353
6	6	0	3.021498	-0.078152	-0.020263
7	6	0	4.145852	0.649812	0.062597
8	1	0	5.125339	0.187824	0.012848
9	1	0	4.109784	1.729618	0.182174
10	1	0	1.643536	1.572363	0.160605
11	1	0	3.106360	-1.156189	-0.140268
12	6	0	-0.862469	-2.109015	-0.042083
13	1	0	-1.179739	-3.144231	-0.054998
14	6	0	0.404393	-1.666396	-0.108656
15	1	0	1.253870	-2.333442	-0.179637
16	8	0	-2.442206	2.074794	-0.011325
17	1	0	-2.525648	3.015794	-0.192310
18	16	0	-2.087182	-0.861614	0.097046

Aldehyde B8



HF (M062X/6-31+G(d,p)) = -423.9821478 Hartrees

Imaginary Frequencies: none found

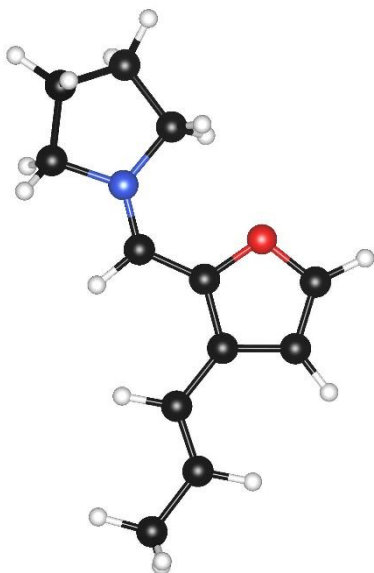
Zero-point correction = 0.165110 (Hartree/Particle)

Thermal correction = 0.129708 Hartrees

Coordinates from last standard orientation:

Center Number	Atomic Number	Atomic Type	Coordinates (Angstroms)		
			X	Y	Z
1	6	0	-0.133036	0.304327	-0.000013
2	6	0	1.134397	-0.213557	-0.000130
3	6	0	1.520053	-1.617991	-0.000032
4	1	0	0.699936	-2.361707	-0.000108
5	6	0	-1.388875	-0.440435	0.000014
6	6	0	-2.604974	0.123106	0.000029
7	6	0	-3.890813	-0.642730	-0.000027
8	1	0	-4.492409	-0.391292	-0.880104
9	1	0	-3.712179	-1.720735	0.000317
10	1	0	-1.322556	-1.526616	0.000017
11	1	0	-2.690278	1.208923	0.000057
12	6	0	1.276827	2.122981	0.000026
13	1	0	1.662900	3.135474	0.000025
14	6	0	-0.022682	1.772252	0.000106
15	1	0	-0.863245	2.455336	0.000226
16	6	0	2.139477	0.898664	-0.000112
17	1	0	2.798702	0.850007	-0.876785
18	1	0	2.798726	0.849840	0.876538
19	1	0	-4.492823	-0.390780	0.879612
20	8	0	2.678874	-1.993520	0.000130

Iminium B9



HF (M062X/6-31+G(d,p)) = -596.3955132Hartrees

Imaginary Frequencies: none found

Zero-point correction = 0.262114 (Hartree/Particle)

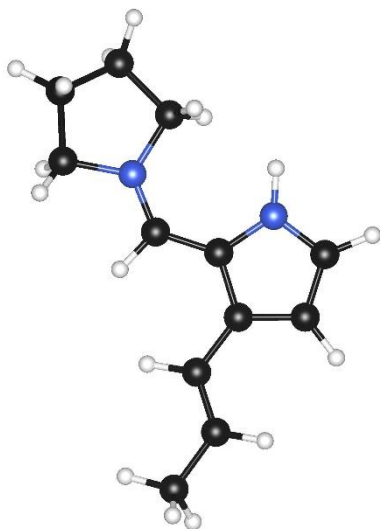
Thermal correction = 0.220898Hartrees

Coordinates from last standard orientation:

Center Number	Atomic Number	Atomic Type	Coordinates (Angstroms)		
			X	Y	Z
1	6	0	-1.767091	0.456765	0.001594
2	6	0	-0.369878	0.497308	0.012797
3	6	0	0.547701	-0.566714	0.037760
4	1	0	0.117143	-1.565920	0.036943
5	7	0	1.848244	-0.508273	0.055056
6	6	0	2.703466	-1.724094	0.048657
7	1	0	2.276199	-2.470158	-0.623574
8	1	0	2.738157	-2.126052	1.067099
9	6	0	4.063769	-1.185160	-0.383141
10	1	0	4.106791	-1.099269	-1.473419
11	1	0	4.878321	-1.832761	-0.056700
12	6	0	4.096202	0.200080	0.270102
13	1	0	4.837956	0.866227	-0.171957
14	1	0	4.313208	0.109886	1.338909
15	6	0	2.675307	0.725484	0.065657
16	1	0	2.327688	1.393829	0.854162
17	1	0	2.550528	1.226623	-0.899420
18	6	0	-2.603004	-0.729608	0.043893
19	6	0	-3.943392	-0.693308	-0.019969
20	6	0	-4.826074	-1.894202	0.024414
21	1	0	-5.443628	-1.944686	-0.878302
22	1	0	-4.251653	-2.818637	0.110616
23	1	0	-2.110727	-1.695563	0.135116
24	1	0	-4.442737	0.270897	-0.111794
25	6	0	-1.033801	2.567152	-0.072601
26	1	0	-0.861297	3.633093	-0.111323

27	6	0	-2.174581	1.821863	-0.053799
28	1	0	-3.181258	2.210601	-0.073046
29	1	0	-5.515101	-1.826764	0.872843
30	8	0	0.063870	1.796646	-0.031717

Iminium B10



HF (M062X/6-31+G(d,p)) = -576.5496683 Hartrees

Imaginary Frequencies: none found

Zero-point correction = 0.275235 (Hartree/Particle)

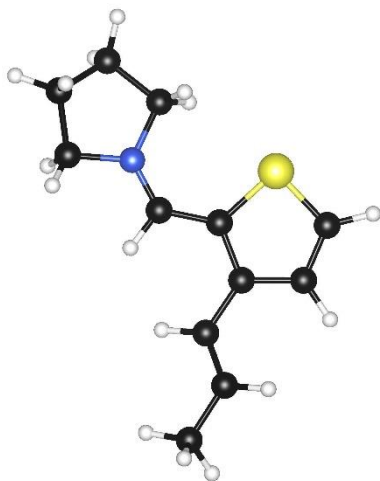
Thermal correction = 0.234419 Hartrees

Coordinates from last standard orientation:

Center Number	Atomic Number	Atomic Type	Coordinates (Angstroms)		
			X	Y	Z
1	6	0	-1.778452	0.496202	0.043162
2	6	0	-0.360193	0.610650	0.009567
3	6	0	0.533384	-0.465978	0.012017
4	1	0	0.074008	-1.451744	-0.005576
5	7	0	1.843218	-0.473223	0.024678
6	6	0	2.636290	-1.728588	-0.010822
7	1	0	2.196220	-2.422490	-0.729016
8	1	0	2.622478	-2.179653	0.987558
9	6	0	4.033451	-1.242039	-0.384665
10	1	0	4.114336	-1.123409	-1.469718
11	1	0	4.807651	-1.936456	-0.056259
12	6	0	4.115499	0.118743	0.314865
13	1	0	4.897180	0.764373	-0.086969
14	1	0	4.298461	-0.014760	1.385210
15	6	0	2.720681	0.710802	0.095855
16	1	0	2.401271	1.356913	0.919241
17	1	0	2.662293	1.253061	-0.856490
18	6	0	-2.534708	-0.745728	0.141124
19	6	0	-3.854294	-0.832774	-0.082415
20	6	0	-4.651104	-2.090237	0.025967
21	1	0	-5.147303	-2.312452	-0.924298

22	1	0	-4.027996	-2.942501	0.305057
23	1	0	-1.998400	-1.651081	0.417971
24	1	0	-4.402327	0.064570	-0.368923
25	6	0	-1.212382	2.673713	-0.093938
26	1	0	-1.199752	3.752988	-0.156469
27	6	0	-2.288823	1.805059	-0.018979
28	1	0	-3.326287	2.101851	0.010389
29	1	0	-5.441494	-1.975098	0.774979
30	7	0	-0.063075	1.969610	-0.069076
31	1	0	0.852561	2.382215	-0.146331

Iminium B11



HF (M062X/6-31+G(d,p)) = -919.3607663 Hartrees

Imaginary Frequencies: none found

Zero-point correction = 0.258647 (Hartree/Particle)

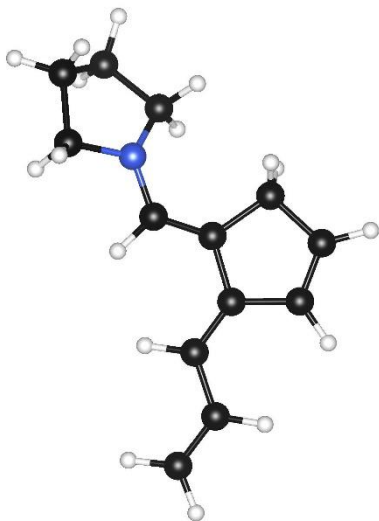
Thermal correction = 0.217046 Hartrees

Coordinates from last standard orientation:

Center Number	Atomic Number	Atomic Type	Coordinates (Angstroms)		
			X	Y	Z
1	6	0	-1.762529	0.325871	0.097154
2	6	0	-0.362399	0.482490	0.069375
3	6	0	0.525181	-0.617074	0.047949
4	1	0	0.060778	-1.601353	0.015090
5	7	0	1.827730	-0.633629	0.044344
6	6	0	2.608753	-1.898288	-0.022249
7	1	0	2.141439	-2.581621	-0.733093
8	1	0	2.611871	-2.352525	0.974547
9	6	0	4.002220	-1.423292	-0.422398
10	1	0	4.059513	-1.291025	-1.507319
11	1	0	4.773986	-2.132585	-0.121044
12	6	0	4.114400	-0.073643	0.293345
13	1	0	4.895931	0.567676	-0.115426
14	1	0	4.316714	-0.222908	1.358200
15	6	0	2.725948	0.541229	0.105548
16	1	0	2.421669	1.194211	0.927459

17	1	0	2.646778	1.088526	-0.840788
18	6	0	-2.459654	-0.951221	0.235010
19	6	0	-3.727384	-1.149250	-0.159370
20	6	0	-4.467947	-2.435907	-0.009555
21	1	0	-4.798925	-2.803122	-0.986321
22	1	0	-3.856240	-3.204166	0.467855
23	1	0	-1.927002	-1.780202	0.695661
24	1	0	-4.268724	-0.331192	-0.634229
25	6	0	-1.550305	2.634189	-0.097167
26	1	0	-1.800906	3.685342	-0.166173
27	6	0	-2.418945	1.581290	0.002836
28	1	0	-3.493236	1.706542	0.042960
29	1	0	-5.370940	-2.283670	0.591047
30	16	0	0.089321	2.167444	-0.070106

Trienamine B12



HF (M062X/6-31+G(d,p)) = -560.0733681 Hartrees

Imaginary Frequencies: none found

Zero-point correction = 0.271641 (Hartree/Particle)

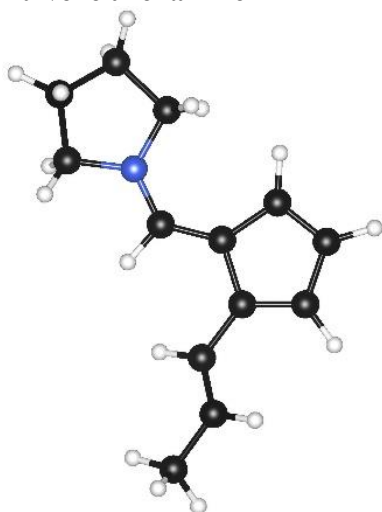
Thermal correction = 0.230718 Hartrees

Coordinates from last standard orientation:

Center Number	Atomic Number	Atomic Type	Coordinates (Angstroms)		
			X	Y	Z
1	6	0	-1.844520	0.325597	-0.027217
2	6	0	-0.384984	0.529063	-0.058253
3	6	0	0.513622	-0.460181	-0.257109
4	1	0	0.150336	-1.471389	-0.447774
5	7	0	1.879807	-0.338735	-0.278135
6	6	0	2.712463	-1.494572	-0.604432
7	1	0	2.544915	-1.813400	-1.637772
8	1	0	2.485642	-2.345316	0.059507
9	6	0	4.129508	-0.980829	-0.362055
10	1	0	4.468233	-0.404485	-1.229743
11	1	0	4.844229	-1.787065	-0.183152

12	6	0	3.939353	-0.058403	0.846672
13	1	0	4.754011	0.656899	0.979887
14	1	0	3.861398	-0.659028	1.759360
15	6	0	2.597354	0.627234	0.559192
16	1	0	2.025501	0.825854	1.473207
17	1	0	2.740584	1.580634	0.034743
18	6	0	-2.512780	-0.842155	0.144514
19	6	0	-3.954495	-0.994414	0.100741
20	6	0	-4.596189	-2.159559	0.282093
21	1	0	-5.677556	-2.224829	0.237788
22	1	0	-4.049259	-3.078233	0.478606
23	1	0	-1.942082	-1.748912	0.341764
24	1	0	-4.546117	-0.102127	-0.097087
25	6	0	-1.486858	2.608780	-0.217529
26	1	0	-1.666828	3.674870	-0.304708
27	6	0	-2.437628	1.663904	-0.186653
28	1	0	-3.502871	1.853790	-0.242282
29	6	0	-0.104400	2.022009	-0.082396
30	1	0	0.542653	2.295941	-0.926624
31	1	0	0.385880	2.399097	0.825819

Fulvene trienamine B12'



HF (M062X/6-31+G(d,p)) = -560.0894673 Hartrees

Imaginary Frequencies: none found

Zero-point correction = 0.272227 (Hartree/Particle)

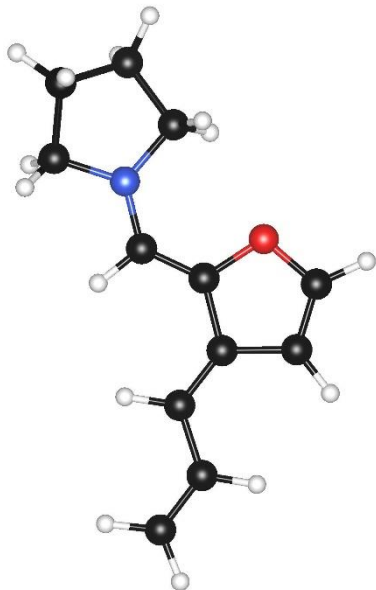
Thermal correction = 0.232627 Hartrees

Coordinates from last standard orientation:

Center Number	Atomic Number	Atomic Type	Coordinates (Angstroms)		
			X	Y	Z
1	6	0	-1.795741	0.569478	0.117825
2	6	0	-0.336929	0.712185	0.067526
3	6	0	0.492483	-0.382459	0.096032
4	1	0	0.022265	-1.363529	0.148795
5	7	0	1.831082	-0.444608	0.060162

6	6	0	2.566638	-1.711555	0.081065
7	1	0	2.078433	-2.445710	-0.565879
8	1	0	2.606695	-2.116386	1.102150
9	6	0	3.958496	-1.308369	-0.402362
10	1	0	3.973413	-1.266496	-1.496576
11	1	0	4.733610	-2.002997	-0.072275
12	6	0	4.117621	0.100372	0.183151
13	1	0	4.889638	0.689904	-0.315059
14	1	0	4.372934	0.034983	1.246151
15	6	0	2.721901	0.712049	0.020124
16	1	0	2.466379	1.412312	0.822162
17	1	0	2.608139	1.234091	-0.939524
18	6	0	-2.525836	-0.692119	0.257233
19	6	0	-3.744172	-0.933834	-0.244963
20	6	0	-4.510629	-2.206380	-0.041179
21	1	0	-4.761658	-2.676445	-0.998742
22	1	0	-3.934690	-2.922641	0.552151
23	1	0	-2.048170	-1.489880	0.830228
24	1	0	-4.222762	-0.159312	-0.844524
25	6	0	-1.262310	2.789185	-0.100948
26	1	0	-1.394539	3.860487	-0.193786
27	6	0	-2.331758	1.829158	0.023122
28	1	0	-3.387865	2.066894	0.071237
29	6	0	-0.061485	2.134645	-0.071487
30	1	0	0.908067	2.602495	-0.157402
31	1	0	-5.457140	-2.019646	0.478915

Trienamine B13



HF (M062X/6-31+G(d,p)) = -595.9714135 Hartrees

Imaginary Frequencies: none found

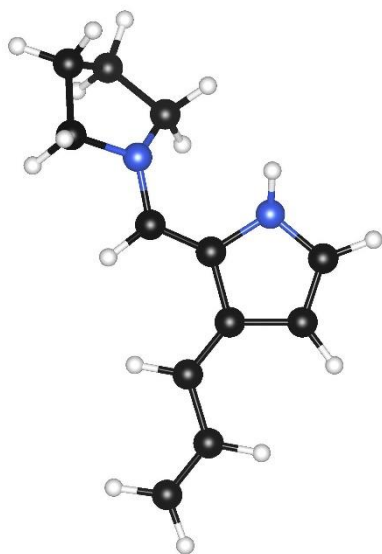
Zero-point correction = 0.247927 (Hartree/Particle)

Thermal correction = 0.206796 Hartrees

Coordinates from last standard orientation:

Center Number	Atomic Number	Atomic Type	Coordinates (Angstroms)		
			X	Y	Z
1	6	0	1.865679	0.326327	0.003330
2	6	0	0.405487	0.417240	-0.010400
3	6	0	-0.517025	-0.572835	-0.020034
4	1	0	-0.128063	-1.587450	-0.020391
5	7	0	-1.872309	-0.484378	-0.020135
6	6	0	-2.722744	-1.670594	0.014291
7	1	0	-2.356519	-2.388546	0.755681
8	1	0	-2.745244	-2.169892	-0.966794
9	6	0	-4.095207	-1.098990	0.367440
10	1	0	-4.174565	-0.969978	1.452313
11	1	0	-4.914936	-1.739843	0.035520
12	6	0	-4.073739	0.268499	-0.325257
13	1	0	-4.818654	0.963760	0.067501
14	1	0	-4.256455	0.142972	-1.398100
15	6	0	-2.640477	0.758531	-0.095623
16	1	0	-2.272944	1.392860	-0.906557
17	1	0	-2.546720	1.324151	0.840538
18	6	0	2.637806	-0.793134	-0.048221
19	6	0	4.082137	-0.791347	-0.001103
20	6	0	4.852725	-1.891467	-0.055484
21	1	0	5.934057	-1.828115	-0.013245
22	1	0	4.414071	-2.882072	-0.143771
23	1	0	2.154955	-1.765665	-0.129787
24	1	0	4.571720	0.177748	0.088403
25	8	0	0.031441	1.766185	0.030357
26	6	0	1.184754	2.481773	0.088771
27	1	0	1.055982	3.554355	0.129784
28	6	0	2.292532	1.723508	0.081011
29	1	0	3.306382	2.091808	0.114660

Trienamine B14



HF (M062X/6-31+G(d,p)) = -576.1149762 Hartrees

Imaginary Frequencies: none found

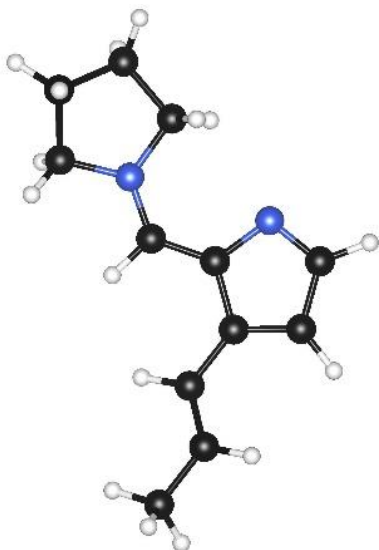
Zero-point correction = 0.260139 (Hartree/Particle)

Thermal correction = 0.219492 Hartrees

Coordinates from last standard orientation:

Center Number	Atomic Number	Atomic Type	Coordinates (Angstroms)		
			X	Y	Z
1	6	0	-1.857374	0.329637	-0.069101
2	6	0	-0.394237	0.471413	-0.174996
3	6	0	0.540909	-0.484268	-0.367254
4	1	0	0.220975	-1.506911	-0.561141
5	7	0	1.905771	-0.250295	-0.374043
6	6	0	2.790119	-1.346045	-0.770950
7	1	0	2.758002	-1.498136	-1.854220
8	1	0	2.486219	-2.288115	-0.283660
9	6	0	4.161611	-0.901258	-0.268604
10	1	0	4.609212	-0.195962	-0.977415
11	1	0	4.850425	-1.738276	-0.135080
12	6	0	3.808419	-0.187359	1.040031
13	1	0	4.599550	0.471970	1.404727
14	1	0	3.595367	-0.929007	1.817740
15	6	0	2.526780	0.571898	0.681584
16	1	0	1.838440	0.682876	1.525516
17	1	0	2.765195	1.577550	0.308714
18	6	0	-2.547372	-0.830942	0.094632
19	6	0	-3.989503	-0.922797	0.156479
20	6	0	-4.674066	-2.068547	0.313091
21	1	0	-5.757423	-2.080904	0.351560
22	1	0	-4.161033	-3.022500	0.404668
23	1	0	-1.993463	-1.762776	0.196688
24	1	0	-4.548124	0.007819	0.065591
25	6	0	-1.311050	2.540073	-0.175460
26	1	0	-1.309558	3.621631	-0.215535
27	6	0	-2.367385	1.699652	-0.124698
28	1	0	-3.403651	1.998590	-0.074287
29	7	0	-0.102148	1.855207	-0.107269
30	1	0	0.703385	2.199012	-0.613207

Fulvene trienamine B14'



HF (M062X/6-31+G(d,p)) = -576.1430189 Hartrees

Imaginary Frequencies: none found

Zero-point correction = 0.260901 (Hartree/Particle)

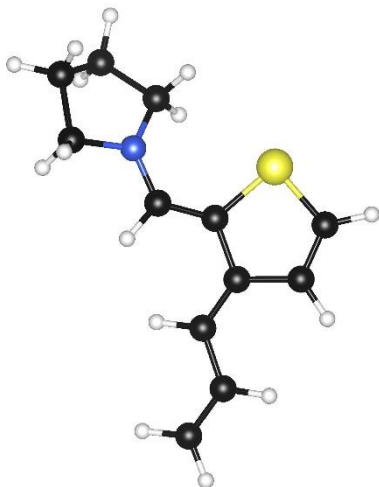
Thermal correction = 0.219145 Hartrees

Coordinates from last standard orientation:

Center Number	Atomic Number	Atomic Type	Coordinates (Angstroms)		
			X	Y	Z
1	6	0	-1.789362	0.552208	0.096862
2	6	0	-0.341784	0.632152	0.077758
3	6	0	0.504137	-0.458528	0.124022
4	1	0	0.050605	-1.446070	0.190651
5	7	0	1.833659	-0.472131	0.089602
6	6	0	2.615041	-1.712988	0.130982
7	1	0	2.131969	-2.486253	-0.472772
8	1	0	2.696542	-2.075106	1.164979
9	6	0	3.978599	-1.280416	-0.404470
10	1	0	3.961237	-1.272819	-1.499510
11	1	0	4.783643	-1.940981	-0.076028
12	6	0	4.104460	0.150419	0.133226
13	1	0	4.846266	0.746292	-0.402044
14	1	0	4.388768	0.126321	1.190923
15	6	0	2.690793	0.718239	-0.017802
16	1	0	2.412950	1.449492	0.742992
17	1	0	2.522357	1.193380	-0.990573
18	6	0	-2.592555	-0.666063	0.196777
19	6	0	-3.866376	-0.781219	-0.200290
20	6	0	-4.691431	-2.024430	-0.060991
21	1	0	-5.051206	-2.372133	-1.035724
22	1	0	-4.115368	-2.831574	0.400446
23	1	0	-2.115742	-1.544376	0.635521
24	1	0	-4.348931	0.080063	-0.662350
25	6	0	-1.027134	2.659903	-0.076715
26	1	0	-0.989100	3.741716	-0.157631
27	6	0	-2.213538	1.860388	0.000545

28	1	0	-3.233669	2.221598	0.013549
29	7	0	0.082299	1.951277	-0.032435
30	1	0	-5.577122	-1.841564	0.557992

Trienammine B15



HF (M062X/6-31+G(d,p)) = -918.9390192 Hartrees

Imaginary Frequencies: none found

Zero-point correction = 0.245074 (Hartree/Particle)

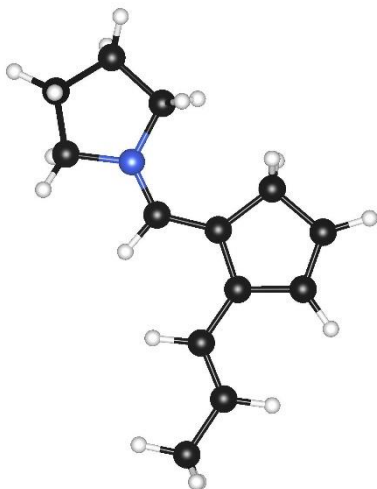
Thermal correction = 0.203768 Hartrees

Coordinates from last standard orientation:

Center Number	Atomic Number	Atomic Type	Coordinates (Angstroms)		
			X	Y	Z
1	6	0	-1.844627	0.167030	-0.029628
2	6	0	-0.389359	0.382493	-0.051990
3	6	0	0.526010	-0.595573	-0.269111
4	1	0	0.145198	-1.590272	-0.503503
5	7	0	1.883339	-0.500346	-0.256770
6	6	0	2.712168	-1.645820	-0.633664
7	1	0	2.551584	-1.914156	-1.682370
8	1	0	2.466974	-2.521194	-0.011944
9	6	0	4.133697	-1.157112	-0.357793
10	1	0	4.502131	-0.583167	-1.214835
11	1	0	4.828206	-1.978773	-0.170488
12	6	0	3.941733	-0.234441	0.850376
13	1	0	4.772614	0.457444	1.004030
14	1	0	3.819960	-0.832512	1.760095
15	6	0	2.631196	0.488791	0.524880
16	1	0	2.061174	0.764655	1.418452
17	1	0	2.815915	1.399486	-0.059094
18	6	0	-2.451657	-1.036818	0.167918
19	6	0	-3.876687	-1.278189	0.081076
20	6	0	-4.454278	-2.471978	0.295324
21	1	0	-5.527436	-2.604531	0.217090
22	1	0	-3.861645	-3.345837	0.553623
23	1	0	-1.836144	-1.897092	0.424366

24	1	0	-4.514889	-0.436010	-0.180173
25	6	0	-1.699716	2.511015	-0.195085
26	1	0	-1.989306	3.552177	-0.261421
27	6	0	-2.524114	1.449401	-0.201789

Iminium B16



HF (M062X/6-31+G(d,p)) = -560.4863791 Hartrees

Imaginary Frequencies: none found

Zero-point correction = 0.285357 (Hartree/Particle)

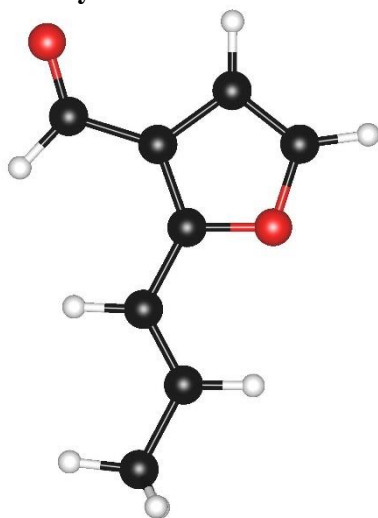
Thermal correction = 0.243778 Hartrees

Coordinates from last standard orientation:

Center Number	Atomic Number	Atomic Type	Coordinates (Angstroms)		
			X	Y	Z
1	6	0	-1.739530	0.453729	-0.001317
2	6	0	-0.353124	0.631638	0.039042
3	6	0	0.536041	-0.456997	0.102536
4	1	0	0.100856	-1.452320	0.162249
5	7	0	1.844733	-0.456937	0.099348
6	6	0	2.638576	-1.708606	0.171844
7	1	0	2.139315	-2.494812	-0.397342
8	1	0	2.713674	-2.013614	1.221575
9	6	0	3.995921	-1.290757	-0.382248
10	1	0	3.977611	-1.305774	-1.476563
11	1	0	4.796095	-1.949315	-0.042291
12	6	0	4.137527	0.144339	0.136993
13	1	0	4.878942	0.728773	-0.409083
14	1	0	4.420559	0.137971	1.193950
15	6	0	2.729424	0.723059	-0.024641
16	1	0	2.479913	1.463064	0.737353
17	1	0	2.581340	1.162490	-1.016865
18	6	0	-2.465457	-0.799850	-0.002483
19	6	0	-3.808811	-0.885411	-0.017673
20	6	0	-4.570793	-2.165599	-0.020972
21	1	0	-5.215600	-2.217840	-0.904730
22	1	0	-3.911064	-3.035152	-0.012679
23	1	0	-1.900452	-1.728344	0.006884

24	1	0	-4.404100	0.025929	-0.028017
25	6	0	-1.411284	2.721100	-0.045676
26	1	0	-1.580467	3.791020	-0.076453
27	6	0	-2.364819	1.768662	-0.054149
28	1	0	-3.430666	1.947750	-0.096404
29	6	0	-0.050083	2.111690	0.017952
30	1	0	0.556740	2.418214	-0.843098
31	1	0	0.474775	2.452027	0.920113
32	1	0	-5.232129	-2.213497	0.850715

Aldehyde C1



HF (M062X/6-31+G(d,p)) = -459.8997539 Hartrees

Imaginary Frequencies: none found

Zero-point correction = 0.142096 (Hartree/Particle)

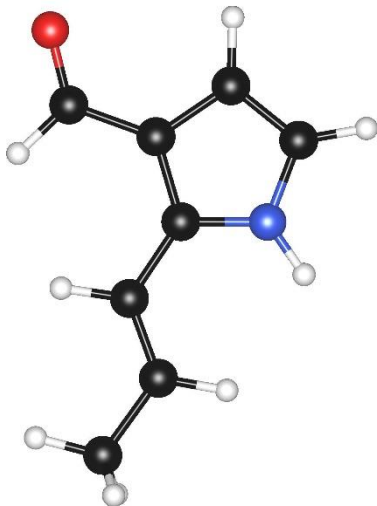
Thermal correction = 0.106772 Hartrees

Coordinates from last standard orientation:

Center Number	Atomic Number	Atomic Type	Coordinates (Angstroms)		
			X	Y	Z
1	6	0	-0.806022	0.402470	-0.000384
2	6	0	-1.945642	-0.312131	0.000038
3	6	0	-3.243033	0.371508	-0.000186
4	1	0	-3.189623	1.481947	-0.000992
5	1	0	-1.959956	-1.398791	0.000649
6	1	0	-0.889709	1.490258	-0.000962
7	6	0	0.536826	-0.140667	-0.000173
8	6	0	1.700695	0.587561	-0.000012
9	6	0	0.939868	-1.527476	-0.000200
10	6	0	2.291320	-1.524967	0.000031
11	1	0	0.299992	-2.397277	-0.000370
12	1	0	3.038733	-2.302341	0.000082
13	6	0	2.003122	2.042417	0.000189
14	1	0	2.585516	2.314909	-0.884710
15	1	0	1.081021	2.624798	0.000013
16	1	0	2.585031	2.314730	0.885463

17	8	0	2.764021	-0.246351	0.000199
18	8	0	-4.315747	-0.193714	0.000427

Aldehyde C2



HF (M062X/6-31+G(d,p)) = -440.0527351 Hartrees

Imaginary Frequencies: none found

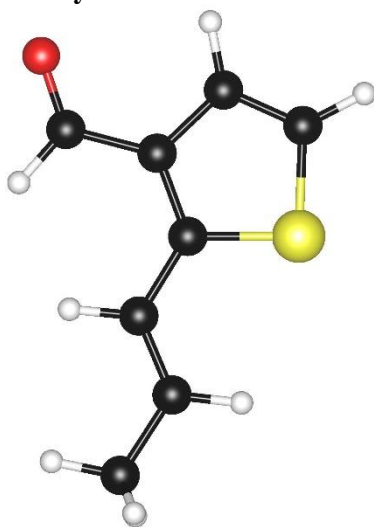
Zero-point correction = 0.154786 (Hartree/Particle)

Thermal correction = 0.118401 Hartrees

Coordinates from last standard orientation:

Center Number	Atomic Number	Atomic Type	Coordinates (Angstroms)		
			X	Y	Z
1	6	0	-0.806453	0.383111	-0.000368
2	6	0	-1.950248	-0.329496	0.000082
3	6	0	-3.241031	0.358683	-0.000175
4	1	0	-3.179161	1.469390	-0.000982
5	1	0	-1.967351	-1.415981	0.000729
6	1	0	-0.899120	1.470634	-0.000955
7	6	0	0.538075	-0.149235	-0.000173
8	6	0	1.703614	0.610340	-0.000011
9	6	0	0.933147	-1.528816	-0.000153
10	6	0	2.299178	-1.563585	0.000034
11	1	0	0.278540	-2.387971	-0.000312
12	1	0	2.988368	-2.393896	0.000033
13	6	0	1.926543	2.087293	0.000198
14	1	0	2.484613	2.405978	-0.886344
15	1	0	0.974723	2.619514	-0.000020
16	1	0	2.484075	2.405785	0.887149
17	8	0	-4.321519	-0.195059	0.000373
18	7	0	2.752514	-0.262048	0.000119
19	1	0	3.722917	0.011588	0.000291

Aldehyde C3



HF (M062X/6-31+G(d,p)) = -782.864751 Hartrees

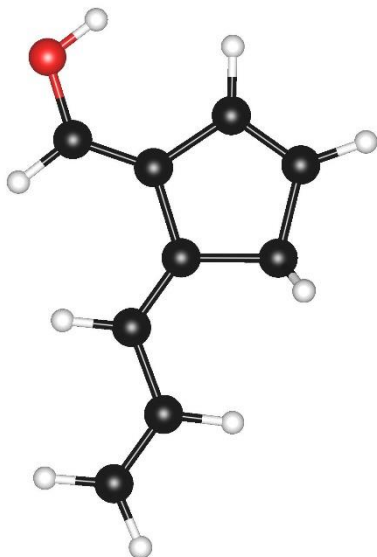
Imaginary Frequencies: none found

Zero-point correction = 0.138356 (Hartree/Particle)

Thermal correction = 0.102913 Hartrees

Coordinates from last standard orientation:

Center Number	Atomic Number	Atomic Type	Coordinates (Angstroms)		
			X	Y	Z
1	6	0	-1.122570	0.413475	-0.000143
2	6	0	-2.237350	-0.339552	0.000080
3	6	0	-3.556431	0.302756	-0.000062
4	1	0	-3.540218	1.414076	-0.000256
5	1	0	-2.223474	-1.425818	0.000363
6	1	0	-1.255161	1.495157	-0.000404
7	6	0	0.248157	-0.077147	-0.000081
8	6	0	1.357798	0.744430	0.000001
9	6	0	0.604945	-1.472177	-0.000100
10	6	0	1.946522	-1.675468	-0.000026
11	1	0	-0.116368	-2.280122	-0.000195
12	1	0	2.481138	-2.614697	-0.000022
13	6	0	1.439914	2.241439	0.000041
14	1	0	1.970802	2.605536	-0.884429
15	1	0	0.445847	2.690125	0.000016
16	1	0	1.970726	2.605494	0.884574
17	8	0	-4.609296	-0.298304	0.000127
18	16	0	2.815948	-0.183116	0.000068

Enol C4

HF (M062X/6-31+G(d,p)) = -423.9631305Hartrees

Imaginary Frequencies: none found

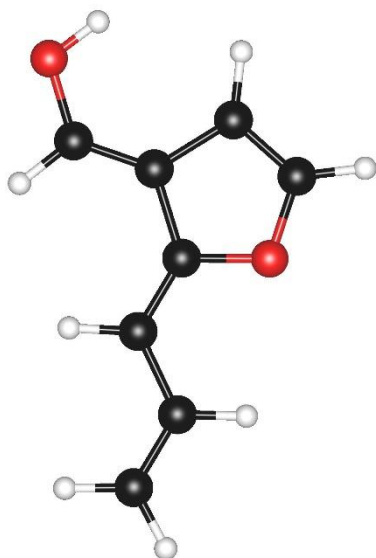
Zero-point correction = 0.165237 (Hartree/Particle)

Thermal correction = 0.129479Hartrees

Coordinates from last standard orientation:

Center Number	Atomic Number	Atomic Type	Coordinates (Angstroms)		
			X	Y	Z
1	6	0	-0.656707	0.529157	-0.000313
2	6	0	-1.904970	-0.205457	-0.000317
3	6	0	-3.097111	0.413076	0.000091
4	1	0	-3.192027	1.495006	0.000384
5	1	0	-1.873206	-1.294198	-0.000726
6	1	0	-0.740816	1.615523	-0.000736
7	6	0	0.579237	-0.015994	0.000049
8	6	0	1.867806	0.726034	-0.000080
9	6	0	0.926677	-1.443364	0.000400
10	6	0	2.256356	-1.617983	0.000281
11	1	0	0.197518	-2.245675	0.000832
12	1	0	2.761187	-2.577652	0.000545
13	6	0	2.043536	2.050239	0.000386
14	1	0	3.039075	2.483475	0.000369
15	1	0	1.206007	2.741264	0.000859
16	6	0	2.991926	-0.302119	-0.000504
17	1	0	3.636920	-0.194995	0.880182
18	1	0	3.635635	-0.195509	-0.882217
19	8	0	-4.312699	-0.185443	0.000093
20	1	0	-4.209200	-1.145234	-0.000198

Enol C5



HF (M062X/6-31+G(d,p)) = -459.862049 Hartrees

Imaginary Frequencies: none found

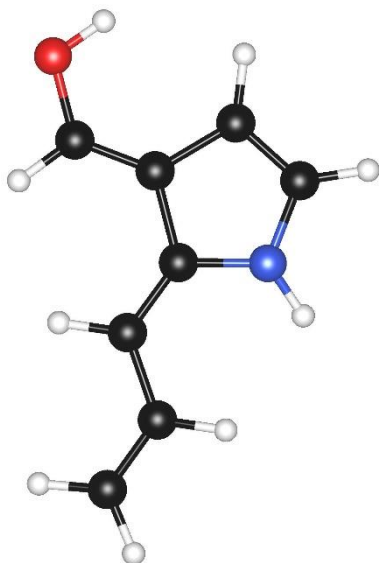
Zero-point correction = 0.141006 (Hartree/Particle)

Thermal correction = 0.105386 Hartrees

Coordinates from last standard orientation:

Center Number	Atomic Number	Atomic Type	Coordinates (Angstroms)		
			X	Y	Z
1	6	0	-0.645009	0.513107	-0.000311
2	6	0	-1.889148	-0.220402	-0.000467
3	6	0	-3.079553	0.397602	0.000399
4	1	0	-3.163770	1.483292	0.001584
5	1	0	-1.874770	-1.307130	-0.001285
6	1	0	-0.714583	1.600312	-0.000105
7	6	0	0.585610	-0.048214	-0.000259
8	6	0	1.872862	0.679530	0.000000
9	6	0	0.966719	-1.459056	-0.000134
10	8	0	2.891284	-0.263280	0.000422
11	6	0	2.306368	-1.498904	0.000336
12	1	0	0.308009	-2.314029	-0.000207
13	1	0	2.997658	-2.329425	0.000655
14	6	0	2.164720	1.982479	-0.000216
15	1	0	3.194700	2.315261	0.000010
16	1	0	1.373638	2.721001	-0.000711
17	8	0	-4.243545	-0.303973	-0.000742
18	1	0	-4.998215	0.291887	0.006533

Enol C6



HF (M062X/6-31+G(d,p)) = -440.0059954 Hartrees

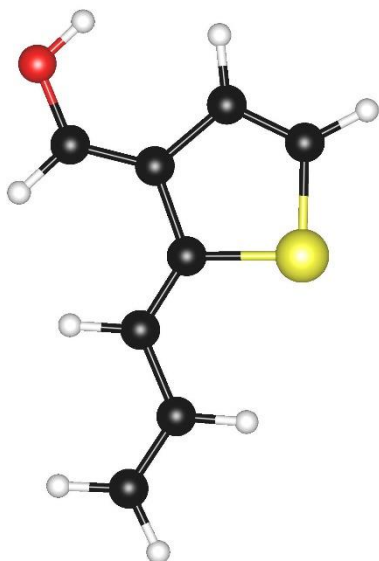
Imaginary Frequencies: none found

Zero-point correction = 0.152594 (Hartree/Particle)

Thermal correction = 0.117225 Hartrees

Coordinates from last standard orientation:

Center Number	Atomic Number	Atomic Type	Coordinates (Angstroms)		
			X	Y	Z
1	6	0	-0.644083	0.509298	-0.000447
2	6	0	-1.887949	-0.224226	-0.000632
3	6	0	-3.079773	0.391077	0.000796
4	1	0	-3.166834	1.476558	0.002498
5	1	0	-1.872166	-1.311002	-0.002011
6	1	0	-0.715933	1.596332	-0.000073
7	6	0	0.588202	-0.052594	-0.000392
8	6	0	1.872976	0.702316	-0.000040
9	6	0	0.954038	-1.468290	-0.000246
10	6	0	2.302438	-1.542486	0.000444
11	1	0	0.276967	-2.308476	-0.000384
12	1	0	2.936660	-2.418586	0.000876
13	6	0	2.093801	2.028942	-0.000369
14	1	0	3.098982	2.434458	-0.000048
15	1	0	1.267319	2.727208	-0.001050
16	8	0	-4.244667	-0.313004	-0.000929
17	1	0	-4.998621	0.283447	0.007505
18	7	0	2.868435	-0.279594	0.000626
19	1	0	3.854014	-0.082973	0.001054

Enol C7

HF (M062X/6-31+G(d,p)) = -782.8262469 Hartrees

Imaginary Frequencies: none found

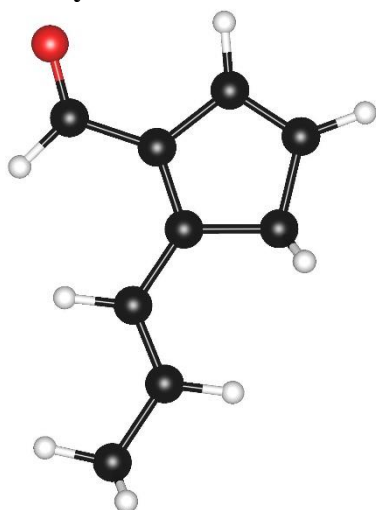
Zero-point correction = 0.137839 (Hartree/Particle)

Thermal correction = 0.101024 Hartrees

Coordinates from last standard orientation:

Center Number	Atomic Number	Atomic Type	Coordinates (Angstroms)		
			X	Y	Z
1	6	0	-0.986210	0.518949	-0.000517
2	6	0	-2.208741	-0.249442	-0.001069
3	6	0	-3.412937	0.342563	0.001037
4	1	0	-3.521740	1.426144	0.003651
5	1	0	-2.174655	-1.335101	-0.003191
6	1	0	-1.101911	1.602027	0.000192
7	6	0	0.269851	0.009621	-0.000595
8	6	0	1.497249	0.848254	-0.000215
9	6	0	0.623468	-1.407149	-0.000604
10	6	0	1.945237	-1.640982	0.000265
11	1	0	-0.111655	-2.202411	-0.000881
12	1	0	2.431071	-2.608284	0.000724
13	6	0	1.594223	2.184578	-0.000719
14	1	0	2.555691	2.684925	-0.000362
15	1	0	0.708368	2.810237	-0.001564
16	8	0	-4.559402	-0.384678	-0.000762
17	1	0	-5.328577	0.192524	0.008869
18	16	0	2.942862	-0.195688	0.000822

Aldehyde C8



HF (M062X/6-31+G(d,p)) = -423.9812446 Hartrees

Imaginary Frequencies: none found

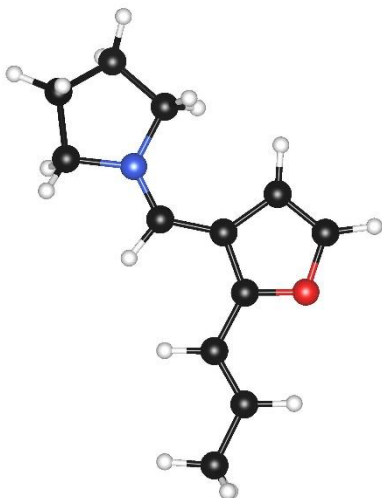
Zero-point correction = 0.164541 (Hartree/Particle)

Thermal correction = 0.128672 Hartrees

Coordinates from last standard orientation:

Center Number	Atomic Number	Atomic Type	Coordinates (Angstroms)		
			X	Y	Z
1	6	0	-0.809016	0.423497	-0.002025
2	6	0	-1.935255	-0.313468	0.000231
3	6	0	-3.246646	0.344971	-0.000648
4	1	0	-3.215960	1.456065	-0.003874
5	1	0	-1.932108	-1.399933	0.003048
6	1	0	-0.917563	1.508658	-0.004529
7	6	0	0.546942	-0.095455	-0.001192
8	6	0	1.689378	0.644532	-0.000237
9	6	0	0.908044	-1.528387	-0.000880
10	6	0	2.244217	-1.654121	0.000339
11	1	0	0.191576	-2.341389	-0.001835
12	1	0	2.806685	-2.579291	0.000563
13	6	0	1.858931	2.128941	0.000963
14	1	0	2.433405	2.452467	-0.874265
15	1	0	0.905118	2.659341	-0.008717
16	6	0	2.869788	-0.288211	0.000843
17	1	0	3.507257	-0.122816	0.880871
18	1	0	3.508437	-0.122969	-0.878363
19	1	0	2.415857	2.453168	0.887303
20	8	0	-4.307625	-0.242137	0.001929

Iminium C9



HF (M062X/6-31+G(d,p)) = -596.4039316 Hartrees

Imaginary Frequencies: none found

Zero-point correction = 0.262326 (Hartree/Particle)

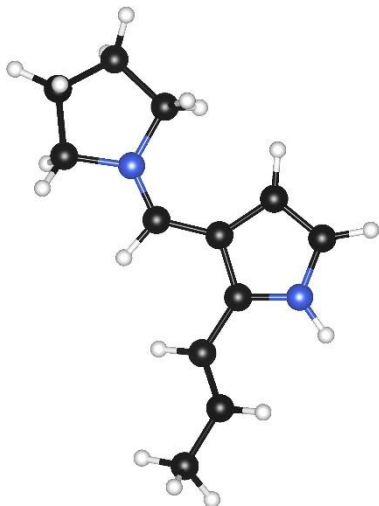
Thermal correction = 0.221163 Hartrees

Coordinates from last standard orientation:

Center Number	Atomic Number	Atomic Type	Coordinates (Angstroms)		
			X	Y	Z
1	6	0	-1.029896	-0.553017	0.031467
2	6	0	0.200158	0.049768	0.040004
3	6	0	1.361853	-0.757862	0.068274
4	1	0	1.245447	-1.841659	0.081058
5	7	0	2.588481	-0.321630	0.075936
6	6	0	3.782286	-1.200811	0.081844
7	1	0	3.601432	-2.072076	-0.550068
8	1	0	3.966629	-1.528914	1.110752
9	6	0	4.888849	-0.273542	-0.412557
10	1	0	4.872621	-0.217486	-1.505503
11	1	0	5.876197	-0.615050	-0.099745
12	6	0	4.496086	1.074416	0.203239
13	1	0	4.971657	1.924742	-0.286613
14	1	0	4.763693	1.098937	1.263845
15	6	0	2.973928	1.108129	0.046074
16	1	0	2.461222	1.644850	0.847905
17	1	0	2.666812	1.525597	-0.919345
18	1	0	0.290263	1.130622	0.020182
19	1	0	-1.061948	-1.642572	0.051452
20	6	0	-2.281402	0.117197	-0.000771
21	6	0	-3.516982	-0.517815	-0.007806
22	6	0	-2.564809	1.536313	-0.033555
23	6	0	-3.907637	1.643132	-0.056993
24	1	0	-1.861789	2.355477	-0.039180
25	1	0	-4.593638	2.474543	-0.085026
26	6	0	-3.944101	-1.937853	0.015124
27	1	0	-4.539039	-2.164906	-0.873957
28	1	0	-3.086170	-2.609543	0.042844
29	1	0	-4.567148	-2.127484	0.893767

30 8 0 -4.484451 0.398500 -0.041248

Iminium C10



HF (M062X/6-31+G(d,p)) = -576.5659099 Hartrees

Imaginary Frequencies: none found

Zero-point correction = 0.275330 (Hartree/Particle)

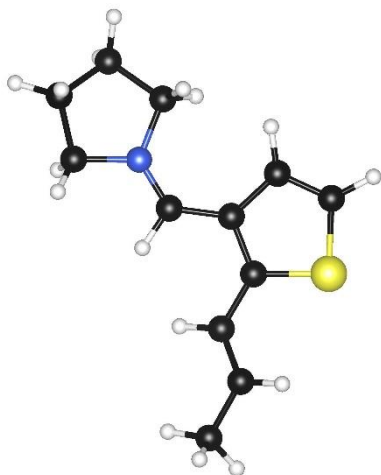
Thermal correction = 0.233933 Hartrees

Coordinates from last standard orientation:

Center Number	Atomic Number	Atomic Type	Coordinates (Angstroms)		
			X	Y	Z
1	6	0	-1.035455	-0.535357	0.009432
2	6	0	0.203500	0.064205	0.032468
3	6	0	1.356139	-0.744369	0.049630
4	1	0	1.235759	-1.827775	0.042462
5	7	0	2.590024	-0.315720	0.069404
6	6	0	3.776238	-1.201227	0.062986
7	1	0	3.595471	-2.057404	-0.589616
8	1	0	3.957019	-1.555251	1.084113
9	6	0	4.891058	-0.271163	-0.408106
10	1	0	4.880549	-0.195323	-1.499969
11	1	0	5.875369	-0.622668	-0.096520
12	6	0	4.501447	1.068234	0.228361
13	1	0	4.983188	1.924532	-0.244980
14	1	0	4.765011	1.073310	1.290326
15	6	0	2.979804	1.110337	0.066258
16	1	0	2.467651	1.636032	0.876139
17	1	0	2.677616	1.549605	-0.891395
18	1	0	0.295975	1.144962	0.034850
19	1	0	-1.062949	-1.626020	0.014032
20	6	0	-2.282589	0.125274	-0.016693
21	6	0	-3.525787	-0.539540	-0.012641
22	6	0	-2.558653	1.539827	-0.046432
23	6	0	-3.910376	1.683390	-0.058770
24	1	0	-1.840095	2.345704	-0.065101

25	1	0	-4.532599	2.564445	-0.085685
26	6	0	-3.860400	-1.992444	0.051421
27	1	0	-4.825478	-2.189400	-0.421248
28	1	0	-3.110914	-2.591754	-0.468367
29	1	0	-3.914111	-2.336304	1.089197
30	7	0	-4.474176	0.414444	-0.037273
31	1	0	-5.467959	0.229233	-0.040633

Iminium C11



HF (M062X/6-31+G(d,p)) = -919.3693188 Hartrees

Imaginary Frequencies: none found

Zero-point correction = 0.258819 (Hartree/Particle)

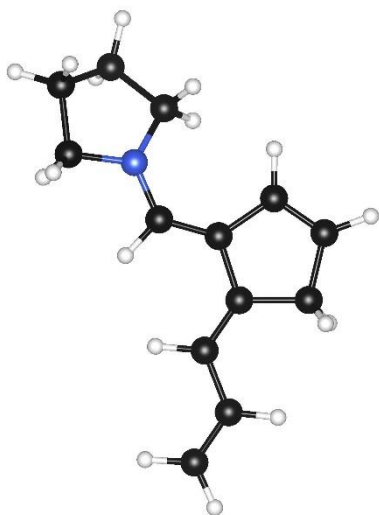
Thermal correction = 0.216855 Hartrees

Coordinates from last standard orientation:

Center Number	Atomic Number	Atomic Type	Coordinates (Angstroms)		
			X	Y	Z
1	6	0	0.681402	0.586010	0.030573
2	6	0	-0.538678	-0.037826	0.041785
3	6	0	-1.711651	0.753549	0.065270
4	1	0	-1.610285	1.838874	0.072778
5	7	0	-2.932478	0.300491	0.074203
6	6	0	-4.137822	1.163495	0.075021
7	1	0	-3.967927	2.034468	-0.560378
8	1	0	-4.328005	1.493561	1.102262
9	6	0	-5.231274	0.219494	-0.416883
10	1	0	-5.212598	0.158847	-1.509553
11	1	0	-6.223598	0.549178	-0.107116
12	6	0	-4.821473	-1.120332	0.205438
13	1	0	-5.284942	-1.979206	-0.281133
14	1	0	-5.090234	-1.143583	1.265786
15	6	0	-3.298718	-1.134344	0.050627
16	1	0	-2.780293	-1.660532	0.855769
17	1	0	-2.984543	-1.552505	-0.912219
18	1	0	-0.616921	-1.119465	0.027975
19	1	0	0.686535	1.676649	0.045461
20	6	0	1.958413	-0.046933	0.002381

21	6	0	3.141810	0.694508	-0.001821
22	6	0	2.202870	-1.467387	-0.024019
23	6	0	3.524684	-1.764229	-0.046067
24	1	0	1.428233	-2.224437	-0.027574
25	1	0	3.994034	-2.737842	-0.070103
26	6	0	3.304046	2.184892	0.026275
27	1	0	4.357267	2.466097	-0.017915
28	1	0	2.801429	2.649040	-0.827348
29	1	0	2.887597	2.604384	0.947097
30	16	0	4.501872	-0.333897	-0.035918

Trienamine C12



HF (M062X/6-31+G(d,p)) = -560.0783088 Hartrees

Imaginary Frequencies: none found

Zero-point correction = 0.271150 (Hartree/Particle)

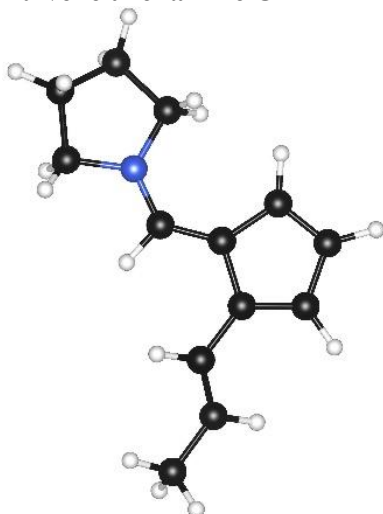
Thermal correction = 0.228525 Hartrees

Coordinates from last standard orientation:

Center Number	Atomic Number	Atomic Type	Coordinates (Angstroms)		
			X	Y	Z
1	6	0	-1.109614	0.654965	-0.030147
2	6	0	0.194354	0.042078	-0.036391
3	6	0	1.329504	0.791170	-0.058162
4	1	0	1.251764	1.877890	-0.070681
5	7	0	2.603294	0.322090	-0.059668
6	6	0	3.787258	1.171440	-0.066801
7	1	0	3.655207	2.024276	0.607247
8	1	0	3.994432	1.559157	-1.076091
9	6	0	4.891084	0.215756	0.389739
10	1	0	4.895083	0.153180	1.483190
11	1	0	5.883446	0.528765	0.057948
12	6	0	4.445490	-1.123153	-0.212183
13	1	0	4.904156	-1.987770	0.272022
14	1	0	4.700688	-1.154890	-1.276804
15	6	0	2.921539	-1.096137	-0.045336

16	1	0	2.399553	-1.619072	-0.857048
17	1	0	2.599093	-1.548608	0.905239
18	1	0	0.265368	-1.041768	-0.019968
19	1	0	-1.124153	1.745695	-0.049179
20	6	0	-2.302215	0.013080	-0.002919
21	6	0	-3.642997	0.649699	0.003076
22	6	0	-2.532552	-1.436011	0.030090
23	6	0	-3.843412	-1.720898	0.056732
24	1	0	-1.738083	-2.174152	0.033627
25	1	0	-4.268828	-2.717858	0.085384
26	6	0	-3.933289	1.955001	-0.024477
27	1	0	-4.962576	2.300515	-0.016659
28	1	0	-3.158830	2.715574	-0.056914
29	6	0	-4.681056	-0.466476	0.044625
30	1	0	-5.347050	-0.427585	-0.826149
31	1	0	-5.316884	-0.391048	0.935432

Fulvene trienamine C12'



HF (M062X/6-31+G(d,p)) = -560.0894486 Hartrees

Imaginary Frequencies: none found

Zero-point correction = 0.272533 (Hartree/Particle)

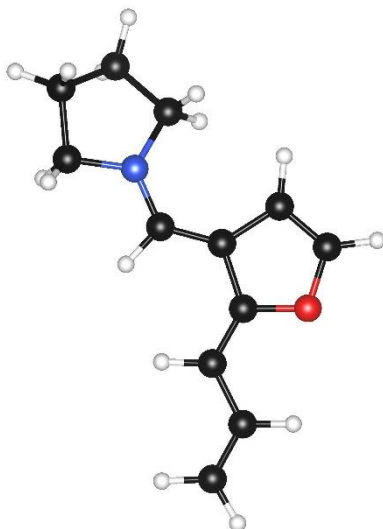
Thermal correction = 0.231392 Hartrees

Coordinates from last standard orientation:

Center Number	Atomic Number	Atomic Type	Coordinates (Angstroms)		
			X	Y	Z
1	6	0	-1.795494	0.560098	-0.147086
2	6	0	-0.336870	0.705420	-0.090116
3	6	0	0.494497	-0.388127	-0.079518
4	1	0	0.028880	-1.370471	-0.145669
5	7	0	1.831237	-0.447230	0.002785
6	6	0	2.572624	-1.711030	-0.021933
7	1	0	2.155421	-2.383212	-0.776822
8	1	0	2.517439	-2.207966	0.956886
9	6	0	4.001041	-1.264448	-0.329892

10	1	0	4.120027	-1.121033	-1.409116
11	1	0	4.747053	-1.986876	0.007461
12	6	0	4.090551	0.082827	0.396651
13	1	0	4.900797	0.717215	0.031999
14	1	0	4.244982	-0.082206	1.468207
15	6	0	2.711514	0.707325	0.159907
16	1	0	2.374384	1.325978	0.998009
17	1	0	2.684937	1.320947	-0.750605
18	6	0	-2.525856	-0.706416	-0.224974
19	6	0	-3.749342	-0.920514	0.277028
20	6	0	-4.516144	-2.200881	0.133019
21	1	0	-5.457848	-2.039910	-0.404197
22	1	0	-3.936860	-2.948249	-0.417085
23	1	0	-2.043837	-1.534220	-0.749745
24	1	0	-4.232961	-0.115335	0.830282
25	6	0	-1.263345	2.788070	-0.036384
26	1	0	-1.395608	3.862998	-0.010343
27	6	0	-0.062468	2.133082	-0.021649
28	1	0	0.907381	2.606429	0.016307
29	6	0	-2.332084	1.822768	-0.115045
30	1	0	-3.388119	2.057488	-0.176693
31	1	0	-4.776464	-2.620009	1.111572

Trienamine C13



HF (M062X/6-31+G(d,p)) = -595.9798717 Hartrees

Imaginary Frequencies: none found

Zero-point correction = 0.247648 (Hartree/Particle)

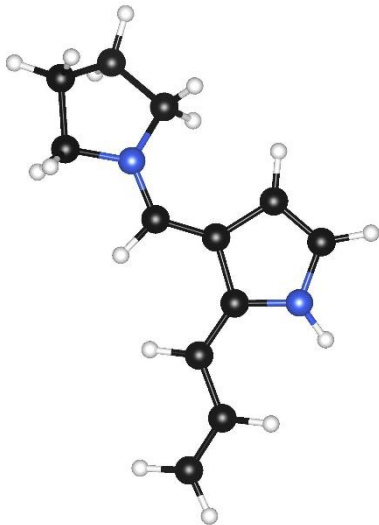
Thermal correction = 0.206087 Hartrees

Coordinates from last standard orientation:

Center Number	Atomic Number	Atomic Type	Coordinates (Angstroms)		
			X	Y	Z
1	6	0	-1.115178	-0.643961	0.028256
2	6	0	0.187212	-0.037183	0.034621
3	6	0	1.321319	-0.790558	0.063178

4	1	0	1.239313	-1.876818	0.082184
5	7	0	2.594317	-0.325973	0.064005
6	6	0	3.776473	-1.179173	0.080529
7	1	0	3.640690	-2.039397	-0.583022
8	1	0	3.981581	-1.554622	1.094580
9	6	0	4.882784	-0.232015	-0.386978
10	1	0	4.886219	-0.180902	-1.480990
11	1	0	5.874183	-0.545041	-0.052602
12	6	0	4.442345	1.114474	0.201753
13	1	0	4.903504	1.972370	-0.291757
14	1	0	4.698564	1.156376	1.265731
15	6	0	2.918245	1.091612	0.036278
16	1	0	2.398502	1.623554	0.843330
17	1	0	2.596626	1.534926	-0.918625
18	1	0	0.258404	1.046751	0.012853
19	1	0	-1.144815	-1.733673	0.048872
20	6	0	-2.299560	0.016325	0.000168
21	6	0	-3.639086	-0.601527	-0.005936
22	6	0	-2.559533	1.453420	-0.030874
23	8	0	-4.575476	0.423566	-0.037251
24	6	0	-3.890727	1.608757	-0.051081
25	1	0	-1.829265	2.248655	-0.037067
26	1	0	-4.510986	2.493022	-0.075059
27	6	0	-4.045218	-1.875883	0.013156
28	1	0	-5.100450	-2.116394	0.004326
29	1	0	-3.322950	-2.681251	0.038809

Trienamine C14



HF (M062X/6-31+G(d,p)) = -576.1231782 Hartrees

Imaginary Frequencies: none found

Zero-point correction = 0.259749 (Hartree/Particle)

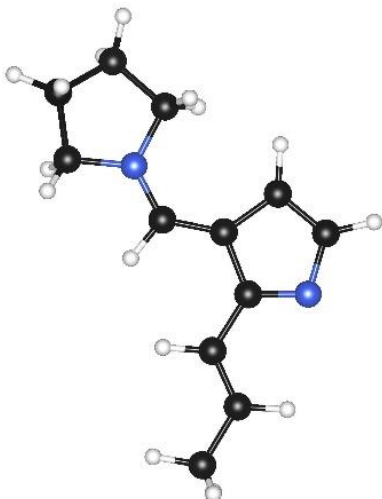
Thermal correction = 0.217801 Hartrees

Coordinates from last standard orientation:

Center Number	Atomic Number	Atomic Type	Coordinates (Angstroms)		
			X	Y	Z

1	6	0	-1.117622	0.645405	-0.014131
2	6	0	0.186211	0.040611	-0.032851
3	6	0	1.320604	0.792825	-0.023717
4	1	0	1.240504	1.879120	0.000643
5	7	0	2.595041	0.326423	-0.035061
6	6	0	3.776555	1.178947	-0.025208
7	1	0	3.648554	2.008122	0.678447
8	1	0	3.972607	1.600951	-1.022952
9	6	0	4.887082	0.211623	0.388023
10	1	0	4.901311	0.111271	1.478547
11	1	0	5.875411	0.539098	0.058175
12	6	0	4.439896	-1.106993	-0.256025
13	1	0	4.904473	-1.986518	0.194616
14	1	0	4.686855	-1.101495	-1.323034
15	6	0	2.917233	-1.090523	-0.076233
16	1	0	2.390169	-1.584273	-0.902901
17	1	0	2.603359	-1.579228	0.859031
18	1	0	0.257517	-1.043383	-0.053094
19	1	0	-1.147533	1.735186	0.003080
20	6	0	-2.301567	-0.018587	-0.013628
21	6	0	-3.642504	0.619790	0.002428
22	6	0	-2.542703	-1.460490	0.004420
23	6	0	-3.876536	-1.653958	0.074055
24	1	0	-1.792646	-2.237183	-0.001203
25	1	0	-4.432069	-2.581096	0.116981
26	6	0	-3.985861	1.917739	-0.101508
27	1	0	-5.022070	2.233512	-0.061308
28	1	0	-3.229142	2.680534	-0.229680
29	7	0	-4.551134	-0.440159	0.138617
30	1	0	-5.529379	-0.336790	-0.073992

Fulvene trienamine C14'

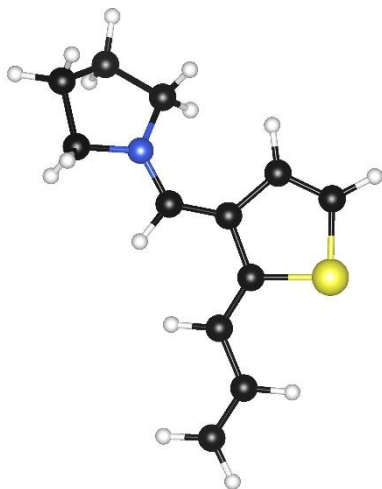


HF (M062X/6-31+G(d,p)) = -576.1377698 Hartrees
 Imaginary Frequencies: none found
 Zero-point correction = 0.261207 (Hartree/Particle)
 Thermal correction = 0.220211 Hartrees

Coordinates from last standard orientation:

Center Number	Atomic Number	Atomic Type	Coordinates (Angstroms)		
			X	Y	Z
1	6	0	-1.768991	0.520421	-0.022940
2	6	0	-0.312468	0.653692	-0.025411
3	6	0	0.532663	-0.432109	-0.011580
4	1	0	0.086054	-1.424761	-0.029224
5	7	0	1.867430	-0.456605	0.018610
6	6	0	2.645620	-1.700682	0.006883
7	1	0	2.226152	-2.404954	-0.716374
8	1	0	2.630738	-2.167335	1.001336
9	6	0	4.051644	-1.222716	-0.354197
10	1	0	4.138716	-1.111996	-1.440255
11	1	0	4.826428	-1.912626	-0.014180
12	6	0	4.120830	0.149819	0.325581
13	1	0	4.904973	0.792812	-0.078411
14	1	0	4.301885	0.025305	1.398391
15	6	0	2.721564	0.728631	0.097859
16	1	0	2.386383	1.376494	0.913449
17	1	0	2.655348	1.294001	-0.840829
18	6	0	-2.530397	-0.731160	0.010468
19	6	0	-3.867743	-0.783402	0.027668
20	6	0	-4.667012	-2.049172	0.061559
21	1	0	-5.331168	-2.116717	-0.807495
22	1	0	-4.020354	-2.931477	0.068373
23	1	0	-1.974411	-1.668174	0.023590
24	1	0	-4.409334	0.161337	0.016814
25	6	0	-1.335649	2.641187	-0.070546
26	1	0	-1.583990	3.695145	-0.099472
27	6	0	-0.087719	2.085836	-0.057100
28	1	0	0.849709	2.619354	-0.086762
29	7	0	-2.352406	1.698960	-0.045650
30	1	0	-5.306348	-2.084965	0.950856

Trienamine C15



HF (M062X/6-31+G(d,p)) = -918.9445892 Hartrees
 Imaginary Frequencies: none found

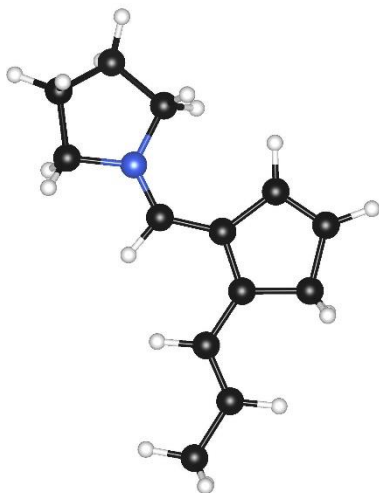
Zero-point correction = 0.244232 (Hartree/Particle)

Thermal correction = 0.200726 Hartrees

Coordinates from last standard orientation:

Center Number	Atomic Number	Atomic Type	Coordinates (Angstroms)		
			X	Y	Z
1	6	0	-0.740436	0.683344	-0.037885
2	6	0	0.547398	0.048767	-0.048990
3	6	0	1.692357	0.788243	-0.058939
4	1	0	1.623839	1.875642	-0.059017
5	7	0	2.957888	0.308802	-0.062584
6	6	0	4.150857	1.148229	-0.050330
7	1	0	4.018509	1.995909	0.629642
8	1	0	4.368689	1.541392	-1.054648
9	6	0	5.241505	0.178446	0.407392
10	1	0	5.234725	0.105091	1.500115
11	1	0	6.239378	0.486356	0.088029
12	6	0	4.790368	-1.150354	-0.212412
13	1	0	5.237992	-2.023656	0.266212
14	1	0	5.053420	-1.172964	-1.275271
15	6	0	3.265590	-1.113281	-0.056648
16	1	0	2.744835	-1.625276	-0.875539
17	1	0	2.933128	-1.567989	0.888939
18	1	0	0.606224	-1.035439	-0.045350
19	1	0	-0.729488	1.773411	-0.045245
20	6	0	-1.952550	0.067424	-0.017329
21	6	0	-3.242343	0.799549	-0.008205
22	6	0	-2.181262	-1.373105	0.008261
23	6	0	-3.476337	-1.725308	0.047238
24	1	0	-1.377290	-2.099335	0.000643
25	1	0	-3.876069	-2.730608	0.074935
26	6	0	-3.462669	2.122614	-0.043831
27	1	0	-4.466077	2.531933	-0.030974
28	1	0	-2.638204	2.825801	-0.088129
29	16	0	-4.592105	-0.368080	0.055863

Iminium C16



HF (M062X/6-31+G(d,p)) = -560.4866441 Hartrees

Imaginary Frequencies: none found

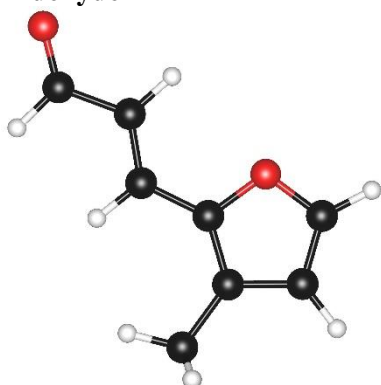
Zero-point correction = 0.284901 (Hartree/Particle)

Thermal correction = 0.243456 Hartrees

Coordinates from last standard orientation:

Center Number	Atomic Number	Atomic Type	Coordinates (Angstroms)		
			X	Y	Z
1	6	0	-1.028839	-0.593724	0.029855
2	6	0	0.194275	0.021660	0.040183
3	6	0	1.366295	-0.773820	0.064398
4	1	0	1.262495	-1.858939	0.071190
5	7	0	2.587056	-0.322542	0.074237
6	6	0	3.791755	-1.186755	0.074070
7	1	0	3.621171	-2.056177	-0.563209
8	1	0	3.980284	-1.518985	1.100891
9	6	0	4.886649	-0.242786	-0.414686
10	1	0	4.869153	-0.179658	-1.507234
11	1	0	5.878268	-0.574330	-0.104655
12	6	0	4.477620	1.096044	0.210229
13	1	0	4.942651	1.955517	-0.273784
14	1	0	4.744994	1.116615	1.270988
15	6	0	2.955231	1.112281	0.053190
16	1	0	2.435646	1.637717	0.857971
17	1	0	2.642880	1.531673	-0.909654
18	1	0	0.275447	1.103047	0.024627
19	1	0	-1.047607	-1.683068	0.046560
20	6	0	-2.290377	0.072602	-0.000969
21	6	0	-3.508027	-0.565760	-0.006145
22	6	0	-2.512724	1.532171	-0.033646
23	6	0	-3.831108	1.776366	-0.058116
24	1	0	-1.728677	2.279622	-0.038183
25	1	0	-4.306914	2.748222	-0.086281
26	6	0	-3.820659	-2.020982	0.020108
27	1	0	-4.419549	-2.292877	-0.855662
28	1	0	-2.932981	-2.654448	0.035185
29	6	0	-4.584474	0.477522	-0.043134
30	1	0	-5.251094	0.385197	0.825951
31	1	0	-5.223914	0.349565	-0.928072
32	1	0	-4.425354	-2.259822	0.901683

Aldehyde D1



HF (M062X/6-31+G(d,p)) = -459.8979071 Hartrees

Imaginary Frequencies: none found

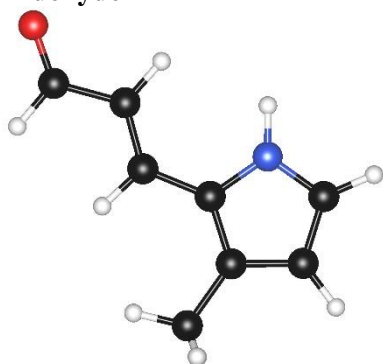
Zero-point correction = 0.142232 (Hartree/Particle)

Thermal correction = 0.107220 Hartrees

Coordinates from last standard orientation:

Center Number	Atomic Number	Atomic Type	Coordinates (Angstroms)		
			X	Y	Z
1	6	0	-0.102481	0.233702	0.000662
2	6	0	1.220485	-0.152536	-0.000293
3	6	0	1.732705	-1.521036	-0.000535
4	1	0	0.973475	-2.327786	-0.001345
5	6	0	-1.344428	-0.515975	0.001103
6	6	0	-2.559712	0.047555	-0.000951
7	6	0	-3.843060	-0.720904	-0.000307
8	1	0	-4.445198	-0.469280	-0.879852
9	1	0	-3.664479	-1.798944	0.000203
10	1	0	-1.244975	-1.598792	0.003158
11	1	0	-2.629402	1.134185	-0.003093
12	6	0	1.104095	2.068347	0.000042
13	1	0	1.192255	3.143044	0.000020
14	6	0	1.999456	1.054762	-0.000831
15	1	0	3.076803	1.120251	-0.001701
16	1	0	-4.444698	-0.468471	0.879380
17	8	0	-0.172167	1.582452	0.000942
18	8	0	2.915149	-1.794664	0.000293

Aldehyde D2



HF (M062X/6-31+G(d,p)) = -440.0507199 Hartrees

Imaginary Frequencies: none found

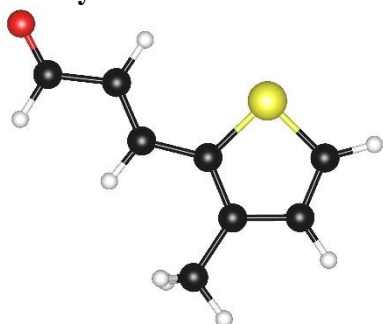
Zero-point correction = 0.154902 (Hartree/Particle)

Thermal correction = 0.118945 Hartrees

Coordinates from last standard orientation:

Center Number	Atomic Number	Atomic Type	Coordinates (Angstroms)		
			X	Y	Z
1	6	0	-0.105054	0.294259	0.006244
2	6	0	1.210306	-0.174614	0.001134
3	6	0	1.629481	-1.571959	-0.000469
4	1	0	0.818978	-2.328335	0.002384
5	6	0	-1.360766	-0.443665	0.011096
6	6	0	-2.590663	0.086088	-0.010487
7	6	0	-3.854805	-0.717756	-0.002341
8	1	0	-4.460024	-0.505008	-0.890045
9	1	0	-3.639599	-1.788958	0.018323
10	1	0	-1.262397	-1.526477	0.033873
11	1	0	-2.717368	1.169269	-0.036964
12	6	0	1.284370	2.070152	-0.000962
13	1	0	1.532334	3.120735	-0.001999
14	6	0	2.079378	0.956498	-0.003712
15	1	0	3.158369	0.920876	-0.008570
16	1	0	-4.469122	-0.473160	0.870804
17	8	0	2.790153	-1.932376	-0.004543
18	7	0	-0.030214	1.656994	0.004617
19	1	0	-0.824369	2.277093	0.013190

Aldehyde D3

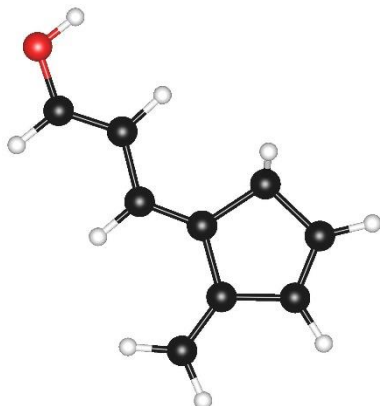


HF (M062X/6-31+G(d,p)) = -782.8633054 Hartrees
 Imaginary Frequencies: none found
 Zero-point correction = 0.138643 (Hartree/Particle)
 Thermal correction = 0.102203 Hartrees

Coordinates from last standard orientation:

Center Number	Atomic Number	Atomic Type	Coordinates (Angstroms)		
			X	Y	Z
1	6	0	0.125050	-0.098312	0.005184
2	6	0	-1.157442	0.424254	0.001208
3	6	0	-1.481629	1.859008	-0.000075
4	1	0	-0.630460	2.565087	0.002036
5	6	0	1.392667	0.625986	0.010374
6	6	0	2.609713	0.066859	-0.010400
7	6	0	3.891835	0.838414	-0.002498
8	1	0	4.491419	0.604729	-0.888674
9	1	0	3.707890	1.915461	0.016113
10	1	0	1.321544	1.711153	0.033079
11	1	0	2.697905	-1.020084	-0.034860
12	6	0	-1.662947	-1.837838	-0.003394
13	1	0	-2.192573	-2.780246	-0.006459
14	6	0	-2.177586	-0.580968	-0.003807
15	1	0	-3.233527	-0.341085	-0.007702
16	1	0	4.497890	0.575842	0.871153
17	8	0	-2.619055	2.281731	-0.003641
18	16	0	0.065899	-1.829320	0.004056

Enol D4



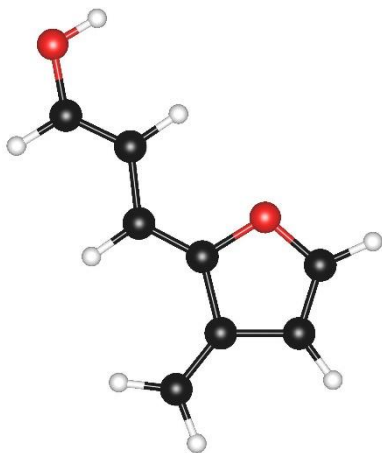
HF (M062X/6-31+G(d,p)) = -423.9608766 Hartrees
 Imaginary Frequencies: none found
 Zero-point correction = 0.165335 (Hartree/Particle)
 Thermal correction = 0.129713 Hartrees

Coordinates from last standard orientation:

Center Number	Atomic Number	Atomic Type	Coordinates (Angstroms)		
			X	Y	Z

1	6	0	0.307748	0.235456	0.000003
2	6	0	-1.115973	-0.173308	0.000008
3	6	0	-1.581025	-1.434547	-0.000016
4	1	0	-0.927563	-2.299945	-0.000044
5	6	0	1.388492	-0.565664	0.000050
6	6	0	2.762105	-0.085795	0.000024
7	6	0	3.835796	-0.887779	-0.000023
8	1	0	4.843590	-0.487803	-0.000031
9	1	0	3.729165	-1.969592	-0.000042
10	1	0	1.256974	-1.647200	0.000096
11	1	0	2.910593	0.993208	0.000053
12	6	0	-1.117312	2.142470	0.000008
13	1	0	-1.458589	3.171293	0.000020
14	6	0	-1.911786	1.063957	0.000031
15	1	0	-2.996822	1.107156	0.000056
16	6	0	0.341184	1.758981	-0.000048
17	1	0	0.862999	2.154564	-0.881057
18	1	0	0.863107	2.154637	0.880862
19	8	0	-2.885229	-1.808447	-0.000021
20	1	0	-3.456991	-1.031371	0.000030

Enol D5



HF (M062X/6-31+G(d,p)) = -459.860336 Hartrees

Imaginary Frequencies: none found

Zero-point correction = 0.141606 (Hartree/Particle)

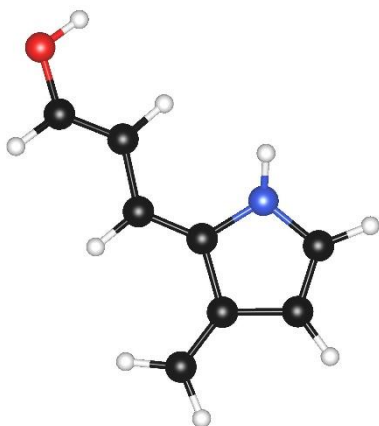
Thermal correction = 0.106401 Hartrees

Coordinates from last standard orientation:

Center Number	Atomic Number	Atomic Type	Coordinates (Angstroms)		
			X	Y	Z
1	6	0	-0.290035	0.179621	-0.000161
2	6	0	1.148336	-0.134971	0.000066
3	6	0	1.691412	-1.366053	-0.000500
4	1	0	1.092822	-2.269758	-0.001466
5	6	0	-1.385739	-0.600844	0.000143
6	6	0	-2.743917	-0.090076	-0.000095
7	6	0	-3.835039	-0.869159	0.000296

8	1	0	-4.832363	-0.444134	0.000123
9	1	0	-3.755690	-1.953254	0.000823
10	1	0	-1.241109	-1.677662	0.000632
11	1	0	-2.855529	0.991872	-0.000602
12	6	0	0.845586	2.094389	0.000045
13	1	0	0.884677	3.173895	-0.000063
14	6	0	1.815253	1.170643	0.000474
15	1	0	2.875187	1.380781	0.000739
16	8	0	-0.412649	1.561089	-0.000437
17	8	0	3.015761	-1.645232	-0.000046
18	1	0	3.531967	-0.829893	0.002076

Enol D6



HF (M062X/6-31+G(d,p)) = -440.0055622 Hartrees

Imaginary Frequencies: none found

Zero-point correction = 0.153962 (Hartree/Particle)

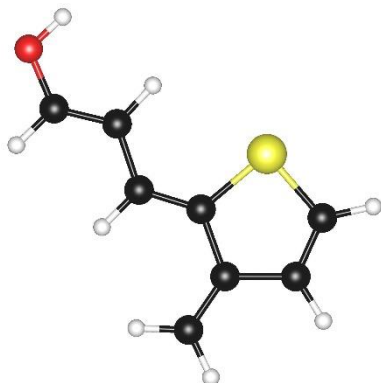
Thermal correction = 0.118574 Hartrees

Coordinates from last standard orientation:

Center Number	Atomic Number	Atomic Type	Coordinates (Angstroms)		
			X	Y	Z
1	6	0	-0.295607	0.228053	-0.009722
2	6	0	1.137291	-0.147054	0.014574
3	6	0	1.612468	-1.406036	-0.037870
4	1	0	0.969735	-2.276401	-0.105473
5	6	0	-1.395569	-0.564194	0.027833
6	6	0	-2.759008	-0.085899	-0.044847
7	6	0	-3.851887	-0.862197	0.039390
8	1	0	-4.849284	-0.444479	-0.034755
9	1	0	-3.768890	-1.936384	0.181251
10	1	0	-1.247622	-1.636430	0.117950
11	1	0	-2.910184	0.983763	-0.194886
12	6	0	0.997276	2.115899	0.019159
13	1	0	1.169402	3.183394	0.024359
14	6	0	1.893356	1.109258	0.058231
15	1	0	2.966441	1.234070	0.084774
16	8	0	2.920665	-1.753140	-0.019156
17	1	0	3.472399	-0.965558	0.062433

18	7	0	-0.297501	1.624841	-0.070725
19	1	0	-1.114722	2.182290	0.112180

Enol D7



HF (M062X/6-31+G(d,p)) = -440.0055622 Hartrees

Imaginary Frequencies: none found

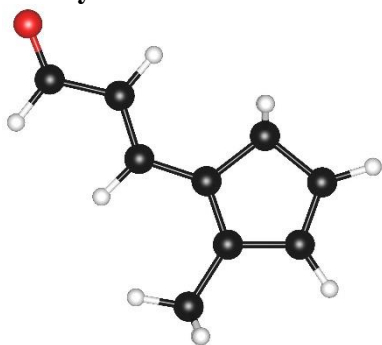
Zero-point correction = 0.153962 (Hartree/Particle)

Thermal correction = 0.118574 Hartrees

Coordinates from last standard orientation:

Center Number	Atomic Number	Atomic Type	Coordinates (Angstroms)		
			X	Y	Z
1	6	0	-0.295607	0.228053	-0.009722
2	6	0	1.137291	-0.147054	0.014574
3	6	0	1.612468	-1.406036	-0.037870
4	1	0	0.969735	-2.276401	-0.105473
5	6	0	-1.395569	-0.564194	0.027833
6	6	0	-2.759008	-0.085899	-0.044847
7	6	0	-3.851887	-0.862197	0.039390
8	1	0	-4.849284	-0.444479	-0.034755
9	1	0	-3.768890	-1.936384	0.181251
10	1	0	-1.247622	-1.636430	0.117950
11	1	0	-2.910184	0.983763	-0.194886
12	6	0	0.997276	2.115899	0.019159
13	1	0	1.169402	3.183394	0.024359
14	6	0	1.893356	1.109258	0.058231
15	1	0	2.966441	1.234070	0.084774
16	8	0	2.920665	-1.753140	-0.019156
17	1	0	3.472399	-0.965558	0.062433
18	7	0	-0.297501	1.624841	-0.070725
19	1	0	-1.114722	2.182290	0.112180

Aldehyde D8



HF (M062X/6-31+G(d,p)) = -423.9805038 Hartrees

Imaginary Frequencies: none found

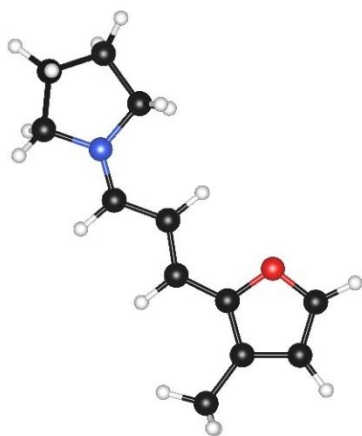
Zero-point correction = 0.164887 (Hartree/Particle)

Thermal correction = 0.129622 Hartrees

Coordinates from last standard orientation:

Center Number	Atomic Number	Atomic Type	Coordinates (Angstroms)		
			X	Y	Z
1	6	0	-0.113819	0.281663	0.000145
2	6	0	1.162129	-0.209571	0.000027
3	6	0	1.559929	-1.621378	0.000172
4	1	0	0.744675	-2.369977	0.000730
5	6	0	-1.360488	-0.466393	0.000303
6	6	0	-2.579191	0.095678	-0.000359
7	6	0	-3.865027	-0.669881	-0.000171
8	1	0	-4.467677	-0.420157	-0.880152
9	1	0	-3.685433	-1.747835	0.000281
10	1	0	-1.292156	-1.552852	0.001034
11	1	0	-2.660568	1.182951	-0.001044
12	6	0	1.448470	2.062390	-0.000150
13	1	0	1.872773	3.058718	-0.000246
14	6	0	2.122967	0.900346	-0.000330
15	1	0	3.196217	0.756685	-0.000626
16	6	0	-0.030677	1.788382	0.000431
17	1	0	-0.527873	2.214458	0.881984
18	1	0	-0.528719	2.215069	-0.880316
19	1	0	-4.467837	-0.419462	0.879507
20	8	0	2.718855	-1.985626	-0.000195

Iminium D9



HF (M062X/6-31+G(d,p)) = -596.3965876 Hartrees

Imaginary Frequencies: none found

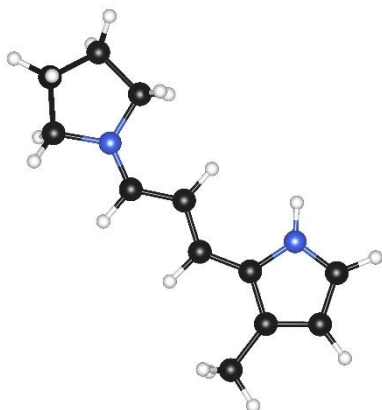
Zero-point correction = 0.262554 (Hartree/Particle)

Thermal correction = 0.221869 Hartrees

Coordinates from last standard orientation:

Center Number	Atomic Number	Atomic Type	Coordinates (Angstroms)		
			X	Y	Z
1	6	0	-1.691202	0.394021	-0.012816
2	6	0	-0.303546	0.598035	-0.018739
3	6	0	0.596327	-0.494073	-0.007672
4	1	0	0.167257	-1.494035	-0.045647
5	7	0	1.895470	-0.464442	0.037045
6	6	0	2.734530	-1.691582	0.011388
7	1	0	2.310201	-2.411734	-0.689907
8	1	0	2.744049	-2.122550	1.018403
9	6	0	4.109605	-1.158707	-0.378783
10	1	0	4.173958	-1.038696	-1.464792
11	1	0	4.909639	-1.827159	-0.058654
12	6	0	4.149937	0.204240	0.320211
13	1	0	4.905457	0.875793	-0.088871
14	1	0	4.349195	0.076851	1.388487
15	6	0	2.736398	0.751832	0.113151
16	1	0	2.387552	1.384245	0.932558
17	1	0	2.641104	1.293913	-0.834105
18	6	0	-2.504530	-0.797624	0.028396
19	6	0	-3.848367	-0.761915	0.013660
20	6	0	-4.721951	-1.967653	0.057456
21	1	0	-5.372979	-1.992958	-0.822630
22	1	0	-4.143765	-2.892735	0.096878
23	1	0	-1.988991	-1.752404	0.077499
24	1	0	-4.342161	0.207859	-0.032419
25	6	0	-1.354447	2.565597	-0.078930
26	1	0	-1.731887	3.575213	-0.114552
27	6	0	-0.116032	2.035754	-0.062814
28	1	0	0.800813	2.600663	-0.093484
29	1	0	-5.380479	-1.923668	0.931391
30	8	0	-2.302198	1.578118	-0.045815

Iminium D10



HF (M062X/6-31+G(d,p)) = -576.5584271 Hartrees

Imaginary Frequencies: none found

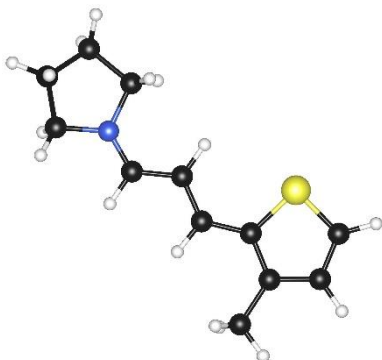
Zero-point correction = 0.275649 (Hartree/Particle)

Thermal correction = 0.235029 Hartrees

Coordinates from last standard orientation:

Center Number	Atomic Number	Atomic Type	Coordinates (Angstroms)		
			X	Y	Z
1	6	0	-1.715324	0.467131	0.108580
2	6	0	-0.312458	0.656429	0.035958
3	6	0	0.560096	-0.454051	0.039368
4	1	0	0.104197	-1.443502	0.041747
5	7	0	1.862572	-0.460094	0.032756
6	6	0	2.665810	-1.709854	0.008394
7	1	0	2.218387	-2.421633	-0.687271
8	1	0	2.670585	-2.138165	1.016632
9	6	0	4.054053	-1.220157	-0.394833
10	1	0	4.118140	-1.121460	-1.483010
11	1	0	4.837344	-1.903678	-0.065053
12	6	0	4.133108	0.154659	0.277179
13	1	0	4.905748	0.797151	-0.146639
14	1	0	4.331238	0.042922	1.347542
15	6	0	2.733916	0.733427	0.062023
16	1	0	2.406191	1.402124	0.861499
17	1	0	2.646888	1.248840	-0.901202
18	6	0	-2.500605	-0.753312	0.250592
19	6	0	-3.759798	-0.889143	-0.190070
20	6	0	-4.588118	-2.119556	-0.018630
21	1	0	-4.913524	-2.501169	-0.991395
22	1	0	-4.039424	-2.905673	0.503848
23	1	0	-2.022684	-1.590694	0.753210
24	1	0	-4.229628	-0.063870	-0.727491
25	6	0	-1.304906	2.673837	-0.108544
26	1	0	-1.579106	3.714586	-0.187584
27	6	0	-0.083146	2.074954	-0.104125
28	1	0	0.855603	2.593148	-0.209052
29	1	0	-5.494926	-1.890597	0.550732
30	7	0	-2.269776	1.692125	0.025655
31	1	0	-3.260362	1.871282	0.119262

Iminium D11



HF (M062X/6-31+G(d,p)) = -919.3596831 Hartrees

Imaginary Frequencies: none found

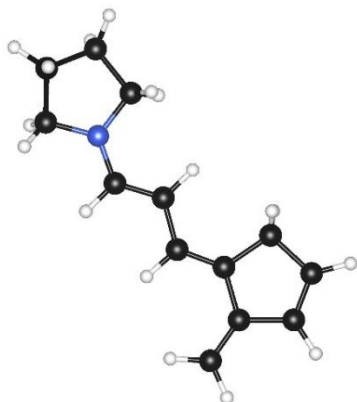
Zero-point correction = 0.258779 (Hartree/Particle)

Thermal correction = 0.216453 Hartrees

Coordinates from last standard orientation:

Center Number	Atomic Number	Atomic Type	Coordinates (Angstroms)		
			X	Y	Z
1	6	0	-1.570318	0.231180	0.100240
2	6	0	-0.202107	0.550798	0.016608
3	6	0	0.744852	-0.512991	-0.002921
4	1	0	0.342243	-1.523576	-0.046115
5	7	0	2.043341	-0.458791	0.010814
6	6	0	2.891327	-1.682015	-0.046452
7	1	0	2.482309	-2.376714	-0.781534
8	1	0	2.881658	-2.149353	0.944114
9	6	0	4.272200	-1.134237	-0.389693
10	1	0	4.363483	-0.986638	-1.470345
11	1	0	5.066727	-1.807939	-0.066854
12	6	0	4.289813	0.211075	0.343229
13	1	0	5.054136	0.894363	-0.028494
14	1	0	4.458034	0.059879	1.413841
15	6	0	2.882025	0.758086	0.105113
16	1	0	2.511155	1.393444	0.912280
17	1	0	2.814315	1.296144	-0.846673
18	6	0	-2.191145	-1.079997	0.254689
19	6	0	-3.427289	-1.378756	-0.176790
20	6	0	-4.087777	-2.703986	0.003423
21	1	0	-4.362173	-3.129434	-0.967207
22	1	0	-3.444743	-3.411183	0.531381
23	1	0	-1.616459	-1.848198	0.767670
24	1	0	-4.001400	-0.616280	-0.704811
25	6	0	-1.142936	2.670485	-0.146636
26	1	0	-1.272210	3.738779	-0.252908
27	6	0	0.017578	1.970910	-0.128059
28	1	0	0.978034	2.451041	-0.241286
29	1	0	-5.017971	-2.587092	0.569381
30	16	0	-2.524866	1.650686	0.037209

Trienamine D12



HF (M062X/6-31+G(d,p)) = -560.073306 Hartrees

Imaginary Frequencies: none found

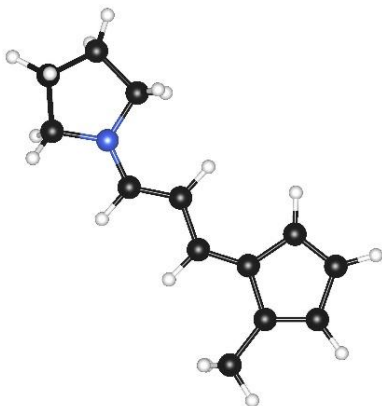
Zero-point correction = 0.271512 (Hartree/Particle)

Thermal correction = 0.232085 Hartrees

Coordinates from last standard orientation:

Center Number	Atomic Number	Atomic Type	Coordinates (Angstroms)		
			X	Y	Z
1	6	0	-1.827852	0.307121	-0.044236
2	6	0	-0.369781	0.541339	-0.108042
3	6	0	0.548475	-0.454960	-0.230683
4	1	0	0.179870	-1.471602	-0.363203
5	7	0	1.909509	-0.376128	-0.225989
6	6	0	2.729982	-1.574981	-0.389007
7	1	0	2.531914	-2.054097	-1.353162
8	1	0	2.518349	-2.304876	0.408446
9	6	0	4.157111	-1.040336	-0.275414
10	1	0	4.486988	-0.649786	-1.244033
11	1	0	4.866153	-1.806099	0.046405
12	6	0	4.003289	0.106225	0.730367
13	1	0	4.830875	0.818540	0.705944
14	1	0	3.929227	-0.298308	1.745606
15	6	0	2.668397	0.740677	0.327816
16	1	0	2.129762	1.175441	1.177995
17	1	0	2.815806	1.529372	-0.423448
18	6	0	-2.471286	-0.871883	0.084874
19	6	0	-3.916767	-1.014796	0.118382
20	6	0	-4.560359	-2.185751	0.240247
21	1	0	-5.643159	-2.239386	0.260034
22	1	0	-4.014014	-3.122157	0.321912
23	1	0	-1.897521	-1.793464	0.178189
24	1	0	-4.505457	-0.101732	0.036190
25	6	0	-1.361238	2.638861	-0.122039
26	1	0	-1.491799	3.714207	-0.155218
27	6	0	-0.181787	1.999846	-0.116530
28	1	0	0.779814	2.496022	-0.157334
29	6	0	-2.513519	1.666933	-0.106781
30	1	0	-3.177486	1.825417	0.752131
31	1	0	-3.133881	1.765635	-1.008252

Fulvene trienammine D12'



HF (M062X/6-31+G(d,p)) = -560.0912156 Hartrees

Imaginary Frequencies: none found

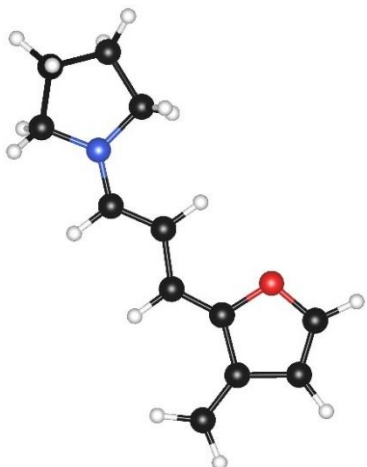
Zero-point correction = 0.271813 (Hartree/Particle)

Thermal correction = 0.230195 Hartrees

Coordinates from last standard orientation:

Center Number	Atomic Number	Atomic Type	Coordinates (Angstroms)		
			X	Y	Z
1	6	0	-1.132369	-0.547330	0.028544
2	6	0	0.172321	0.040776	0.036827
3	6	0	1.289492	-0.742770	0.061365
4	1	0	1.177782	-1.826743	0.073689
5	7	0	2.568300	-0.313685	0.067162
6	6	0	3.730101	-1.198576	0.066680
7	1	0	3.566911	-2.046889	-0.605195
8	1	0	3.927305	-1.588094	1.076092
9	6	0	4.858394	-0.275103	-0.395063
10	1	0	4.858583	-0.210690	-1.488324
11	1	0	5.842190	-0.618761	-0.068909
12	6	0	4.456515	1.075110	0.212129
13	1	0	4.940178	1.926107	-0.271335
14	1	0	4.714836	1.096440	1.276125
15	6	0	2.933025	1.097355	0.047304
16	1	0	2.426237	1.637058	0.856143
17	1	0	2.624809	1.551183	-0.906094
18	1	0	0.261487	1.122698	0.019997
19	1	0	-1.165068	-1.639215	0.048955
20	6	0	-2.324065	0.111288	-0.001303
21	6	0	-3.644430	-0.533435	-0.007354
22	6	0	-3.903273	1.753644	-0.060399
23	1	0	-4.407674	2.712233	-0.089997
24	6	0	-3.877234	-2.012989	0.024040
25	1	0	-4.948165	-2.230451	0.001535
26	1	0	-3.416804	-2.514614	-0.835080
27	6	0	-4.577746	0.455427	-0.042327
28	1	0	-5.652407	0.311020	-0.054757
29	6	0	-2.559581	1.554257	-0.035735
30	1	0	-1.791935	2.317623	-0.042166
31	1	0	-3.463250	-2.469034	0.930932

Trienamine D13



HF (M062X/6-31+G(d,p)) = -595.9750923 Hartrees

Imaginary Frequencies: none found

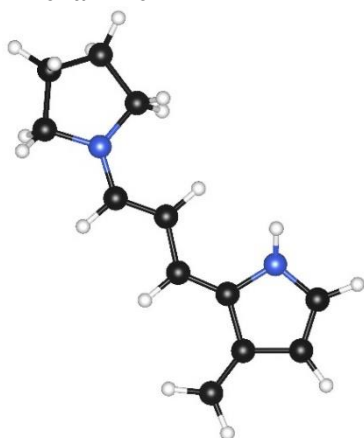
Zero-point correction = 0.248397 (Hartree/Particle)

Thermal correction = 0.207832 Hartrees

Coordinates from last standard orientation:

Center Number	Atomic Number	Atomic Type	Coordinates (Angstroms)		
			X	Y	Z
1	6	0	1.797682	0.277345	0.029812
2	6	0	0.348016	0.508579	0.077283
3	6	0	-0.566238	-0.498594	0.155267
4	1	0	-0.191104	-1.516858	0.243521
5	7	0	-1.920853	-0.416906	0.148842
6	6	0	-2.762880	-1.607594	0.255292
7	1	0	-2.510516	-2.181208	1.152461
8	1	0	-2.629705	-2.259802	-0.621717
9	6	0	-4.176118	-1.027483	0.296687
10	1	0	-4.423209	-0.723444	1.319425
11	1	0	-4.930561	-1.740239	-0.042727
12	6	0	-4.056776	0.204845	-0.607008
13	1	0	-4.855934	0.933379	-0.455248
14	1	0	-4.069347	-0.102875	-1.658021
15	6	0	-2.676749	0.765811	-0.249525
16	1	0	-2.186144	1.258137	-1.096906
17	1	0	-2.739684	1.486364	0.578314
18	6	0	2.536750	-0.849373	-0.074597
19	6	0	3.984544	-0.866065	-0.081179
20	6	0	4.732993	-1.975679	-0.191211
21	1	0	5.816026	-1.928216	-0.190079
22	1	0	4.277618	-2.958337	-0.285765
23	1	0	2.012351	-1.796474	-0.165483
24	1	0	4.476688	0.100107	0.011485
25	6	0	1.448436	2.473715	0.129376
26	1	0	1.810686	3.489859	0.175958
27	6	0	0.208780	1.966524	0.112985
28	1	0	-0.699600	2.545863	0.159158
29	8	0	2.422219	1.509987	0.089329

Trienamine D14



HF (M062X/6-31+G(d,p)) = -576.1195168 Hartrees

Imaginary Frequencies: none found

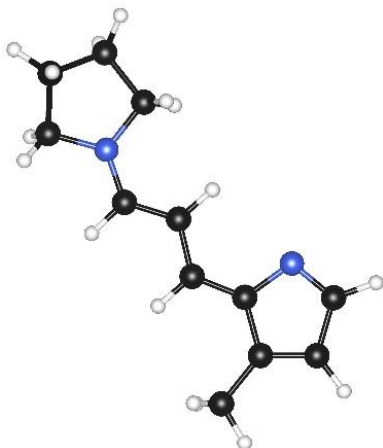
Zero-point correction = 0.260292 (Hartree/Particle)

Thermal correction = 0.218647 Hartrees

Coordinates from last standard orientation:

Center Number	Atomic Number	Atomic Type	Coordinates (Angstroms)		
			X	Y	Z
1	6	0	-1.810461	0.316915	-0.034383
2	6	0	-0.354818	0.552447	-0.068468
3	6	0	0.545656	-0.463681	-0.202131
4	1	0	0.157590	-1.469790	-0.355128
5	7	0	1.900709	-0.397330	-0.182714
6	6	0	2.729631	-1.584096	-0.388730
7	1	0	2.508527	-2.050918	-1.353832
8	1	0	2.547630	-2.326488	0.403448
9	6	0	4.153748	-1.033379	-0.309481
10	1	0	4.455489	-0.639631	-1.285961
11	1	0	4.878368	-1.792021	-0.006196
12	6	0	4.015744	0.112785	0.699461
13	1	0	4.835766	0.832526	0.651241
14	1	0	3.971940	-0.289704	1.717252
15	6	0	2.666019	0.734211	0.329715
16	1	0	2.147783	1.178683	1.186761
17	1	0	2.784754	1.509948	-0.439995
18	6	0	-2.499792	-0.849051	0.122349
19	6	0	-3.935742	-0.967312	0.036303
20	6	0	-4.643952	-2.089881	0.258505
21	1	0	-5.722863	-2.107526	0.156254
22	1	0	-4.153370	-3.017354	0.542018
23	1	0	-1.934629	-1.751935	0.333561
24	1	0	-4.492017	-0.074859	-0.255716
25	6	0	-1.404166	2.564316	-0.132656
26	1	0	-1.681360	3.607893	-0.185625
27	6	0	-0.177222	2.007402	-0.079641
28	1	0	0.752625	2.552505	-0.117696
29	7	0	-2.389412	1.579512	-0.170448
30	1	0	-3.343193	1.759356	0.096688

Fulvene trienamine D14'



HF (M062X/6-31+G(d,p)) = -576.1425105 Hartrees

Imaginary Frequencies: none found

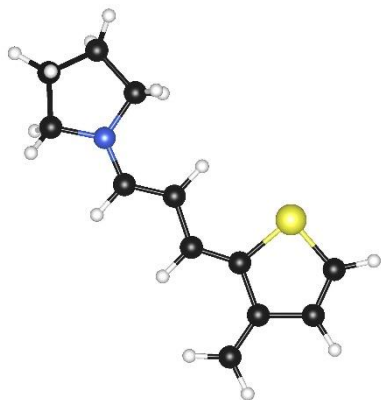
Zero-point correction = 0.260696 (Hartree/Particle)

Thermal correction = 0.219094 Hartrees

Coordinates from last standard orientation:

Center Number	Atomic Number	Atomic Type	Coordinates (Angstroms)		
			X	Y	Z
1	6	0	-1.141246	-0.596119	0.031325
2	6	0	0.149582	0.000656	0.039750
3	6	0	1.274935	-0.776097	0.066868
4	1	0	1.176179	-1.861574	0.081518
5	7	0	2.544636	-0.331557	0.072374
6	6	0	3.719892	-1.199588	0.072125
7	1	0	3.565533	-2.054286	-0.593545
8	1	0	3.925110	-1.579071	1.083541
9	6	0	4.833002	-0.262274	-0.398232
10	1	0	4.827619	-0.202290	-1.491732
11	1	0	5.822713	-0.591388	-0.075037
12	6	0	4.414475	1.084367	0.205665
13	1	0	4.885180	1.940083	-0.282071
14	1	0	4.675772	1.112860	1.268784
15	6	0	2.890633	1.086302	0.044767
16	1	0	2.376389	1.621970	0.850567
17	1	0	2.572978	1.528400	-0.910210
18	1	0	0.201975	1.084358	0.020312
19	1	0	-1.193510	-1.686367	0.051390
20	6	0	-2.322825	0.088962	0.000288
21	6	0	-3.664220	-0.481480	-0.010936
22	6	0	-3.659380	1.769595	-0.057142
23	1	0	-4.005512	2.798977	-0.084300
24	6	0	-4.001087	-1.940113	0.015772
25	1	0	-5.083429	-2.085694	-0.014318
26	1	0	-3.566988	-2.466631	-0.841201
27	6	0	-4.507846	0.589242	-0.047762
28	1	0	-5.590577	0.573713	-0.065994
29	7	0	-2.385025	1.489703	-0.029087
30	1	0	-3.622201	-2.420807	0.924356

Trienammine D15



HF (M062X/6-31+G(d,p)) = -918.9403592 Hartrees

Imaginary Frequencies: none found

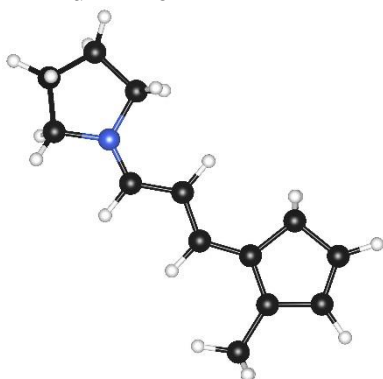
Zero-point correction = 0.244624 (Hartree/Particle)

Thermal correction = 0.202883 Hartrees

Coordinates from last standard orientation:

Center Number	Atomic Number	Atomic Type	Coordinates (Angstroms)		
			X	Y	Z
1	6	0	-1.640185	0.073354	-0.027715
2	6	0	-0.215382	0.446174	-0.092488
3	6	0	0.753541	-0.496227	-0.296318
4	1	0	0.435806	-1.510709	-0.534960
5	7	0	2.101909	-0.349431	-0.254567
6	6	0	2.987775	-1.471173	-0.575418
7	1	0	2.852962	-1.789304	-1.613814
8	1	0	2.770246	-2.328589	0.079401
9	6	0	4.383723	-0.909852	-0.304025
10	1	0	4.747470	-0.372512	-1.186433
11	1	0	5.105528	-1.690992	-0.056832
12	6	0	4.133857	0.074114	0.843850
13	1	0	4.934229	0.806313	0.969856
14	1	0	4.015208	-0.471934	1.785904
15	6	0	2.803341	0.720849	0.451116
16	1	0	2.209612	1.047790	1.311632
17	1	0	2.968527	1.587333	-0.204573
18	6	0	-2.174422	-1.162144	0.129944
19	6	0	-3.591008	-1.464054	0.139215
20	6	0	-4.103814	-2.696164	0.284062
21	1	0	-5.174302	-2.866426	0.288038
22	1	0	-3.460041	-3.564552	0.399687
23	1	0	-1.496624	-2.000586	0.278885
24	1	0	-4.277694	-0.625719	0.021012
25	6	0	-1.217676	2.570489	-0.095188
26	1	0	-1.347265	3.643870	-0.129701
27	6	0	-0.056286	1.897127	-0.062476
28	1	0	0.901303	2.400308	-0.087275
29	16	0	-2.642444	1.542923	-0.119138

Iminium D16



HF (M062X/6-31+G(d,p)) = -560.4807685 Hartrees

Imaginary Frequencies: none found

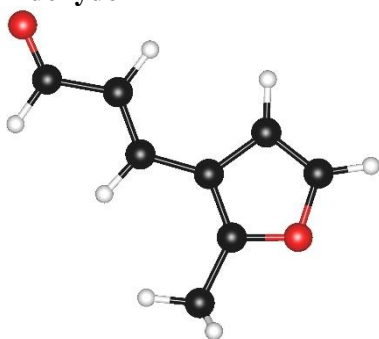
Zero-point correction = 0.285113 (Hartree/Particle)

Thermal correction = 0.243995 Hartrees

Coordinates from last standard orientation:

Center Number	Atomic Number	Atomic Type	Coordinates (Angstroms)		
			X	Y	Z
1	6	0	-1.717095	0.429196	-0.021872
2	6	0	-0.342112	0.639454	-0.059523
3	6	0	0.562277	-0.458225	-0.075570
4	1	0	0.131964	-1.454031	-0.157742
5	7	0	1.861905	-0.450077	-0.008842
6	6	0	2.667160	-1.700070	-0.062392
7	1	0	2.258924	-2.366730	-0.823707
8	1	0	2.608818	-2.186015	0.917625
9	6	0	4.077164	-1.196147	-0.349851
10	1	0	4.207686	-1.027708	-1.423401
11	1	0	4.836514	-1.905296	-0.018283
12	6	0	4.118772	0.130844	0.415012
13	1	0	4.918083	0.794256	0.082754
14	1	0	4.250001	-0.051274	1.486018
15	6	0	2.738931	0.734626	0.150346
16	1	0	2.367417	1.356224	0.966951
17	1	0	2.719172	1.305948	-0.783549
18	6	0	-2.433715	-0.822021	0.023850
19	6	0	-3.778781	-0.903923	0.048627
20	6	0	-4.548182	-2.178613	0.089844
21	1	0	-5.217818	-2.244224	-0.774511
22	1	0	-3.893102	-3.051794	0.095956
23	1	0	-1.869512	-1.751487	0.041870
24	1	0	-4.365164	0.014683	0.039430
25	6	0	-1.249778	2.748868	-0.081187
26	1	0	-1.380741	3.822763	-0.111097
27	6	0	-0.080904	2.092603	-0.100157
28	1	0	0.891155	2.559525	-0.160320
29	6	0	-2.387947	1.775526	-0.024451
30	1	0	-3.005094	1.910801	0.873480
31	1	0	-3.060828	1.879772	-0.885753
32	1	0	-5.185541	-2.207582	0.980119

Aldehyde E1



HF (M062X/6-31+G(d,p)) = -459.8995532 Hartrees

Imaginary Frequencies: none found

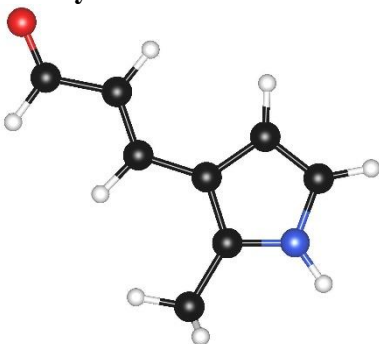
Zero-point correction = 0.142296 (Hartree/Particle)

Thermal correction = 0.107131 Hartrees

Coordinates from last standard orientation:

Center Number	Atomic Number	Atomic Type	Coordinates (Angstroms)		
			X	Y	Z
1	6	0	0.757427	0.479038	0.000182
2	6	0	1.879217	-0.265634	0.000242
3	6	0	3.190157	0.391113	0.000018
4	1	0	3.160620	1.502534	0.000196
5	1	0	1.854113	-1.351415	0.000341
6	1	0	0.844920	1.564908	0.000153
7	6	0	-0.585896	-0.033882	0.000150
8	6	0	-1.811344	0.587159	-0.000172
9	6	0	-2.075144	-1.632149	-0.000056
10	1	0	-2.366082	-2.671372	-0.000074
11	6	0	-2.095239	2.056040	0.000046
12	1	0	-2.671399	2.338803	0.885890
13	1	0	-1.176452	2.645768	-0.005341
14	6	0	-2.779071	-0.467913	-0.000346
15	1	0	-3.854673	-0.366105	-0.000679
16	1	0	-2.680602	2.337126	-0.880234
17	8	0	-0.749684	-1.388813	0.000298
18	8	0	4.250798	-0.196547	-0.000377

Aldehyde E2

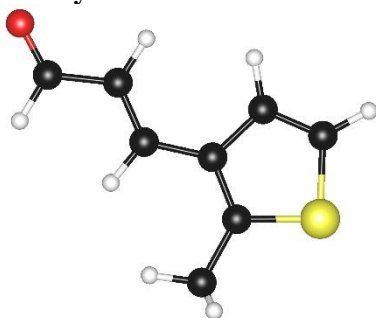


HF (M062X/6-31+G(d,p)) = -440.0524551 Hartrees
 Imaginary Frequencies: none found
 Zero-point correction = 0.154487 (Hartree/Particle)
 Thermal correction = 0.119864 Hartrees

Coordinates from last standard orientation:

Center Number	Atomic Number	Atomic Type	Coordinates (Angstroms)		
			X	Y	Z
1	6	0	0.766700	0.423655	0.000034
2	6	0	1.907996	-0.297987	0.000017
3	6	0	3.205147	0.376714	0.000043
4	1	0	3.156322	1.487253	0.000432
5	1	0	1.932152	-1.385188	-0.000079
6	1	0	0.857839	1.509478	0.000201
7	6	0	-0.580048	-0.075399	-0.000051
8	6	0	-1.788044	0.620376	-0.000211
9	6	0	-2.231841	-1.593432	0.000077
10	1	0	-2.669754	-2.580565	0.000073
11	6	0	-1.976274	2.107023	0.000060
12	1	0	-2.529711	2.428712	0.887419
13	1	0	-1.024122	2.641650	-0.008778
14	6	0	-2.824018	-0.346691	-0.000049
15	1	0	-3.886814	-0.150321	-0.000192
16	1	0	-2.544729	2.426711	-0.878420
17	8	0	4.277124	-0.193160	-0.000104
18	7	0	-0.883114	-1.421716	0.000082
19	1	0	-0.204084	-2.165991	0.000082

Aldehyde E3



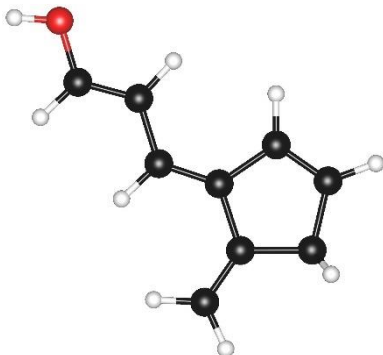
HF (M062X/6-31+G(d,p)) = -782.865599 Hartrees
 Imaginary Frequencies: none found
 Zero-point correction = 0.138198 (Hartree/Particle)
 Thermal correction = 0.101369 Hartrees

Coordinates from last standard orientation:

Center Number	Atomic Number	Atomic Type	Coordinates (Angstroms)		
			X	Y	Z
1	6	0	0.926549	0.528431	0.004386
2	6	0	2.022446	-0.254338	-0.001684

3	6	0	3.356248	0.354682	0.000700
4	1	0	3.366117	1.466059	0.006957
5	1	0	1.975204	-1.340983	-0.008455
6	1	0	1.073545	1.609800	0.009277
7	6	0	-0.454458	0.101149	0.003767
8	6	0	-1.564857	0.924653	0.001802
9	6	0	-2.575878	-1.174312	-0.002870
10	1	0	-3.320406	-1.958495	-0.004191
11	6	0	-1.508831	2.428055	-0.002066
12	1	0	-0.923428	2.810688	0.839358
13	1	0	-1.060345	2.808791	-0.925064
14	6	0	-2.779074	0.177589	-0.002331
15	1	0	-3.762245	0.634147	-0.003921
16	1	0	-2.514497	2.845869	0.076027
17	8	0	4.394619	-0.271324	-0.003606
18	16	0	-0.907735	-1.576296	0.001789

Enol E4



HF (M062X/6-31+G(d,p)) = -423.9613425 Hartrees

Imaginary Frequencies: none found

Zero-point correction = 0.164473 (Hartree/Particle)

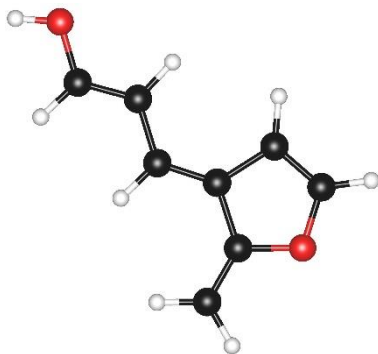
Thermal correction = 0.127394 Hartrees

Coordinates from last standard orientation:

Center Number	Atomic Number	Atomic Type	Coordinates (Angstroms)		
			X	Y	Z
1	6	0	-0.495803	-0.672379	0.000000
2	6	0	0.289802	-1.887812	0.000000
3	6	0	-0.278206	-3.101898	0.000000
4	1	0	-1.359432	-3.231789	0.000000
5	1	0	1.375079	-1.832658	0.000000
6	1	0	-1.578649	-0.797508	0.000000
7	6	0	0.000000	0.584507	0.000000
8	6	0	-0.792347	1.842581	0.000000
9	6	0	1.412743	0.987475	0.000000
10	6	0	1.534225	2.323023	0.000000
11	1	0	2.241479	0.288904	0.000000
12	1	0	2.473112	2.865432	0.000000
13	6	0	-2.122602	1.966041	0.000000
14	1	0	-2.595308	2.943513	0.000000
15	1	0	-2.779518	1.101496	0.000000

16	6	0	0.190523	3.006337	0.000000
17	1	0	0.057711	3.645802	0.881276
18	1	0	0.057711	3.645802	-0.881276
19	8	0	0.471436	-4.237600	0.000000
20	1	0	-0.093685	-5.015454	0.000000

Enol E5



HF (M062X/6-31+G(d,p)) = -459.8632432 Hartrees

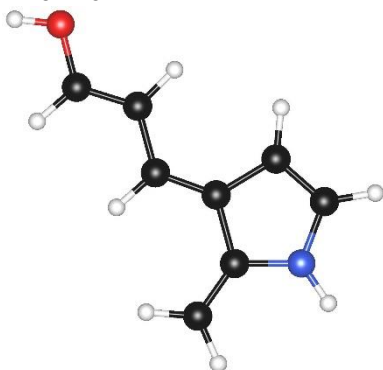
Imaginary Frequencies: none found

Zero-point correction = 0.142086 (Hartree/Particle)

Thermal correction = 0.107406 Hartrees

Coordinates from last standard orientation:

Center Number	Atomic Number	Atomic Type	Coordinates (Angstroms)		
			X	Y	Z
1	6	0	-0.600001	0.610946	-0.000201
2	6	0	-1.834554	-0.144729	-0.000349
3	6	0	-3.037133	0.451659	0.000217
4	1	0	-3.155020	1.531409	0.000775
5	1	0	-1.761903	-1.230844	-0.000899
6	1	0	-0.655176	1.696268	-0.000185
7	6	0	0.623157	0.057730	-0.000100
8	6	0	1.969529	0.663833	0.000030
9	6	0	2.107376	-1.589701	0.000130
10	1	0	2.362596	-2.639932	0.000176
11	6	0	2.285502	1.969956	-0.000039
12	1	0	3.321318	2.289499	0.000098
13	1	0	1.523122	2.741514	-0.000229
14	6	0	2.872117	-0.490595	0.000180
15	1	0	3.951270	-0.456522	0.000298
16	8	0	0.766127	-1.325243	-0.000058
17	8	0	-4.239556	-0.171850	0.000232
18	1	0	-4.114733	-1.129244	-0.000629

Enol E6

HF (M062X/6-31+G(d,p)) = -440.0057536 Hartrees

Imaginary Frequencies: none found

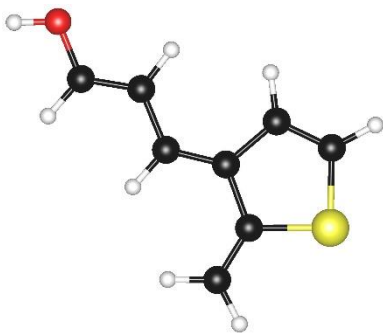
Zero-point correction = 0.154170 (Hartree/Particle)

Thermal correction = 0.119075 Hartrees

Coordinates from last standard orientation:

Center Number	Atomic Number	Atomic Type	Coordinates (Angstroms)		
			X	Y	Z
1	6	0	-0.610640	0.578955	-0.023314
2	6	0	-1.858502	-0.152608	0.070809
3	6	0	-3.056304	0.429598	-0.099515
4	1	0	-3.162545	1.482863	-0.341697
5	1	0	-1.824113	-1.213285	0.322858
6	1	0	-0.666976	1.658552	-0.133800
7	6	0	0.616551	0.021210	0.018802
8	6	0	1.942188	0.694943	-0.003443
9	6	0	2.253453	-1.559738	-0.041401
10	1	0	2.643959	-2.568572	-0.069135
11	6	0	2.180910	2.016548	0.067434
12	1	0	3.196208	2.396756	0.049875
13	1	0	1.377800	2.740901	0.150916
14	6	0	2.923287	-0.391938	-0.073716
15	1	0	3.995609	-0.266025	-0.104359
16	8	0	-4.266651	-0.174267	0.002308
17	1	0	-4.155069	-1.104405	0.234657
18	7	0	0.879156	-1.361374	0.096398
19	1	0	0.228594	-2.024853	-0.296514

Enol E7



HF (M062X/6-31+G(d,p)) = -782.8287946 Hartrees

Imaginary Frequencies: none found

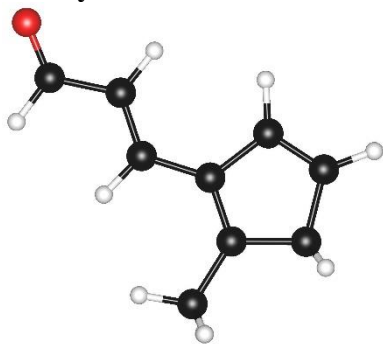
Zero-point correction = 0.138604 (Hartree/Particle)

Thermal correction = 0.102369 Hartrees

Coordinates from last standard orientation:

Center Number	Atomic Number	Atomic Type	Coordinates (Angstroms)		
			X	Y	Z
1	6	0	-0.776382	0.695943	0.000325
2	6	0	-1.987905	-0.094670	0.000202
3	6	0	-3.206017	0.472105	0.000281
4	1	0	-3.346590	1.549220	0.000405
5	1	0	-1.901783	-1.181183	0.000088
6	1	0	-0.897243	1.778124	0.001081
7	6	0	0.479469	0.208589	-0.000337
8	6	0	1.741082	0.991546	0.000040
9	6	0	2.561326	-1.216600	0.000870
10	1	0	3.242414	-2.057930	0.001400
11	6	0	1.838727	2.333243	-0.000901
12	1	0	2.811264	2.813168	-0.000310
13	1	0	0.967491	2.978709	-0.002260
14	6	0	2.890008	0.082417	0.001290
15	1	0	3.911303	0.445293	0.002230
16	8	0	-4.392011	-0.175997	0.000280
17	1	0	-4.250600	-1.131271	0.000165
18	16	0	0.834874	-1.538850	-0.000979

Aldehyde E8

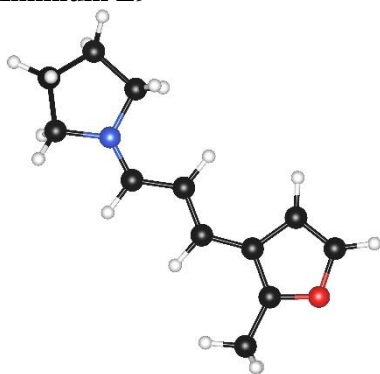


HF (M062X/6-31+G(d,p)) = -423.9849446 Hartrees
 Imaginary Frequencies: none found
 Zero-point correction = 0.164944 (Hartree/Particle)
 Thermal correction = 0.129505 Hartrees

Coordinates from last standard orientation:

Center Number	Atomic Number	Atomic Type	Coordinates (Angstroms)		
			X	Y	Z
1	6	0	-0.783936	0.448481	-0.000704
2	6	0	-1.911605	-0.292869	0.000066
3	6	0	-3.224794	0.354874	-0.000212
4	1	0	-3.200271	1.466582	-0.001543
5	1	0	-1.898095	-1.380196	0.001020
6	1	0	-0.894318	1.533762	-0.001640
7	6	0	0.562284	-0.070200	-0.000395
8	6	0	1.719611	0.652694	-0.000061
9	6	0	2.401169	-1.545595	0.000111
10	1	0	3.001699	-2.447050	0.000162
11	6	0	1.898859	2.137522	0.000340
12	1	0	2.471941	2.451439	-0.878529
13	1	0	0.949439	2.675010	-0.003794
14	6	0	2.854222	-0.277537	0.000309
15	1	0	3.892817	0.035867	0.000602
16	6	0	0.900997	-1.538314	-0.000290
17	1	0	0.493266	-2.051522	-0.881488
18	1	0	0.492892	-2.051432	0.880794
19	1	0	2.464499	2.451871	0.883906
20	8	0	-4.284339	-0.237333	0.000690

Iminium E9



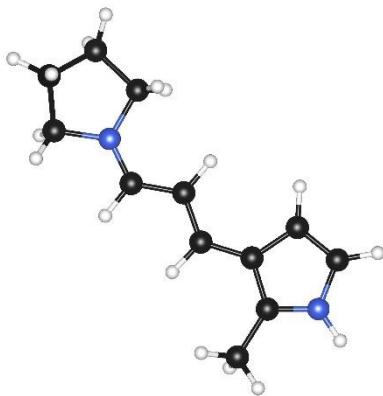
HF (M062X/6-31+G(d,p)) = -596.4064371 Hartrees
 Imaginary Frequencies: none found
 Zero-point correction = 0.262403 (Hartree/Particle)
 Thermal correction = 0.221077 Hartrees

Coordinates from last standard orientation:

Center Number	Atomic Number	Atomic Type	Coordinates (Angstroms)		
			X	Y	Z

1	6	0	1.067826	0.654190	0.032542
2	6	0	-0.152866	0.026918	0.040890
3	6	0	-1.327905	0.810419	0.067953
4	1	0	-1.236381	1.896558	0.079228
5	7	0	-2.545869	0.346055	0.076087
6	6	0	-3.758645	1.197117	0.079817
7	1	0	-3.598347	2.070909	-0.554361
8	1	0	-3.951912	1.524111	1.107571
9	6	0	-4.843555	0.243520	-0.412981
10	1	0	-4.825364	0.185758	-1.505832
11	1	0	-5.838823	0.562574	-0.101462
12	6	0	-4.419460	-1.093802	0.205218
13	1	0	-4.874971	-1.956051	-0.282923
14	1	0	-4.686831	-1.122361	1.265827
15	6	0	-2.896776	-1.091897	0.048913
16	1	0	-2.371843	-1.615112	0.851841
17	1	0	-2.578526	-1.505002	-0.914828
18	1	0	-0.209130	-1.056038	0.021419
19	1	0	1.108211	1.741835	0.051912
20	6	0	2.313776	0.000439	0.000831
21	6	0	3.615183	0.486863	-0.010463
22	6	0	3.616160	-1.743616	-0.055159
23	1	0	3.800517	-2.807780	-0.079301
24	6	0	4.060073	1.911360	0.010020
25	1	0	4.651299	2.135352	-0.882142
26	1	0	3.220958	2.607947	0.045912
27	6	0	4.450553	-0.660083	-0.046819
28	1	0	5.530330	-0.681981	-0.064474
29	1	0	4.694615	2.096558	0.881095
30	8	0	2.330136	-1.368530	-0.027084

Iminium E10



HF (M062X/6-31+G(d,p)) = -576.5614715 Hartrees

Imaginary Frequencies: none found

Zero-point correction = 0.275266 (Hartree/Particle)

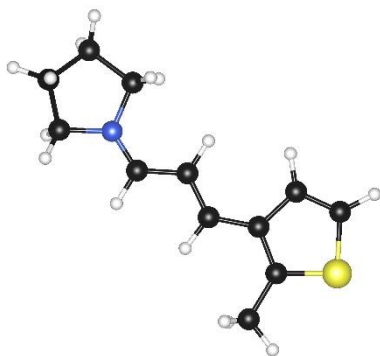
Thermal correction = 0.234156 Hartrees

Coordinates from last standard orientation:

Center	Atomic	Atomic	Coordinates (Angstroms)
--------	--------	--------	-------------------------

Number	Number	Type	X	Y	Z
1	6	0	1.063741	0.531954	0.022623
2	6	0	-0.179461	-0.073439	0.035485
3	6	0	-1.328448	0.735181	0.059310
4	1	0	-1.203342	1.817893	0.064651
5	7	0	-2.566558	0.312474	0.071735
6	6	0	-3.746649	1.205778	0.072953
7	1	0	-3.560518	2.066517	-0.572170
8	1	0	-3.926611	1.552476	1.096807
9	6	0	-4.866957	0.287251	-0.407804
10	1	0	-4.856845	0.222767	-1.500395
11	1	0	-5.849282	0.641062	-0.092622
12	6	0	-4.485762	-1.061168	0.214579
13	1	0	-4.972166	-1.909584	-0.268081
14	1	0	-4.749920	-1.075860	1.276291
15	6	0	-2.963899	-1.109672	0.053650
16	1	0	-2.457301	-1.646752	0.860098
17	1	0	-2.663773	-1.542578	-0.907950
18	1	0	-0.286133	-1.153296	0.024581
19	1	0	1.092279	1.621442	0.038004
20	6	0	2.322472	-0.076296	-0.006220
21	6	0	3.591016	0.553678	-0.007728
22	6	0	3.877646	-1.680240	-0.058502
23	1	0	4.267890	-2.687957	-0.086817
24	6	0	3.840567	2.028901	0.029530
25	1	0	4.909072	2.232833	-0.051009
26	1	0	3.339551	2.541873	-0.796629
27	6	0	4.552078	-0.460558	-0.040059
28	1	0	5.624873	-0.334234	-0.049861
29	1	0	3.486756	2.467104	0.967841
30	7	0	2.552562	-1.446284	-0.037435
31	1	0	1.845373	-2.165257	-0.049742

Iminium E11



HF (M062X/6-31+G(d,p)) = -919.3709258 Hartrees

Imaginary Frequencies: none found

Zero-point correction = 0.258864 (Hartree/Particle)

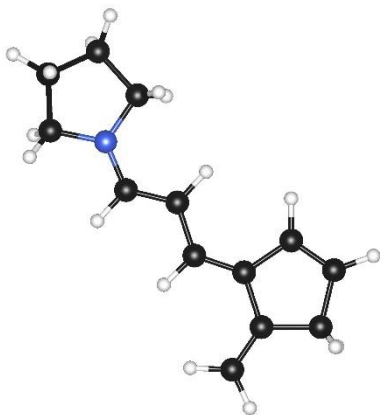
Thermal correction = 0.216555 Hartrees

Coordinates from last standard orientation:

Center Number	Atomic Number	Atomic Type	Coordinates (Angstroms)		
			X	Y	Z

1	6	0	0.828413	0.722743	0.030469
2	6	0	-0.381840	0.073524	0.045192
3	6	0	-1.570133	0.836593	0.066215
4	1	0	-1.494818	1.923990	0.070199
5	7	0	-2.780878	0.353823	0.076442
6	6	0	-4.006571	1.186368	0.073891
7	1	0	-3.857996	2.060100	-0.563223
8	1	0	-4.207531	1.514082	1.099906
9	6	0	-5.075321	0.214367	-0.418196
10	1	0	-5.052519	0.151934	-1.510710
11	1	0	-6.076392	0.519664	-0.111547
12	6	0	-4.633374	-1.113586	0.207633
13	1	0	-5.073925	-1.984972	-0.278008
14	1	0	-4.903924	-1.141303	1.267437
15	6	0	-3.110138	-1.089293	0.056733
16	1	0	-2.581253	-1.600118	0.865157
17	1	0	-2.782501	-1.503622	-0.903357
18	1	0	-0.434289	-1.010866	0.035257
19	1	0	0.820470	1.813593	0.042148
20	6	0	2.113556	0.132595	0.001951
21	6	0	3.328102	0.827772	-0.007210
22	6	0	4.057398	-1.378007	-0.049961
23	1	0	4.706523	-2.243788	-0.072335
24	6	0	3.455068	2.323327	0.017167
25	1	0	4.504400	2.615087	-0.040565
26	1	0	2.934512	2.783516	-0.827822
27	6	0	4.430984	-0.055738	-0.036778
28	1	0	5.463943	0.270274	-0.048274
29	1	0	3.044001	2.741033	0.941357
30	16	0	2.365037	-1.591835	-0.026460

Trienamine E12



HF (M062X/6-31+G(d,p)) = -560.0793104 Hartrees

Imaginary Frequencies: none found

Zero-point correction = 0.271272 (Hartree/Particle)

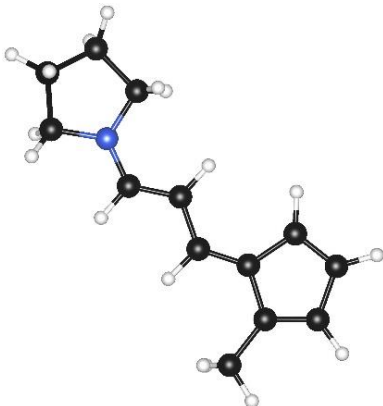
Thermal correction = 0.228995 Hartrees

Coordinates from last standard orientation:

Center	Atomic	Atomic	Coordinates (Angstroms)
--------	--------	--------	-------------------------

Number	Number	Type	X	Y	Z
1	6	0	-1.136738	0.696726	-0.029104
2	6	0	0.167393	0.076363	-0.037190
3	6	0	1.308037	0.815608	-0.063138
4	1	0	1.239352	1.902977	-0.079077
5	7	0	2.577405	0.335833	-0.064900
6	6	0	3.770153	1.172923	-0.077968
7	1	0	3.645493	2.033808	0.587092
8	1	0	3.983481	1.548100	-1.090637
9	6	0	4.862919	0.210121	0.390120
10	1	0	4.862953	0.156962	1.484076
11	1	0	5.859418	0.510124	0.058753
12	6	0	4.405446	-1.129324	-0.201819
13	1	0	4.853693	-1.994412	0.291185
14	1	0	4.663924	-1.172776	-1.265244
15	6	0	2.881134	-1.085339	-0.040540
16	1	0	2.356355	-1.608304	-0.850464
17	1	0	2.550140	-1.527861	0.911752
18	1	0	0.225229	-1.008859	-0.018606
19	1	0	-1.155075	1.787629	-0.047696
20	6	0	-2.312790	0.040429	-0.001203
21	6	0	-3.661898	0.651546	0.006906
22	6	0	-3.972939	-1.649129	0.052101
23	1	0	-4.449479	-2.623367	0.076834
24	6	0	-3.999286	1.951910	-0.011998
25	1	0	-5.040794	2.256152	-0.002774
26	1	0	-3.253020	2.739607	-0.038059
27	6	0	-4.614287	-0.473171	0.040408
28	1	0	-5.690105	-0.333774	0.053256
29	6	0	-2.475179	-1.469507	0.027641
30	1	0	-2.000185	-1.920410	0.910394
31	1	0	-2.025006	-1.951372	-0.851777

Fulvene trienaine E12'

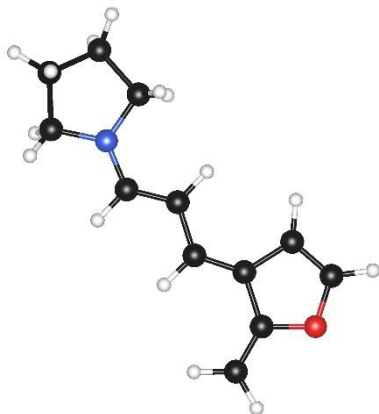


HF (M062X/6-31+G(d,p)) = -560.0912156 Hartrees
 Imaginary Frequencies: none found
 Zero-point correction = 0.271814 (Hartree/Particle)
 Thermal correction = 0.230197 Hartrees

Coordinates from last standard orientation:

Center Number	Atomic Number	Atomic Type	Coordinates (Angstroms)		
			X	Y	Z
1	6	0	-1.132359	-0.547378	0.028635
2	6	0	0.172335	0.040713	0.037266
3	6	0	1.289509	-0.742835	0.061532
4	1	0	1.177812	-1.826813	0.073492
5	7	0	2.568307	-0.313723	0.067482
6	6	0	3.730157	-1.198531	0.066895
7	1	0	3.566748	-2.047108	-0.604591
8	1	0	3.927779	-1.587659	1.076379
9	6	0	4.858202	-0.275125	-0.395569
10	1	0	4.857839	-0.210908	-1.488841
11	1	0	5.842174	-0.618672	-0.069828
12	6	0	4.456555	1.075167	0.211609
13	1	0	4.939936	1.926112	-0.272227
14	1	0	4.715431	1.096672	1.275466
15	6	0	2.932965	1.097340	0.047589
16	1	0	2.426614	1.636964	0.856760
17	1	0	2.624160	1.551219	-0.905589
18	1	0	0.261489	1.122643	0.020912
19	1	0	-1.165092	-1.639267	0.048779
20	6	0	-2.324033	0.111284	-0.001140
21	6	0	-3.644396	-0.533426	-0.007600
22	6	0	-2.559540	1.554259	-0.035497
23	6	0	-3.903212	1.753678	-0.060509
24	1	0	-1.791888	2.317618	-0.041899
25	1	0	-4.407576	2.712287	-0.090149
26	6	0	-3.877273	-2.012959	0.023949
27	1	0	-4.948221	-2.230344	0.001328
28	1	0	-3.416797	-2.514809	-0.835018
29	6	0	-4.577702	0.455462	-0.042663
30	1	0	-5.652365	0.311090	-0.055304
31	1	0	-3.463442	-2.468855	0.930980

Trienammine E13



HF (M062X/6-31+G(d,p)) = -595.9781919 Hartrees

Imaginary Frequencies: none found

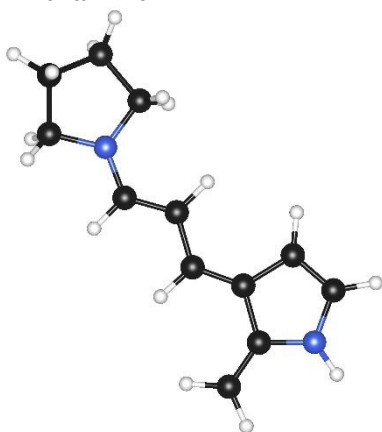
Zero-point correction = 0.247817 (Hartree/Particle)

Thermal correction = 0.206159 Hartrees

Coordinates from last standard orientation:

Center Number	Atomic Number	Atomic Type	Coordinates (Angstroms)		
			X	Y	Z
1	6	0	-1.150482	0.733600	-0.031192
2	6	0	0.145015	0.104943	-0.038036
3	6	0	1.289715	0.838323	-0.062832
4	1	0	1.230847	1.926266	-0.077863
5	7	0	2.554690	0.347002	-0.064257
6	6	0	3.754793	1.172983	-0.073757
7	1	0	3.638317	2.032315	0.594972
8	1	0	3.971803	1.550627	-1.084843
9	6	0	4.838766	0.198248	0.390306
10	1	0	4.838701	0.141168	1.484075
11	1	0	5.837897	0.490275	0.059652
12	6	0	4.368385	-1.134769	-0.206064
13	1	0	4.809116	-2.005723	0.283374
14	1	0	4.625508	-1.176680	-1.269901
15	6	0	2.844746	-1.077413	-0.043074
16	1	0	2.313894	-1.593396	-0.853213
17	1	0	2.510529	-1.518553	0.908490
18	1	0	0.182098	-0.979735	-0.019119
19	1	0	-1.197529	1.820382	-0.051851
20	6	0	-2.327768	0.082803	-0.001624
21	6	0	-3.715626	0.575124	0.007986
22	6	0	-3.665614	-1.682805	0.052640
23	1	0	-3.836389	-2.750030	0.076356
24	6	0	-4.147459	1.850305	-0.011207
25	1	0	-5.207588	2.075883	-0.000920
26	1	0	-3.457409	2.686584	-0.037509
27	6	0	-4.519508	-0.649704	0.043728
28	1	0	-5.597817	-0.704789	0.059733
29	8	0	-2.354323	-1.311679	0.027139

Trienamine E14



HF (M062X/6-31+G(d,p)) = -576.1207353Hartrees

Imaginary Frequencies: none found

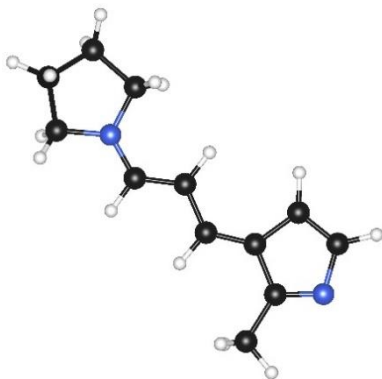
Zero-point correction = 0.260177 (Hartree/Particle)

Thermal correction = 0.218584 Hartrees

Coordinates from last standard orientation:

Center Number	Atomic Number	Atomic Type	Coordinates (Angstroms)		
			X	Y	Z
1	6	0	-1.147217	0.704635	0.000538
2	6	0	0.157289	0.087435	-0.027876
3	6	0	1.300043	0.816200	0.076473
4	1	0	1.234240	1.896341	0.202694
5	7	0	2.570531	0.332573	0.052214
6	6	0	3.760030	1.172207	0.072709
7	1	0	3.669969	1.948959	0.839082
8	1	0	3.921750	1.664292	-0.899426
9	6	0	4.872941	0.165574	0.365570
10	1	0	4.919365	-0.028533	1.442382
11	1	0	5.853775	0.512907	0.033718
12	6	0	4.392616	-1.087629	-0.378211
13	1	0	4.855253	-2.007940	-0.015540
14	1	0	4.618226	-0.993329	-1.445737
15	6	0	2.872512	-1.071650	-0.166665
16	1	0	2.325279	-1.455434	-1.038617
17	1	0	2.566831	-1.666880	0.707262
18	1	0	0.223198	-0.989559	-0.163161
19	1	0	-1.188341	1.791179	0.036667
20	6	0	-2.327818	0.048755	-0.013549
21	6	0	-3.701586	0.607826	-0.041564
22	6	0	-3.820803	-1.659093	0.155788
23	1	0	-4.127834	-2.692298	0.255218
24	6	0	-4.057402	1.896720	-0.206231
25	1	0	-5.102533	2.185589	-0.215440
26	1	0	-3.320302	2.681030	-0.340567
27	6	0	-4.587068	-0.551489	0.103963
28	1	0	-5.666641	-0.516261	0.122864
29	7	0	-2.469768	-1.358030	0.002327
30	1	0	-1.768801	-1.928817	0.451153

Fulvene trienamine E14'



HF (M062X/6-31+G(d,p)) = -576.138208 Hartrees

Imaginary Frequencies: none found

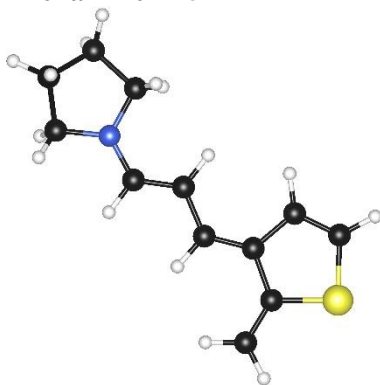
Zero-point correction = 0.260572 (Hartree/Particle)

Thermal correction = 0.218975 Hartrees

Coordinates from last standard orientation:

Center Number	Atomic Number	Atomic Type	Coordinates (Angstroms)		
			X	Y	Z
1	6	0	-1.124805	-0.524237	0.028073
2	6	0	0.175620	0.060634	0.036302
3	6	0	1.290971	-0.730905	0.062381
4	1	0	1.171225	-1.814051	0.075887
5	7	0	2.567785	-0.310860	0.068536
6	6	0	3.726049	-1.203421	0.071548
7	1	0	3.555573	-2.054312	-0.594643
8	1	0	3.919371	-1.586134	1.083716
9	6	0	4.858867	-0.288677	-0.395402
10	1	0	4.857910	-0.227913	-1.488803
11	1	0	5.840575	-0.637988	-0.069469
12	6	0	4.467005	1.065802	0.208823
13	1	0	4.955790	1.911993	-0.277577
14	1	0	4.726484	1.088455	1.272413
15	6	0	2.943780	1.099153	0.044938
16	1	0	2.440328	1.643503	0.852166
17	1	0	2.638320	1.549885	-0.910212
18	1	0	0.265994	1.142392	0.018550
19	1	0	-1.163657	-1.615865	0.048357
20	6	0	-2.315932	0.138575	-0.001676
21	6	0	-3.639592	-0.497214	-0.008892
22	6	0	-2.608376	1.562736	-0.036500
23	6	0	-3.962471	1.649657	-0.059915
24	1	0	-1.897223	2.377327	-0.043819
25	1	0	-4.573426	2.543143	-0.088285
26	6	0	-3.910320	-1.969375	0.024033
27	1	0	-4.988739	-2.130269	-0.013811
28	1	0	-3.449062	-2.481907	-0.827078
29	7	0	-4.594052	0.388297	-0.042770
30	1	0	-3.520363	-2.426689	0.939976

Trienamine E15



HF (M062X/6-31+G(d,p)) = -918.9451571 Hartrees

Imaginary Frequencies: none found

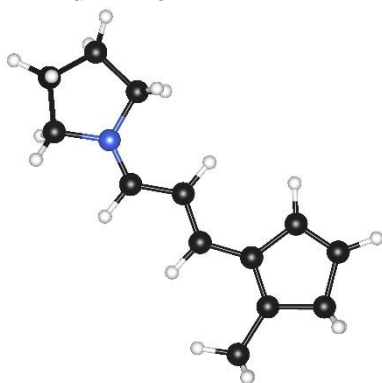
Zero-point correction = 0.244509 (Hartree/Particle)

Thermal correction = 0.201144 Hartrees

Coordinates from last standard orientation:

Center Number	Atomic Number	Atomic Type	Coordinates (Angstroms)		
			X	Y	Z
1	6	0	-0.904449	0.848680	-0.035707
2	6	0	0.374340	0.191099	-0.050000
3	6	0	1.538101	0.897517	-0.067011
4	1	0	1.503511	1.986538	-0.072611
5	7	0	2.787721	0.376503	-0.071522
6	6	0	4.009690	1.171801	-0.067592
7	1	0	3.907548	2.033227	0.600365
8	1	0	4.244949	1.543136	-1.076453
9	6	0	5.063311	0.168702	0.405691
10	1	0	5.049996	0.108963	1.499206
11	1	0	6.072905	0.436169	0.086552
12	6	0	4.565848	-1.150474	-0.199578
13	1	0	4.979063	-2.033600	0.291784
14	1	0	4.832449	-1.196168	-1.260854
15	6	0	3.042588	-1.055648	-0.051400
16	1	0	2.506793	-1.556347	-0.867592
17	1	0	2.688440	-1.488640	0.896372
18	1	0	0.400287	-0.895516	-0.042328
19	1	0	-0.896851	1.938833	-0.043648
20	6	0	-2.112719	0.244530	-0.011227
21	6	0	-3.440987	0.897337	0.008059
22	6	0	-4.035899	-1.383803	0.059527
23	1	0	-4.631724	-2.287372	0.086978
24	6	0	-3.680938	2.223209	-0.015189
25	1	0	-4.698562	2.597339	0.004997
26	1	0	-2.883016	2.956432	-0.055702
27	6	0	-4.492259	-0.122731	0.054293
28	1	0	-5.544707	0.136373	0.078043
29	16	0	-2.287805	-1.531013	0.012272

Iminium E16



HF (M062X/6-31+G(d,p)) = -560.4940946 Hartrees

Imaginary Frequencies: none found

Zero-point correction = 0.285296 (Hartree/Particle)

Thermal correction = 0.244124 Hartrees

Coordinates from last standard orientation:

Center Number	Atomic Number	Atomic Type	Coordinates (Angstroms)		
			X	Y	Z
1	6	0	1.050474	0.600880	0.029048
2	6	0	-0.181101	-0.017489	0.038623
3	6	0	-1.347808	0.772659	0.065486
4	1	0	-1.244281	1.857721	0.076372
5	7	0	-2.574357	0.324044	0.074431
6	6	0	-3.774617	1.191121	0.079290
7	1	0	-3.604868	2.061218	-0.557618
8	1	0	-3.963140	1.524223	1.106063
9	6	0	-4.873454	0.251832	-0.410438
10	1	0	-4.858669	0.193769	-1.503345
11	1	0	-5.863919	0.583290	-0.096478
12	6	0	-4.465252	-1.091247	0.206107
13	1	0	-4.932726	-1.947362	-0.281606
14	1	0	-4.731213	-1.116785	1.267176
15	6	0	-2.942703	-1.107640	0.047772
16	1	0	-2.424758	-1.638050	0.850893
17	1	0	-2.631318	-1.526845	-0.915908
18	1	0	-0.258488	-1.099964	0.021048
19	1	0	1.064196	1.690586	0.047219
20	6	0	2.299293	-0.054039	-0.001204
21	6	0	3.534538	0.569719	-0.007357
22	6	0	3.997449	-1.672574	-0.056040
23	1	0	4.517506	-2.622908	-0.082144
24	6	0	3.846733	2.026383	0.016253
25	1	0	4.441554	2.291085	-0.863977
26	1	0	2.960065	2.660142	0.036065
27	6	0	4.570681	-0.448767	-0.041525
28	1	0	5.632666	-0.233378	-0.052921
29	6	0	2.506428	-1.545173	-0.032106
30	1	0	2.055414	-2.012549	-0.917759
31	1	0	2.080605	-2.045493	0.848001
32	1	0	4.457908	2.259006	0.894444

Part V – References

- (1) Brazil, R. The Origin of Homochirality. *Chemistry World*. October 2015.
- (2) Elks, J.; Ganellin, C. R. *Dictionary of Drugs: Chemical Data, Structures and Bibliographies*, 1st ed.; Springer-Science+Business Media B.V., 1990.
- (3) Inxight Drugs <https://drugs.ncats.io/substances> (accessed Jan 7, 2021).
- (4) Thayer, A. M. Centering on Chirality. *Chem. Eng. News* **2007**, *85*, 11–19.
- (5) Clayden, J.; Greeves, N.; Warren, S.; Wothers, P. *Organic Chemistry*, 7th ed.; Oxford University Press: New York, 2008.
- (6) Anslyn, E. V.; Dougherty, D. A. *Modern Physical Organic Chemistry*; University Science Books, 2006.
- (7) Diels, O.; Alder, K. Synthesen in Der Hydroaromatischen Reihe. *Justus Liebig's Ann. der Chemie* **1928**, *460* (1), 98–122. <https://doi.org/10.1002/jlac.19284600106>.
- (8) Diels, O.; Alder, K. Synthesen in Der Hydro-Aromatischen Reihe, II. Mitteilung: Über Cantharidin. *Berichte der Dtsch. Chem. Gesellschaft (A B Ser.* **1929**, *62* (3), 554–562. <https://doi.org/10.1002/cber.19290620318>.
- (9) The Nobel Prize in Chemistry 1950 - NobelPrize.org <https://www.nobelprize.org/prizes/chemistry/1950/summary/> (accessed Apr 2, 2020).
- (10) Carey, F. A.; Sundberg, R. J. *Advanced Organic Chemistry Part A: Structure and Mechanisms*, 5th ed.; Springer New York LLC, 2007.
- (11) Carey, F. A.; Sundberg, R. J. *Advanced Organic Chemistry Part B: Reactions and Synthesis*, 5th ed.; Springer New York LLC, 2007.
- (12) Fleming, I. *Frontier Orbitals and Organic Chemical Reactions*, 16th ed.; John Wiley & Sons: London, 2007.
- (13) Fukui, K. Recognition of Stereochemical Paths by Orbital Interaction. *Acc. Chem. Res.* **1971**, *4* (2), 57–64. <https://doi.org/10.1021/ar50038a003>.
- (14) Woodward, R. B.; Hoffmann, R. Stereochemistry of Electrocyclic Reactions. *J. Am. Chem. Soc.* **1965**, *87* (2), 395–397. <https://doi.org/10.1021/ja01080a054>.

- (15) Woodward, R. B.; Hoffmann, R. The Conservation of Orbital Symmetry. *Angew. Chemie Int. Ed. English* **1969**, 8 (11), 781–853. <https://doi.org/10.1002/anie.196907811>.
- (16) The Nobel Prize in Chemistry 1981 - NobelPrize.org <https://www.nobelprize.org/prizes/chemistry/1981/summary/> (accessed Apr 7, 2020).
- (17) Zimmerman, H. E. On Molecular Orbital Correlation Diagrams, the Occurrence of Möbius Systems in Cyclization Reactions, and Factors Controlling Ground- and Excited-State Reactions. I. *J. Am. Chem. Soc.* **1966**, 88 (7), 1564–1565. <https://doi.org/10.1021/ja00959a052>.
- (18) Dewar, M. J. S. A Molecular Orbital Theory of Organic Chemistry-VIII. Romanticity and Electrocyclic Reactions. *Tetrahedron* **1966**, 22 (SUPPL. 8), 75–92. [https://doi.org/10.1016/S0040-4020\(01\)82171-2](https://doi.org/10.1016/S0040-4020(01)82171-2).
- (19) Hoffmann, R.; Woodward, R. B. Orbital Symmetries and Endo-Exo Relationships in Concerted Cycloaddition Reactions. *J. Am. Chem. Soc.* **1965**, 87 (19), 4388–4389. <https://doi.org/10.1021/ja00947a033>.
- (20) García, J. I.; Mayoral, J. A.; Salvatella, L. Do Secondary Orbital Interactions Really Exist? *Acc. Chem. Res.* **2000**, 33 (10), 658–664. <https://doi.org/10.1021/ar0000152>.
- (21) Arrieta, A.; Cossío, F. P.; Lecea, B. Direct Evaluation of Secondary Orbital Interactions in the Diels-Alder Reaction between Cyclopentadiene and Maleic Anhydride. *J. Org. Chem.* **2001**, 66 (18), 6178–6180. <https://doi.org/10.1021/jo0158478>.
- (22) Wannere, C. S.; Paul, A.; Herges, R.; Houk, K. N.; Schaefer, H. F.; Von Ragué Schleyer, P. The Existence of Secondary Orbital Interactions. *J. Comput. Chem.* **2007**, 28 (1), 344–361. <https://doi.org/10.1002/jcc.20532>.
- (23) Cookson, R. C.; Drake, B. V.; Hudec, J.; Morrison, A. The Adduct of Tropone and Cyclopentadiene: A New Type of Cyclic Reaction. *Chem. Commun.* **1966**, No. 1, 15–16. <https://doi.org/10.1039/C19660000015>.
- (24) Itô, S.; Fujise, Y.; Okuda, T.; Inoue, Y. Reaction of Tropone with Cyclopentadiene. *Bull. Chem. Soc. Jpn.* **1966**, 39 (6), 1351–1351. <https://doi.org/10.1246/bcsj.39.1351>.

- (25) Salem, L. Intermolecular Orbital Theory of the Interaction between Conjugated Systems. I. General Theory. *J. Am. Chem. Soc.* **1968**, *90* (3), 543–552. <https://doi.org/10.1021/ja01005a001>.
- (26) Salem, L. Intermolecular Orbital Theory of the Interaction between Conjugated Systems. II. Thermal and Photochemical Cycloadditions. *J. Am. Chem. Soc.* **1968**, *90* (3), 553–566. <https://doi.org/10.1021/ja01005a002>.
- (27) Houk, K. N.; Woodward, R. B. Cycloaddition Reactions of Cycloheptatriene and 2,5-Dimethyl-3,4-Diphenylcyclopentadienone. *J. Am. Chem. Soc.* **1970**, *92* (13), 4143–4145. <https://doi.org/10.1021/ja00716a073>.
- (28) Dunn, L. C.; Houk, K. N. The Regioselectivity of [6+4] Cycloadditions of Dienamines to Fulvenes. *Tetrahedron Lett.* **1978**, *19* (37), 3411–3414. [https://doi.org/10.1016/S0040-4039\(00\)70533-8](https://doi.org/10.1016/S0040-4039(00)70533-8).
- (29) Liu, C. Y.; Mareda, J.; Houk, K. N.; Fronczek, F. R. Intramolecular [8 + 2] Cycloadditions of Alkenylheptafulvenes. *J. Am. Chem. Soc.* **1983**, *105* (22), 6714–6715. <https://doi.org/10.1021/ja00360a029>.
- (30) Saha, P.; Saikia, A. K. Ene Cyclization Reaction in Heterocycle Synthesis. *Organic and Biomolecular Chemistry*. Royal Society of Chemistry April 25, 2018, pp 2820–2840. <https://doi.org/10.1039/c8ob00429c>.
- (31) Bakhtiari, A.; Safaei-Ghomi, J. Effects of Chiral Ligands on the Asymmetric Carbonyl-Ene Reaction. *Synlett* **2019**, *30* (15), 1738–1764. <https://doi.org/10.1055/s-0037-1611875>.
- (32) Jensen, A. W.; Mohanty, D. K.; Dilling, W. L. The Growing Relevance of Biological Ene Reactions. *Bioorganic and Medicinal Chemistry*. Elsevier Ltd March 1, 2019, pp 686–691. <https://doi.org/10.1016/j.bmc.2019.01.020>.
- (33) Chai, Y.; Hong, S. P.; Lindsay, H. A.; McFarland, C.; McIntosh, M. C. New Aspects of the Ireland and Related Claisen Rearrangements. *Tetrahedron* **2002**, *58* (15), 2905–2928. [https://doi.org/10.1016/S0040-4020\(02\)00164-3](https://doi.org/10.1016/S0040-4020(02)00164-3).
- (34) Castro, A. M. M. Claisen Rearrangement over the Past Nine Decades. *Chem. Rev.* **2004**, *104* (6), 2939–3002. <https://doi.org/10.1021/cr020703u>.

- (35) Serrano-Molina, D.; Martín-Castro, A. M. Tandem Sequences Involving Michael Additions and Sigmatropic Rearrangements. *Synth.* **2016**, *48* (20), 3459–3469. <https://doi.org/10.1055/s-0035-1562554>.
- (36) West, T. H.; Spoehrle, S. S. M.; Kasten, K.; Taylor, J. E.; Smith, A. D. Catalytic Stereoselective [2,3]-Rearrangement Reactions. *ACS Catalysis*. American Chemical Society October 29, 2015, pp 7446–7479. <https://doi.org/10.1021/acscatal.5b02070>.
- (37) Rycek, L.; Hudlicky, T. Applications of the Wittig-Still Rearrangement in Organic Synthesis. *Angew. Chemie Int. Ed.* **2017**, *56* (22), 6022–6066. <https://doi.org/10.1002/anie.201611329>.
- (38) Wang, F.; Wang, J.; Zhang, Y.; Yang, J. The [1,2]- and [1,4]-Wittig Rearrangement. *Tetrahedron*. Elsevier Ltd January 31, 2020, p 130857. <https://doi.org/10.1016/j.tet.2019.130857>.
- (39) Tantillo, D. J. Speeding Up Sigmatropic Shifts - To Halve or to Hold. *Acc. Chem. Res.* **2016**, *49* (4), 741–749. <https://doi.org/10.1021/acs.accounts.6b00029>.
- (40) Wu, H.; Wang, Q.; Zhu, J. Recent Advances in Catalytic Enantioselective Rearrangement. *European J. Org. Chem.* **2019**, *2019* (10), 1964–1980. <https://doi.org/10.1002/ejoc.201801799>.
- (41) The IUPAC Compendium of Chemical Terminology <https://goldbook.iupac.org/> (accessed Feb 3, 2020).
- (42) Eder, U.; Sauer, G.; Wiechert, R. New Type of Asymmetric Cyclization to Optically Active Steroid CD Partial Structures. *Angew. Chemie Int. Ed. English* **1971**, *10* (7), 496–497. <https://doi.org/10.1002/anie.197104961>.
- (43) Hajos, Z. G.; Parrish, D. R. Asymmetric Synthesis of Bicyclic Intermediates of Natural Product Chemistry. *J. Org. Chem.* **1974**, *39* (12), 1615–1621. <https://doi.org/10.1021/jo00925a003>.
- (44) List, B.; Lerner, R. A.; Barbas, C. F. Proline-Catalyzed Direct Asymmetric Aldol Reactions [13]. *J. Am. Chem. Soc.* **2000**, *122* (10), 2395–2396. <https://doi.org/10.1021/ja994280y>.
- (45) Ahrendt, K. A.; Borths, C. J.; MacMillan, D. W. C. New Strategies for Organic Catalysis: The First Highly Enantioselective Organocatalytic Diels - Alder Reaction [16]. *J. Am. Chem. Soc.* **2000**, *122* (17), 4243–4244. <https://doi.org/10.1021/ja000092s>.

- (46) Dalko, P. I.; Moisan, L. Enantioselective Organocatalysis. *Angewandte Chemie - International Edition*. John Wiley & Sons, Ltd October 15, 2001, pp 3726–3748. [https://doi.org/10.1002/1521-3773\(20011015\)40:20<3726::AID-ANIE3726>3.0.CO;2-D](https://doi.org/10.1002/1521-3773(20011015)40:20<3726::AID-ANIE3726>3.0.CO;2-D).
- (47) Dalko, P. I.; Moisan, L. In the Golden Age of Organocatalysis. *Angewandte Chemie - International Edition*. John Wiley & Sons, Ltd October 4, 2004, pp 5138–5175. <https://doi.org/10.1002/anie.200400650>.
- (48) List, B. Introduction: Organocatalysis. *Chemical Reviews*. American Chemical Society December 2007, pp 5413–5415. <https://doi.org/10.1021/cr078412e>.
- (49) MacMillan, D. W. C. The Advent and Development of Organocatalysis. *Nature* **2008**, *455* (7211), 304–308. <https://doi.org/10.1038/nature07367>.
- (50) Shirakawa, S.; Maruoka, K. Recent Developments in Asymmetric Phase-Transfer Reactions. *Angew. Chemie - Int. Ed.* **2013**, *52* (16), 4312–4348. <https://doi.org/10.1002/anie.201206835>.
- (51) Tan, J.; Yasuda, N. Contemporary Asymmetric Phase Transfer Catalysis: Large-Scale Industrial Applications. *Organic Process Research and Development*. American Chemical Society November 20, 2015, pp 1731–1746. <https://doi.org/10.1021/acs.oprd.5b00304>.
- (52) Taylor, M. S.; Jacobsen, E. N. Asymmetric Catalysis by Chiral Hydrogen-Bond Donors. *Angewandte Chemie - International Edition*. John Wiley & Sons, Ltd February 27, 2006, pp 1520–1543. <https://doi.org/10.1002/anie.200503132>.
- (53) Doyle, A. G.; Jacobsen, E. N. Small-Molecule H-Bond Donors in Asymmetric Catalysis. *Chem. Rev.* **2007**, *107* (12), 5713–5743. <https://doi.org/10.1021/cr068373r>.
- (54) Held, F. E.; Tsogoeva, S. B. Asymmetric Cycloaddition Reactions Catalyzed by Bifunctional Thiourea and Squaramide Organocatalysts: Recent Advances. *Catalysis Science and Technology*. Royal Society of Chemistry February 1, 2016, pp 645–667. <https://doi.org/10.1039/c5cy01894c>.
- (55) Chauhan, P.; Mahajan, S.; Kaya, U.; Hack, D.; Enders, D. Bifunctional Amine-Squaramides: Powerful Hydrogen-Bonding Organocatalysts for Asymmetric Domino/Cascade Reactions. *Adv. Synth. Catal.* **2015**, *357* (2–3), 253–281. <https://doi.org/10.1002/adsc.201401003>.

- (56) Mukherjee, S.; Yang, J. W.; Hoffmann, S.; List, B. Asymmetric Enamine Catalysis. *Chemical Reviews*. American Chemical Society 2007, pp 5471–5569. <https://doi.org/10.1021/cr0684016>.
- (57) Erkkilä, A.; Majander, I.; Pihko, P. M. Iminium Catalysis. **2007**, 5416–5470.
- (58) Melchiorre, P.; Marigo, M.; Carlone, A.; Bartoli, G. Asymmetric Aminocatalysis - Gold Rush in Organic Chemistry. *Angew. Chemie - Int. Ed.* **2008**, 47 (33), 6138–6171. <https://doi.org/10.1002/anie.200705523>.
- (59) Bertelsen, S.; Jørgensen, K. A. Organocatalysis - After the Gold Rush. *Chemical Society Reviews*. The Royal Society of Chemistry July 21, 2009, pp 2178–2189. <https://doi.org/10.1039/b903816g>.
- (60) Pihko, P. M.; Majander, I.; Erkkilä, A. Enamine Catalysis. In *Asymmetric Organocatalysis*; List, B., Ed.; Springer-Verlag Berlin Heidelberg: Berlin, 2010; pp 29–75.
- (61) Enders, D.; Niemeier, O.; Henseler, A. Organocatalysis by N-Heterocyclic Carbenes. *Chemical Reviews*. American Chemical Society December 2007, pp 5606–5655. <https://doi.org/10.1021/cr068372z>.
- (62) Erkkilä, A.; Majander, I.; Pihko, P. M. Iminium Catalysis. *Chem. Rev.* **2007**, 107 (12), 5416–5470. <https://doi.org/10.1021/cr068388p>.
- (63) Beeson, T. D.; Mastracchio, A.; Hong, J.-B.; Ashton, K.; MacMillan, D. W. C. Enantioselective Organocatalysis Using SOMO Activation. *Science (80-.)*. **2007**, 316 (5824).
- (64) Devery, J. J.; Conrad, J. C.; MacMillan, D. W. C.; Flowers, R. A. Mechanistic Complexity in Organo-SOMO Activation. *Angew. Chemie - Int. Ed.* **2010**, 49 (35), 6106–6110. <https://doi.org/10.1002/anie.201001673>.
- (65) Buzzetti, L.; Crisenza, G. E. M.; Melchiorre, P. Mechanistic Studies in Photocatalysis. *Angewandte Chemie - International Edition*. Wiley-VCH Verlag March 18, 2019, pp 3730–3747. <https://doi.org/10.1002/anie.201809984>.
- (66) Holden, C. M.; Melchiorre, P. Photochemistry and Excited-State Reactivity of Organocatalytic Intermediates. In *Photochemistry*; Royal Society of Chemistry, 2020; Vol. 47, pp 344–378. <https://doi.org/10.1039/9781788016520-00344>.

- (67) Jensen, K. L.; Dickmeiss, G.; Jiang, H.; Albrecht, L.; Jørgensen, K. A. The Diarylprolinol Silyl Ether System: A General Organocatalyst. *Acc. Chem. Res.* **2012**, *45* (2), 248–264. <https://doi.org/10.1021/ar200149w>.
- (68) Jiang, H.; Albrecht, L.; Jørgensen, K. A. Aminocatalytic Remote Functionalization Strategies. *Chem. Sci.* **2013**, *4* (6), 2287–2300. <https://doi.org/10.1039/c3sc50405k>.
- (69) Donslund, B. S.; Johansen, T. K.; Poulsen, P. H.; Halskov, K. S.; Jørgensen, K. A. The Diarylprolinol Silyl Ethers: Ten Years After. *Angew. Chemie - Int. Ed.* **2015**, *54* (47), 13860–13874. <https://doi.org/10.1002/anie.201503920>.
- (70) Zimmerman, H. E.; Traxler, M. D. The Stereochemistry of the Ivanov and Reformatsky Reactions. I. *J. Am. Chem. Soc.* **1957**, *79* (8), 1920–1923. <https://doi.org/10.1021/ja01565a041>.
- (71) Bahmanyar, S.; Houk, K. N.; Martin, H. J.; List, B. Quantum Mechanical Predictions of the Stereoselectivities of Proline-Catalyzed Asymmetric Intermolecular Aldol Reactions. *J. Am. Chem. Soc.* **2003**, *125* (9), 2475–2479. <https://doi.org/10.1021/ja028812d>.
- (72) Allemann, C.; Gordillo, R.; Clemente, F. R.; Cheong, P. H. Y.; Houk, K. N. Theory of Asymmetric Organocatalysis of Aldol and Related Reactions: Rationalizations and Predictions. *Acc. Chem. Res.* **2004**, *37* (8), 558–569. <https://doi.org/10.1021/ar0300524>.
- (73) Lam, Y. H.; Grayson, M. N.; Holland, M. C.; Simon, A.; Houk, K. N. Theory and Modeling of Asymmetric Catalytic Reactions. *Acc. Chem. Res.* **2016**, *49* (4), 750–762. <https://doi.org/10.1021/acs.accounts.6b00006>.
- (74) Para, N. A.; MacMillan, D. W. C. New Strategies in Organic Catalysis: The First Enantioselective Organocatalytic Friedel-Crafts Alkylation [18]. *J. Am. Chem. Soc.* **2001**, *123* (18), 4370–4371. <https://doi.org/10.1021/ja015717g>.
- (75) Allemann, C.; Gordillo, R.; Clemente, F. R.; Cheong, P. H. Y.; Houk, K. N. Theory of Asymmetric Organocatalysis of Aldol and Related Reactions: Rationalizations and Predictions. *Acc. Chem. Res.* **2004**, *37* (8), 558–569. <https://doi.org/10.1021/ar0300524>.
- (76) Gordillo, R.; Houk, K. N. Origins of Stereoselectivity in Diels-Alder Cycloadditions Catalyzed by

- Chiral Imidazolidinones. *J. Am. Chem. Soc.* **2006**, *128* (11), 3543–3553. <https://doi.org/10.1021/ja0525859>.
- (77) Notz, W.; List, B. Catalytic Asymmetric Synthesis of Anti-1,2-Diols [1]. *Journal of the American Chemical Society*. American Chemical Society August 2, 2000, pp 7386–7387. <https://doi.org/10.1021/ja001460v>.
- (78) List, B.; Pojarliev, P.; Castello, C. Proline-Catalyzed Asymmetric Aldol Reactions between Ketones and α -Unsubstituted Aldehydes. *Org. Lett.* **2001**, *3* (4), 573–575. <https://doi.org/10.1021/ol006976y>.
- (79) Northrup, A. B.; MacMillan, D. W. C. The First Direct and Enantioselective Cross-Aldol Reaction of Aldehydes. *J. Am. Chem. Soc.* **2002**, *124* (24), 6798–6799. <https://doi.org/10.1021/ja0262378>.
- (80) Pidathala, C.; Hoang, L.; Vignola, N.; List, B. Direct Catalytic Asymmetric Enolexo Aldolizations. *Angew. Chemie - Int. Ed.* **2003**, *42* (24), 2785–2788. <https://doi.org/10.1002/anie.200351266>.
- (81) Mangion, I. K.; Northrup, A. B.; MacMillan, D. W. C. The Importance of Iminium Geometry Control in Enamine Catalysis: Identification of a New Catalyst Architecture for Aldehyde-Aldehyde Couplings. *Angew. Chemie - Int. Ed.* **2004**, *43* (48), 6722–6724. <https://doi.org/10.1002/anie.200461851>.
- (82) List, B. The Direct Catalytic Asymmetric Three-Component Mannich Reaction [21]. *Journal of the American Chemical Society*. American Chemical Society September 27, 2000, pp 9336–9337. <https://doi.org/10.1021/ja001923x>.
- (83) List, B.; Pojarliev, P.; Biller, W. T.; Martin, H. J. The Proline-Catalyzed Direct Asymmetric Three-Component Mannich Reaction: Scope, Optimization, and Application to the Highly Enantioselective Synthesis of 1,2-Amino Alcohols. *J. Am. Chem. Soc.* **2002**, *124* (5), 827–833. <https://doi.org/10.1021/ja0174231>.
- (84) Hayashi, Y.; Tsuboi, W.; Shoji, M.; Suzuki, N. Application of High Pressure Induced by Water-Freezing to the Direct Catalytic Asymmetric Three-Component List-Barbas-Mannich Reaction. *J. Am. Chem. Soc.* **2003**, *125* (37), 11208–11209. <https://doi.org/10.1021/ja0372513>.
- (85) Hayashi, Y.; Tsuboi, W.; Ashimine, I.; Urushima, T.; Shoji, M.; Sakai, K. The Direct and

- Enantioselective, One-Pot, Three-Component, Cross-Mannich Reaction of Aldehydes. *Angew. Chemie - Int. Ed.* **2003**, *42* (31), 3677–3680. <https://doi.org/10.1002/anie.200351813>.
- (86) Notz, W.; Tanaka, F.; Watanabe, S. I.; Chowdari, N. S.; Turner, J. M.; Thayumanavan, R.; Barbas, C. F. The Direct Organocatalytic Asymmetric Mannich Reaction: Unmodified Aldehydes as Nucleophiles. *J. Org. Chem.* **2003**, *68* (25), 9624–9634. <https://doi.org/10.1021/jo0347359>.
- (87) Ibrahim, I.; Casas, J.; Córdova, A. Direct Catalytic Enantioselective α -Aminomethylation of Ketones. *Angew. Chemie - Int. Ed.* **2004**, *43* (47), 6528–6531. <https://doi.org/10.1002/anie.200460678>.
- (88) Enders, D.; Grondal, C.; Vrettou, M.; Raabe, G. Asymmetric Synthesis of Selectively Protected Amino Sugars and Derivatives by a Direct Organocatalytic Mannich Reaction. *Angew. Chemie - Int. Ed.* **2005**, *44* (26), 4079–4083. <https://doi.org/10.1002/anie.200500810>.
- (89) List, B.; Pojarliev, P.; Martin, H. J. Efficient Proline-Catalyzed Michael Additions of Unmodified Ketones to Nitro Olefins. *Org. Lett.* **2001**, *3* (16), 2423–2425. <https://doi.org/10.1021/ol015799d>.
- (90) Betancort, J. M.; Sakthivel, K.; Thayumanavan, R.; Barbas, C. F. Catalytic Enantioselective Direct Michael Additions of Ketones to Alkylidene Malonates. *Tetrahedron Lett.* **2001**, *42* (27), 4441–4444. [https://doi.org/10.1016/S0040-4039\(01\)00793-6](https://doi.org/10.1016/S0040-4039(01)00793-6).
- (91) Melchiorre, P.; Jørgensen, K. A. Direct Enantioselective Michael Addition of Aldehydes to Vinyl Ketones Catalyzed by Chiral Amines. *J. Org. Chem.* **2003**, *68* (11), 4151–4157. <https://doi.org/10.1021/jo026837p>.
- (92) Fonseca, M. T. H.; List, B. Catalytic Asymmetric Intramolecular Michael Reaction of Aldehydes. *Angew. Chemie - Int. Ed.* **2004**, *43* (30), 3958–3960. <https://doi.org/10.1002/anie.200460578>.
- (93) Hayashi, Y.; Gotoh, H.; Tamura, T.; Yamaguchi, H.; Masui, R.; Shoji, M. Cysteine-Derived Organocatalyst in a Highly Enantioselective Intramolecular Michael Reaction. *J. Am. Chem. Soc.* **2005**, *127* (46), 16028–16029. <https://doi.org/10.1021/ja055740s>.
- (94) Bøgevig, A.; Juhl, K.; Kumaragurubaran, N.; Zhuang, W.; Jørgensen, K. A. Direct Organo-Catalytic Asymmetric α -Amination of Aldehydes—A Simple Approach to Optically Active α -Amino

- Aldehydes, A-Amino Alcohols, and A-Amino Acids. *Angew. Chemie Int. Ed.* **2002**, *41* (10), 1790–1793. [https://doi.org/10.1002/1521-3773\(20020517\)41:10<1790::AID-ANIE1790>3.0.CO;2-Y](https://doi.org/10.1002/1521-3773(20020517)41:10<1790::AID-ANIE1790>3.0.CO;2-Y).
- (95) List, B. Direct Catalytic Asymmetric α -Amination of Aldehydes. *J. Am. Chem. Soc.* **2002**, *124* (20), 5656–5657. <https://doi.org/10.1021/ja0261325>.
- (96) Kumaragurubaran, N.; Juhl, K.; Zhuang, W.; Bøgevig, A.; Jørgensen, K. A. Direct L-Proline-Catalyzed Asymmetric α -Amination of Ketones. *J. Am. Chem. Soc.* **2002**, *124* (22), 6254–6255. <https://doi.org/10.1021/ja026412k>.
- (97) Vogt, H.; Vanderheiden, S.; Bräse, S. Proline-Catalysed Asymmetric Amination of α,α -Disubstituted Aldehydes: Synthesis of Configurationally Stable Enantioenriched α -Aminoaldehydes. *Chem. Commun.* **2003**, *3* (19), 2448–2449. <https://doi.org/10.1039/b305465a>.
- (98) Zhong, G. A Facile and Rapid Route to Highly Enantiopure 1,2-Diols by Novel Catalytic Asymmetric α -Aminoxylation of Aldehydes. *Angew. Chemie - Int. Ed.* **2003**, *42* (35), 4247–4250. <https://doi.org/10.1002/anie.200352097>.
- (99) Brown, S. P.; Brochu, M. P.; Sinz, C. J.; MacMillan, D. W. C. The Direct and Enantioselective Organocatalytic α -Oxidation of Aldehydes. *J. Am. Chem. Soc.* **2003**, *125* (36), 10808–10809. <https://doi.org/10.1021/ja037096s>.
- (100) Hayashi, Y.; Yamaguchi, J.; Sumiya, T.; Shoji, M. Direct Proline-Catalyzed Asymmetric α -Aminoxylation of Ketones. *Angew. Chemie - Int. Ed.* **2004**, *43* (9), 1112–1115. <https://doi.org/10.1002/anie.200353085>.
- (101) Juhl, K.; Jørgensen, K. A. The First Organocatalytic Enantioselective Inverse-Electron-Demand Hetero-Diels-Alder Reaction. *Angew. Chemie - Int. Ed.* **2003**, *42* (13), 1498–1501. <https://doi.org/10.1002/anie.200250652>.
- (102) Wabnitz, T. C.; Saaby, S.; Jørgensen, K. A. The First Catalytic Inverse-Electron Demand Hetero-Diels-Alder Reaction of Nitroso Alkenes Using Pyrrolidine as an Organocatalyst. *Org. Biomol. Chem.* **2004**, *2* (6), 828–834. <https://doi.org/10.1039/b316518c>.
- (103) Jen, W. S.; Wiener, J. J. M.; MacMillan, D. W. C. New Strategies for Organic Catalysis: The First

- Enantioselective Organocatalytic 1,3-Dipolar Cycloaddition [20]. *Journal of the American Chemical Society*. American Chemical Society October 11, 2000, pp 9874–9875. <https://doi.org/10.1021/ja005517p>.
- (104) Hayashi, Y.; Gotoh, H.; Hayashi, T.; Shoji, M. Diphenylprolinol Silyl Ethers as Efficient Organocatalysts for the Asymmetric Michael Reaction of Aldehydes and Nitroalkenes. *Angew. Chemie - Int. Ed.* **2005**, *44* (27), 4212–4215. <https://doi.org/10.1002/anie.200500599>.
- (105) Franzén, J.; Marigo, M.; Fielenbach, D.; Wabnitz, T. C.; Kjærsgaard, A.; Jørgensen, K. A. A General Organocatalyst for Direct α -Functionalization of Aldehydes: Stereoselective C-C, C-N, C-F, C-Br, and C-S Bond-Forming Reactions. Scope and Mechanistic Insights. *J. Am. Chem. Soc.* **2005**, *127* (51), 18296–18304. <https://doi.org/10.1021/ja056120u>.
- (106) Brandau, S.; Landa, A.; Franzén, J.; Marigo, M.; Jørgensen, K. A. Organocatalytic Conjugate Addition of Malonates to α,β -Unsaturated Aldehydes: Asymmetric Formal Synthesis of (-)-Paroxetine, Chiral Lactams, and Lactones. *Angew. Chemie - Int. Ed.* **2006**, *45* (26), 4305–4309. <https://doi.org/10.1002/anie.200601025>.
- (107) Enders, D.; Hüttl, M. R. M.; Grondal, C.; Raabe, G. Control of Four Stereocentres in a Triple Cascade Organocatalytic Reaction. *Nature* **2006**, *441* (7095), 861–863. <https://doi.org/10.1038/nature04820>.
- (108) Seebach, D.; Grošelj, U.; Badine, D. M.; Schweizer, W. B.; Beck, A. K. Isolation and X-Ray Structures of Reactive Intermediates of Organocatalysis with Diphenylprolinol Ethers and with Imidazolidinones a Survey and Comparison with Computed Structures and with 1-Acyl-Imidazolidinones: The 1,5-Repulsion and the Geminal-Diaryl Effect at Work. *Helv. Chim. Acta* **2008**, *91* (11), 1999–2034. <https://doi.org/10.1002/hlca.200890216>.
- (109) Grošelj, U.; Seebach, D.; Badine, D. M.; Schweizer, W. B.; Beck, A. K.; Krossing, I.; Klose, P.; Hayashi, Y.; Uchimaru, T. Structures of the Reactive Intermediates in Organocatalysis with Diarylprolinol Ethers. *Helv. Chim. Acta* **2009**, *92* (7), 1225–1259. <https://doi.org/10.1002/hlca.200900179>.

- (110) Schmid, M. B.; Zeitler, K.; Gschwind, R. M. Formation and Stability of Prolinol and Prolinol Ether Enamines by NMR: Delicate Selectivity and Reactivity Balances and Parasitic Equilibria. *J. Am. Chem. Soc.* **2011**, *133* (18), 7065–7074. <https://doi.org/10.1021/ja111544b>.
- (111) Schmid, M. B.; Zeitler, K.; Gschwind, R. M. Distinct Conformational Preferences of Prolinol and Prolinol Ether Enamines in Solution Revealed by NMR. *Chem. Sci.* **2011**, *2* (9), 1793–1803. <https://doi.org/10.1039/c1sc00274k>.
- (112) Dinér, P.; Kjærsgaard, A.; Lie, M. A.; Jørgensen, K. A. On the Origin of the Stereoselectivity in Organocatalysed Reactions with Trimethylsilyl-Protected Diarylprolinol. *Chem. - A Eur. J.* **2008**, *14* (1), 122–127. <https://doi.org/10.1002/chem.200701244>.
- (113) Dinér, P.; Nielsen, M.; Marigo, M.; Jørgensen, K. A. Enantioselective Organocatalytic Conjugate Addition of N Heterocycles to α,β -Unsaturated Aldehydes. *Angew. Chemie - Int. Ed.* **2007**, *46* (12), 1983–1987. <https://doi.org/10.1002/anie.200604854>.
- (114) Seebach, D.; Gilmour, R.; Grošelj, U.; Deniau, G.; Sparr, C.; Ebert, M. O.; Beck, A. K.; McCusker, L. B.; Šišak, D.; Uchimaru, T. Stereochemical Models for Discussing Additions to α,β -Unsaturated Aldehydes Organocatalyzed by Diarylprolinol or Imidazolidinone Derivatives - Is There an “(E)/(Z)-Dilemma”? *Helv. Chim. Acta* **2010**, *93* (4), 603–634. <https://doi.org/10.1002/hlca.201000069>.
- (115) Halskov, K. S.; Donslund, B. S.; Paz, B. M.; Jørgensen, K. A. Computational Approach to Diarylprolinol-Silyl Ethers in Aminocatalysis. *Acc. Chem. Res.* **2016**, *49* (5), 974–986. <https://doi.org/10.1021/acs.accounts.6b00008>.
- (116) Hayashi, Y.; Okamura, D.; Yamazaki, T.; Ameda, Y.; Gotoh, H.; Tsuzuki, S.; Uchimaru, T.; Seebach, D. A Theoretical and Experimental Study of the Effects of Silyl Substituents in Enantioselective Reactions Catalyzed by Diphenylprolinol Silyl Ether. *Chem. - A Eur. J.* **2014**, *20* (51), 17077–17088. <https://doi.org/10.1002/chem.201403514>.
- (117) Gotoh, H.; Masui, R.; Ogino, H.; Shoji, M.; Hayashi, Y. Enantioselective Ene Reaction of Cyclopentadiene and α,β -Enals Catalyzed by a Diphenylprolinol Silyl Ether. *Angew. Chemie - Int.*

- Ed.* **2006**, *45* (41), 6853–6856. <https://doi.org/10.1002/anie.200602925>.
- (118) Hayashi, Y.; Toyoshima, M.; Gotoh, H.; Ishikawa, H. Diphenylprolinol Silyl Ether Catalysis in an Asymmetric Formal Carbo [3 + 3] Cycloaddition Reaction via a Domino Michael/Knoevenagel Condensation. *Org. Lett.* **2009**, *11* (1), 45–48. <https://doi.org/10.1021/ol802330h>.
- (119) Landa, A.; Puente, Á.; Santos, J. I.; Vera, S.; Oiarbide, M.; Palomo, C. Catalytic Conjugate Additions of Geminal Bis(Sulfone)s: Expanding the Chemistry of Sulfones as Simple Alkyl Anion Equivalents. *Chem. - A Eur. J.* **2009**, *15* (44), 11954–11962. <https://doi.org/10.1002/chem.200902094>.
- (120) Alba, A. N.; Companyó, X.; Moyano, A.; Rios, R. Formal Highly Enantioselective Organocatalytic Addition of Alkyl Anions to α,β -Unsaturated Aldehydes: Application to the Synthesis of Isotope-Enantiomers. *Chem. - A Eur. J.* **2009**, *15* (42), 11095–11099. <https://doi.org/10.1002/chem.200901806>.
- (121) Vega-Peñaloza, A.; Paria, S.; Bonchio, M.; Dell'Amico, L.; Companyó, X. Profiling the Privileges of Pyrrolidine-Based Catalysts in Asymmetric Synthesis: From Polar to Light-Driven Radical Chemistry. *ACS Catal.* **2019**, *9* (7), 6058–6072. <https://doi.org/10.1021/acscatal.9b01556>.
- (122) Gotoh, H.; Uchimaru, T.; Hayashi, Y. Two Reaction Mechanisms via Iminium Ion Intermediates: The Different Reactivities of Diphenylprolinol Silyl Ether and Trifluoromethyl-Substituted Diarylprolinol Silyl Ether. *Chem. - A Eur. J.* **2015**, *21* (35), 12337–12346. <https://doi.org/10.1002/chem.201500326>.
- (123) Dell'Amico, L.; Rassu, G.; Zambrano, V.; Sartori, A.; Curti, C.; Battistini, L.; Pelosi, G.; Casiraghi, G.; Zanardi, F. Exploring the Vinylogous Reactivity of Cyclohexenylidene Malononitriles: Switchable Regioselectivity in the Organocatalytic Asymmetric Addition to Enals Giving Highly Enantioenriched Carbabicyclic Structures. *J. Am. Chem. Soc.* **2014**, *136* (31), 11107–11114. <https://doi.org/10.1021/ja5054576>.
- (124) Hughes, D. L. Asymmetric Organocatalysis in Drug Development - Highlights of Recent Patent Literature. *Org. Process Res. Dev.* **2018**, *22* (5), 574–584.

- <https://doi.org/10.1021/acs.oprd.8b00096>.
- (125) Reyes-Rodríguez, G. J.; Rezayee, N. M.; Vidal-Albalat, A.; Jørgensen, K. A. Prevalence of Diarylprolinol Silyl Ethers as Catalysts in Total Synthesis and Patents. *Chem. Rev.* **2019**, *119* (6), 4221–4260. <https://doi.org/10.1021/acs.chemrev.8b00583>.
- (126) Haindl, M. H.; Schmid, M. B.; Zeitler, K.; Gschwind, R. M. What Is Your Actual Catalyst? TMS Cleavage Rates of Diarylprolinol Silyl Ethers Studied by in Situ NMR. *RSC Adv.* **2012**, *2* (14), 5941–5943. <https://doi.org/10.1039/c2ra20860a>.
- (127) Companyó, X.; Burés, J. Distribution of Catalytic Species as an Indicator to Overcome Reproducibility Problems. *J. Am. Chem. Soc.* **2017**, *139* (25), 8432–8435. <https://doi.org/10.1021/jacs.7b05045>.
- (128) Thomas R. Hoye; Brian M. Eklov; Troy D. Ryba; Mikhail Voloshin, A.; Yao, L. J. No-D NMR (No-Deuterium Proton NMR) Spectroscopy: A Simple Yet Powerful Method for Analyzing Reaction and Reagent Solutions. *Org. Lett.* **2004**, *6*, 953–956. <https://doi.org/10.1021/OL049979+>.
- (129) Brunner, H.; Bügler, J.; Nuber, B. Enantioselective Catalysis 98. Preparation of 9-Amino(9-Deoxy)Cinchona Alkaloids. *Tetrahedron: Asymmetry* **1995**, *6* (7), 1699–1702. [https://doi.org/10.1016/0957-4166\(95\)00215-B](https://doi.org/10.1016/0957-4166(95)00215-B).
- (130) Cassani, C.; Martín-Rapún, R.; Arceo, E.; Bravo, F.; Melchiorre, P. Synthesis of 9-Amino(9-Deoxy)Epi Cinchona Alkaloids, General Chiral Organocatalysts for the Stereoselective Functionalization of Carbonyl Compounds. *Nat. Protoc.* **2013**, *8* (2), 325–344. <https://doi.org/10.1038/nprot.2012.155>.
- (131) Melchiorre, P.; Bravo Lara, F.; Martin, R. Cinchona Alkaloid Derivatives, Their Process of Preparation and Their Use as Catalysts. EP 2 687 527 A1, 2014.
- (132) Xie, J.-W.; Chen, W.; Li, R.; Zeng, M.; Du, W.; Yue, L.; Chen, Y.-C.; Wu, Y.; Zhu, J.; Deng, J.-G. Highly Asymmetric Michael Addition to α,β -Unsaturated Ketones Catalyzed by 9-Amino-9-Deoxyepiquinine. *Angew. Chemie Int. Ed.* **2007**, *46* (3), 389–392. <https://doi.org/10.1002/anie.200603612>.

- (133) McCooey, S. H.; Connon, S. J. Readily Accessible 9-Epi-Amino Cinchona Alkaloid Derivatives Promote Efficient, Highly Enantioselective Additions of Aldehydes and Ketones to Nitroolefins. *Org. Lett.* **2007**, *9* (4), 599–602. <https://doi.org/10.1021/ol0628006>.
- (134) Liu, T. Y.; Cui, H. L.; Zhang, Y.; Jiang, K.; Du, W.; He, Z. Q.; Chen, Y. C. Organocatalytic and Highly Enantioselective Direct α -Amination of Aromatic Ketones. *Org. Lett.* **2007**, *9* (18), 3671–3674. <https://doi.org/10.1021/ol701648x>.
- (135) Jiang, L.; Chen, Y. C. Recent Advances in Asymmetric Catalysis with Cinchona Alkaloid-Based Primary Amines. *Catalysis Science and Technology*. The Royal Society of Chemistry June 23, 2011, pp 354–365. <https://doi.org/10.1039/c0cy00096e>.
- (136) Bertelsen, S.; Marigo, M.; Brandes, S.; Dinér, P.; Jørgensen, K. A. Dienamine Catalysis: Organocatalytic Asymmetric γ -Amination of α,β -Unsaturated Aldehydes. *J. Am. Chem. Soc.* **2006**, *128* (39), 12973–12980. <https://doi.org/10.1021/ja064637f>.
- (137) Hong, B. C.; Wu, M. F.; Tseng, H. C.; Liao, J. H. Enantioselective Organocatalytic Formal [3 + 3]-Cycloaddition of α,β -Unsaturated Aldehydes and Application to the Asymmetric Synthesis of (-)-Isopulegol Hydrate and (-)-Cubebaol. *Org. Lett.* **2006**, *8* (11), 2217–2220. <https://doi.org/10.1021/ol060486+>.
- (138) Hong, B. C.; Tseng, H. C.; Chen, S. H. Synthesis of Aromatic Aldehydes by Organocatalytic [4+2] and [3+3] Cycloaddition of α,β -Unsaturated Aldehydes. *Tetrahedron* **2007**, *63* (13), 2840–2850. <https://doi.org/10.1016/j.tet.2007.01.039>.
- (139) Hong, B. C.; Wu, M. F.; Tseng, H. C.; Huang, G. F.; Su, C. F.; Liao, J. H. Organocatalytic Asymmetric Robinson Annulation of α,β -Unsaturated Aldehydes: Applications to the Total Synthesis of (+)-Palitantin. *J. Org. Chem.* **2007**, *72* (22), 8459–8471. <https://doi.org/10.1021/jo701477v>.
- (140) De Figueiredo, R. M.; Fröhlich, R.; Christmann, M. Amine-Catalyzed Cyclizations of Tethered α,β -Unsaturated Carbonyl Compounds. *Angew. Chemie - Int. Ed.* **2008**, *47* (8), 1450–1453. <https://doi.org/10.1002/anie.200704688>.

- (141) Marcos, V.; Alemán, J. Old Tricks, New Dogs: Organocatalytic Dienamine Activation of α,β -Unsaturated Aldehydes. *Chem. Soc. Rev.* **2016**, *45* (24), 6812–6832. <https://doi.org/10.1039/c6cs00438e>.
- (142) Halskov, K. S.; Donslund, B. S.; Barfüsser, S.; Jørgensen, K. A. Organocatalytic Asymmetric Formation of Steroids. *Angew. Chemie Int. Ed.* **2014**, *53* (16), 4137–4141. <https://doi.org/10.1002/anie.201400203>.
- (143) Mose, R.; Jensen, M. E.; Preegel, G.; Jørgensen, K. A. Direct Access to Multifunctionalized Norcamphor Scaffolds by Asymmetric Organocatalytic Diels-Alder Reactions. *Angew. Chemie - Int. Ed.* **2015**, *54* (46), 13630–13634. <https://doi.org/10.1002/anie.201507348>.
- (144) Jia, Z. J.; Jiang, H.; Li, J. L.; Gschwend, B.; Li, Q. Z.; Yin, X.; Grouleff, J.; Chen, Y. C.; Jørgensen, K. A. Trienamines in Asymmetric Organocatalysis: Diels-Alder and Tandem Reactions. *J. Am. Chem. Soc.* **2011**, *133* (13), 5053–5061. <https://doi.org/10.1021/ja1112194>.
- (145) Jiang, H.; Gschwend, B.; Albrecht, Ł.; Hansen, S. G.; Jørgensen, K. A. Asymmetric Trienamine Catalysis for the Construction of Structurally Rigid Cyclic α,α -Disubstituted Amino Acid Derivatives. *Chem. - A Eur. J.* **2011**, *17* (33), 9032–9036. <https://doi.org/10.1002/chem.201101539>.
- (146) Jia, Z. J.; Zhou, Q.; Zhou, Q. Q.; Chen, P. Q.; Chen, Y. C. Exo-Selective Asymmetric Diels-Alder Reaction of 2,4-Dienals and Nitroalkenes by Trienamine Catalysis. *Angew. Chemie - Int. Ed.* **2011**, *50* (37), 8638–8641. <https://doi.org/10.1002/anie.201102013>.
- (147) Jiang, H.; Cruz, D. C.; Li, Y.; Lauridsen, V. H.; Jørgensen, K. A. Asymmetric Organocatalytic Thio-Diels-Alder Reactions via Trienamine Catalysis. *J. Am. Chem. Soc.* **2013**, *135* (13), 5200–5207. <https://doi.org/10.1021/ja4007244>.
- (148) Zhang, S. J.; Zhang, J.; Zhou, Q. Q.; Dong, L.; Chen, Y. C. Aminocatalytic Asymmetric Exo-Diels-Alder Reaction with Methiodide Salts of Mannich Bases and 2,4-Dienals to Construct Chiral Spirocycles. *Org. Lett.* **2013**, *15* (4), 968–971. <https://doi.org/10.1021/ol4002015>.
- (149) Liu, J. X.; Zhou, Q. Q.; Deng, J. G.; Chen, Y. C. An Asymmetric Normal-Electron-Demand Aza-Diels-Alder Reaction via Trienamine Catalysis. *Org. Biomol. Chem.* **2013**, *11* (47), 8175–8178.

- <https://doi.org/10.1039/c3ob41698d>.
- (150) Portalier, F.; Bourdreux, F.; Marrot, J.; Moreau, X.; Coeffard, V.; Greck, C. Merging Oxidative Dearomatization and Aminocatalysis: One-Pot Enantioselective Synthesis of Tricyclic Architectures. *Org. Lett.* **2013**, *15* (22), 5642–5645. <https://doi.org/10.1021/ol402546h>.
- (151) Li, Y.; López-Delgado, F. J.; Jørgensen, D. K. B.; Nielsen, R. P.; Jiang, H.; Jørgensen, K. A. Trienamine-Mediated Asymmetric [4+2]-Cycloaddition of α,β -Unsaturated Ester Surrogates Applying 4-Nitro-5-Styrylisoxazoles. *Chem. Commun.* **2014**, *50* (99), 15689–15691. <https://doi.org/10.1039/c4cc08171d>.
- (152) Gómez, C. V.; Cruz, D. C.; Mose, R.; Jørgensen, K. A. Organocatalytic Cascade Reactions: Diversity-Oriented Synthesis for the Construction of Hydroisoquinoline Scaffolds. *Chem. Commun.* **2014**, *50* (45), 6035–6038. <https://doi.org/10.1039/c4cc01231c>.
- (153) Li, X.; Lin, M. H.; Han, Y.; Wang, F.; Cheng, J. P. Asymmetric Diels-Alder Reaction of 3-Olefinic Benzofuran-2-Ones and Polyenals: Construction of Chiral Spirocyclic Benzofuran-2-Ones. *Org. Lett.* **2014**, *16* (1), 114–117. <https://doi.org/10.1021/ol403094a>.
- (154) Donslund, B. S.; Nielsen, R. P.; Mønsted, S. M. N.; Jørgensen, K. A. Benzofulvenes in Trienamine Catalysis: Stereoselective Spiroindene Synthesis. *Angew. Chemie Int. Ed.* **2016**, *55* (37), 11124–11128. <https://doi.org/10.1002/anie.201605079>.
- (155) Halskov, K. S.; Johansen, T. K.; Davis, R. L.; Steurer, M.; Jensen, F.; Jørgensen, K. A. Cross-Trienamines in Asymmetric Organocatalysis. *J. Am. Chem. Soc.* **2012**, *134* (31), 12943–12946. <https://doi.org/10.1021/ja3068269>.
- (156) Dieckmann, A.; Breugst, M.; Houk, K. N. Zwitterions and Unobserved Intermediates in Organocatalytic Diels-Alder Reactions of Linear and Cross-Conjugated Trienamines. *J. Am. Chem. Soc.* **2013**, *135* (8), 3237–3242. <https://doi.org/10.1021/ja312043g>.
- (157) Liu, Y.; Nappi, M.; Arceo, E.; Vera, S.; Melchiorre, P. Asymmetric Catalysis of Diels-Alder Reactions with in Situ Generated Heterocyclic Ortho -Quinodimethanes. *J. Am. Chem. Soc.* **2011**, *133* (38), 15212–15218. <https://doi.org/10.1021/ja206517s>.

- (158) Liu, Y.; Nappi, M.; Escudero-Adán, E. C.; Melchiorre, P. Multicatalytic Asymmetric Synthesis of Complex Tetrahydrocarbazoles via a Diels-Alder/Benzoin Reaction Sequence. *Org. Lett.* **2012**, *14* (5), 1310–1313. <https://doi.org/10.1021/ol300192p>.
- (159) Skrzyńska, A.; Przydacz, A.; Albrecht, Ł. Organocatalytic Nonclassical Trienamine Activation in the Remote Alkylation of Furan Derivatives. *Org. Lett.* **2015**, *17* (22), 5682–5685. <https://doi.org/10.1021/acs.orglett.5b02979>.
- (160) Przydacz, A.; Skrzyńska, A.; Albrecht, Ł. Breaking Aromaticity with Aminocatalysis: A Convenient Strategy for Asymmetric Synthesis. *Angew. Chemie - Int. Ed.* **2019**, *58* (1), 63–73. <https://doi.org/10.1002/anie.201808197>.
- (161) Stiller, J.; Poulsen, P. H.; Cruz, D. C.; Dourado, J.; Davis, R. L.; Jørgensen, K. A. Organocatalytic [4+2] Addition Reactions via Tetraenamine Intermediate. *Chem. Sci.* **2014**, *5* (5), 2052–2056. <https://doi.org/10.1039/c4sc00081a>.
- (162) He, X. L.; Zhao, H. R.; Duan, C. Q.; Du, W.; Chen, Y. C. Remote Asymmetric Oxa-Diels-Alder Reaction of 5-Allylic Furfurals via Dearomatizative Tetraenamine Catalysis. *Org. Lett.* **2018**, *20* (3), 804–807. <https://doi.org/10.1021/acs.orglett.7b03942>.
- (163) Yang, Q. Q.; Xiao, W.; Du, W.; Ouyang, Q.; Chen, Y. C. Asymmetric [4+2] Annulations to Construct Norcamphor Scaffolds with 2-Cyclopentenone via Double Amine-Thiol Catalysis. *Chem. Commun.* **2018**, *54* (9), 1129–1132. <https://doi.org/10.1039/c7cc09221k>.
- (164) Zhou, Q. Q.; Xiao, Y. C.; Yuan, X.; Chen, Y. C. Asymmetric Diels-Alder Reactions of 2,4,6-Trientials via Tetraenamine Catalysis. *Asian J. Org. Chem.* **2014**, *3* (4), 545–549. <https://doi.org/10.1002/ajoc.201400015>.
- (165) Jurberg, I. D.; Chatterjee, I.; Tannert, R.; Melchiorre, P. When Asymmetric Aminocatalysis Meets the Vinylogy Principle. *Chem. Commun.* **2013**, *49* (43), 4869–4883. <https://doi.org/10.1039/c3cc41270a>.
- (166) Klier, L.; Tur, F.; Poulsen, P. H.; Jørgensen, K. A. Asymmetric Cycloaddition Reactions Catalysed by Diarylprolinol Silyl Ethers. *Chem. Soc. Rev.* **2017**, *46* (4), 1080–1102.

- <https://doi.org/10.1039/c6cs00713a>.
- (167) Hayashi, Y.; Gotoh, H.; Honma, M.; Sankar, K.; Kumar, I.; Ishikawa, H.; Konno, K.; Yui, H.; Tsuzuki, S.; Uchimaru, T. Organocatalytic, Enantioselective Intramolecular [6 + 2] Cycloaddition Reaction for the Formation of Tricyclopentanoids and Insight on Its Mechanism from a Computational Study. *J. Am. Chem. Soc.* **2011**, *133* (50), 20175–20185. <https://doi.org/10.1021/ja108516b>.
- (168) Mose, R.; Pregel, G.; Larsen, J.; Jakobsen, S.; Iversen, E. H.; Jørgensen, K. A. Organocatalytic Stereoselective [8+2] and [6+4] Cycloadditions. *Nat. Chem.* **2017**, *9* (5), 487–492. <https://doi.org/10.1038/nchem.2682>.
- (169) Zhou, Z.; Wang, Z. X.; Zhou, Y. C.; Xiao, W.; Ouyang, Q.; Du, W.; Chen, Y. C. Switchable Regioselectivity in Amine-Catalysed Asymmetric Cycloadditions. *Nat. Chem.* **2017**, *9* (6), 590–594. <https://doi.org/10.1038/nchem.2698>.
- (170) Donslund, B. S.; Monleón, A.; Palazzo, T. A.; Christensen, M. L.; Dahlgaard, A.; Erickson, J. D.; Jørgensen, K. A. Organocatalytic Enantioselective Higher-Order Cycloadditions of In Situ Generated Amino Isobenzofulvenes. *Angew. Chemie - Int. Ed.* **2018**, *57* (5), 1246–1250. <https://doi.org/10.1002/anie.201710694>.
- (171) Donslund, B. S.; Jessen, N. I.; Bertuzzi, G.; Giardinetti, M.; Palazzo, T. A.; Christensen, M. L.; Jørgensen, K. A. Catalytic Enantioselective [10+4] Cycloadditions. *Angew. Chemie - Int. Ed.* **2018**, *57* (40), 13182–13186. <https://doi.org/10.1002/anie.201807830>.
- (172) McLeod, D.; Izzo, J. A.; Jørgensen, D. K. B.; Lauridsen, R. F.; Jørgensen, K. A. Development and Investigation of an Organocatalytic Enantioselective [10 + 2] Cycloaddition. *ACS Catal.* **2020**, *10* (18), 10784–10793. <https://doi.org/10.1021/acscatal.0c03378>.
- (173) Bertuzzi, G.; Thøgersen, M. K.; Giardinetti, M.; Vidal-Albalat, A.; Simon, A.; Houk, K. N.; Jørgensen, K. A. Catalytic Enantioselective Hetero-[6+4] and-[6+2] Cycloadditions for the Construction of Condensed Polycyclic Pyrroles, Imidazoles, and Pyrazoles. *J. Am. Chem. Soc.* **2019**, *141* (7), 3288–3297. <https://doi.org/10.1021/jacs.8b13659>.

- (174) Frankowski, S.; Skrzyńska, A.; Albrecht, Ł. Inverting the Reactivity of Troponoid Systems in Enantioselective Higher-Order Cycloaddition. *Chem. Commun.* **2019**, *55* (78), 11675–11678. <https://doi.org/10.1039/c9cc05638f>.
- (175) Wheeler, S. E.; Houk, K. N.; Schleyer, P. V. R.; Allen, W. D. A Hierarchy of Homodesmotic Reactions for Thermochemistry. *J. Am. Chem. Soc.* **2009**, *131* (7), 2547–2560. <https://doi.org/10.1021/ja805843n>.
- (176) Wheeler, S. E. Homodesmotic Reactions for Thermochemistry. *Wiley Interdiscip. Rev. Comput. Mol. Sci.* **2012**, *2* (2), 204–220. <https://doi.org/10.1002/wcms.72>.
- (177) Zhao, Y.; Truhlar, D. G. The M06 Suite of Density Functionals for Main Group Thermochemistry, Thermochemical Kinetics, Noncovalent Interactions, Excited States, and Transition Elements: Two New Functionals and Systematic Testing of Four M06-Class Functionals and 12 Other Function. *Theor. Chem. Acc.* **2008**, *120* (1–3), 215–241. <https://doi.org/10.1007/s00214-007-0310-x>.
- (178) Petersson, G. A.; Bennett, A.; Tensfeldt, T. G.; Al-Laham, M. A.; Shirley, W. A.; Mantzaris, J. A. Complete Basis Set Model Chemistry. I. The Total Energies of Closed-Shell Atoms and Hydrides of the First-Row Elements. *J. Chem. Phys.* **1988**, *89* (4), 2193–2218. <https://doi.org/10.1063/1.455064>.
- (179) Petersson, G. A.; Al-Laham, M. A. A Complete Basis Set Model Chemistry. II. Open-Shell Systems and the Total Energies of the First-Row Atoms. *J. Chem. Phys.* **1991**, *94* (9), 6081–6090. <https://doi.org/10.1063/1.460447>.
- (180) Frisch, M. J.; Trucks, G. W.; Schlegel, H. B.; Scuseria, G. E.; Robb, M. a.; Cheeseman, J. R.; Scalmani, G.; Barone, V.; Petersson, G. a.; Nakatsuji, H.; Li, X.; Caricato, M.; Marenich, a. V.; Bloino, J.; Janesko, B. G.; Gomperts, R.; Mennucci, B.; Hratchian, H. P.; Ortiz, J. V.; Izmaylov, a. F.; Sonnenberg, J. L.; Williams; Ding, F.; Lipparini, F.; Egidi, F.; Goings, J.; Peng, B.; Petrone, A.; Henderson, T.; Ranasinghe, D.; Zakrzewski, V. G.; Gao, J.; Rega, N.; Zheng, G.; Liang, W.; Hada, M.; Ehara, M.; Toyota, K.; Fukuda, R.; Hasegawa, J.; Ishida, M.; Nakajima, T.; Honda, Y.; Kitao, O.; Nakai, H.; Vreven, T.; Throssell, K.; Montgomery Jr., J. a.; Peralta, J. E.; Ogliaro, F.; Bearpark,

- M. J.; Heyd, J. J.; Brothers, E. N.; Kudin, K. N.; Staroverov, V. N.; Keith, T. a.; Kobayashi, R.; Normand, J.; Raghavachari, K.; Rendell, a. P.; Burant, J. C.; Iyengar, S. S.; Tomasi, J.; Cossi, M.; Millam, J. M.; Klene, M.; Adamo, C.; Cammi, R.; Ochterski, J. W.; Martin, R. L.; Morokuma, K.; Farkas, O.; Foresman, J. B.; Fox, D. J. G09. 2009, p Gaussian 09, Gaussian, Inc., Wallin.
- (181) Tenderholt, A. L. QMForge, version 2.1
<https://sourceforge.net/projects/qmforge/files/qmforge/QMForge-2.1/%0A>.
- (182) Momma, K.; Izumi, F. VESTA 3 for Three-Dimensional Visualization of Crystal, Volumetric and Morphology Data. *J. Appl. Crystallogr.* **2011**, *44* (6), 1272–1276.
<https://doi.org/10.1107/S0021889811038970>.
- (183) Fuson, R. C. The Principle of Vinylogy. *Chem. Rev.* **1935**, *16* (1), 1–27.
<https://doi.org/10.1021/cr60053a001>.
- (184) Nurkkala, L. J.; Steen, R. O.; Friberg, H. K. J.; Häggström, J. A.; Bernhardt, P. V.; Riley, M. J.; Dunne, S. J. The Effects of Pendant vs. Fused Thiophene Attachment upon the Luminescence Lifetimes and Electrochemistry of Tris(2,2'-Bipyridine)Ruthenium(II) Complexes. *Eur. J. Inorg. Chem.* **2008**, *2008* (26), 4101–4110. <https://doi.org/10.1002/ejic.200800456>.
- (185) Škorić, I.; Kikaš, I.; Kovács, M.; Šindler-Kulyk, M.; Horváth, O. Synthesis, Spectroscopic Characterization and Photophysics of New Functionalized 2,3-Distyrylfurans: Substituent and Solvent Effects on Their Photobehavior. *J. Photochem. Photobiol. A Chem.* **2010**, *211* (2–3), 152–161. <https://doi.org/10.1016/j.jphotochem.2010.02.013>.
- (186) Zhen, W.; Wang, F.; Zhao, M.; Du, Z.; Li, X. Rhodium(III)-Catalyzed Oxidative C-H Functionalization of Azomethine Ylides. *Angew. Chemie - Int. Ed.* **2012**, *51* (47), 11819–11823.
<https://doi.org/10.1002/anie.201207204>.
- (187) Xu, C.; Li, H.; He, X.; Du, W.; Chen, Y. Asymmetric Direct Remote Michael Addition Reactions of Allyl Furfurals via Dearomative Trienammine and Tetraenammine Catalysis. *Asian J. Org. Chem.* **2019**, *8* (7), 1037–1040. <https://doi.org/10.1002/ajoc.201900197>.
- (188) Longuet-Higgins, H. C. The Electronic Structure of Thiophene and Related Molecules. *Trans.*

- Faraday Soc.* **1949**, *45* (0), 173–179. <https://doi.org/10.1039/tf9494500173>.
- (189) Bak, B.; Christensen, D.; Hansen-Nygaard, L.; Rastrup-Andersen, J. The Structure of Thiophene. *J. Mol. Spectrosc.* **1961**, *7* (1–6), 58–63. [https://doi.org/10.1016/0022-2852\(61\)90341-1](https://doi.org/10.1016/0022-2852(61)90341-1).
- (190) Jones, D.; Guerra, M.; Favaretto, L.; Modelli, A.; Fabrizio, M.; Distefano, G. Determination of the Electronic Structure of Thiophene Oligomers and Extrapolation to Polythiophene. *J. Phys. Chem.* **1990**, *94* (15), 5761–5766. <https://doi.org/10.1021/j100378a030>.
- (191) Gribble, G. W. Recent Developments in Indole Ring Synthesis - Methodology and Applications. *J. Chem. Soc. Perkin Trans. 1* **2000**, No. 7, 1045–1075. <https://doi.org/10.1039/a909834h>.
- (192) Cacchi, S.; Fabrizi, G. Synthesis and Functionalization of Indoles through Palladium-Catalyzed Reactions. *Chem. Rev.* **2005**, *105* (7), 2873–2920. <https://doi.org/10.1021/cr040639b>.
- (193) Humphrey, G. R.; Kuethe, J. T. Practical Methodologies for the Synthesis of Indoles. *Chem. Rev.* **2006**, *106* (7), 2875–2911. <https://doi.org/10.1021/cr0505270>.
- (194) Ewing, J.; Hughes, G. K.; Ritchie, E.; Taylor, W. C. An Alkaloid Related to Dehydrolaudanosoline. *Nature* **1952**, *169* (4302), 618–619. <https://doi.org/10.1038/169618b0>.
- (195) Williams, D. E.; Davies, J.; Patrick, B. O.; Bottriell, H.; Tarling, T.; Roberge, M.; Andersen, R. J. Cladoniamides A-G, Tryptophan-Derived Alkaloids Produced in Culture by *Streptomyces Uncialis*. *Org. Lett.* **2008**, *10* (16), 3501–3504. <https://doi.org/10.1021/ol801274c>.
- (196) Du, Y. L.; Ding, T.; Patrick, B. O.; Ryan, K. S. Xenocladoniamide F, Minimal Indolotryptoline from the Cladoniamide Pathway. *Tetrahedron Lett.* **2013**, *54* (41), 5635–5638. <https://doi.org/10.1016/j.tetlet.2013.08.017>.
- (197) Randriambola, L.; Quirion, J. C.; Kan-Fan, C.; Husson, H. P. Structure of Goniomitine, a New Type of Indole Alkaloid. *Tetrahedron Lett.* **1987**, *28* (19), 2123–2126. [https://doi.org/10.1016/S0040-4039\(00\)96059-3](https://doi.org/10.1016/S0040-4039(00)96059-3).
- (198) De Simone, F.; Gertsch, J.; Waser, J. Catalytic Selective Cyclizations of Aminocyclopropanes: Formal Synthesis of Aspidospermidine and Total Synthesis of Goniomitine. *Angew. Chemie - Int. Ed.* **2010**, *49* (33), 5767–5770. <https://doi.org/10.1002/anie.201001853>.

- (199) Bin, H.; Wang, K.; Yang, D.; Yang, X.; Xie, J.; Zhou, Q. Scalable Enantioselective Total Synthesis of (–)-Goniomitine. *Angew. Chemie Int. Ed.* **2019**, *58* (4), 1174–1177. <https://doi.org/10.1002/anie.201812822>.
- (200) Jeon, K. I.; Xu, X.; Aizawa, T.; Lim, J. H.; Jono, H.; Kwon, D. S.; Abe, J. I.; Berk, B. C.; Li, J. D.; Yan, C. Vinpocetine Inhibits NF-KB-Dependent Inflammation via an IKK-Dependent but PDE-Independent Mechanism. *Proc. Natl. Acad. Sci. U. S. A.* **2010**, *107* (21), 9795–9800. <https://doi.org/10.1073/pnas.0914414107>.
- (201) Kim, D. S.; Park, W. J.; Jun, C. H. Metal-Organic Cooperative Catalysis in C-H and C-C Bond Activation. *Chemical Reviews*. American Chemical Society July 12, 2017, pp 8977–9015. <https://doi.org/10.1021/acs.chemrev.6b00554>.
- (202) Mcleod, D.; Thøgersen, M. K.; Jessen, N. I.; Jørgensen, K. A.; Jamieson, C. S.; Xue, X. S.; Houk, K. N.; Liu, F.; Hoffmann, R. Expanding the Frontiers of Higher-Order Cycloadditions. *Acc. Chem. Res.* **2019**, *52* (12), 3488–3501. <https://doi.org/10.1021/acs.accounts.9b00498>.
- (203) Kim, H. J.; Ruzsyczky, M. W.; Choi, S. H.; Liu, Y. N.; Liu, H. W. Enzyme-Catalysed [4+2] Cycloaddition Is a Key Step in the Biosynthesis of Spinosyn A. *Nature* **2011**, *473* (7345), 109–112. <https://doi.org/10.1038/nature09981>.
- (204) Raju, R.; Piggott, A. M.; Conte, M. M.; Capon, R. J. Heronamides A - C, New Polyketide Macrolactams from an Australian Marine-Derived Streptomyces Sp. A Biosynthetic Case for Synchronized Tandem Electrocyclization. *Org. Biomol. Chem.* **2010**, *8* (20), 4682–4689. <https://doi.org/10.1039/c0ob00267d>.
- (205) Zhang, B.; Wang, K. B.; Wang, W.; Wang, X.; Liu, F.; Zhu, J.; Shi, J.; Li, L. Y.; Han, H.; Xu, K.; Qiao, H. Y.; Zhang, X.; Jiao, R. H.; Houk, K. N.; Liang, Y.; Tan, R. X.; Ge, H. M. Enzyme-Catalysed [6+4] Cycloadditions in the Biosynthesis of Natural Products. *Nature* **2019**, *568* (7750), 122–126. <https://doi.org/10.1038/s41586-019-1021-x>.
- (206) Jamieson, C. S.; Ohashi, M.; Liu, F.; Tang, Y.; Houk, K. N. The Expanding World of Biosynthetic Pericyclases: Cooperation of Experiment and Theory for Discovery. *Natural Product Reports*.

- Royal Society of Chemistry May 1, 2019, pp 698–713. <https://doi.org/10.1039/c8np00075a>.
- (207) Zhou, Z.; Wang, Z. X.; Zhou, Y. C.; Xiao, W.; Ouyang, Q.; Du, W.; Chen, Y. C. Switchable Regioselectivity in Amine-Catalysed Asymmetric Cycloadditions. *Nat. Chem.* **2017**, *9* (6), 590–594. <https://doi.org/10.1038/nchem.2698>.
- (208) Preethalayam, P.; Krishnan, K. S.; Thulasi, S.; Chand, S. S.; Joseph, J.; Nair, V.; Jaroschik, F.; Radhakrishnan, K. V. Recent Advances in the Chemistry of Pentafulvenes. *Chem. Rev.* **2017**, *117* (5), 3930–3989. <https://doi.org/10.1021/acs.chemrev.6b00210>.
- (209) De Mico, A.; Margarita, R.; Parlanti, L.; Vescovi, A.; Piancatelli, G. A Versatile and Highly Selective Hypervalent Iodine (III)/ 2,2,6,6-Tetraniethyl-1-Piperidinyloxy-Mediated Oxidation of Alcohols to Carbonyl Compounds. *J. Org. Chem.* **1997**, *62* (20), 6974–6977. <https://doi.org/10.1021/jo971046m>.
- (210) Luzzio, F. A.; Fitch, R. W.; Moore, W. J.; Mudd, K. J. A Facile Oxidation of Alcohols Using Pyridinium Chlorochromate/Silica Gel. *J. Chem. Educ.* **1999**, *76* (7), 974–975. <https://doi.org/10.1021/ed076p974>.
- (211) Erden, I.; Sabol, J.; Gubeladze, A.; Ruiz, A. An Expedient Synthesis of 6-Vinylfulvene. *Turkish J. Chem.* **2013**, *37* (4), 519–524. <https://doi.org/10.3906/kim-1302-74>.
- (212) Meyer, S. D.; Schreiber, S. L. Acceleration of the Dess-Martin Oxidation by Water. *J. Org. Chem.* **1994**, *59* (24), 7549–7552. <https://doi.org/10.1021/jo00103a067>.
- (213) Erden, I.; Xu, F. P.; Sadoun, A.; Smith, W.; Sheff, G.; Ossun, M. Scope and Limitations of Fulvene Syntheses. Preparation of 6-Vinyl-Substituted and -Functionalized Fulvenes. First Examples of Nucleophilic Substitution on a 6-(Chloromethyl)Fulvene. *J. Org. Chem.* **1995**, *60* (4), 813–820. <https://doi.org/10.1021/jo00109a010>.
- (214) Erden, I.; Gronert, S.; Keeffe, J. R.; Ma, J.; Ocal, N.; Gärtner, C.; Soukup, L. L. Effect of Allylic Groups on SN2 Reactivity. *J. Org. Chem.* **2014**, *79* (14), 6410–6418. <https://doi.org/10.1021/jo501157s>.
- (215) Erden, I.; Gronert, S.; Cabrera, G.; Coskun, N.; Tapken, M. Diverse Modes of Reactivity of 6-

- (Chloromethyl)-6-Methylfulvene. *European J. Org. Chem.* **2017**, 2017 (20), 2925–2931. <https://doi.org/10.1002/ejoc.201700442>.
- (216) Chen, G.; Wang, Z.; Wu, J.; Ding, K. Facile Preparation of α -Aryl Nitriles by Direct Cyanation of Alcohols with TMSCN under the Catalysis of InX₃. *Org. Lett.* **2008**, 10 (20), 4573–4576. <https://doi.org/10.1021/ol801812a>.
- (217) Kosarych, Z.; Cohen, T. Rapid, High-Yield Cleavage of Enol and Dienol Methyl Ethers under Mild Conditions Using Chlorotrimethylsilane/Sodium Iodide. *Tetrahedron Lett.* **1980**, 21, 3959–3962.
- (218) Ireland, R. E.; Mueller, R. H. The Claisen Rearrangement of Allyl Esters. *J. Am. Chem. Soc.* **1972**, 94 (16), 5897–5898. <https://doi.org/10.1021/ja00771a062>.
- (219) Ireland, R. E.; Willard, A. K. LW STERBOSELBCTIVE GENERATION OF ESTER BNOLATES. *Tetrahedron Lett.* **1975**, 463978 (3975), 3975–3978.
- (220) Ireland, R. E.; Mueller, R. H.; Willard, A. K. The Ester Enolate Claisen Rearrangement. Stereochemical Control through Stereoselective Enolate Formation. *J. Am. Chem. Soc.* **1976**, 98 (10), 2868–2877. <https://doi.org/10.1021/ja00426a033>.
- (221) Majumdar, K. C.; Nandi, R. K. The Claisen Rearrangement in the Syntheses of Bioactive Natural Products. *Tetrahedron* **2013**, 69 (34), 6921–6957. <https://doi.org/10.1016/j.tet.2013.06.003>.
- (222) Heathcock, C. H.; Buse, C. T.; Kleschick, W. A.; Pirrung, M. C.; Sohn, J. E.; Lampe, J. Acyclic Stereoselection. 7. Stereoselective Synthesis of 2-Alkyl-3-Hydroxy Carbonyl Compounds by Aldol Condensation. *J. Org. Chem.* **1980**, 45 (6), 1066–1081. <https://doi.org/10.1021/jo01294a030>.
- (223) Ireland, R. E.; Wipf, P.; Armstrong, J. D. Stereochemical Control in the Ester Enolate Claisen Rearrangement. 1. Stereoselectivity in Silyl Ketene Acetal Formation. *J. Org. Chem.* **1991**, 56 (2), 650–657. <https://doi.org/10.1021/jo00002a030>.
- (224) Podunavac, M.; Lacharity, J. J.; Jones, K. E.; Zakarian, A. Stereodivergence in the Ireland-Claisen Rearrangement of α -Alkoxy Esters. *Org. Lett.* **2018**, 20 (16), 4867–4870. <https://doi.org/10.1021/acs.orglett.8b02011>.
- (225) Enders, D.; Knopp, M.; Schiffers, R. Asymmetric [3.3]-Sigmatropic Rearrangements in Organic

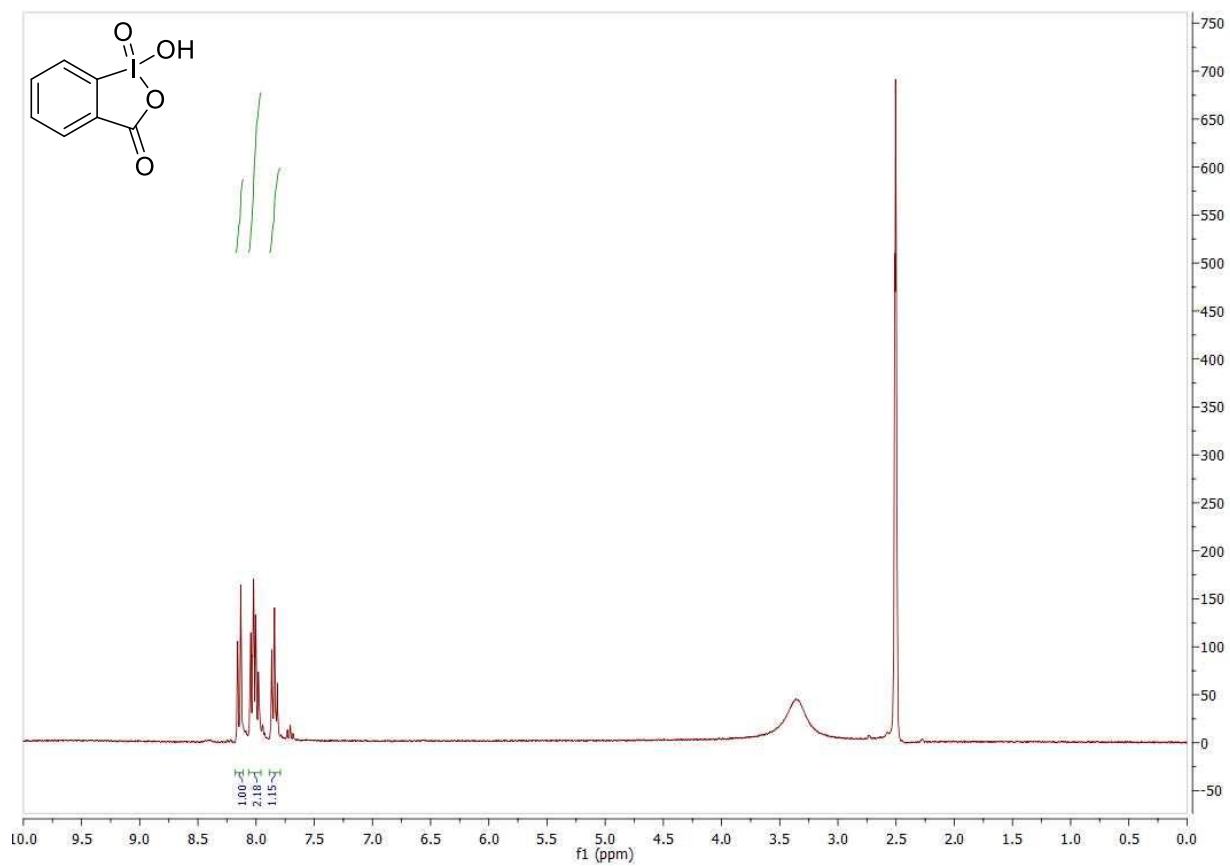
- Synthesis. *Tetrahedron Asymmetry* **1996**, 7 (7), 1847–1882.
- (226) Corey, E. J.; Lee, D. H. Highly Enantioselective and Diastereoselective Ireland-Claisen Rearrangement of Achiral Allylic Esters. *J. Am. Chem. Soc.* **1991**, 113 (10), 4026–4028. <https://doi.org/10.1021/ja00010a074>.
- (227) De Filippis, V.; Pozzi, N.; Acquasaliente, L.; Artusi, I.; Pontarollo, G.; Peterle, D. Protein Engineering by Chemical Methods: Incorporation of Nonnatural Amino Acids as a Tool for Studying Protein Folding, Stability, and Function. *Pept. Sci.* **2018**, 110 (5), e24090. <https://doi.org/10.1002/pep2.24090>.
- (228) Vagner, J.; Qu, H.; Hruby, V. J. Peptidomimetics, a Synthetic Tool of Drug Discovery. *Current Opinion in Chemical Biology*. Elsevier Current Trends June 1, 2008, pp 292–296. <https://doi.org/10.1016/j.cbpa.2008.03.009>.
- (229) Neises, B.; Steglich, W. Simple Method for the Esterification of Carboxylic Acids. *Angew. Chemie Int. Ed. English* **1978**, 17 (7), 522–524. <https://doi.org/10.1002/anie.197805221>.
- (230) Wang, H. Chiral Phase-Transfer Catalysts with Hydrogen Bond: A Powerful Tool in the Asymmetric Synthesis. *Catalysts* **2019**, 9 (3). <https://doi.org/10.3390/catal9030244>.
- (231) O'Donnell, M. J.; Wu, S.; Huffman, J. C. A New Active Catalyst Species for Enantioselective Alkylation by Phase-Transfer Catalysis. *Tetrahedron* **1994**, 50 (15), 4507–4518. [https://doi.org/10.1016/S0040-4020\(01\)89382-0](https://doi.org/10.1016/S0040-4020(01)89382-0).
- (232) Lygo, B.; Wainwright, P. G. A New Class of Asymmetric Phase-Transfer Catalysts Derived from Cinchona Alkaloids - Application in the Enantioselective Synthesis of α -Amino Acids. *Tetrahedron Lett.* **1997**, 38 (49), 8595–8598. [https://doi.org/10.1016/S0040-4039\(97\)10293-3](https://doi.org/10.1016/S0040-4039(97)10293-3).
- (233) Krištofiková, D.; Filo, J.; Mečiarová, M.; Šebesta, R. Why Do Thioureas and Squaramides Slow down the Ireland–Claisen Rearrangement? *Beilstein J. Org. Chem.* **2019**, 15 (1), 2948–2957. <https://doi.org/10.3762/bjoc.15.290>.
- (234) Furniss, B. S.; Hannaford, A. J.; Smith, P. W. G.; Tatchell, A. R. *Vogel's TEXTBOOK OF PRACTICAL ORGANIC CHEMISTRY*, 5th ed.; Longman Scientific & Technical: Essex, UK, 1989.

- <https://doi.org/10.1002/pola.1991.080290821>.
- (235) Frigerio, M.; Santagostino, M.; Sputore, S. A User-Friendly Entry to 2-Iodoxybenzoic Acid (IBX). *J. Org. Chem.* **1999**, *64* (12), 4537–4538. <https://doi.org/10.1021/jo9824596>.
- (236) Bailey, D. J.; O'Hagan, D.; Tavasli, M. A Short Synthesis of (S)-2-(Diphenylmethyl) Pyrrolidine, a Chiral Solvating Agent for NMR Analysis. *Tetrahedron Asymmetry* **1997**, *8* (1), 149–153. [https://doi.org/10.1016/S0957-4166\(96\)00495-8](https://doi.org/10.1016/S0957-4166(96)00495-8).
- (237) Ho, C. Y.; Chen, Y. C.; Wong, M. K.; Yang, D. Fluorinated Chiral Secondary Amines as Catalysts for Epoxidation of Olefins with Oxone. *J. Org. Chem.* **2005**, *70* (3), 898–906. <https://doi.org/10.1021/jo048378t>.
- (238) Wang, Z.; Wang, C.; Zhou, L.; Sun, J. L-Pipecolinic Acid Derived Lewis Base Organocatalyst for Asymmetric Reduction of N-Aryl Imines by Trichlorosilane: Effects of the Side Amide Group on Catalytic Performances. *Org. Biomol. Chem.* **2013**, *11* (5), 787–797. <https://doi.org/10.1039/c2ob26772a>.
- (239) Yu, L.; Li, P. New Simple Primary Amine-Thiourea Organocatalysts and Their Application in Asymmetric Conjugate Addition. *Tetrahedron Lett.* **2014**, *55* (27), 3697–3700. <https://doi.org/10.1016/j.tetlet.2014.05.006>.
- (240) Kim, H. Y.; Oh, K. Highly Diastereo- and Enantioselective Aldol Reaction of Methyl α -Isocyanoacetate: A Cooperative Catalysis Approach. *Org. Lett.* **2011**, *13* (6), 1306–1309. <https://doi.org/10.1021/ol103104y>.
- (241) Isobe, T.; Fukuda, K.; Ishikawa, T. Simple Preparation of Chiral 1,3-Dimethyl-2-Iminoimidazolidines (Monocyclic Guanidines) and Applications to Asymmetric Alkylative Esterification. *Tetrahedron Asymmetry* **1998**, *9* (10), 1729–1735. [https://doi.org/10.1016/S0957-4166\(98\)00152-9](https://doi.org/10.1016/S0957-4166(98)00152-9).
- (242) Isobe, T.; Fukuda, K.; Ishikawa, T. Modified Guanidines as Potential Chiral Superbases. 1. Preparation of 1,3-Disubstituted 2-Iminoimidazolidines and the Related Guanidines through Chloroamidine Derivatives. *J. Org. Chem.* **2000**, *65* (23), 7770–7773.

<https://doi.org/10.1021/jo000744v>.

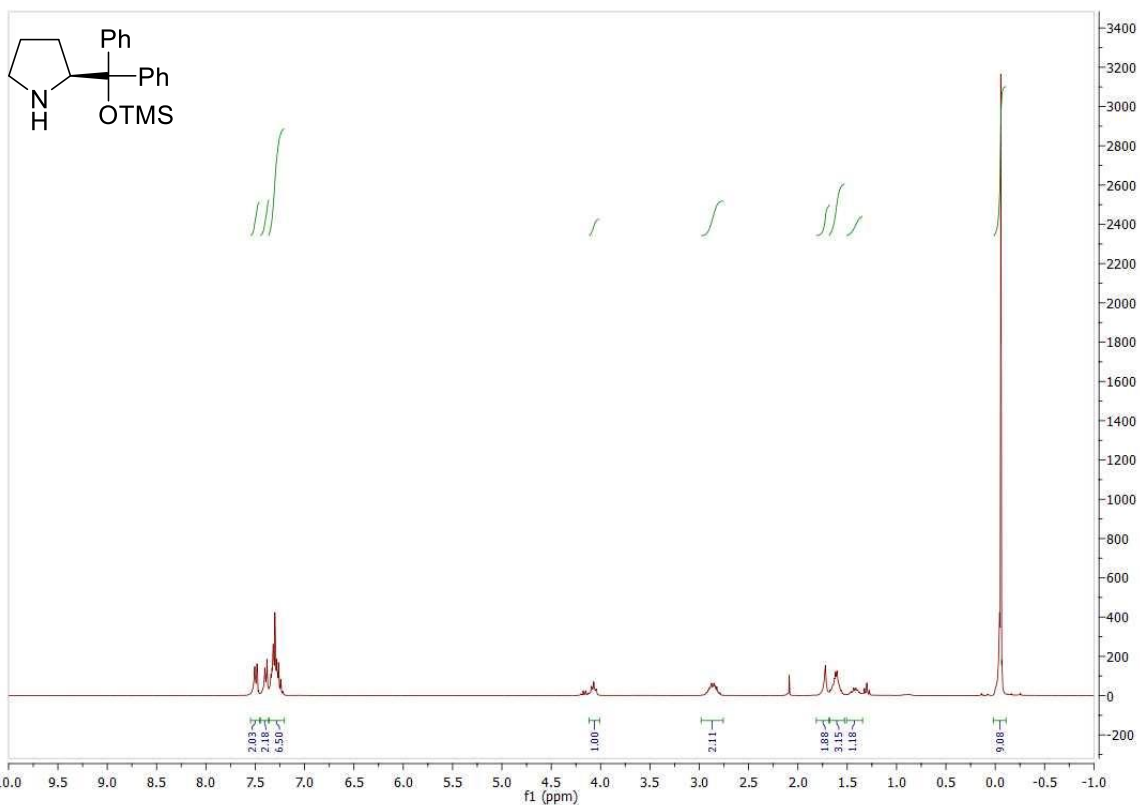
- (243) Dahlin, N.; Bøgevig, A.; Adolfsson, H. N-Arenesulfonyl-2-Aminomethylpyrrolidines - Novel Modular Ligands and Organocatalysts for Asymmetric Catalysis. *Adv. Synth. Catal.* **2004**, *346* (9–10), 1101–1105. <https://doi.org/10.1002/adsc.200404098>.
- (244) Cao, C. L.; Ye, M. C.; Sun, X. L.; Tang, Y. Pyrrolidine-Thiourea as a Bifunctional Organocatalyst: Highly Enantioselective Michael Addition of Cyclohexanone to Nitroolefins. *Org. Lett.* **2006**, *8* (14), 2901–2904. <https://doi.org/10.1021/ol060481c>.
- (245) Wilson, R. M.; Thalji, R. K.; Bergman, R. G.; Ellman, J. A. Enantioselective Synthesis of a PKC Inhibitor via Catalytic C-H Bond Activation. *Org. Lett.* **2006**, *8* (8), 1745–1747. <https://doi.org/10.1021/ol060485h>.
- (246) Pirovano, V.; Arpini, E.; Dell'Acqua, M.; Vicente, R.; Abbiati, G.; Rossi, E. Gold(I)-Catalyzed Synthesis of Tetrahydrocarbazoles via Cascade [3,3]-Propargylic Rearrangement/[4+2] Cycloaddition of Vinylindoles and Propargylic Esters. *Adv. Synth. Catal.* **2016**, *358* (3), 403–409. <https://doi.org/10.1002/adsc.201500913>.
- (247) Monari, M.; Montroni, E.; Nitti, A.; Lombardo, M.; Trombini, C.; Quintavalla, A. Highly Stereoselective [4+2] and [3+2] Spiroannulations of 2-(2-Oxoindolin-3-ylidene)Acetic Esters Catalyzed by Bifunctional Thioureas. *Chem. - A Eur. J.* **2015**, *21* (31), 11038–11049. <https://doi.org/10.1002/chem.201500676>.
- (248) Cokun, N.; Erden, I. An Efficient Catalytic Method for Fulvene Synthesis. *Tetrahedron* **2011**, *67* (45), 8607–8614. <https://doi.org/10.1016/j.tet.2011.09.036>.

Part VI – Annexes

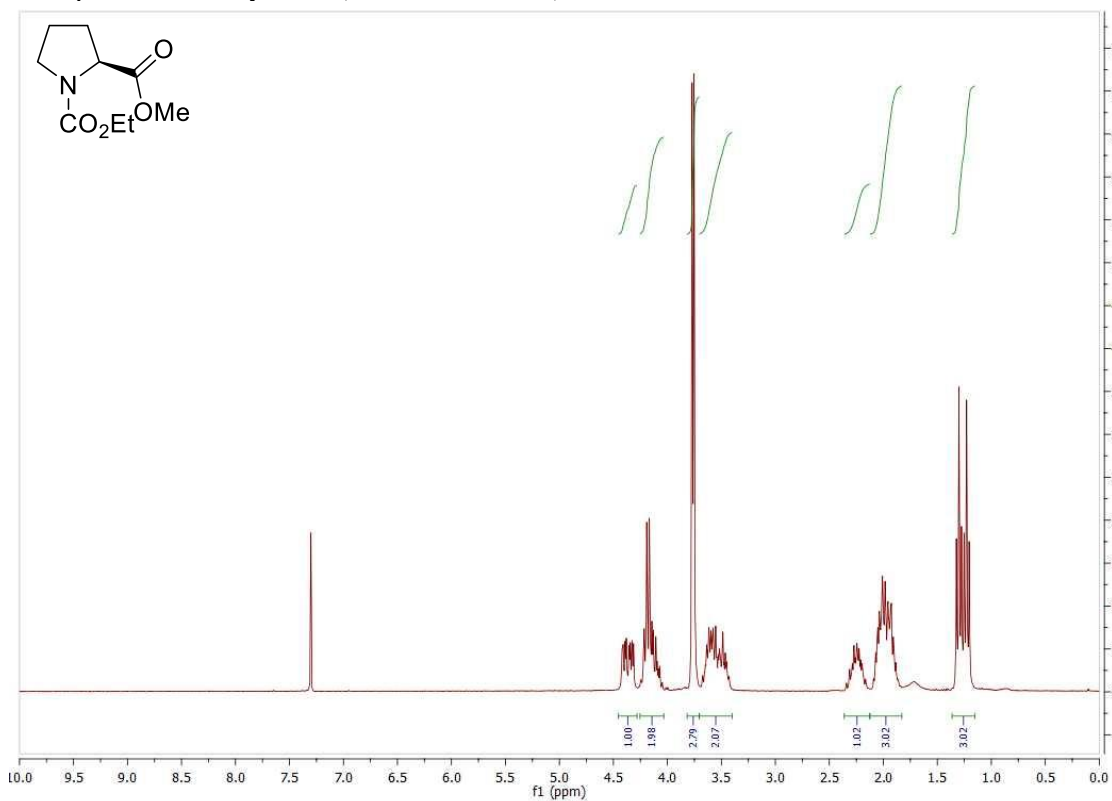


¹H NMR spectra of IBX (300 MHz in DMSO-d₆).

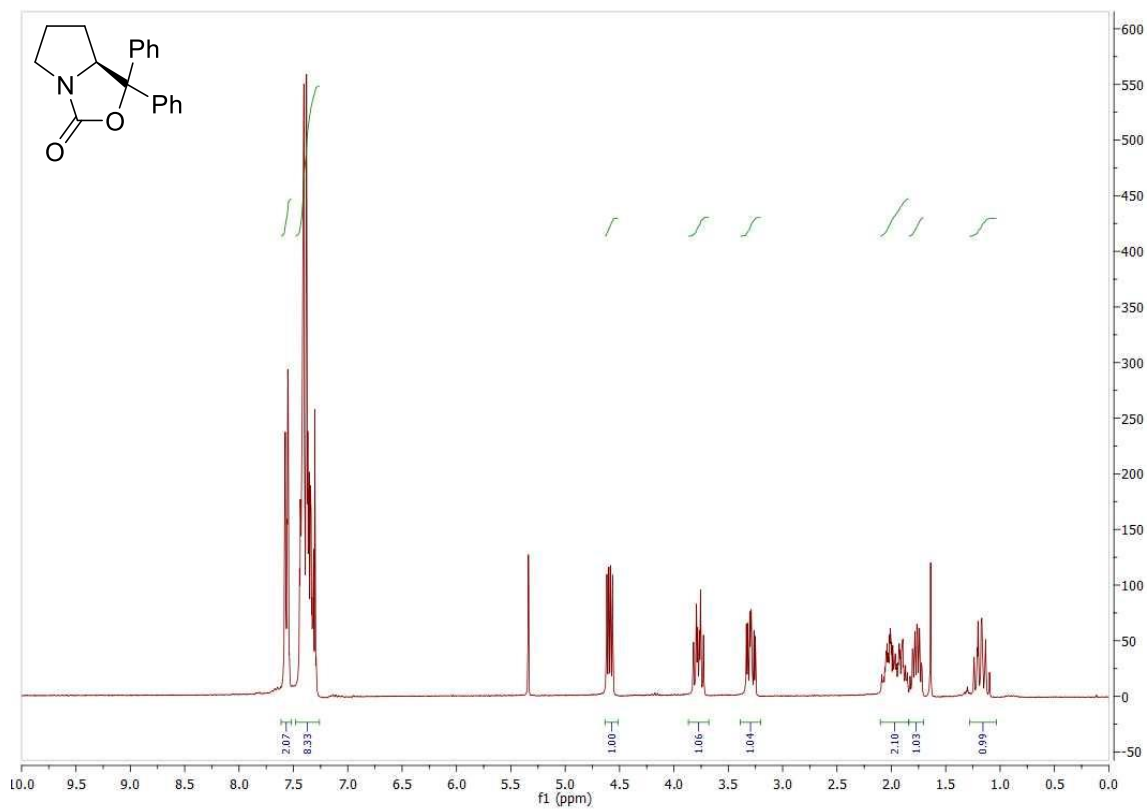
NMR Spectra of Catalysts



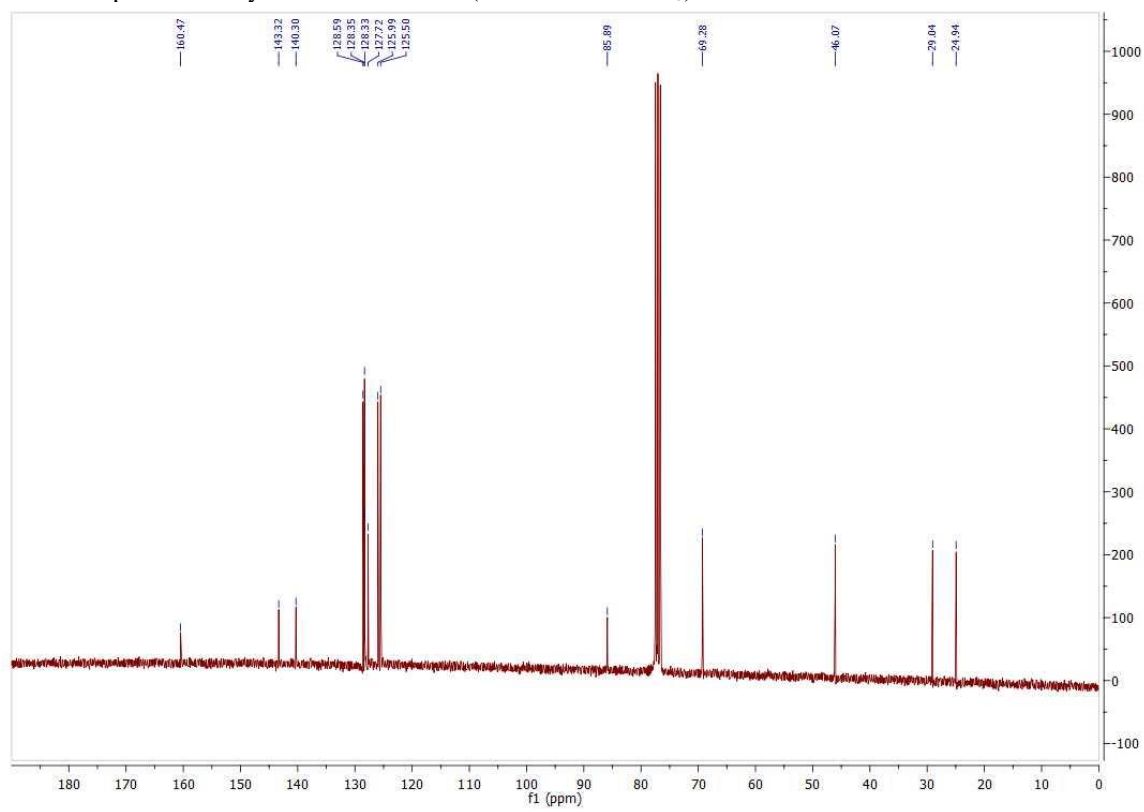
¹H NMR spectrum of catalyst **IIIa** (300 MHz in CDCl₃).



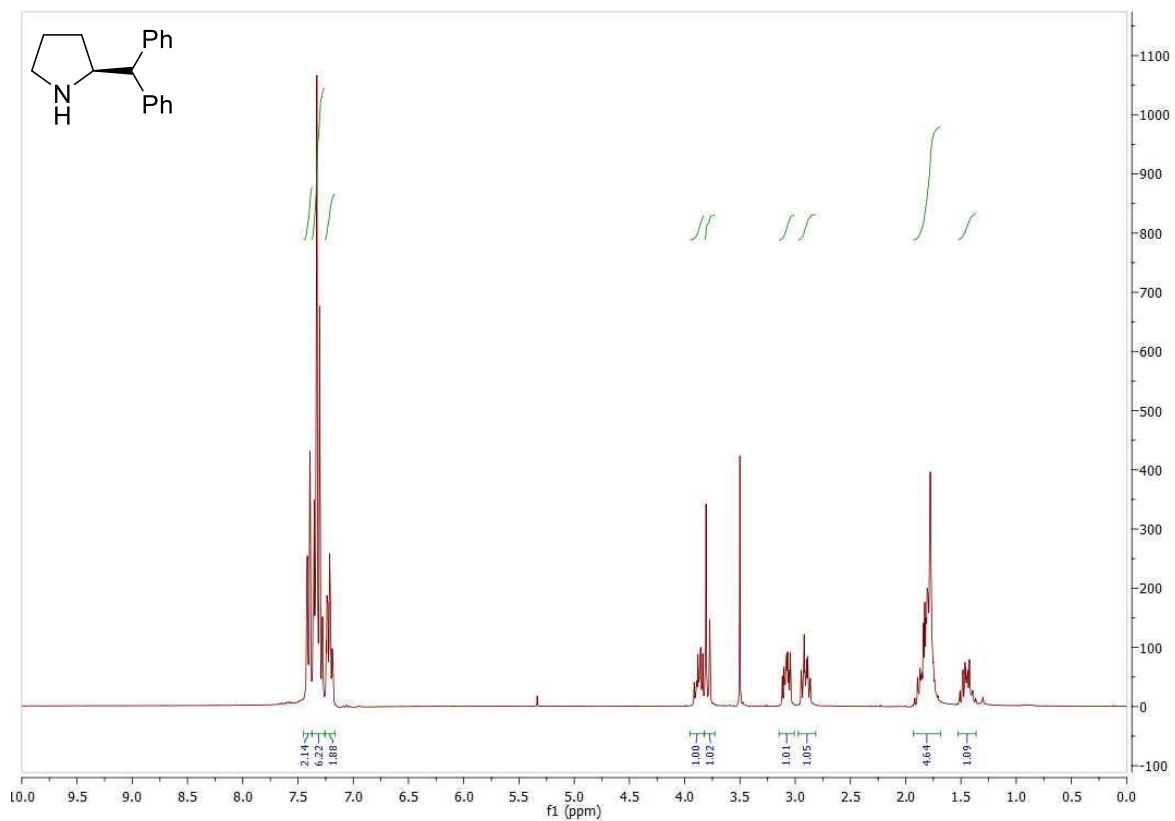
¹H NMR spectrum of carbamate **179** (300 MHz in CDCl₃).



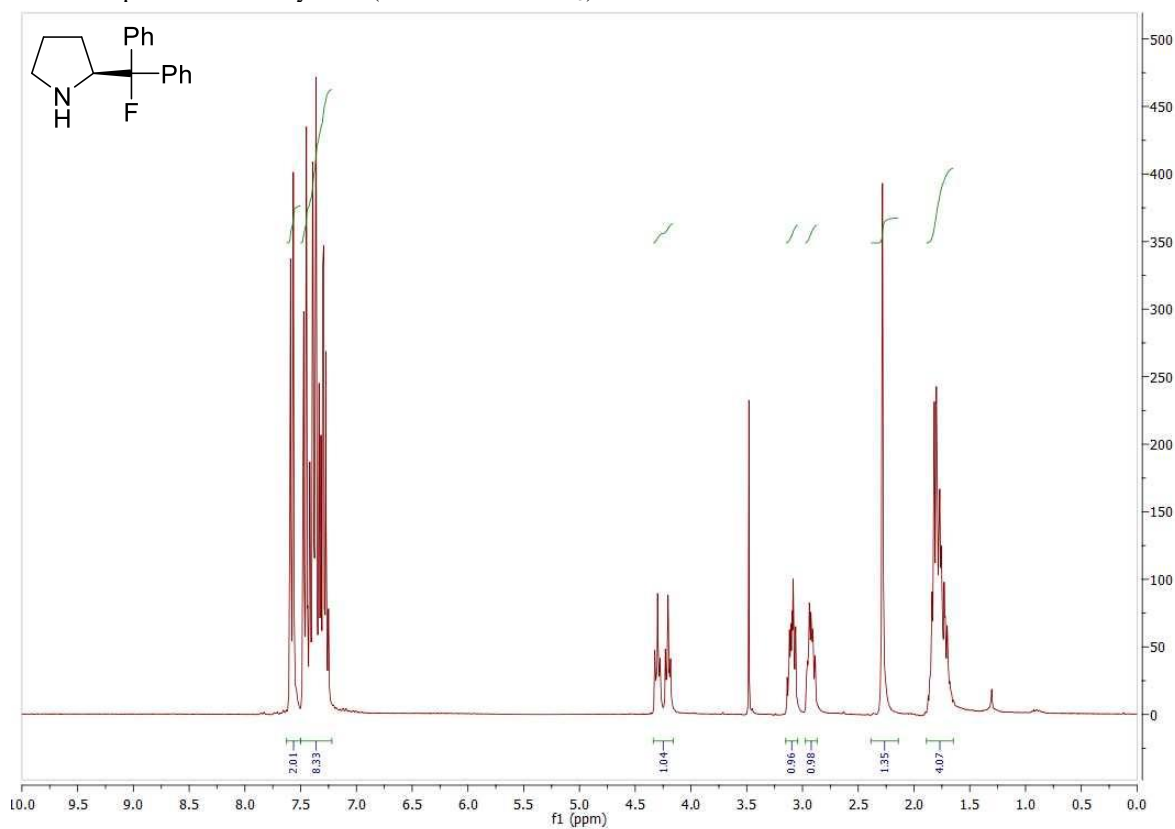
¹H NMR spectrum of cyclic carbamate **180** (300 MHz in CDCl₃).



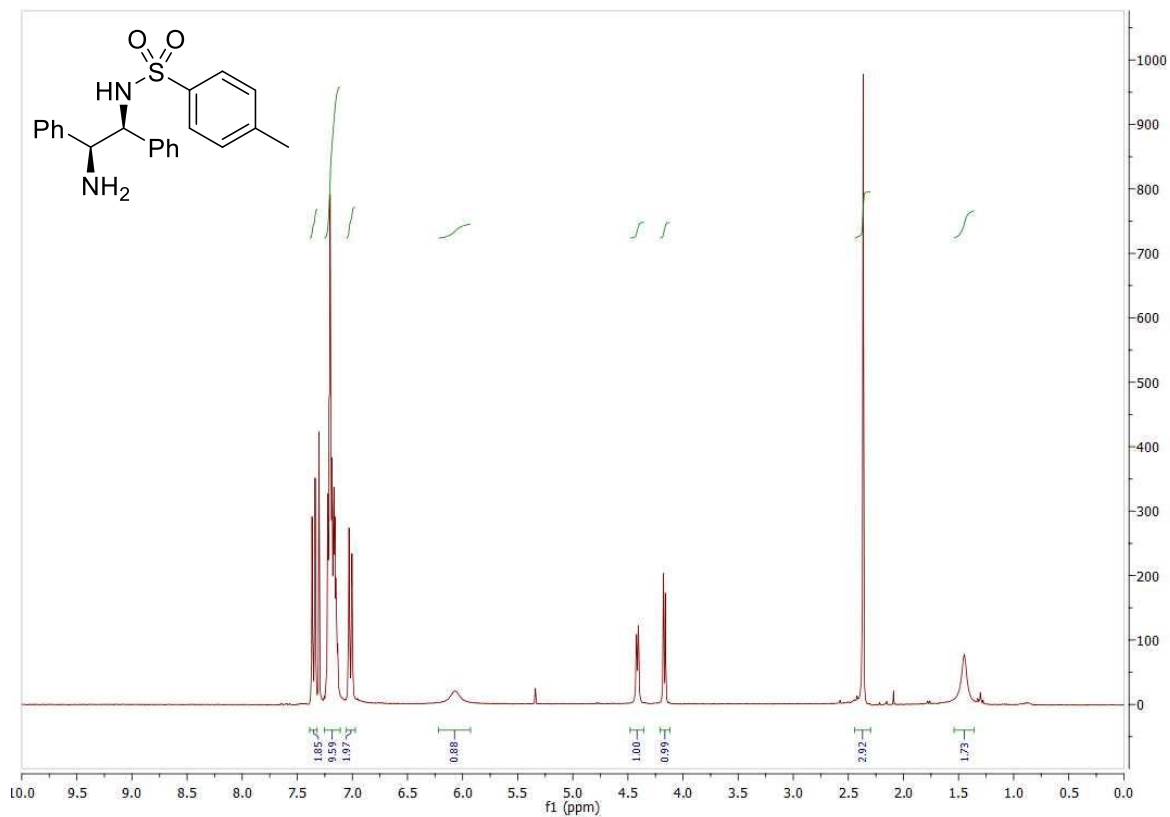
¹³C NMR spectrum of cyclic carbamate **180** (75 MHz in CDCl₃).



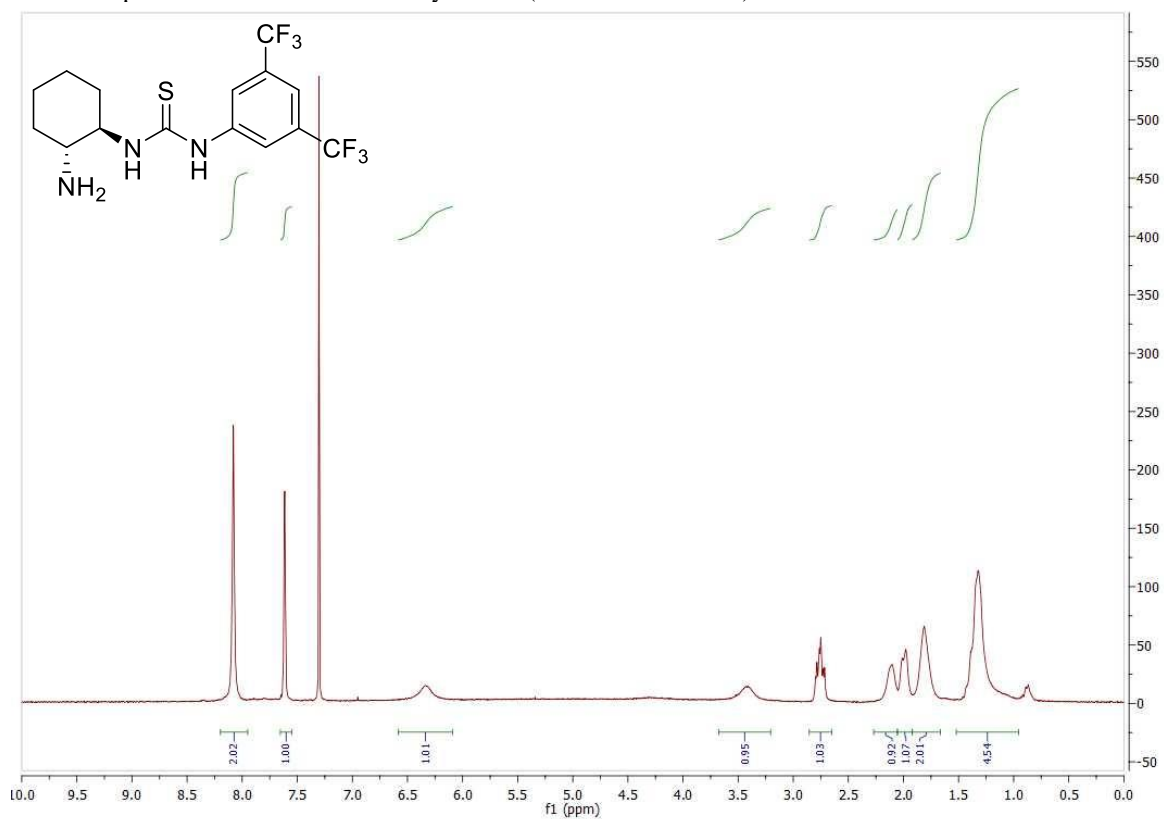
^1H NMR spectrum of catalyst **IV** (300 MHz in CDCl_3).



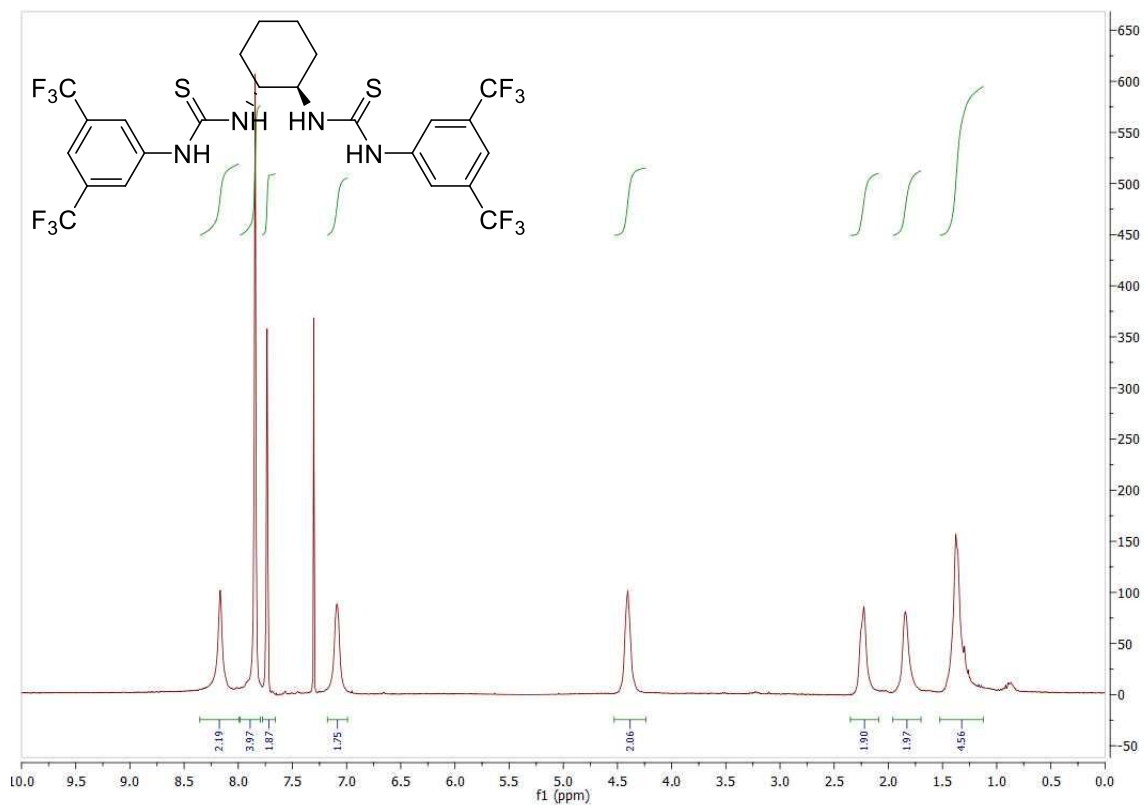
^1H NMR spectrum of catalyst **XII** (300 MHz in CDCl_3).



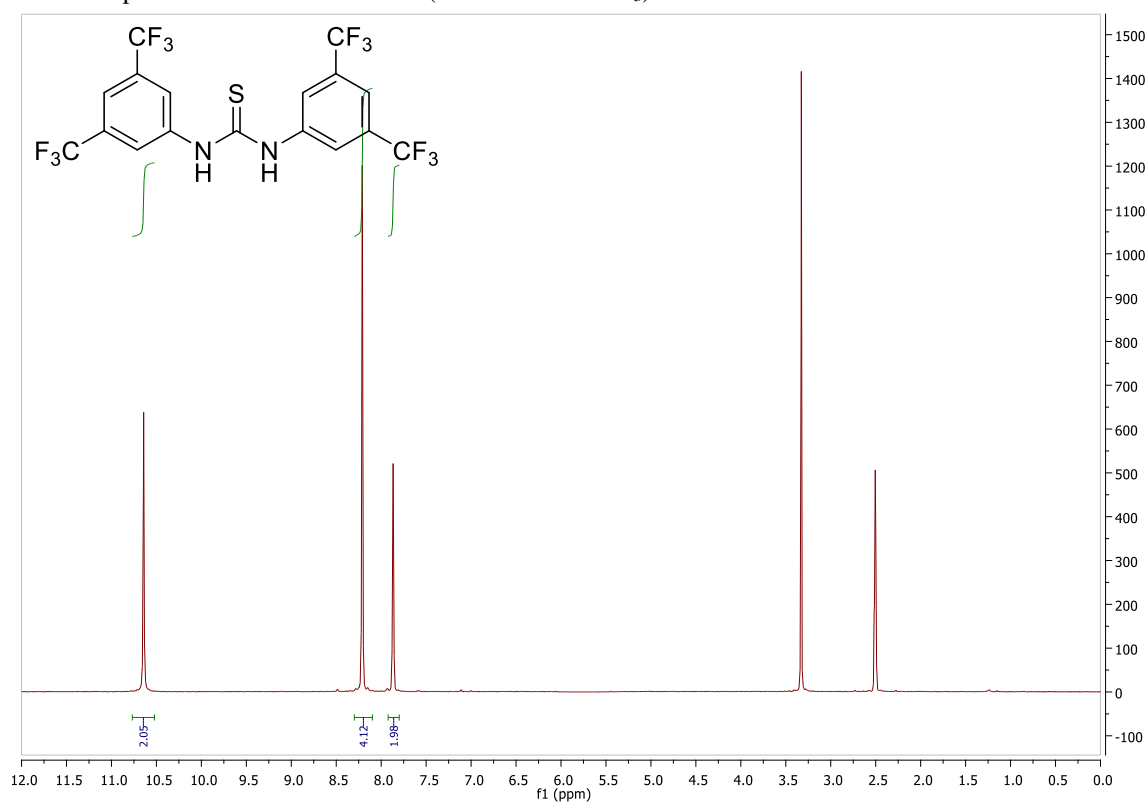
¹H NMR spectrum of bifunctional catalyst **XIII** (300 MHz in CDCl₃).



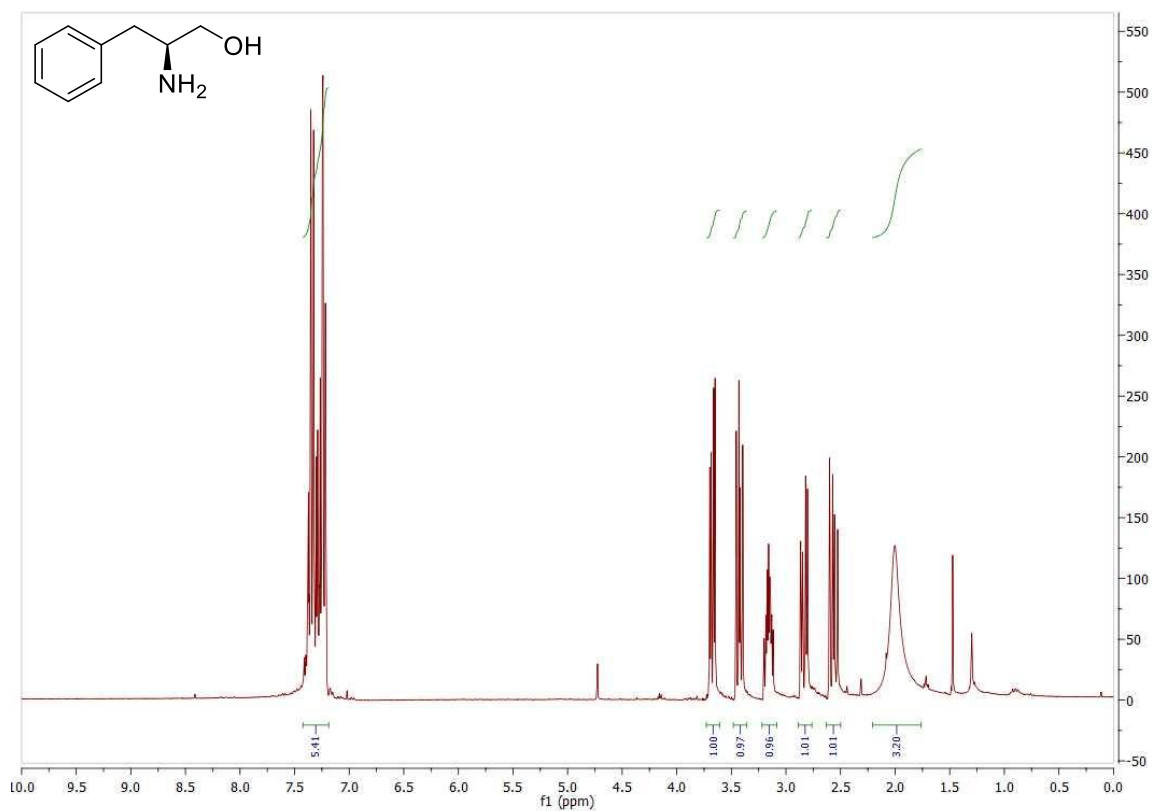
¹H NMR spectrum of bifunctional catalyst **XIV** (300 MHz in CDCl₃).



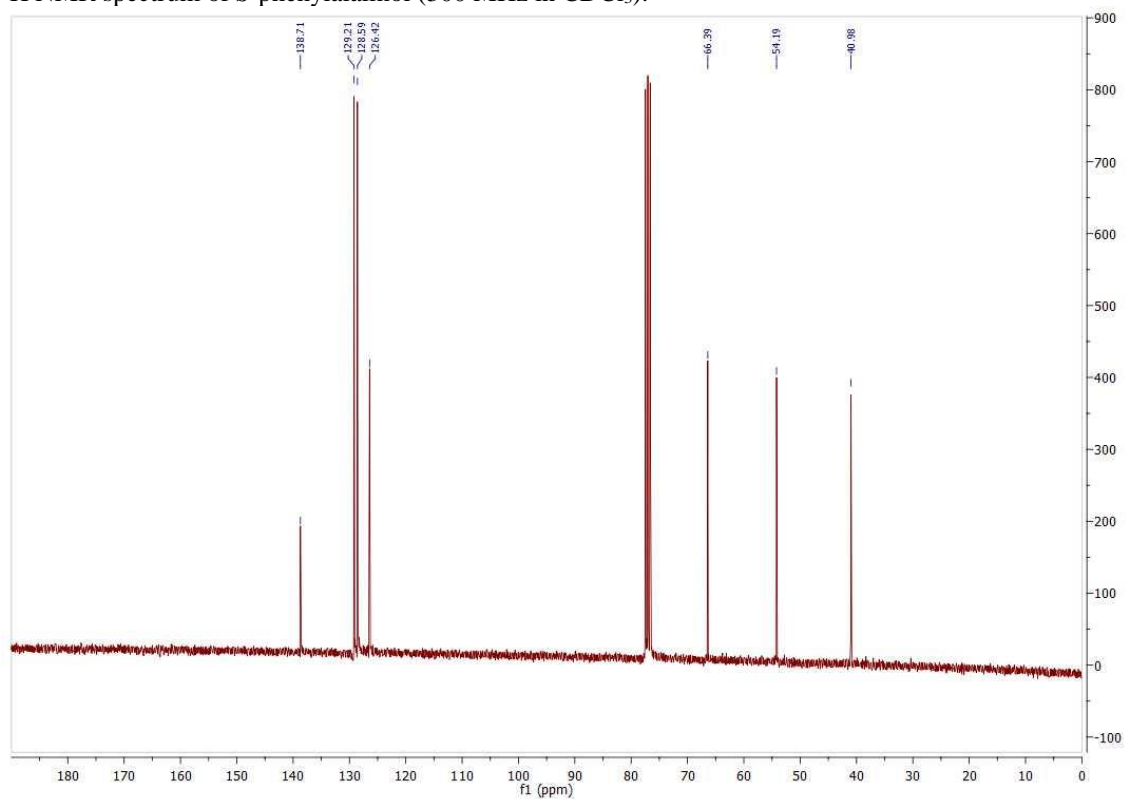
¹H NMR spectrum of bithiourea **XXI** (300 MHz in CDCl₃).



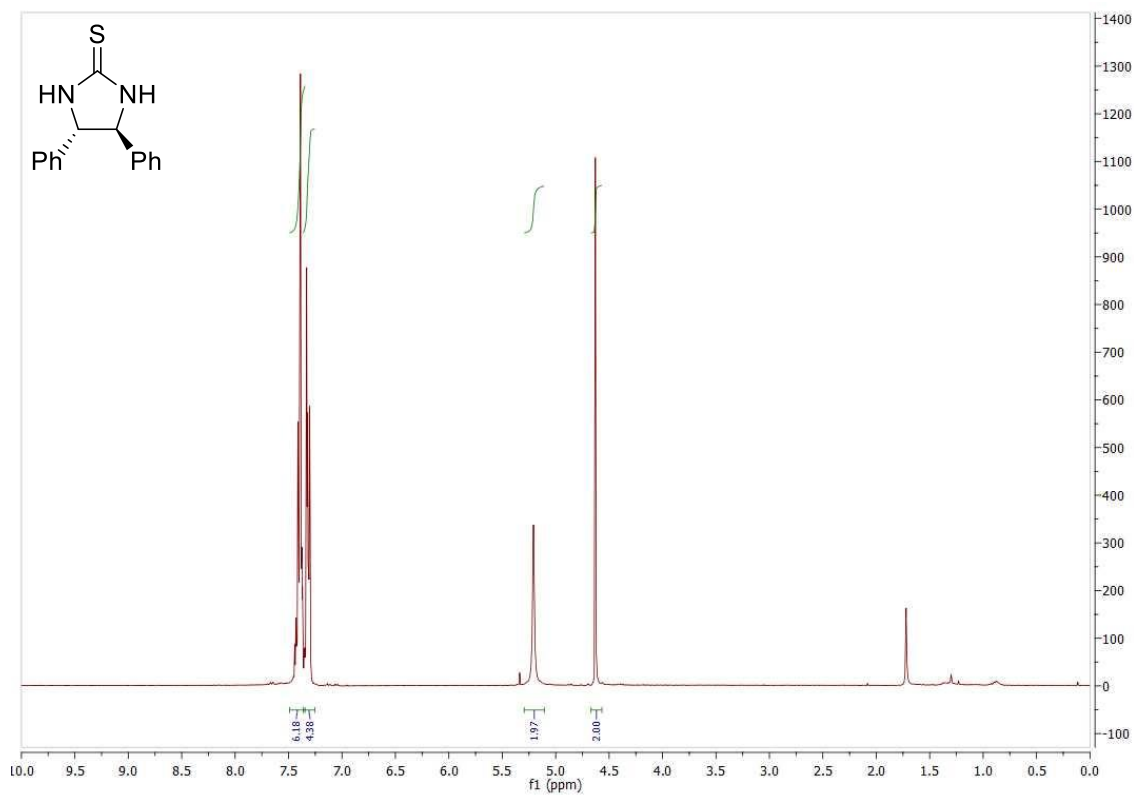
¹H NMR spectrum of thiourea **XIX** (300 MHz in DMSO-d₆).



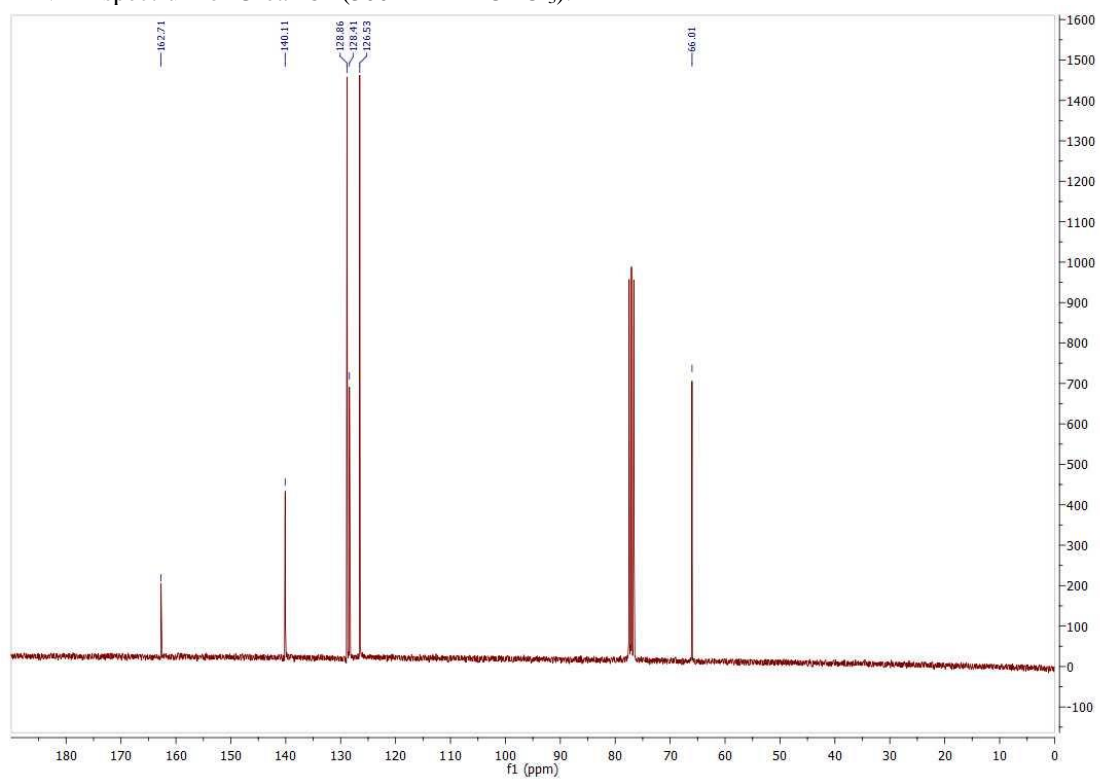
¹H NMR spectrum of *S*-phenylalalinol (300 MHz in CDCl₃).



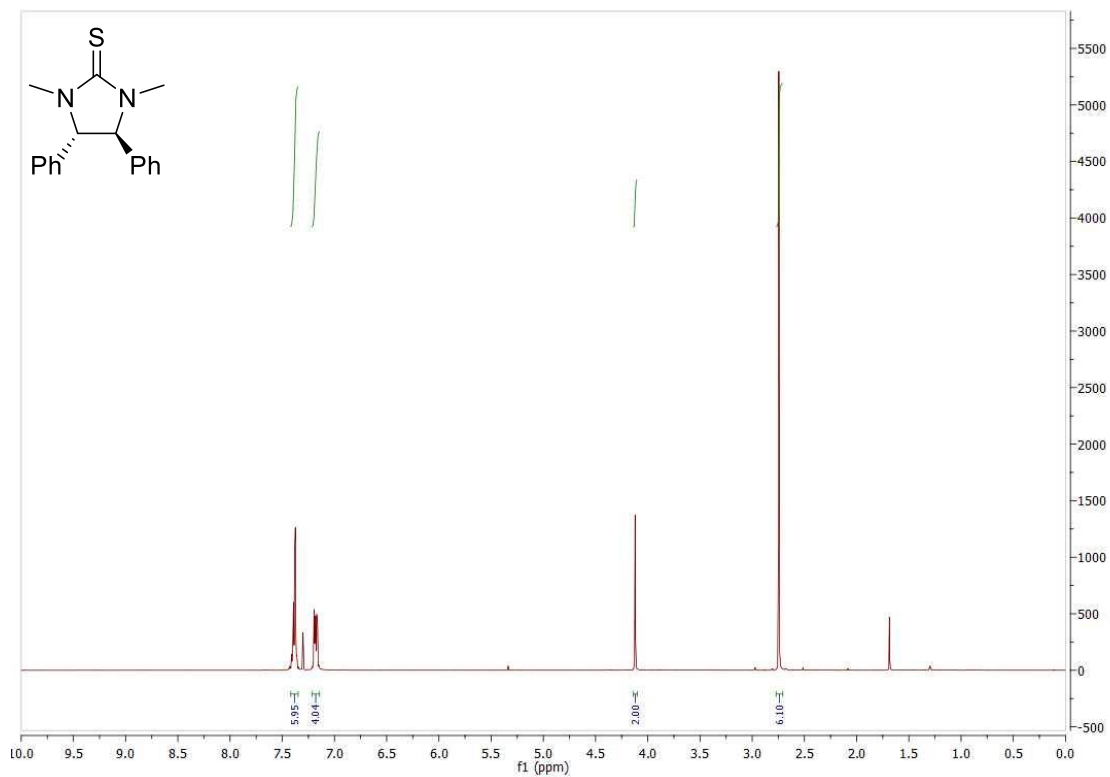
¹³C NMR spectrum of *S*-phenylalalinol (75 MHz in CDCl₃).



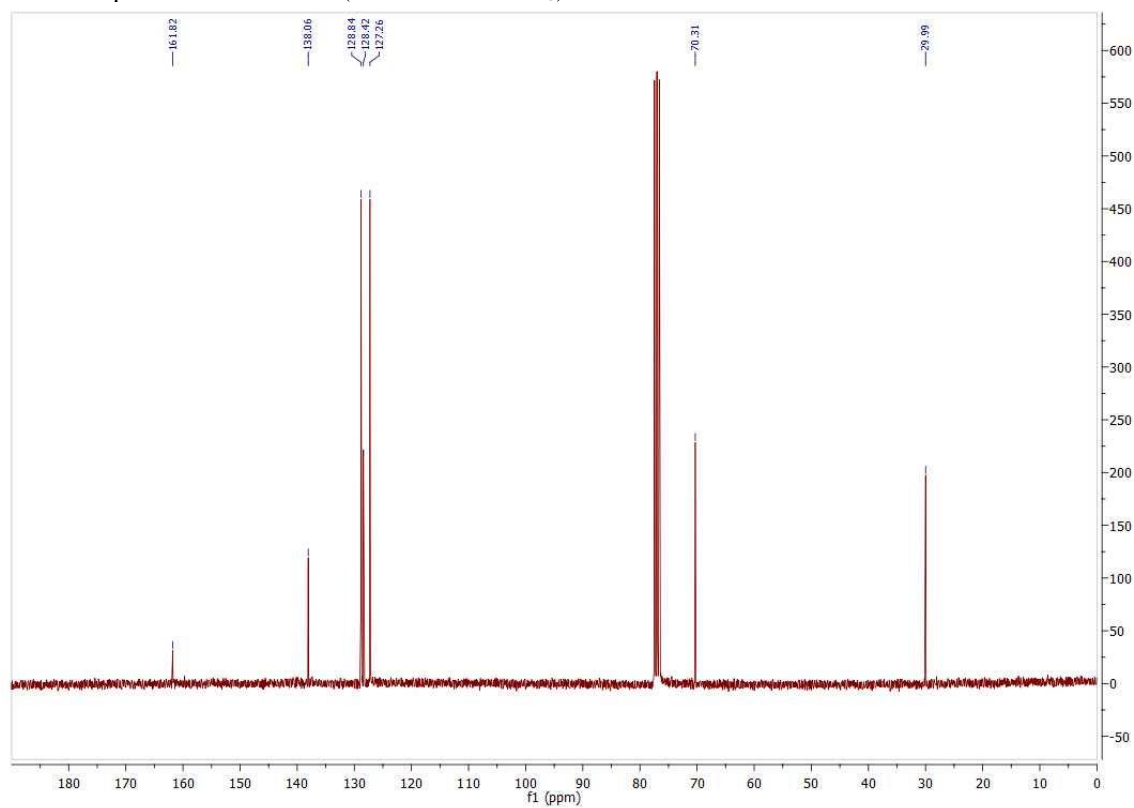
^1H NMR spectrum of Urea **181** (300 MHz in CDCl_3).



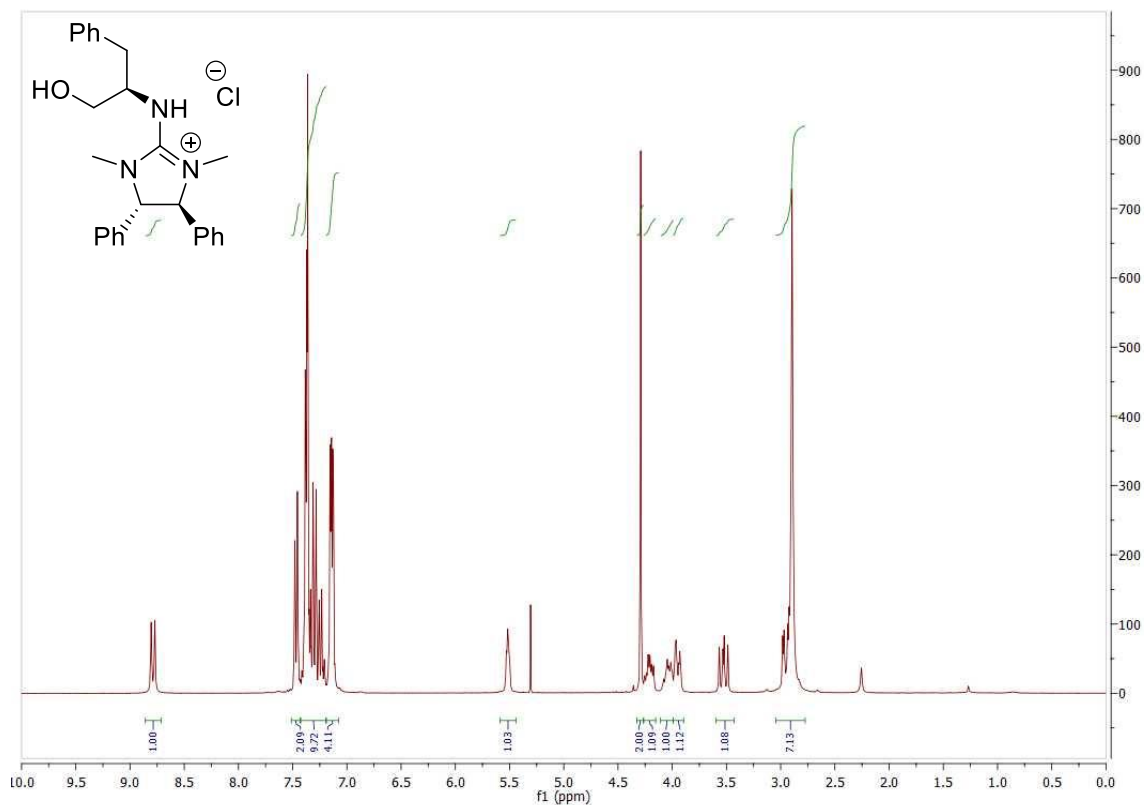
^{13}C NMR spectrum of Urea **181** (75 MHz in CDCl_3).



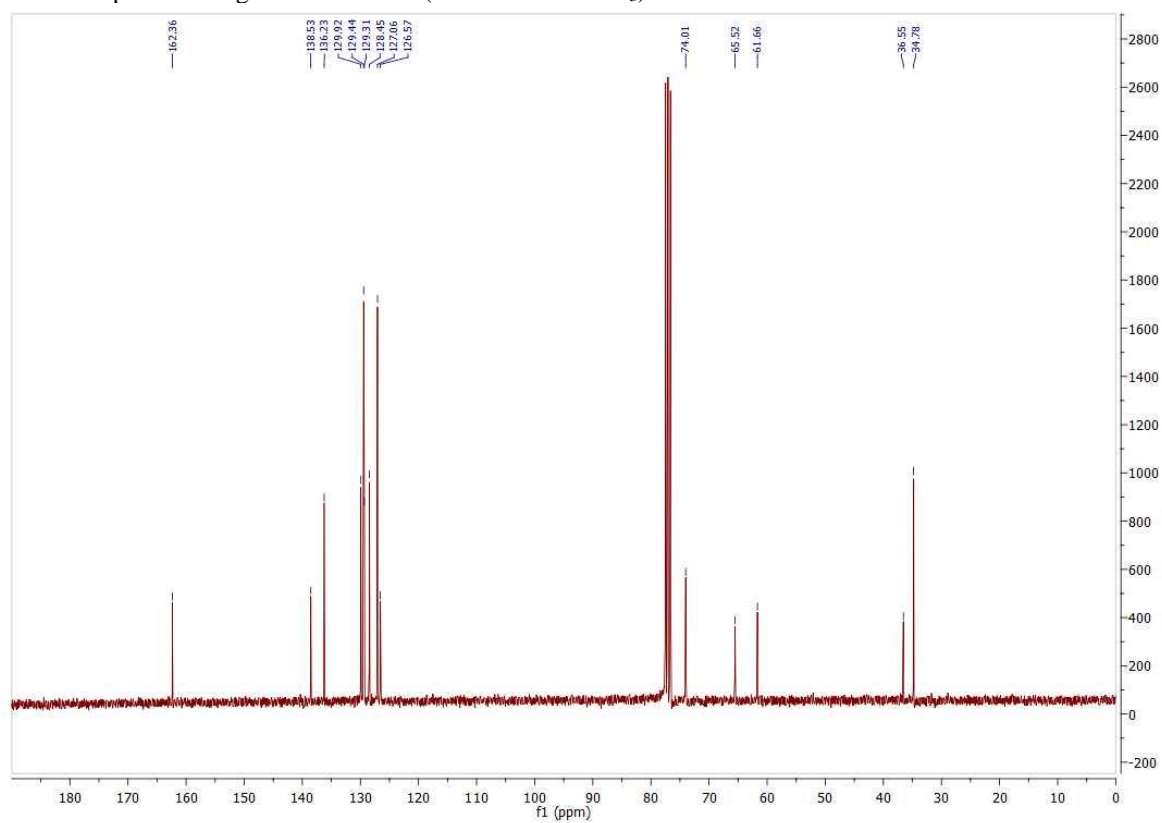
¹H NMR spectrum of Urea **182** (300 MHz in CDCl₃).



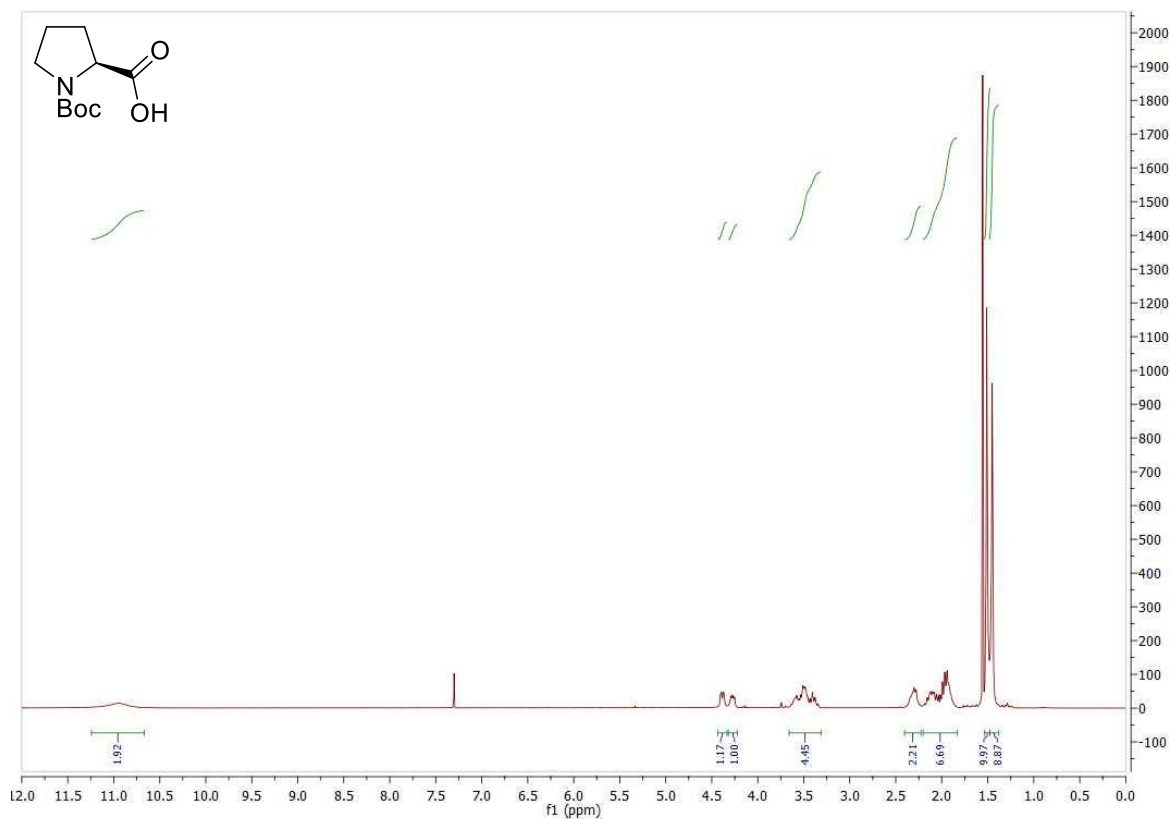
¹³C NMR spectrum of Urea **182** (75 MHz in CDCl₃).



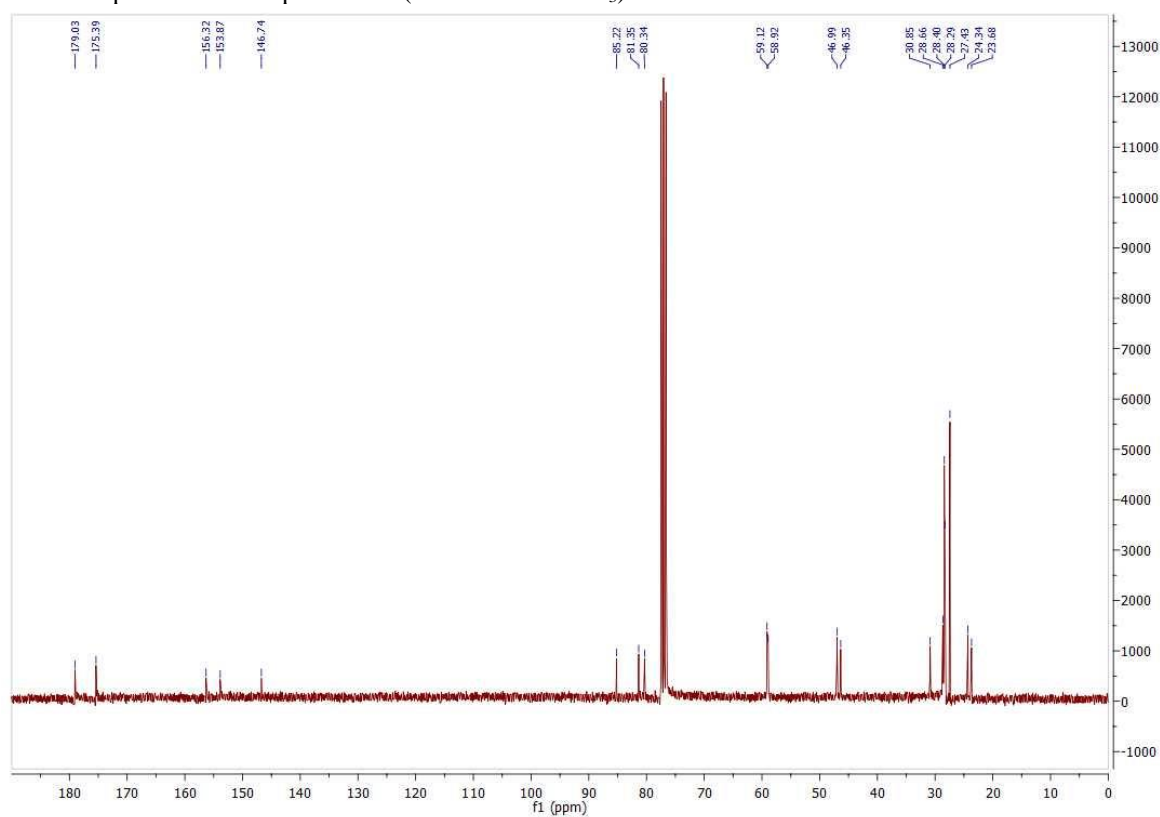
¹H NMR spectrum of guanidinium **XX** (300 MHz in CDCl₃).



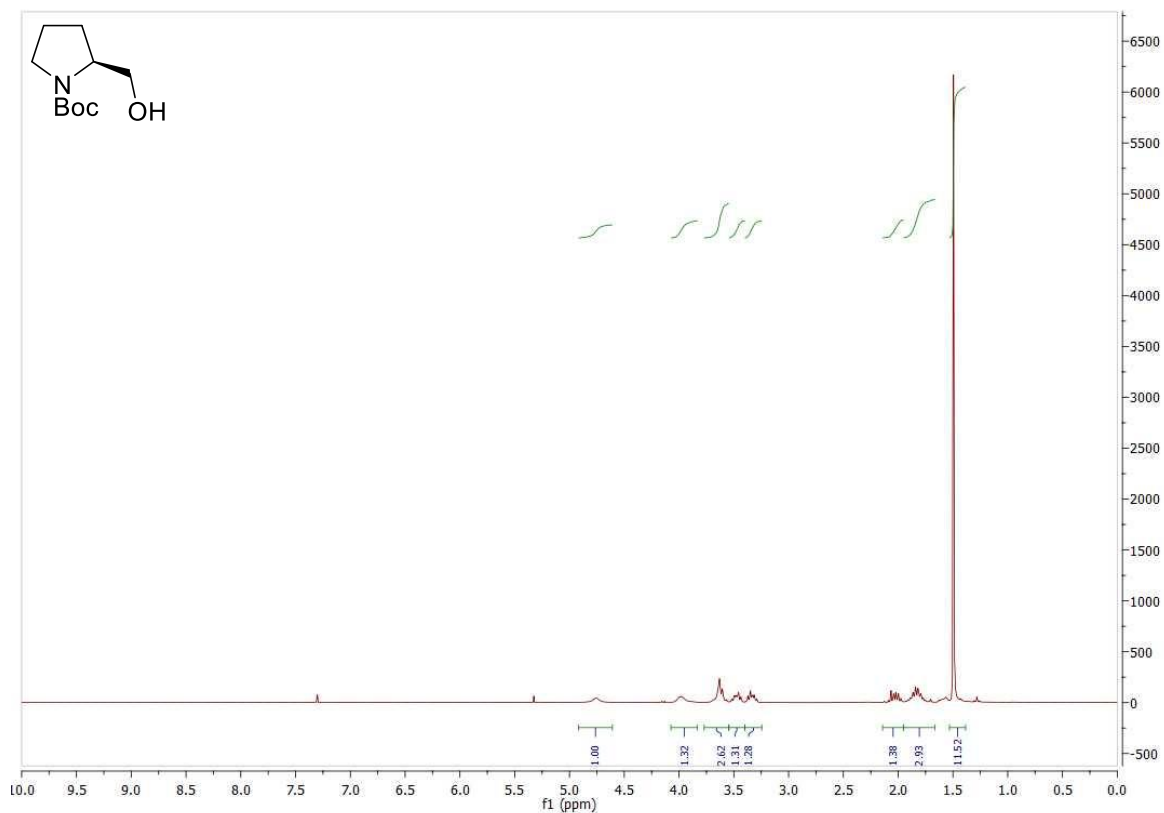
¹³C NMR spectrum of guanidinium **XX** (75 MHz in CDCl₃).



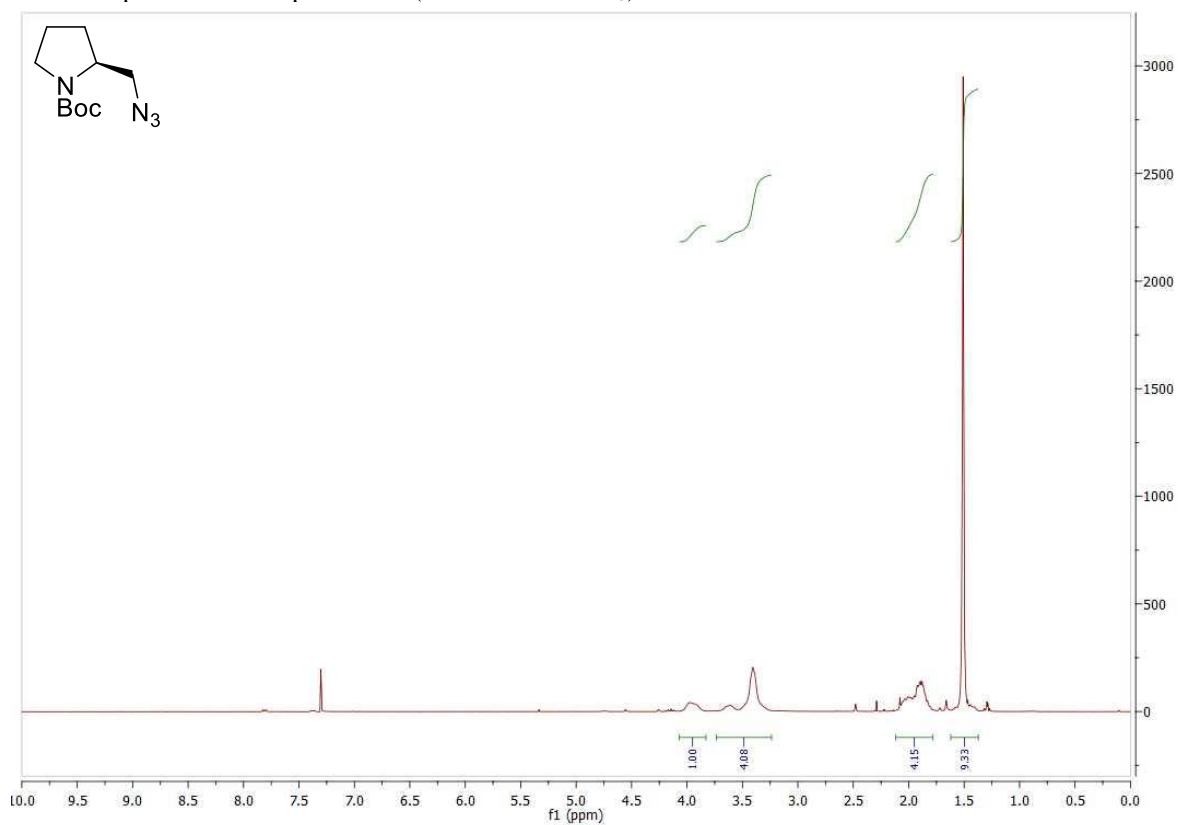
¹H NMR spectrum of compound **184** (300 MHz in CDCl₃).



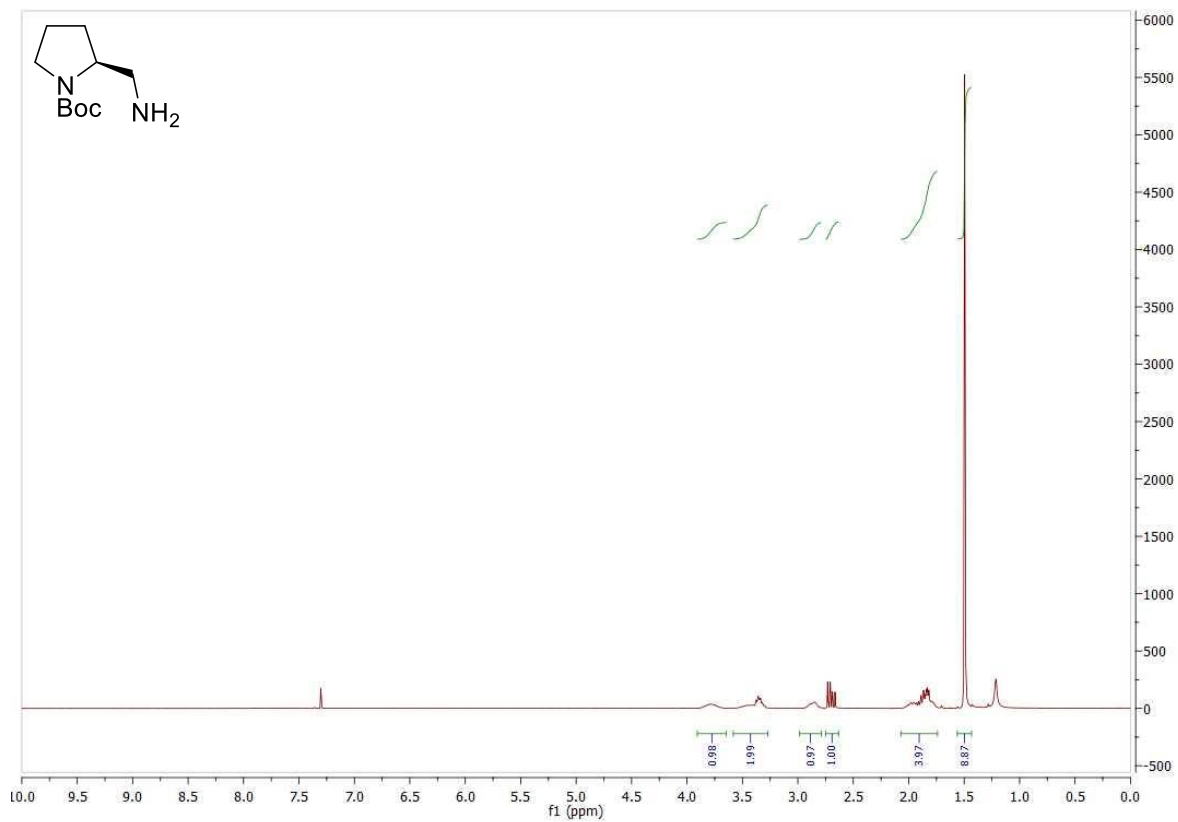
¹³C NMR spectrum of compound **184** (75 MHz in CDCl₃).



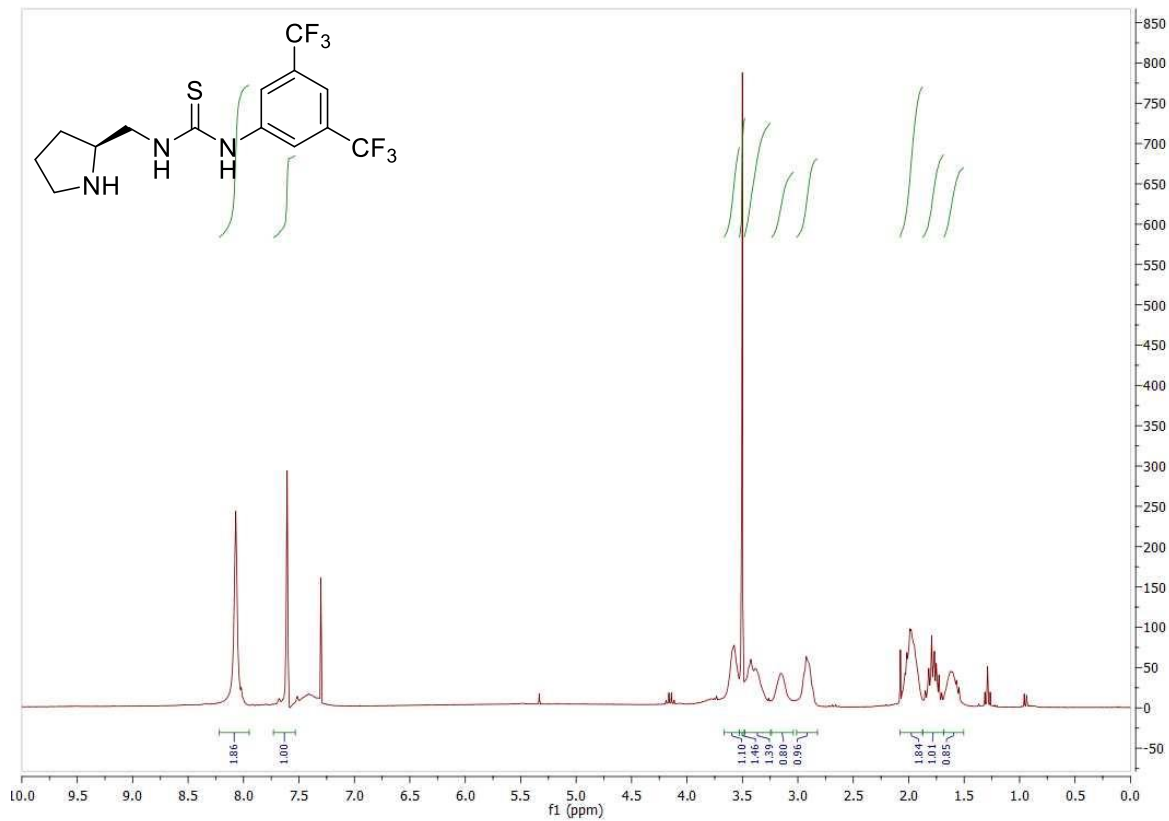
¹H NMR spectrum of compound **185** (300 MHz in CDCl₃).



¹H NMR spectrum of compound **187** (300 MHz in CDCl₃).

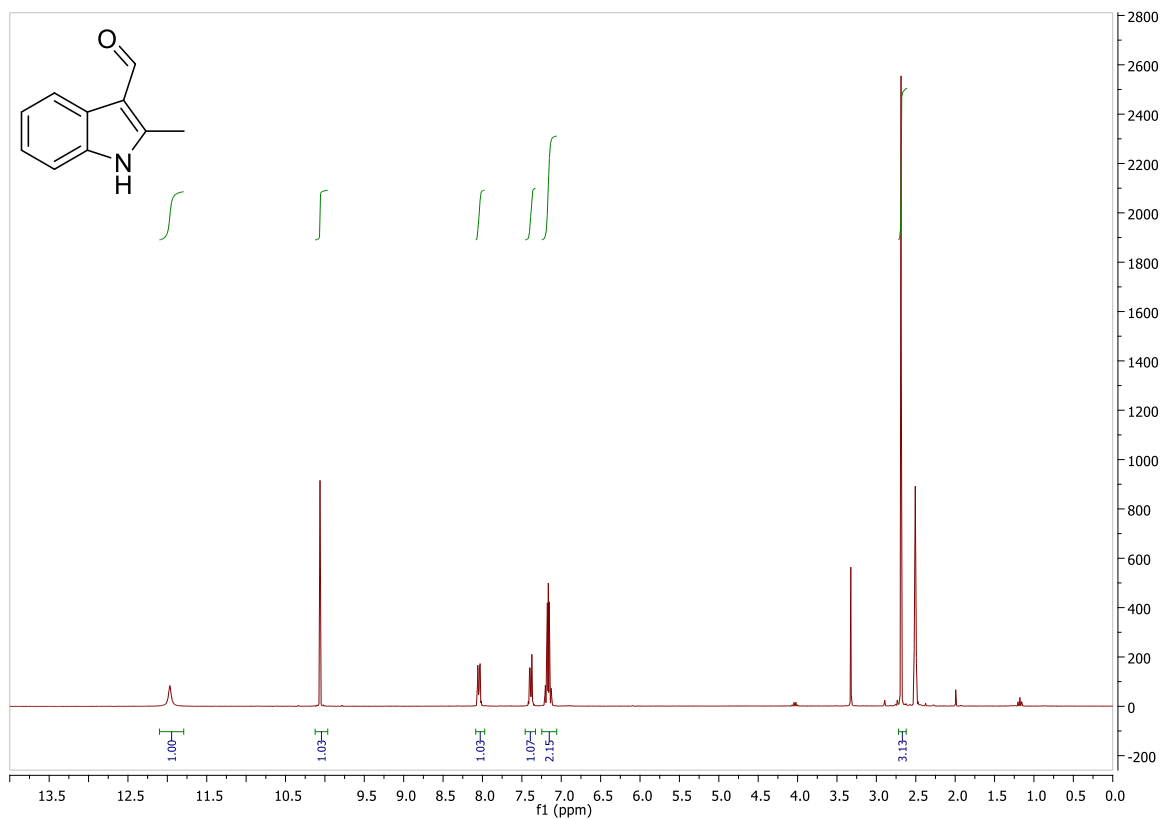


¹H NMR spectrum of compound **188** (300 MHz in CDCl₃).

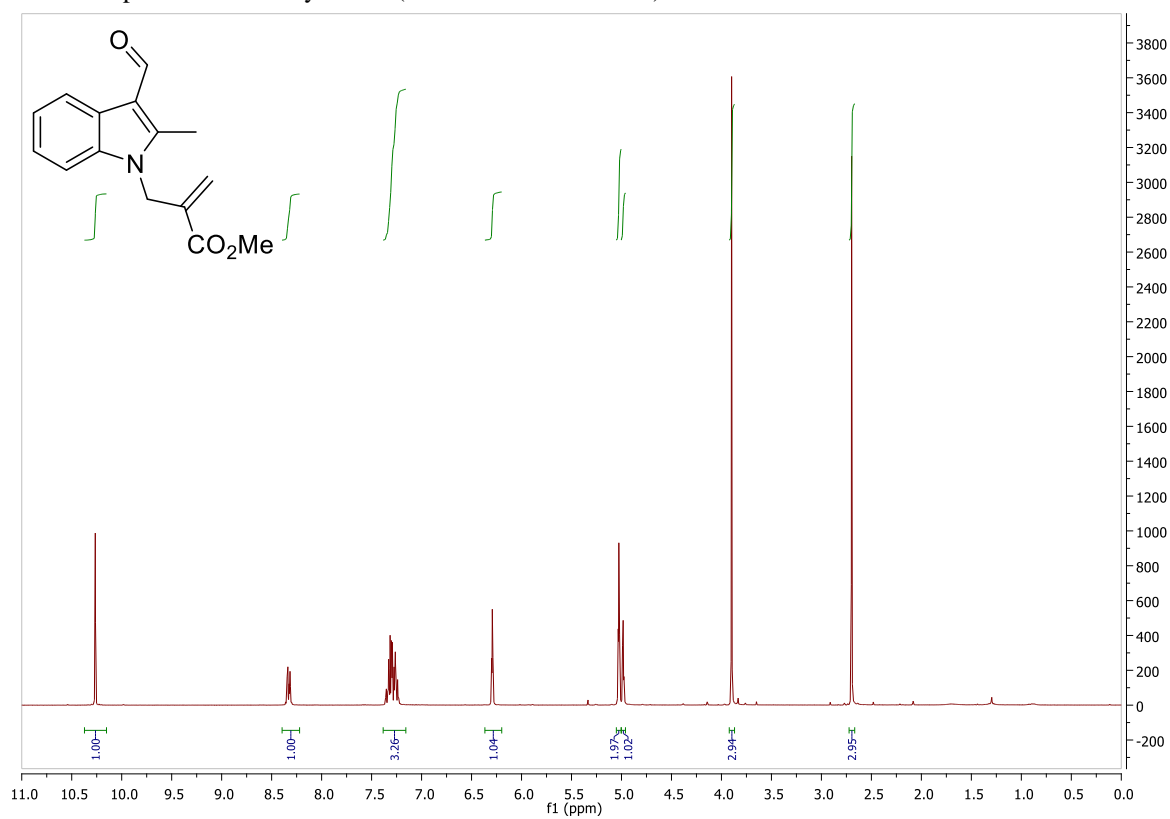


¹H NMR spectrum of bifunctional aminocatalyst **XV** (300 MHz in CDCl₃).

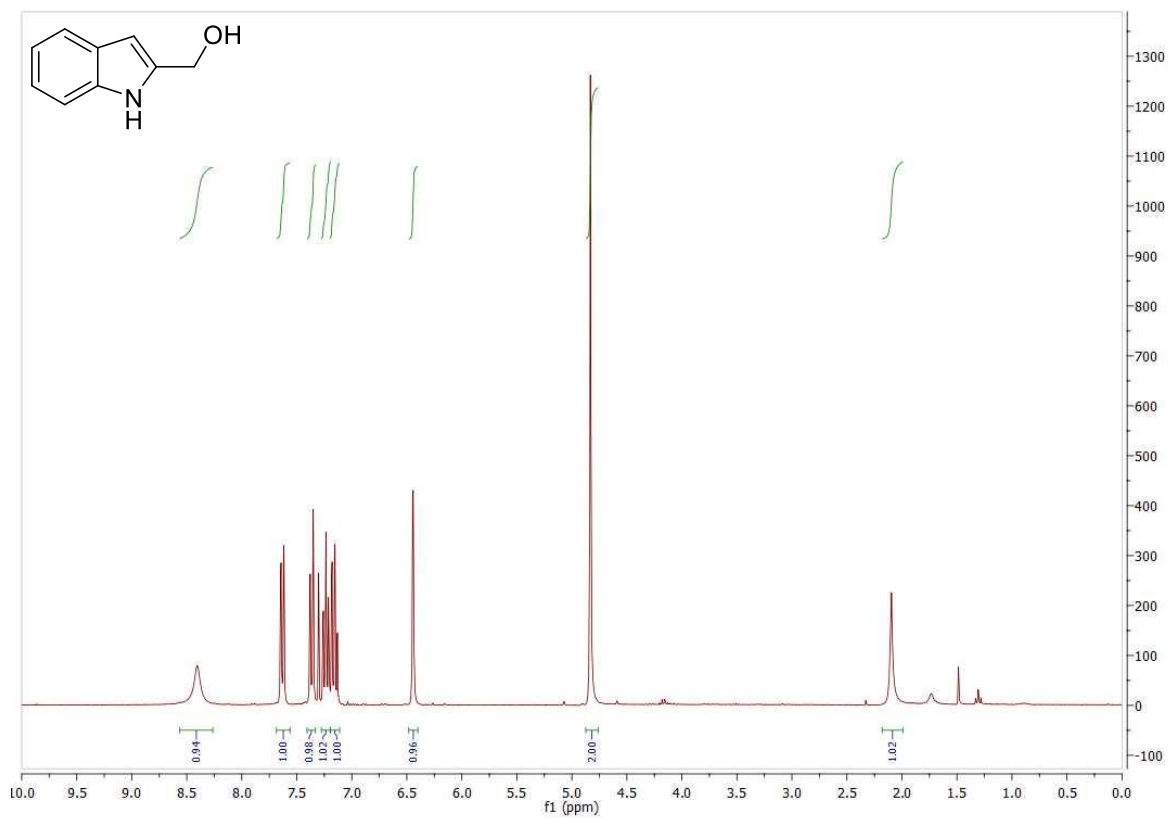
NMR Spectra for the Synthesis of Dihydropyrido[1,2-a]indole Scaffolds



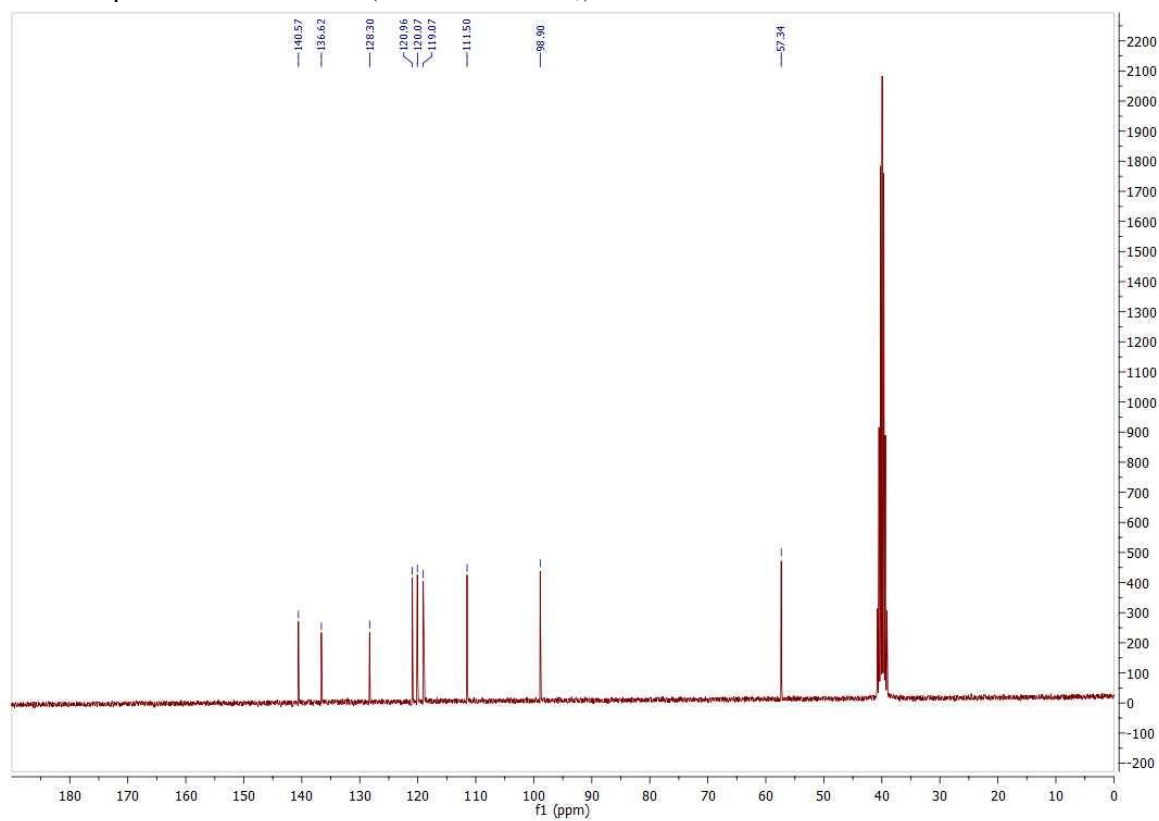
¹H NMR spectrum of aldehyde **189** (300 MHz in DMSO-d₆).



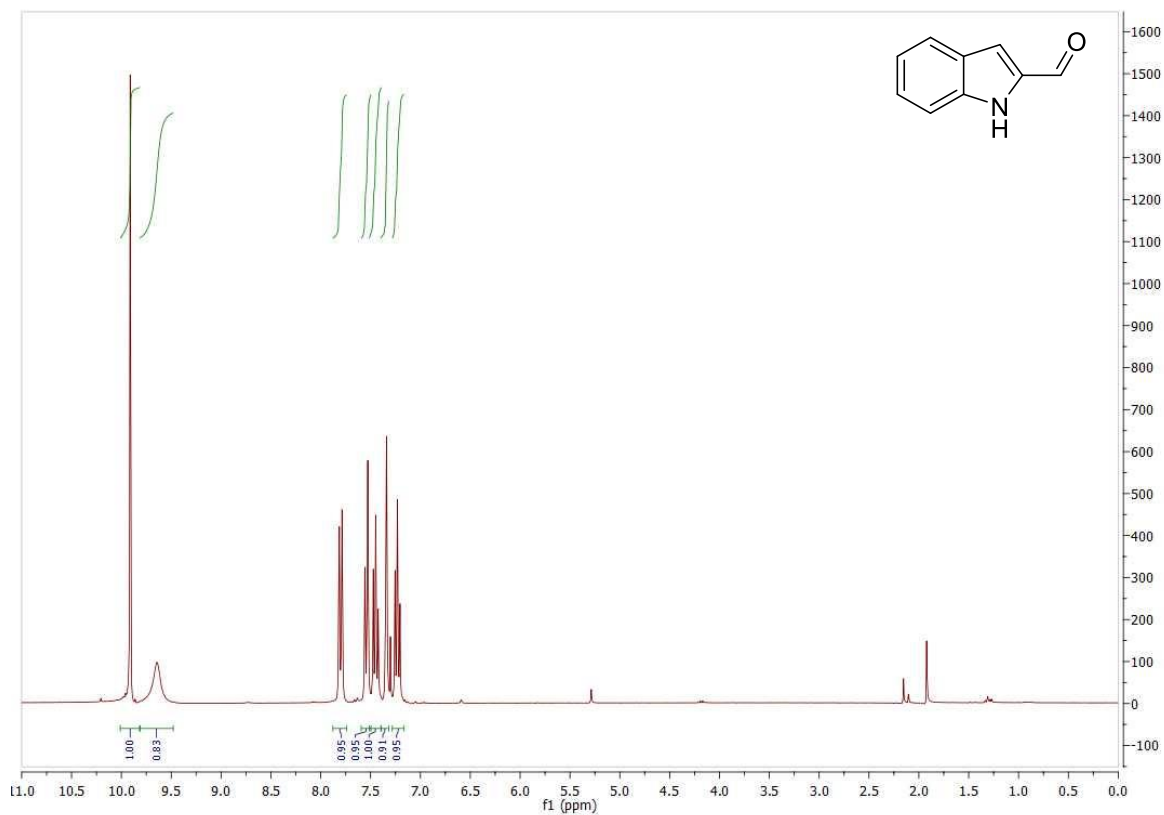
¹H NMR spectrum of compound **131** (300 MHz in CDCl₃).



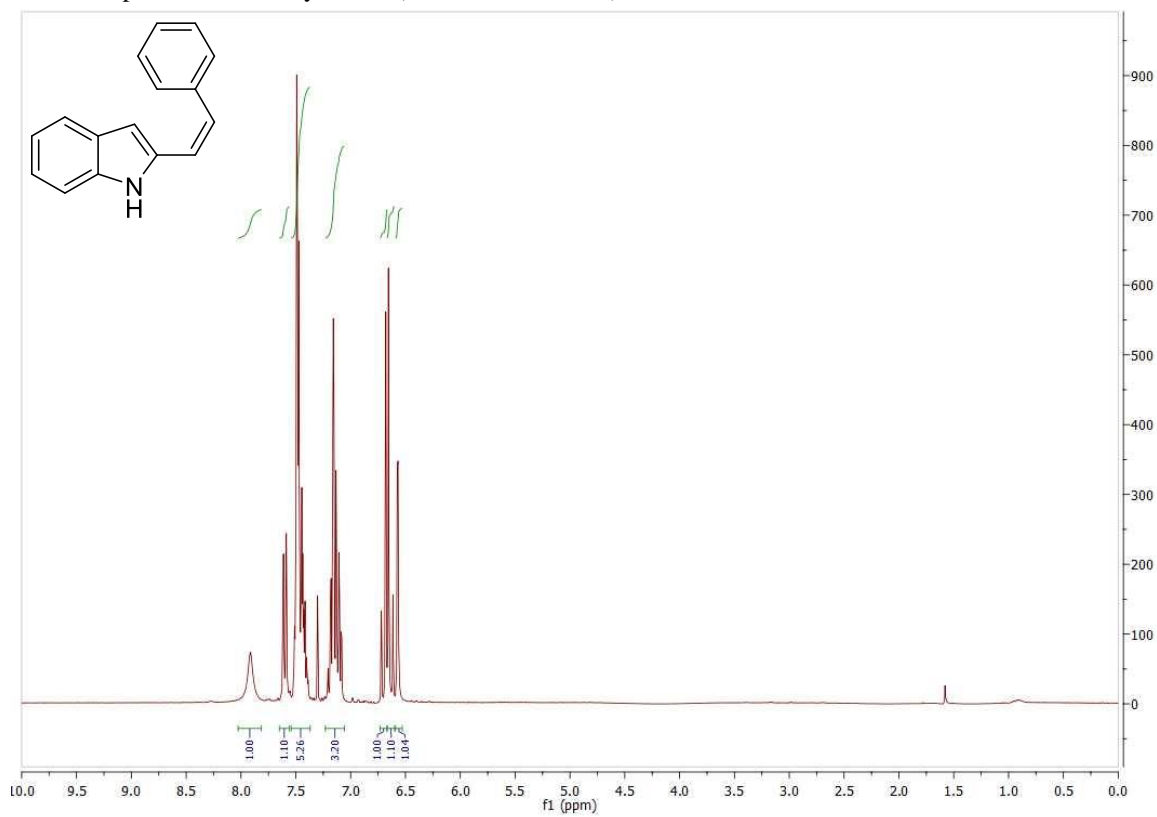
¹H NMR spectrum of alcohol **190** (300 MHz in CDCl₃).



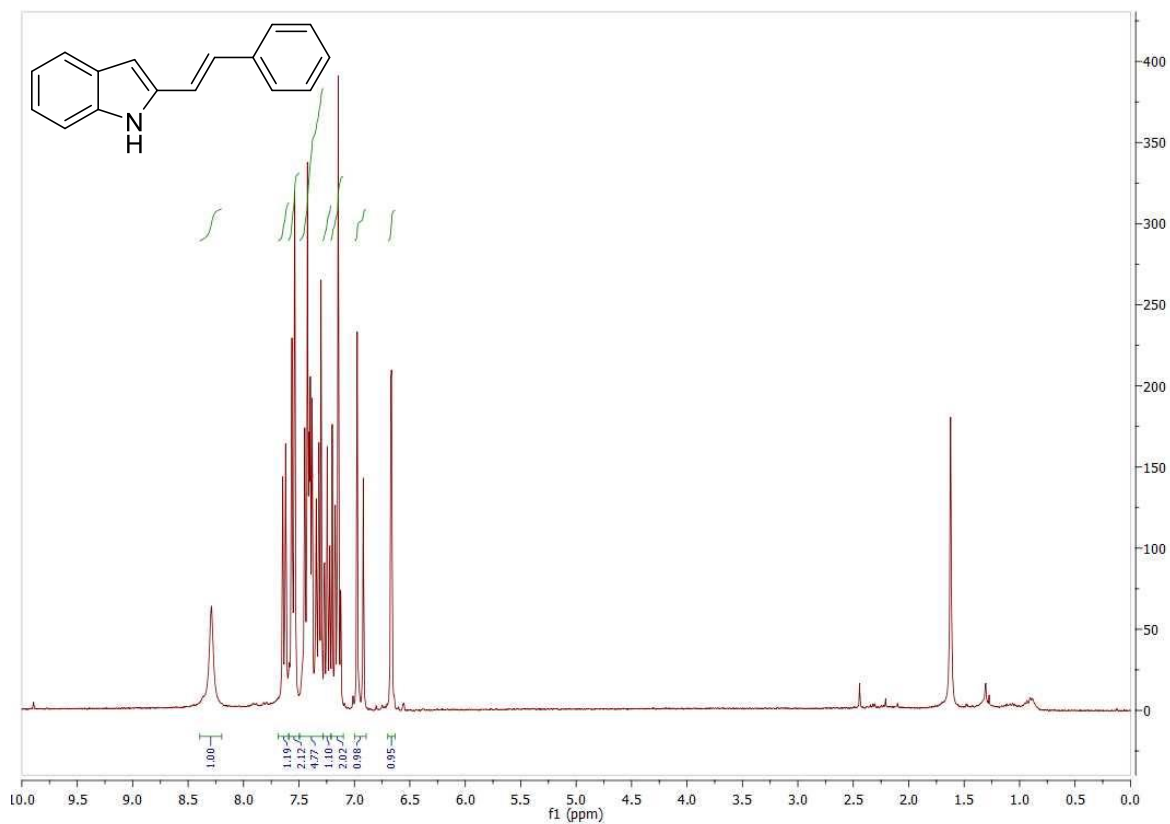
¹³C NMR spectrum of alcohol **190** (75 MHz in DMSO).



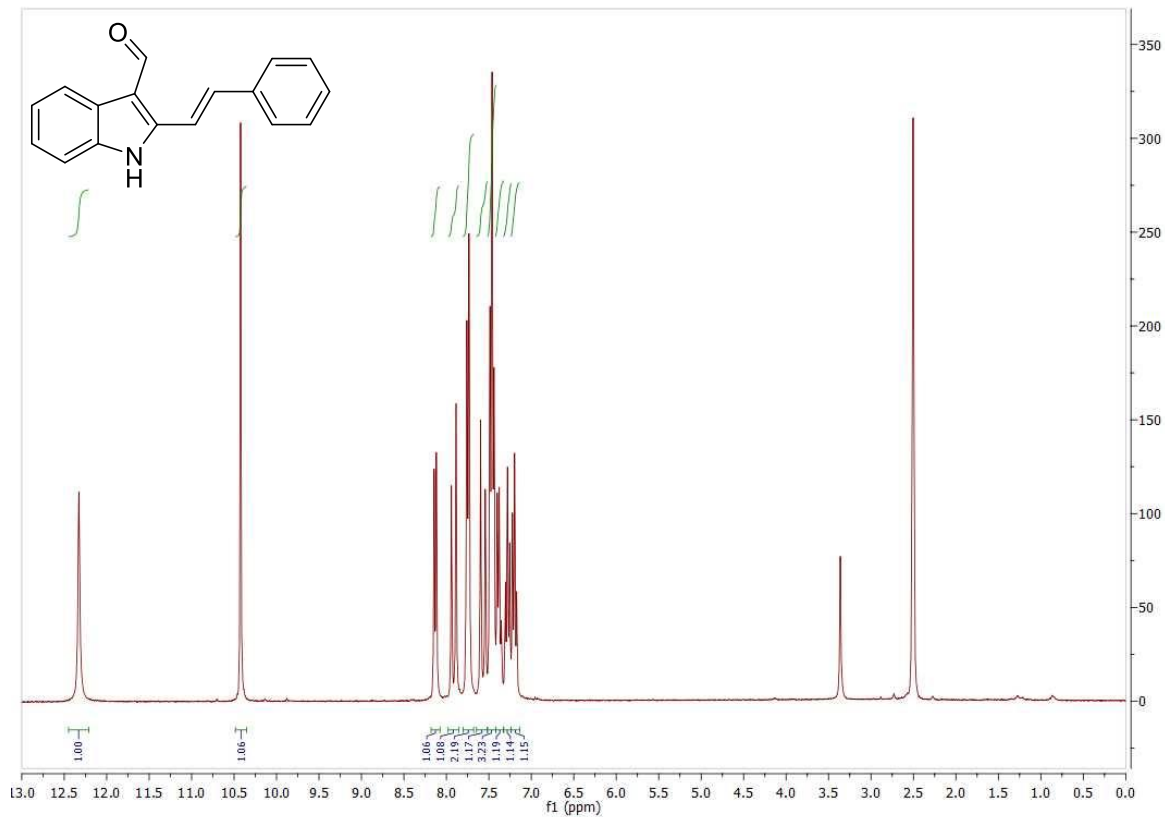
¹H NMR spectrum of aldehyde **191** (300 MHz in CDCl₃).



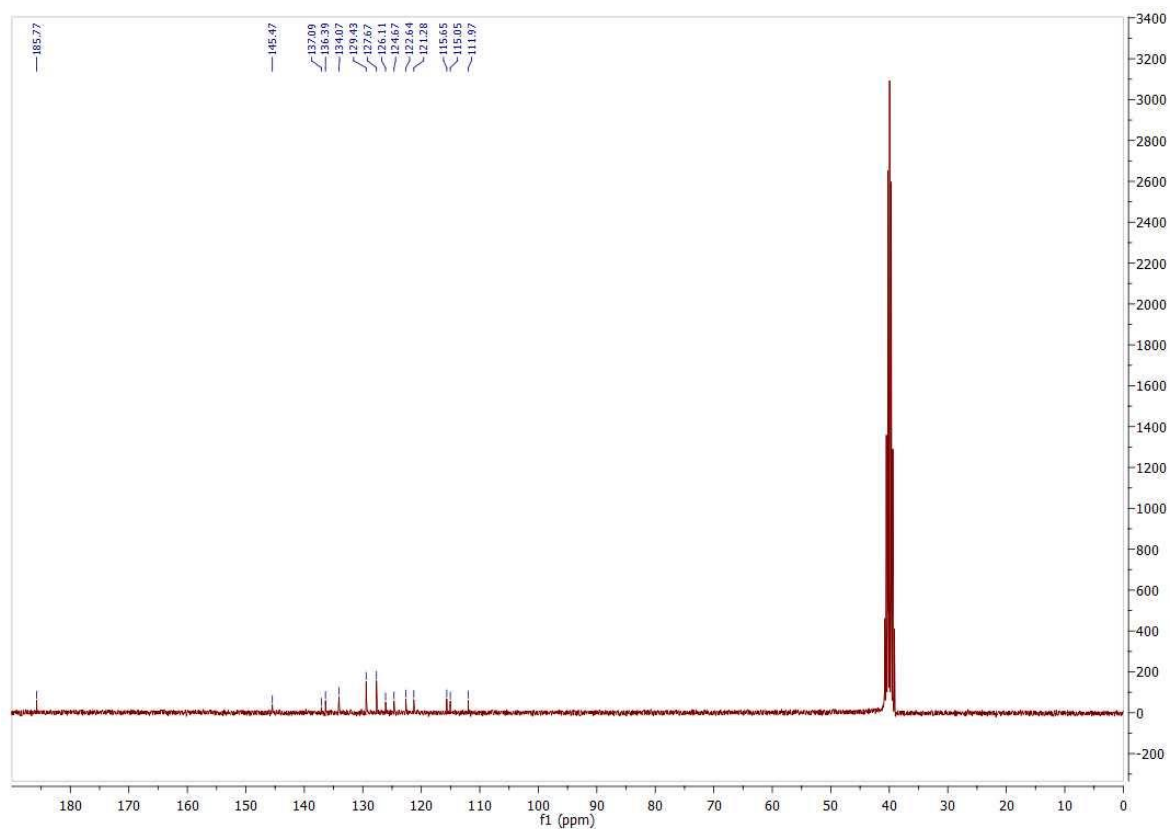
¹H NMR spectrum of compound **Z-192** (300 MHz in CDCl₃).



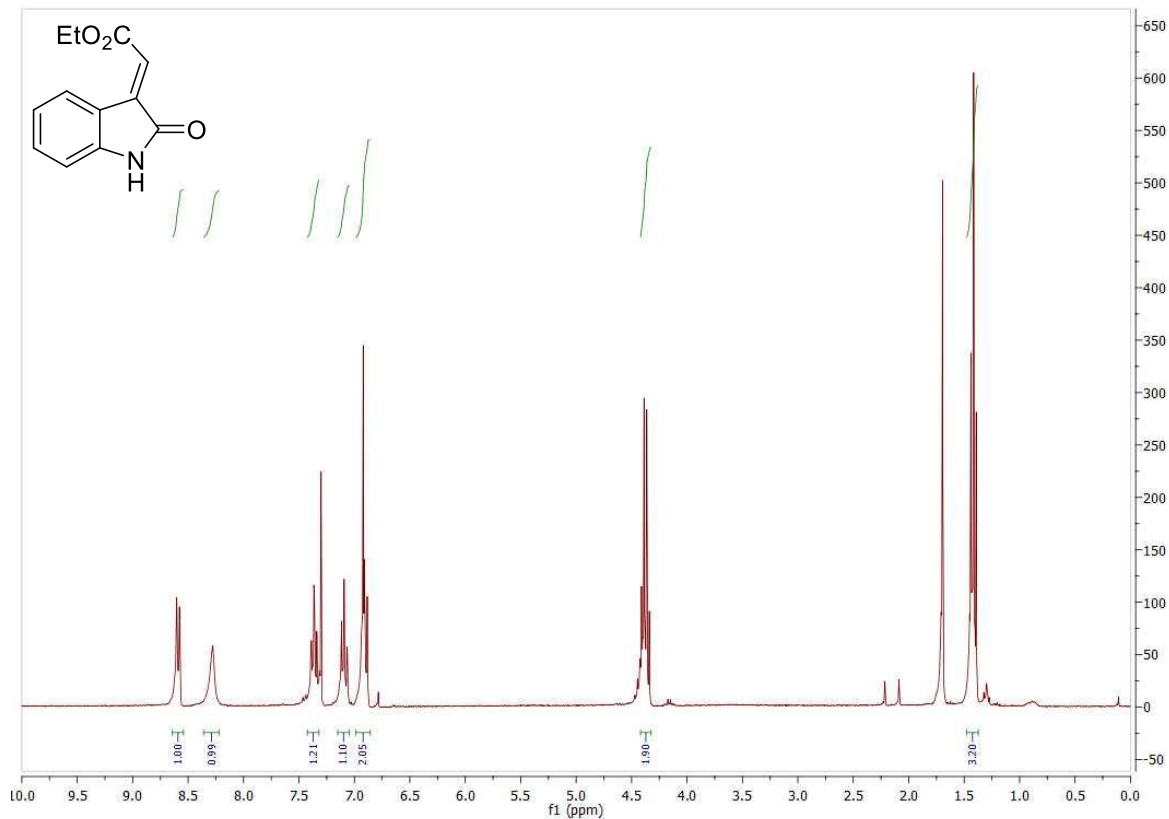
¹H NMR spectrum of compound **E-192** (300 MHz in CDCl₃).



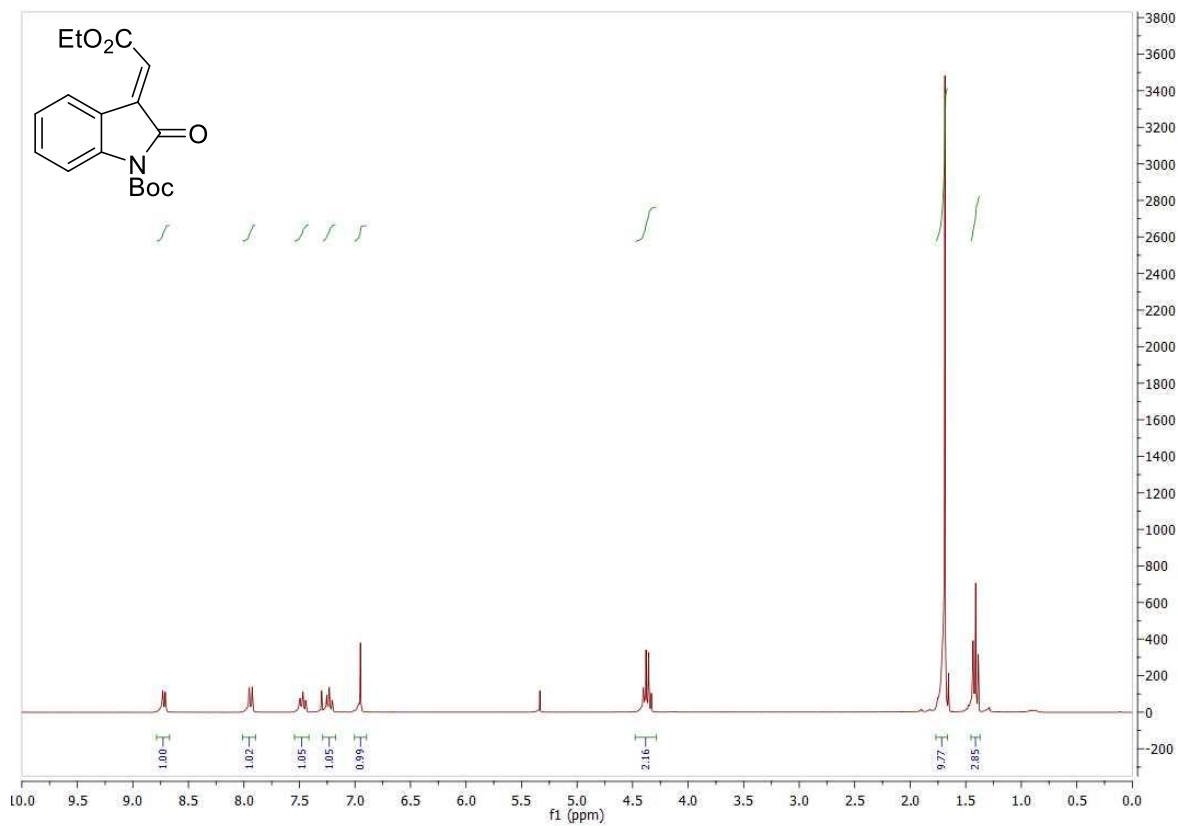
¹H NMR spectrum of compound **134** (300 MHz in DMSO-d₆).



¹³C NMR spectrum of compound **134** (75 MHz in DMSO-d6).

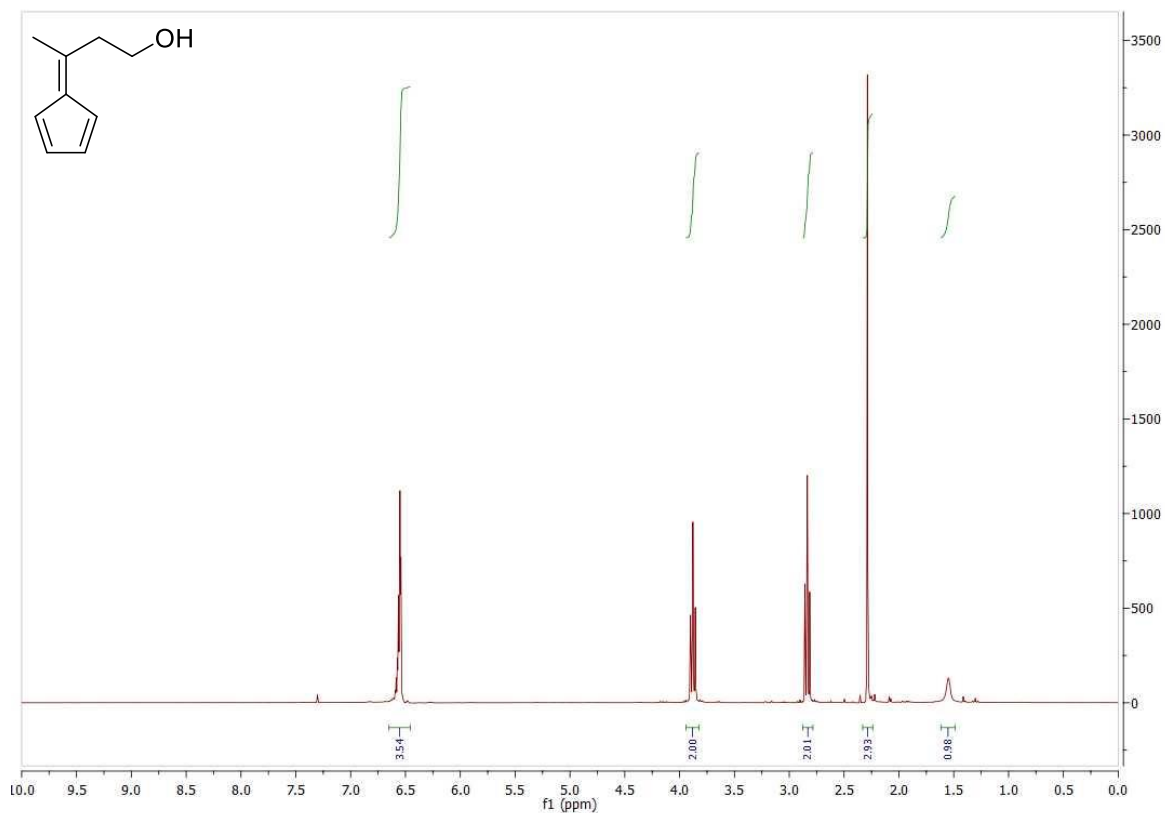


¹H NMR spectrum of 3-olefinic oxindole **193** (300 MHz in CDCl₃).

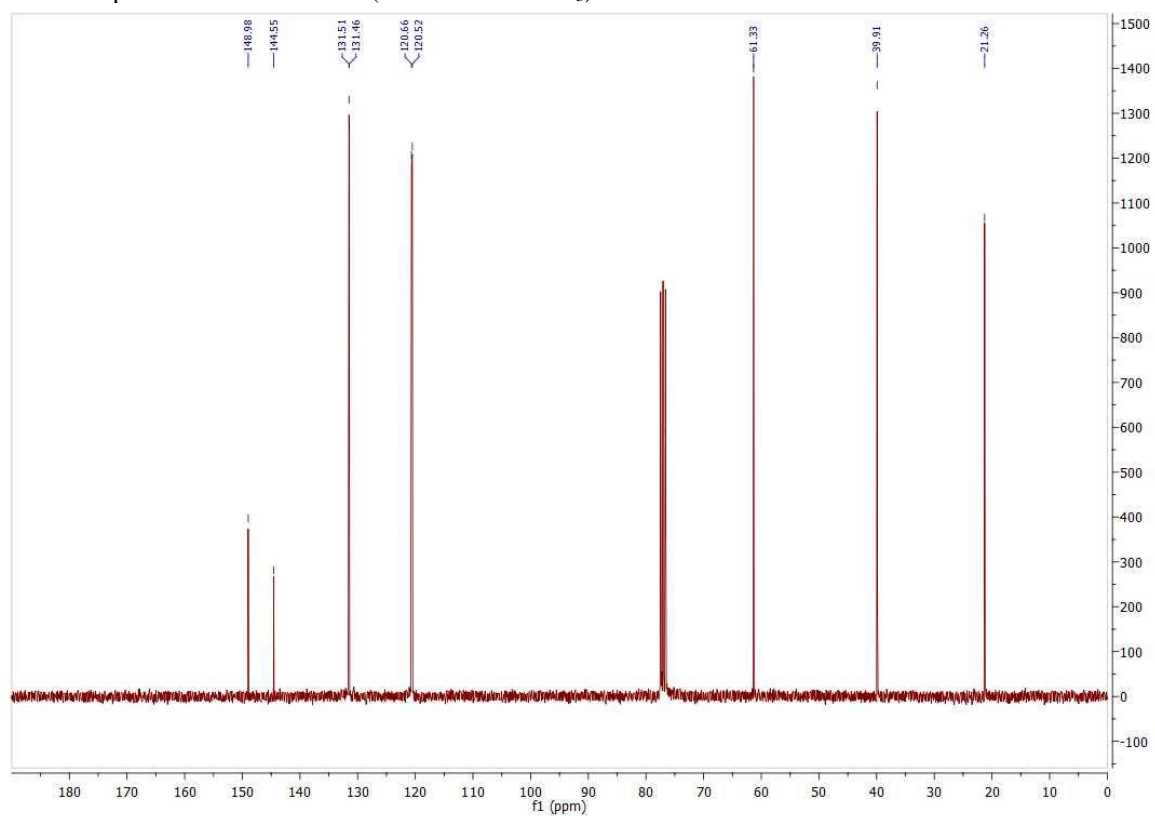


^1H NMR spectrum of 3-olefinic oxindole **67** (300 MHz in CDCl_3).

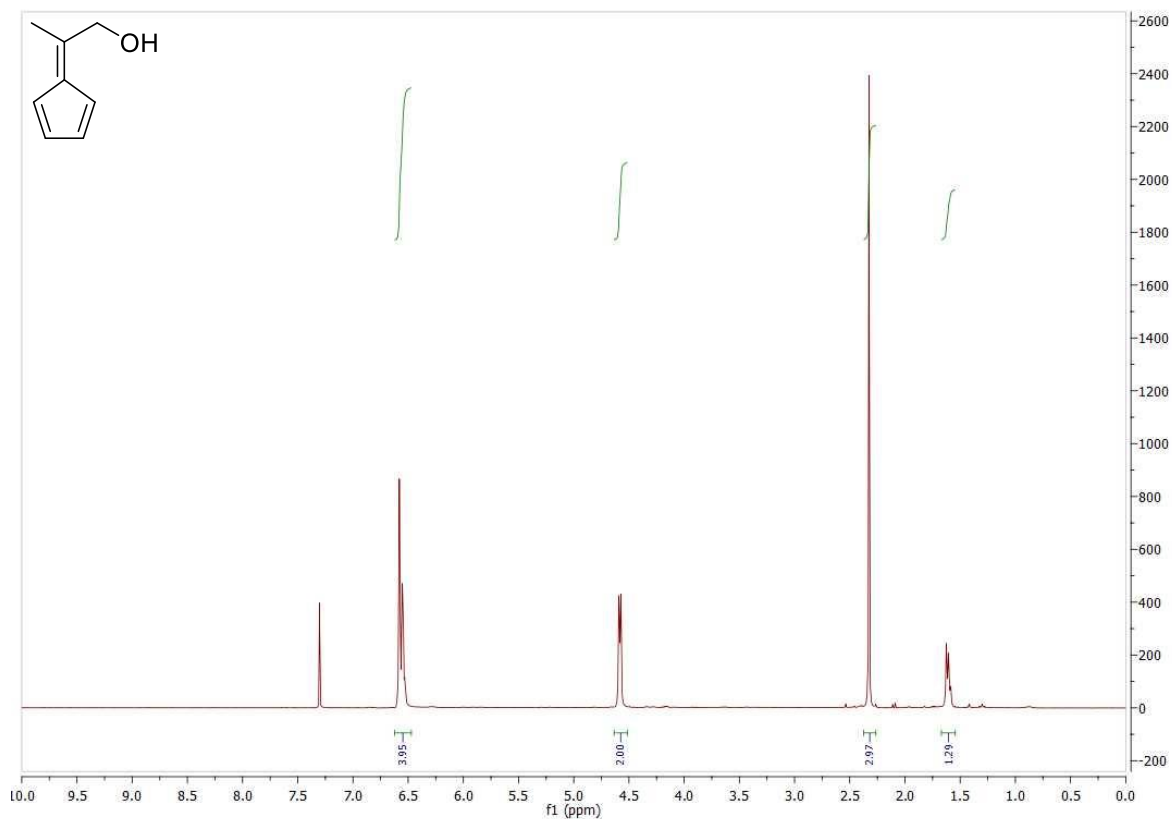
NMR Spectra for the High Order Cycloadditions



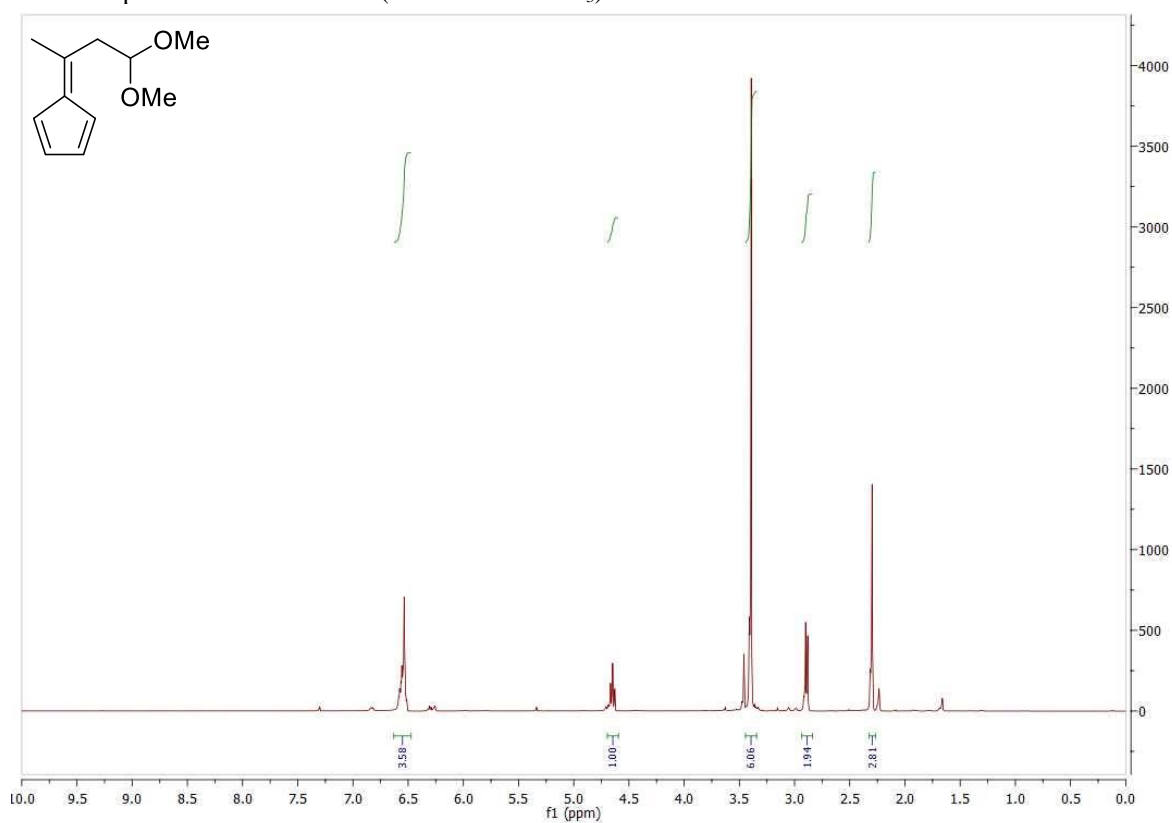
¹H NMR spectrum of fulvene **146** (300 MHz in CDCl₃).



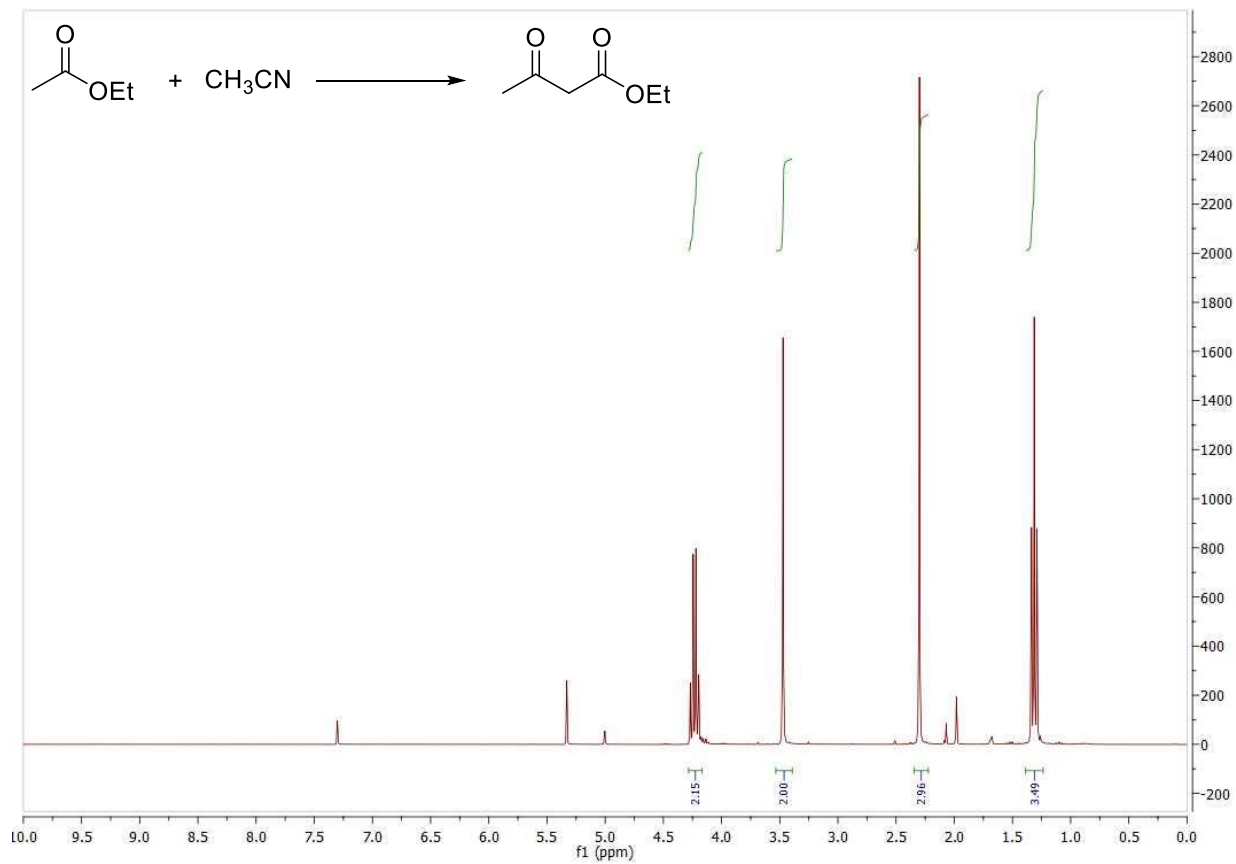
¹³C NMR spectrum of fulvene **146** (75 MHz in CDCl₃).



¹H NMR spectrum of fulvene **157** (300 MHz in CDCl₃).

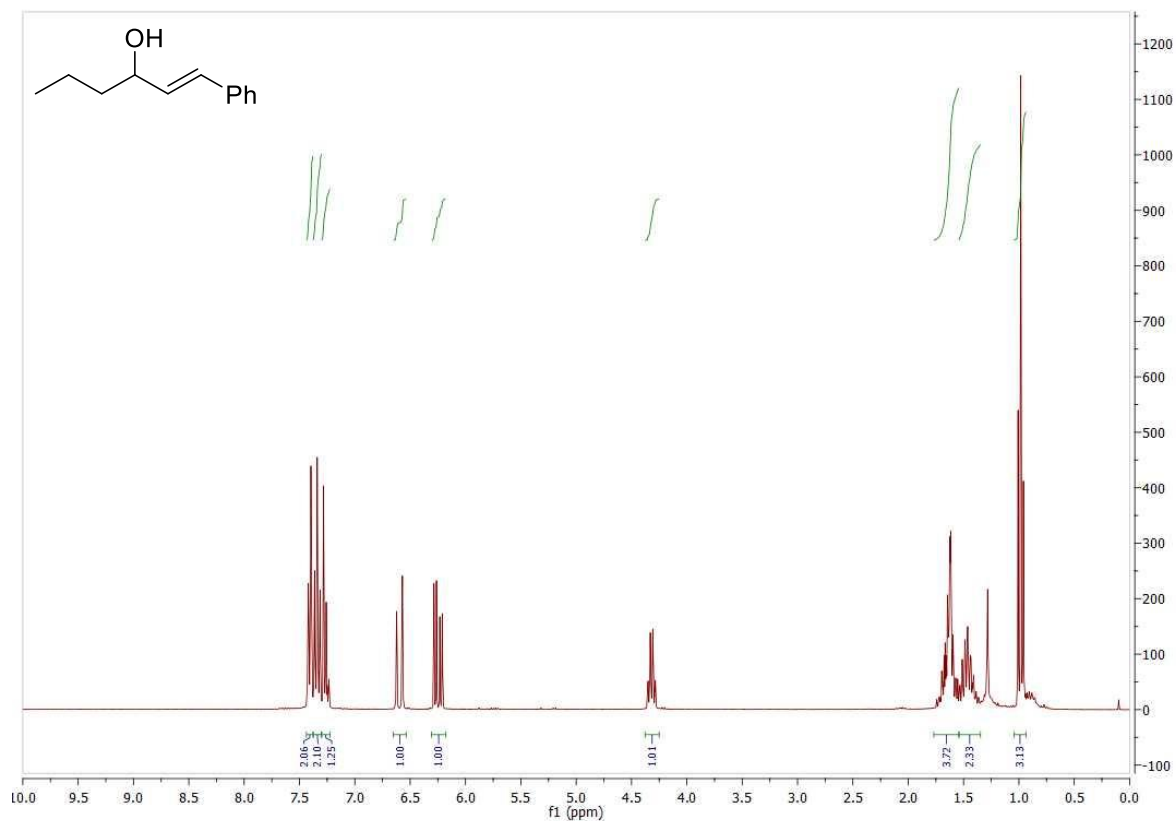


¹H NMR spectrum of fulvene **162** (300 MHz in CDCl₃).

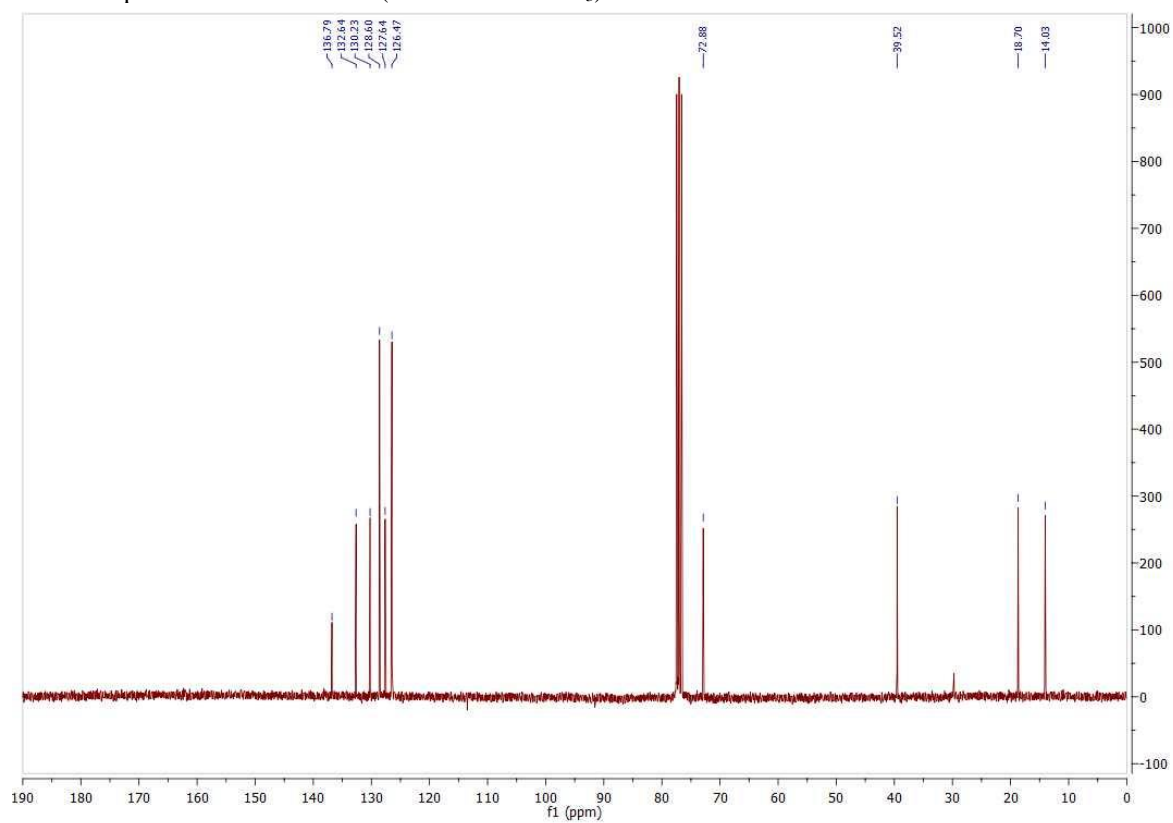


^1H NMR spectrum of the product from the attempted synthesis of **159** (300 MHz in CDCl_3).

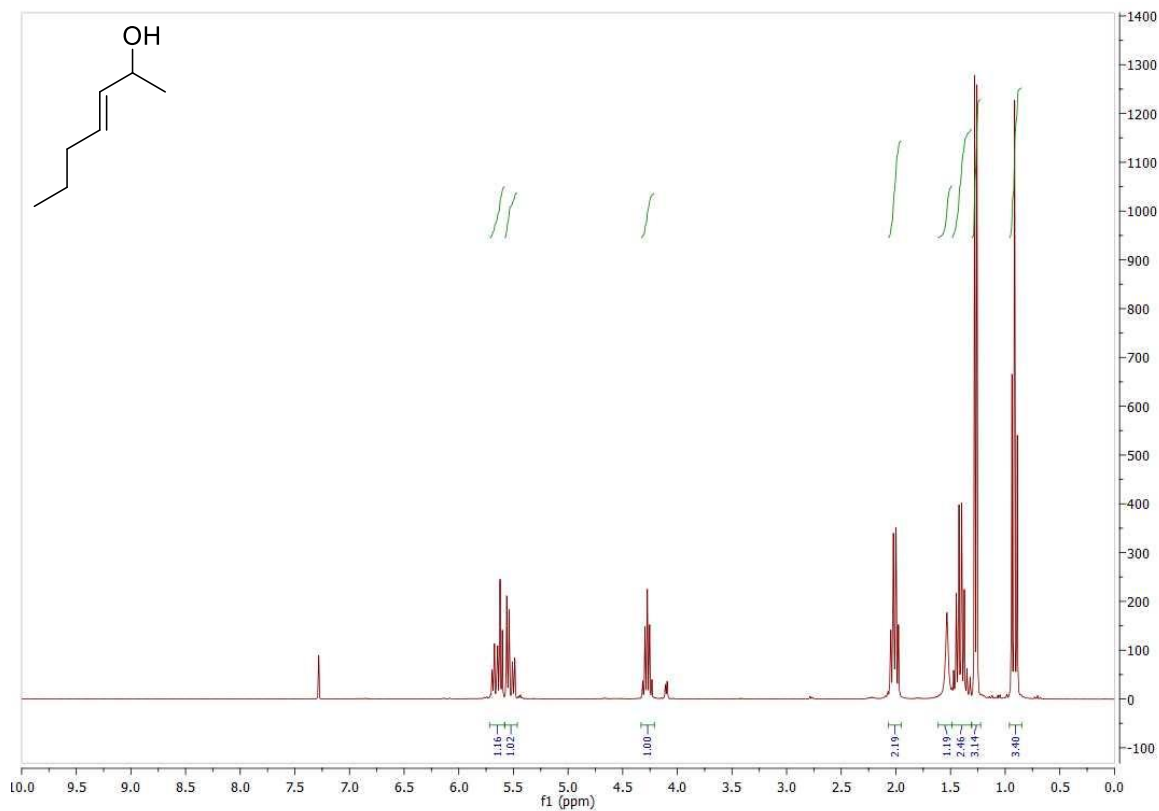
NMR Spectra of Ireland-Claisen Rearrangement



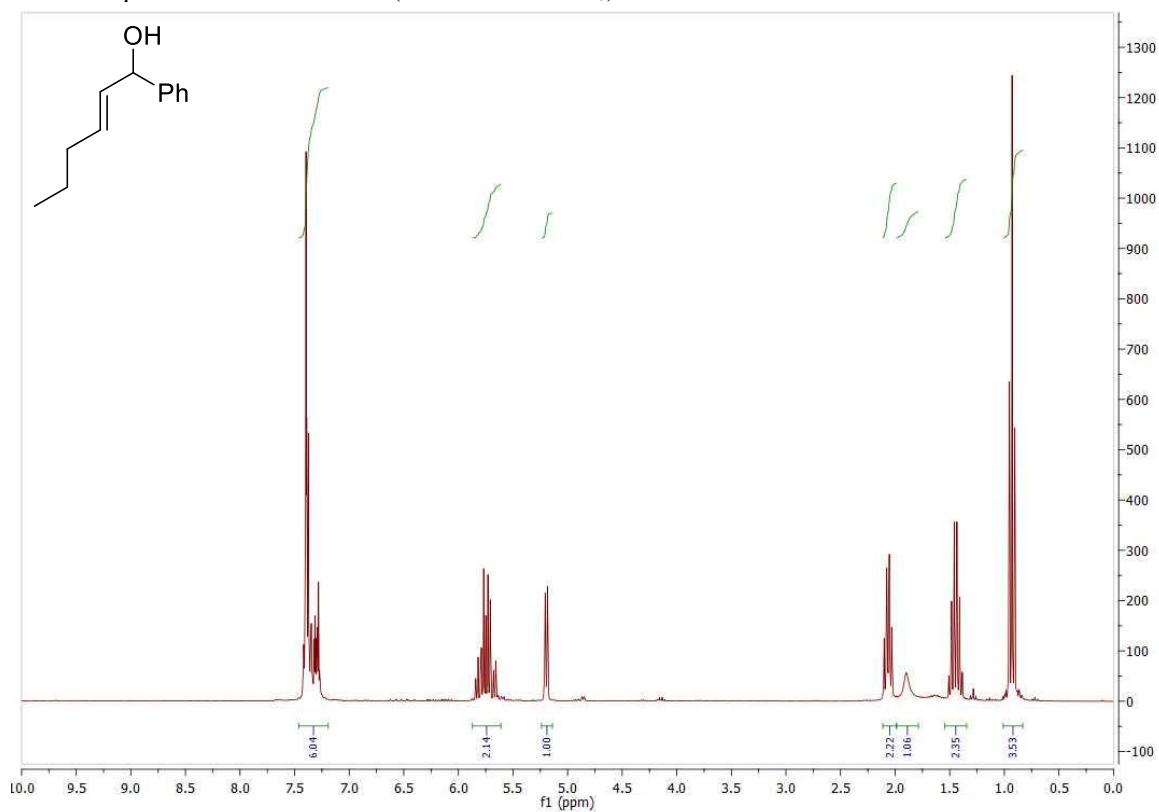
^1H NMR spectrum of alcohol **171** (300 MHz in CDCl_3).



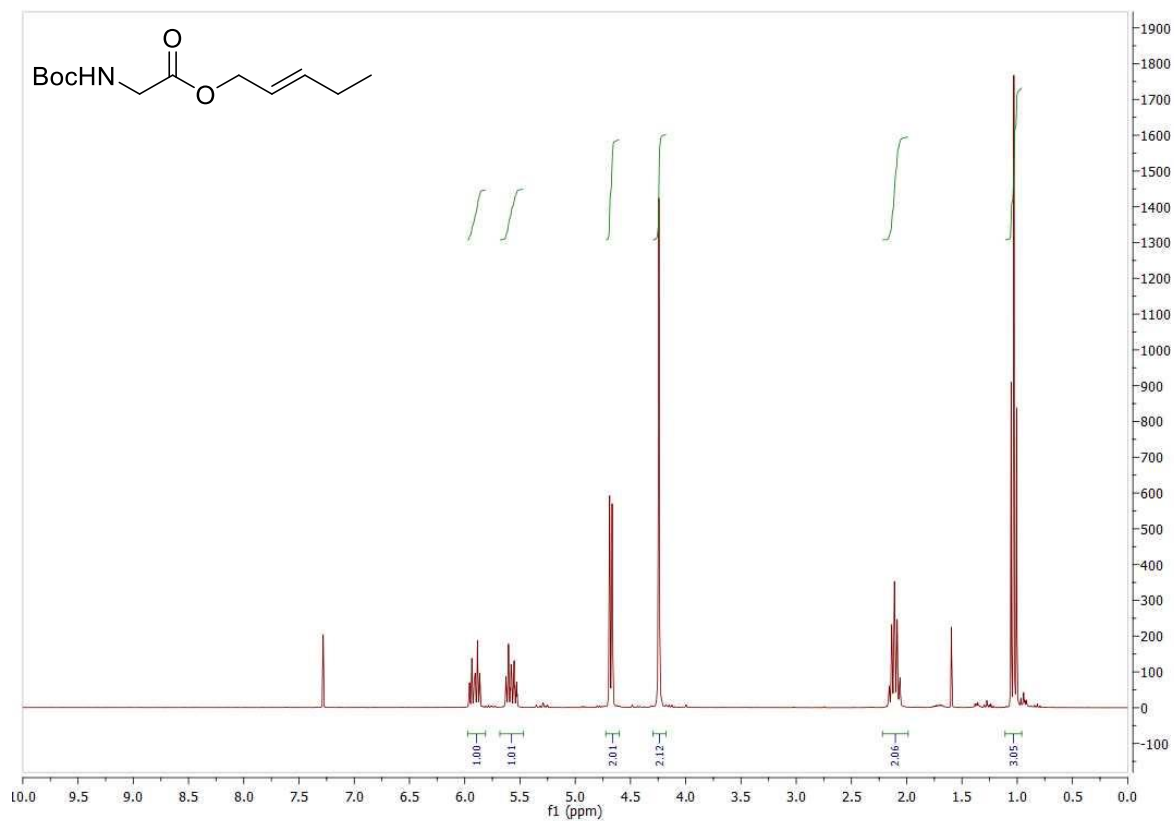
^{13}C NMR spectrum of alcohol **171** (75 MHz in CDCl_3).



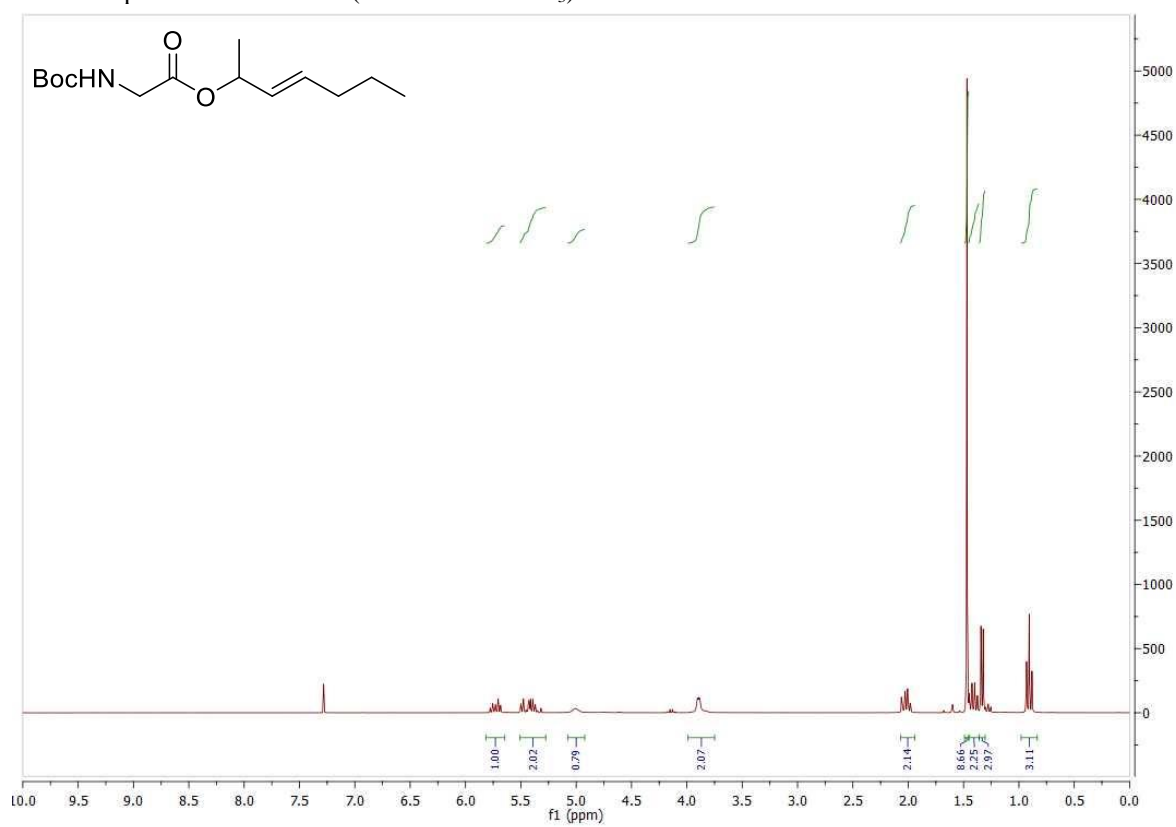
¹H NMR spectrum of alcohol **194a** (300 MHz in CDCl₃).



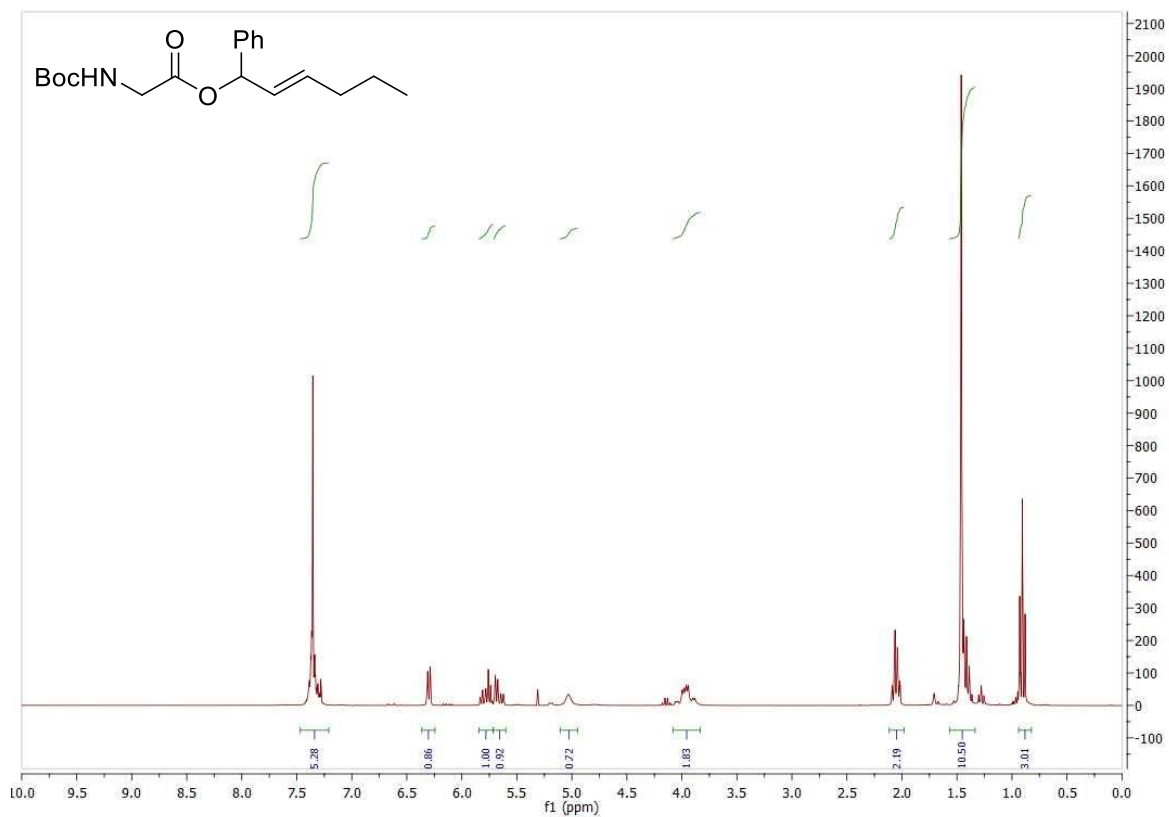
¹H NMR spectrum of alcohol **194b** (300 MHz in CDCl₃).



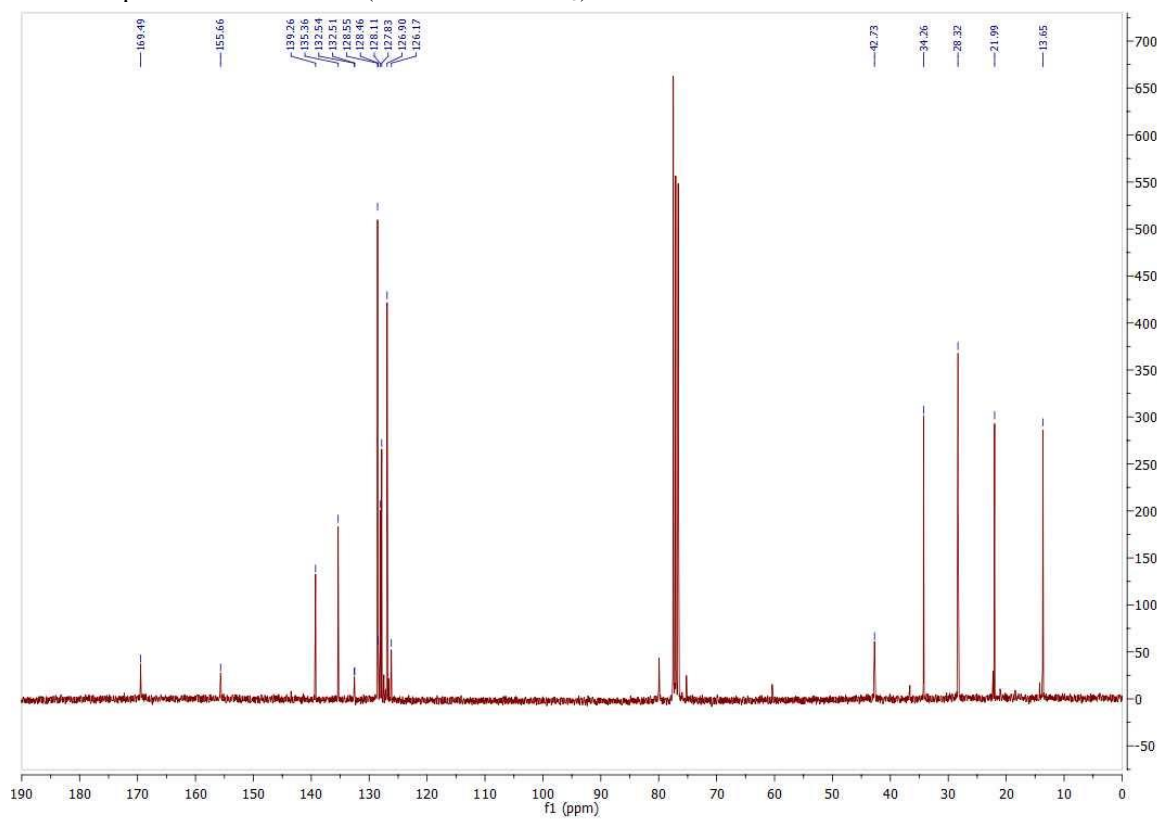
^1H NMR spectrum of ester **169** (300 MHz in CDCl_3).



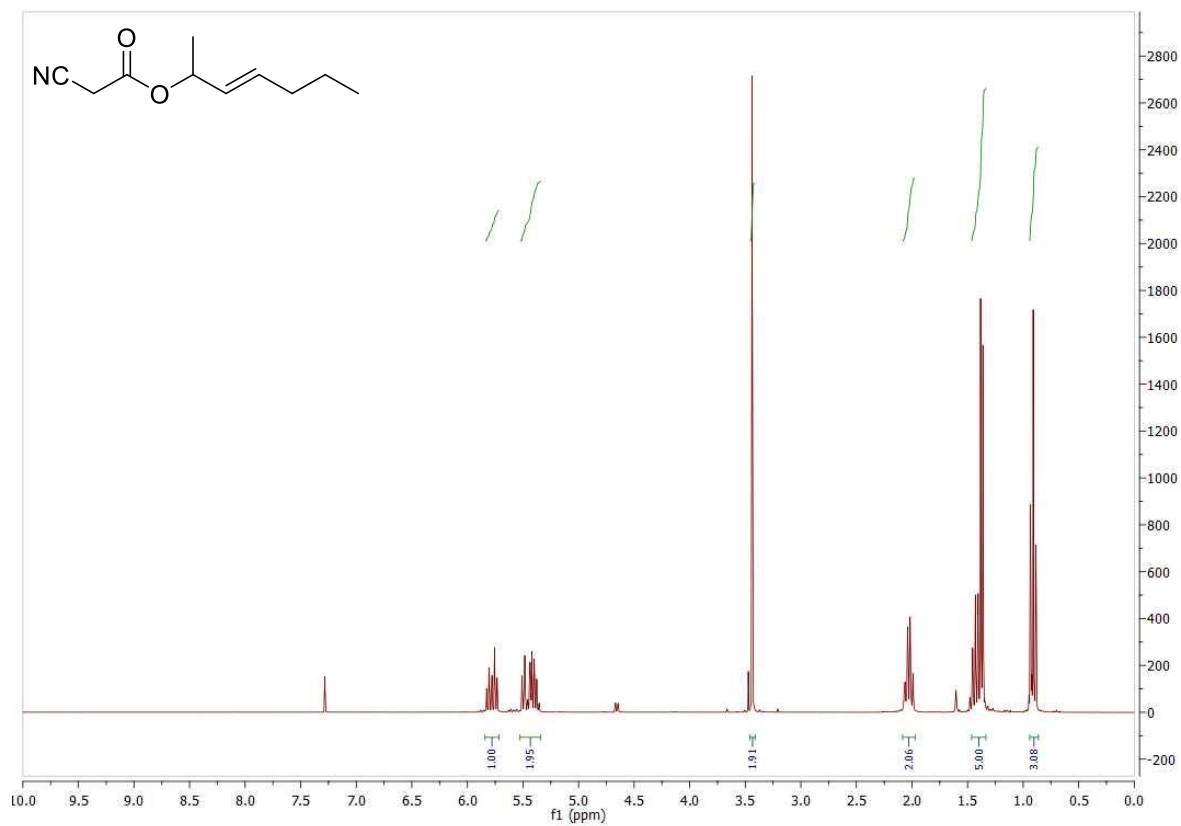
^1H NMR spectrum of ester **169a** (300 MHz in CDCl_3).



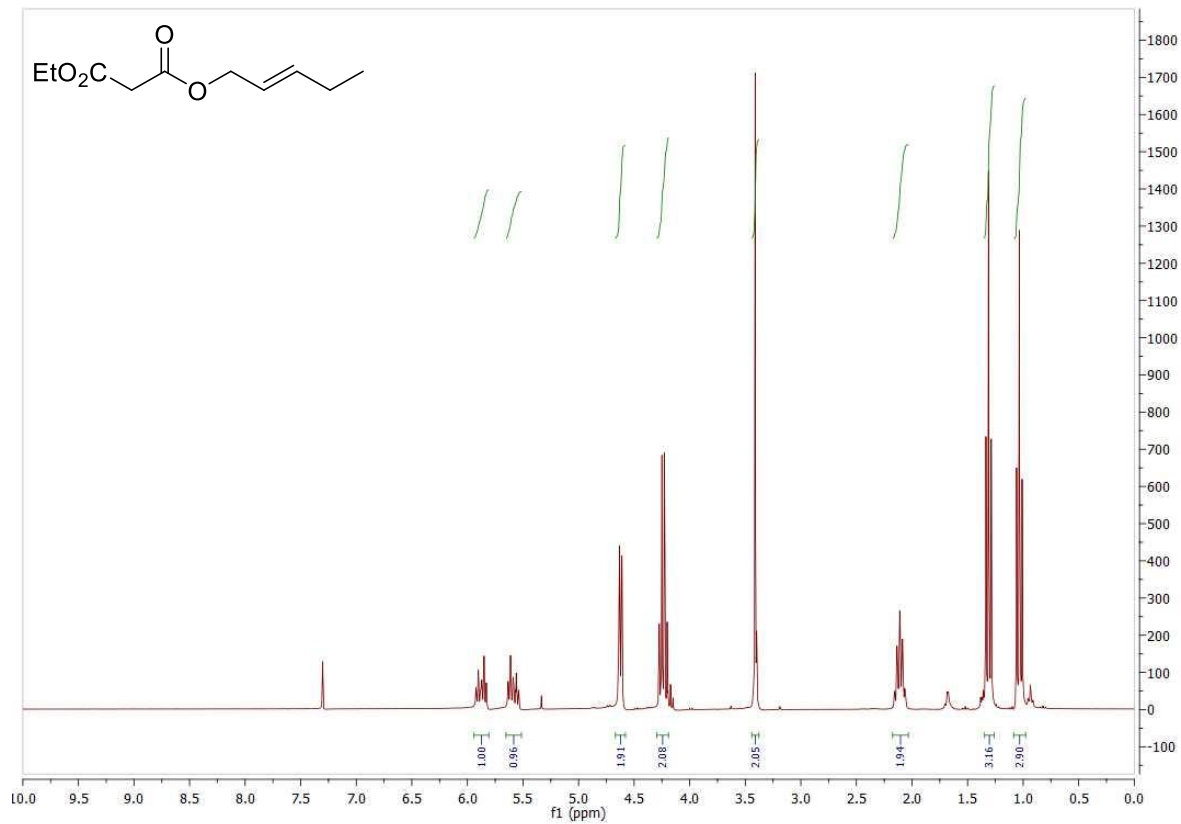
¹H NMR spectrum of ester **169b** (300 MHz in CDCl₃).



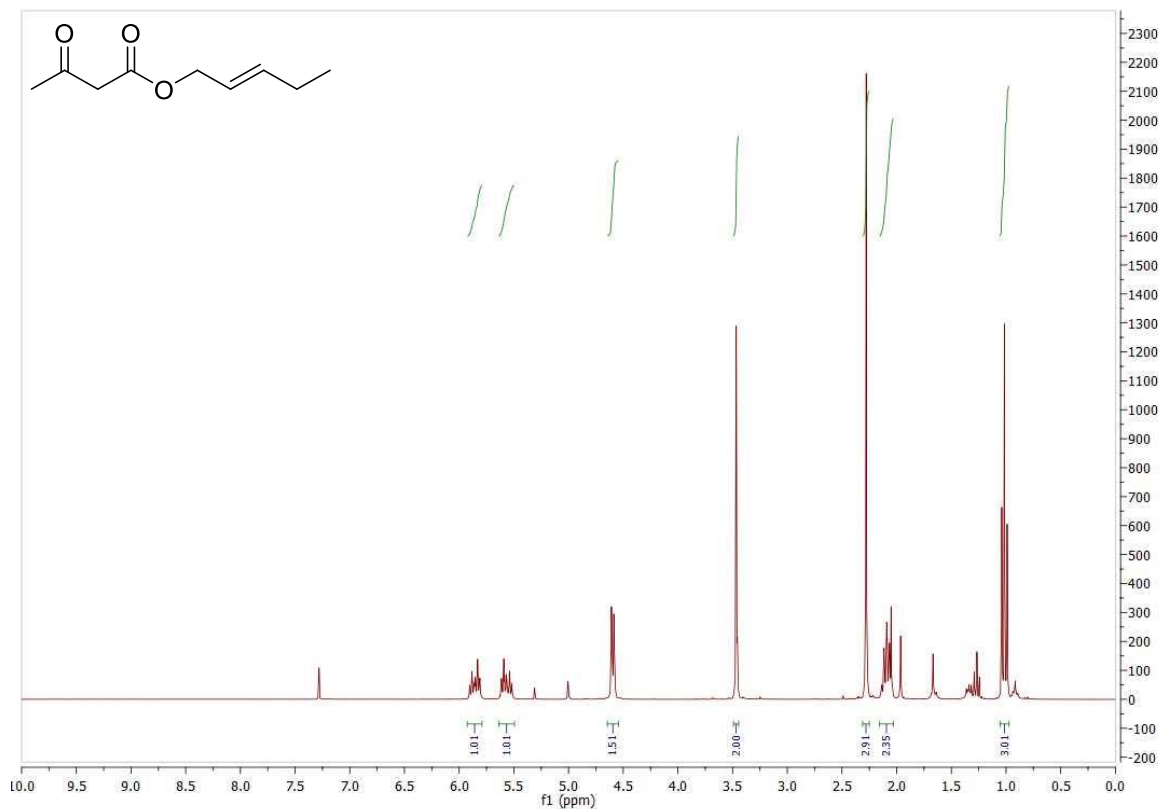
¹³C NMR spectrum of ester **169b** (300 MHz in CDCl₃).



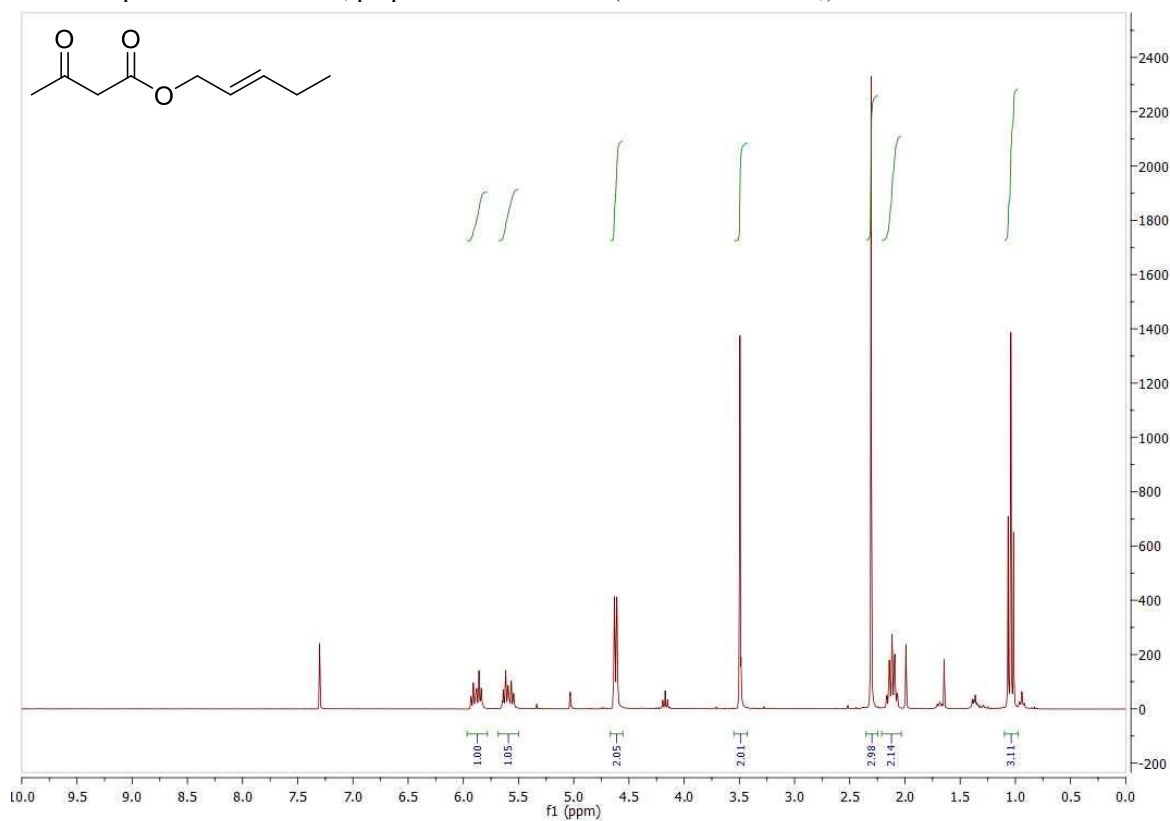
¹H NMR spectrum of ester **173** (300 MHz in CDCl₃).



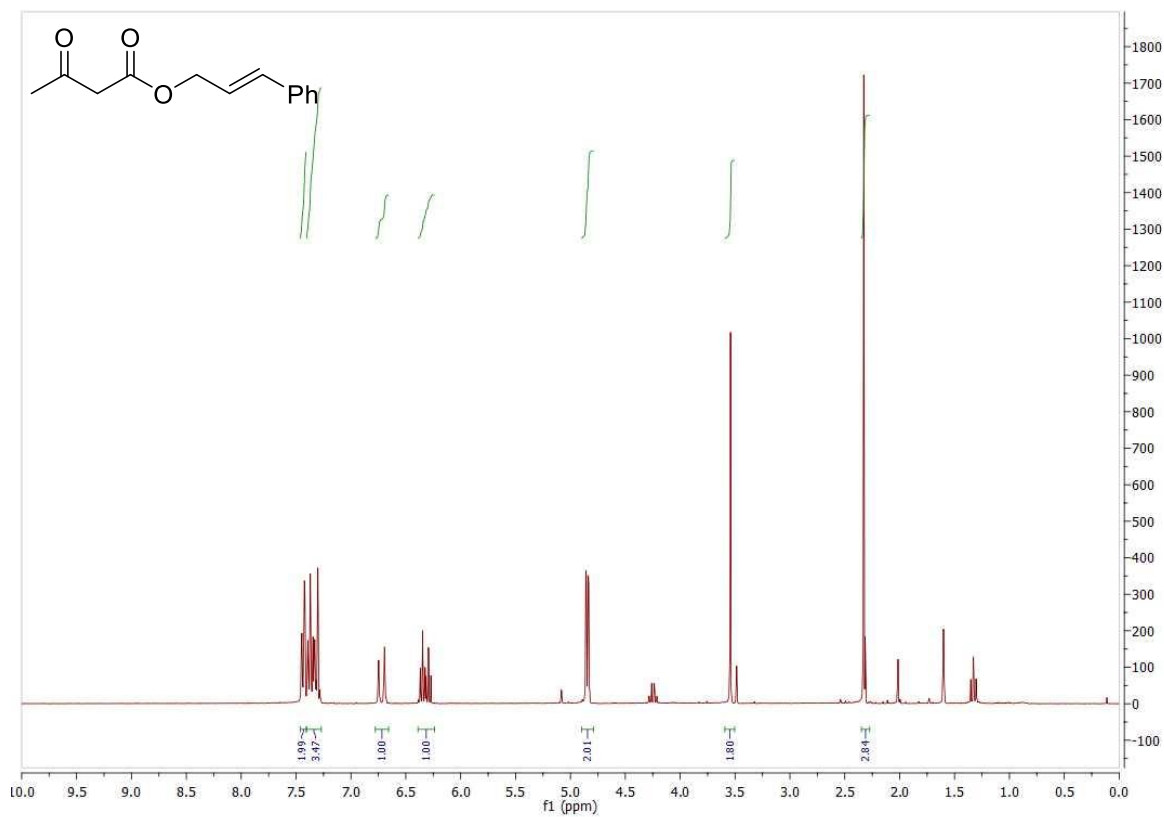
¹H NMR spectrum of ester **178** (300 MHz in CDCl₃).



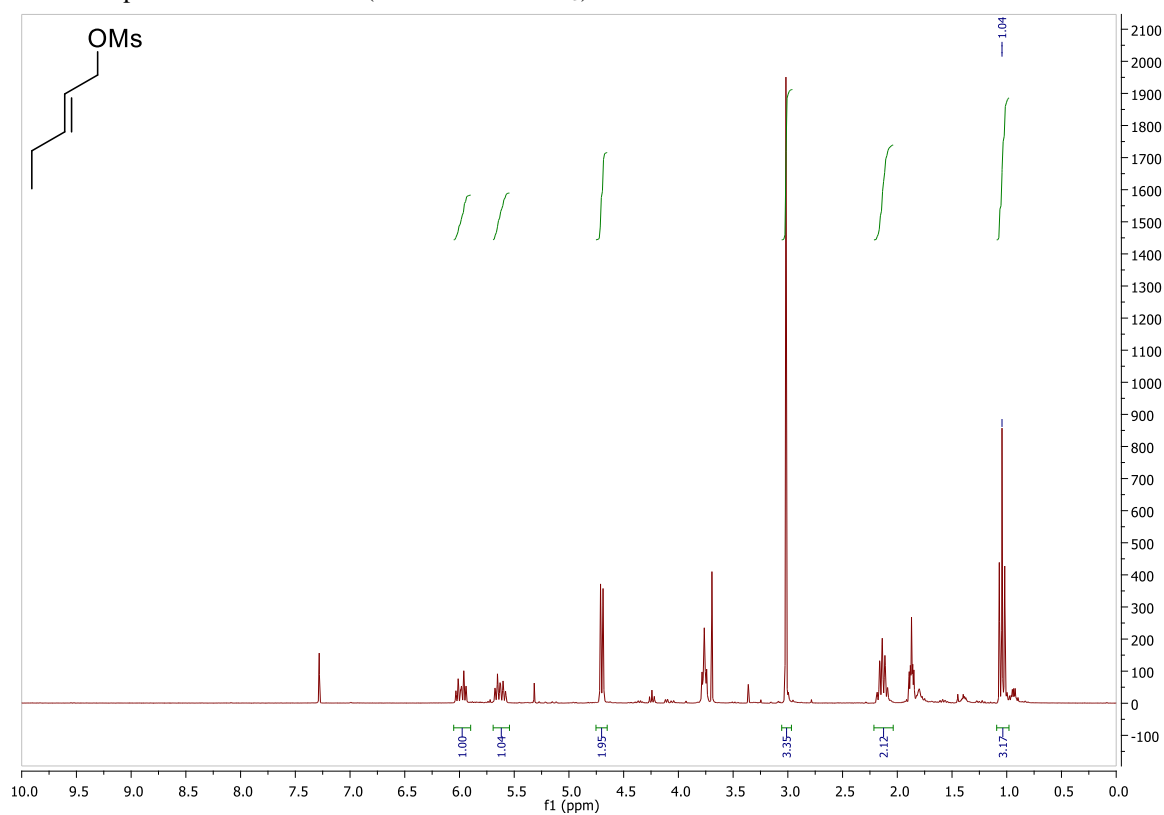
¹H NMR spectrum of ester **175**, prepared via Method A (300 MHz in CDCl₃).



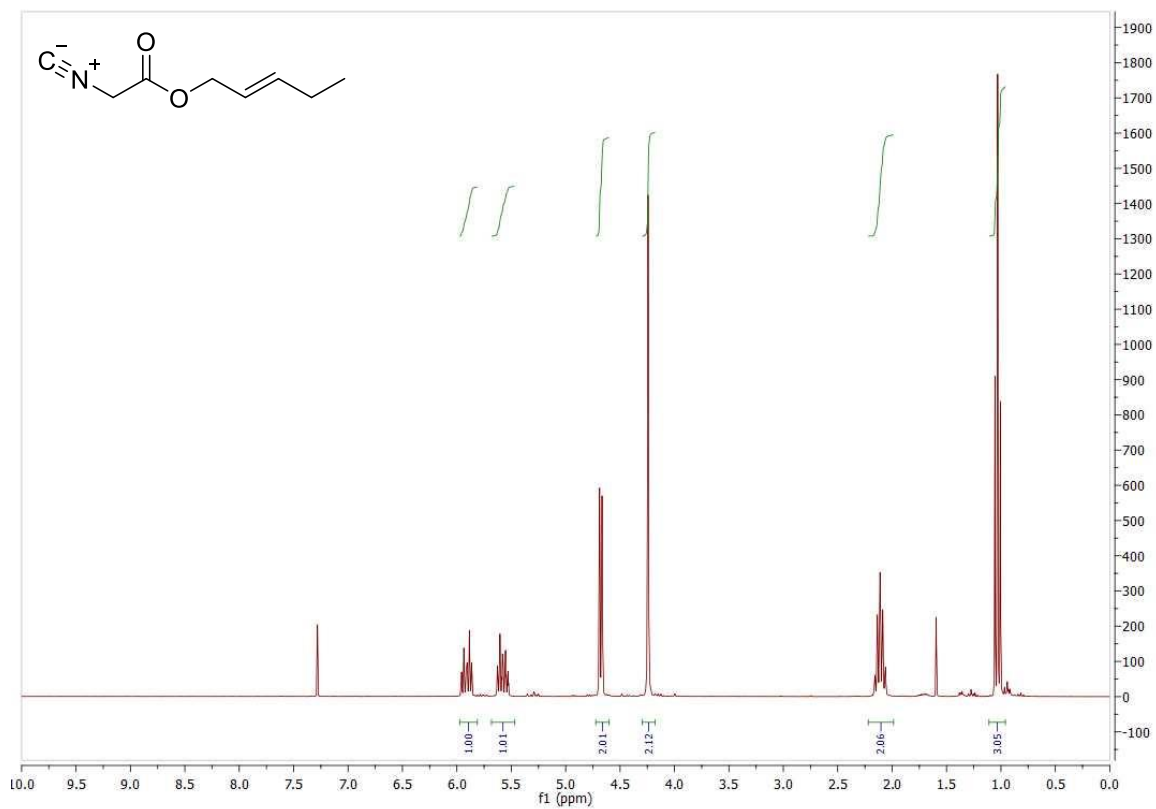
¹H NMR spectrum of ester **175**, prepared via Method B (300 MHz in CDCl₃).



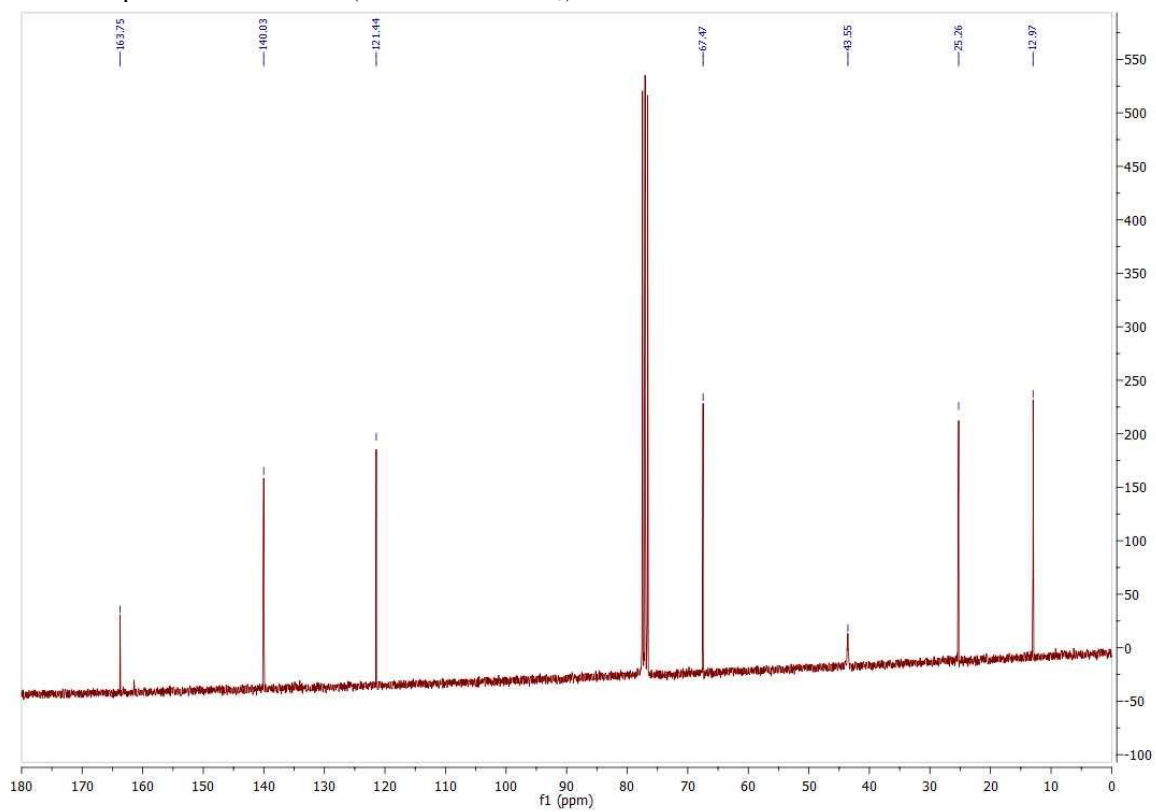
^1H NMR spectrum of ester **175b** (300 MHz in CDCl_3).



^1H NMR spectrum of mesylated alcohol **195** (300 MHz in CDCl_3).



¹H NMR spectrum of ester **177** (300 MHz in CDCl₃).



¹³C NMR spectrum of ester **177** (75 MHz in CDCl₃).